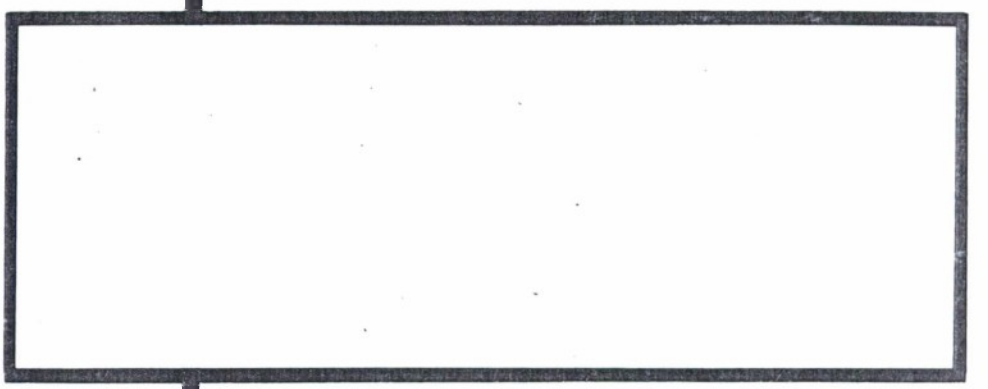

SCIENCE SERVICES DIVISION

TEXAS INSTRUMENTS
INCORPORATED
6000 LEMMON AVENUE
P O BOX 5621 • DALLAS TEXAS

Copy # 14

LASA DATA ANALYSIS AND MCF SUPPORT

FINAL REPORT

AF19(628)5167

by

Harry Lake, Project Manager

George Hair, Project Scientist

Don Crouch
Bill Johnson
Terry Harley
Jim Wrenn

TEXAS INSTRUMENTS INCORPORATED
Science Services Division
P. O. Box 5621
Dallas, Texas 75222

31 August 1966

Contract No.: MIT Subcontract No. 325
under Prime Contract No.
AF 19(628)-5167 (ARPA Order 512)

Prepared for

Massachusetts Institute of Technology Lincoln Laboratory
Lexington, Massachusetts

Work Sponsored by the U.S. Advanced Research Project Agency of the Department of Defense

Project VELA UNIFORM

ABSTRACT

With the objective of determining optimum design criteria for predetection multichannel filters for use at the subarray level at the LASA, a study was conducted of the characteristics of the ambient noise fields and instrument responses of five selected subarrays.

Characteristics of the ambient noise fields which relate to design of multichannel filters and which were studied include

- Coherence as a function of distance between seismometers as well as a function of frequency
- Power density as a function of frequency and wavenumber
- Isotropicity of noise fields
- Similarity of noise fields at widely separated subarrays
- Similarity of daytime noise fields and nighttime noise fields

Characteristics of individual instrument responses studied include

- Variation among elements of a particular subarray in amplitude and phase response at selected frequencies
- Variation with time in amplitude and phase response of each instrument at 1 cps
- Degree to which phase responses can be equalized by minimum-phase equalization filters

Based on the measured characteristics of the noise fields and instrument responses, 14 multichannel filters were developed and compared as to degree of improvement in signal-to-noise ratio. These filters were designed in such a way that only one design criterion differed for each pair compared, thus allowing evaluation of that criterion's effect on filter performance.

A multichannel filter, of a design determined by the comparison experiments to be optimum for subarray predetection filtering, was developed for each of five subarrays. These filters were evaluated

Accepted for the Air Force
Franklin C. Hudson
Chief, Lincoln Laboratory Office

as to frequency-wavenumber response, attenuation of ambient noise and signal distortion. Five multichannel filters of a slightly different design also were developed. These filters achieve greater signal-to-noise improvement in the case of signals with horizontal velocity components above 20 km/sec.

These multichannel filters, and certain others of interest, were punched on paper tape for on-line evaluation with the Digital Multichannel Filter System at LASA.

A processing procedure for detecting signals at either subarray or full-array level is recommended and illustrated by application to selected events at those subarrays under consideration.

TABLE OF CONTENTS

LIST OF APPENDIXES

LIST OF TABLES

LIST OF TABLES (CONTD.)

LIST OF ILLUSTRATIONS

LIST OF ILLUSTRATIONS (CONTD)

LIST OF ILLUSTRATIONS (CONTD)

LIST OF ILLUSTRATIONS (CONTD)

LIST OF ILLUSTRATIONS (CONTD)

LIST OF ILLUSTRATIONS (CONTD)

LIST OF ILLUSTRATIONS (CONTD)

LIST OF ILLUSTRATIONS (CONTD)

SECTION I

INTRODUCTION AND SUMMARY

A. INTRODUCTION

The objective of the study conducted under MIT Lincoln Laboratory Subcontract 325, AF 19 (628)-5167 Prime, was the specification of design criteria for optimum predetection multichannel filters to be used at the subarray level on the Large Aperture Seismic Array (LASA). Certain characteristics of the ambient noise fields and the instrument responses, and the variability of both factors with time were investigated since they bear directly on the problem of optimum filter design. Multichannel filters of the type determined to be optimum for predetection processing were developed for five subarrays and were evaluated through a comparison of response characteristics, noise attenuation and lack of signal distortion.

A number of both daytime and nighttime ambient noise samples were used to study and compare noise fields and to develop measured-noise multichannel filters. Routine 1-cps calibrations spanning one month were employed to study the time-stability of instrument responses, and a special multifrequency calibration was employed to study variation in response among the instruments within selected subarrays. The remainder of the data ensemble consisted of recordings of several teleseismic P-waves which were used for filter evaluation. Direct copies of LASA field tapes were used for the entire data ensemble.

Since the objective was the determination of the optimum type of MCF for predetection processing and was not the actual development of such filters for all 21 subarrays, only five of the subarrays were selected for study and filter development. These five were selected to give the maximum separation between subarrays and hence a good representation of the differing conditions across the LASA. This number of subarrays was considered to be both economical and adequate for the purposes of the investigation. Demultiplexing to individual records of each channel to be processed was necessary and desirable due to the multiplexed format in which the data was received and the small number of subarrays to be processed. The bulk of data processing was accomplished on the IBM 7044 computer, with a small amount of filter application and detection processing accomplished on the TIAC* (Texas Instruments Automatic Computer).

---

*Trademark of Texas Instruments Incorporated

While the data ensemble was being collected and prepared for analysis, the wavenumber resolution of a LASA subarray was measured by designing two multichannel filters from theoretical noise and signal models. In one case the noise was modeled as a disk in the wavenumber plane and the signal as a point source from which energy propagated from North to South across the subarray at an apparent horizontal velocity of 18 km/sec. In another case the noise was modeled as an annulus in the wavenumber plane and the signal as having an infinite apparent horizontal velocity. These two filters were fully described and analyzed in Special Report No. 1 and Special Report No. 2*. After an inspection of the filter responses, the conclusion was that directional signal models and distributed signal models were justified by the subarray wavenumber resolution below 2.0 cps.

Optimum design criteria for subarray predetection multichannel filters were determined by designing and comparing a number of filters for one subarray. Only one design parameter differed for the pair of filters being compared in each case, thereby allowing an exact assessment of the effect on filter performance of that design parameter.

Multichannel filters were developed for five subarrays, according to the criteria determined by the comparisons previously made, to be optimum for predetection-filtering for 12-km/sec and higher velocity signals. These filters were evaluated by computing their transfer functions and wavenumber responses and by measuring attenuation of ambient noise as a function of frequency. Distortion of teleseismic signals, or lack thereof, was estimated by applying each filter to several signals and comparing with both a single seismometer and an average trace.

A detection processing procedure was illustrated by application to three teleseismic signals at each of the five subarrays. This procedure consisted of squaring the output of a Wiener MCF and integrating over a moving time gate. Earlier work on another project** has indicated this procedure to be equally as good as the analysis-of-variance procedure or the quadratic processor procedure. Since the technique just illustrated is more easily and economically implemented than the other two procedures, it is recommended for use in signal detection.

---

* Texas Instruments Incorporated, 1966: LASA Data Analysis and MCF Support, Special Rpt. No. 1, Feb 24.

Texas Instruments Incorporated, 1966: LASA Data Analysis and MCF Support, Special Rpt. No. 2, Apr.

** Texas Instruments Incorporated, 1966: Array Research Final Rpt., Matrix-Multiply Detection Processing of Array Data, May 24.

Included in this report are two appendixes containing lists of filter weights for all multichannel filters developed in the course of this project and lists of those average correlation functions used in designing the five final filters.

The five optimum filters designed to pass all signals of apparent horizontal velocity greater than 12 km/sec were punched into paper tape for input to the on-line digital MCF system. Additionally, five multichannel filters of exactly the same design as the disk signal model filters, except for the use of infinite velocity signal models in design, were also supplied on punched tape. These filters provide better noise attenuation at the expense of some signal attenuation (above 1 cps) below 20 km/sec in apparent horizontal velocity. MCF 11 and MCF 12 were also punched.

B. AMBIENT NOISE CHARACTERISTICS

Although a complete characterizaton of LASA's ambient noise field was not the intent of this project, certain characteristics of the noise field were investigated. Those characteristics investigated were especially significant in determining the optimum type of predetection processing.

Noise coherence as a function of frequency and distance was studied first since this characteristic determines whether multichannel filters can achieve greater noise reduction than a simple beam-steer operation. If the noise in the signal frequency band were not coherent between seismometers, then beam-steering in combination with optimum Wiener frequency-filtering would provide all the S/N improvement possible. The ambient noise was found to be coherent to a significant degree in the signal frequency band (0.5 cps to 3.0 cps). Coherence was measured by developing and applying both single-channel and multichannel spatial prediction filters and measuring the percentage of the noise predictable as a frequency function.

Coherence generally fell off as distance increased between the seismometer whose output was predicted and the seismometer whose output was filtered. However, some noise in the signal band was still predictable at distances of 3.5 km, the subarray radius.

In Section II the results of the noise characterization are presented in detail. In addition to spatial coherence measurements, estimates of the stationarity of the coherent noise component are presented through comparisons of the percent predictable at the time of filter design and the percent predictable six days later. Frequency-wavenumber spectra of representative daytime and nighttime noise samples are presented. Comparison of day and night noise has indicated that multichannel filters designed from an average of daytime and nighttime noise correlations would perform satisfactorily and that specific day and night filters would be unnecessary.

Power density spectra of noise recorded on the center seismometer 500 ft deep and noise recorded on the seismometers 200 ft deep indicated that the noise was identical below 1.5 cps. Above 1.5 cps the center seismometer recorded less noise than did the shallower seismometers; this difference increased almost linearly with the frequency to 7 db at 5.0 cps.

C. VARIATIONS IN INSTRUMENT RESPONSE

Differences in response characteristics of the seismometer-amplifier package from instrument to instrument are of interest in the MCF design problem because if uncompensated, these differences can cause serious signal attenuation. This signal attenuation is due to the fact that theoretical and, therefore, perfectly equalized signal models are usually used in filter development. Two solutions are readily available, however: single-channel filters may be designed from multifrequency calibration data to equalize the response of each instrument to some reference, or the response variations as determined from the calibration analysis may be incorporated into the signal model. The latter method is more easily accomplished and was used for the development of the response-compensated MCF (Section IV, paragraph C).

To test the feasibility of compensating for differences in instrument response by this method and to determine the seriousness of the differences, a special multifrequency calibration of each of five subarrays was conducted. Analysis of this calibration is presented in Section III-B. The differences in both phase and amplitude response were found to be large at all frequencies except near 1.0 cps. Compensation for these differences would clearly improve broadband signal response of the predetection multichannel filters.

Another important instrument response characteristic to MCF design is the instrument's variation with time. If there is significant variation with time, multichannel filters must be redesigned at frequent intervals. Nine calibrations (at 1.0 cps) of each of the 125 instruments being considered were obtained and analyzed to estimate the time-stationarity of each instrument's response. These nine calibrations covered one month and during this period each instrument was found to have a very stable response, except for occasional sudden changes for individual instruments. These sudden changes in response are largely unexplained, although from their nature it is believed that they are due primarily to adjustments, repairs or replacements of the instrument components. Several, but not all, instruments within a subarray would simultaneously experience these sudden response changes which usually better equalized those instruments whose amplitude responses at 1.0 cps deviated most from unity.

These step-like changes in instrument response were very numerous during November 1965. There was such poor correlation for many instruments between the responses at the end of November and the 1-cps response measured in March 1966 when the multifrequency calibrations were run that it was deemed impractical to include compensation for instrument response variations in the design of the five multichannel filters to be supplied for the on-line digital system.

An evaluation of an equalization technique which models the response variation among instruments as the effect of a minimum-phase filter was conducted using a multifrequency calibration test recorded with the Texas Instruments Digital Field System (DFS)* during May 1965. The technique consists of designing for each channel a minimum-phase whitening filter from the ratio of the amplitude response of that channel to the amplitude response of an arbitrary reference channel. Evaluation primarily was concerned with the degree of phase response equalization obtained with this method. Good improvement was obtained at all frequencies, the greatest improvement being near the 1-cps damped resonant frequency of the seismometer. Variations of $\pm 20^\circ$ were typically reduced to less than $\pm 5^\circ$.

D. DETERMINATION OF OPTIMUM DESIGN PARAMETERS FOR PREDETECTION MULTICHANNEL FILTERS

Thirteen multichannel filters were designed and evaluated in order to determine the effects of each design parameter on the S/N ratio improvement capability of each filter. These filters were designed so that only one design parameter differed for each pair to be compared. The pairs of filters were compared as to transfer function, frequency-wavenumber response, ambient noise attenuation, and signal distortion or attenuation. Signal distortion was not considered an undesirable effect as was signal attenuation since the filters were to be used only for predetection-filtering. The specific design parameters whose effects were compared were

- Ring-model (5 and 8) multichannel filters vs 25-channel maximum-likelihood multichannel filters
- Use of an infinite velocity signal model vs use of a disk signal model
- Simulation of instrument response differences in the signal model vs an equalized signal model

*Trademark of Texas Instruments Incorporated

- Variable S/N ratio (permitting filtering on a frequency basis as well as on a velocity basis) vs a constant S/N
- Use of measured-noise statistics vs use of a theoretical noise model
- 1-sec filters vs 2-sec filters vs 6-sec filters
- Whitened measured noise vs nonwhitened measured noise
- Use of daytime noise statistics vs use of nighttime noise statistics

Results of these comparisons are presented and discussed in detail in Section IV.

E. DEVELOPMENT AND EVALUATION OF PREDETECTION MULTI-CHANNEL FILTERS

On the basis of the comparisons of various design parameters, an MCF considered to be optimum for predetection-filtering at the LASA subarray level was developed for each of the five subarrays.

Five-channel ring-model filters were developed in each case. The noise models consisted of weighted and averaged daytime and nighttime noise correlations which had been whitened. The noise was whitened by convolving the measured correlation set with the autocorrelation of a 5-point whitening filter developed from the average of all autocorrelation functions.

Noise correlations were computed for ±40 lags, but the whitening operation limited the available length to ±36 lags. For this reason all filters are 37 points, or 1.85-sec, long.

The signal models simulated a disk in wavenumber space with a radius corresponding to 12 km/sec and were band-limited from 1.0 cps to 3.0 cps. Differing instrument responses were not simulated in the signal models since comparison of November 1965 and March 1966 calibrations at 1.0 cps had indicated significantly different responses for many of the instruments. Also, the filter comparison discussed in Section IV, paragraph C.7 showed that a filter incorporating relative responses estimated from March calibrations into the signal model yielded a S/N ratio improvement 2 or 3 db less than a filter designed from an equalized signal model when both filters were applied to November events. A total signal energy to total noise power ratio of 4 was used for all filter design. Since the noise was prewhitened and the signal model was band-limited, the effective S/N ratio in the signal frequency band was actually nearer to 10 or 12.

These filters were evaluated through computation of transfer functions and frequency-wavenumber responses and through comparison to straight summation as to ambient noise attenuation. Filter response was always within ±1.5 db of unity at velocities greater than 12 km/sec in the frequency band of 1.0 to 3.0 cps. In addition to frequency-filtering outside the signal band, these filters can achieve considerable noise attenuation on a velocity basis.

The wavenumber responses of all filters were remarkably similar. Since average noise statistics were used in filter design, this similarity in response is an indication that the long-term average noise statistics are very similar across the LASA. At 1.5 cps and above, all responses were uniformly low outside the 12-km/sec disk, as would be expected if the majority of the noise at these frequencies was incoherent.

Attenuation of ambient noise in the signal band from 1.0 to 3.0 cps ranged from 3 to 6 db less than that obtained by averaging all 25 channels. This is not particularly surprising in view of the fact that the filters are constrained to pass a very large region in wavenumber space precluding the $\sqrt{n}$ improvement in S/N attained by averaging the predominantly random noise in this frequency band. For this reason, a filter identical to the MCF in all respects, except that the disk signal model was replaced with an infinite velocity signal model, was also developed for each of the five subarrays. Previous comparison of a disk signal model filter with an infinite velocity signal model filter showed that the latter filter achieved up to 5 db more reduction in ambient noise in the signal band. Thus, the five infinite velocity filters may be expected to achieve about 3 db more noise reduction in the signal band but will attenuate signals with apparent horizontal velocities of 20 km/sec or more by less than 1 db at 1.0 cps.

Infinite velocity filters would be preferred, therefore, as predetection filters for high-velocity teleseismic events since they provide more improvement in S/N ratio. Additional improvement could probably be obtained by using directional point source signal models if the objective were designing filters to monitor particular geographical regions.

The poorer than straight summation noise attenuation in the signal band attained with infinite velocity signal model filters strongly suggests that detection at the LASA subarray level is primarily limited by the high-velocity (above 8 km/sec) mantle P-wave noise. A study of this noise in regard to its composition, time-stationarity, spatial-stationarity, coherence, and frequency-wavenumber characteristics is now underway on the Large Array Signal and Noise Analysis project for AFTAC. It is expected that, when the characteristics of the high-velocity noise field are better understood, multichannel filters which will achieve a significant reduction in this noise component can be devised for application to the large array.

The signal detection procedure recommended is a square-and-integrate operation following application of a Wiener MCF. This procedure is illustrated in Section V by applying it to three teleseismic P-wave signals at each of the five subarrays. A relatively constant level output is obtained preceding the P-wave, and an abrupt and proportionately very large increase in the output is seen at the time of P-wave arrival. The events selected for this illustration ranged in reported magnitude from 4.6 for the Mariana event to 5.0 for the Algerian event. A clear indication of the arrival of coherent teleseismic energy was obtained at each event.

SECTION II

AMBIENT NOISE CHARACTERISTICS

A. NOISE COHERENCE STUDIES

1. Purposes

The purposes of these studies were to determine the predictability of LASA noise, on a subarray basis, in the seismic band of 0.0 to 5.0 cps as a function of both distance and the number of seismometers used, and to obtain a preliminary estimate of the time-stability of the noise.

2. Method

Two noise samples approximately 4 min long were obtained for subarray F-3. The first sample (noise sample A) was recorded on 21 May 1965 at 07:07 MST and the second one (noise sample B) was recorded on 26 May 1965 at 22:01 MST. The two samples were decimated by 4 to give a Nyquist frequency of 5.2 cps, and were approximately whitened by designing a whitening filter for seismometer 32 (for each noise sample) and applying that filter to all 25 channels. Figure II-1 shows part of the two resampled and whitened noise samples.

Two sets of filters to predict the center seismometer were designed for noise sample A:

- Single-channel filters for distances from 0.5 to 3.5 km
- Multichannel filters using either rings or arms of the array

The filters are described in Table II-1.

All filters were then applied to noise sample A and almost all of the filters were applied to noise sample B (Table II-1). The error trace was obtained as the reference trace (center seismometer) minus the reference trace prediction. Bartlett-smoothed autocorrelations of the error and reference traces were computed and Fourier-transformed to obtain spectral estimates. The ratio of the error to the reference spectrum was obtained to measure the predictability as a function of frequency for each filter.

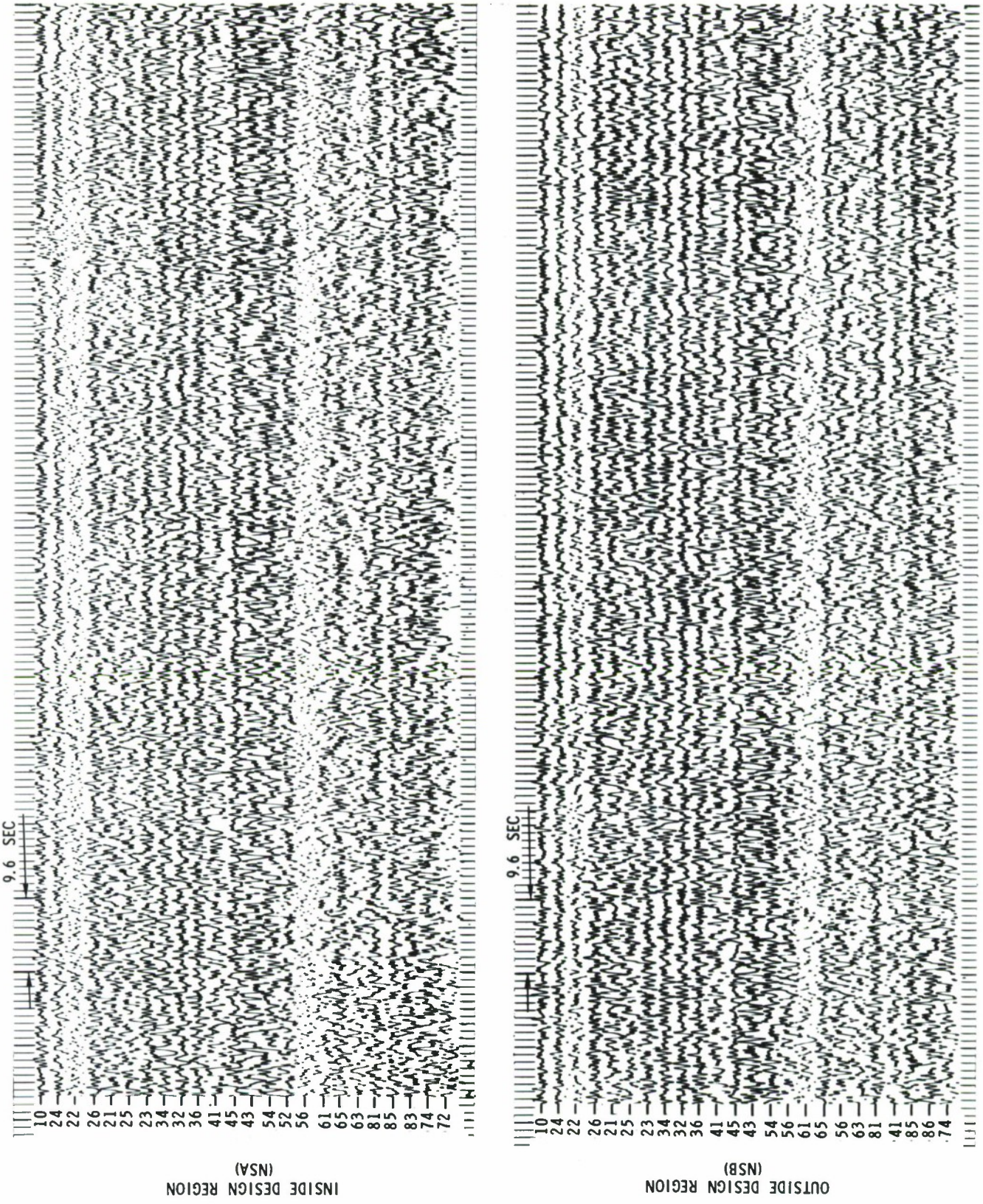

Figure II-1. Noise Samples A and B Recorded at Subarray F-3

Table II-1

DESCRIPTION OF THE PREDICTION FILTERS

Filter	Description	Applied to NS A	Applied to NS B
1	Single-channel, 1/2 km from center seismometer	Yes	Yes
2	Single-channel, 1 km from center seismometer	Yes	No
3	Single-channel, 1-1/2 km from center seismometer	Yes	Yes
4	Single-channel, 2 km from center seismometer	Yes	No
5	Single-channel, 2-1/2 km from center seismometer	Yes	Yes
6	Single-channel, 3 km from center seismometer	Yes	Yes
7	Single-channel, 3-1/2 km from center seismometer	Yes	Yes
8	4-channel, ring 2, 1/2 km from center seismometer	Yes	Yes
9	5-channel, rings 3 and 4, 1 and 1-1/2 km from center seismometer	Yes	Yes
10	5-channel, rings 5 and 6, 2 and 2-1/2 km from center seismometer	Yes	No
11	5-channel, rings 7 and 8, 3 and 3-1/2 km from center seismometer	Yes	No
12	9-channel "arm" case using seismometers 1/2, 1-1/2 and 2-1/2 km from center seismometer along arms 1, 3 and 5	Yes	No

B. DISCUSSION OF RESULTS

1. Application of Prediction Filters to Noise Sample A

a. Single-Channel Prediction

Figure II-2 shows the reference trace and the reference trace prediction (noise sample A) for the seven single-channel filters. Two observations can be made:

- The predicted output had much less high frequency than was actually present which implies that the high-frequency noise was mainly incoherent. Considering the noise field to consist of coherent and incoherent noise, then the frequency response of the prediction filter will be

$$H(f) = \frac{\Phi_c(f)}{\Phi_c(f) + \Phi_i(f)}$$

  where $\Phi_c(f)$ and $\Phi_i(f)$ are the coherent and incoherent noise sources, respectively. As $\Phi_c(f) \rightarrow 0$, then $H(f) \rightarrow 0$ and the filter essentially turns off or becomes a band-pass filter which rejects the high frequency. Since the high-frequency energy was not passed by the filters, it must have been mainly incoherent.

- The predictability of the low-frequency energy decreases with increasing distance.

Figures II-3 through II-5 show the error-to-reference spectral ratios. A highly predictable peak is seen at 0.25 cps for which the prediction decreased as a function of distance (indicated in Figure II-2 and shown in Figure II-6). The predictability decreased rapidly to about 0.6 cps and then decreased more slowly to essentially no predictability at about 1.4 cps for seismometers spaced 0.5 km apart. At 3.5 km these figures are 0.4 and 1.0 cps, respectively.

At higher frequencies, predictable energy existed at 2.4, 2.8 and 3.2 cps and to some extent at 1.75 and 3.65 cps. The predictability of these peaks also decreased with distance; the 2.4-cps and 2.8-cps peaks disappeared at 1.5 km and the 3.2-cps peak disappeared at 2.0 km.

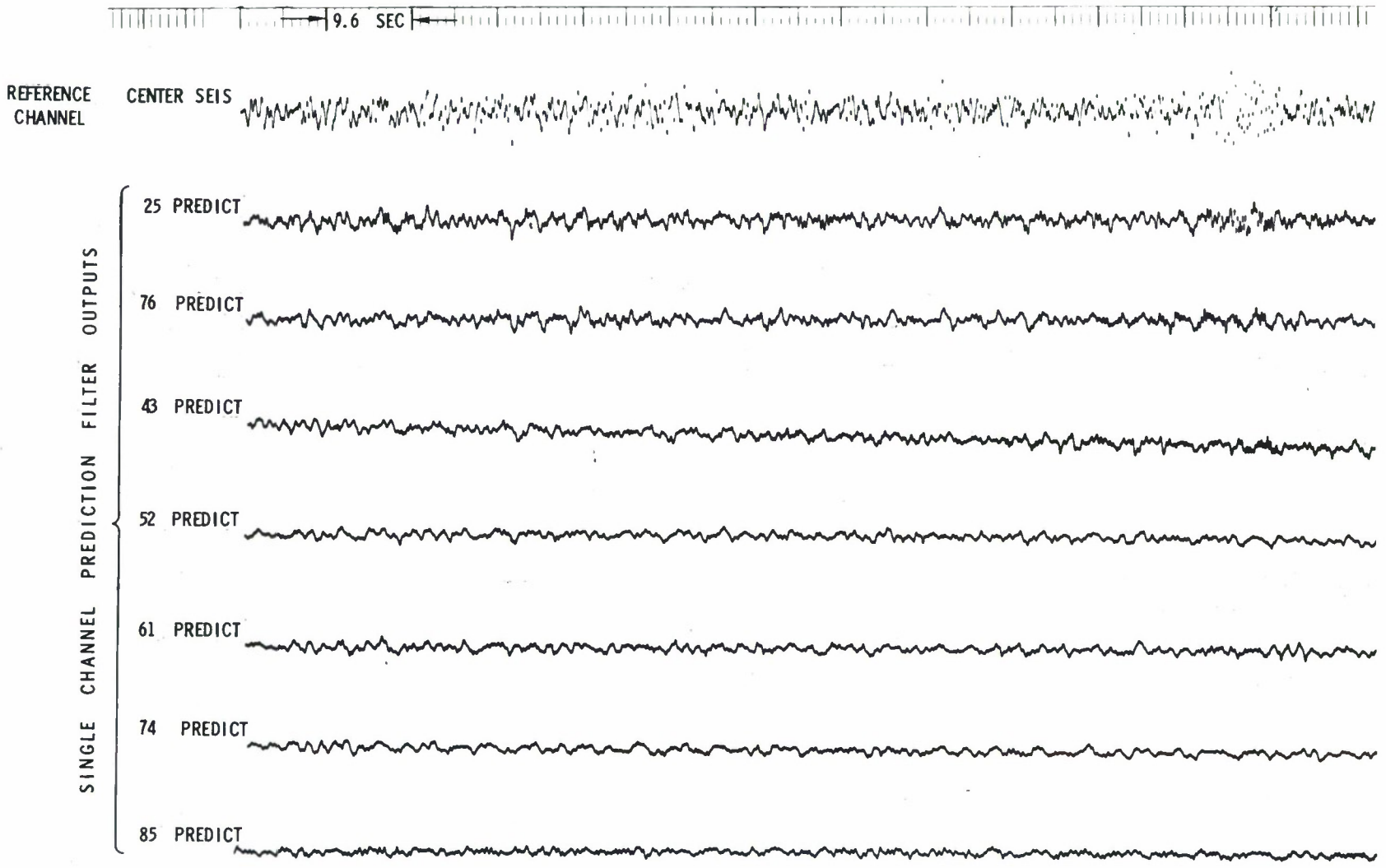

Figure II-2. Center Seismometer and Single-Channel Predictions of Same (NSA)

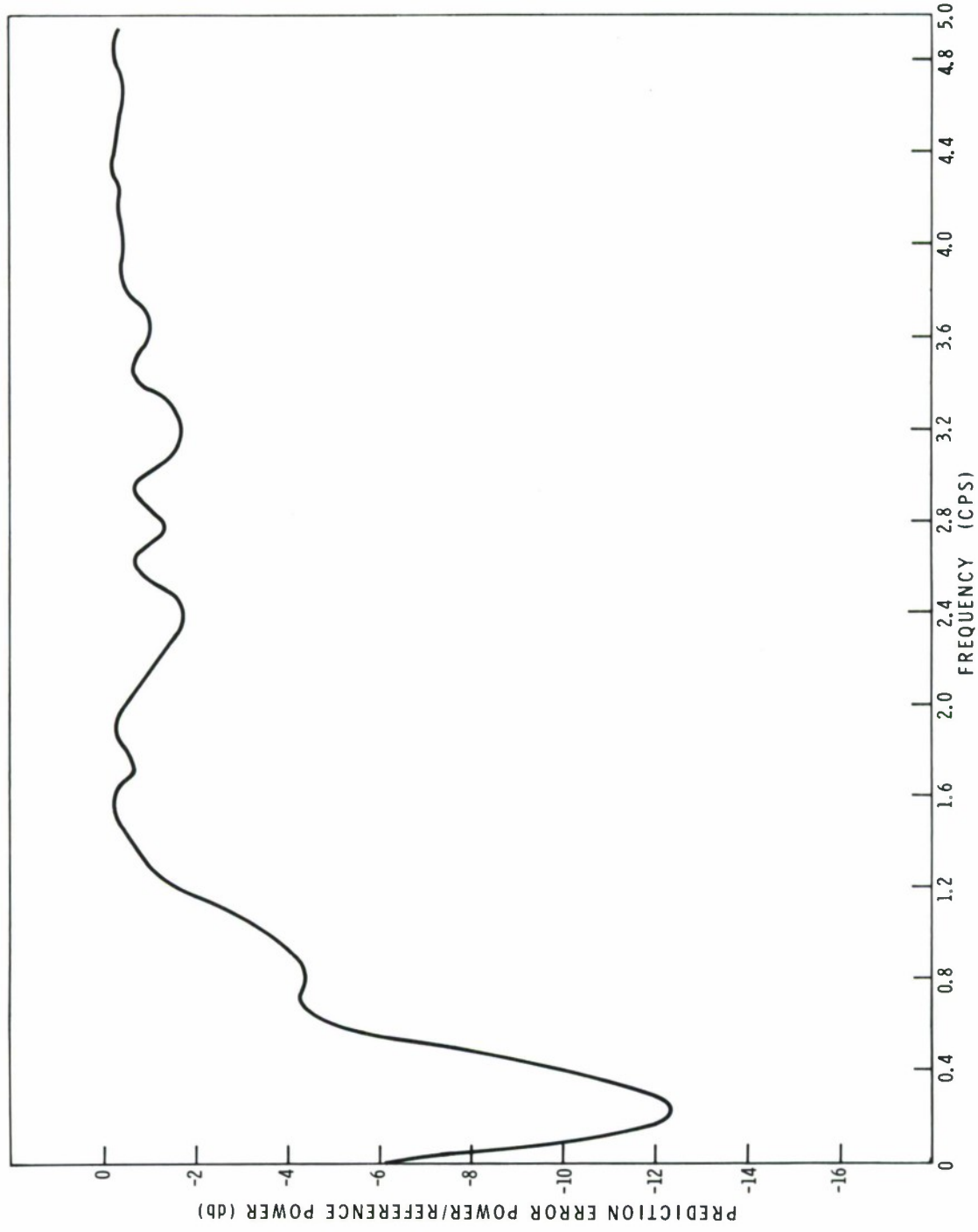

Figure II-3. Single-Channel Prediction of the Center Seismometer Using Seismometer 25 (NSA)

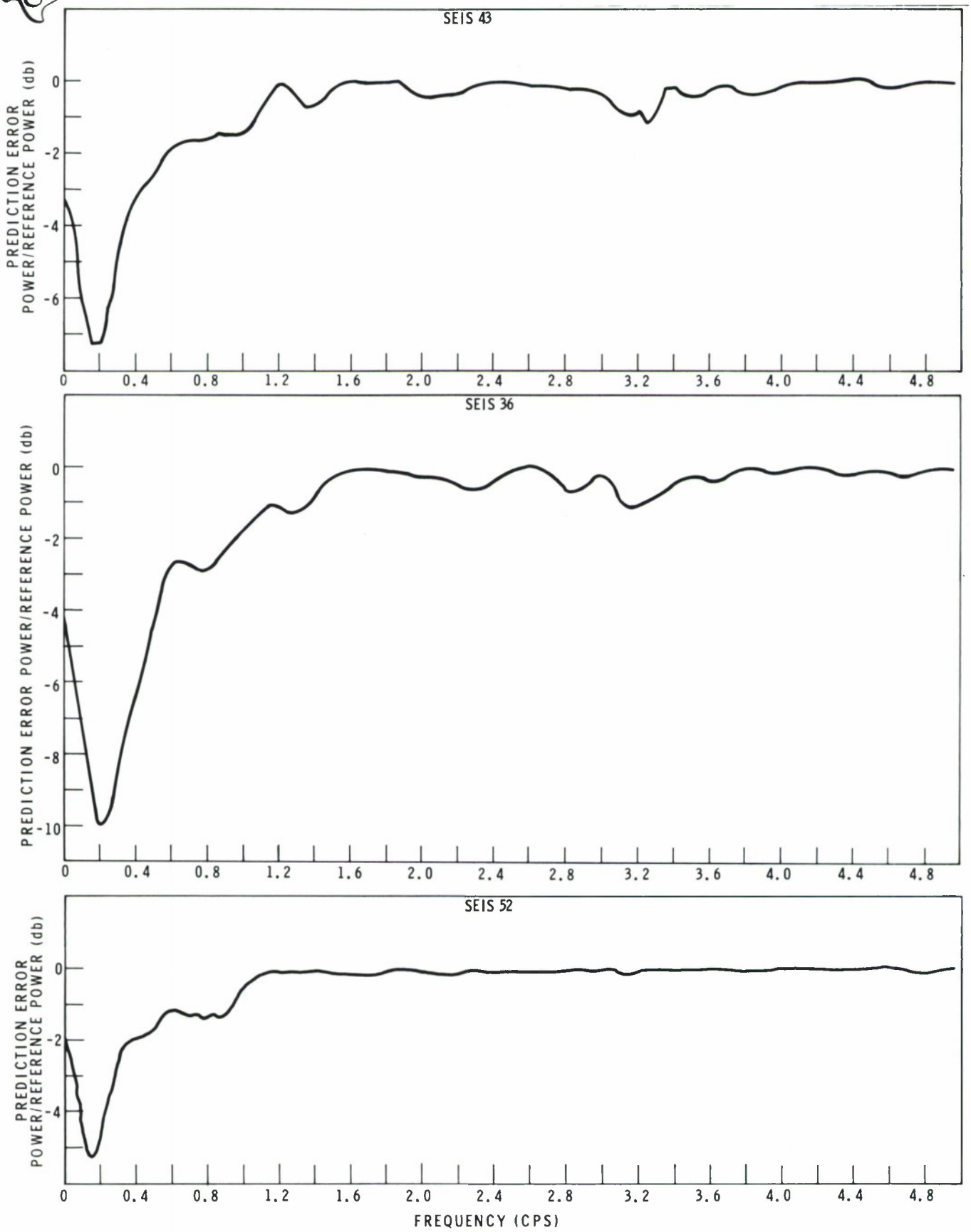

Figure II-4. Single-Channel Prediction of the Center Seismometer Using Seismometers 36, 43, 52 (NSA)

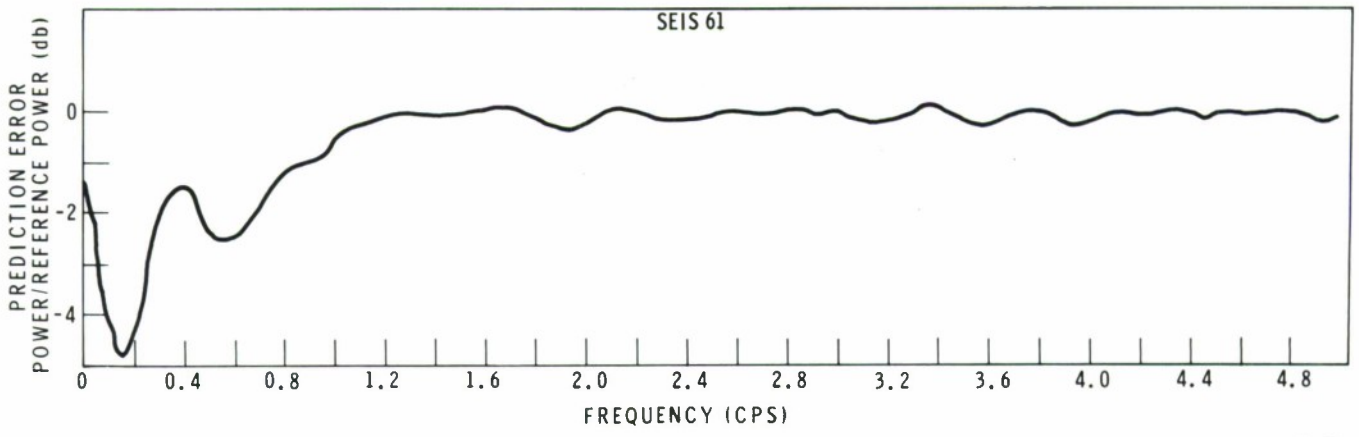

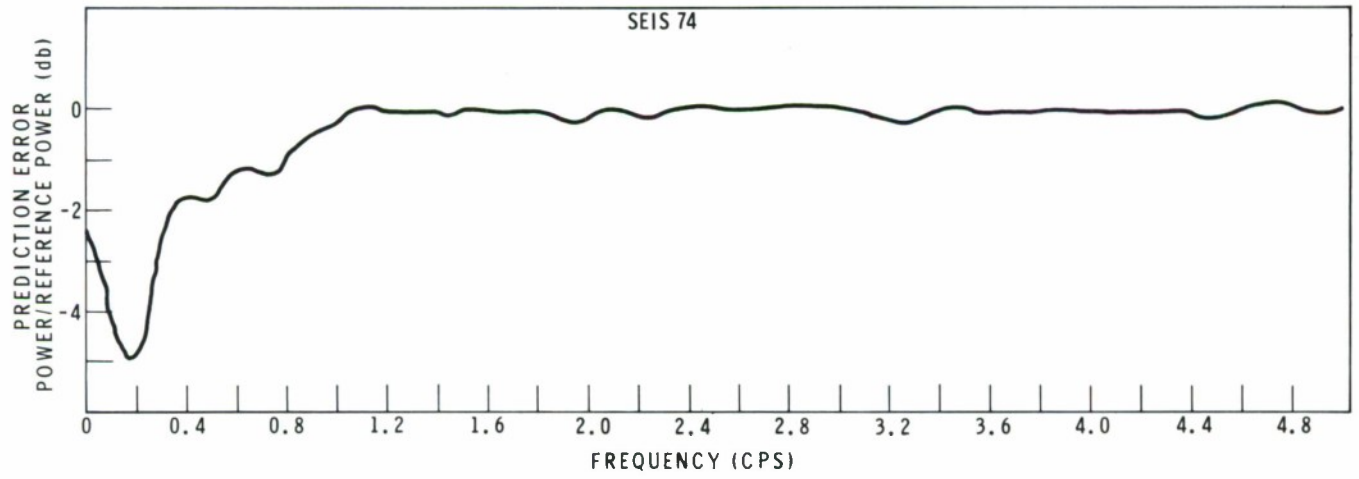

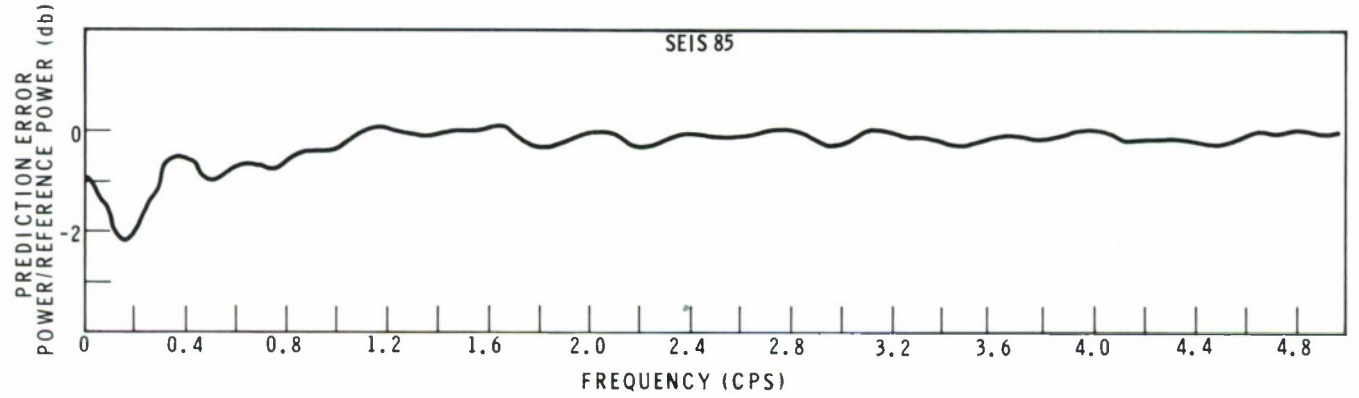

Figure II-5. Single-Channel Prediction of the Center Seismometer Using Seismometers 61, 74, 85 (NSA)

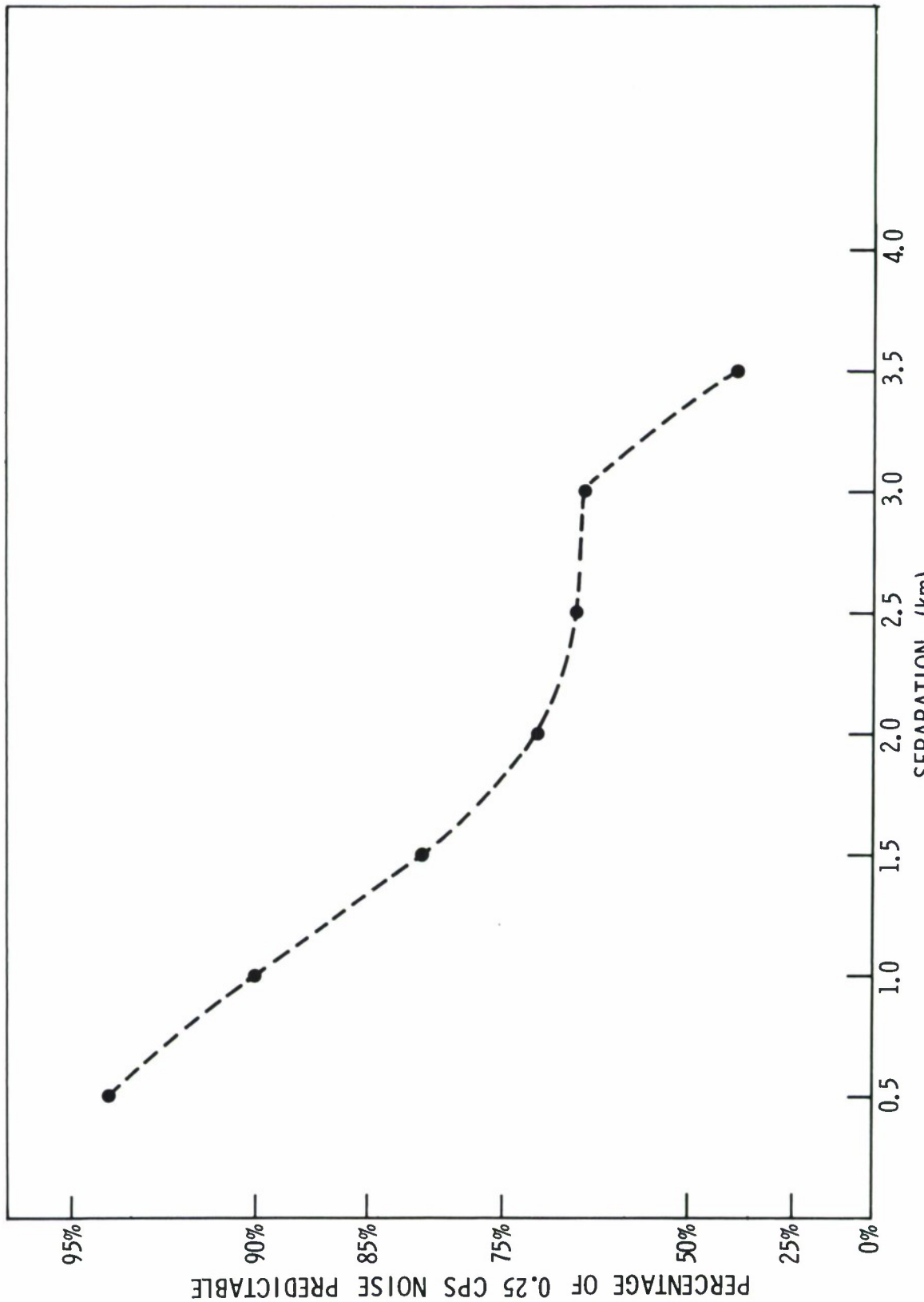

Figure II-6. Predictability of 0.25-cps Peak as a Function of Distance (NSA)

b. Multichannel Prediction

The reference trace and the reference trace prediction for the four ring filters and the 9-channel arm filter are shown in Figure II-7. Figures II-8 and II-9 show the error-to-reference spectral ratios for the ring filters and Figure II-10 shows the ratio for the arm filter.

Regarding the set of ring filters

- The predictable peaks seen for the single-channel data were better defined by the multichannel filters. Also, additional peaks at 2.1, 4.1 and 4.7 cps were observed.
- The degree of predictability was a function of distance again.
- The predictions were better by 2 to 3 db than were the corresponding single-channel predictions.

It can be concluded that the coherent component of the noise is either multimode or multisource energy (or both), because of the improved prediction obtained by using additional channels and because of the decrease in predictability with distance.

For the 9-channel filter (Figure II-10) the error-to-reference spectral ratio suggests that 1- or 2-db prediction has been obtained at all frequencies. However, this prediction probably was not real, but due to the total number of filter points becoming large, with respect to the length of the data; i.e., the prediction was becoming more deterministic than statistical due to the fewer degrees of freedom in filter design.

2. Application of Prediction Filters to Noise Sample B

a. Single-Channel Prediction

The reference trace and the reference trace prediction (noise sample B) for five single-channel filters are shown in Figure II-11. Figures II-12 and II-13 show the error-to-reference spectral ratios. Very little noise in noise sample B was predictable, using the filters designed from noise sample A. At 0.25 cps there was about 50-percent prediction, but at other frequencies, except for the 0.5-km filter, there was no prediction. Above about 2.0 cps there was actually more power in the error than in the reference trace, especially for the close-in filters.

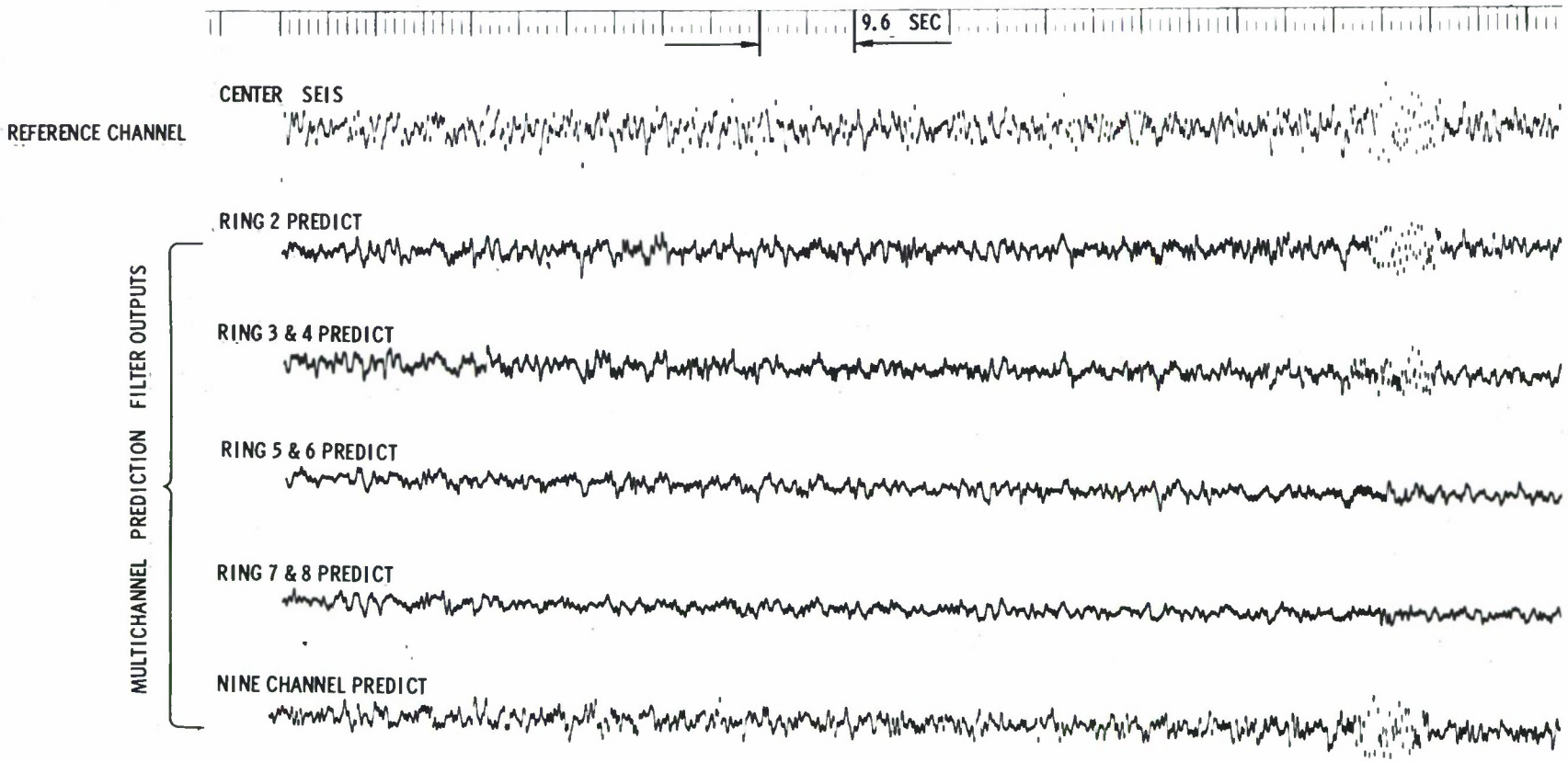

Figure II-7. Center Seismometer and Multichannel Prediction of Same (NSA)

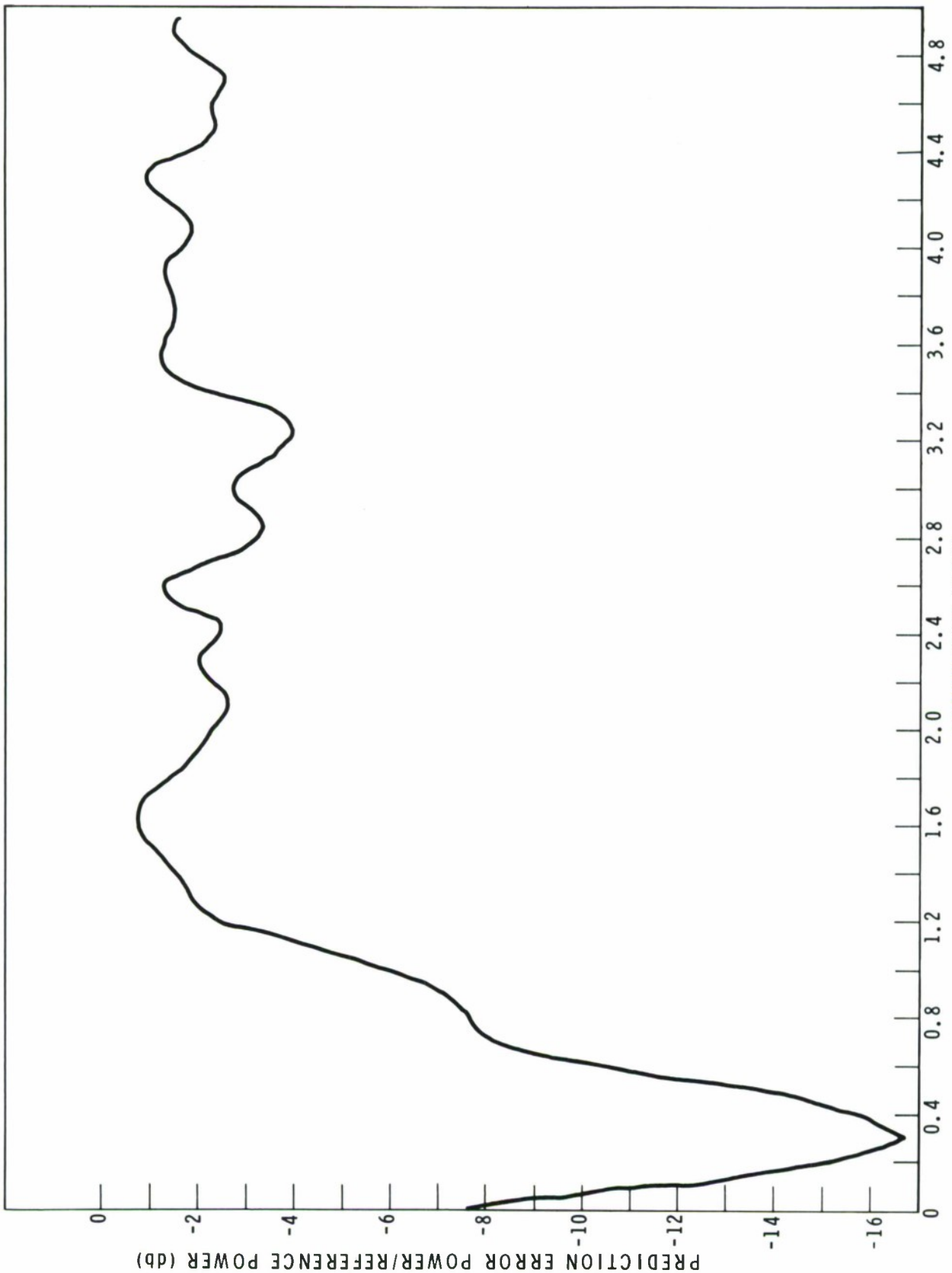

Figure II-8. Four-Channel Prediction of the Center Seismometer Using Ring 2 (NSA)

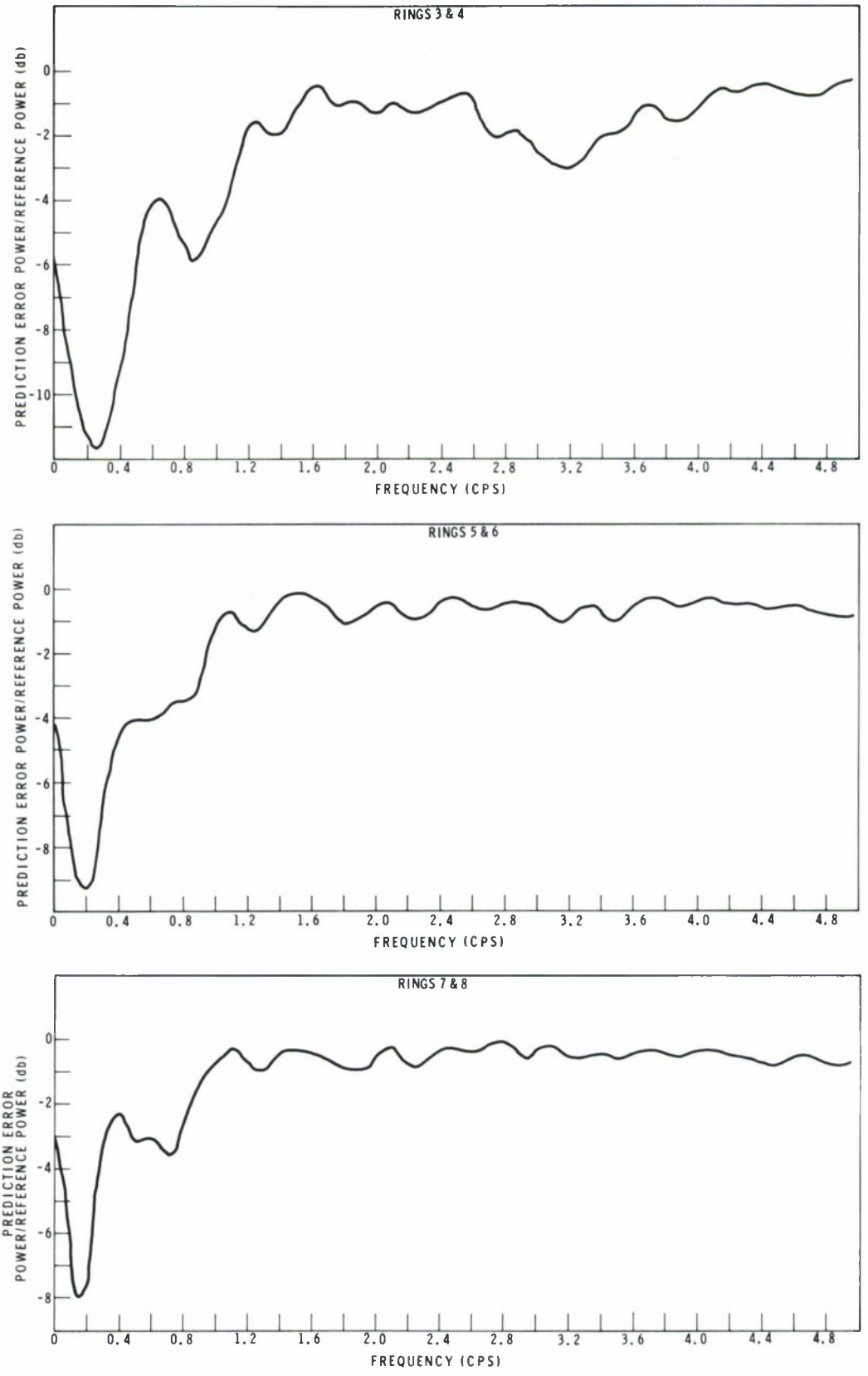

Figure II-9. Multichannel Prediction of the Center Seismometer Using Rings 3 and 4 (5 Channels), 5 and 6 (5 Channels), and 7 and 8 (4 Channels), Respectively (NSA)

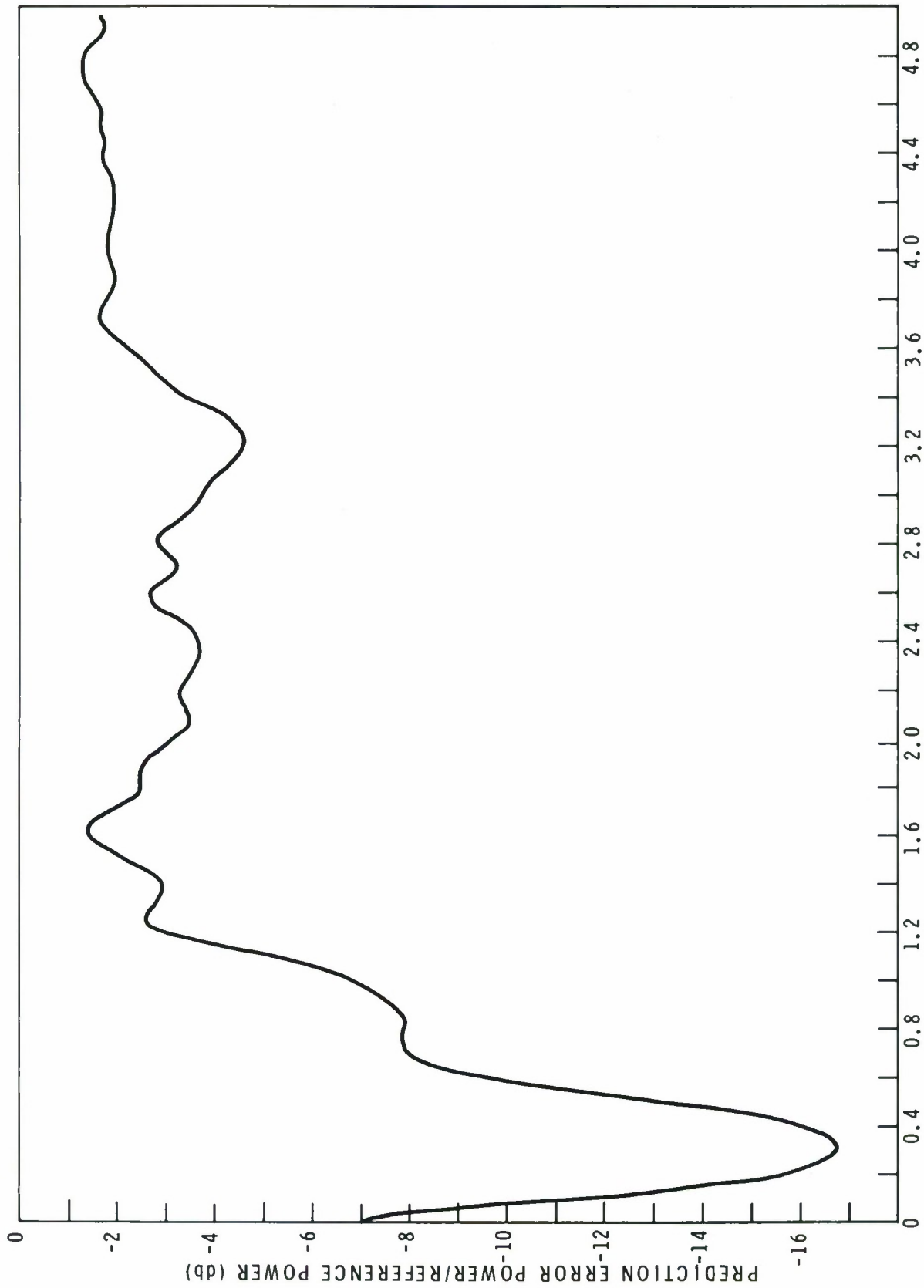

Figure II-10. Multichannel Prediction of Center Seismometer Using 9-Channel "Arm" Configuration (NSA)

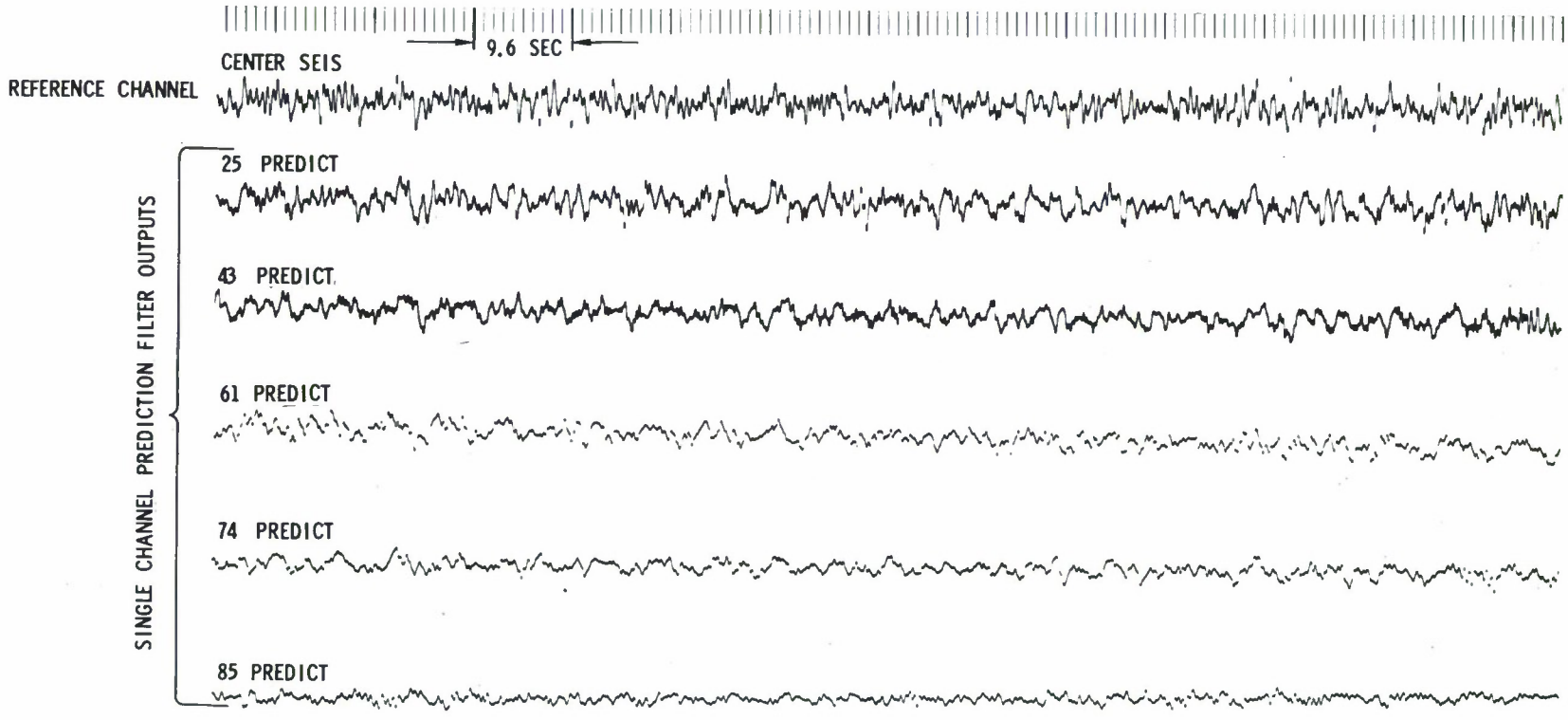

Figure II-11. Center Seismometer and Single-Channel Prediction of Same (NSB)

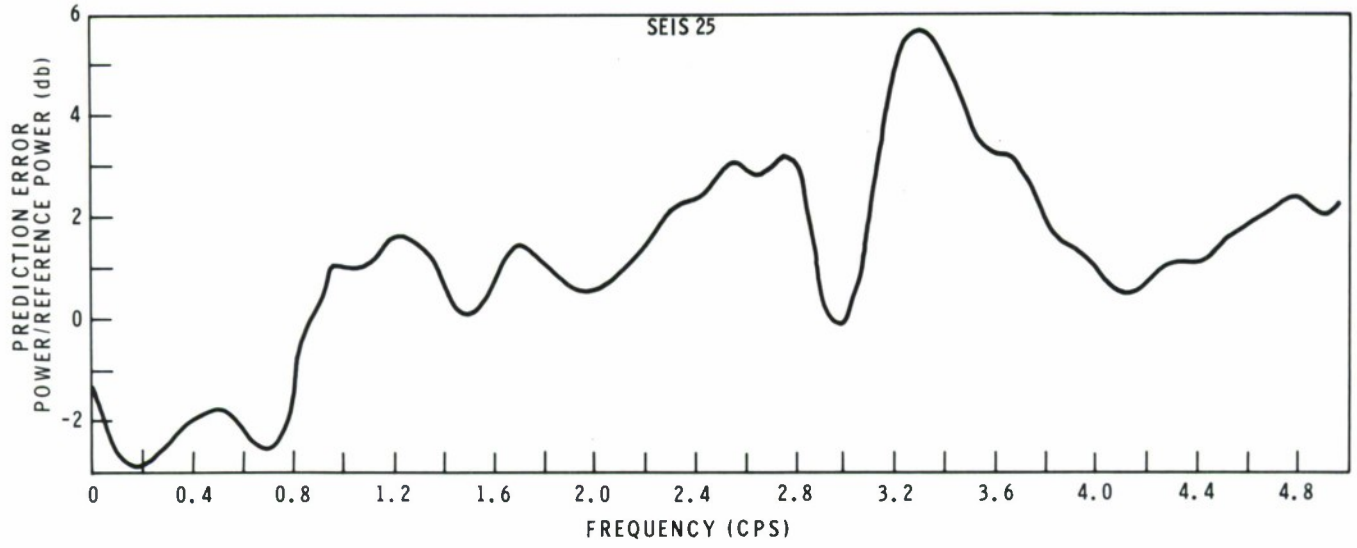

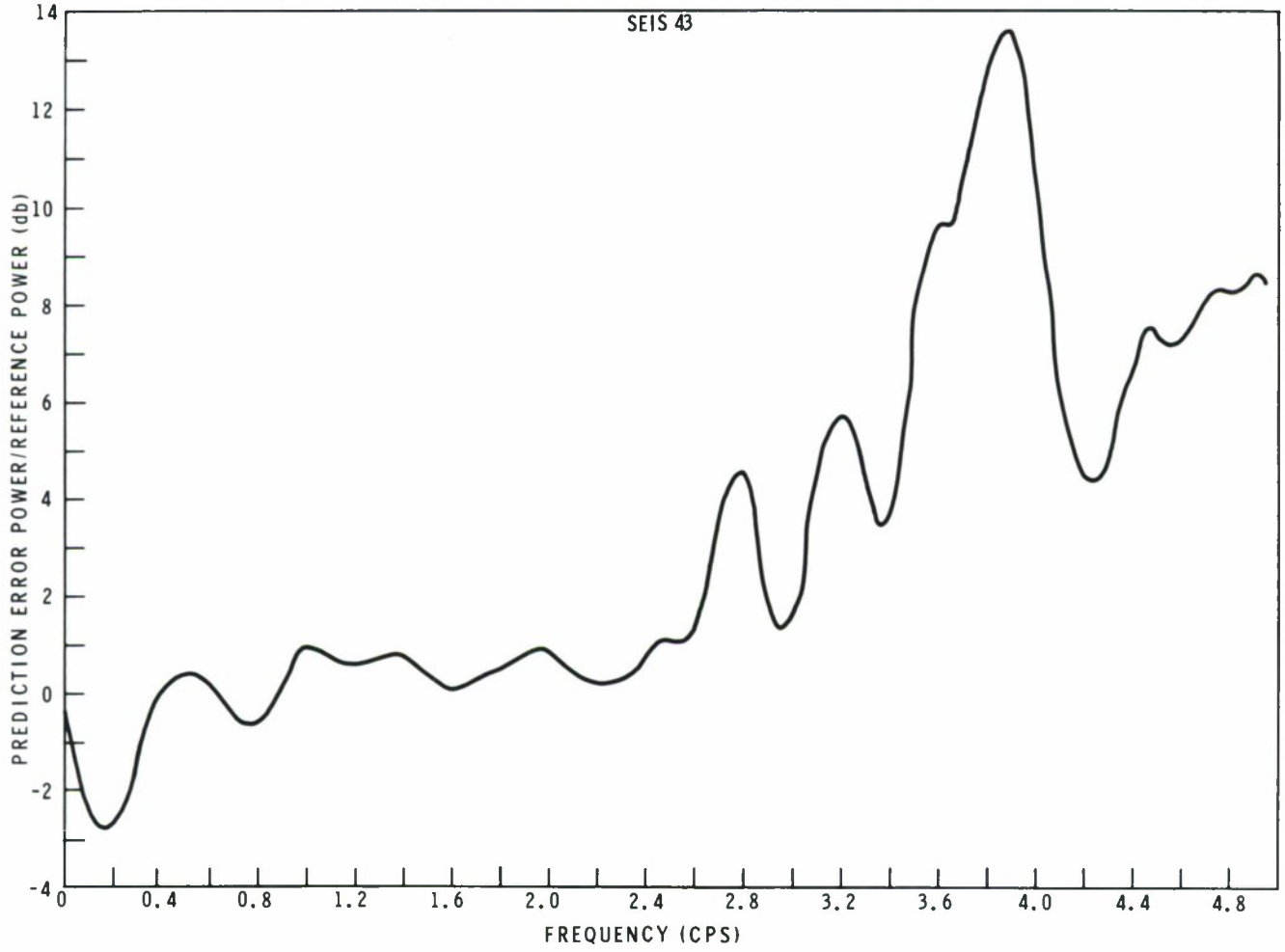

Figure II-12. Single-Channel Prediction of Center Seismometer Using Seismometers 25, and 43, Respectively (NSB)

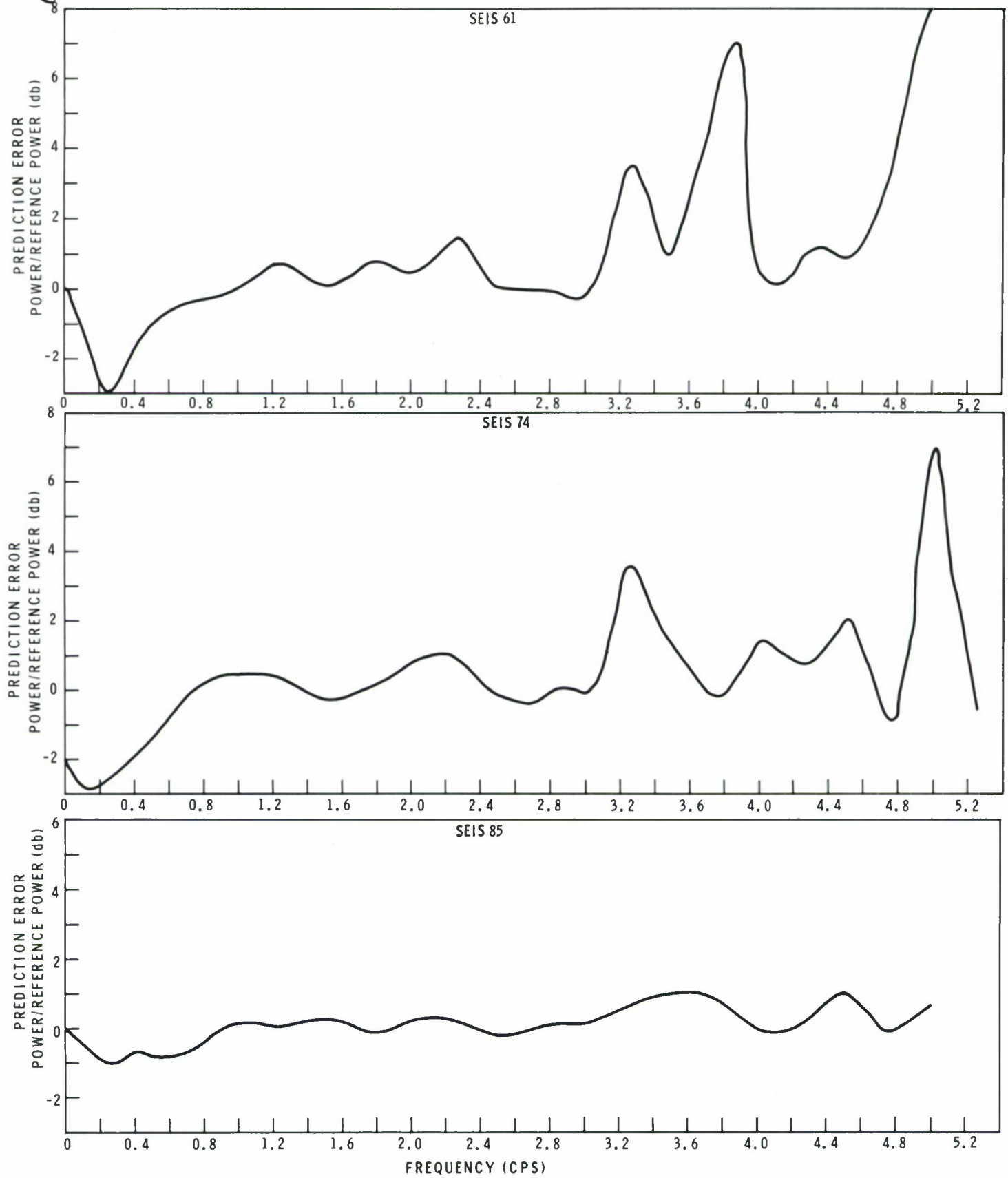

Figure II-13. Single-Channel Prediction of Seismometer Using Seismometers 61, 74, and 85, Respectively (NSB)

The apparently poor prediction at the 0.25-cps peak was probably partly due to differences in the relative power of the reference trace and traces used in the prediction. As an example, for noise sample A the 0.5-km seismometer had about 6 db more power than the center seismometer at 0.25 cps, but for noise sample B, the two seismometers had about equal power (Figure II-14). Thus, about 6 db of the decrease in predictability for noise sample B could be explained. Combining this with the prediction obtained brings noise sample A and noise sample B into reasonably good agreement. Adding 6 db to the 0.25-cps prediction for other noise sample B distances would also bring these sample B values into fair agreement with those of noise sample A. (This is not unreasonable because of the difference in depth between the center seismometer and the other seismometer.) Thus, it appears that at 0.25 cps the noise was reasonably time-stationary.

Above 2.0 cps the noise does not appear to be time-stationary. Figure II-15 shows the coherence between the center seismometer and the 0.5-km seismometer for both noise sample A and noise sample B. There were coherent peaks for both noise samples, but they occurred at different frequencies for each sample. Thus, the filter designed from noise sample A would be ineffective in predicting the coherent peaks in noise sample B. Note that noise sample A was recorded at 07:07 MST and noise sample B at 10:01 MST so that the difference in the high-frequency energy is reasonable.

b. Multichannel Prediction

The reference trace and the two ring predictions of the reference trace are shown in Figure II-16. Figure II-17 shows the error-to-reference spectral ratios. These data corroborate previous observations that the 0.25-cps peak was reasonably time-stationary, but the high-frequency (above 2.0 cps) noise was not. Also, the improvement obtained over single-channel prediction again indicates a multimode or multisource (or both) noise field at 0.25 cps.

C. CONCLUSIONS

From this analysis can be concluded that for subarray F-3

- There was a peak at 0.25 cps which was both highly predictable and fairly time-stationary
- There were predictable peaks at higher frequencies (notably 2.4, 2.8 and 3.2 cps) which were predictable but not time-stationary
- Where the noise was predictable, it was either multimode or multisource (or both) energy

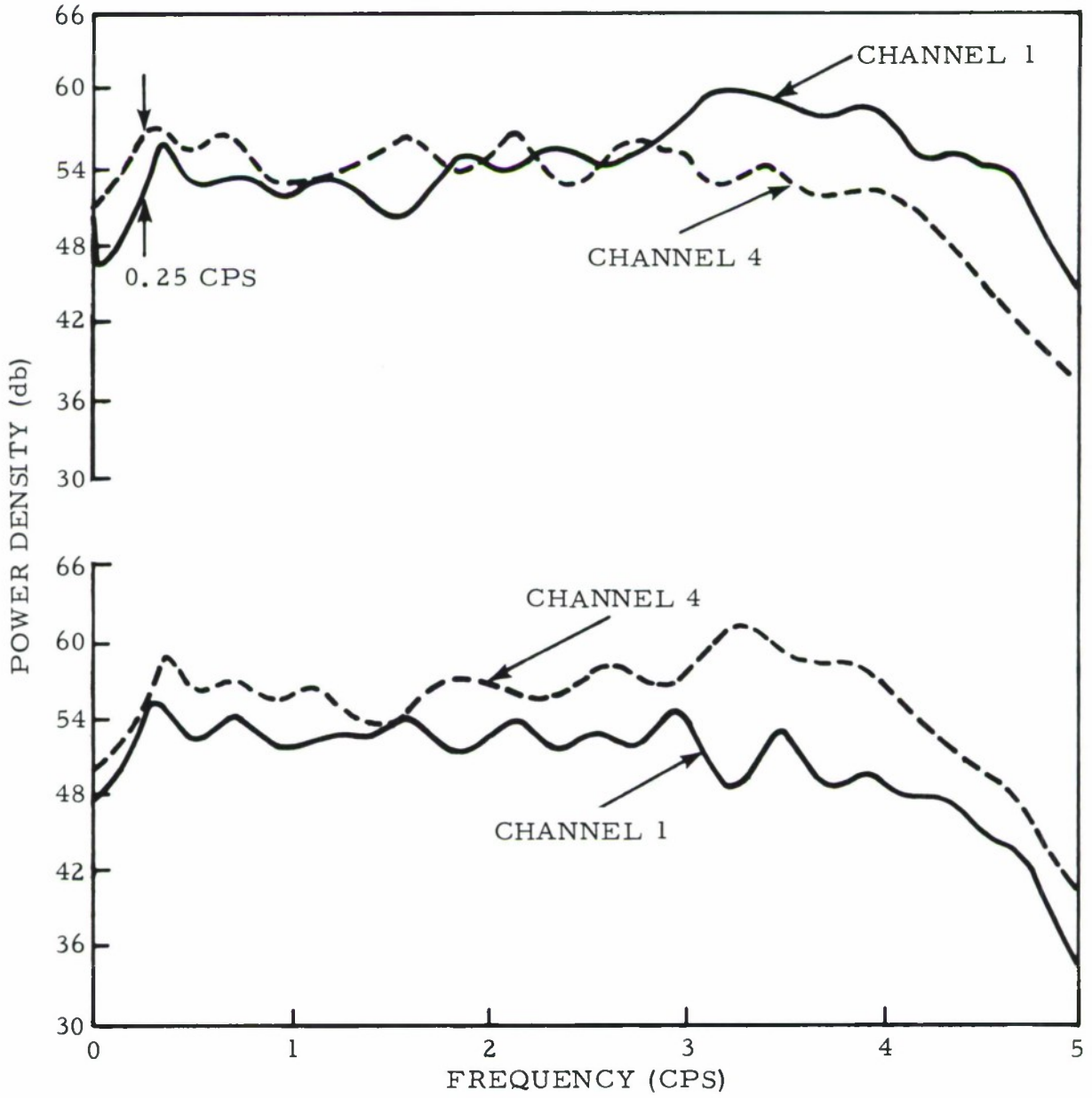

Figure II-14. Comparison of Power Density at 0.25 cps on Channels 1 and 4 for NSA and NSB, respectively

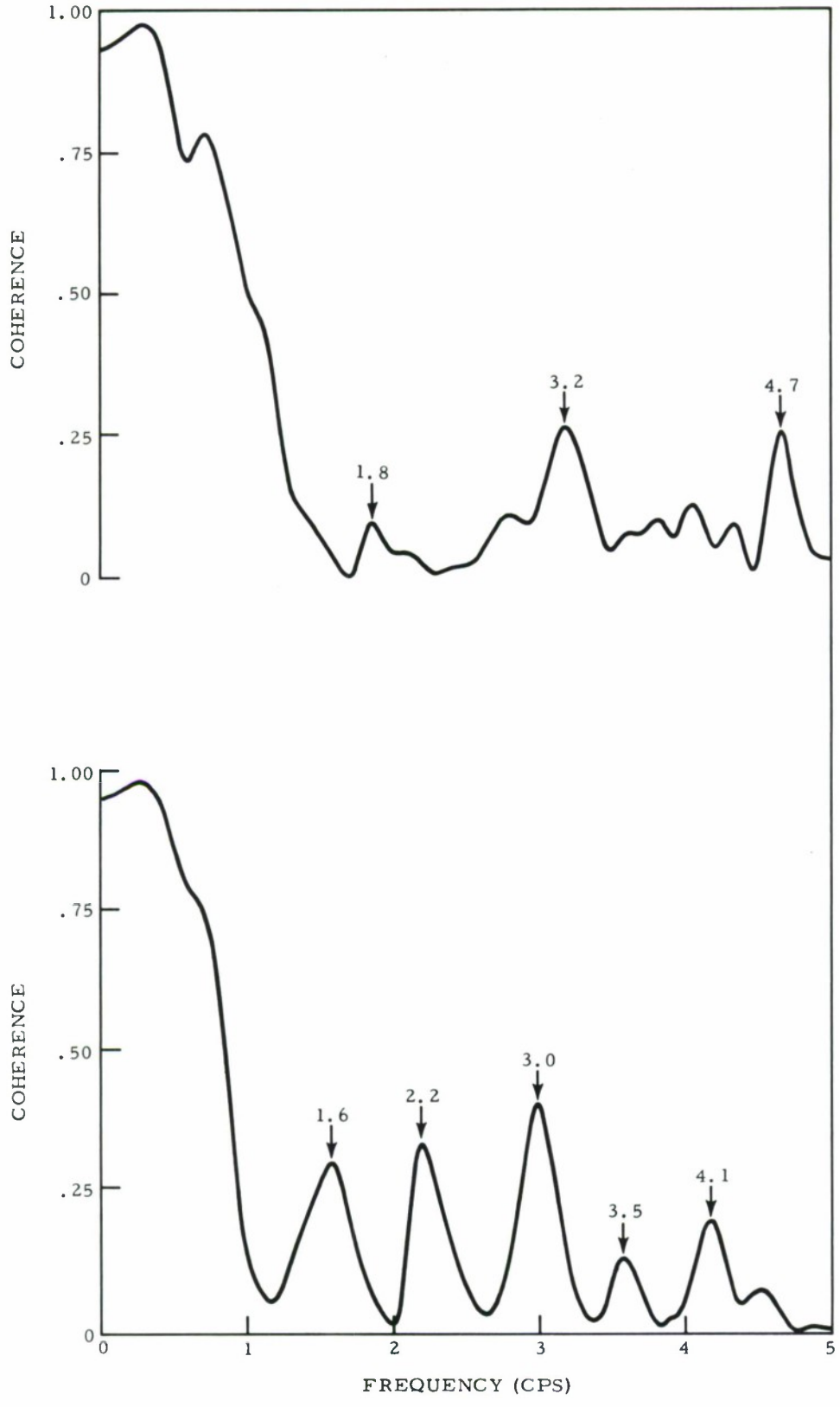

Figure II-15. Coherence Between Channels 1 and 4 for NSA and NSB, Respectively

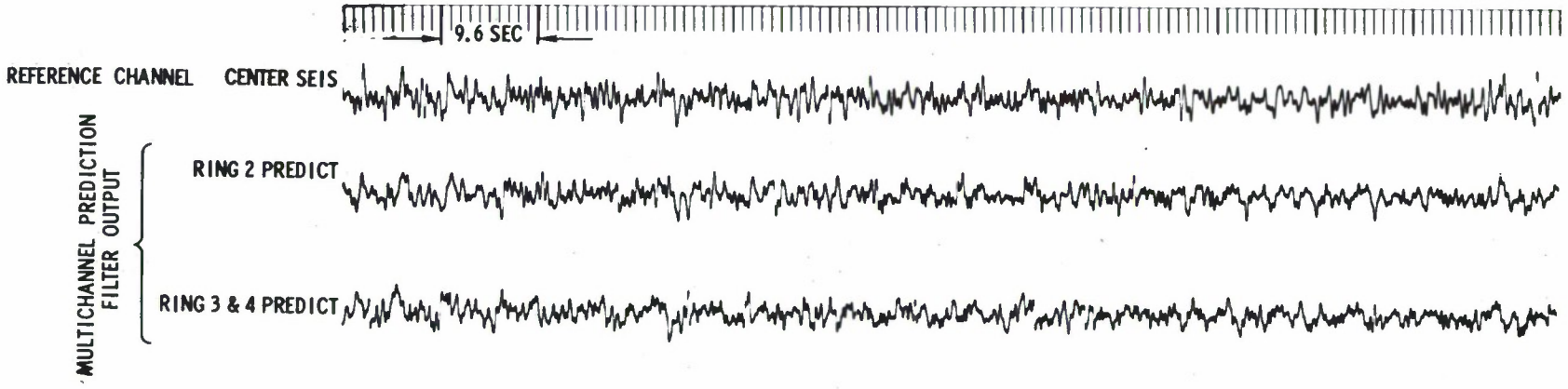

Figure II-16. Center Seismometer and Multichannel Prediction of Same (NSB)

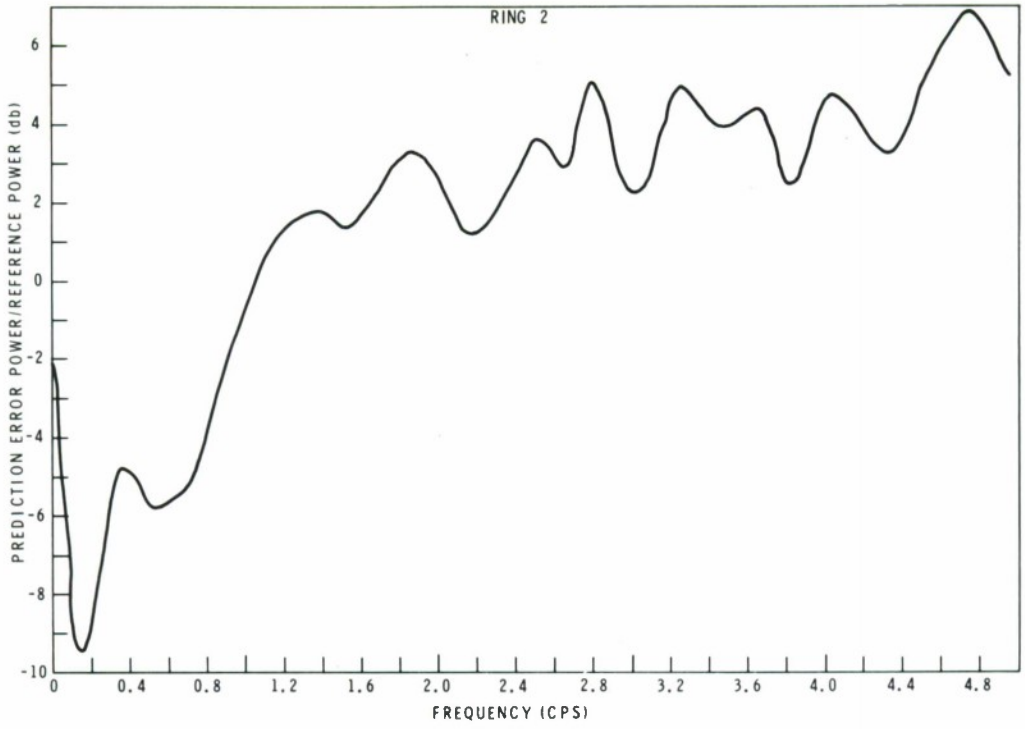

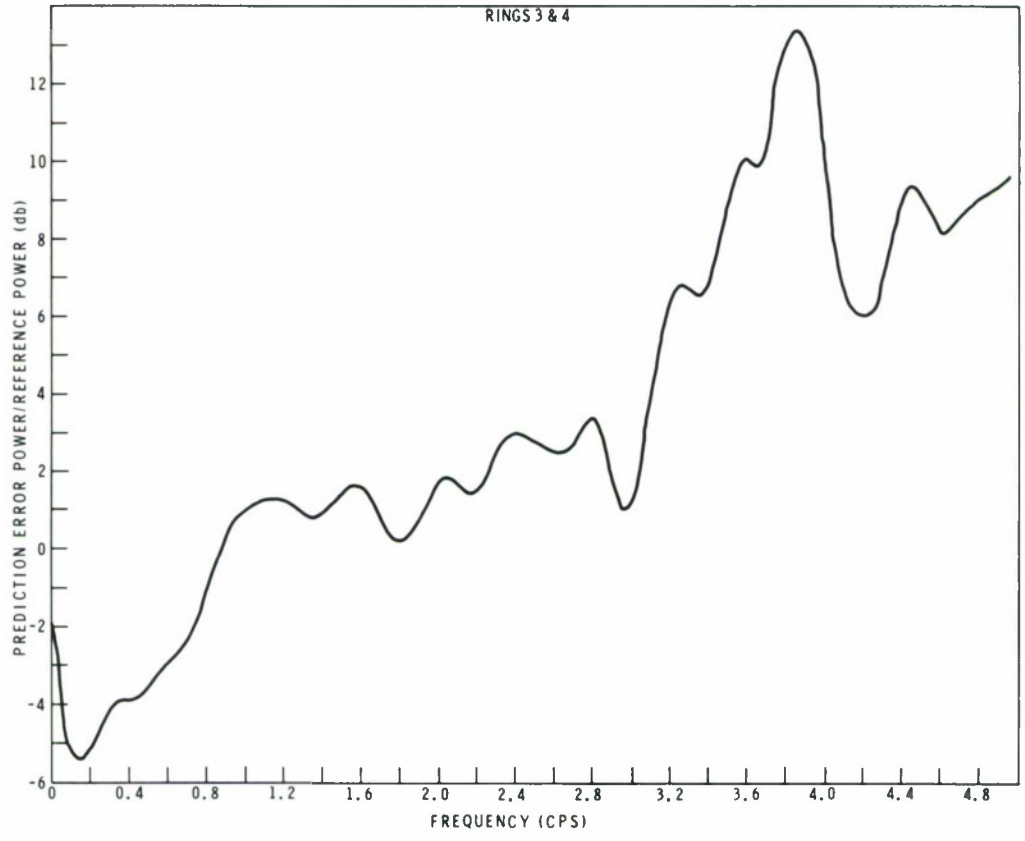

Figure II-17. Multichannel Prediction of center Seismometer Using Ring 2 (4 Channels) and Rings 3 and 4 (Channels), Respectively (NSB)

D. COMPARISON OF DAYTIME AND NIGHTTIME NOISE STATISTICS

Two noise samples were selected for use in comparing day and night noise statistics. Noise sample D was recorded at the F-3 subarray on 24 November 1965 between 03:21 and 03:24 MST. Noise sample F was recorded at the F-3 subarray on 24 March 1966 between 12:47 and 12:50 MST. The frequency-wavenumber spectrum of the nighttime noise sample D is shown in Figure II-18 for frequencies in 0.25-cps increments (from 0.25 cps to 1.00 cps). Figure II-19 shows the $f\text{-}\vec{k}$ spectrum at a frequency of 1.50 cps. The $f\text{-}\vec{k}$ spectrum for the daytime noise sample F was computed by a different process and the frequencies (at which peaks occured in the spectrum) shown in Figure II-20 are 0.3 cps and 0.8 cps. The two sets of spectra are similar, indicating there is no significant change in the noise field between day and night or from November to March.

At 0.3 cps the daytime sample has a high-velocity noise source situated to the northeast of the subarray. All other noise sources are down about 9 db or more from this source. The 0.25-cps nighttime noise spectrum shows these same features. The nighttime noise peak is broader than the daytime peak, but the nighttime peak at a higher frequency (0.50 cps) is broader than the 0.3-cps daytime peak. This indicates that the difference is mainly due to the difference in frequencies at which the spectra of the two samples are plotted. The difference in size is noticed also between the 0.75-cps nighttime spectrum and the 0.8-cps daytime spectrum. The primary difference between the day and night spectra occurs at 0.75 cps where the high velocity night noise is essentially isotropic and the high velocity day noise (at 0.8 cps) is from the west. However, the 2 km/sec noise sources to the northwest and west are present in both samples.

These spectra indicate a rather stable noise field between day and night over a period of several months.

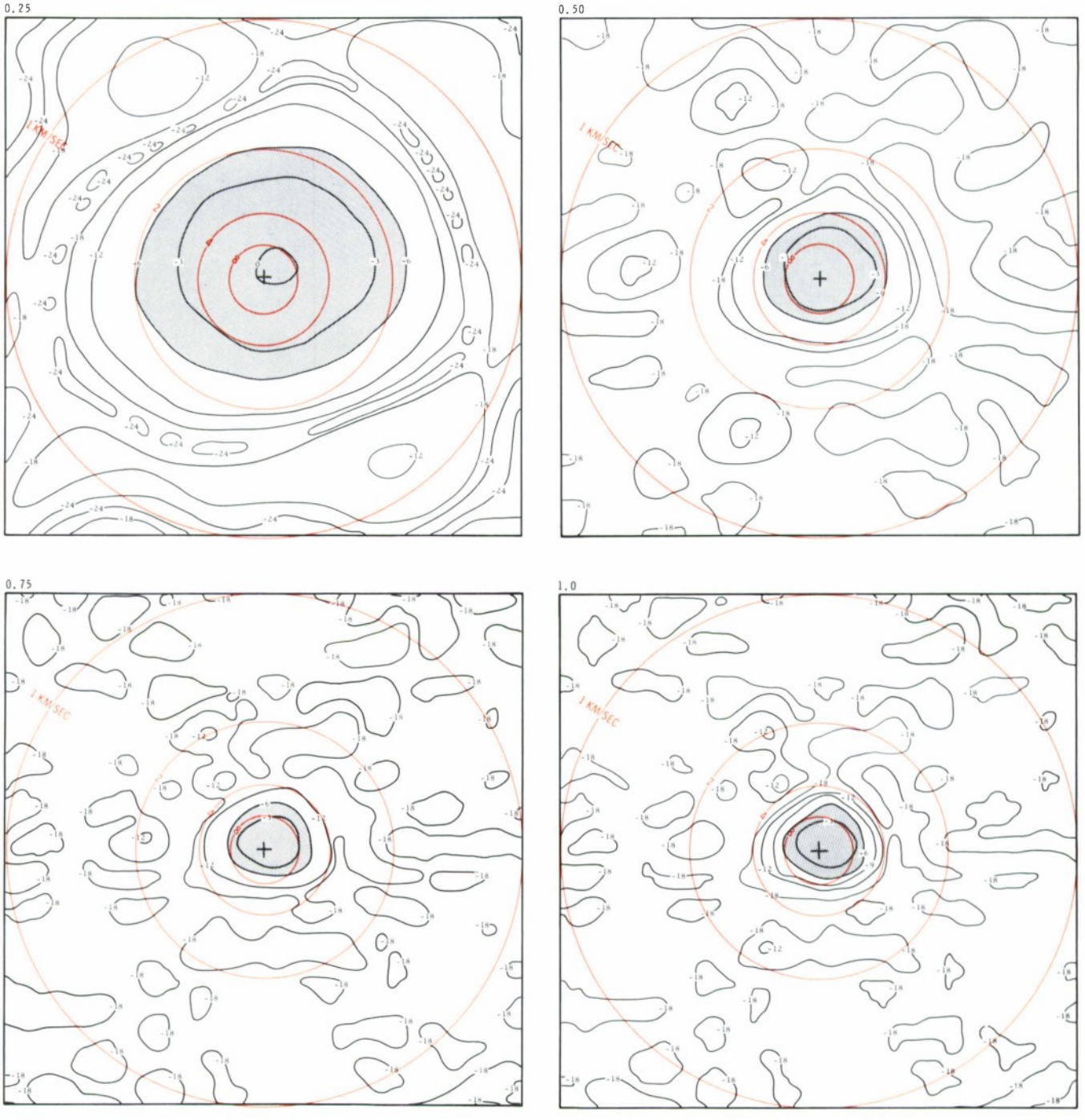

Figure II-18. Frequency-Wavenumber Spectra of Nighttime Noise Sample D; f = 0.25 cps, 0.50 cps, 0.75 cps and 1.00 cps

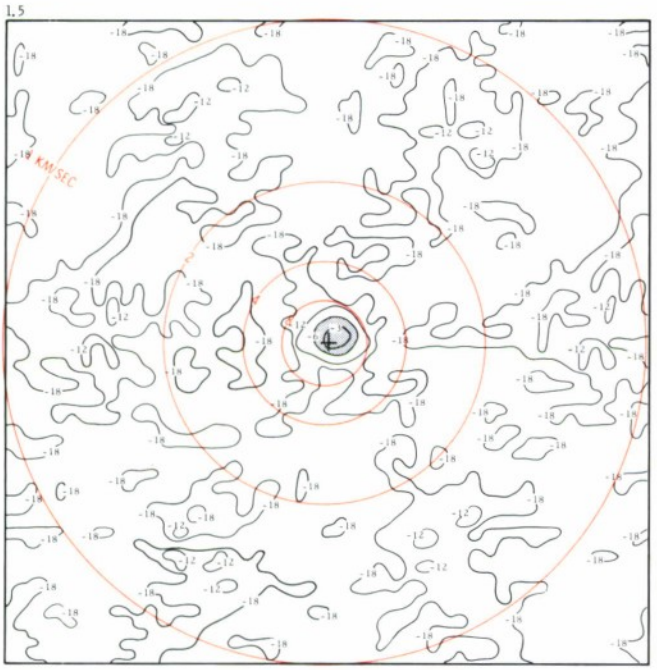

Figure II-19. Frequency-Wavenumber Spectrum of Nighttime Noise Sample D; f = 1.50 cps

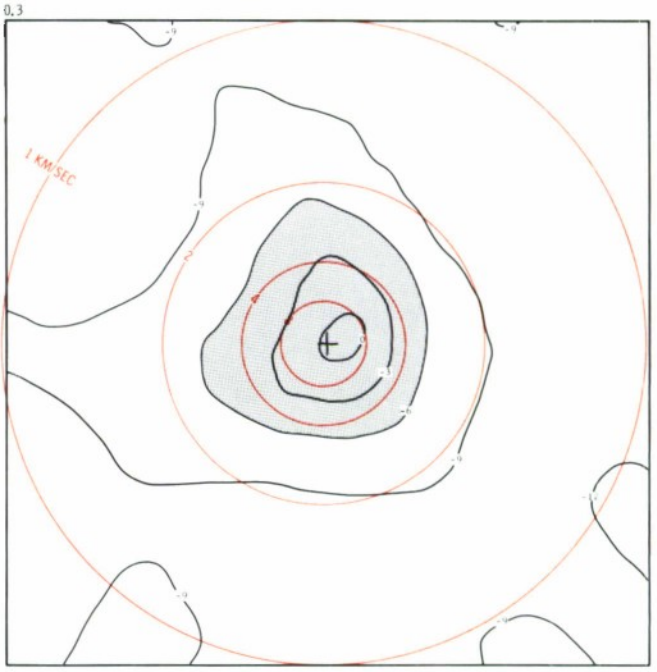

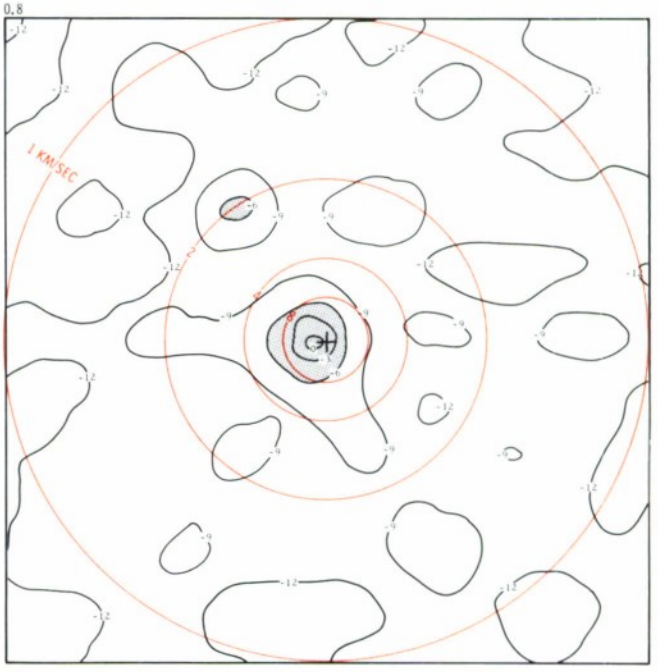

Figure II-20. Frequency-Wavenumber Spectra of Daytime Noise Sample F; f = 0.3, 0.8 cps

SECTION III

INSTRUMENT RESPONSE VARIATIONS

A. TIME-STATIONARITY AT 1 CPS

1. Purpose

A study was made to determine if the LASA seismometer amplitude and phase responses are stable as functions of time. Time-stability of seismometer responses is a necessary requirement for effective on-line multichannel filtering.

2. Data Used

Nine 1-cps calibrations covering a 1-month period (2 November - 1 December 1965) were chosen for subarrays F-3, F-4, C-3, E-2, and F-2. All 25 seismometers from each subarray were demultiplexed, and a few channels from each subarray for each calibration were plotted to check the data. The signal-to-noise (S/N) ratios were large (40 db or more) on all seismometers. Table III-1a lists each subarray's calibration length, which was constant for all nine calibrations.

Table III-1a

LENGTH OF CALIBRATION FOR EACH SUBARRAY	
Subarray	Length of Calibration (No. of cycles)
F-3	36
F-4	40
C-3	16
E-2	29
F-2	36

In addition, a 1-cps calibration performed in mid-March was obtained for each subarray. Table III-1b gives the date for each subarray's calibration.

The seismometer or channel numbers used in the text refer to the sequence in which the channels are recorded on the LASA field tape for a particular subarray.

Table III-1b

1-CPS CALIBRATION FOR EACH SUBARRAY	
Subarray	Date
F-3	10 March 1966
F-4	14 March 1966
C-3	11 March 1966
E-2	15 March 1966
F-2	9 March 1966

3. Method

After the calibrations were demultiplexed, gate lengths (Table III-1a) were chosen and Fourier transforms were computed on a 0.001-cps increment for all seismometers in each subarray in order to determine the precise calibration frequency. An integral number of cycles were chosen (within visual accuracy) to avoid end effects in the transform. The amplitude and phase at the peak (i.e., calibration) frequency were then used as estimates of the seismometer amplitude and phase responses.

To remove possible variations due to changes in the signal input, the seismometers were referenced to channel 1. (No reference trace was available, so channel 1 was arbitrarily chosen.) That is, the amplitude and phase responses relative to channel 1 were studied:

$$A_i^R = \frac{A_i}{A_1} \qquad i = 2, \ldots 25$$

$$\phi_i^R = \phi_i - \phi_1$$

Note that a change in the response of channel 1 (but no other channel) between calibrations would change all the above values and thus give artificial variation, as was observed on two occasions.

To quantitatively measure the stability of the seismometer over a 1-month period, the means and variances of the amplitude and phase responses were computed according to

$$\bar{x} = \frac{1}{n} \sum^{n} x_i$$

$$S^2 = \frac{1}{n-1} \sum^{n} (x_i - \bar{x})^2$$

(where n = 9, except for F-2, where n = 8) and the standard deviation (S) was plotted for each seismometer.

Also, the amplitude and phase responses of the 1 December 1965 calibration were compared with those of mid-March 1966. Percentage changes in amplitude responses and absolute changes in phase responses were tabulated and compared with corresponding changes over the 1-month period.

4. Results

a. Stability of Calibration Frequency

Table III-2 lists the calibration frequencies of the five subarrays for each calibration as determined from the Fourier transforms. Note that F-3 has a significant change in frequency (.022 cps) between 5 November and 16 November. The reason for the change is not known, but it may have been due to replacing the F-3 oscillator between the two dates.

All other calibrations change by not more than 0.001 cps. These small changes could probably be explained by temperature or humidity changes. Table III-2 also lists the calibration frequencies of the March calibrations which were special calibrations; there is no reason that these should agree with the others. However, since the values will be relevant in later discussions, they are listed in the table.

b. Amplitude and Phase Variations Over the 2 November to 1 December Period

In general, with a few exceptions the amplitude and phase responses showed good time-stability over the 1-month period. An attempt

Note: Refer to end of Section III for Tables III-2 through III-27.

was made to explain all anomalously large variations by relating them either to low-quality input data or to modifications to the seismometer-amplifier system as reported in the LASA logs (provided by Mr. Royce Brown), or by infering a possible explanation from the nature of the variations.

A discussion of each subarray follows, with accompanying tables and figures when necessary.

Subarray F-3 (Tables III-3 and III-4) was unique because it had a shift in calibration frequency which was accompanied by large variations in amplitude responses and small variations in phase responses. The amplitude variations probably were partly due to the shift in calibration frequency and partly due to a lowering of the channel 1 gain on 12 November (as reported in the LASA logs). Because channel gains are not altered unless they exceed certain specifications, the major part of the variations probably were due to the gain change on channel 1. The small phase variations probably were due to the shift in calibration frequency.

There are four anomalously high amplitude ratio values corresponding to channels 10, 14, 18, and 25 for the 16 November calibration. The playback of the calibration did not show any input data problems on these channels and verified the relative amplitude ratios obtained from the transforms. The station logs did not have any reference to channel adjustments, although it appears these four rather high-gain channels may have been balanced. Thus, no definite explanation for the high values can be given.

The phase difference corresponding to channel 21 shows a large 16° change between 5 November and 16 November. Again, neither the playback nor the station logs provided the explanation for this change.

Table III-5 gives the phase means, variances and standard deviations for all nine calibrations and the amplitude for the six calibrations after the shift in calibration frequency and gain adjustment to channel 1. Figures III-1 and III-2 show the standard deviations in graph form. The one anomalously high value on channels 10, 14, 18 and 25 cause their amplitude standard deviations to be relatively large. For other channels, amplitude response standard deviations are less than 4 percent. The phase response standard deviations are less than 1.8° for all seismometers other than channel 21.

Subarray F-4 (Tables III-6 and III-7) generally had good stability. The channel 10 and channel 24 amplitude ratios were high and low, respectively,

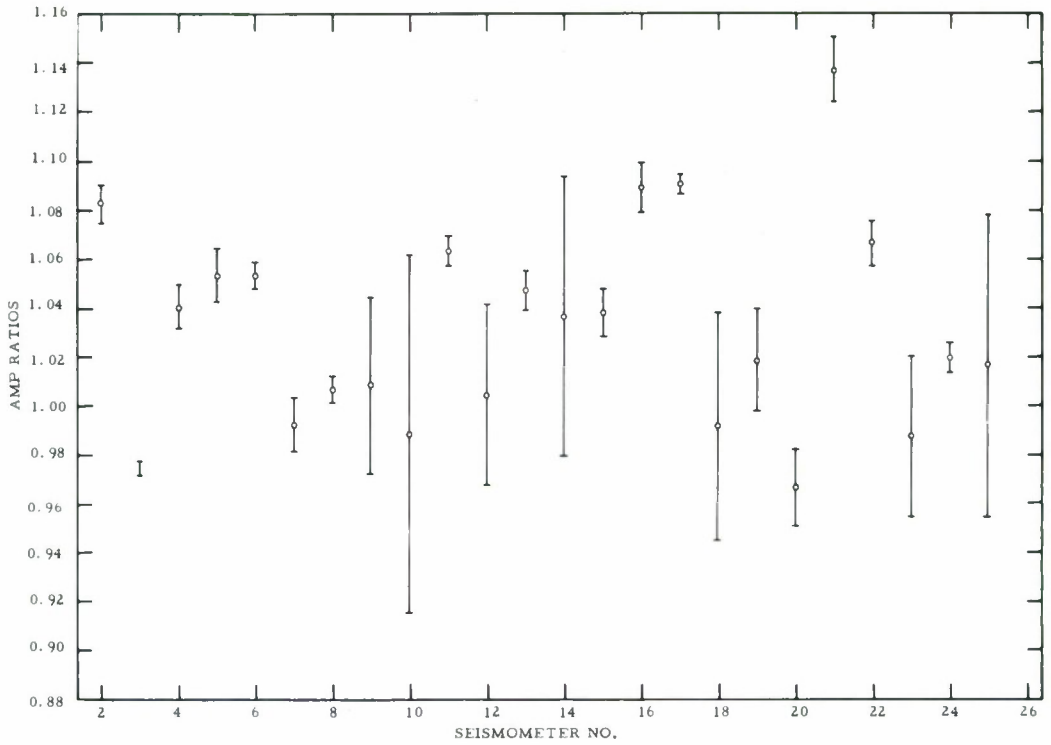

Figure III-1. Seismometer Amplitude Response Variations Over A One Month Period. Subarray F-3

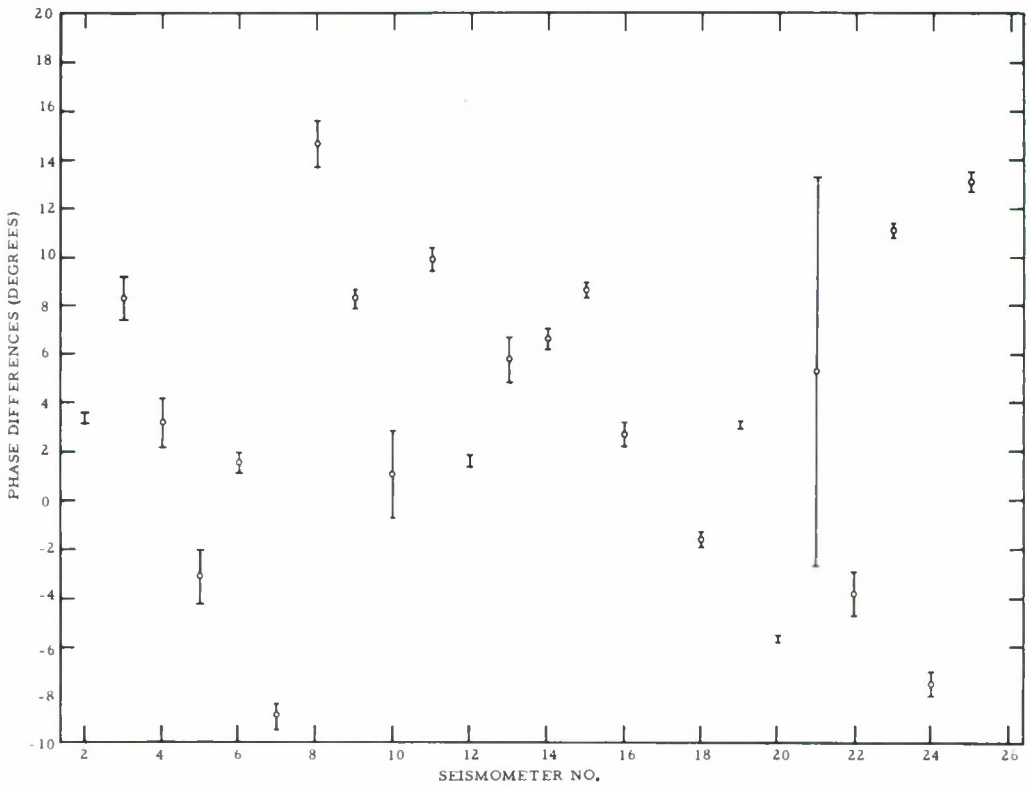

Figure III-2. Seismometer Phase Response Variations Over A One Month Period. Subarray F-3

for the 2 November calibration. Again, no explanation was available. The phase differences for channel 2 had relatively low values on 2 November and 21 November. No explanation was available for these values. The channel 11 phase difference had much less stability than the other channels, suggesting that some component of the seismometer-amplifier system may have been deteriorating.

Table III-8 gives the means, variances and standard deviations for all 24 amplitude ratios and phase differences. Figures III-3 and III-4 show the standard deviations in graph form. The amplitude response standard deviations were less than 5 percent on all channels and the phase response standard deviations were less than 0.4° on all but channels 2 and 11.

Subarray C-3 (Tables III-9 and III-10) had excellent stability in amplitude responses except for a large abrupt change between 16 November and 20 November. This change was not explainable from the station logs, nor could it be attributed to a variation in the channel 1 response. (The change varied from zero on channel 2 to 0.29 on channels 11 and 13.) Because the change varied from seismometer to seismometer and because the changes balanced the gains at 1 cps across the array, the most likely explanation is that the seismometer-amplifier systems were manually adjusted.

The phase differences were stable except for the channel 10 response which changed about 10° between 16 November and 20 November. This change probably was related to the amplitude change discussed above. Also, a change of about 2° in the phase response of channel 1 may be inferred between 3 November and 5 November, as shown by the 2° change in all 24 ratios.

The amplitude means, variances and standard deviations are not presented because of the apparently manually caused change. The phase data (after the 2° phase shift on channel 1 was removed) are given in Table III-11 and are plotted in Figure III-5. Except for channel 10, the phase response standard deviations were less than 0.4°.

Subarray E-2 (Tables III-12 and III-13) had stable amplitude and phase responses, except for eight seismometers which had abrupt amplitude changes between 23 November and 24 November. Again, these changes appear to be due to manual adjustments of these comparatively high-gain systems.

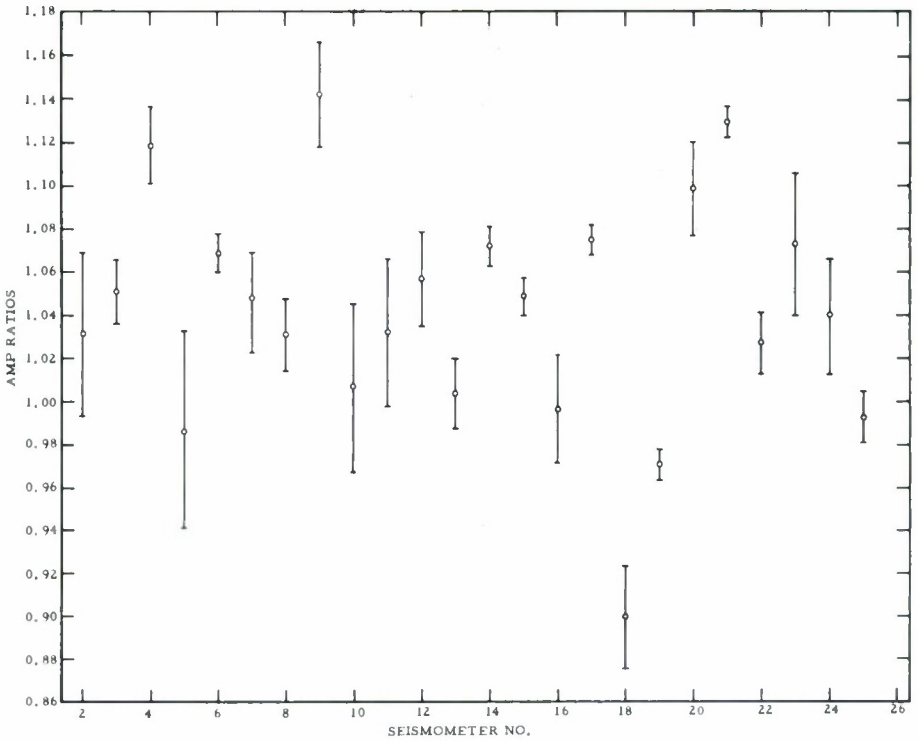

Figure III-3. Seismometer Amplitude Response Variations Over A One Month Period. Subarray F-4

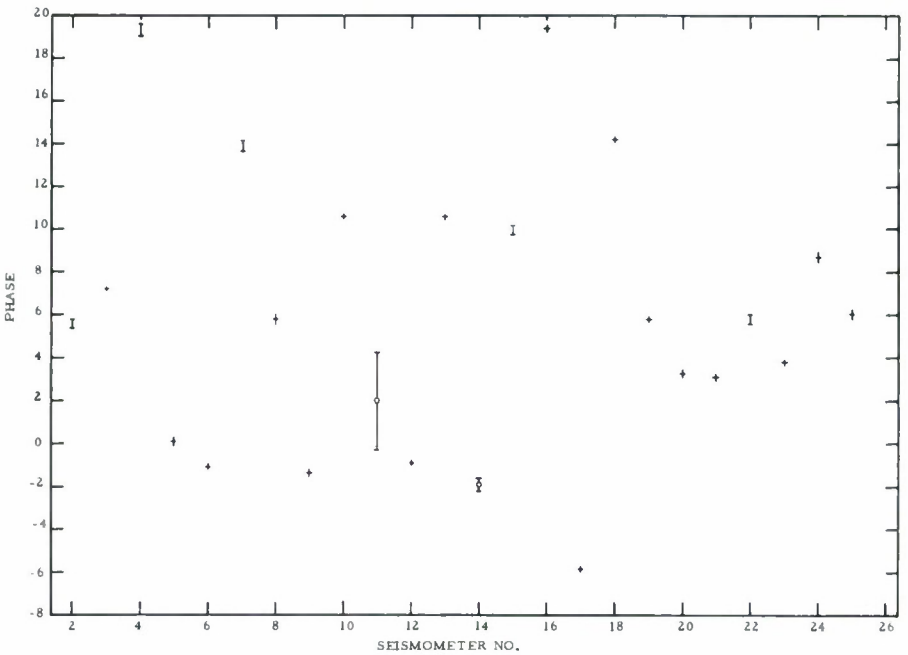

Figure III-4. Seismometer Phase Response Variations Over A One Month Period. Subarray F-4

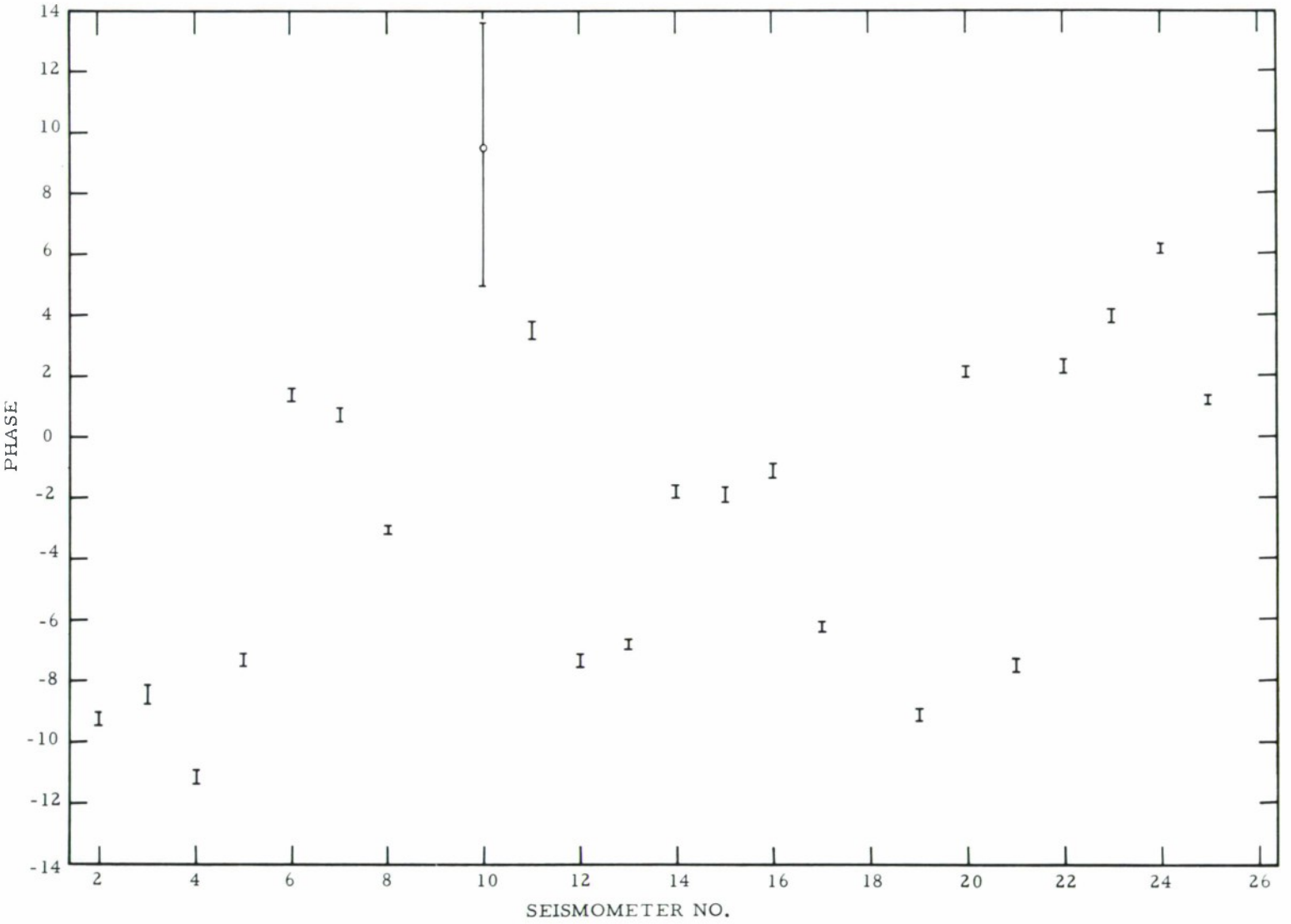

Figure III-5. Seismometer Amplitude Response Variations Over A One Month Period. Subarray C-3

Table III-14 gives the means, variances and standard deviations for both the amplitude and phase responses, except for the eight seismometers discussed above, and Figures III-6 and III-7 present the data in graph form. Amplitude response standard deviations were less than 3.5 percent and the phase response deviations were less than 0.3°.

Subarray F-2 (Tables III-15 and III-16) amplitude responses were stable except for the last calibration on 2 December which was different for nearly every seismometer. However, since the differences were not regular, it appears that they were natural variations due to some physical cause. The phase responses were stable.

Table III-17 gives the means, variances and standard deviations for the amplitude and phase responses, and Figures III-8 and III-9 present in graph form the standard deviations from the mean. Amplitude response standard deviations were less than 6 percent and phase response deviations were less than 0.6°.

c. Comparisons of 1 December and Mid-March Calibrations

The amplitude and phase responses for the 1 December 1965 calibration are compared with those of the March calibration in Tables III-18 through III-22; Table III-23 summarizes the variations. About two-thirds of the amplitude response variations were less than 10 percent, and one-third of the phase response variations were less than 2°. For the 1-month data, essentially all amplitude and phase responses were within these limits (neglecting the abrupt amplitude response changes observed on subarrays C-3 and E-2).

Most of the remaining amplitude response variations were between 10 and 20 percent, but ranged up to a maximum of 65 percent (channel 10, subarray F-3). Most of the remaining phase response variations were between 2° and 10°, but ranged up to a maximum of 41° (channel 6, subarray F-3). Because of the substantial number of large variations, instrument response differences were not included in the five multichannel filters designed for on-line application (Section V).

As shown in Table III-2, the calibration frequencies were about 0.02 cps different for the two sets of data. This difference could explain a significant part of the phase response variations. (Absolute phase responses,

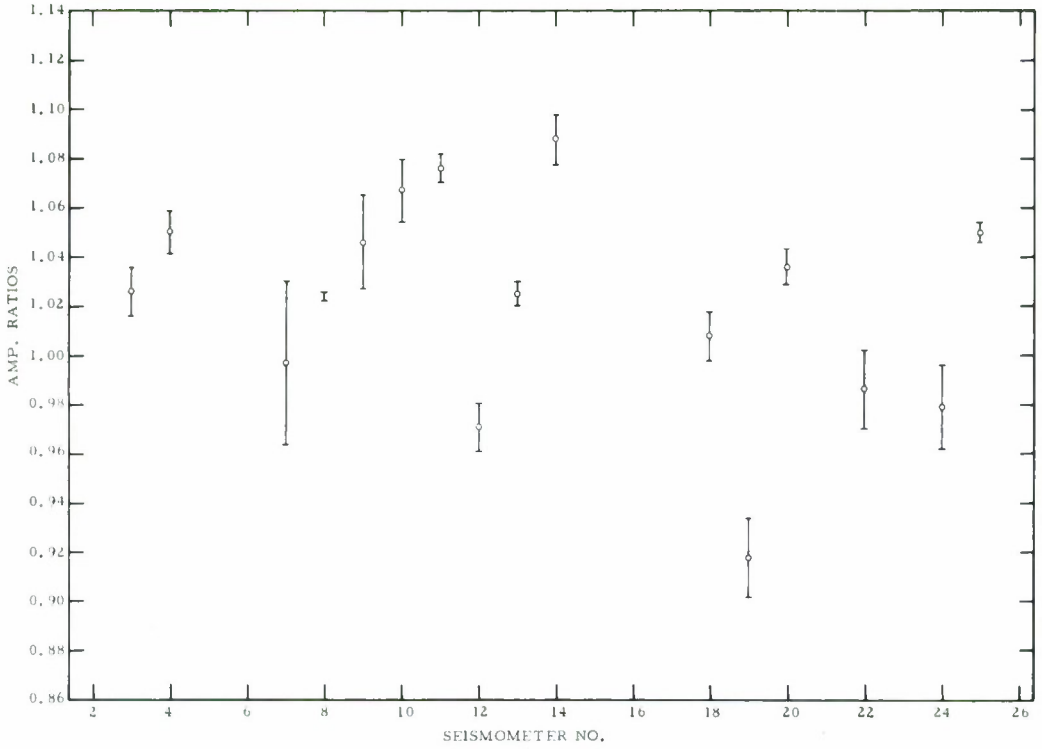

Figure III-6. Seismometer Amplitude Response Variations Over A One Month Period. Subarray E-2

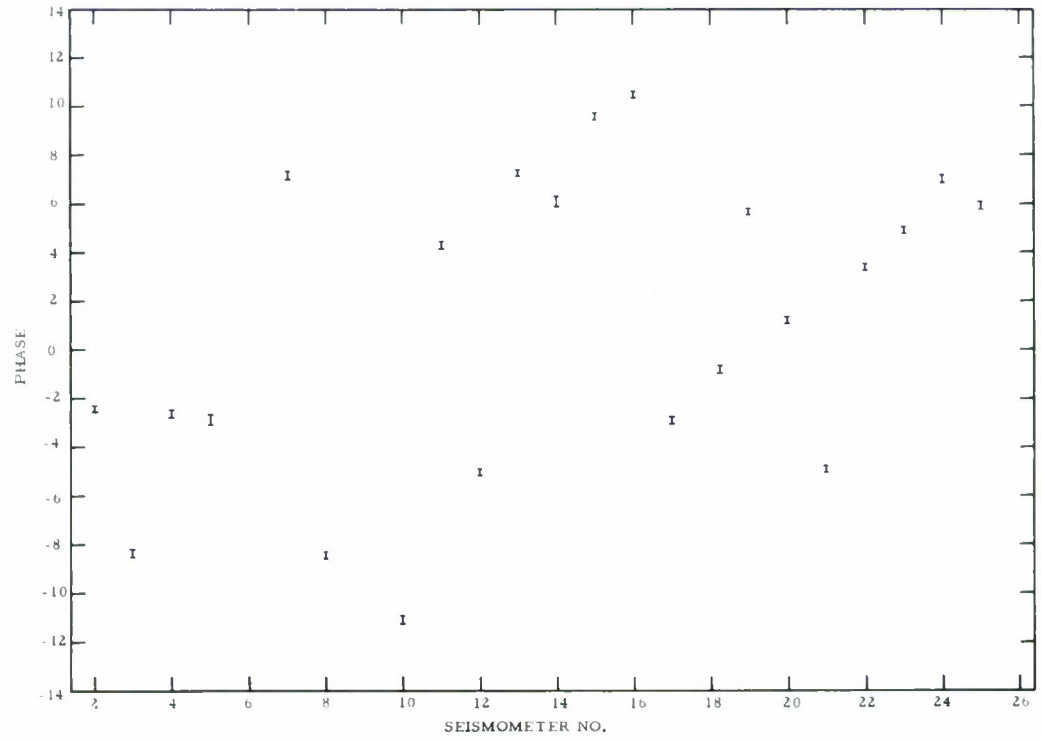

Figure III-7. Seismometer Phase Response Variations Over A One Month Period. Subarray E-2

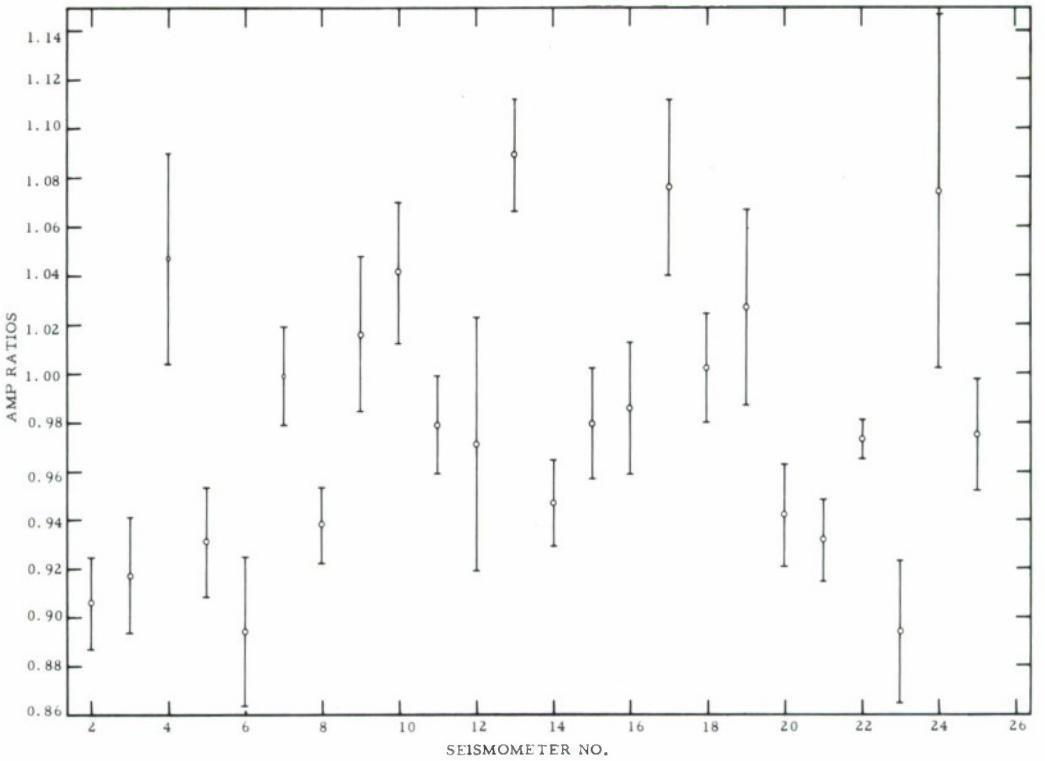

Figure III-8. Seismometer Amplitude Response Variations Over A One Month Period. Subarray F-2

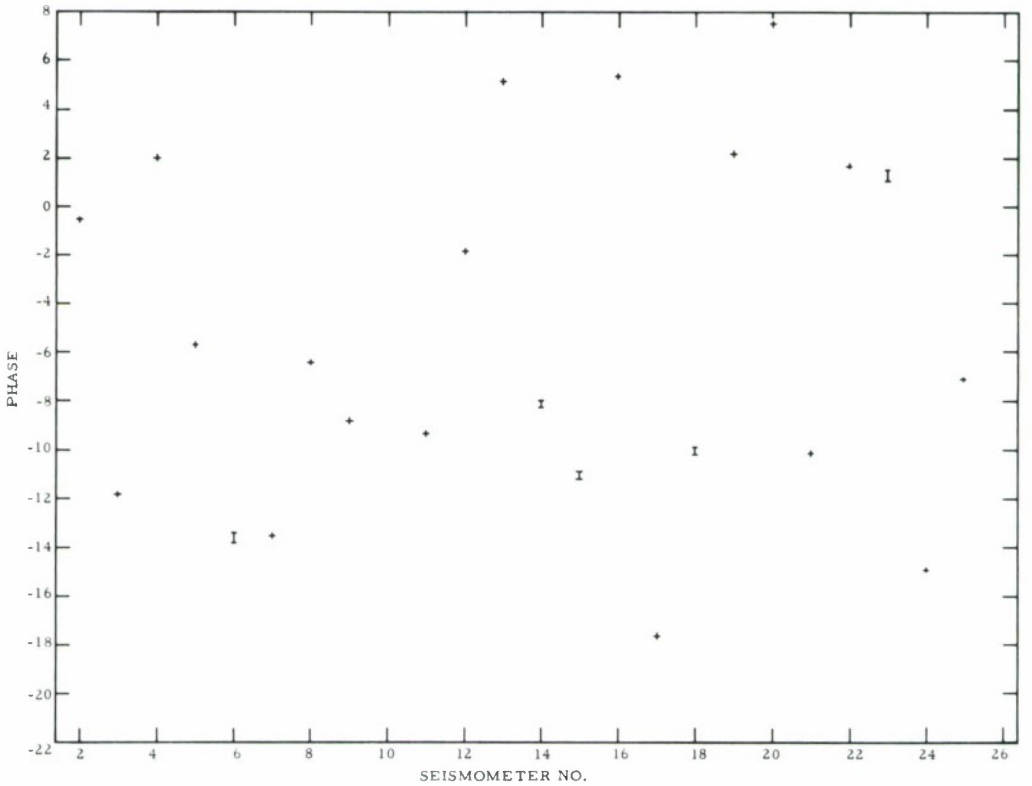

Figure III-9. Seismometer Phase Response Variations Over A One Month Period. Subarray F-2

obtained from the March 1966 calibrations where a reference channel was included, varied quite rapidly in the neighborhood of 1 cps.) Otherwise, differences in phase and amplitude response probably were due to one or a combination of the following:

- Natural variations due to environmental changes and/or instrument drift
- Replacement of components
- Manual adjustments

Necessary information was not available to determine which one or a combination of these three was the major cause for the large variations observed in both amplitude and phase responses. Thus, at present, no conclusion can be made about the stability of seismometer responses over the longer 3-1/2 month period.

5. Summary

The time-stability at 1 cps of all seismometers from each of five subarrays was studied by analyzing their amplitude and phase responses relative to the center seismometers. Nine calibrations recorded over a 1-month period (2 November - 1 December 1965) were used in the study. The analysis showed that the seismometers generally had good time-stability in both amplitude and phase responses over the 1-month period. With the exception of a few seismometers, amplitude response standard deviations (neglecting the abrupt changes discussed below) were less than 5 percent and phase response standard deviations were less than 2°. These deviations were small enough that they would not have significantly reduced the effectiveness of an on-line system.

In addition to the normal variations the following abrupt variations were observed:

- Variations due to changes in the seismometer-amplifier system
- For six amplitude responses and four phase responses, larger-than-normal variations which had no immediate explanation
- For subarrays C-3 (all seismometers) and E-2 (eight seismometers) abrupt changes in amplitude responses (by as much as 30 percent) which were most likely due to manual adjustments to the seismometer system

The relative amplitude and phase responses of the 1 December calibration were compared with responses obtained for a mid-March 1966 calibration on all five subarrays. Variations significantly larger than those seen over the 1-month period were observed. Many were large enough to affect the performance of an on-line MCF system. However, the information necessary to determine the major cause of the variations was not available. Thus, at present, no conclusion can be made about the stability of the seismometer responses over the 3-1/2 month period.

B. MULTIFREQUENCY CALIBRATION ANALYSIS

1. Purpose

This study is to investigate the instrument responses of 125 seismometers as determined by an analysis of one multifrequency calibration of each seismometer. The results of this investigation were used to experimentally determine the improvement in MCF performance to be obtained by incorporating these measured responses into the MCF design. The response variations between instruments within each subarray and estimates of relative instrument responses are presented.

The calibration data for this analysis was specially recorded during March 1966 from five subarrays (F-3, F-4, C-3, E-2, and F-2) at 11 different frequencies. The calibration signal length at each frequency was approximately 150 sec and was recorded at a high S/N ratio.

2. Method

The LASA digital tapes containing the calibrations were de-multiplexed, at 11 different calibration frequencies, to obtain 26 traces for each of the five subarrays. The 26 traces consisted of one calibration reference trace and the recorded output of each 25 seismometers in each subarray. The reference trace and the traces of two selected instruments were Calcomp-plotted for each subarray to determine the starting time and the length of each frequency calibration and to check for abnormalities in the data. A gate length of an integral number of cycles was chosen for each frequency. To determine the exact calibration frequencies, the reference traces were Fourier-transformed in increments of 0.002 cps over a frequency band centered on the nominal frequency. Each energy-density spectrum was plotted and the frequency at maximum amplitude was selected. Results of

this analysis are shown in Table III-24. (Two subarrays were not calibrated at certain frequencies.) The digital tape containing the 0.4- and 0.6-cps calibrations for F-3 was damaged and the 6.0-cps calibration of F-2 was not received.

For each calibration, after exact calibration frequencies had been determined, the Fourier transforms were calculated for each channel at the corresponding calibration frequency. Each data gate began at a zero crossing and contained an integral number of cycles. This process yielded the phase spectra and amplitude spectra for all of the 125 channels at 11 frequencies/channel. The center seismometer of each subarray was chosen as a reference; responses were not referenced to the calibration reference channel because of large phase differences observed between the reference channel and the other channels. Since the cause of this phase shift was unknown and only relative responses were required, it was decided that the center seismometer was preferable as reference. For each frequency, differences in the phase spectrum for the center seismometer and the phase spectra for the other 24 seismometers were formed. Relative amplitude response was measured by dividing the amplitude spectra of the remaining 24 seismometers by the amplitude spectrum of the center seismometer. By this means, relative phase and amplitude responses were obtained for all 125 channels at 11 frequencies/channel.

Since the calibration frequencies did not contain all frequencies of interest, the relative responses were estimated by fitting a polynomial to the calibration results of each seismometer and evaluating this polynomial at increments of 0.25 cps. The method of least squares was employed to obtain the coefficients of a polynomial of the form

$$f(X) = A_o + A_1X + A_2X^2 + \ldots + A_nX^n$$

An investigation was made to determine the degree polynomial best suited for this estimation. The set of measured relative responses for one channel was used to fit polynomials of degree 3 through 9. It was found that a polynomial of degree 5 fit both the amplitude and phase responses very accurately (less than 2-percent error) and still yielded values which were well-behaved between the measured points. Then, when the responses for a complete subarray were estimated by being fitted to a degree 5 polynomial, the results were likewise satisfactory. Tables III-25 and III-26 contain comparisons between the measured relative amplitude and phase responses and the polynomial-estimated relative amplitude and phase responses for selected channels.

The relative phase and amplitude responses of channel 22, subarray F-3, represent the best results. The relative phase response of channel 12, subarray C-3, and the relative amplitude response of both channel 17, subarray F-4, and channel 12, subarray C-3, are typical results. Poorest results for the 125 channels are the relative phase response of seismometer 6, subarray E-2, and seismometer 17, subarray F-4, and the relative amplitude response of seismometer 6, subarray E-2.

The relative phase responses and the polynomials which were fit to these responses are further illustrated in Figures III-10 and III-11. The maximum difference between measured relative phase and polynomial-estimated phase was 1° for most of the 125 seismometers, which is sufficiently accurate for application. In Figure III-10, seismometer 18 of subarray E-2 and seismometer 6 of subarray F-2 are representative of the seismometers for which the best results were obtained; seismometer 12 of subarray C-3 is representative of a typical result. The poorest polynomial fits were obtained for six seismometers (6, 12, 17, 19, 23, and 25) of subarray F-4. Figure III-11 presents the measured phase responses and the polynomial-estimated phase responses for three of these instruments. The difference in measured relative phase responses and polynomial-estimated responses was less than 4° for all six seismometers.

Figures III-10 and III-11 indicate that certain of the polynomials have large excursions between 4.0 and 6.0 cps, that are not justified by the measured data. However, these variations were not considered in the signal model design since the signal model was band-limited from 0.5 to 4.0 cps.

3. Results

Relative phase and amplitude responses as a function of frequency are represented in Figures C-1 through C-10, Appendix C. Each figure contains six plots, each of which presents the relative phase or amplitude responses for the four channels from one of the six arms of the subarray. No relation was observed between the relative responses of instruments within any one particular arm of the subarray, nor between relative responses of channels equidistant from the center of the subarray.

A more visual illustration of the response variations among the 25 seismometers of subarray F-3 is presented in Figures C-11 through C-14, Appendix C. Most relative responses are well-behaved for frequencies below

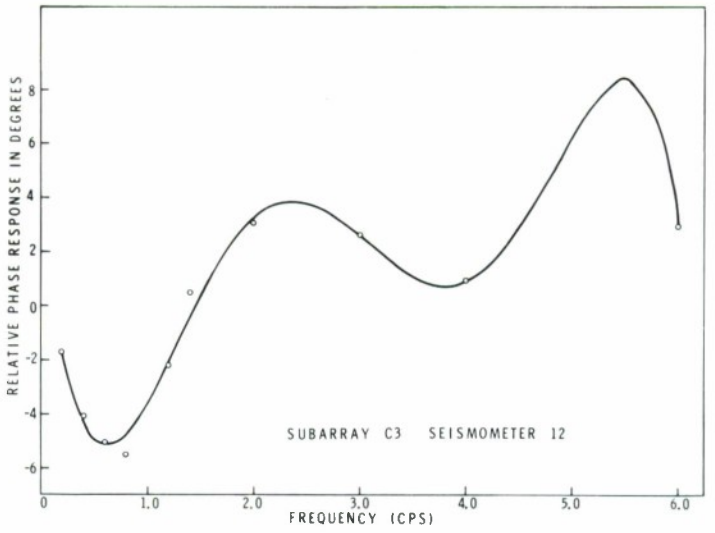

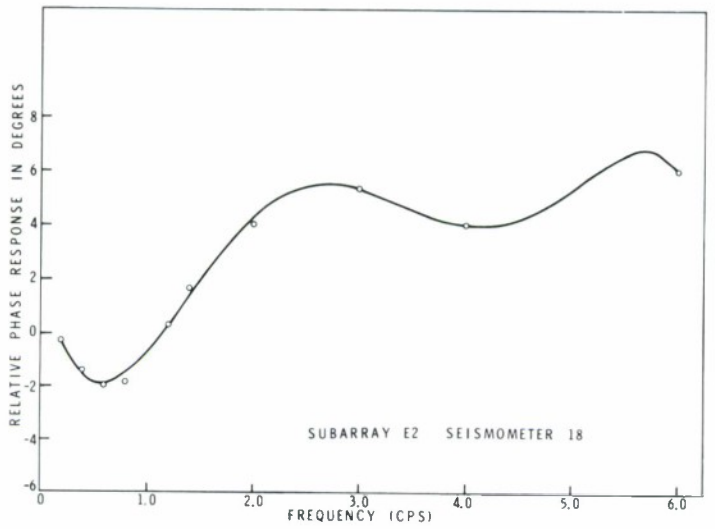

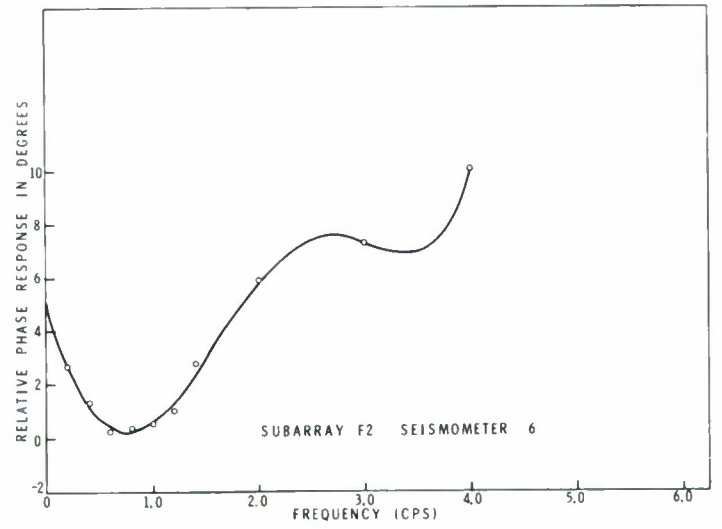

Figure III-10. Comparison of Relative Phase Responses and Polynomial Fit

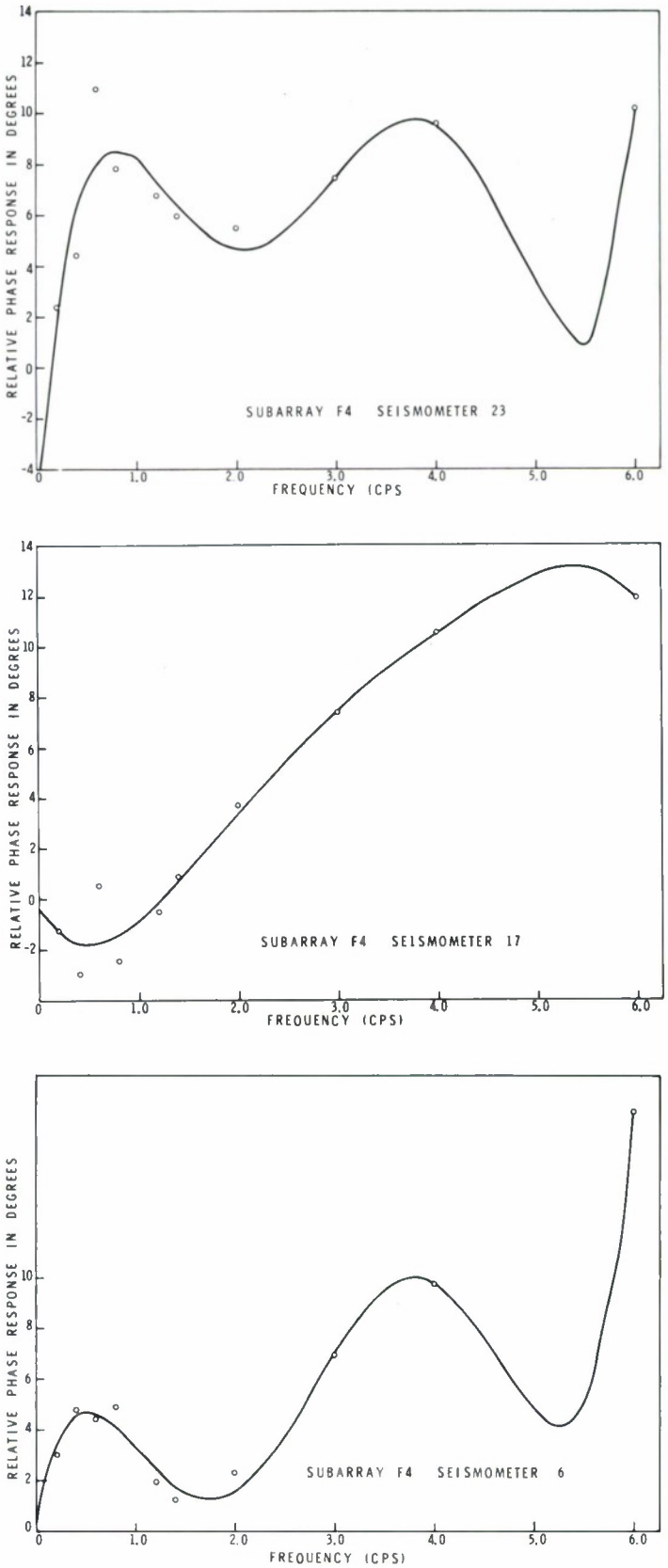

Figure III-11. Comparison of Relative Phase Responses and Polynomial Fit for Subarray F-4

3 cps. The exceptions are seismometer 16 of subarray C-3 (Figure C-8) and seismometer 6 of subarray F-3 (Figure C-1). Also, the amplitude response for channel 24 of subarray E-2 (Figure C-4) has an abrupt deflection at 1.0 cps, and the phase response for channel 6 of subarray F-3 (Figure C-6) is less than that for the other instruments.

The means, standard deviations and extremes of the relative phase and amplitude responses for each subarray at all calibration frequencies are illustrated in Figures III-12 through III-16. The phase response of channel 16 of subarray C-3 and the phase and amplitude responses of channel 6 of subarray F-3 were not included in determining these values (for reasons previously mentioned). Of interest is the fact that the minimum standard deviation from the mean amplitude response occurs at 1 cps for every subarray. This is not surprising since the damped resonant frequency of each seismometer is approximately 1 cps.

All figures indicate substantial variations in both relative phase and amplitude responses within each subarray for frequencies greater than 3 cps. For frequencies below 3 cps the relative responses differ noticeably from seismometer to seismometer as Figures C-1 through C-14 illustrate. However, the standard deviations from the mean are less than those at the higher frequencies.

4. Conclusions

From this multifrequency calibration analysis, it has been determined that there are strong variations in phase and amplitude responses among the seismometers within a subarray. These variations are very pronounced at frequencies greater than 3 cps. It is apparent that equalization of these response differences would result in significant improvement in MCF performance. These variations also would also seriously distort frequency-wavenumber spectra computed without proper compensation for instrument response differences.

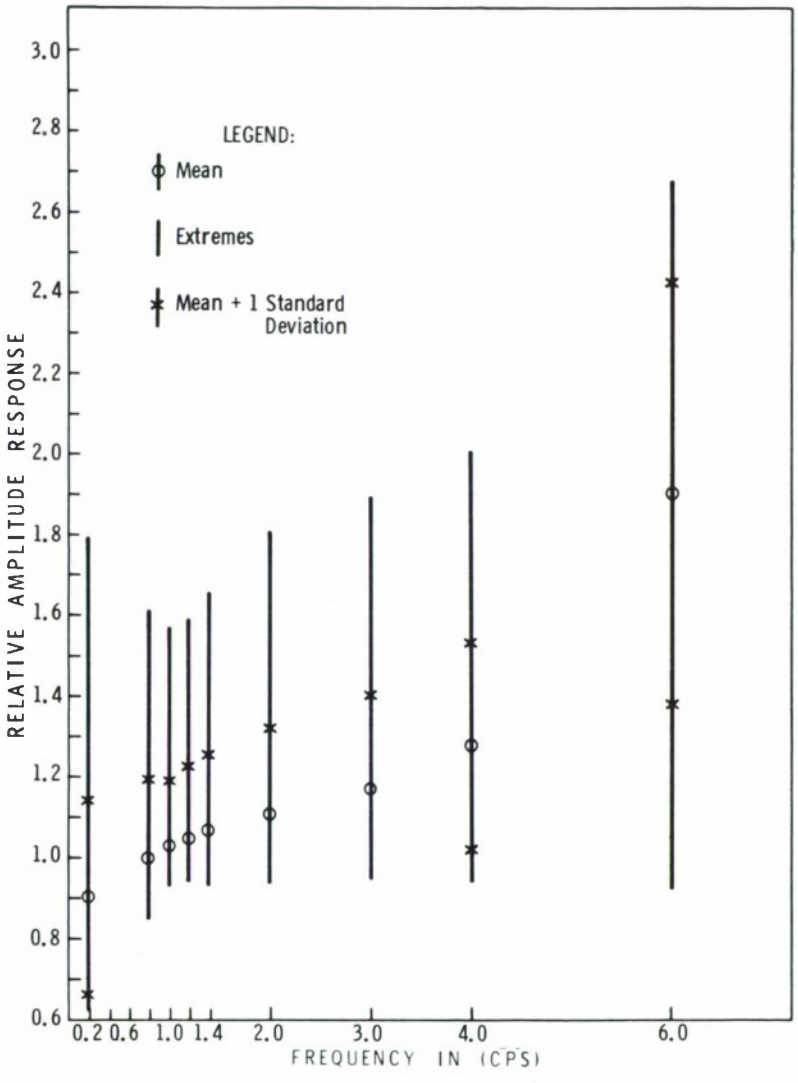

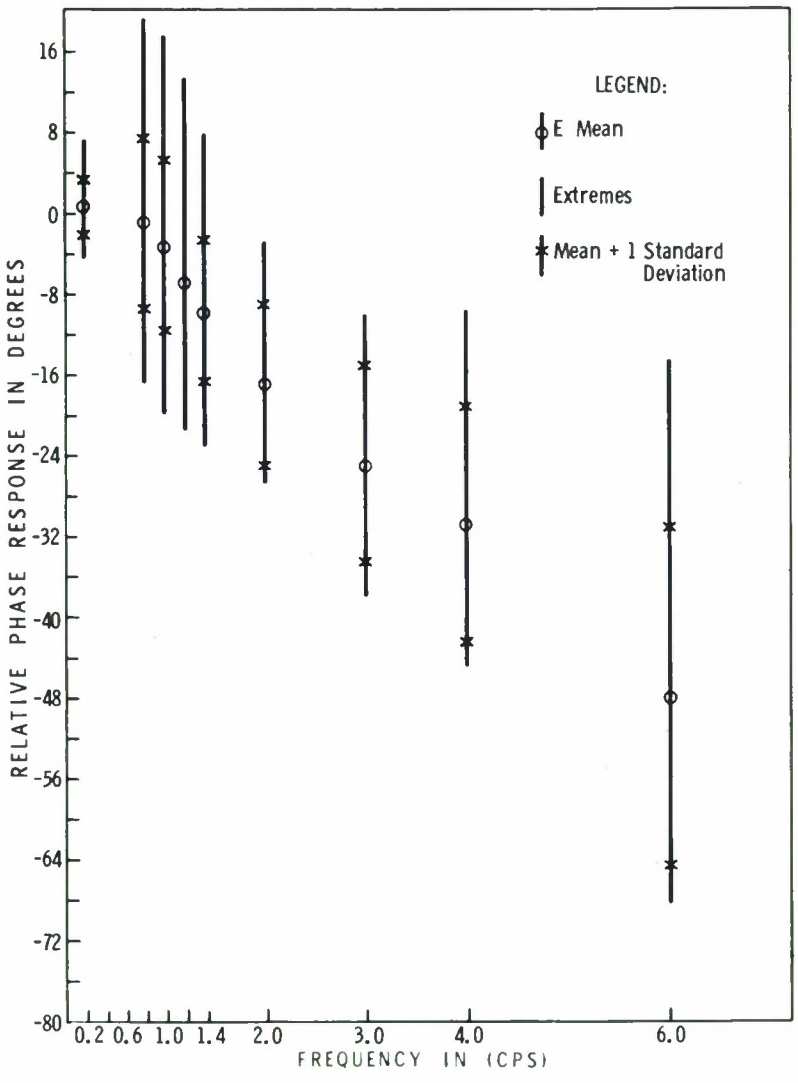

Figure III-12. An Illustration of the Mean, Standard Deviations and Extremes of Relative Phase and Amplitude Responses for Subarray F-3

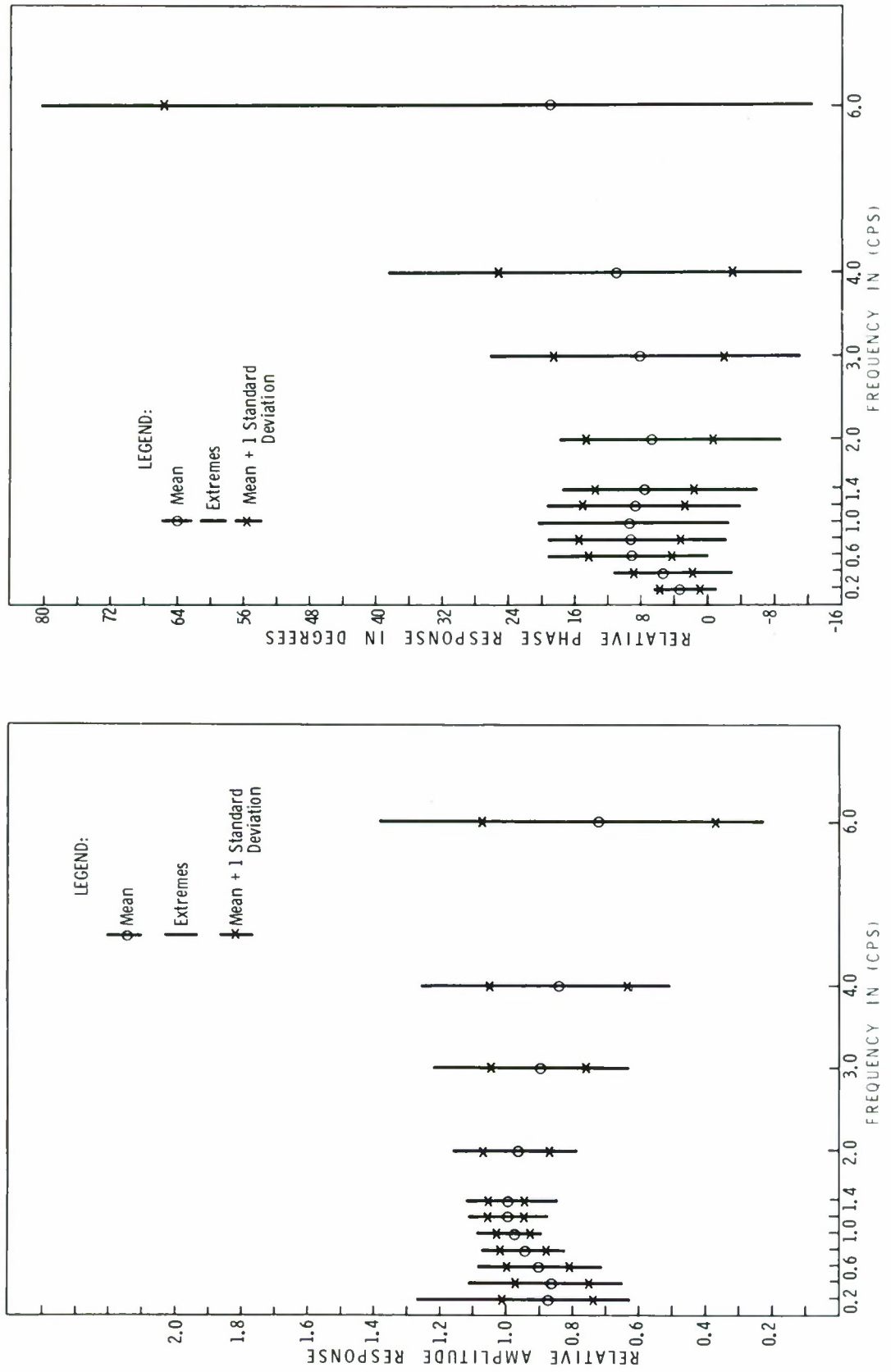

Figure III-13. An Illustration of the Mean, Standard Deviations and Extremes of Relative Phase and Amplitude Responses for Subarray F-4

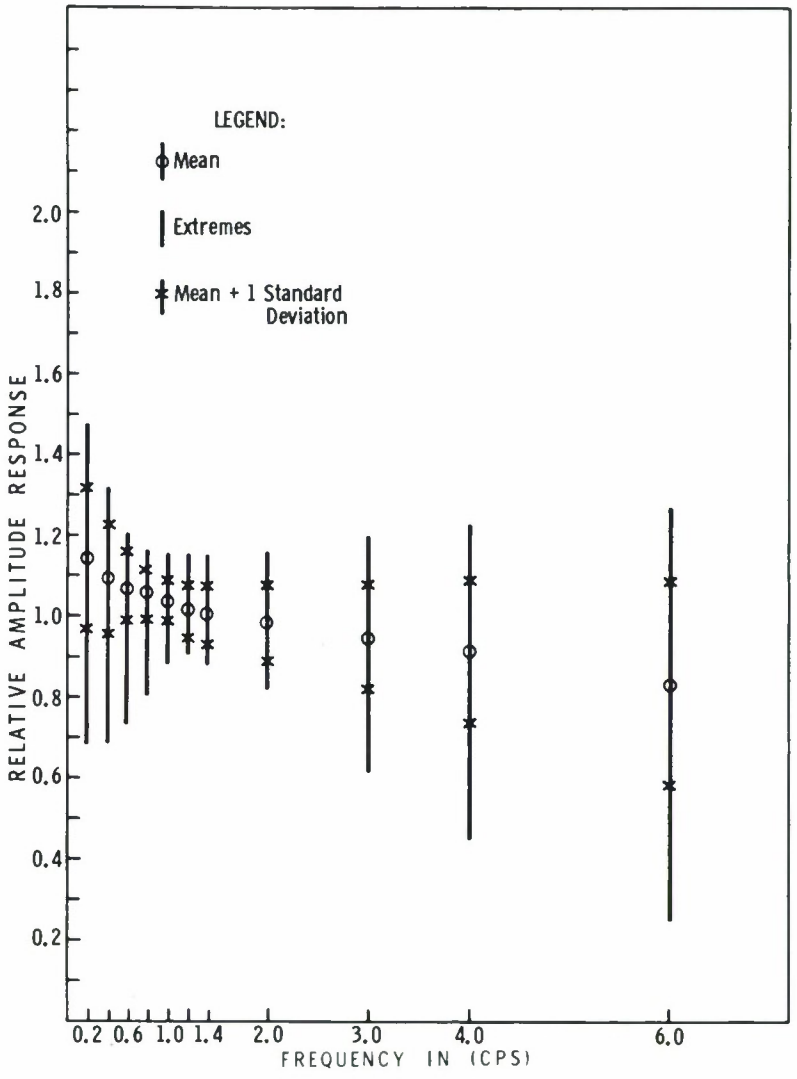

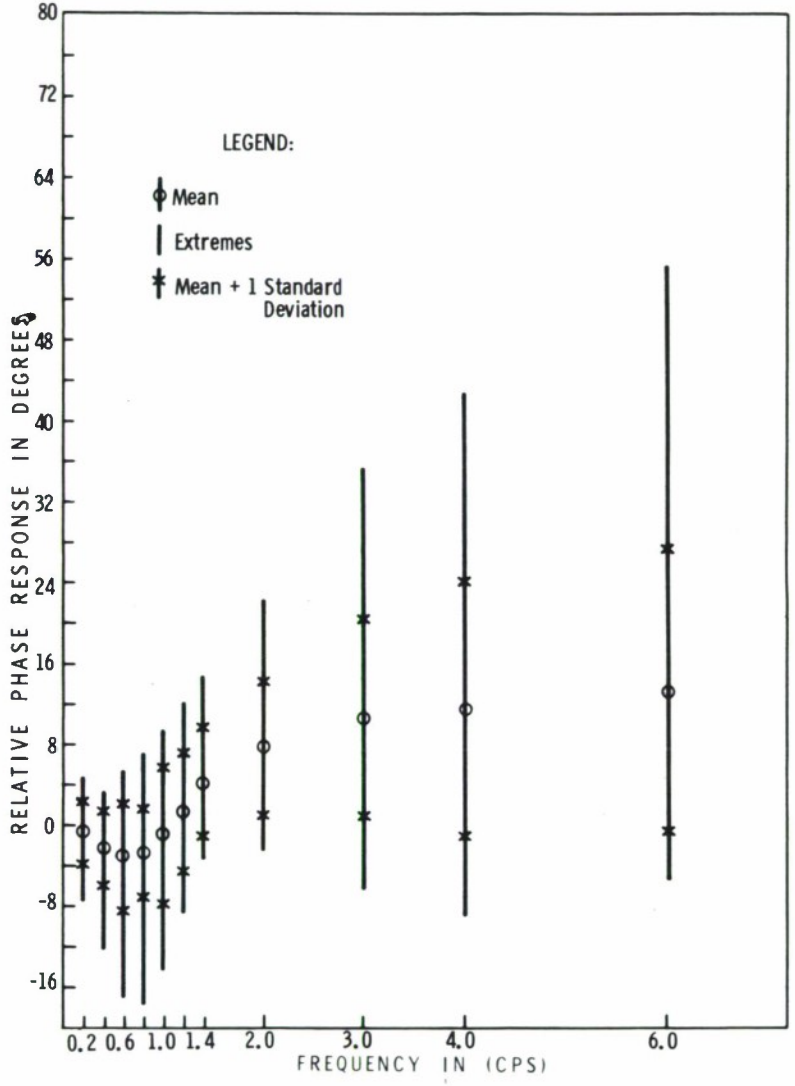

Figure III-14. An Illustration of the Mean, Standard Deviations and Extremes of Relative Phase and Amplitude Responses for Subarray C-3

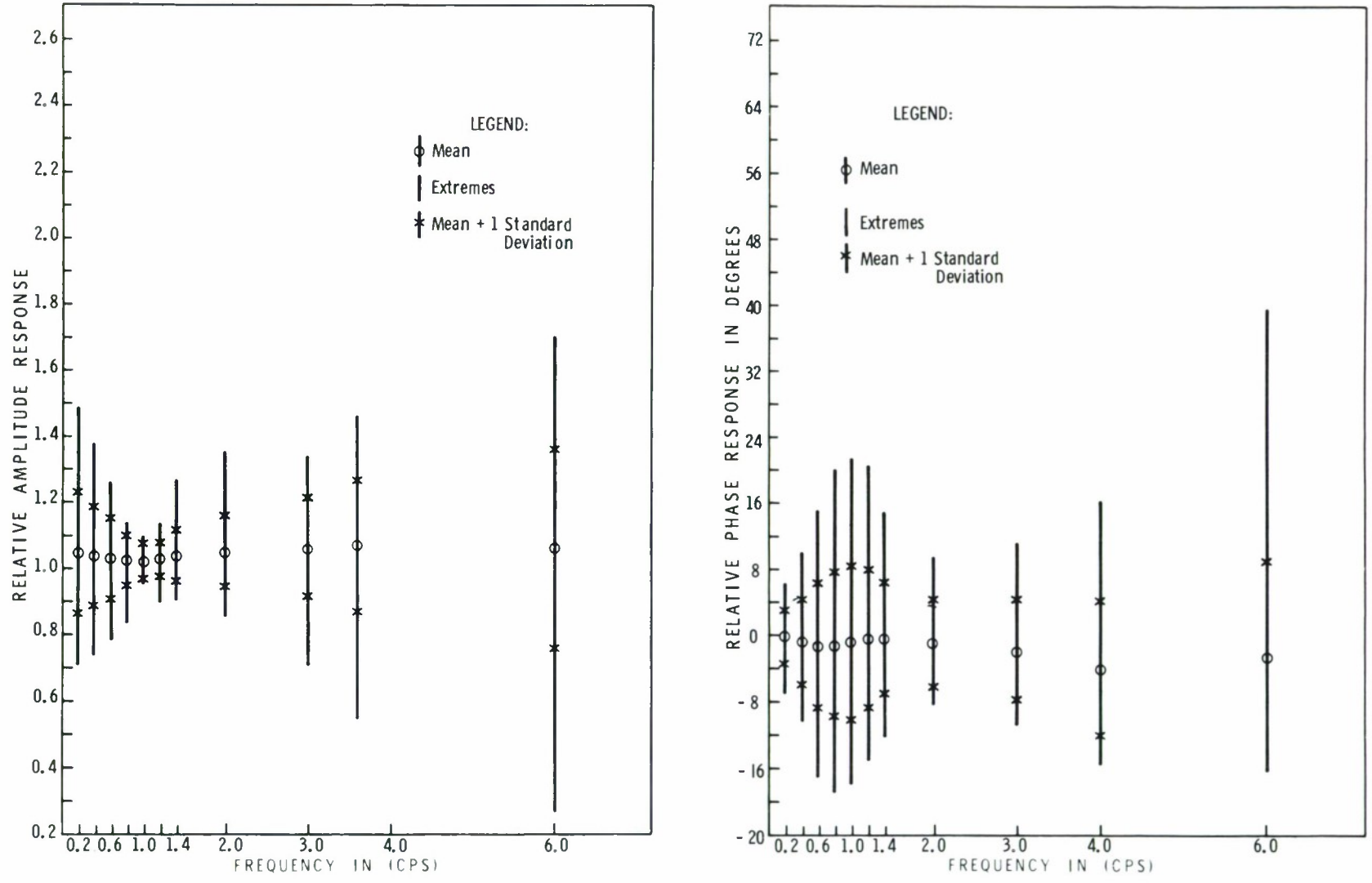

Figure III-15. An Illustration of the Mean, Standard Deviations and Extremes of Relative Phase and Amplitude Responses for Subarray E-2

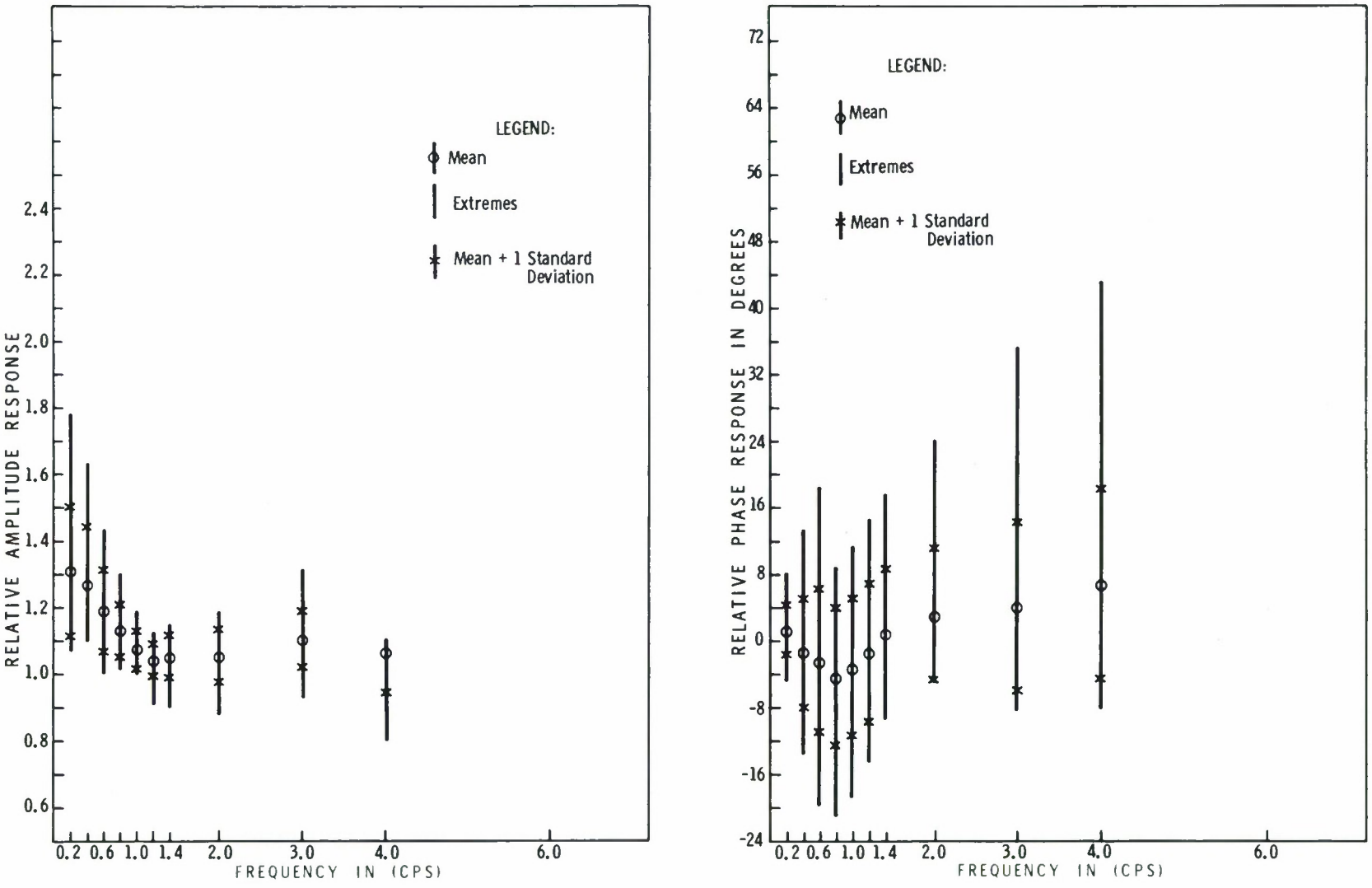

Figure III-16. An Illustration of the Mean, Standard Deviations and Extremes of Relative Phase and Amplitude Responses for Subarray F-2

C. DEVELOPMENT OF INSTRUMENT RESPONSE EQUALIZATION FILTERS FOR THE B1 SUBARRAY

Significant differences in phase and amplitude responses exist among the instruments within the LASA. The response variation from channel to channel within a particular subarray must be properly compensated for in the design of multichannel filters for that subarray in order to achieve maximum S/N improvement. Response variations within the array also make invalid the assumption of space-stationarity which is necessary to the computation of frequency-wavenumber spectra.

1. Purpose

The experiment described herein was designed to investigate the development of digital equalization filters which would compensate for differences in phase and amplitude responses. These filters were designed on the assumption that the response differences could be modeled as having been produced by minimum-phase filters. Calibration data recorded by Texas Instruments Digital Field System (DFS)* on 13 May 1965 during the engineering and seismological evaluation of subarray B1** was used to specify filter response.

The filters were evaluated on the basis of their ability to equalize phase response to that of an arbitrarily chosen reference seismometer. Whereas phase responses varied as much as 37° at 1 cps, as determined from the calibration, application of the equalization filters reduced this variation to 7°. In general, considerable reduction in the phase response variation from instrument to instrument was achieved at all frequencies for the 22 channels for which equalization filters were developed.

---

*Trade of Texas Instruments Incorporated.

*Texas Instruments, 1965, Large Aperture Seismic Array: Final Specifications Rpt., Contract AF33(657)-13899, August.

2. Filter Design

All channels were calibrated on a 0.1-cps frequency increment from 0.5 cps to 1.5 cps and at 2.5, 3.0, 4.0, 5.0, 6.0, and 7.0 cps. Two channels, seismometers 10 and 33, were not used for this test because of large deviations from the average, which were believed to be due to other causes. Calibration data were recorded digitally on a 0.024-sec/sample basis. All calibrations were Fourier-transformed and amplitude and phase responses plotted. Channel 5, which corresponded to seismometer 44 for the DFS recording format, was chosen as reference channel since its amplitude response seemed to be representative of the average response. Table III-27 presents the recording format used for this data.

The ratio of the amplitude response for the i^{th} channel to the amplitude response of channel 5 was formed at each calibration frequency. Then, a least-squares fit of a third- to seventh-degree polynomial, depending upon which appeared to fit best (but usually a fifth-degree) was made to estimate the amplitude ratio function for each of the 22 channels to be equalized to channel 5. Evaluation of each polynomial on 0.05-cps increments yielded the required estimate of the amplitude response ratio functions. Figure III-17 shows in decibels the relative amplitude responses of the reference channel and channels 10 (35) and 25 (53), which are representative of the remaining channel responses.

Table III-27

TRACE IDENTIFICATION			
Channel No.	Seismometer No.	Channel No.	Seismometer No.
1	71	14	26
2	31	15	33
3	10	16	73
4	24	17	51
5	44	18	21
6	84	19	64
7	82	20	62
8	42	21	25
9	22	22	55
10	35	23	66
11	75	24	23
12	86	25	53
13	46		

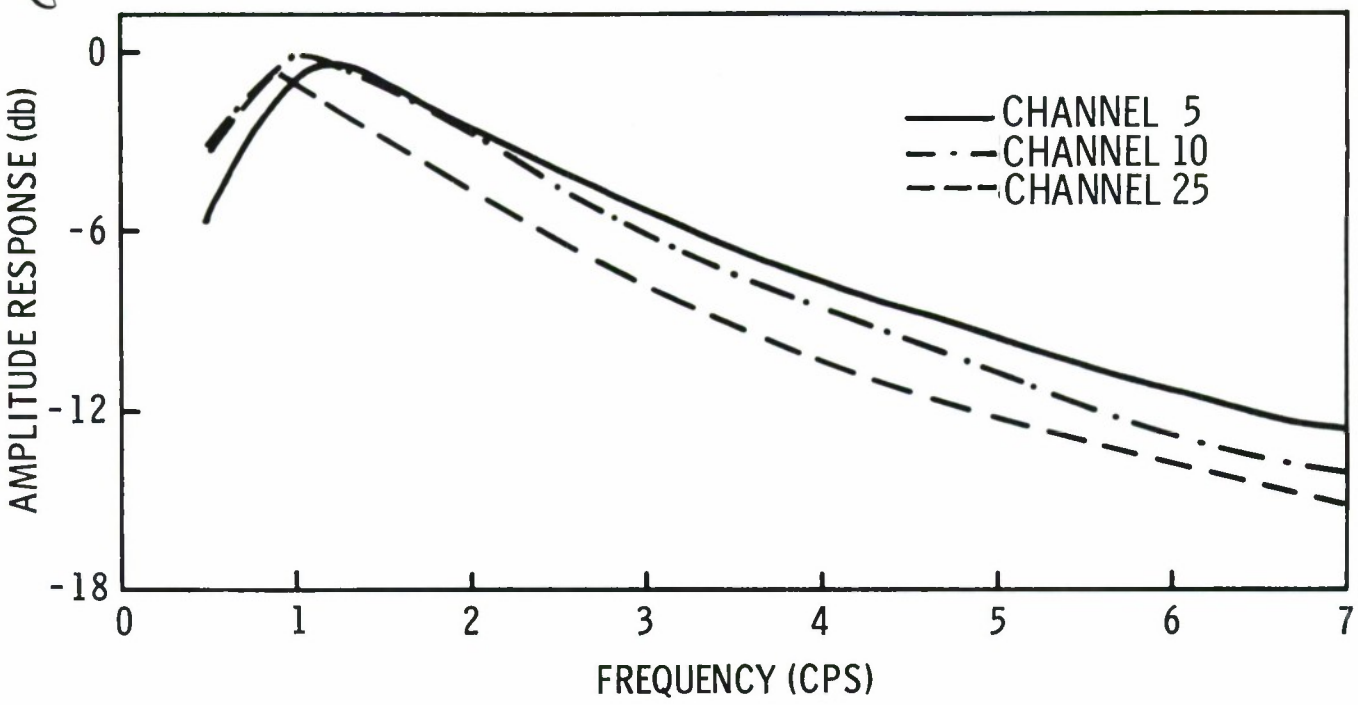

Figure III-17. Relative Amplitude Responses for 13 May 1965 Calibration Data

The requirements for equalization filters in this case were that each be minimum phase and that its amplitude response be the reciprocal of the estimated amplitude response ratio function for that channel. The existing program for designing minimum-phase whitening filter designs in the time domain. Input to the program is an autocorrelation function of the time series to be whitened. The square of the amplitude-response ratio function was Fourier-transformed as indicated below to obtain the proper function for input to this program:

$$\Phi_{ii}(n\Delta\tau) = \sum_{m=-416}^{416} \left(\frac{A_i(m\Delta f)}{A_5(m\Delta f)} \right)^2 e^{j2\pi m\Delta f m\Delta t} \quad \Delta f \; n=0, 1, \ldots . 28$$

where

$\Phi_{ii}(n\Delta\tau)$ = "autocorrelation" function corresponding to channel i

$A_i(m\Delta f)$ = amplitude response of channel i

Δf = 0.05 cps

$\Delta\tau$ = 0.072 sec

The 22 autocorrelation functions were input to the filter design program and a 29-point equalization filter developed for each. These filters were applied to the channels for which they were designed for two sets of calibrations. One calibration was that used in estimating relative amplitude responses, and the other was the same-type calibration which was performed 2 weeks later. The degree of equalization achieved was very nearly the same, indicating very little change in instrument responses over the 2-week period.

3. Filter Evaluation

The relative phase responses for the 22 channels studied are presented in Figure III-18(a-d). This figure series also shows relative phase following application of equalization filters. Relative phase was measured by Fourier-transforming the calibration data after equalization filtering. Only the six discrete frequencies -- 0.5, 0.7, 1.0, 1.5, 2.5, and 3.0 cps — were examined, although a continuous curve estimate of the relative phase was sketched through the measured values. Almost all channels show considerable improvement in similarity of phase response to that for channel 5. Those which show the least improvement are always the channels for which the phase response closely agrees (within $\pm 5^\circ$) with that for channel 5 before equalization.

The relative phase following application of equalization filters is shown for both sets of calibration data in Figure III-19(a-d). The close agreement at all frequencies for all channels, except channel 21, demonstrates the stability of instrument response over the 2-week interval. The behavior of channel 21 is unexplained but may be due to the replacing or adjusting of some component associated with this channel between calibrations.

Figure III-20 presents the range of variation in relative phase response among the 22 channels for the calibration set used in filter design and the same data after equalization. Variations of as much as 38° at 1.0 cps before filtering have been reduced to less than 4° by equalization. While marked improvement has been achieved at all frequencies, the greatest percentage of improvement has been obtained at 1.0 cps. This better filter performance at 1.0 cps may indicate that the assumption that the differences in seismometer-amplifier responses may be modeled as the effect of a minimum-phase filter is better approximated at 1.0 cps. Figure III-21 shows the same comparisons for the second set of calibrations. Very similar results were obtained, since there was little change in relative phase response between calibrations.

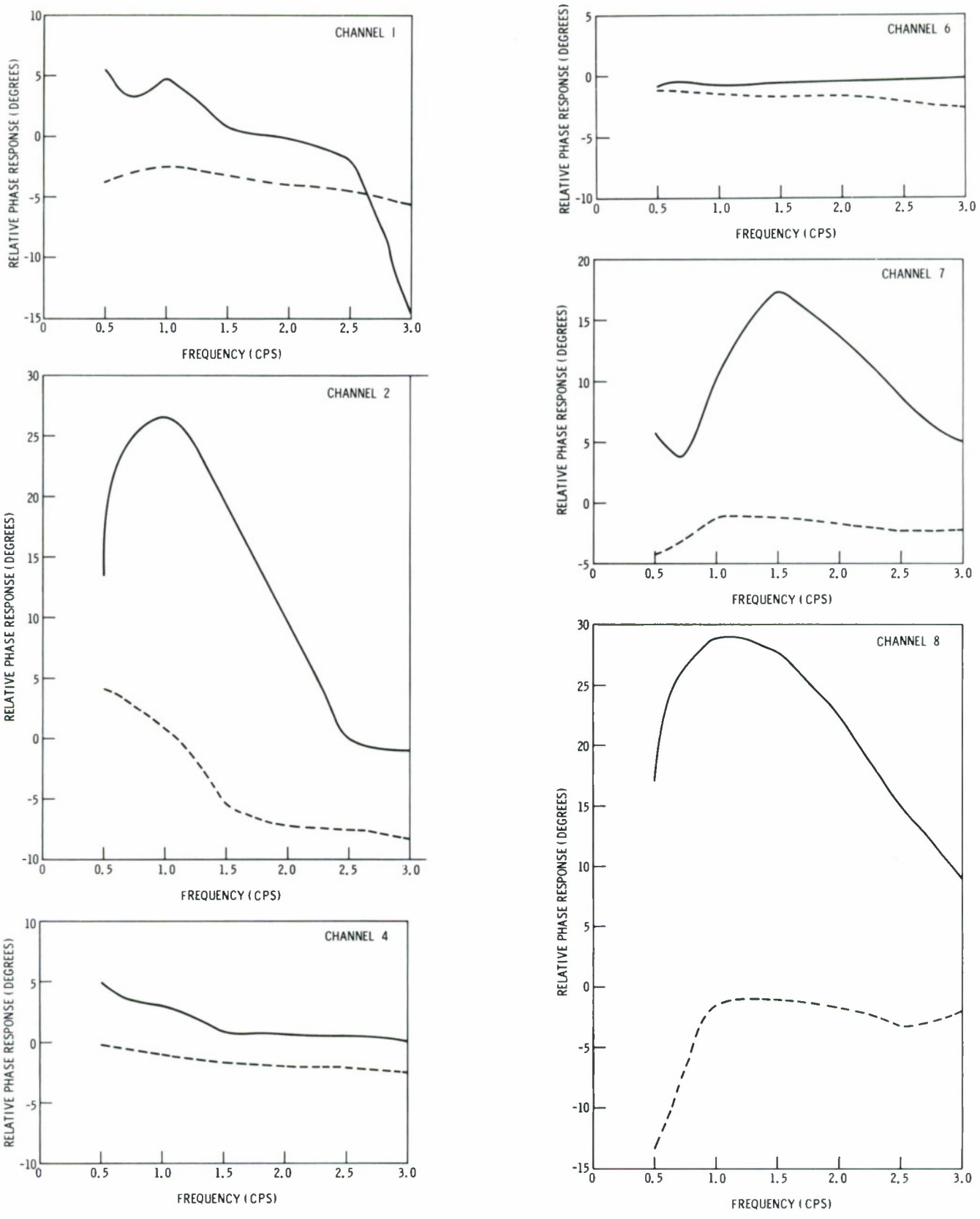

Figure III-18a. Phase Responses for May 13, 1965 Relative to Channel 5 Before (solid curve) and After (dashed curve) Filtering

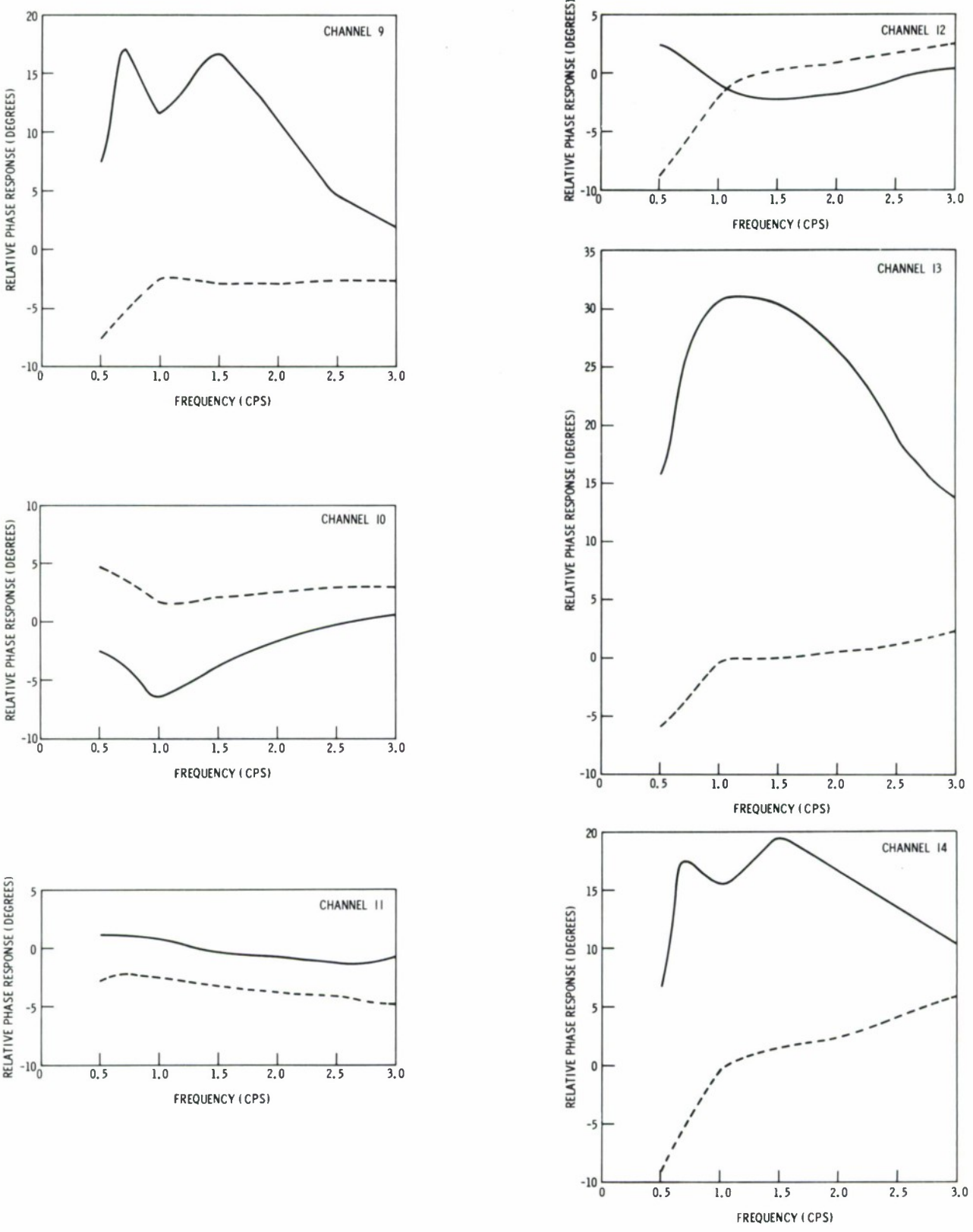

Figure III-18b. Phase Responses for May 13, 1965 Relative to Channel 5 Before (solid curve) and After (dashed curve) Filtering

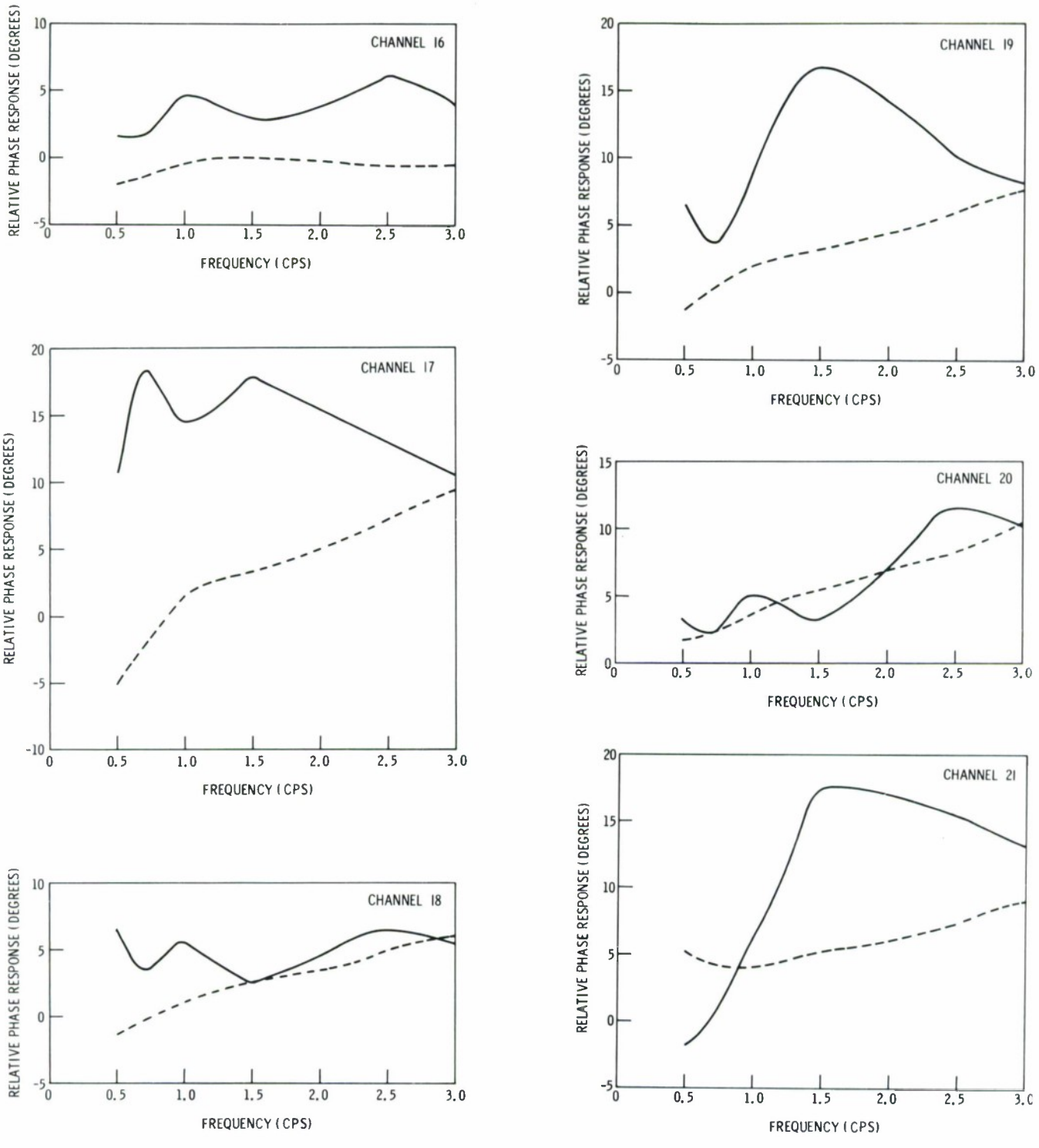

Figure III-18c. Phase Responses for May 13, 1965 Relative to Channel 5 Before (solid curve) and After (dashed curve) Filtering

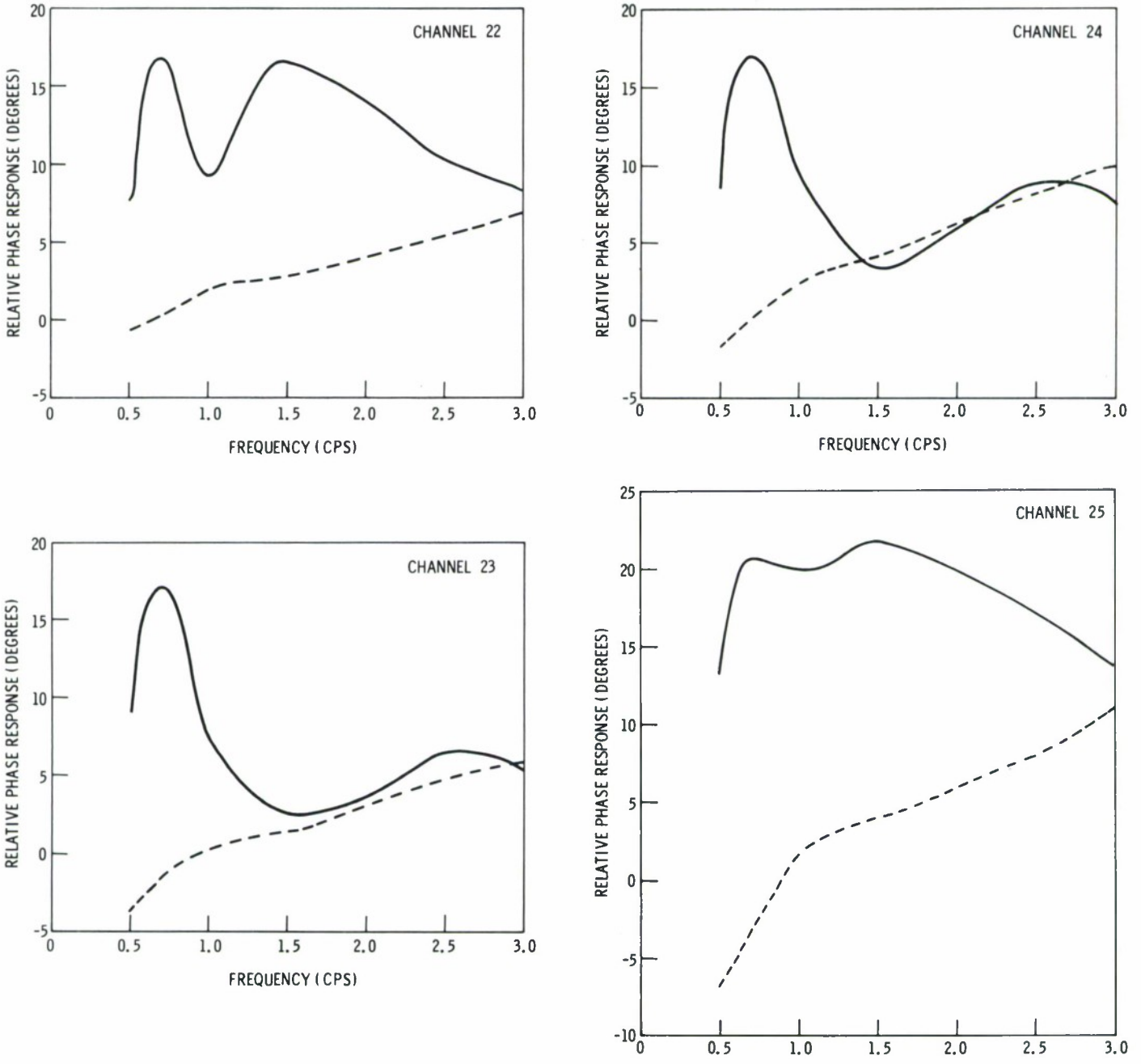

Figure III-18d. Phase Responses for May 13, 1965 Relative to Channel 5 Before (solid curve) and After (dashed curve) Filtering

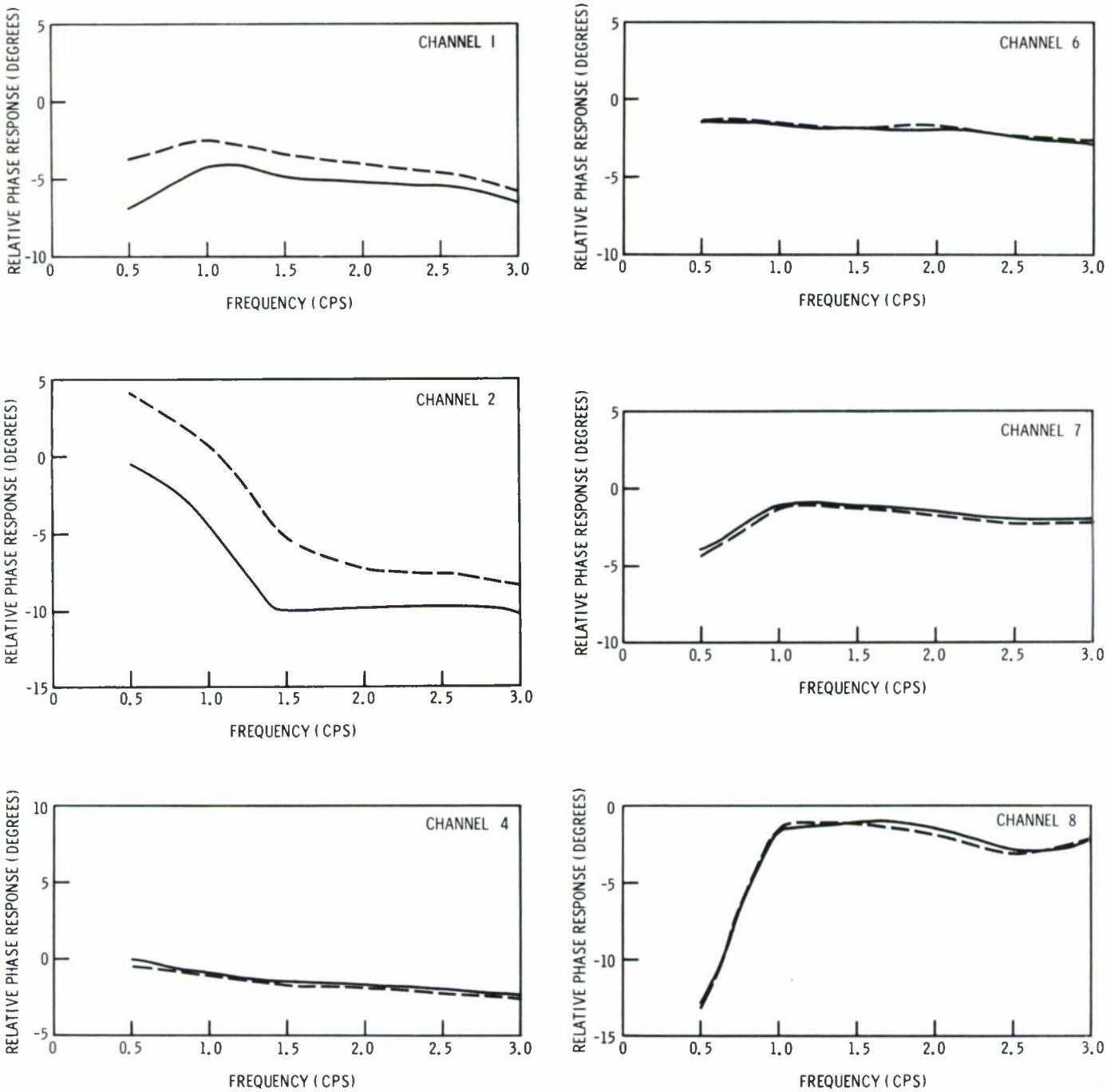

Figure III-19a. Comparison of Phase Responses for 13 May (dashed curve) and 27 May 1965 (solid curve) Relative to Channel 5 After Filtering

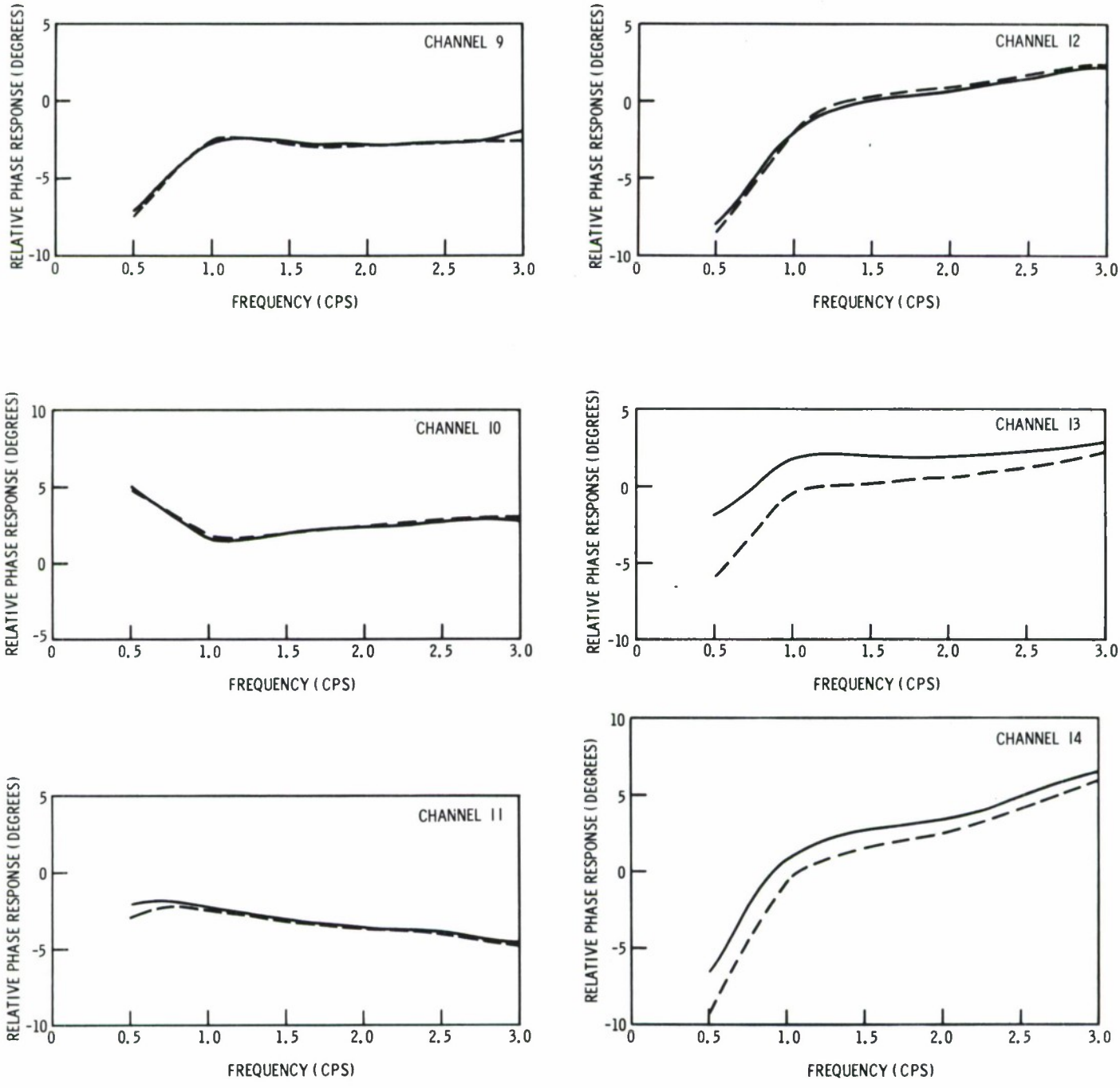

Figure III-19b. Comparison of Phase Responses for 13 May (dashed curve) and 27 May 1965 (solid curve) Relative to Channel 5 After Filtering

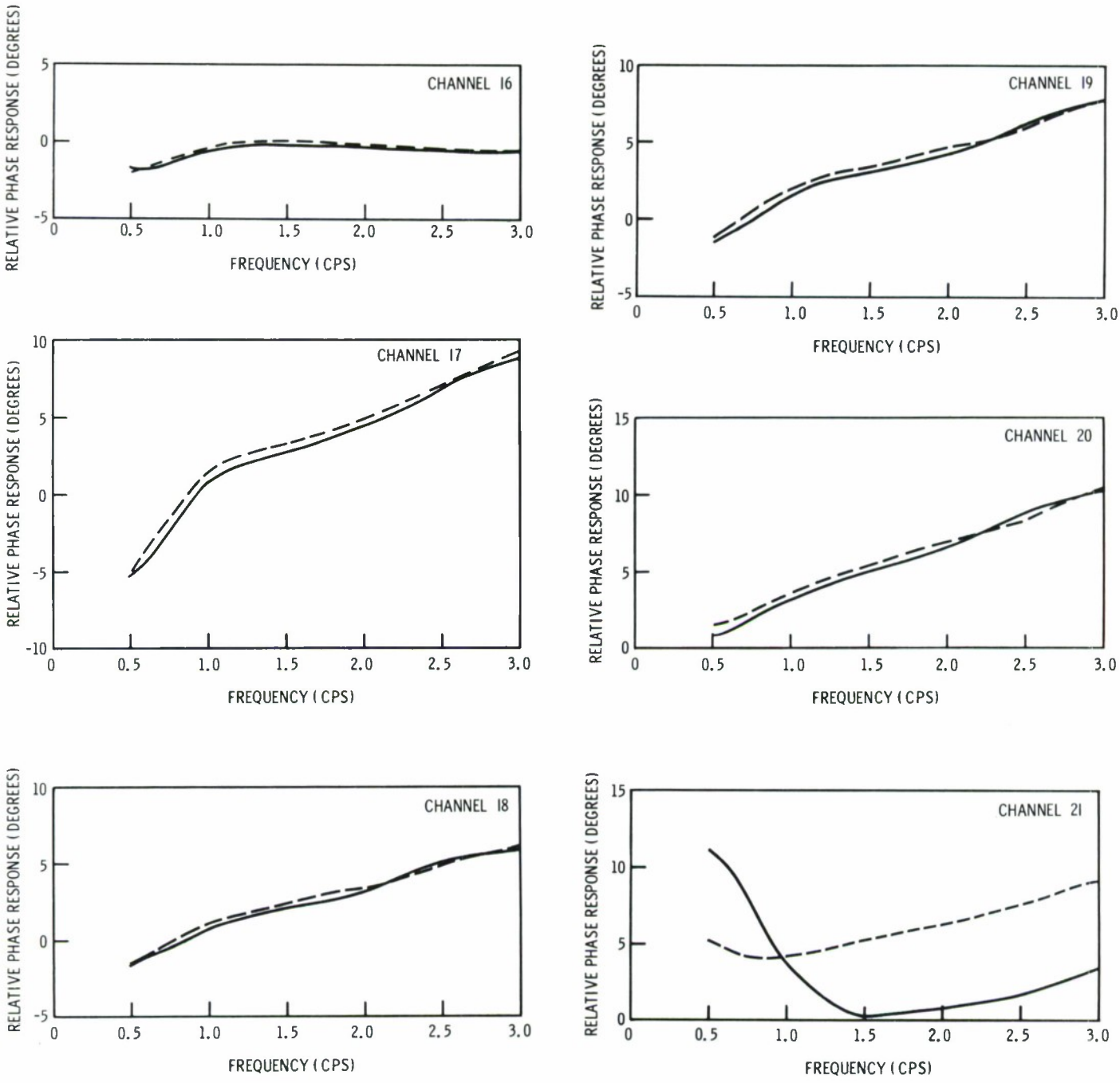

Figure III-19c. Comparison of Phase Responses for 13 May (dashed curve) and 27 May 1965 (solid curve) Relative to Channel 5 After Filtering

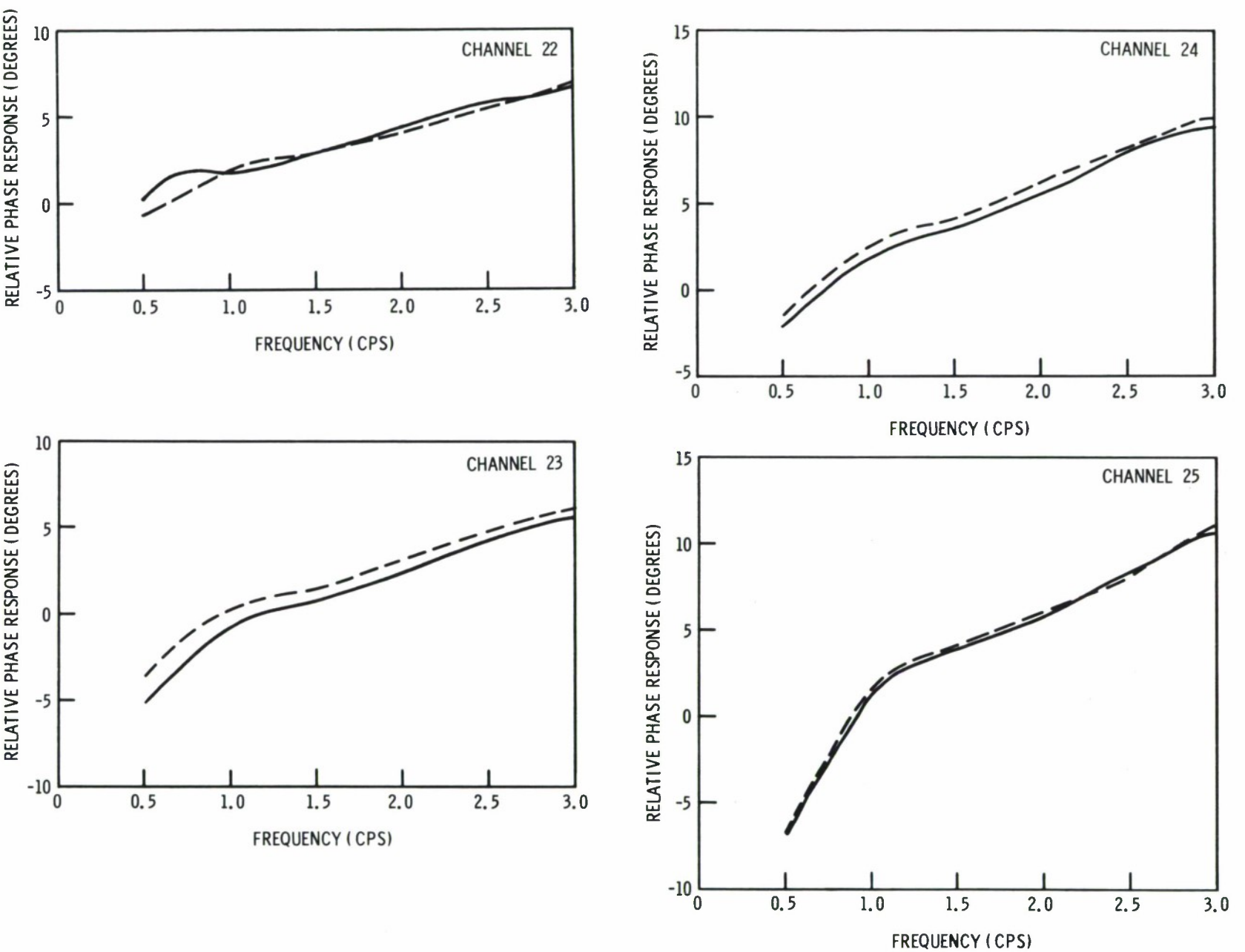

Figure III-19d. Comparison of Phase Responses for 13 May (dashed curve) and 27 May 1965 (solid curve) Relative to Channel 5 After Filtering

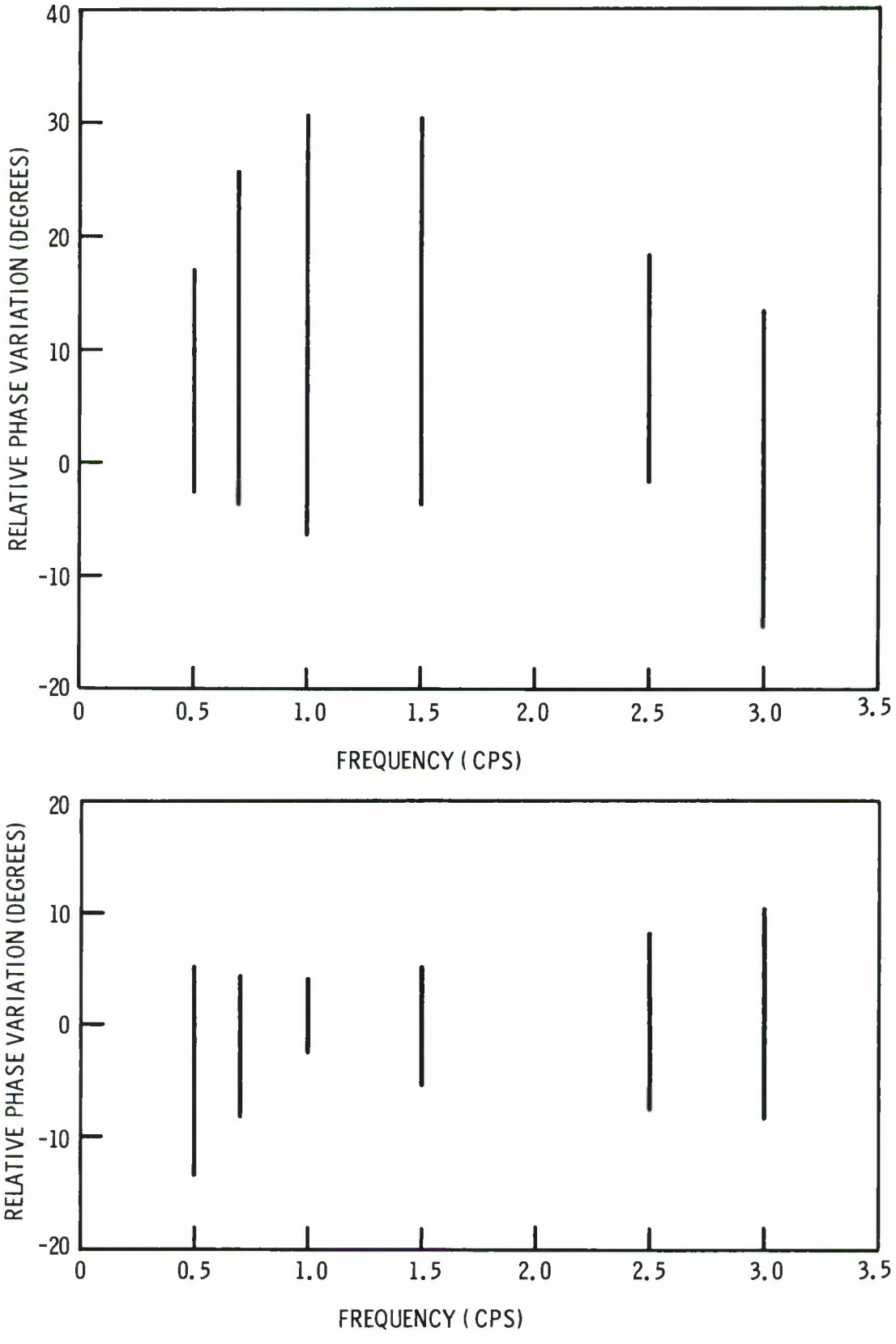

Figure III-20. Seismometer Phase Response Variations Relative to Channel 5 for 13 May 1965 Before (upper figure) and After Filtering

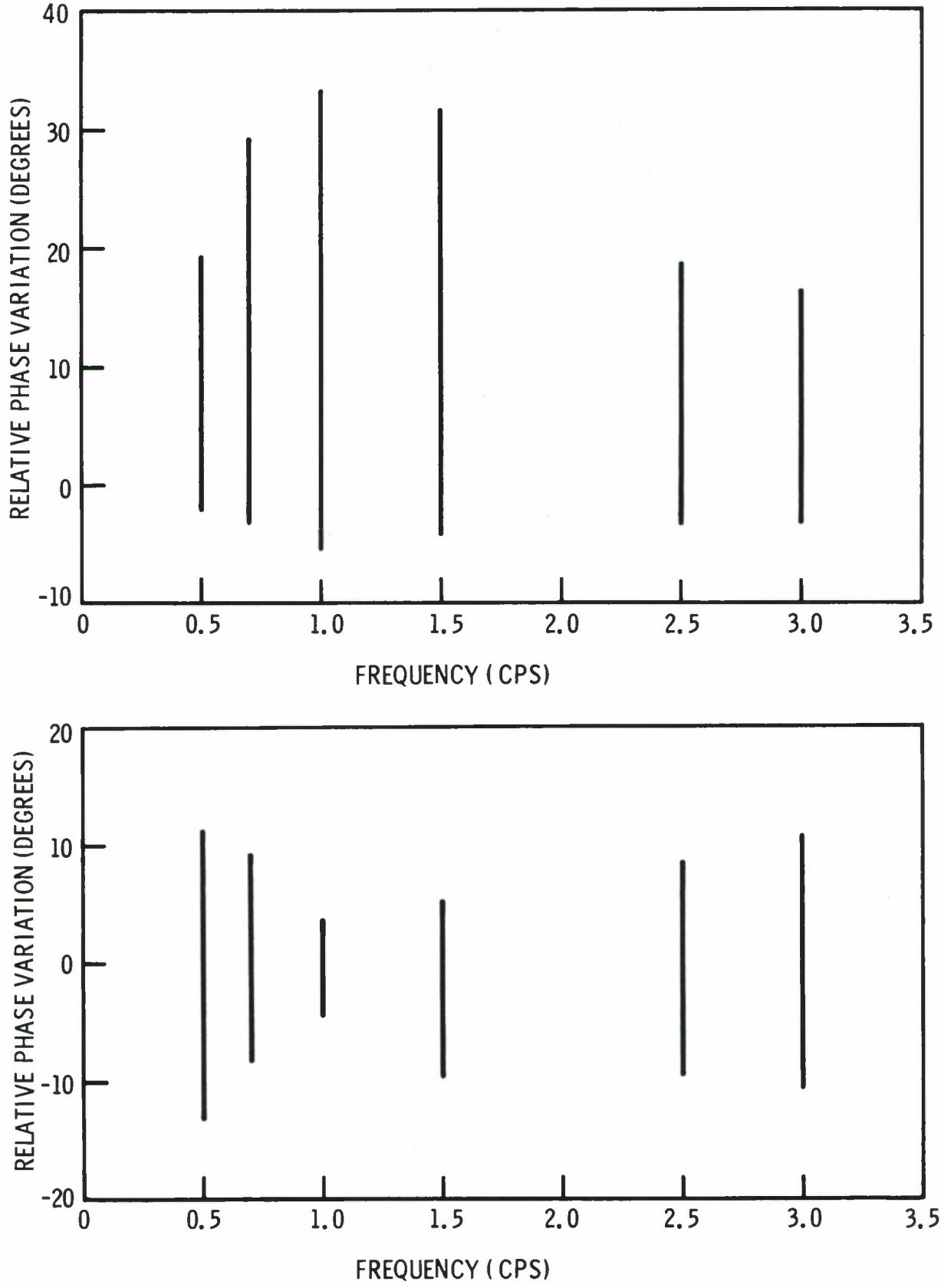

Figure III-21. Seismometer Phase Response Variations Relative to Channel 5 for 27 May 1965 Before (upper figure) and After Filtering

Table III-2

CALIBRATION FREQUENCY IN CPS FOR SUBARRAYS AND THE MID-MARCH CALIBRATIONS

SUBARRAYS	CALIBRATION FREQUENCY IN CPS								
	11-2-65	11-3-65	11-5-65	11-16-65	11-20-65	11-21-65	11-23-65	11-24-65	12-1-65
F-3	0.966	0.966	0.966	0.987	0.987	0.987	0.987	0.987	0.988
F-4	0.983	0.983	0.984	0.984	0.984	0.984	0.984	0.984	0.984
C-3	0.978	0.978	0.979	0.979	0.978	0.979	0.979	0.979	0.978
E-2	0.974	0.974	0.974	0.975	0.975	0.975	0.975	0.975	0.975
F-2	0.992	0.992	0.992	0.992	0.992	0.992		0.992	0.992

MID-MARCH CALIBRATIONS

SUBARRAY	DATE	CALIBRATION FREQUENCY IN CPS
F-3	Mar 10/66	1.006
F-4	Mar 14/66	1.000
C-3	Mar 11/66	1.002
E-2	Mar 15/66	0.980
F-2	Mar 9/66	1.000

Table III-3

SUBARRAY F-3 AMPLITUDE RATIOS									
Seis	Nov 2	Nov 3	Nov 5	Nov 16	Nov 20	Nov 21	Nov 23	Nov 24	Dec 1
2	0.900	0.910	0.902	1.083	1.084	1.084	1.091	1.084	1.068
3	0.906	0.908	0.908	0.978	0.974	0.972	0.978	0.973	0.972
4	0.866	0.873	0.862	1.042	1.043	1.042	1.049	1.042	1.022
5	0.895	0.901	0.888	1.055	1.055	1.057	1.063	1.055	1.032
6	0.863	0.871	0.866	1.046	1.058	1.053	1.059	1.055	1.045
7	0.839	0.845	0.831	0.988	0.998	1.001	1.005	0.989	0.976
8	0.853	0.855	0.839	1.006	1.011	1.002	1.012	1.007	0.998
9	0.878	0.888	0.863	0.959	1.029	1.034	1.042	1.022	0.964
10	0.944	0.950	0.951	1.138	0.959	0.956	0.962	0.964	0.953
11	0.909	0.916	0.909	1.065	1.064	1.063	1.071	1.063	1.052
12	0.944	0.953	0.939	0.984	1.015	1.032	1.047	1.004	0.945
13	0.871	0.874	0.871	1.050	1.049	1.049	1.056	1.047	1.031
14	0.955	0.962	0.954	1.152	1.015	1.017	1.022	1.011	0.997
15	0.889	0.899	0.884	1.036	1.041	1.042	1.050	1.041	1.019
16	0.915	0.920	0.917	1.092	1.043	1.093	1.098	1.092	1.070
17	0.861	0.872	0.873	1.090	1.091	1.090	1.096	1.091	1.084
18	0.934	0.942	0.930	1.088	0.973	0.974	0.980	0.971	0.963
19	0.905	0.912	0.890	1.002	1.019	1.032	1.051	1.013	0.992
20	0.824	0.841	0.823	0.969	0.971	0.973	0.978	0.970	0.935
21	1.014	1.023	1.009	1.144	1.147	1.134	1.135	1.149	1.115
22	0.887	0.874	0.865	1.062	1.065	1.073	1.076	1.067	1.050
23	0.868	0.875	0.860	0.993	1.001	1.002	1.011	0.999	0.970
24	0.875	0.885	0.872	1.017	1.022	1.023	1.027	1.020	1.008
25	0.974	0.984	0.971	1.139	0.998	0.999	1.006	0.996	0.961

Table III-4

SUBARRAY F-3 PHASE DIFFERENCES									
Seis	Nov 2	Nov 3	Nov 5	Nov 16	Nov 20	Nov 21	Nov 23	Nov 24	Dec 1
2	3.05	3.07	3.20	3.51	3.53	3.52	3.54	3.54	3.60
3	7.01	7.07	7.08	8.85	8.92	8.85	8.96	8.87	8.93
4	1.79	1.88	1.93	3.86	3.90	3.94	3.92	3.88	4.01
5	-4.54	-4.65	-4.55	-2.35	-2.38	-2.34	-2.28	-2.36	-2.16
6	1.07	1.07	1.12	1.82	1.84	1.83	1.79	1.84	1.87
7	-9.26	-9.27	-9.23	-8.26	-8.29	-8.27	-8.36	-8.37	-8.29
8	15.32	13.83	13.16	13.71	14.64	15.66	14.84	15.43	15.87
9	7.89	7.92	7.74	8.58	8.54	8.59	8.59	8.54	8.65
10	3.04	3.01	3.03	-0.48	-0.50	-0.43	-0.38	-0.38	-0.14
11	9.30	9.31	9.36	10.22	10.27	10.28	10.28	10.28	10.38
12	1.40	1.34	1.37	1.85	1.82	1.79	1.82	1.84	2.01
13	4.57	4.62	4.69	6.42	6.46	6.46	6.46	6.47	6.62
14	6.26	6.29	6.09	6.78	7.08	6.99	7.02	7.07	6.55
15	9.08	9.14	9.11	8.48	8.53	8.54	8.37	8.56	8.68
16	2.17	2.15	2.12	3.19	3.20	3.15	3.17	3.17	3.24
17	19.88	19.86	20.02	19.37	19.55	19.35	19.52	19.49	19.60
18	-2.00	-1.93	-1.94	-1.38	-1.35	-1.35	-1.33	-1.30	-1.40
19	3.35	3.37	3.35	3.18	3.14	3.15	3.22	3.19	3.20
20	-5.64	-5.67	-5.66	-5.40	-5.44	-5.46	-5.40	-5.46	-5.42
21	16.14	16.14	16.18	-0.50	0.16	0.19	0.15	0.13	0.30
22	-4.82	-4.97	-5.02	-3.17	-3.12	-3.17	-3.09	-3.10	-3.01
23	10.75	10.78	10.78	11.41	11.43	11.40	11.48	11.47	11.25
24	-6.60	-6.56	-6.66	-7.75	-7.76	-7.77	-7.75	-7.77	-7.74
25	12.64	12.62	12.62	13.35	13.50	13.45	13.53	13.47	13.56

Table III-5

SUBARRAY F-3 MEANS, VARIANCES AND STANDARD DEVIATIONS OF AMPLITUDE RATIOS AND PHASE DIFFERENCES

	AMPLITUDE			PHASE		
Seis	Mean	Variance	Std. Dev.	Mean	Variance	Std. Dev.
2	1.082	0.000058	0.008	3.39	0.0492	0.22
3	0.974	0.000008	0.003	8.28	0.8511	0.92
4	1.040	0.000085	0.009	3.23	1.0553	1.02
5	1.053	0.000114	0.011	-3.06	1.2914	1.13
6	1.053	0.000035	0.006	1.58	0.1394	0.37
7	0.993	0.000113	0.011	-8.62	0.2255	0.47
8	1.006	0.000028	0.005	14.71	0.9170	0.96
9	1.008	0.001361	0.036	8.33	0.1371	0.37
10	0.988	0.005368	0.073	1.14	3.2120	1.79
11	1.063	0.000038	0.006	9.96	0.2331	0.48
12	1.004	0.001375	0.037	1.69	0.0629	0.25
13	1.047	0.000071	0.008	5.86	0.8642	0.93
14	1.036	0.003320	0.058	6.68	0.1534	0.39
15	1.038	0.000109	0.010	8.74	0.0790	0.28
16	1.089	0.000098	0.010	2.84	0.2711	0.52
17	1.090	0.000015	0.004	19.62	0.0565	0.24
18	0.991	0.002265	0.048	-1.55	0.0926	0.30
19	1.018	0.000449	0.021	3.23	0.0084	0.09
20	0.966	0.000241	0.016	-5.50	0.0133	0.11
21	1.136	0.000139	0.012	5.43	64.7064	8.04
22	1.066	0.000084	0.009	-3.71	0.8391	0.91
23	0.988	0.001133	0.033	11.22	0.1198	0.34
24	1.019	0.000043	0.006	-7.37	0.3294	0.57
25	1.016	0.003853	0.062	13.19	0.1854	0.43

Table III-6

SUBARRAY F-4 AMPLITUDE RATIOS									
Seis	Nov 2	Nov 3	Nov 5	Nov 16	Nov 20	Nov 21	Nov 23	Nov 24	Dec 1
2	1.010	1.066	1.057	0.987	1.023	1.035	1.016	1.003	0.990
3	1.070	1.069	1.068	1.049	1.050	1.045	1.036	1.034	1.030
4	1.139	1.141	1.136	1.118	1.121	1.128	1.108	1.103	1.086
5	1.046	1.048	1.042	0.967	0.971	0.968	0.961	0.956	0.925
6	1.073	1.066	1.072	1.086	1.076	1.070	1.064	1.065	1.050
7	1.082	1.081	1.069	1.033	1.046	1.039	1.032	1.032	1.019
8	1.053	1.048	1.049	1.032	1.032	1.027	1.021	1.013	1.008
9	1.172	1.177	1.168	1.136	1.137	1.133	1.126	1.114	1.111
10	1.097	1.029	1.022	0.996	0.998	0.997	0.990	0.980	0.956
11	1.074	1.078	1.078	1.008	1.020	1.018	1.010	1.007	0.993
12	1.086	1.086	1.084	1.049	1.052	1.049	1.042	1.044	1.024
13	1.020	1.020	1.019	1.003	1.009	1.003	0.997	0.995	0.972
14	1.075	1.050	1.077	1.081	1.080	1.076	1.072	1.072	1.067
15	1.059	1.055	1.056	1.048	1.051	1.059	1.044	1.034	1.035
16	1.038	1.018	1.026	1.001	0.988	0.984	0.978	0.974	0.966
17	1.074	1.066	1.069	1.087	1.085	1.079	1.073	1.071	1.069
18	0.910	0.924	0.946	0.894	0.898	0.893	0.887	0.888	0.860
19	0.979	0.978	0.980	0.974	0.973	0.967	0.976	0.968	0.958
20	1.126	1.122	1.125	1.083	1.103	1.100	1.090	1.085	1.001
21	1.126	1.125	1.128	1.146	1.140	1.133	1.127	1.128	1.126
22	1.022	1.012	1.025	1.062	1.029	1.024	1.019	1.017	1.030
23	1.111	1.116	1.111	1.061	1.066	1.061	1.056	1.054	1.020
24	0.975	1.018	1.045	1.059	1.060	1.055	1.048	1.048	1.049
25	0.996	1.007	1.008	1.003	0.995	0.988	0.983	0.980	0.975

Table III-7

SUBARRAY F-4 PHASE DIFFERENCES									
Seis	Nov 2	Nov 3	Nov 5	Nov 16	Nov 20	Nov 21	Nov 23	Nov 24	Dec 1
2	1.49	6.78	5.42	7.52	6.65	3.86	6.30	6.30	6.45
3	7.09	7.16	7.08	7.26	7.15	7.16	7.23	7.18	7.20
4	19.48	19.37	19.19	19.92	19.14	19.15	19.18	18.87	19.03
5	0.12	-0.13	0.05	0.44	0.15	0.11	0.19	0.15	0.11
6	-1.15	-0.93	-1.16	-0.81	-1.18	-1.15	-1.16	-1.25	-1.31
7	13.87	13.95	13.85	14.53	13.93	13.94	13.95	13.45	13.91
8	5.69	5.89	5.77	6.29	5.95	5.80	5.77	5.29	5.65
9	-1.27	-1.37	-1.20	-1.54	-1.30	-1.29	-1.29	-1.30	-1.46
10	10.86	10.71	10.73	10.65	10.59	10.61	10.61	10.24	10.55
11	-1.41	-1.78	1.36	4.05	3.92	3.57	3.99	2.75	1.80
12	-0.95	-0.81	-0.77	-0.74	-0.86	-0.79	-0.84	-1.18	-0.96
13	10.54	10.69	10.58	10.89	10.53	10.54	10.54	10.35	10.43
14	-2.70	-1.85	-1.93	-1.51	-1.75	-1.81	-1.72	-2.10	-1.89
15	9.87	9.90	9.50	10.34	10.14	9.90	10.11	10.15	9.91
16	19.31	19.46	19.34	19.81	19.37	19.29	19.40	19.05	19.41
17	-5.77	-5.68	-5.77	-5.69	-5.84	-5.94	-5.83	-6.08	-5.92
18	14.36	14.59	14.72	14.11	14.07	13.95	14.12	14.10	14.25
19	5.87	5.79	5.97	6.00	5.93	5.85	5.91	5.56	5.84
20	3.21	3.09	3.34	3.73	3.19	3.19	3.18	3.36	3.09
21	3.03	3.20	3.11	3.10	3.16	3.21	3.25	2.77	3.19
22	5.77	5.86	5.81	6.31	5.74	5.78	5.79	5.61	5.70
23	3.66	3.79	3.82	3.99	3.79	3.74	3.77	3.84	3.67
24	9.31	8.21	8.57	8.59	8.84	8.79	8.86	8.12	8.72
25	5.73	6.09	6.34	6.23	6.22	6.19	6.26	5.78	6.14

Table III-8

SUBARRAY F-4 MEANS, VARIANCES AND STANDARD DEVIATIONS OF AMPLITUDE RATIOS AND PHASE DIFFERENCES						
	AMPLITUDE			PHASE		
Seis	Mean	Variance	Std. Dev	Mean	Variance	Std. Dev
2	1.031	0.001453	0.038	5.57	3.3763	1.84
3	1.051	0.000232	0.015	7.17	0.0035	0.06
4	1.119	0.000329	0.018	19.26	0.0924	0.30
5	0.987	0.002076	0.046	0.13	0.0219	0.15
6	1.069	0.000095	0.009	-1.12	0.0246	0.16
7	1.048	0.000544	0.023	13.93	0.0752	0.27
8	1.031	0.000309	0.018	5.79	0.0708	0.26
9	1.142	0.000589	0.024	-1.34	0.0109	0.10
10	1.007	0.001596	0.039	10.62	0.0286	0.17
11	1.032	0.001181	0.034	2.03	5.1544	2.26
12	1.057	0.000495	0.022	-0.88	0.0185	0.14
13	1.004	0.000245	0.016	10.57	0.0236	0.15
14	1.072	0.000091	0.009	-1.92	0.1120	0.33
15	1.049	0.000089	0.009	9.98	0.0577	0.24
16	0.997	0.000623	0.025	19.38	0.0395	0.19
17	1.075	0.000052	0.007	-5.84	0.0165	0.13
18	0.900	0.000592	0.024	14.25	0.0662	0.26
19	0.971	0.000056	0.007	5.86	0.0168	0.13
20	1.099	0.000491	0.022	3.26	0.0392	0.19
21	1.130	0.000054	0.007	3.11	0.0211	0.14
22	1.027	0.000212	0.014	5.82	0.0390	0.19
23	1.073	0.001067	0.033	3.79	0.0097	0.09
24	1.040	0.000735	0.027	8.67	0.1277	0.36
25	0.993	0.000143	0.012	6.11	0.0454	0.21

Table III-9

SUBARRAY C-3 AMPLITUDE RATIOS									
Seis	Nov 2	Nov 3	Nov 5	Nov 16	Nov 20	Nov 21	Nov 23	Nov 24	Dec 1
2	1.061	1.062	1.041	1.044	1.044	1.039	1.031	1.044	1.044
3	1.062	1.081	1.092	1.092	1.003	0.996	0.990	1.005	1.016
4	1.207	1.196	1.196	1.194	0.987	0.982	0.972	0.997	1.009
5	1.037	1.036	1.034	1.034	0.968	0.960	0.951	0.966	0.968
6	1.276	1.273	1.265	1.268	1.126	1.119	1.113	1.121	1.122
7	1.307	1.302	1.306	1.311	0.965	0.958	0.953	0.978	1.000
8	1.067	1.063	1.073	1.075	1.051	1.042	1.036	1.057	1.069
9	1.228	1.219	1.212	1.214	0.978	0.970	0.962	0.978	0.996
10	1.117	1.007	1.123	1.125	0.998	0.988	0.978	0.998	1.017
11	1.302	1.297	1.309	1.309	1.018	1.009	1.000	1.033	1.084
12	1.246	1.240	1.242	1.243	1.010	0.997	0.989	1.014	1.050
13	1.301	1.293	1.293	1.292	1.002	0.990	0.985	1.007	1.038
14	1.047	1.046	1.043	1.043	0.957	0.949	0.942	0.965	0.988
15	1.200	1.202	1.195	1.196	1.105	1.099	1.091	1.113	1.127
16	1.033	1.030	1.028	1.028	0.955	0.949	0.941	0.964	0.987
17	1.162	1.156	1.163	1.163	0.974	0.967	0.959	0.985	1.015
18	1.085	1.087	1.085	1.088	0.969	0.964	0.960	0.970	0.937
19	1.129	1.129	1.117	1.117	1.017	1.012	1.007	1.019	1.026
20	1.102	1.099	1.100	1.100	1.083	1.073	1.068	1.086	1.100
21	1.269	1.264	1.269	1.268	0.972	0.963	0.957	0.968	0.994
22	1.165	1.164	1.157	1.157	1.010	1.006	1.003	1.009	1.002
23	1.178	1.178	1.174	1.174	1.051	1.043	1.036	1.058	1.076
24	1.083	1.079	1.081	1.084	1.053	1.044	1.037	1.065	1.100
25	1.074	1.070	1.067	1.070	1.040	1.032	1.025	1.043	1.058

Table III-10

SUBARRAY C-3 PHASE DIFFERENCES									
Seis	Nov 2	Nov 3	Nov 5	Nov 16	Nov 20	Nov 21	Nov 23	Nov 24	Dec 1
2	-11.14	-10.98	-8.94	-8.74	-9.31	-9.43	-9.23	-9.44	-9.34
3	-10.83	-10.82	-8.81	-8.69	-8.16	-8.23	-8.08	-8.24	-8.16
4	-12.78	-12.92	-10.87	-10.77	-11.25	-11.27	-11.19	-11.37	-11.26
5	-9.16	-9.33	-7.20	-7.08	-7.54	-7.42	-7.38	-7.54	-7.51
6	-0.53	-0.42	1.69	1.63	1.27	1.25	1.33	1.26	1.08
7	-1.77	-1.81	0.35	0.25	-0.07	0.06	0.00	-0.07	-0.19
8	-5.17	-5.33	-3.08	-3.16	-2.94	-2.99	-2.86	2.93	-2.97
9	-20.32	-20.39	-18.42	-18.11	-18.09	-18.26	-17.84	-18.14	-18.05
10	2.67	5.38	3.59	3.54	13.34	13.72	13.45	13.69	12.70
11	1.85	1.88	3.91	3.83	3.37	3.53	3.33	3.18	3.01
12	-9.10	-9.21	-7.12	-7.12	-7.48	-7.42	-7.37	-7.51	-7.45
13	-8.50	-8.75	-6.72	-6.73	-6.85	-6.84	-6.80	-6.98	-6.82
14	-3.92	-3.86	-1.54	-1.41	-2.03	-2.06	-1.94	-2.02	-1.94
15	-3.87	-3.95	-1.64	-1.57	-2.07	-2.10	-1.95	-1.89	-1.86
16	-2.95	-3.19	-0.77	-0.73	-1.25	-1.23	-1.20	-1.16	-1.13
17	-8.22	-8.34	-6.05	-5.97	-6.22	-6.49	-6.26	-6.27	-6.15
18	12.04	12.00	14.53	14.18	13.94	13.97	13.88	14.01	14.02
19	-11.17	-11.32	-9.00	-8.85	-9.27	-9.29	-9.05	-9.20	-9.10
20	0.12	-0.12	2.29	2.13	2.04	2.05	2.07	2.08	2.28
21	-9.67	-9.76	-7.68	-7.71	-7.41	-7.38	-7.38	-7.52	-7.14
22	0.19	0.19	2.57	2.60	2.17	2.07	2.10	2.17	2.29
23	1.77	1.78	4.22	4.15	3.93	3.98	3.86	3.95	4.14
24	4.13	4.06	6.46	6.24	6.06	6.10	6.03	6.15	6.27
25	-0.86	-0.89	1.37	1.15	1.14	1.22	1.05	1.15	1.20

Table III-11

SUBARRAY C-3 MEANS, VARIANCES AND STANDARD DEVIATIONS FOR PHASE DIFFERENCES			
Seis	Mean	Variance	Std. Dev.
2	-9.17	0.0584	0.24
3	-8.44	0.1082	0.32
4	-11.07	0.0561	0.23
5	-7.35	0.0294	0.17
6	1.39	0.0425	0.21
7	0.08	0.0326	0.18
8	-3.04	0.0199	0.14
9	-18.18	0.0343	0.18
10	9.56	21.7735	4.66
11	3.54	0.1145	0.33
12	-7.30	0.0288	0.16
13	-6.77	0.0169	0.13
14	-1.85	0.0519	0.22
15	-1.87	0.0310	0.17
16	-1.06	0.0401	0.20
17	-6.21	0.0234	0.15
18	14.06	0.0372	0.19
19	-9.13	0.0237	0.15
20	2.10	0.0156	0.12
21	-7.51	0.0421	0.20
22	2.26	0.0375	0.19
23	3.97	0.0267	0.16
24	6.16	0.0187	0.13
25	1.17	0.0080	0.08

Table III-12

SUBARRAY E-2 AMPLITUDE RATIOS									
Seis	Nov 2	Nov 3	Nov 5	Nov 16	Nov 20	Nov 21	Nov 23	Nov 24	Dec 1
2	1.085	1.082	1.093	1.115	1.107	1.109	1.111	1.036	1.040
3	1.019	1.022	1.020	1.033	1.037	1.039	1.035	1.027	1.005
4	1.037	1.038	1.046	1.060	1.057	1.058	1.057	1.057	1.043
5	1.152	1.147	1.151	1.147	1.146	1.149	1.146	1.015	1.007
6	1.143	1.149	1.147	1.139	1.140	1.140	1.140	0.993	0.977
7	1.034	1.041	1.034	0.979	0.994	0.994	0.983	0.966	0.944
8	1.023	1.025	1.023	1.025	1.022	1.024	1.024	1.026	1.023
9	1.069	1.070	1.060	1.044	1.045	1.046	1.042	1.034	1.006
10	1.079	1.078	1.077	1.065	1.065	1.071	1.067	1.064	1.034
11	1.080	1.079	1.077	1.079	1.076	1.077	1.077	1.075	1.059
12	0.983	0.979	0.984	0.971	0.968	0.969	0.969	0.970	0.950
13	1.023	1.020	1.024	1.032	1.027	1.028	1.027	1.027	1.015
14	1.098	1.096	1.095	1.085	1.089	1.091	1.090	1.087	1.063
15	1.124	1.121	1.124	1.128	1.131	1.133	1.130	1.025	1.016
16	1.121	1.119	1.123	1.122	1.120	1.123	1.120	0.991	0.968
17	1.181	1.180	1.181	1.171	1.173	1.177	1.176	0.987	0.969
18	1.011	1.007	1.006	1.014	1.014	1.015	1.013	1.009	0.982
19	0.940	0.936	0.935	0.917	0.911	0.911	0.911	0.911	0.888
20	1.041	1.039	1.039	1.036	1.038	1.038	1.037	1.035	1.016
21	1.108	1.104	1.112	1.142	1.137	1.136	1.136	1.040	1.032
22	1.006	1.006	1.003	0.980	0.978	0.980	0.981	0.981	0.956
23	1.111	1.109	1.105	1.104	1.101	1.103	1.102	1.003	0.994
24	1.005	1.004	0.997	0.972	0.972	0.971	0.968	0.967	0.959
25	1.047	1.043	1.047	1.054	1.056	1.053	1.052	1.054	1.047

Table III-13

SUBARRAY E-2 PHASE DIFFERENCES									
Seis	Nov 2	Nov 3	Nov 5	Nov 16	Nov 20	Nov 21	Nov 23	Nov 24	Dec 1
2	-2.47	-2.40	-2.48	-2.60	-2.41	-2.40	-2.48	-2.37	-2.48
3	-8.45	-8.35	-8.40	-8.55	-8.32	-8.22	-8.30	-8.32	-8.30
4	-2.83	-2.49	-2.58	-2.66	-2.52	-2.45	-2.56	-2.54	-2.57
5	-3.12	-2.83	-2.92	-2.84	-2.87	-2.80	-2.90	-2.99	-2.48
6	26.16	26.17	26.13	26.10	26.37	26.44	26.35	26.43	26.40
7	7.00	7.19	7.10	7.04	7.20	7.19	7.15	7.11	7.19
8	-8.67	-8.40	-8.46	-8.53	-8.38	-8.30	-8.41	-8.37	-8.33
9	-14.62	-14.27	-14.42	-14.48	-14.36	-14.20	-14.30	-14.21	-14.23
10	-11.00	-11.03	-11.15	-11.33	-11.05	-10.97	-11.24	-11.16	-11.17
11	4.25	4.33	4.36	4.10	4.36	4.32	4.23	4.29	4.22
12	-4.89	-4.94	-4.90	-5.18	-4.98	-4.93	-5.02	-4.98	-5.03
13	7.37	7.48	7.41	7.18	7.31	7.28	7.30	7.33	7.27
14	6.11	6.28	5.81	6.15	6.11	6.41	5.90	6.03	5.83
15	9.43	9.70	9.55	9.57	9.77	9.81	9.67	9.66	9.53
16	10.27	10.52	10.47	10.49	10.60	10.52	10.51	10.55	10.57
17	-3.10	-2.82	-2.90	-3.01	-2.81	-2.75	-2.90	-2.71	-2.70
18	-0.75	-0.74	-0.84	-0.96	-0.81	-0.79	-0.87	-0.84	-0.86
19	5.57	5.71	5.67	5.53	5.75	5.78	5.65	5.75	5.61
20	1.09	1.35	1.25	1.15	1.22	1.21	1.15	1.19	1.15
21	-5.10	-4.80	-4.94	-5.18	-5.00	-4.90	-4.98	-4.93	-4.92
22	3.35	3.36	3.40	3.27	-3.50	3.54	3.43	3.52	3.49
23	4.91	5.00	4.91	4.74	4.92	4.97	4.80	4.96	4.86
24	7.05	7.15	7.03	6.76	7.13	7.10	6.87	6.96	7.02
25	5.81	5.96	5.92	5.93	5.81	5.92	5.88	5.85	5.88

Table III-14

SUBARRAY E-2 MEANS, VARIANCES AND STANDARD DEVIATIONS OF AMPLITUDE RATIOS AND PHASE DIFFERENCES

	AMPLITUDE			PHASE		
Seis	Mean	Variance	Std. Dev.	Mean	Variance	Std. Dev.
2				-2.45	0.0048	0.07
3	1.026	0.000117	0.010	-8.36	0.0095	0.10
4	1.050	0.000088	0.009	-2.58	0.0124	0.11
5				-2.86	0.0299	0.17
6				26.29	0.0218	0.14
7	0.997	0.001122	0.033	7.13	0.0053	0.07
8	1.024	0.000002	0.001	-8.43	0.0127	0.11
9	1.046	0.000365	0.019	-14.34	0.0120	0.19
10	1.067	0.000185	0.013	-11.12	0.0142	0.12
11	1.076	0.000043	0.006	4.27	0.0070	0.08
12	0.971	0.000102	0.010	-4.98	0.0078	0.08
13	1.025	0.000024	0.005	7.33	0.0075	0.08
14	1.088	0.000106	0.010	6.07	0.0406	0.22
15				9.63	0.0149	0.12
16				10.50	0.0090	0.09
17				-2.86	0.0184	0.13
18	1.008	0.000104	0.010	-0.83	0.0045	0.06
19	0.918	0.000271	0.016	5.67	0.0075	0.08
20	1.036	0.000058	0.008	1.20	0.0056	0.07
21				-4.97	0.0126	0.11
22	0.986	0.000273	0.016	3.43	0.0083	0.09
23				4.89	0.0070	0.08
24	0.979	0.000305	0.017	7.01	0.0161	0.12
25	1.050	0.000021	0.004	5.88	0.0283	0.14

Table III-15

SUBARRAY F-2 AMPLITUDE RATIOS								
Seis	Nov 2	Nov 3	Nov 5	Nov 16	Nov 20	Nov 21	Nov 24	Dec 1
2	0.919	0.927	0.919	0.899	0.888	0.886	0.890	0.930
3	0.908	0.906	0.911	0.912	0.903	0.902	0.916	0.976
4	1.076	1.078	1.073	1.055	1.045	1.047	1.052	0.944
5	0.931	0.927	0.934	0.946	0.936	0.939	0.955	0.879
6	0.864	0.868	0.908	0.901	0.895	0.899	0.860	0.955
7	1.000	1.001	0.999	0.989	0.981	0.982	0.991	1.045
8	0.936	0.938	0.937	0.947	0.943	0.941	0.958	0.903
9	1.026	1.023	1.031	1.030	1.016	1.018	1.045	0.940
10	1.070	1.079	1.066	1.032	1.029	1.029	1.033	0.990
11	0.992	0.995	0.989	0.967	0.957	0.957	0.966	1.011
12	0.917	0.912	0.932	0.984	0.975	0.976	1.003	1.070
13	1.095	1.096	1.090	1.073	1.073	1.071	1.072	1.138
14	0.963	0.971	0.959	0.934	0.929	0.936	0.929	0.965
15	0.995	0.978	0.983	0.969	0.960	0.960	0.973	1.032
16	1.013	1.024	1.007	0.964	0.959	0.960	0.960	0.998
17	1.095	1.104	1.087	1.072	1.064	1.065	1.075	1.142
18	1.007	1.011	1.004	0.990	0.981	0.980	0.990	1.050
19	1.064	1.067	1.057	1.026	1.017	1.020	1.027	0.941
20	0.956	0.960	0.951	0.926	0.922	0.922	0.926	0.977
21	0.948	0.950	0.946	0.931	0.921	0.923	0.938	0.898
22	0.978	0.979	0.977	0.978	0.969	0.969	0.982	0.956
23	0.925	0.933	0.920	0.876	0.865	0.865	0.866	0.903
24	1.104	1.109	1.103	1.101	1.085	1.090	1.104	0.898
25	0.992	0.995	0.987	0.974	0.969	0.971	0.988	0.924

Table III-16

SUBARRAY F-2 PHASE DIFFERENCES								
Seis	Nov 2	Nov 3	Nov 5	Nov 16	Nov 20	Nov 21	Nov 24	Dec 1
2	-0.56	-0.64	-0.55	-0.51	-0.49	-0.58	-0.47	-0.60
3	-11.71	-11.87	-11.71	-11.82	-11.83	-11.91	-11.78	-11.88
4	1.97	1.86	1.93	1.99	1.97	1.96	2.03	2.04
5	-5.65	-5.73	-5.60	-5.72	-5.70	-5.70	-5.64	-5.75
6	-13.68	-13.90	-13.62	-13.56	-13.50	-14.04	-13.62	-13.52
7	-13.53	-13.55	-13.44	-13.54	-13.52	-13.64	-13.53	-13.54
8	-6.38	-6.44	-6.35	-6.30	-6.41	-6.42	-6.35	-6.39
9	-8.79	-9.02	-8.77	-8.72	-8.79	-8.73	-8.68	-8.67
10	-6.31	-6.40	-6.37	-5.41	-5.20	-5.20	-5.10	-6.04
11	-9.30	-9.39	-9.28	-9.30	-9.29	-9.38	-9.50	-9.16
12	-1.85	-1.97	-1.92	-1.85	-1.88	-1.82	-1.78	-1.80
13	5.24	5.09	5.25	5.19	5.20	5.26	-5.28	5.16
14	-8.05	-8.21	-8.20	-8.07	-8.15	-8.20	-8.11	-8.14
15	-10.95	-10.99	-11.03	-10.93	-11.01	-11.05	-10.98	-10.99
16	5.52	5.30	5.32	5.47	5.40	5.39	5.50	5.46
17	-17.52	-17.73	-17.55	-17.56	-17.60	-17.67	-17.59	-17.62
18	-9.99	-10.14	-10.08	-10.00	-10.03	-10.12	-9.99	-10.06
19	2.13	1.94	2.04	2.23	2.22	2.25	2.24	2.24
20	7.58	7.43	7.43	7.57	7.57	7.48	7.56	7.52
21	-10.00	-10.15	-10.08	-10.08	-10.11	-10.16	-10.10	-10.09
22	1.74	1.58	1.59	1.54	1.78	1.76	1.85	1.91
23	1.28	1.25	1.23	1.38	1.47	1.50	1.32	0.74
24	-14.85	-15.02	-14.86	-14.92	-14.91	-14.91	-14.92	-14.94
25	-7.03	-7.14	-7.10	-7.07	-7.08	-7.07	-7.03	-6.97

Table III-17

SUBARRAY F-2 MEANS, VARIANCES AND STANDARD DEVIATIONS OF AMPLITUDE RATIOS AND PHASE DIFFERENCES

	AMPLITUDE			PHASE		
Seis	Mean	Variance	Std. Dev.	Mean	Variance	Std. Dev.
2	0.906	0.000381	0.019	-0.55	0.0033	0.05
3	0.917	0.000589	0.024	-11.81	0.0057	0.08
4	1.047	0.001883	0.043	1.97	0.0032	0.05
5	0.931	0.000517	0.023	-5.69	0.0026	0.05
6	0.894	0.000961	0.031	-13.68	0.0318	0.19
7	0.999	0.000414	0.020	-13.54	0.0029	0.05
8	0.438	0.000252	0.015	-6.39	0.0032	0.06
9	1.016	0.001026	0.032	-8.77	0.0122	0.11
10	1.041	0.000848	0.029	-5.75	0.3356	0.58
11	0.979	0.000408	0.020	-9.28	0.0078	0.08
12	0.971	0.002726	0.052	-1.86	0.0040	0.06
13	1.089	0.000517	0.023	5.21	0.0041	0.06
14	0.947	0.000349	0.018	-8.14	0.0037	0.06
15	0.980	0.000534	0.023	-10.99	0.0016	0.04
16	0.986	0.000767	0.028	5.42	0.0066	0.08
17	1.076	0.001357	0.036	-17.61	0.0047	0.07
18	1.002	0.000521	0.022	-10.05	0.0034	0.06
19	1.027	0.001636	0.040	2.16	0.0133	0.11
20	0.942	0.000451	0.021	7.52	0.0040	0.06
21	0.932	0.000318	0.018	-10.10	0.0024	0.05
22	0.973	0.000076	0.008	1.72	0.0182	0.13
23	0.894	0.000854	0.029	1.27	0.0558	0.23
24	1.074	0.005118	0.072	-14.92	0.0027	0.05
25	0.975	0.000528	0.023	-7.06	0.0026	0.05

Table III-18

CHANGES IN AMPLITUDE AND PHASE RESPONSE BETWEEN 1 DEC 1965 AND MAR 1966, SUBARRAY F-3

Seis	AMPLITUDE			PHASE		
	Dec 1	March	% Change	Dec. 1	March	Diff
2	1.068	0.929	-13.00	3.60	-5.88	9.48
3	0.972	0.931	-4.30	8.93	-0.69	9.62
4	1.022	1.009	-1.30	4.01	-5.74	9.75
5	1.032	1.045	1.20	-2.16	-7.40	5.24
6	1.045	1.172	12.1	1.87	-39.21	41.08
7	0.976	0.978	0.20	-8.29	-19.78	11.49
8	0.998	0.980	-1.80	15.87	4.90	10.97
9	0.964	1.568	61.60	8.65	1.92	6.73
10	0.953	1.570	64.75	-0.14	-5.27	5.13
11	1.052	0.983	17.02	10.38	0.87	9.51
12	0.943	1.009	6.90	2.01	-1.11	3.12
13	1.031	0.952	-7.60	6.62	-7.60	14.22
14	0.997	0.991	-0.60	6.55	4.33	2.22
15	1.019	1.025	0.50	8.68	1.15	7.53
16	1.070	0.959	-10.30	3.24	-7.65	10.89
17	1.084	0.959	-11.50	19.60	17.43	2.17
18	0.963	0.989	2.60	-1.40	-11.28	9.88
19	0.992	1.002	1.00	3.20	-1.44	4.64
20	0.935	0.953	1.80	-5.42	-13.69	8.27
21	1.115	0.999	-10.40	0.30	-9.52	9.82
22	1.050	1.052	0.20	-3.01	-13.48	10.47
23	0.920	0.975	5.90	11.25	-0.24	11.49
24	1.008	1.015	0.70	-7.74	-17.42	9.68
25	0.961	0.964	0.30	13.56	9.48	4.08

Table III-19

CHANGES IN AMPLITUDE AND PHASE RESPONSE BETWEEN 1 DEC 1965 AND MAR 1966, SUBARRAY F-4

	AMPLITUDE			PHASE		
Seis	Dec. 1	March	% Change	Dec. 1	March	Diff.
2	0.990	0.904	-8.70	6.45	11.93	-5.48
3	1.030	1.011	-1.90	7.20	14.37	-7.17
4	1.086	0.932	-14.20	19.03	18.68	0.35
5	0.925	1.086	-17.40	0.11	-2.54	2.65
6	1.050	1.028	-2.10	-1.31	3.24	-4.55
7	1.019	0.983	-3.50	13.91	18.30	-4.39
8	1.008	1.006	-0.20	5.65	10.15	-4.50
9	1.111	0.992	-10.70	-1.46	6.78	-8.24
10	0.956	1.071	12.00	10.55	18.42	-7.87
11	0.993	0.961	-3.20	1.80	8.77	-6.97
12	1.024	0.989	-3.40	-0.96	7.18	-1.14
13	0.972	0.985	1.30	10.43	10.69	-0.26
14	1.067	1.058	-0.80	-1.89	3.72	-5.61
15	1.035	0.992	-4.20	9.91	16.93	-7.02
16	0.966	0.943	-2.30	19.41	20.55	-1.14
17	1.069	0.898	-16.00	-5.92	-1.79	-4.13
18	0.860	0.981	14.10	14.25	11.04	3.21
19	0.958	0.964	0.60	5.84	12.21	-6.37
20	1.001	0.993	-0.80	3.09	8.41	-5.32
21	1.126	0.918	-18.50	3.19	8.78	-5.59
22	1.030	0.906	-12.40	5.70	1.67	4.03
23	1.020	0.946	-7.40	3.67	7.58	-3.91
24	1.049	0.896	-14.60	8.72	7.55	1.17
25	0.975	0.960	1.50	6.14	7.08	-0.94

Table III-20

CHANGES IN AMPLITUDE AND PHASE RESPONSE
BETWEEN 1 DEC 1965 AND MARCH 1966, SUBARRAY C-5

	AMPLITUDE			PHASE		
Seis	Dec. 1	March	% Change	Dec. 1	March	Diff
2	1.044	0.996	-4.60	-9.34	-8.21	1.13
3	1.016	1.030	1.40	-8.16	-5.33	2.83
4	1.009	1.015	0.60	-11.26	-7.18	-4.08
5	0.968	1.000	3.20	-7.51	-2.33	-5.18
6	1.122	1.047	-6.70	1.08	1.95	-0.87
7	1.000	1.000	0.00	-0.19	1.93	-2.12
8	1.069	0.999	-6.50	-2.97	-5.21	2.24
9	0.996	0.968	-2.80	-18.05	-14.44	-3.61
10	1.017	1.151	13.20	12.70	3.75	8.95
11	1.084	1.082	-0.20	3.01	9.40	-6.39
12	1.050	1.045	0.50	-7.45	-8.27	0.82
13	1.038	1.043	0.50	-6.82	-4.17	-2.65
14	0.988	0.999	1.10	-1.94	5.64	-7.58
15	1.127	1.042	7.60	-1.86	4.05	-5.91
16	0.987	0.986	-0.10	-1.13	7.58	-8.71
17	1.015	1.078	6.30	-6.15	-4.49	-1.66
18	0.937	0.880	-6.10	14.02	8.26	6.76
19	1.026	1.069	4.20	-9.10	-9.91	0.81
20	1.100	1.080	-1.80	2.28	-1.69	3.97
21	0.994	1.059	6.50	-7.14	-3.02	-4.12
22	1.002	1.044	4.20	2.29	1.55	0.74
23	1.076	1.071	-0.50	4.14	5.39	-1.25
24	1.100	1.078	-2.20	6.27	6.57	-0.30
25	1.058	1.111	5.30	1.20	-1.03	2.23

Table III-21

CHANGES IN AMPLITUDE AND PHASE RESPONSE BETWEEN 1 DEC 1965 AND MAR 1966, SUBARRAY E-2

	AMPLITUDE			PHASE		
Seis	Dec. 1	March	% Change	Dec. 1	March	Diff
2	1.040	1.053	1.20	-2.48	-8.06	5.58
3	1.005	1.070	6.50	-8.30	-11.82	3.52
4	1.043	1.019	-2.40	-2.57	-7.03	4.46
5	1.007	1.020	1.30	-2.48	-3.14	0.66
6	0.977	0.995	1.80	26.40	21.90	4.50
7	0.944	1.090	15.50	7.19	4.65	2.54
8	1.023	0.990	-3.20	-8.33	-13.16	4.83
9	1.006	1.037	3.10	-14.23	-18.12	3.89
10	1.034	1.083	4.90	-11.17	-15.49	4.32
11	1.059	1.068	0.90	4.22	1.68	2.54
12	0.950	1.041	9.50	-5.03	-7.99	2.96
13	1.015	1.015	0.00	7.27	8.81	-1.54
14	1.063	1.101	3.60	5.83	3.60	2.23
15	1.016	1.026	1.00	9.53	1.89	7.64
16	0.968	1.000	3.20	10.57	8.82	1.75
17	0.969	1.033	6.40	-2.70	-5.61	2.91
18	0.982	1.038	5.60	-0.86	-1.08	0.22
19	0.888	1.080	21.60	5.61	-0.72	6.33
20	1.016	1.063	4.60	1.15	0.53	0.62
21	1.032	1.003	-2.90	-4.92	-7.81	2.89
22	0.956	0.970	1.40	3.49	2.35	1.14
23	0.994	1.003	0.90	4.86	4.73	0.13
24	0.959	0.967	0.80	7.02	9.91	-2.89
25	1.047	0.885	-15.30	5.88	7.51	1.63

Table III-22

CHANGES IN AMPLITUDE AND PHASE RESPONSE BETWEEN 1 DEC 1965 AND MAR 1966, SUBARRAY F-2

	AMPLITUDE			PHASE		
Seis	Dec. 1	March	% Change	Dec. 1	March	Diff.
2	0.930	1.079	16.00	-0.60	11.52	-12.12
3	0.976	1.094	11.80	-11.88	-12.45	0.57
4	0.944	1.054	11.70	2.04	5.24	-3.20
5	0.879	1.002	14.00	-5.75	-9.04	3.29
6	0.955	1.100	15.20	-13.52	0.50	-14.02
7	1.045	1.196	14.40	-13.54	-14.27	0.73
8	0.903	1.044	15.70	-6.39	-7.32	0.93
9	0.940	1.071	14.00	-8.67	-3.59	-5.08
10	0.990	1.118	12.90	-6.04	-1.57	-4.47
11	1.011	1.118	10.60	-9.16	-8.04	-1.12
12	1.070	1.097	2.50	-1.80	-3.12	1.32
13	1.138	1.058	-7.00	5.16	11.00	-5.84
14	0.965	1.084	12.30	-8.14	-8.33	0.19
15	1.032	1.148	11.30	-10.99	-9.30	-1.69
16	0.998	1.091	9.30	5.46	4.49	0.97
17	1.142	1.097	-3.90	-17.62	-18.59	0.97
18	1.050	1.161	10.60	-10.06	-8.88	-1.18
19	0.941	1.068	13.50	2.24	7.29	-5.05
20	0.977	1.077	10.30	7.52	9.59	-2.07
21	0.898	1.019	13.50	-10.09	-11.06	0.97
22	0.956	1.092	13.60	1.91	2.81	-0.90
23	0.903	1.012	12.10	0.74	-0.75	1.49
24	0.898	1.004	11.80	-14.94	-15.25	-0.31
25	0.924	1.071	15.90	-6.97	-8.07	1.10

Table III-23

COMPARISON OF 1 DEC 1965 AND MID-MARCH 1966 CALIBRATION			
Amplitude		Phase	
Percent Change	No. of Channels	Diff.	No. of Channels
<5	61	<2	37
5-10	18	2-5	39
10-15	28	5-10	35
15-20	10	>10	9
>20	3		

Table III-24

CALIBRATION FREQUENCIES				
F-2	F-3	C-3	F-4	E-2
0.202	0.202	0.200	0.202	0.202
0.398	—	0.398	0.400	0.398
0.600	—	0.598	0.598	0.598
0.802	0.802	0.802	0.800	0.802
1.000	1.006	1.002	1.000	0.980
1.204	1.198	1.206	1.198	1.178
1.424	1.418	1.430	1.420	1.406
2.028	2.016	2.012	2.006	2.012
3.040	3.030	3.020	3.024	3.014
4.000	4.000	4.000	4.000	3.984
—	6.000	6.006	6.004	6.000

Table III-25a

COMPARISON OF MEASURED RELATIVE RESPONSES AND POLYNOMIAL-ESTIMATED RELATIVE RESPONSES

FREQUENCY	MEASURED RELATIVE PHASE RESPONSE	ESTIMATED RELATIVE PHASE RESPONSE	DIFFERENCE	MEASURED RELATIVE AMPLITUDE RESPONSE	ESTIMATED RELATIVE AMPLITUDE RESPONSE	DIFFERENCE
Subarray C-3 Seismometer 12						
0.200	0.140	0.207	-0.067	1.2286	1.2239	0.0047
0.398	-4.810	-5.429	0.619	1.1495	1.1586	-0.0091
0.598	-8.340	-8.074	-0.266	1.1059	1.1077	-0.0018
0.802	-9.510	-8.568	-0.942	1.0784	1.0687	-0.0097
1.206	-5.650	-5.945	0.295	1.0184	1.0204	-0.0020
1.430	-2.960	-3.727	0.767	1.0032	1.0057	-0.0025
2.012	0.420	0.855	-0.435	0.9926	0.9914	0.0012
3.020	0.750	0.747	0.003	1.0010	1.0012	-0.0002
4.000	0.980	0.952	0.028	1.0205	1.0204	0.0001
6.006	-1.400	-1.397	0.003	0.9827	0.9827	-0.0000
Subarray F-4 Seismometer 17						
0.202	-1.170	-1.361	0.191	1.1410	1.1308	0.0102
0.400	-3.040	-1.757	-1.283	1.0767	1.0972	-0.0205
0.598	0.530	-1.752	2.282	1.0833	1.0754	0.0079
0.800	-2.530	-1.429	-1.101	1.0607	1.0617	-0.0010
1.198	-0.550	-1.678	-0.382	1.0550	1.0491	0.0059
1.420	0.850	0.750	0.100	1.0488	1.0458	0.0030
2.006	3.700	3.393	0.307	1.0284	1.0365	-0.0081
3.024	7.340	7.495	-0.155	1.0106	1.0072	0.0034
4.000	10.570	10.528	0.042	1.0023	1.0031	-0.0008
6.004	11.920	11.922	-0.002	0.9277	0.9277	0.0000

Table III-25b

POLYNOMIAL - ESTIMATED RELATIVE RESPONSES				
FREQUENCY	C-3 (212) RELATIVE PHASE RESPONSE	C-3 (212) RELATIVE AMPLITUDE RESPONSE	F-4 (217) RELATIVE PHASE RESPONSE	F-4 (217) RELATIVE AMPLITUDE RESPONSE
0.0	10.038	1.3081	-0.431	0.9267
0.25	-1.555	1.2059	-1.499	0.9254
0.50	-7.099	1.1309	-1.798	0.9173
0.75	-8.607	1.0775	-1.534	0.9034
1.00	-7.673	1.0409	-0.876	0.8852
1.25	-5.521	1.0169	0.038	0.8637
1.50	-3.038	1.0024	1.101	0.8400
1.75	-0.817	0.9946	2.230	0.8151
2.00	0.796	0.9915	3.366	0.7900
2.25	1.669	0.9915	4.470	0.7654
2.50	1.839	0.9935	5.517	0.7419
2.75	1.467	0.9968	6.498	0.7200
3.00	0.804	1.0009	7.411	0.7002
3.25	0.145	1.0054	8.261	0.6826
3.50	-0.211	1.0102	9.059	0.6673
3.75	-0.003	1.0153	9.812	0.6542
4.00	0.952	1.0204	10.528	0.6430
4.25	2.719	1.0254	11.204	0.6331
4.50	5.200	1.0299	11.831	0.6240
4.75	8.093	1.0333	12.385	0.6145
5.00	10.858	1.0345	12.828	0.6036
5.25	12.664	1.0322	13.099	0.5900
5.50	12.358	1.0247	13.118	0.5720
5.75	8.419	1.0094	12.777	0.5477
6.00	-1.082	0.9835	11.940	0.5151

Table III-26a

COMPARISON OF MEASURED RELATIVE RESPONSES AND POLYNOMIAL - ESTIMATED RELATIVE RESPONSES

FREQUENCY	MEASURED RELATIVE PHASE RESPONSE	ESTIMATED RELATIVE PHASE RESPONSE	DIFFERENCE	MEASURED RELATIVE AMPLITUDE RESPONSE	ESTIMATED RELATIVE AMPLITUDE RESPONSE	DIFFERENCE
Subarray F-3 Seismometer 22						
0.202	-3.740	-3.766	0.026	1.0859	1.0873	-0.0014
0.802	-11.634	-11.634	-0.126	1.0608	1.0530	0.0078
1.006	-13.480	-13.518	0.038	1.0517	1.0518	-0.00005
1.198	-15.110	-15.140	0.030	1.0493	1.0546	-0.0053
1.418	-16.840	-16.925	0.085	1.0548	1.0622	-0.0074
2.016	-22.010	-21.946	-0.064	1.1107	1.1018	0.0089
3.030	-31.730	-31.740	0.010	1.2096	1.2130	-0.0034
4.000	-40.750	-40.750	0.0002	1.3697	1.3688	0.0008
6.000	-66.190	-66.190	-0.0002	2.2228	2.2229	-0.00003
Subarray E-2 Seismometer 6						
0.202	6.330	4.244	2.086	0.7167	0.7126	0.0042
0.398	9.720	12.234	-2.514	0.7428	0.7323	0.0147
0.598	14.830	16.929	-2.099	0.7930	0.8055	-0.0125
0.802	19.820	18.883	0.937	0.8773	0.9109	-0.0336
1.178	20.340	17.225	3.114	1.1460	1.1235	0.0225
1.406	14.590	14.118	0.471	1.2751	1.2357	0.0394
2.012	0.040	3.137	-3.097	1.3563	1.3985	-0.0422
3.014	-8.830	-10.310	1.480	1.3285	1.3132	0.0153
3.984	-12.500	-12.106	-0.394	1.3405	1.3441	-0.0036
6.000	-12.970	-12.986	0.016	1.3707	1.3706	0.0001

Table III-26b

POLYNOMIAL - ESTIMATED RELATIVE RESPONSES				
FREQUENCY	F-3 RELATIVE PHASE RESPONSE	F-3 RELATIVE AMPLITUDE RESPONSE	E-2 (26) RELATIVE PHASE RESPONSE	E-2 (26) RELATIVE AMPLITUDE RESPONSE
0.00	0.298	1.1105	-8.344	0.7753
0.25	-4.597	1.0827	6.553	0.7112
0.50	-8.264	1.0642	15.017	0.7645
0.75	-11.113	1.0542	18.617	0.8822
1.00	-13.466	1.0517	18.693	1.0241
1.25	-15.566	1.0560	16.367	1.1613
1.50	-17.587	1.0661	12.568	1.2749
1.75	-19.645	1.0812	8.039	1.3546
2.00	-21.804	1.1004	3.358	1.3974
2.25	-24.084	1.1233	-1.045	1.4061
2.50	-26.475	1.1491	-4.875	1.3880
2.75	-28.944	1.1778	-7.955	1.3537
3.00	-31.441	1.2091	-10.208	1.3152
3.25	-33.912	1.2432	-11.644	1.2852
3.50	-36.309	1.2806	-12.340	1.2752
3.75	-38.593	1.3221	-12.427	1.2946
4.00	-40.750	1.3688	-12.074	1.3486
4.25	-42.797	1.4225	-11.469	1.4379
4.50	-44.789	1.4849	-10.806	1.5561
4.75	-46.835	1.5587	-10.268	1.6894
5.00	-49.098	1.6469	-10.008	1.8146
5.25	-51.811	1.7529	-10.139	1.8979
5.50	-55.285	1.8810	-10.710	1.8935
5.75	-59.914	2.0359	-11.698	1.7423
6.00	-66.190	2.2229	-12.986	1.3706

SECTION IV

DETERMINATION OF OPTIMUM MCF DESIGN PARAMETERS

Presented in this section are results of the evaluation and comparison of 13 multichannel filters (MCF) for the purpose of determining an optimum combination of design parameters. The series of filters was developed in such a way that pairs of filters could be compared, with only a single design parameter differing between the two filters.

The evaluation was based on four types of measurements, with more or fewer measurements for certain filters: impulse response, frequency response, frequency-wavenumber ($f\text{-}\vec{k}$) response, and ambient seismic-noise attenuation. Four of the filters were applied to recorded P-wave signals and the degree of signal distortion was estimated.

A brief description of each filter is presented first and a list of the comparisons are presented in a table. Also, a general description of the four basic measurements is presented, leaving exceptions to be mentioned within the appropriate section.

A. DESCRIPTION OF FILTERS

Each filter used in determining the optimum MCF design parameters, their characteristics and comparisons are listed in Table IV-1. All filters are 1.0 sec long unless otherwise noted. The filters were designed for the LASA standard subarray shown in Figure IV-1. The F-3 subarray from which the noise samples were taken is oriented so that the subarray arm containing the number 1 seismometer of each ring is 6° west of north.

The 25-channel noise samples were obtained by retaining each of the 25 seismometer outputs as a separate channel. The 8-ring noise samples were obtained by summing the noise output of all the seismometers on a given ring for each of the eight rings shown in Figure IV-1. The 5-ring noise samples were obtained by summing rings 3 and 4, rings 5 and 6 and rings 7 and 8 of the 8-ring noise sample. (In discussing ring-model filters, the terms channel and ring will be used interchangeably.)

The filters designed using this ring-forming technique, being linear filters, are such that the set of filter weights listed for a particular ring may be applied either to each seismometer output on the corresponding ring or to the ring sum.

Table IV-1

SUMMARY OF MULTICHANNEL FILTER CHARACTERISTICS

MCF	LENGTH (SEC)	NUMBER OF CHANNELS	SIGNAL-TO-NOISE RATIO	TYPE OF SIGNAL MODEL	TYPE OF NOISE MODEL	SUBARRAY CONFIGURATION	COMPARED WITH
3	1.0	25	N/A	INFINITE VELOCITY MAXIMUM-LIKELIHOOD	MEASURED NIGHT NOISE MODEL SINGLE SAMPLE 150 SEC, 11/24/65	SUBARRAY F3 25 CHANNEL	5,6
4	1.0	8	4:1	INFINITE VELOCITY SIGNAL MODEL	MEASURED NIGHT NOISE MODEL SINGLE SAMPLE 150 SEC, 11/24/65	SUBARRAY F3 8 CHANNEL RING MODEL	5,8
5	1.0	8	4:1	12 KM/SEC → ∞ DISK SIGNAL MODEL	MEASURED NIGHT NOISE MODEL SINGLE SAMPLE 150 SEC, 11/24/65	SUBARRAY F3 8 CHANNEL RING MODEL	3,4,6
6	1.0	5	4:1	12 KM/SEC → ∞ DISK SIGNAL MODEL	MEASURED NIGHT NOISE MODEL SINGLE SAMPLE 150 SEC, 11/24/65	SUBARRAY F3 5 CHANNEL RING MODEL	3,7,11
7	1.0	5	4:1	12 KM/SEC → ∞ DISK SIGNAL MODEL	THEORETICAL NOISE MODEL 1 → 8 KM/SEC	SUBARRAY F3 5 CHANNEL RING MODEL	6
8	0.8	8	4:1	INFINITE VELOCITY SIGNAL MODEL	WHITENED, MEASURED NIGHT NOISE MODEL, SINGLE SAMPLE 150 SEC, 11/24/65	SUBARRAY F3 8 CHANNEL RING MODEL	4
9	1.0	5	4:1	INFINITE VELOCITY SIGNAL MODEL	MEASURED NIGHT NOISE MODEL 150 SEC, AVERAGE OF 7 SAMPLES	SUBARRAY F3 5 CHANNEL RING MODEL	10
10	1.0	5	4:1	INFINITE VELOCITY SIGNAL MODEL	MEASURED DAY NOISE MODEL 150 SEC, AVERAGE OF 4 SAMPLES	SUBARRAY F3 5 CHANNEL RING MODEL	9
11	1.0	5	VARIABLE	DISK SIGNAL MODEL, 12 KM/SEC → ∞ THEORETICAL AMPLITUDE RESPONSE	MEASURED NIGHT NOISE MODEL 150 SEC, 11/24/65	SUBARRAY F3 5 CHANNEL RING MODEL	6,12
12	1.0	5	VARIABLE	DISK SIGNAL MODEL DATA 12 KM/SEC → ∞ WITH INSTRUMENT RESPONSES INCORPORATED	MEASURED NIGHT NOISE MODEL 150 SEC, 11/24/65	SUBARRAY F3 5 CHANNEL RING MODEL	11
13	1.0	5	4:1	INFINITE VELOCITY SIGNAL MODEL	MEASURED NIGHT NOISE MODEL 330 SEC, 11/24/65	SUBARRAY F3 5 CHANNEL RING MODEL	14,15
14	2.0	5	4:1	INFINITE VELOCITY SIGNAL MODEL	MEASURED NIGHT NOISE MODEL 330 SEC, 11/24/65	SUBARRAY F3 5 CHANNEL RING MODEL	13,15
15	5.6	5	4:1	INFINITE VELOCITY SIGNAL MODEL	MEASURED NIGHT NOISE MODEL 330 SEC, 11/24/65	SUBARRAY F3 5 CHANNEL RING MODEL	13,14

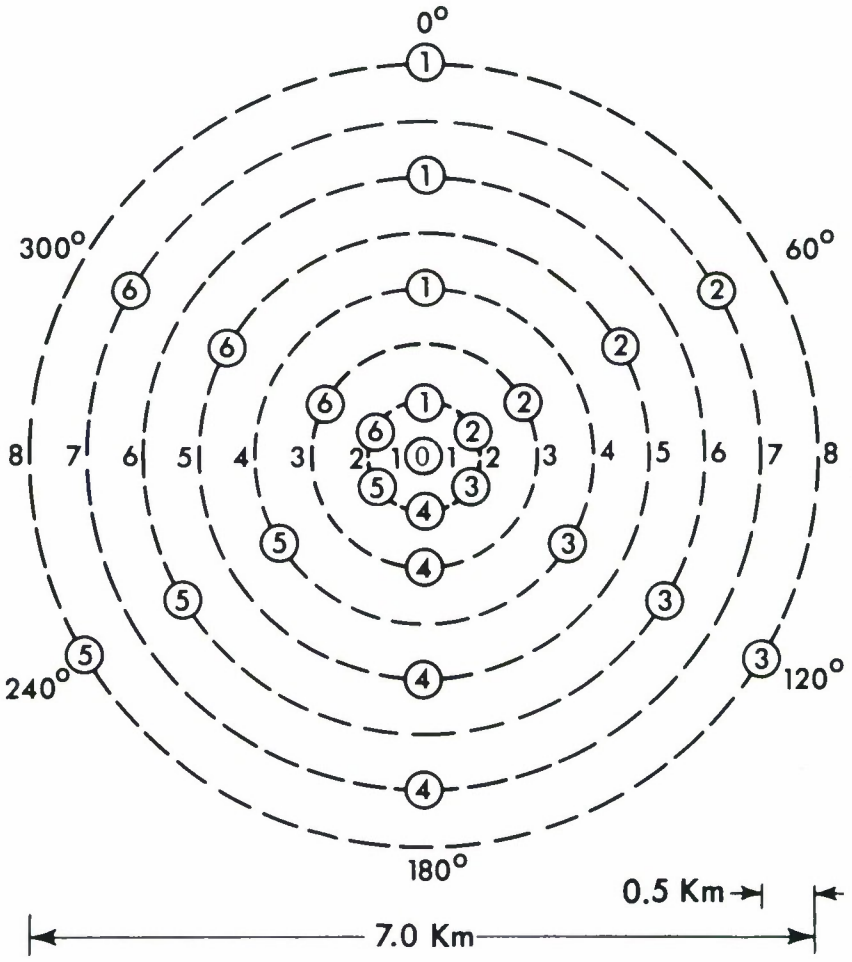

NOTE:
Seismometer No. 10 Is 500' Deep
Seismometers 21-65 Are 200' Deep

Figure IV-1. LASA Standard Subarray

Several noise samples were used in designing the filters. Noise sample B is a 330-sec noise sample recorded at the F-3 subarray on 24 November 1965 between 03:18 and 03:24 MST (Figure IV-2). Noise sample D used in designing most of the short filters is the last 150 sec of sample B. Noise sample A used only in evaluating the filters is the 150 sec immediately preceding sample D. Noise sample C is a 150-sec sample recorded at F-3 about 25 hours earlier (23 November 1965 between 02:19 and 02:22 MST).

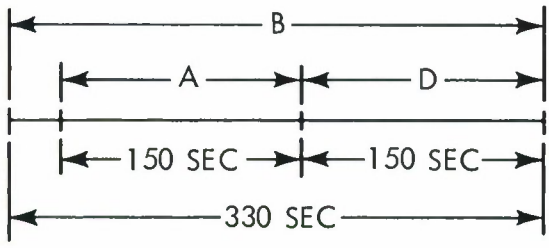

Noise Sample Recorded
24 November 1965 Between
02:18 and 02:24 MST

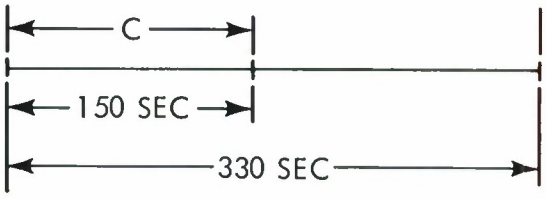

Noise Sample Recorded
23 November 1965 Between
01:19 and 01:22 MST

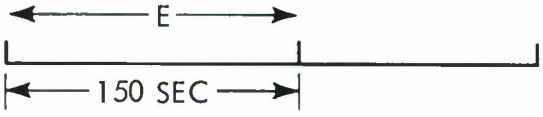

Noise Sample Recorded
31 March 1966 Between
13:58 and 14:01 MST

Figure IV-2. Noise Samples Used in Designing and Evaluating Multichannel Filters

1. Design Parameters for MCF-3

MCF-3 is a 25-channel maximum-likelihood filter, i.e., an MCF constrained to have an impulse response of exactly a unit impulse which thus permits no distortion of broadband infinite velocity signals. The effective signal model (no signal model as such is required) for the maximum-likelihood filter design is an infinite velocity model with an infinite S/N ratio.

The noise used in designing this filter was noise sample D. The mean-square-error as a function of filter length generated by the standard MCF design program is not meaningful in this case.

MCF-3 was used for comparison with MCF-5 and MCF-6, both ring-model filters for which the signal model was a disk in wavenumber space.

2. Design Parameters for MCF-4

MCF-4 is an 8-ring MCF utilizing an infinite velocity signal model. The method of summing the channels into eight rings was described in previous paragraphs. The signal correlations for simulating an infinite velocity set are all identical. The noise sample D autocorrelation for channel 1 was used to generate this set and scaled to give a S/N ratio of 4 on channel 1.

This filter was used in the comparison between an infinite velocity signal model and a disk signal model (MCF-5) and in the comparison between the use of whitened noise (MCF-8) and the use of nonwhitened noise (MCF-4).

3. Design Parameters for MCF-5

MCF-5 is an 8-ring disk signal model MCF. The signal model corresponds to constant power density over a disk in wavenumber space ($\vec{k}$-space) with a radius corresponding to a horizontal component velocity of 12 km/sec. The signal spectrum was shaped to the average spectrum of the 5-ring noise sample D. This spectrum differs very little from the average spectrum of the 25-channel noise sample. The noise sample used in designing MCF-5 was noise sample D, and the S/N ratio was 4.

This filter was used for comparison with the maximum-likelihood filter (MCF-3) and was used for comparison with an MCF designed with an infinite velocity signal model (MCF-4).

4. Design Parameters for MCF-6

MCF-6 is a 5-ring disk signal model MCF. The disk signal model and the noise model (measured correlations from noise sample D) are the same as those used in the design of MCF-5 except that the eight rings were summed into five rings, as described in previous paragraphs. Again, the signal spectrum was shaped to give a constant S/N ratio of 4.

This filter was used in several comparisons: between the disk signal ring-model filter design and the maximum-likelihood filter design (MCF-3); between using measured-noise statistics for the noise model (MCF-6) and using a theoretical noise model (MCF-7); between an MCF designed with a constant S/N ratio (MCF-6) which does not frequency-filter and an MCF designed with a S/N ratio which varies with frequency (MCF-11), thus permitting frequency-filtering as well as velocity-filtering.

5. Design Parameters for MCF-7

MCF-7 is a 5-ring filter designed from a theoretical noise model. The noise model corresponds to constant power density within an annulus in $\vec{k}$-space with an inner radius corresponding to a velocity of 8 km/sec and an outer radius corresponding to a velocity of 1 km/sec. The spectrum of the signal model used for the design of MCF-5 and MCF-6 was used also for the signal and noise spectral models for MCF-7. The S/N ratio was 4 at all frequencies.

MCF-7 was used in the comparison between using a theoretical noise model and using measured-noise statistics (MCF-6) for filter design.

6. Design Parameters for MCF-8

MCF-8 is an 8-ring filter designed from a noise model of whitened measured correlations from noise sample D. To whiten the noise spectrum, a 5-point whitening filter was designed from the noise sample D autocorrelation of channel 1. The 8-channel correlations were convolved with the autocorrelation of the whitening filter. This resulted in a correlation set exactly equivalent to the set which would have been obtained by applying the whitening filter to each channel and then computing the correlation functions. The infinite velocity signal model consisted of a set of correlations, each identical to the whitened-noise autocorrelation of channel 1.

In the whitening process, the correlations were necessarily shortened. Consequently, MCF-8 is only 0.8 sec long.

This filter was used in the comparison between using whitened measured-noise statistics and using nonwhitened measured-noise statistics (MCF-6) for the noise model in MCF design.

7. Design Parameters for MCF-9

MCF-9 is a 5-ring filter designed from an infinite velocity signal model and a measured nighttime noise model. The noise model was obtained by calculating the 5-ring correlations of seven separate noise samples recorded at the F-3 subarray between 01:00 and 05:35 MST and between 5 November 1965 and 1 December 1965. A 150-sec portion of each recorded sample was used to compute the correlations. The seven correlation sets were summed to obtain the average nighttime noise correlations used to design the filter. Each of the signal correlations for the infinite velocity model were identical to the channel 1 noise autocorrelation. The S/N ratio was 4.

MCF-9 was one of the filters used to determine the noise reduction gains to be attained by applying multichannel filters designed from daytime noise statistics (MCF-10) during the day and multichannel filters designed from nighttime noise statistics (MCF-9) during the night.

8. Design Parameters for MCF-10

MCF-10 is a 5-ring filter designed from an infinite velocity signal model and a measured daytime noise model. The four daytime noise samples used were recorded at the F-3 subarray between 11:00 and 17:00 MST and between 24 March 1966 and 5 April 1966. A 5-channel correlation set was computed for each noise sample, and the four sets were then summed to produce a single 5-channel noise correlation set. The noise autocorrelation for channel 1 was used to form an infinite velocity signal correlation set with S/N ratio equal to 4.

This filter was used in the comparison between the effects of using daytime or nighttime (MCF-9) noise statistics.

9. Design Parameters for MCF-11 and MCF-12

MCF-11 and MCF-12 were designed for a 5-channel ring-model subarray configuration. The noise model was identical for each, consisting of a correlation set computed over a 150-sec interval (noise sample D) recorded at subarray F-3. Both filters were designed with a disk signal model in order to pass the $\vec{k}$ - space region from 12 km/sec to infinite velocity. However, the signal model for MCF-12 incorporated variations in instrument responses. The signal model for each filter was band-limited from 1.0 to 2.25 cps. The total signal energy to total noise power ratio was set to 2 to insure a S/N ratio greater than 1 everywhere within the disk in $\vec{k}$-space.

MCF-11 and MCF-12 were directly compared to evaluate the decrease in signal distortion or attenuation to be achieved by correcting the signal model to include instrument response variations. MCF-11 was compared also with MCF-6 to determine the effectiveness of frequency-filtering combined with velocity-filtering.

10. Design Parameters for MCF-13, MCF-14 and MCF-15

MCF-13, MCF-14 and MCF-15 were designed for a 5-channel ring model subarray configuration. The noise model consisted of a correlation set computed over a 330-sec interval (noise sample B) of ambient noise recorded at the F-3 subarray. The signal model consisted of a point in $\vec{k}$-space corresponding to an infinite velocity signal. A constant signal-to-organized-noise ratio of 4 was used. The three filters differed only in length: MCF-13 was 1-sec long, MCF-14 was 2 sec long and MCF-15 was 5.65-sec long. The signal model was not corrected for variations in instrument responses.

MCF-13, MCF-14 and MCF-15 were directly compared to examine the relationship between noise rejection capabilities and filter length.

B. CALCULATION OF FILTER RESPONSES

1. Impulse Response

The impulse response of each filter was calculated on a 0.05-sec increment over the length of the filter. All filters were designed at this sample rate from data recorded at the same rate.

2. Frequency Response

The frequency response of all filters was calculated from 0.00 cps to 10.00 cps in 0.25-cps increments except for the 5.6-sec filter (MCF-15) and the 1-sec (MCF-13) and 2-sec (MCF-14) filters compared with it. These three responses were calculated on a 0.05-cps increment.

3. Frequency-Wavenumber Response

The f-$\vec{k}$ response of each filter was calculated in 0.25-cps increments from 0.25 cps to 1.50 cps, and up to 2.00 cps in some cases. However, the wavenumber responses are presented only for frequencies of 0.25, 0.50, 1.00, and 1.50 cps. The responses at these frequencies are representative in character and correspond to the signal and noise areas of primary interest. Velocity rings are overlaid in red on each plot. In all cases the velocity at the edge of each plot corresponds to 1.0 km/sec.

The contour levels used vary from plot to plot because of great differences in complexity of the contour plots. In general, each plot is contoured in 6-db increments to a level which seemed appropriate for that plot. Contours around areas of very low response are not shown if they are fairly narrow and do not correspond to some known noise peak. Also, in general, the contour of -3 db is shown only around the peak response at the origin.

The $f\text{-}\vec{k}$ responses for the ring-model multichannel filters have hexagonal or triangular symmetry. However, due to the coarse wavenumber increment used, differences appear in the contour levels of symmetrically corresponding features.

The $f\text{-}\vec{k}$ response at 1.50 cps shows an area slightly larger than a unit cell. The k_x and k_y shown have a maximum value of 1.50 cycles/km at the edge. The unit cell has a maximum k_x of 1.154 cycles/km and a maximum k_y of 1.333 cycles/km.

The frequency-wavenumber spectrum of noise sample D is shown in Figure II-18 (Section II) for comparison with the $f\text{-}\vec{k}$ responses of the filters.

4. Noise Attenuation

Most of the multichannel filters were applied to two noise samples. As mentioned in paragraph B, noise samples A and D were recorded at the F-3 subarray between 03:18 and 03:24 MST on 24 November 1965 (Figure IV-2). Noise sample C was recorded between 02:19 and 02:22 MST the previous day (23 November 1965) and noise sample E was recorded between 13:58 and 14:01 MST on 31 March 1966.

The noise attenuation of each filter was calculated as the ratio of the MCF output power density spectrum to the input noise power density spectrum. Three methods of representing the input noise were chosen.

- Summing the input noise traces, dividing by the number of seismometers used to obtain the noise, and calculating the power density spectrum of this trace. This power density spectrum is actually the spectrum of the noise filtered by a straight sum process. The ratio of an MCF output power density spectrum to the straight-sum power density spectrum will be referred to as an MCF/ST SUM ratio.
- Calculating the power density spectrum of the noise on the center channel input. The ratio of the MCF output power density spectrum to this center channel input power density spectrum will be referred to as an MCF/CC ratio.
- Calculating the average of the power density spectra of the 25 noise traces originally used to obtain the ring-summed noise samples. The ratio of the MCF output power density spectrum to this average spectrum will be referred to as an MCF/AVG ratio.

When it is necessary to refer to the ratios calculated by any two or all three of these methods, they may be termed noise attenuation plots.

After calculating the MCF/AVG noise ratio for a few filters, it was decided that no extra information was gained from this technique. The ratios are shown for the four filters for which they were computed.

It should be noted that all the filters were designed to estimate the signal at the center channel.

5. Other Responses

In some cases the random noise response is shown as a function of frequency. The response represents the MCF output power relative to input power when the input consists of unit power random-noise on all channels.

Also, for some filters the mean-square-error vs frequency is shown. The mean-square-error is, in general, a very reasonable quantity by which to rate the overall performance of a multichannel processing system. The objective for using such a system is to combine several channel outputs (each containing both signal and noise) in a linear fashion so that the resultant single output is the best possible estimate of the expected signal. The linear combination of these channel outputs is accomplished by sets of filter weights derived from an iterative solution to the Wiener optimum multichannel theory. These weights are constrained to yield the minimum average power difference (mean-square-error) between the expected output signal and its estimate, assuming given signal and noise models and given length for each set of weights. A measure of the quality of this estimation is the average power of the difference, or error, between the expected signal and its estimate. This error may be thought of as the sum of the error in estimating the expected signal caused by the presence of noise and that caused by distortion in the estimated signal. Therefore, if signal distortion is negligible, the reduction in the mean-square-error is a direct measure of the reduction in total noise power achieved.

C. COMPARISON OF FILTERS

Comparisons between the filters described in the previous paragraphs will now be discussed. In most cases the only difference between the two filters being compared is a single design parameter. The filter design parameters and a list of comparisons are summarized in Table IV-1.

1. Comparison of Maximum-Likelihood (MCF-3), 8-Ring (MCF-5) and 5-Ring (MCF-6) Models

The maximum-likelihood filter (MCF-3) was compared with both an 8-ring filter (MCF-5) and a 5-ring filter (MCF-6) which were designed from the same measured noise (noise sample D) used to design MCF-3. MCF-5 and MCF-6 were designed from the same signal model which was a disk in wavenumber space with a radius corresponding to 12 km/sec.

As mentioned before, MCF-3 was constrained to have an impulse response of exactly a unit impulse. An indication of the constraint accuracy is given by the figures presenting impulse response and frequency response measurement. The impulse response (Figure IV-6) has a zero time value of 1.0000000 and all other points are less than 4.82×10^{-8} in magnitude. The phase response (Figure IV-6) is $0.00^\circ \pm 0.005^\circ$ at every calculated frequency (0.00 cps to 10.00 cps in 0.25-cps increments), and the amplitude response varies between 0.99999972 and 1.0000001.

The mean-square-error as a function of filter length generated by the standard MCF design program is not meaningful in this case.

The frequency-wavenumber ($f\text{-}\vec{k}$) response of MCF-3 is shown in Figure IV-16. Examination of the $f\text{-}\vec{k}$ spectra of noise sample D (Figure II-18, Section II) from which this filter was designed shows a source of high-velocity noise to the northeast. This peak accounts for the rapid falloff of the filter response toward the northeast.

At 0.25 cps the main response lobe centered at the origin in $\vec{k}$-space is very broad, being down less than 3 db at 3 km/sec. At 0.50 cps the main response lobe is much narrower than at 0.25 cps, but the response has no deep holes except at a few spots outside the 2-km/sec ring. At 1.00 cps the main peak is still narrower and the nearby reject zone is much deeper than at 0.50 cps.

Several sharp reject areas which appear in the $f\text{-}\vec{k}$ response deserve comment. Outside of the main noise peak, the noise power is so low that the $f\text{-}\vec{k}$ spectra plots (Figure II-18, Section II) of noise sample D are dominated by the spectral window which appears on the plots as peaks of about -12 db. Therefore, it is possible that there are other weak, though coherent, noise sources which do not appear on the $f\text{-}\vec{k}$ spectra plots and that MCF-3 has designed to reject these noise components. However, most of the holes shown on the MCF-3 response remain at constant $\vec{k}$ as the frequency increases, indicating a possible array geometry effect. Since the transform of a discrete function is the sum of a finite and usually small number of periodic functions which are harmonics of one function, the transform may be expected to have an oscillating character which is basically a function of the sample interval of the original variable. The severity of the oscillation, the peak-to-trough amplitude variation, generally decreases as the number of samples increases. For the $f\text{-}\vec{k}$ response, the number of samples is small so that the oscillatory character might be expected to be noticeable for the transform of some functions, i.e., for the $f\text{-}\vec{k}$ response of some filters at certain frequencies. Furthermore, the original samples are unevenly located in x-y space, making almost impossible calculating by hand the variation to be expected in the $f\text{-}\vec{k}$ response due to this sampling problem. It should be noted that this oscillatory response is not erroneous, but is the actual transform of the original discrete function in x-y space.

The wavenumber spectrum for 1.50 cps shows the same trends noted at 1.00 cps, viz., sharper main lobe, and a few deep holes at the same wavenumbers as before.

The noise attenuation plots for MCF-3 are shown in Figure IV-24 as MCF/ST SUM ratio and in Figure IV-32 as MCF/CC ratio. At frequencies below 0.5 cps, MCF-3 achieves more noise attenuation than the straight sum process, with a maximum difference between the two processes of 10.5 db at 0.16 cps for noise sample D and 10.0 at 0.16 cps for noise sample A. At high frequencies the rejection of MCF-3 is about 10 db less than that of a straight sum.

MCF-5 is the constant S/N ratio ring-model filter designed from a disk signal model and the same noise sample used in the design of MCF-3. The impulse and frequency responses of MCF-5 are shown in Figure IV-8, and the mean-square-error reduction is shown in Figure IV-14. The impulse response has a peak of 0.96 amplitude at zero time, but also has a doublet of 0.1 amplitude on the right end. This doublet results from the periodic component of increasing amplitude in the frequency response.

The f-$\vec{k}$ response is shown in Figure IV-18. At 0.50 cps the response drops sharply at velocities just below 12 km/sec, having a deep reject zone around 4 km/sec. This sharp drop is necessary because of the high-velocity noise source. Since the noise source is slightly broader in $\vec{k}$-space than is the signal model, the MCF is able to reduce substantially the total noise power by a sharp response peak at high velocity. The response behaves in a similar manner at 0.25 cps and 1.00 cps. At 1.50 cps the main noise source is narrower than the signal model, and the filter is unable to reject much of the main noise source.

MCF-6 is a 5-ring MCF with constant S/N ratio. It was designed from the same disk signal model and measured noise as that of MCF-5. The impulse and frequency responses are shown in Figure IV-9 and the reduction in mean-square-error is shown in Figure IV-14. There is no significant difference between these responses and those of MCF-5.

The noise attenuation plots for both MCF-5 (Figures IV-26, IV-34 and IV-41) and MCF-6 (Figures IV-27, IV-35 and IV-42) have several characteristics in common with the plots for most of the other filters. Some of the general characteristics will be described now.

An examination of the MCF/CC ratios indicates that at some frequencies, usually the high frequencies, the MCF noise power output is greater than the center channel noise power input. However, a comparison of the MCF/CC ratios and the MCF/AVG ratios indicates that above 2.5 cps the noise power on the center channel is 6 or 7 db below the average noise power in sample D and is 8 to 10 db below the average noise power in sample A.

This difference between the center channel noise power and the average input noise power results in multichannel filters whose noise power output at high frequencies is greater than the center channel noise power input but is less than the average noise power input. The difference between the spectrum of the center seismometer (at a 500-ft depth) and the maximum and minimum of the spectra from the six seismometers on ring 2 (at a 200-ft depth) is shown in Figure IV-3. The difference between the spectrum of the center channel input and that of the output of the straight sum process is shown in Figure IV-4.

Figures IV-3 and IV-4 indicate that the bulk of the noise is below 1.0 cps. Above 1.0 cps the power density is more than 20 db below the peak power. Because so much of the noise power is concentrated at these low frequencies, filters designed in the time domain may be expected to concentrate on this frequency band and neglect the response at the higher frequencies. In general, the MCF/AVG ratios show that at low frequencies the filters have high attenuation. The attenuation decreases with increasing frequency until 1.5 cps to 2.0 cps; at the higher frequencies the noise becomes more random and the noise attenuation ratio decreases toward the straight sum limit of -14 db. The plots actually remain 3 or 4 db above this limit; this difference seems to be caused by a change in the S/N ratio as described below.

The disk signal model filters were designed by shaping the signal model to the spectra average of noise sample D. The ratio of the total signal power to total noise power on channel 1 was set to 4. The great bulk of noise power is below 1.5 cps; at these low frequencies the channel 1 noise power spectrum is virtually identical to the average noise power spectrum. However, at high frequencies the channel 1 noise power spectrum is about 8 to 10 db below the average power spectrum. Setting the S/N ratio to 4 adds another 6 db to the signal spectrum, giving a total of 14 to 16 db, or a S/N ratio of about 32. This variation in S/N ratio allows the filter some frequency-filtering. Since the S/N ratio increases with increasing frequency, the effect will be to allow the MCF to pass more high-frequency information than would normally be passed by a straight sum process.

Another characteristic in some of the plots of relative noise attenuation is the periodicity at frequencies above 1.0 or 2.0 cps. This periodicity may be attributed to spectral window effects when generating the signal spectrum from the noise autocorrelation for which the low-frequency peak dominates the spectrum. Thus, at high frequencies, in addition to the gradual increase in S/N ratio, there is a periodic variation which produces more frequency-filtering that results in periodicity as observed in the noise attenuation plots.

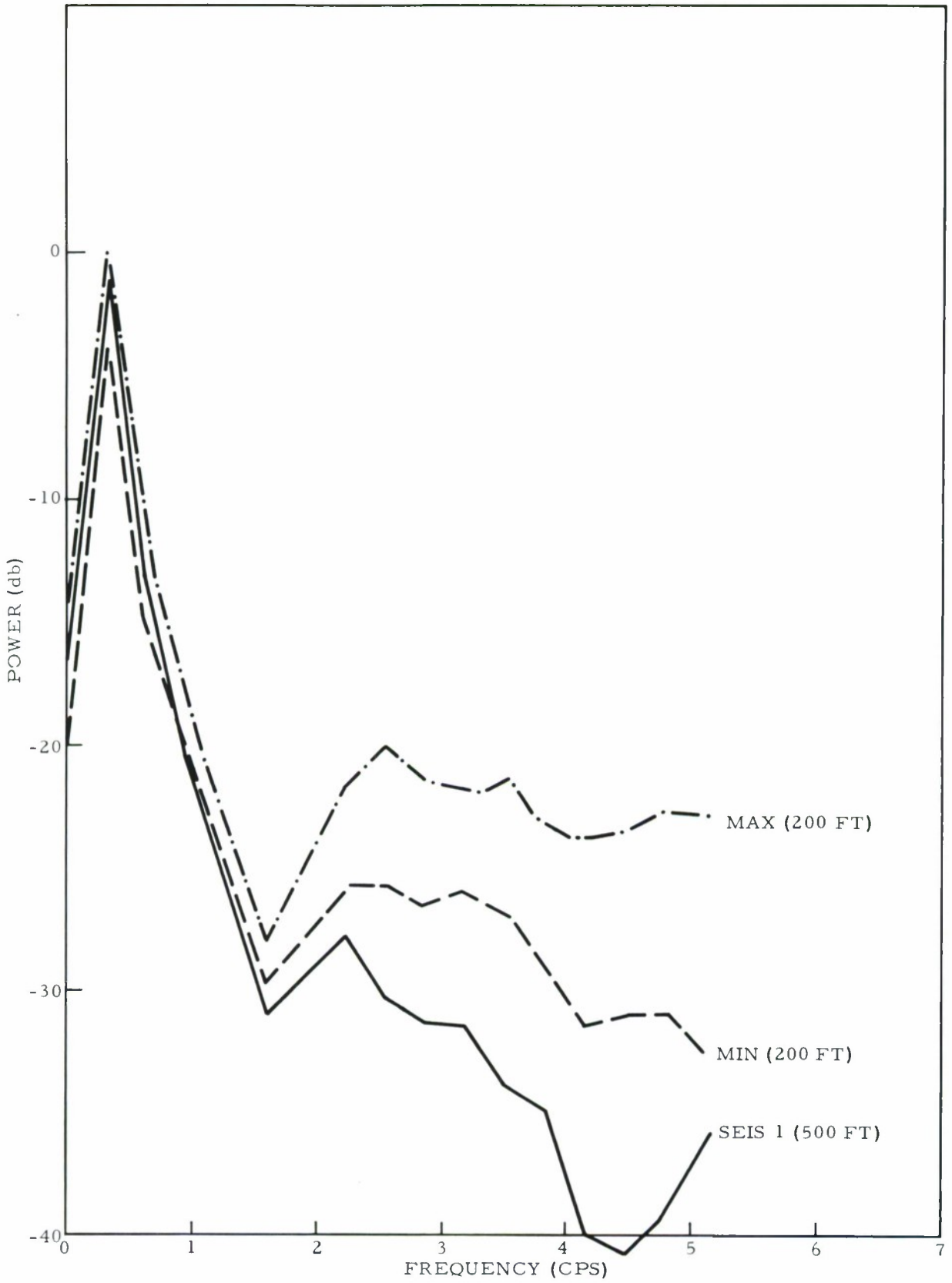

Figure IV-3. Power Density Spectra for the Center Seismometer and the Maximum and Minimum of the Six Seismometers on Ring 2 for a Nighttime Noise Sample

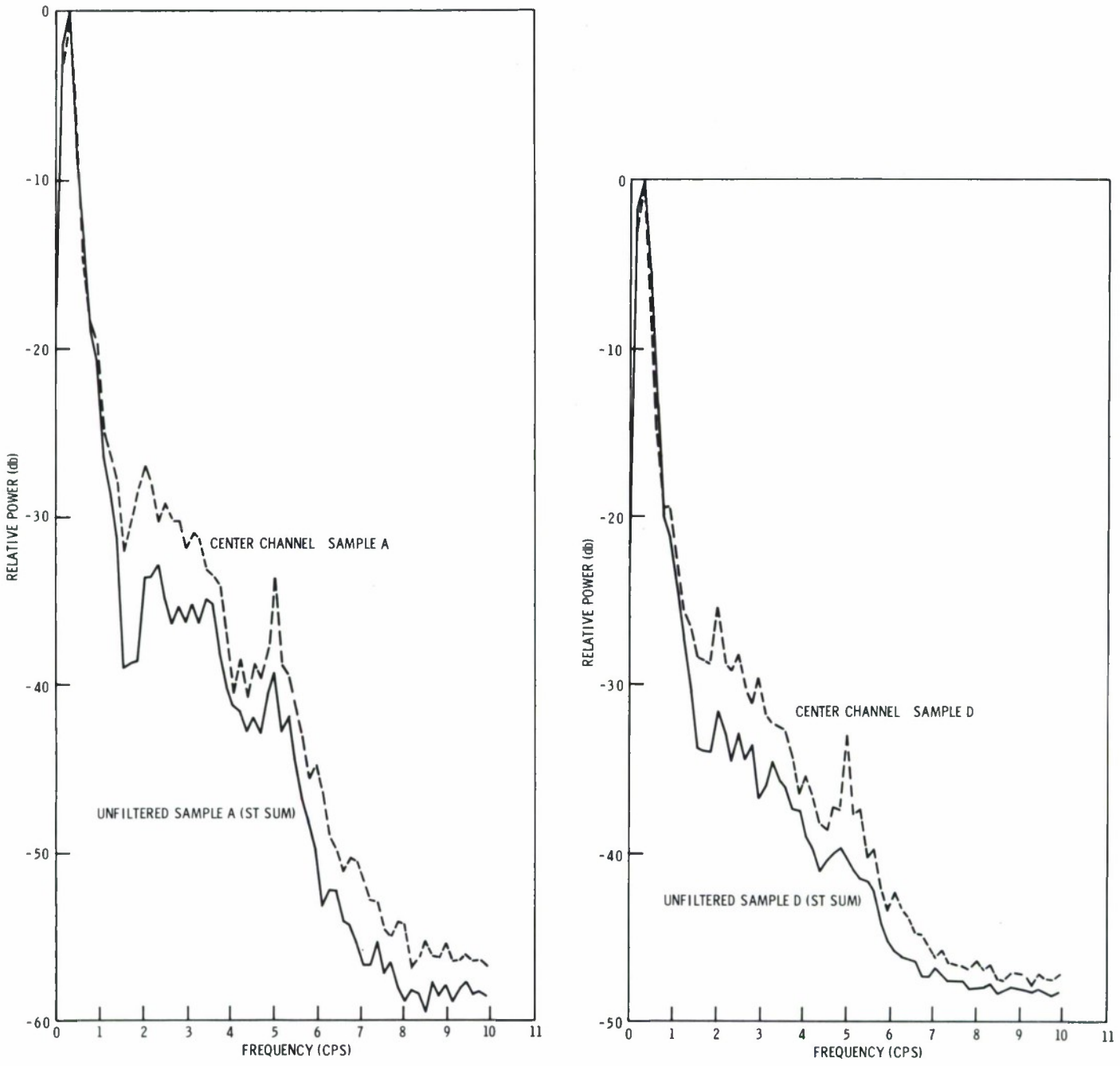

Sample A

Sample D

Figure IV-4. Straight Sum and Center Channel Power Density Spectra

The MCF/ST SUM ratios show results similar to those of the MCF/AVG ratios, i.e., for most of the filters the ratios are about +4 to +6 db from 2.5 cps to 5.0 cps, indicating that at these frequencies the straight sum process has 4 to 6 db greater noise rejection than the multichannel filters.

Many of the attenuation curves slope sharply downward at 5.0 cps. In every case the curves were calculated to higher frequencies and show only a sharp dip at 5.0 cps with the general level of the curve above 5.0 cps returning to the level of the curve below 5.0 cps. Examination of the center channel spectra and of the straight-sum trace spectra for samples D and A reveals large peaks at 5.0 cps. This noise component apparently was coherent across the array and some rejection was possible on the basis of wavenumber.

Similarly, the large dip in the noise sample D spectrum between 1.5 cps and 2.0 cps results in less attenuation than at adjacent frequencies as evidenced by most of the noise attenuation plots.

As previously mentioned, these characteristics of the noise attenuation plots are common to most of the filters.

The results of analyzing the $f\text{-}\vec{k}$ responses of MCF-3 (Figure IV-16) and MCF-5 (Figure IV-18) indicate that at the two lower frequencies (0.25 cps and 0.50 cps) the response to high velocities falls off much more rapidly with decreasing velocity and to a lower value in the rejection zone for MCF-5 than for MCF-3. However, at low velocities (below 2 km/sec) MCF-3 remains lower than MCF-5 which comes back up to -6 db at 0.25 cps and to +6 db at 0.50 cps. At 1.00 cps, MCF-3 continues to fall off rapidly, dropping to -6 db over about 90 percent of the azimuth between 6 and 7 km/sec; in some directions MCF-3 drops to -18 db at the same velocities. MCF-5 only drops to -6 db, and over less than half the azimuth at 6 km/sec; at 3 km/sec it is back to 0 db and, except for a -6 db rejection ring around 1.6 km/sec, the response is high (above 0 db) over most of the region at velocities below 3 km/sec. At 1.50 cps, integration of the two responses over the area inside the 2-km/sec circle would appear to show much less power in the MCF-3 response than in the MCF-5 response. The MCF-3 response has a sharp peak at infinite velocity whereas MCF-5 is flat, within ±3 db at velocities above approximately 4 km/sec.

The MCF-6 response (Figure IV-19) has a sharper, more isotropic peak at high velocity and stays lower at low velocity than does the response of either MCF-3 or MCF-5 at 0.25 cps. At 0.50 cps, the response of MCF-6 falls off more rapidly and drops to a lower value than the MCF-3 response; however, it is about the same as the MCF-5 response in this respect. MCF-6 does not have peaks at low velocity which rise as high as those of MCF-5, but MCF-6 seems to have a larger area in $\vec{k}$-space above 0 db. Again, MCF-6 is more isotropic than MCF-5 or MCF-3. At 1.00 cps,

the response of MCF-6 has a more uniform rejection ring around 4 km/sec than does that of MCF-5. Furthermore, the MCF-6 response does not come back up as much at 2 km/sec as does that of MCF-5. At 1.6 km/sec MCF-5 has a rejection ring which MCF-6 does not have, though MCF-6 appears to be trying to reject around this velocity. At this frequency, MCF-3 falls off much more sharply from high velocity to a much lower value in most directions than does MCF-6; but to the south and northeast, MCF-3 has very little rejection at velocities above 2 km/sec. Below 2 km/sec the MCF-3 response is above 0 db over a large area of $\vec{k}$-space. At 1.50 cps, MCF-6 attempts to form a rejection ring around 5 km/sec whereas MCF-5 does very little at this velocity. Both filter responses rise between 4 and 3 km/sec; however, below 2 km/sec, MCF-6 seems to hold its response down over a much larger area in $\vec{k}$-space than does MCF-5. MCF-3 has a good rejection zone between 4 and 8 km/sec in most directions, though again it is far from isotropic (having little rejection in the north at any velocity). MCF-3 also tends to fall off rapidly in the signal area, being down more than 6 db in some places at velocities greater than 12 km/sec.

In general, the f-$\vec{k}$ response of MCF-6 seems to be as good as, or better than, MCF-5 at the four frequencies examined. The response at high velocity usually falls off more rapidly and the response at low velocity is generally lower for MCF-6 than for MCF-5. Furthermore, MCF-6 is considerably more isotropic than MCF-5.

MCF-3 and MCF-6 are not as easily compared. MCF-6 generally has sharper falloff from the signal area and a deeper rejection zone adjacent to the signal area at the two lowest frequencies. Over all $\vec{k}$-space, MCF-6 obviously has greater rejection at 0.25 cps and appears to have greater overall rejection at 0.50 cps also. But at the two highest frequencies, the situation changes slightly. MCF-3 has generally sharper falloff from high velocity. The total rejection at velocities below 2 km/sec is hard to determine, but MCF-6 appears to do better than MCF-3. The sharp falloff of MCF-3 at high frequencies is offset by its lack of isotropy. The isotropic response at high velocities should compensate for the slightly shallower rejection zone of MCF-6.

Examination of the noise attenuation plots (Figures IV-24, IV-26, IV-27, IV-32, IV-34, and IV-35) allows further comparison among the filters. Compared to the straight sum process for sample D, MCF-6 does better than MCF-5 at most frequencies below 1.5 cps. The exceptions are at 0.16 cps where MCF-5 is about 1 db better than MCF-6 and at 0.79 cps where MCF-5 is again about 1 db better than MCF-6. Around 1.5 cps, MCF-6 has a much smaller peak, the difference being about 5 db. Above 1.5 cps, the two filters perform similarly at frequencies up to 5.0 cps. The comparison of the two filters for sample A is about the same as that described for sample D.

Again comparing MCF/ST SUM ratios for sample D, MCF-3 has about 4.5 db more attenuation at 0.16 cps than does MCF-6 and about 1.2 db more at 0.32 cps. At 0.48 cps the two filters perform about the same, but above 0.5 cps MCF-6 has more attenuation than MCF-3, except at 0.79 cps. The improvement of MCF-6 over MCF-3 is about 5 db from 2.0 cps to 5.0 cps. Again, for sample A similar results are obtained.

This difference in noise attenuation at high frequencies compared to a straight sum process between ring-model and maximum-likelihood filters is easily explained. As mentioned above, most of the filters have from 4 to 6 db less rejection than does the straight sum process at high frequencies. However, those filters are ring-model filters for which a few traces were straight-summed before input. The resulting straight-sum noise rejection cannot be directly calculated because the number of traces summed into a ring varies from ring to ring. But considering an average of about 3 traces per ring for the 8-ring filters, one would expect about 5 db more random noise rejection from an 8-ring filter than from a 25-channel filter. Comparing the MCF/ST SUM ratio for MCF-3 with that for MCF-4, which is an 8-ring filter designed from an infinite velocity signal model, a difference of about 5 db is observed at high frequencies.

Comparing MCF/ST SUM ratios of MCF-6 for samples A and D shows about the same attenuation for both samples at 0.16 cps (0.2 db more attenuation for sample A), with slightly less attenuation for sample A at other frequencies. The differences between the two samples are about the same as those for MCF-3, except that at 0.16 cps MCF-3 has 0.5 db less attenuation for sample A than for sample D.

A comparison of the MCF/CC ratios for MCF-5 and MCF-6 shows the same results as the MCF/ST SUM ratios. Likewise, comparison of the MCF/CC ratios for MCF-3 and MCF-6 shows results similar to the MCF/ST SUM ratios.

Thus, in a very narrow, very low frequency band (frequencies below 0.4 cps) the MCF-3 has from 1 to 4.5 db greater attenuation than MCF-6. At higher frequencies MCF-6 has greater attenuation, the average difference being from 3 to 5 db between 2.0 and 5.0 cps.

Other techniques can greatly improve the attenuation of the 5-ring MCF at frequencies below 0.4 cps, as will be shown later.

In addition to the response measurements, an estimation of signal distortion was obtained for MCF-3 and MCF-6 by applying each filter to teleseismic events. Figure IV-5 shows the center seismometer, the straight sum output and the MCF-3, -6, -11, and -12 output traces for each event used. (Some filters were not applied to every event.) The distortion of the signal seems to be negligible for both filters. Another noteworthy feature is the superiority of MCF-6 over MCF-3 with regard to noise rejection.

This comparison indicates that the 5-ring MCF designed from a disk signal model does better than the 8-ring disk signal model MCF and performs comparably to a maximum-likelihood filter. Furthermore, the ring-model filter has the advantage of an isotropic passband in the area of $\vec{k}$-space corresponding to velocities above 12 km/sec, a feature which the maximum-likelihood filter does not have. These results led to the choice of the 5-ring, disk signal model MCF over the maximum-likelihood design.

2. Comparison of Infinite Velocity (MCF-4) and Disk Signal Models (MCF-5)

MCF-4, an 8-ring filter designed from measured noise and an infinite velocity signal model, was compared with MCF-5, an 8-ring filter designed from the same measured noise as for MCF-4 and from a disk signal model with the same power spectrum as the average of the 5-channel noise autopower spectra.

The impulse and frequency responses of MCF-4 are shown in Figure IV-7. The peak at zero time has an amplitude of 0.96 and the side lobes are less than 0.03 in magnitude. The mean-square-error reduction is shown in Figure IV-15.

The $f\text{-}\vec{k}$ response of MCF-4 is shown in Figure IV-17. At 0.25 cps the filter is unable to cut very sharply, but does have a rejection ring at a low wavenumber value which corresponds to the high-velocity noise source. At 0.50 cps the rejection zone appears at higher velocity, probably due to the increasing resolution. Except for a few deep rejection regions, the response is quite high at velocities below 2.5 km/sec. However, the noise $f\text{-}\vec{k}$ spectrum (Figure II-18, Section II) shows very little noise at these velocities. The response at 1.00 cps is similar to that at lower frequencies. At 1.50 cps the filter response is down even at infinite velocity. At this frequency the center channel noise autopower density spectrum from which the signal model was formed has dropped 1 to 2 db below the average noise power density spectrum, causing a decrease in the S/N ratio. Furthermore, the high-velocity noise source is concentrated in a very small area in $\vec{k}$-space and the resolution is insufficient to enable the filter to reject the noise without some rejection at infinite velocity.

MCF-5 is identical to MCF-4 except that MCF-5 was designed from a disk signal model rather than from an infinite velocity signal model. The impulse and frequency responses are shown in Figure IV-8 and were explained in the previous paragraphs.

The first comparison is that of the f-$\vec{k}$ responses of the two filters (Figures IV-17 and IV-18). At 0.25 cps the MCF-5 response falls more sharply and goes to a lower value in some directions than does that of MCF-4. Furthermore, at velocities below about 1.5 km/sec the MCF-4 response comes up quite high, with peaks of +12 db. The MCF-5 response has a few small +6-db peaks at low velocity; however, over all the area of $\vec{k}$-space shown, corresponding to velocities below 2 km/sec, the MCF-5 response is considerably lower than that of MCF-4. At 0.50 cps MCF-5 still has a sharper falloff and deeper rejection ring between 3 and 4 km/sec. MCF-5 stays lower (between 1.7 and 3.0 km/sec) than MCF-4, but MCF-4 is still slightly more isotropic than MCF-5. At 1.00 cps MCF-4 has a deeper, more uniform rejection zone of 6 to 12 db around 2 km/sec and extending to about 1.6 km/sec than MCF-5. The rejection zone of MCF-5 is from about 1.7 to 1.4 km/sec. At 1.50 cps a major problem arises in MCF-4: the response is down more than 6 db over the entire signal area in $\vec{k}$-space. This signal rejection was explained above.

Both filters have little rejection at velocities below 8 km/sec, but the response of MCF-5 seems to be slightly lower at these velocities.

MCF-4 behaves well at all frequencies but the highest, although it does not have as sharp a response at high velocities or as much rejection at low velocities as does MCF-5 at the two low frequencies. At 1.00 cps MCF-4 is about the same as MCF-5, but at 1.50 cps MCF-4 attenuates the signal. This problem might be reduced by the use of a signal model identical in form to the average autopower spectrum rather than to an individual channel so that there would be less variation in S/N ratio. The chief advantage of MCF-4 over MCF-5 is its greater isotropy; the chief disadvantage, besides the signal attenuation at 1.50 cps, is the more gradual falloff of its response with increasing velocity.

The noise attenuation plots show about the same results in comparing the two filters with each other, whether by MCF/ST SUM ratios (Figures IV-25 and IV-26) or by MCF/CC ratios (Figures IV-33 and IV-34) and whether using sample A or sample D.

At the two lowest frequencies (0.16 and 0.32 cps) the ratios are the same for both filters. As frequency increases, the attenuation of MCF-5 becomes less than that of MCF-4 until at about 1.5 cps where it is about 1.5 to 2.0 db less than that of MCF-4. From 1.5 to 5.0 cps the ratios are similar, with each filter alternately having the greater attenuation. Thus, on the basis of noise attenuation, MCF-4 seems to do better than MCF-5.

The comparison of these two filters indicates that MCF-5 maintains a much better signal passband at all frequencies than does MCF-4. The slight improvement in noise attenuation of MCF-4 over MCF-5 in a small frequency band (1.5 to 2.0 cps) is not sufficient to offset MCF-4's disadvantage of 6 db or more attenuation in the signal area of $\vec{k}$-space. Thus, the disk signal model results in a better filter than an infinite velocity signal model.

3. Comparison of a Theoretical Noise Model (MCF-7) and Measured-Noise Statistics (MCF-6)

A 5-ring filter (MCF-7) designed from a theoretical annular noise model in an area of $\vec{k}$-space corresponding to an annulus between the velocities of 1 and 8 km/sec was compared with a 5-ring filter (MCF-6) designed from measured noise. The same disk signal model was used for both filters.

The impulse and frequency responses of MCF-7 are shown in Figure IV-10 and the mean-square-error reduction is shown in Figure IV-14. Since both the signal and noise are perfectly isotropic, the impulse response is perfectly symmetrical and the phase angle of the frequency response is $0.0^\circ \pm 0.05^\circ$ everywhere. The location of the two doublets on the impulse response corresponds to the half-cycle-per-unit-frequency periodicity in the frequency response; their character as doublets results from the increasing amplitude of the envelope of the frequency response.

The f-$\vec{k}$ response shown in Figure IV-20 deserves comment. The two major differences between this response and the others previously discussed are that the response is not as sharply peaked at high velocities nor does it have any high spots at low velocities. Both characteristics are due to the difference in noise model. In the earlier cases, the actual measured noise was similar in shape and location in $\vec{k}$-space to the signal model. In order to reject noise, the filter had to have a response which would fall off very rapidly at velocities just below 12 km/sec. Furthermore, since there was very little noise at low velocities, the response was allowed to rise at low velocities, if necessary, to improve the rapid falloff at the higher velocities. In MCF-7, there is complete separation between signal and noise and much less need for rapid falloff from the high-velocity response. Since the noise covers the low-velocity region, the response must stay down at these velocities.

The noise attenuation plots for MCF-7 are shown in Figures IV-28, IV-36 and IV-43. The shape of these plots is different from the ones previously examined. The MCF/ST SUM ratios show that MCF-7 is, at most, only about 2 or 3 db better than a straight sum process. Since the MCF was designed from models which have all signal and no noise at high velocity, it will make no effort to attenuate actual noise at high velocity. But the two noise samples to which the filter was applied contain mostly high-velocity noise at low frequency. Thus, the filter will not attenuate much of the noise in these samples.

The responses of MCF-6 were explained in a preceding paragraph. Comparing the $f\text{-}\vec{k}$ responses of the two filters shows that the MCF-7 response falls off with decreasing velocity much more slowly than that of MCF-6. The broad response lobe at high velocity would pass a large amount of noise. The performance of MCF-7 at low velocities is markedly superior to that of MCF-6, but previous analysis has pointed out the lack of major low-velocity noise sources.

The noise attenuation plots (Figures IV-27, IV-28, IV-35, IV-36, IV-42, and IV-43) show that at the very low frequencies MCF-6 has about 4 to 5 db more attenuation than does MCF-7.

In summary, MCF-7 lacks the sharp falloff in $f\text{-}\vec{k}$ response from high velocities needed for the actual noise field, and has less noise attenuation than does MCF-6 at low frequencies where there is the bulk of the noise. These factors indicate that measured-noise statistics should be used in the design of the filters.

4. Comparison Between the Use of Nonwhitened Noise (MCF-4) and the Use of Whitened Noise (MCF-8)

An 8-ring filter (MCF-4) designed from an infinite velocity signal model and measured noise was compared with an 8-ring filter (MCF-8) designed from an infinite velocity signal model and whitened noise obtained by whitening the noise correlations used in designing MCF-4. The infinite velocity signal model used for MCF-8 was obtained from the whitened noise autocorrelation for channel 1.

The impulse and frequency responses of MCF-8 are shown in Figure IV-11 and the mean-square-error reduction is shown in Figure IV-15. The amplitude response has a variation of less than approximately 0.25 db between 0.0 and 5.0 cps. This small variation indicates that the use of whitened noise reduces the S/N ratio variations which allow frequency-filtering.

The f-$\vec{k}$ response in Figure IV-21 shows a peak at infinite velocity surrounded by a rejection ring of 12 to 24 db between 2 and 3 km/sec at 0.25 cps. The peak narrows and the ring moves in at 0.50 cps and again at 1.00 cps, though the ring is breaking up and goes down only to -18 db. Finally at 1.50 cps the first ring is only down 12 db, but the falloff from high velocity is very sharp.

At low velocities below 4 km/sec the response is, in general, lower than for the nonwhitened noise filters. At 0.50 cps this response is up around -3 to +3 db over much of the area between 1 and 2 km/sec where there is little noise. However, at other frequencies the response is as high as 0 db only twice; both of the peaks are very narrow with rapid falloff and occur at 1.00 cps at a velocity less than 1 km/sec.

The noise attenuation plots are shown in Figures IV-29 and IV-37. The chief difference between these ratios and those of the nonwhitened noise filters is that these ratios are relatively flat over the entire frequency range. The MCF/ST SUM ratio for sample D shows about 4.5-db improvement for the MCF at the two lowest frequencies measured (0.16 and 0.32 cps) and shows 4.5 and 3.7 db for the two lowest frequencies on sample A. The MCF/CC ratios show that the MCF delivers 6.2- and 7.0-db improvement over the center channel on sample D at the two lowest frequencies while it gives 6.5 db at each frequency on sample A.

The impulse and frequency responses (Figure IV-7) and the f-$\vec{k}$ response (Figure IV-17) of MCF-4 were described in paragraph C.2.

An examination of the f-$\vec{k}$ responses (Figures IV-17 and IV-21) of the two filters shows that the response of MCF-8 falls off from high velocities more rapidly than that of MCF-4. Also, MCF-8 has a noticeably deeper rejection zone around the high-velocity peak. This rejection is good even at 1.50 cps where MCF-4 has no rejection between 2 and 8 km/sec. MCF-8 has a response peak at infinite velocity rather than a rejection area as has MCF-4.

The f-$\vec{k}$ response of MCF-8 seems to be much better than that of MCF-4, maintaining a sharp response peak at high velocities and at all frequencies considered. It should be noted that with this infinite velocity signal model obtained from a correlation set identical in form to that of the center channel noise autocorrelation, the filters were unable to maintain a high response over the entire $\vec{k}$-space area within the 12-km/sec circle at 1.50 cps.

The noise attenuation plots are shown in Figures IV-25, IV-29, IV-33, and IV-37. A comparison of the MCF/ST SUM ratios for the two filters shows that MCF-8 has more attenuation than MCF-4 at all frequencies except the first (0.16 cps). At 0.16 cps the attenuation of MCF-4 is 3 db better for sample A and 2.5 db better for sample D. From 1.0 to 5.0 cps MCF-8 has an average of about 7-db improvement over MCF-4 for sample D and about 5 db for sample A. Similar results are obtained from the MCF/CC ratio comparison except that at 0.32 cps for sample D, MCF-4 is still better than MCF-8, but only by about 0.25 db. Also, at 5.0 cps MCF-4 has a sharp dip in the ratio which goes about 0.75 db below that of MCF-8 for sample D and about 2.25 db below for sample A. This dip was explained in the earlier paragraph on noise attenuation (paragraph B.4).

These comparisons indicate that substantial (3 to 10 db) improvement in noise attenuation was obtained over almost the entire frequency range of interest by whitening the noise correlations before designing the filter. Furthermore, significant improvement in the $f\text{-}\vec{k}$ response resulted from the whitening process. These results indicate that the noise used in the filter design should be whitened.

5. Comparison of Nighttime (MCF-9) and Daytime (MCF-10) Noise Statistics

This study was made to determine if noise reduction could be significantly improved by applying a filter designed from nighttime noise samples to nighttime noise and applying a filter designed from daytime noise samples to daytime noise. Two 5-ring filters were designed from infinite velocity signal models, but from different noise samples. The nighttime filter (MCF-9) was designed from an average of seven noise samples recorded between 01:00 and 06:00 MST while the daytime filter (MCF-10) was designed from an average of four noise samples recorded between 11:00 and 17:00 MST.

The impulse and frequency responses of MCF-9 shown in Figure IV-12 indicate that this technique of averaging correlations over several noise samples produces a filter less prone to frequency-filtering than does the single sample design. MCF-9 has an amplitude response flat within +0 and about -0.5 db. The mean-square-error reduction is shown in Figure IV-15.

The $f\text{-}\vec{k}$ response of MCF-9 shown in Figure IV-22 follows the pattern already described for filters designed from a single nonwhitened noise sample at 0.25, 0.50 and 1.00 cps. A slight difference is noted at 1.50 cps. The previously mentioned filters had trouble separating signal and noise at high velocities because the high-velocity noise peak was so narrow that it almost matched the signal model. In order to reject the noise, the filter either had to reject extremely high velocities, resulting in a response which was down 3 to 6 db at infinite velocity as in the case of the

infinite velocity filter (MCF-4), or had to compromise and pass signal, resulting in less than 3-db rejection at lower velocities (8 to 12 km/sec). The process of averaging the correlations produced a model with a more uniform spectrum over the frequency range of interest. Thus, the high-velocity noise peak in $\vec{k}$-space does not seem to narrow down drastically at 1.50 cps as it did with the single sample. The resulting filter response remains above -3 db over most of the area within the 12-km/sec velocity ring, but drops as low as -18 db at 8 km/sec.

The noise attenuation plots are shown in Figures IV-30 and IV-38. MCF-9 and MCF-10 (applied to a different pair of noise samples than were the other filters) were designed from an average of noise samples and were applied to one sample of each type. Sample A was the sample used for the other filters and, being recorded between 03:18 and 03:21 MST, was chosen as the nighttime noise sample. Though not used in the design of MCF-9, sample A is immediately adjacent to one of the seven noise samples used. In the design of MCF-10, four daytime noise samples of 150-sec duration were used. One of these samples was chosen to represent the daytime noise in the measurement of noise attenuation. This daytime sample (sample E) is a 150-sec section of a noise sample recorded between 13:58 and 14:01 MST.

In summary, the noise attenuation plots show the results of applying a filter (MCF-9) designed from nighttime noise to a nighttime noise sample (sample A) and to a daytime noise sample (sample E).

A comparison of the MCF/ST SUM ratios for the two samples shows that at 0.16 cps the nighttime filter improvement in noise rejection over a straight sum process is about 0.5 db better for the nighttime sample than for the daytime sample. At 0.32 and 0.48 cps the behavior for both samples is the same. Above 0.48 cps the MCF/ST SUM ratio for the nighttime sample becomes increasingly better over a small band of frequencies than does that for the daytime sample with a maximum improvement of about 5 db from 1.0 to 1.5 cps. Above 1.5 cps the two ratios approach the same value at about 1.9 cps and closely follow each other up to 5.0 cps.

Figure IV-13 shows the impulse and frequency responses of MCF-10. This filter has an amplitude response flat within +0 and about -0.5 db from 0.0 to 5.0 cps. The mean-square-error reduction is shown in Figure IV-15.

The $f\text{-}\vec{k}$ response shown in Figure IV-23 is very similar to that of MCF-9 except that at 1.50 cps MCF-10 has a rejection ring around 7 km/sec which is 12 to 18 db below that for MCF-9. Other features of the $f\text{-}\vec{k}$ response follow the patterns already discussed for the other filters.

Noise attenuation plots are shown in Figures IV-31 and IV-39. At 0.16 and 0.32 cps the daytime filter MCF/ST SUM ratio is about 1 db better for the daytime sample than that for the nighttime sample. From about 0.5 to 1.0 cps the daytime filter works better on the nighttime sample, the ratio showing about 3-db improvement over the daytime sample at about 0.75 cps. From 1.2 to 5.0 cps the two ratios follow each other in general.

Comparing the $f\text{-}\vec{k}$ responses of the two filters (Figures IV-22 and IV-23), they are similar at 0.25 cps, except that the response of MCF-9 remains high over a wider area of $\vec{k}$-space at high velocity, but drops more sharply to a lower value than does that of MCF-10. The response of MCF-9 is generally lower at the low velocities than is the response of MCF-10. At 0.50 cps MCF-9 keeps its peak at high velocity sharper than does MCF-10, but the MCF-9 response does not fall as sharply or fall to such low values in its first rejection ring as does that of MCF-10. However, at velocities below 3 km/sec MCF-9 has a generally lower response than does MCF-10. At 1.00 cps the response of MCF-9 is higher over most of $\vec{k}$-space than is the response of MCF-10. Between 2 and 3 km/sec MCF-10 seems to be trying to reject some noise whereas MCF-9 does nothing noticeable in this frequency. At 1.50 cps MCF-9 exhibits a sharp falloff below 12 km/sec and a deep rejection ring between 6 and 8 km/sec. In achieving this deep rejection, the response was allowed to come up quite high around 3 km/sec. MCF-10, not having the deep rejection ring, does not rise quite as high as 3 km/sec.

These responses indicate that the noise does vary from day to night or from month to month: the nighttime noise samples were recorded in November 1965 while the daytime samples were recorded four months later in late March and early April 1966.

The noise attenuation plots are shown in Figures IV-30, IV-31, IV-38, and IV-39. A comparison of the MCF/ST SUM ratios shows that, in general, the daytime filter (MCF-10) performs better on the daytime noise (sample E) than does the nighttime filter; however, the difference is only 1 db at 0.16 cps. At 0.32 cps both filters are the same, but the nighttime filter is about 1 db better at 0.48 cps. At higher frequencies, the daytime filter is slightly better than the nighttime filter, with about 5- or 6-db improvement from 1 to 2 cps. Considering the nighttime noise (sample A), the nighttime filter is almost 1 db better than the daytime filter at 0.16 cps, about 0.5 db better at 0.32 cps, about 0.5 db better at 0.48 cps, and generally worse at higher frequencies. The MCF/CC ratios agree that the nighttime filter does better than the daytime filter in filtering daytime noise at a couple of frequencies, being a fraction less than 1 db better at 0.16 cps and 0.48 cps. At the other frequencies the daytime filter does better.

At the low frequencies below 0.5 cps, both filters do comparable work on both samples. At the frequencies above 1.0 cps, the daytime filter seems to do better on both samples. This suggests that the daytime filter, unlike the nighttime filter, was designed from noise samples containing slightly more power at the high frequencies.

On the whole, the difference in performance between the two filters does not seem sufficient to warrant separate filters for daytime and nighttime use. In fact, since the daytime samples were recorded about four months after the nighttime samples, it is further concluded that a filter designed from an average of several noise samples may be expected to perform consistently well over a period of several months. These results indicate that the filters should be designed from an average of several noise samples.

6. Comparison of Constant (MCF-6) and Variable (MCF-11) Signal-To-Noise Ratios

Multichannel filters described in previous paragraphs have utilized signal models whose power spectra have been shaped to approximate the spectrum of the noise model. This shaping procedure is normally followed to insure that the filter has a good transient response. It also insures that MCF rejection of a particular frequency is on a velocity basis rather than due to spectral differences between signal and noise. A constant multiplier is usually applied to the signal model to achieve a desired S/N ratio. The following study was initiated to determine the extent to which detection capabilities could be enhanced by allowing the MCF to reject on both a frequency and velocity basis.

MCF-6 and MCF-11 were used to perform this evaluation. They were identical in design, except for the shape of the signal model power spectrum. Both are 1.0 sec long and are designed for the 5-channel ring model case. The noise model in each case was from a 150-sec section of data recorded on 24 December 1965 at approximately 03:00 MST (noise sample D). No equalization to incorporate instrument response variations was performed. Both filters used a disk signal model designed to pass the $\vec{k}$-space region from 12 km/sec to infinite velocity. This type of signal model introduces less P-wave distortion in the medium-velocity range (12 to 20 km/sec) than does infinite velocity signal models which generally are 6 to 12 db down at these velocities. MCF-6 was described previously in this section, being used in a comparison between a measured-noise model and a theoretically derived noise model. Also, figures pertaining to MCF-6 were presented and will be referred to during this discussion.

MCF-6 used a constant signal-to-organized-noise ratio of 4. The signal model spectrum was shaped to resemble the noise model spectrum at all frequencies. Therefore, this MCF would be expected to achieve noise rejection primarily on a velocity basis. This is verified by the wavenumber responses previously presented in Figure IV-19. Arrivals with apparent horizontal velocities above 12 km/sec are essentially unattenuated at all frequencies. Noise rejection occurs primarily in the velocity range from 4 to 8 km/sec for all frequencies. An additional reject occurs between 1 and 2 km/sec.

MCF-11 used a theoretical shaping function for the signal model passing the frequency band from 1.0 to 2.25 cps. The theoretical input function is shown on Figure IV-44 overlaid with the amplitude response of the weighted stack of the filters. An additional S/N factor of 2 was used to insure that signal power would exceed noise power at all points in the $\vec{k}$-space passband. The filter is allowed to reject noise on a frequency basis at all frequencies outside the defined passband. Inside this band, rejection is a combination of velocity- and frequency-filtering which varies as a function of the relative power in the signal and noise spectra at any frequency.

Figure IV-44 is a three-part figure showing the impulse response of MCF-11 and the amplitude and phase responses obtained by taking the Fourier transform of the impulse response. As the parts of this figure indicate, the MCF response resembles a bandpass filter in many respects. Amplitude response peaks in the higher frequency reject regions are apparently due to low spectral power in the noise spectrum and to spectral window effects. The spectral window is created when the inverse transform of the frequency-domain-shaped spectrum is taken. The exact inverse transform, in this case, requires a ±2-sec time domain function. However, this function was truncated to a ±1-sec function for the signal model. Also, the reject regions of the signal model were restrained to a -30 db level.

Figure IV-45 shows the mean-square-error reduction achieved in the design of MCF-11. Total noise power was reduced to less than 1 percent of the input mean-square value. The mean-square-error curve for MCF-6 (Figure IV-14) indicated total noise power reduced to 5.5 percent of the original. These figures assume no signal distortion. Obviously, total noise power has been reduced to an additional 6 db with MCF-11.

Wavenumber responses for MCF-11 (Figure IV-46) indicate attenuation greater than 12 db at all points in $\vec{k}$-space for frequencies located outside the signal model passband. For example at 0.25 cps, infinite velocity energy is down 48 db from unity and falls off further to a low of 60 db between 8 and 12 km/sec. All points in the $\vec{k}$-plane are at least 24 db down from unity. Comparatively, MCF-6 (Figure IV-19) passes energy at velocities greater than 12 km/sec with less than 3-db rejection and is generally 18 db down between 2 and 4 km/sec.

At 0.5 cps MCF-11 is down at least 9 db over the entire $\vec{k}$-plane, including the high-velocity region, and ranges to 48 db down between 1 and 2 km/sec. MCF-6 is less than 3 db down from infinity to 8 km/sec with rejection regions 18 to 30 db down between 2 and 4 km/sec.

In the passband of the signal model at 1.00 cps, MCF-11 is within 3 db of unity to 8 km/sec and down 12 to 30 db between 2 and 4 km/sec. MCF-6 is similar, although the region between 2 and 4 km/sec is less than 12 db down.

At 1.5 cps MCF-6 rejects very little in the $\vec{k}$-plane at velocities greater than 2 km/sec. MCF-11 still passes the disk from 12 km/sec to infinity with less than 3-db attenuation, but generally rejects the region between 2 and 8 km/sec by amounts varying from 12 to 24 db.

Summarizing the wavenumber response comparisons, it appears that allowing MCF-11 to filter the spectral regions of high-noise energy on a frequency basis has enabled that filter to concentrate its capability to velocity-filter on the low-velocity noise energy contained in the passband, thereby achieving improved overall noise-rejection capability. The passband is designed to encompass the frequency range expected for P-phase body-wave energy, thus signal energy should be passed without significant attenuation from 12 km/sec to infinity.

Both filters were applied to noise samples A and D. Figure IV-47 illustrates a section of noise from each sample, showing the center seismometer (ring 1), the straight sum output and the filtered outputs from MCF-6, -11 and -12. MCF-12 will be discussed later. The MCF-6 output shows a 6- to 9-db reduction in the dominant 5-sec microseism compared with ring 1 and the straight sum. MCF-11 has removed all visible evidence of this low-frequency energy.

Power spectra were computed for ring 1, the straight sum and the MCF-6 and MCF-11 outputs over the total noise interval for both noise samples. The relative noise rejection as a function of frequency was computed by forming the ratio of power density at each frequency between each MCF output trace and the center seismometer (ring 1). Also computed was the ratio between each output MCF trace and the straight sum trace. The ratios for MCF-6 are shown in Figures IV-35 and IV-27 and those for MCF-11 are in Figure IV-48.

The ratios allow comparison of MCF performance over noise not included in the MCF design. Superior noise rejection is evident at all frequencies for MCF-11 when compared with MCF-6. The dominant 5-sec microseism is especially attenuated, with MCF-11 yielding 20 db greater rejection than MCF-6 over this region. Performance is consistent in and out of the design interval, indicating a relative insensitivity to minor noise field variations with the ring models. The increased noise rejection achieved by MCF-11 (as described by these ratios) is consistent with the mean-square-error and frequency-wavenumber plot indications.

Signal distortion was evaluated by apply MCF-6 and MCF-11 to 3 teleseismic events. Figure IV-5 shows the center seismometer, the straight sum output and the MCF-3, -6, -11 and -12 output traces for each event. Of particular interest was relative noise rejection, signal distortion (both amplitude and phase) and possible precursor effects introduced by the frequency-filtering capabilities of MCF-11. Noise rejection is markedly superior for MCF-11 compared with MCF-6, and signal amplitude and phase distortion seem negligible for both. A slight precursor is discernible for MCF-11; however, it does not appear to be of major concern. For purposes of event detection, a slight precursor is of relatively small consequence if a large gain in S/N ratio can be achieved.

In conclusion, it appears that event detection capabilities can be increased substantially by the use of an MCF incorporating a combination of velocity- and frequency-filtering characteristics as opposed to velocity-filtering alone.

7. Comparison Between Equalized and Unequalized Signal Models

MCF-11 was designed using an idealized signal model, i.e., the assumption was made that amplitude and phase responses were identical for each channel. The noise model, having been constructed from measured noise, contains departures from this idealized case due to existing variations in the instrument responses. Depending upon their extent, such variations were utilized by MCF-11 to achieve noise rejection. However, signals recorded by these instruments were affected by the same variations and were also distorted to some extent by the MCF.

MCF-12 was designed in a fashion similar to MCF-11; both used band-limited disk signal models to pass the $\vec{k}$-space area from 12 km/sec to infinity, both used measured noise from subarray F-3 (noise sample D) and both had S/N ratios of 2. However, the signal model for MCF-12 was perturbed to incorporate the F-3 instrument response variations described in Section III. Therefore, signals also containing these same variations should be undistorted by the MCF.

The design of MCF-12 resulted in a total noise power decrease to 1.8 percent of the input mean-square value (Figure IV-45) as compared with 1.0 percent obtained with MCF-11. The difference is a result of prohibiting MCF-12 from using the noise variations due to instrument responses as a basis for rejection. However, actual S/N improvement with MCF-12 should be comparable to that for MCF-11 due to the expected decrease in signal distortion.

The evaluation of the impulse response for MCF-12 required a departure from previously used methods. The impulse response was obtained by convolving the filter for each channel with an impulse that had been perturbed to incorporate the instrument response variations for the channel and then summing the convolved outputs. Figure IV-49 shows the impulse, amplitude and phase response of MCF-12. The signal model perturbations have caused considerable character change from the MCF-11 impulse response (Figure IV-44). The bandpass character remains evident in the amplitude response, although superimposed on a curve describing the instrument response. Some spectral window effects are also present due to the signal model truncation. (The signal model was shaped in the frequency domain and the exact inverse transform required a ±2-sec time domain representation).

The signal distortion (2 to 3 db) in the passband apparently is caused by several factors: the truncation of the time domain signal model to ±1 sec, a relatively low S/N ratio of 2:1 and the rather narrow signal bandwidth with high roll-off rates on both sides. The low overall S/N ratio causes difficulty when high-velocity noise is concentrated in a small section of the signal passband, creating a situation where the S/N ratio is actually less than 1 and the MCF is caused to reject. The existence of such noise is indicated by the behavior of the MCF-3 $f\text{-}\vec{k}$ response (Figure IV-16) which suggests a high-velocity noise peak in the northeast quadrant.

Frequency-wavenumber plots for MCF-12 are presented in Figure IV-50. The departure from ring-model symmetry is a result of the perturbation of the signal model to include the instrument response variations. Considerably greater noise rejection is evident with MCF-11 (Figure IV-46) at 0.25 cps (40 db more rejection at 8 km/sec, and 18 db more at infinite velocity). Both filters are comparable at 0.5 cps except at infinite velocity where MCF-12 is 6 db down from MCF-11. At 1.0 cps both filters exhibit some signal distortion across the 12-km/sec disk, with MCF-12 down 3 db lower than MCF-11. The multichannel filters' responses are comparable through the remainder of the $\vec{k}$-plane. At 1.5 cps, responses for both filters are very similar, indicative of the relatively less coherent noise field at this frequency.

In summary, the $f\text{-}\vec{k}$ comparisons indicate a reduced capability in noise rejection accompanied by increased signal distortion in the passband for MCF-12. The former effect was expected, since the design departure from an idealized signal model eliminated some basis for noise rejection. However, the latter effect is undesirable. Measures taken to minimize such distortion in designing the final filters include a broader signal passband

with lower roll-off rates, longer (± 1.8-sec) filters (thus minimizing the effects of truncation), and whitening of the noise model to stabilize S/N ratios through the passband.

MCF-12 was applied to noise samples A and D (Figure IV-47). Its noise rejection appears to be roughly comparable with that for MCF-11. Spectral ratios were computed for the MCF-12 output with both the center seismometer (ring 1) and the straight sum output (average) and are presented in Figure IV-51. Again, its noise rejection is comparable with that of MCF-11 (Figure IV-48).

Figure IV-5 illustrated the relative signal distortions obtained when MCF-11 and -12 were applied to three teleseismic events. Rejection of the noise preceding each event is comparable for the two filters. However, the MCF-12 filtered output indicates signal distortion to the extent of 3 to 6 db of loss in amplitude as compared to the MCF-11 output. This is directly contrary to the initial hypothesis, viz., that signal distortion would be decreased by incorporating the instrument response variations in the signal model. Part of the observed distortion occurs due to the filter impulse and frequency responses just described. An additional and perhaps equally important cause is the evidence presented in Section III concerning the observed changes in the relative instrument response variations from November 1965 (when the 1.0-cps calibrations were first taken) to March 1966 (when the multifrequency calibrations were conducted). Especially with F-3, large changes occurred in the responses of instruments during this period, making the responses measured in March nonrepresentative for other time periods. For this reason, it was decided to exclude the response variations from the final filter design.

8. Effect of Filter Length on Noise Rejection Properties (MCF-13, -14, -15)

This study was conducted to determine the variation in noise rejection properties when the time span of the optimum MCF is increased. LASA subarray F-3, reduced to a 5-channel ring model, was used. A measured-noise model was constructed from a 330-sec sample of noise (sample B) recorded on 24 December 1965 at approximately 03:00 MST. The signal model was a point in $\vec{k}$-space corresponding to an infinite velocity signal. A constant signal-to-organized-noise ratio of 4 was used. Three filters were developed: MCF-13 (1-sec long), MCF-14 (2-sec long) and MCF-15 (5.65-sec long).

The three filters were compared in terms of their responses and noise rejection capabilities. Figure IV-52 illustrates the relative reduction in the mean-square-error obtained with the design of each filter. Total mean-square-error reduction is comparable in all cases, with MCF-13 providing 94.9 percent reduction and MCF-15 yielding 97.5 percent reduction. Since the initial mean-square-error corresponds to the total noise power, assuming no signal distortion, this represents a reduction in total noise power to 5.1 percent and 2.5 percent of the initial value, respectively.

The filter transient responses are presented in Figure IV-53. The figure has three parts: the impulse responses for each filter, the amplitude responses and the phase responses. The impulse responses were formed from a weighted sum of the five individual filters in each MCF. The amplitude and phase responses correspond to the Fourier transform of the impulse responses. MCF-15 yields the best approximation to an ideal impulse, with side-lobe peak amplitude lower than 1 percent of the main-lobe peak amplitude.

The amplitude and phase responses are correspondingly flat (amplitude within 1 db of unity from 0.0 to 8.0 cps, within 2 db from 8.0 to 10.0 cps and less than 3° phase shift at all frequencies). However, MCF-14 and MCF-13 also have impulsive responses with side-lobe peak amplitudes less than 10 percent of main-lobe peak amplitudes, and have correspondingly flat amplitude and phase responses between 0.0 and 5.0 cps. The shorter filters maintain less control between 5.0 and 10.0 cps, but maximum deviation is still only 4 db in amplitude (MCF-14) and 20° in phase (MCF-13). An interesting fact is that MCF-13 maintains a flatter amplitude response and allows the phase to vary while MCF-14 suppresses phase shift at the expense of amplitude. Very little power was present in the design spectrum at these higher frequencies. Consequently, the multichannel filters concentrated on increasing S/N ratio at the lower frequencies, at the expense of controlling the higher frequencies.

Figure IV-54 presents the relative power spectrum of the center seismometer in the ring model for the design-interval noise sample. This figure also indicates that spectral power in the region above 5.0 cps ranges from 30 db to more than 50 db below peak power. Instrument response characteristics have not been removed from these curves.

The random-noise response is presented as a frequency function for each MCF in Figure IV-55. Also indicated is the reduction obtainable for

random noise by the straight sum process. Each MCF shows a rapidly increasing response with decreasing frequency below 1.0 cps where, in previous reports*, the ratio of random noise to coherent noise has been shown to be small.

Figures IV-56, IV-57 and IV-58 present the wavenumber response evaluation for MCF-13, -14 and -15, respectively, at frequencies 0.25, 0.50, 1.0, and 1.5 cps. Regions of more than 18-db rejection are shaded. In general, contour levels shown are in 6-db increments, although the -6 db contour generally was omitted from the more complex plots for clarity. The ±3-db contour levels are included only at the centers of each plot.

In general, these response curves show fairly sharp peaks around the origin in $\vec{k}$-space which corresponds to the infinite velocity signal model. Since P-phase arrivals with epicentral angles between 80° and 100° will exhibit apparent horizontal velocities greater than 20 km/sec, P-phase signal attenuation is limited in all cases to less than 6 db and usually is less than 3 db.

At 0.25 and 0.50 cps, noise rejection is primarily in the region from 1 to 4 km/sec for all three filters, although additional rejection at 4 km/sec is obtained with MCF-15 at 0.5 cps. The region from 2 to 4 km/sec generally is rejected by MCF-15 and MCF-14 at 1.0 cps, but the shorter MCF-13 has a rejection ring in the 1.5 km/sec region. This type of tradeoff, or compromise, will occur when different filter lengths are compared, since each filter is constrained by design to be the optimum filter for a given length. In this case, optimum is defined to mean the set of filter points that achieve the maximum reduction in mean-square-error. Therefore, filters of different lengths may satisfy this restriction by rejecting different regions in $\vec{k}$-space, according to their capabilities. Variations in the reject regions, however, generally will occur only at frequencies where noise power is relatively small over the whole $\vec{k}$-plane and where such tradeoffs are reasonably small-order. Figure IV-52 indicated that all three filters achieved approximately equal reductions in total noise power. The $\vec{k}$-space region between 4 and 7 km/sec is attenuated by all three filters at 1.5 cps.

Comparison of the three filters in terms of wavenumber response leads to the conclusion that MCF-15 achieves the best rejection

*Texas Instruments Incorporated, 1966: LASA Data Analysis and MCF Support, Spec Rpt No. 1 (Feb) and No. 2 (Apr).

at both low and high frequencies. However, both MCF-14 and MCF-13 have comparable responses, and it is probable that the increase in total noise rejection is not sufficient to warrant the increased cost of design and application. An overall improvement in noise rejection is apparently achieved with increased filter length, although this may not necessarily be true for specific frequencies or areas in $\vec{k}$-space.

The three filters were applied to noise samples B (part of the design interval) and C (recorded 25 hours earlier). Figure IV-59 shows the center seismometer (ring 1) of the subarray, the straight sum trace and each of the three MCF output traces for the two noise samples. Little difference is apparent in MCF performance for the two noise samples, indicating that the filters are not highly tuned to the noise contained in the design interval. This relative insensitivity to minor variations in the noise field is a particularly advantageous feature of a ring model which makes no assumptions as to noise directionality. In both cases MCF-15 generally has rejected the low-frequency noise better than MCF-14 and MCF-13, but all three filters have achieved from 6 to 12 db greater rejection of the predominate low-frequency noise energy than has the straight sum. Cancellation of the less-coherent high-frequency energy is roughly equivalent for MCF-15 and the straight sum, with somewhat less rejection achieved by MCF-14 and MCF-13 as might be expected after examination of the random noise responses presented earlier. It should be noted that the center seismometer is buried about 500 ft deep and the other seismometers are buried 200 ft deep, and thus the center seismometer does not necessarily give a representative indication of the high-frequency energy content across the subarray (Figure IV-3).

Power density spectra using a 150-sec data gate were computed for each of the traces illustrated in Figure IV-59. The relative power density spectra for the input noise sample (ring 1), the straight sum output and the three MCF outputs are shown in Figure IV-54. The relative noise rejection as a frequency function was computed by forming the ratio of power density at each frequency between each output MCF trace and the center seismometer. These curves are shown in Figure IV-60 for noise samples B and C. Also computed was the ratio between each output MCF trace and the straight sum output. These ratios are presented in Figure IV-61 for noise samples B and C.

Figure IV-60 indicates comparable noise rejection performance with the two noise samples and about 1-db measurable deterioration outside the design area over the frequency range from 0.0 to 5.0 cps. The behavior of each MCF is markedly similar, with differences in degree of rejection only.

Figure IV-61 follows the same trend of similarity in behavior and about 1-db deterioration in performance outside the design interval. Also, the relative performance of the three filters and the straight sum trace are compared. Superior performance is evident for the filters in the region of greatest noise power (below 1.0 cps). Above 1.0 cps MCF-15 and the straight sum are roughly equivalent while MCF-14 and MCF-13 show 3- to 5-db less rejection. These results compare favorably with the results of applying the filters (Figure IV-59) and the random noise responses (Figure IV-55). However, Figure IV-54 indicates that the actual noise rejection at these higher frequencies is relatively insignificant when compared with the rejection at frequencies where maximum power is concentrated.

In summary, the effect of increasing the length of the MCF is apparently an increase in overall noise rejection and specifically an improvement in the higher frequency energy rejection. This is probably because the filter design constrains each MCF to reject first the energy which more easily minimizes the mean-square-error (i.e., the large quantities of low-velocity low-frequency energy) and later achieves the relatively minor gains possible at the higher frequencies. The gains are minor, however, especially for the nearly 6-to-1 increase in filter length (in one instance), and generally would not be economically justifiable. The remarkable stability in the noise rejection as a frequency function indicates that differences in MCF performance as a function of filter length are primarily a matter of degree rather than emphasis.

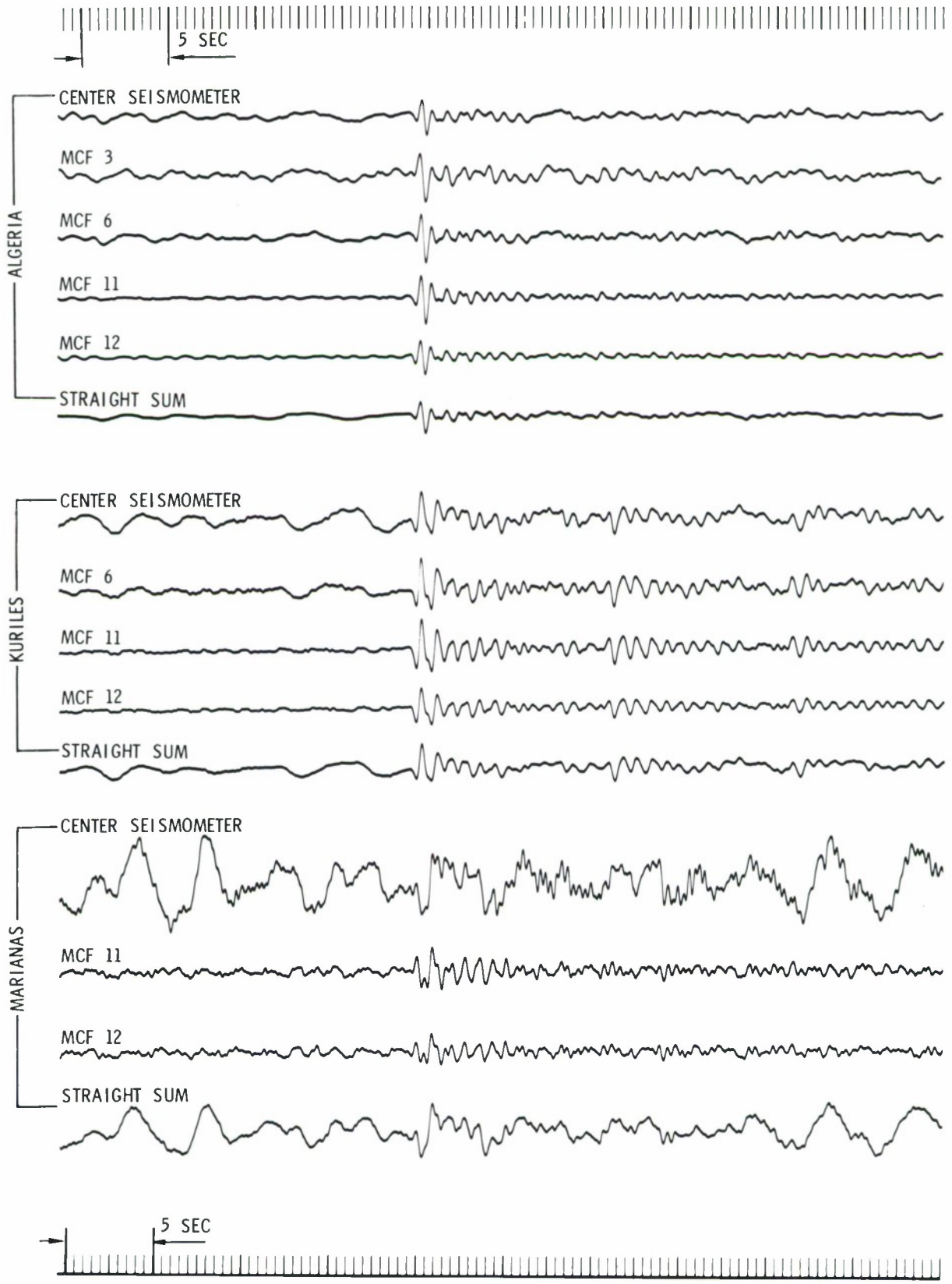

Figure IV-5. Signal Applications

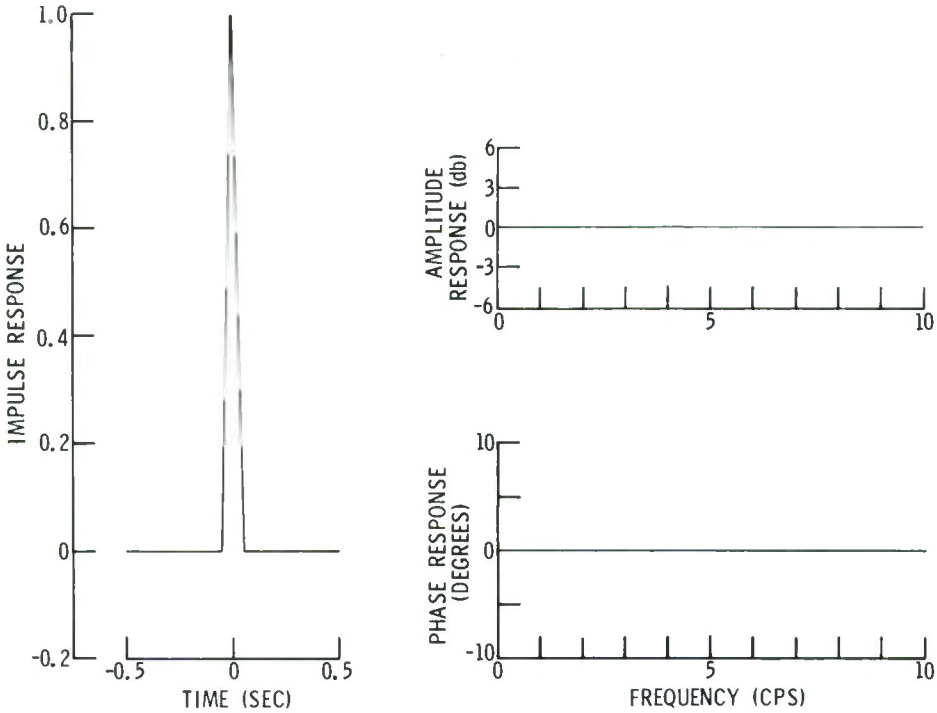

Figure IV-6. Impulse and Frequency Response of MCF-3

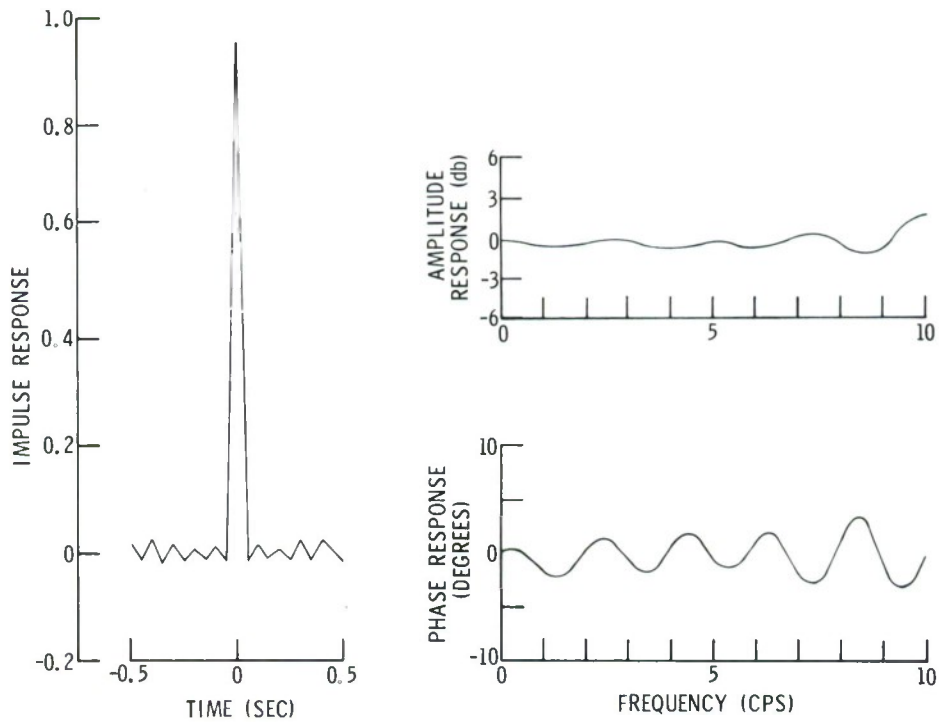

Figure IV-7. Impulse and Frequency Response of MCF-4

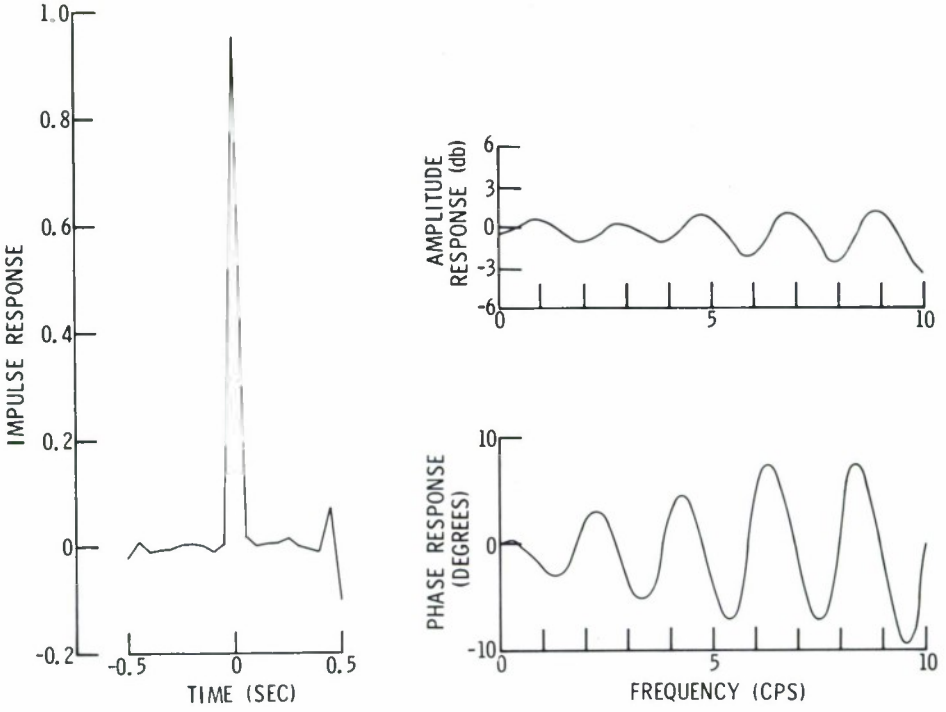

Figure IV-8. Impulse and Frequency Response of MCF-5

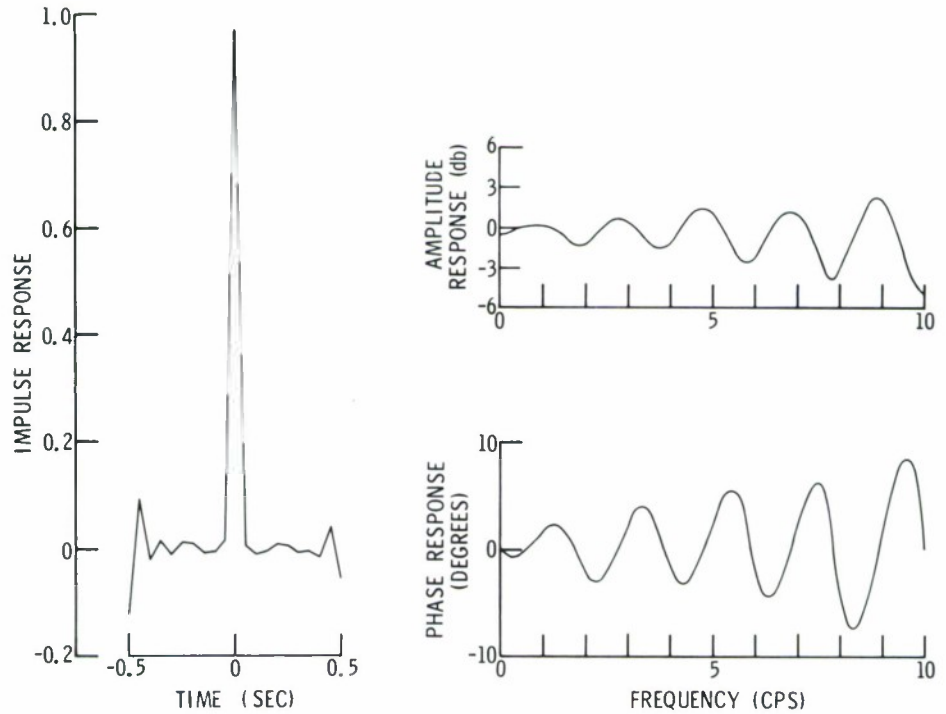

Figure IV-9. Impulse and Frequency Response of MCF-6

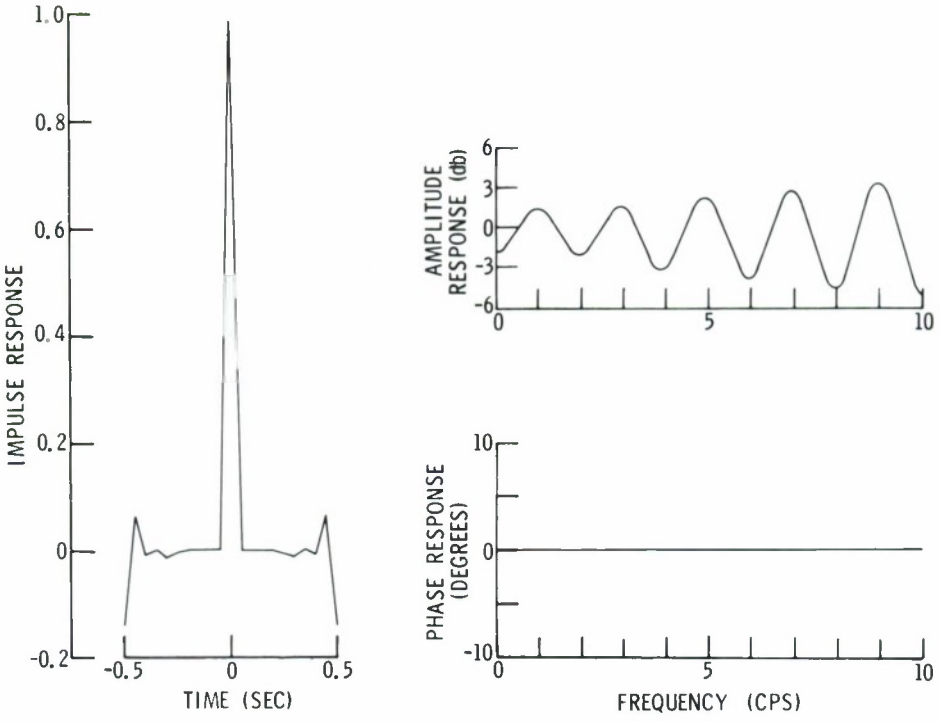

Figure IV-10. Impulse and Frequency Response of MCF-7

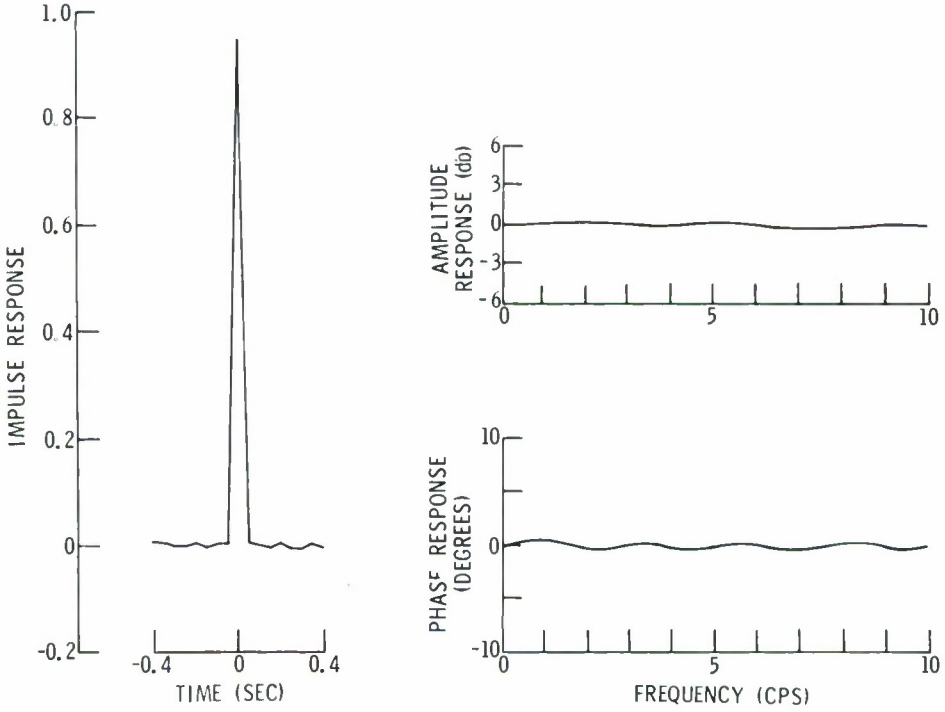

Figure IV-11. Impulse and Frequency Response of MCF-8

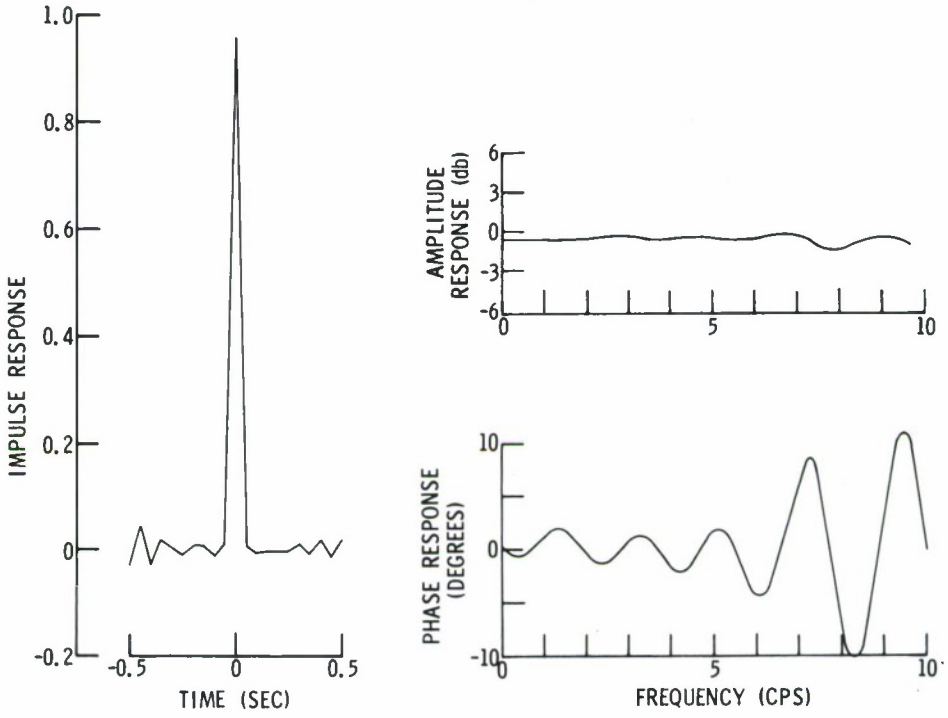

Figure IV-12. Impulse and Frequency Response of MCF-9

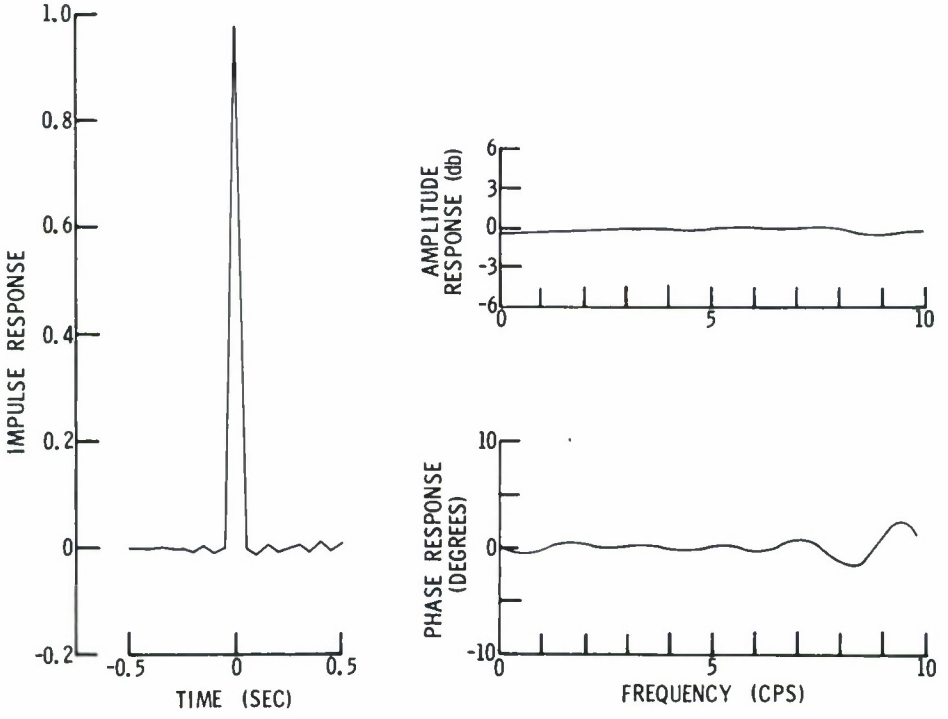

Figure IV-13. Impulse and Frequency Response of MCF-10

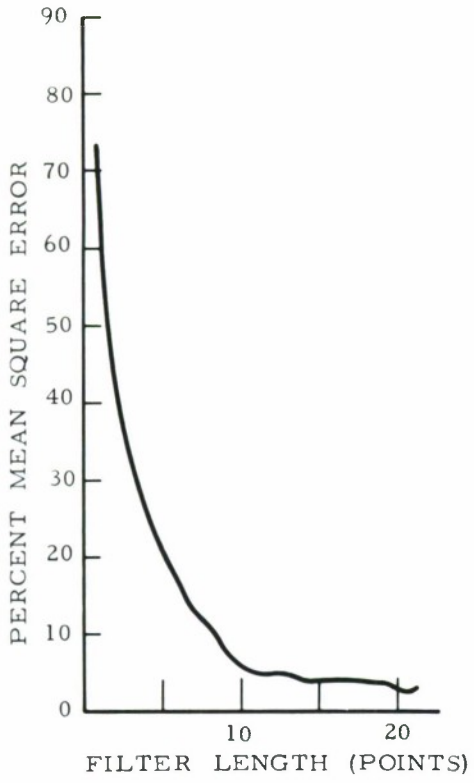

MCF-4

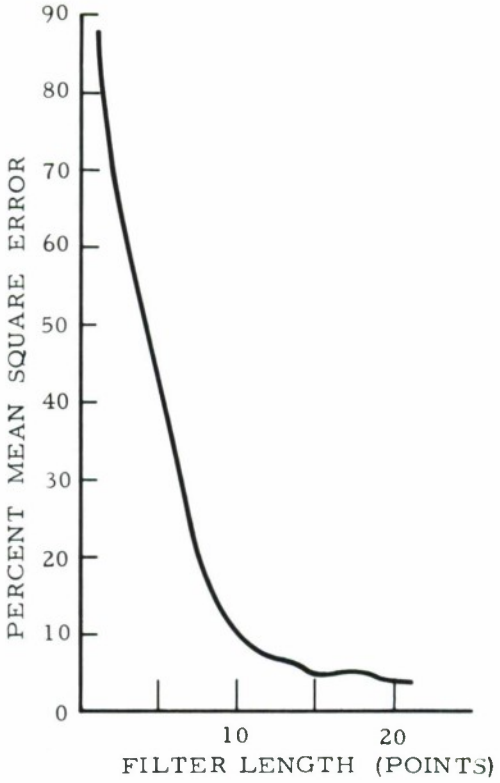

MCF-5

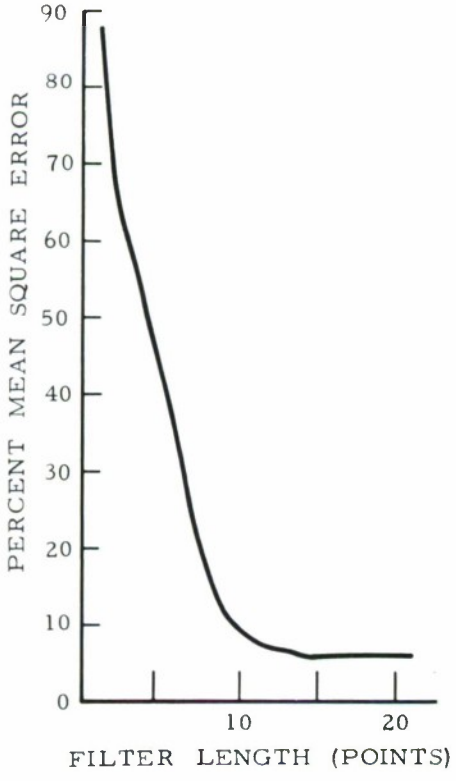

MCF-6

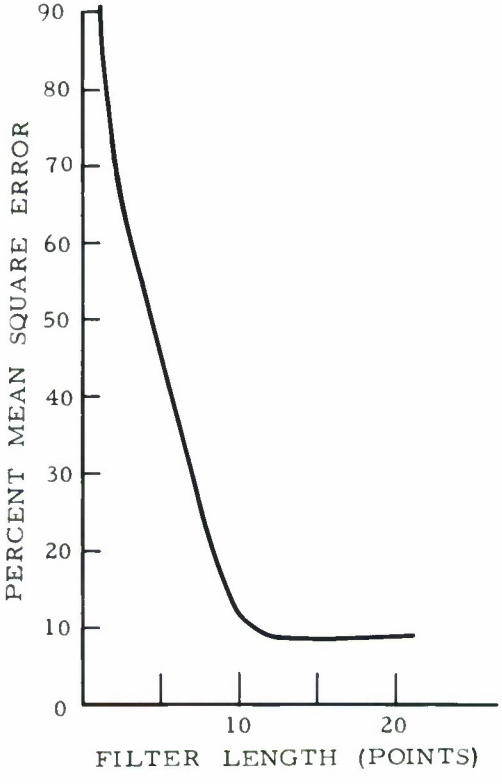

MCF-7

Figure IV-14. Percent Mean-Square-Error

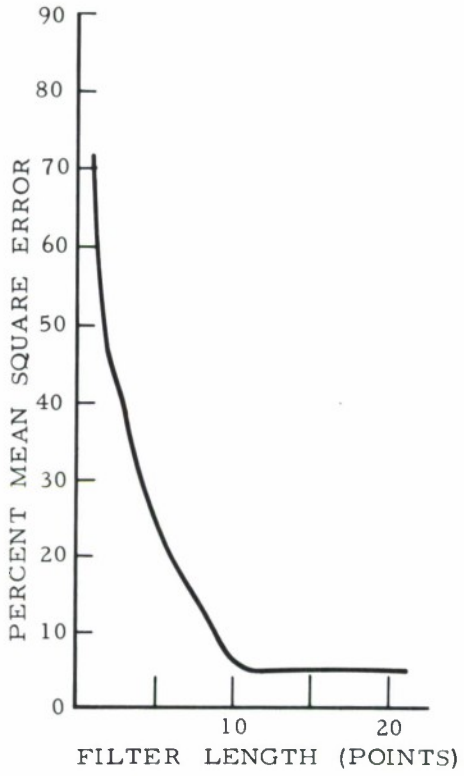

MCF-8

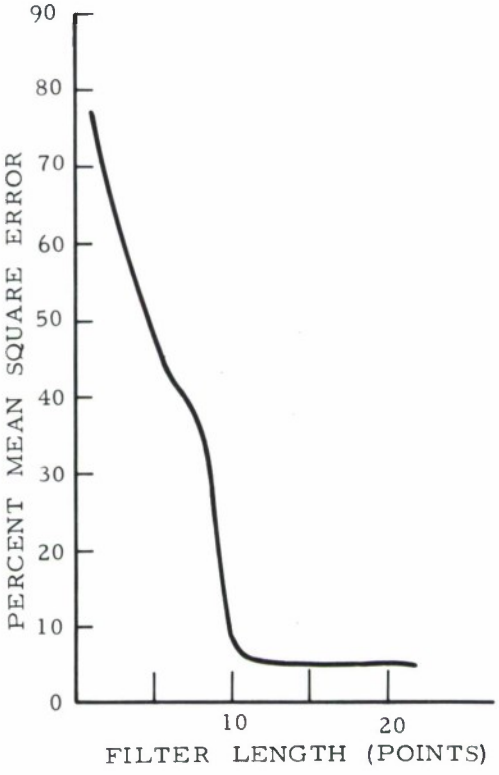

MCF-9

Figure IV-15. Percent Mean-Square-Error

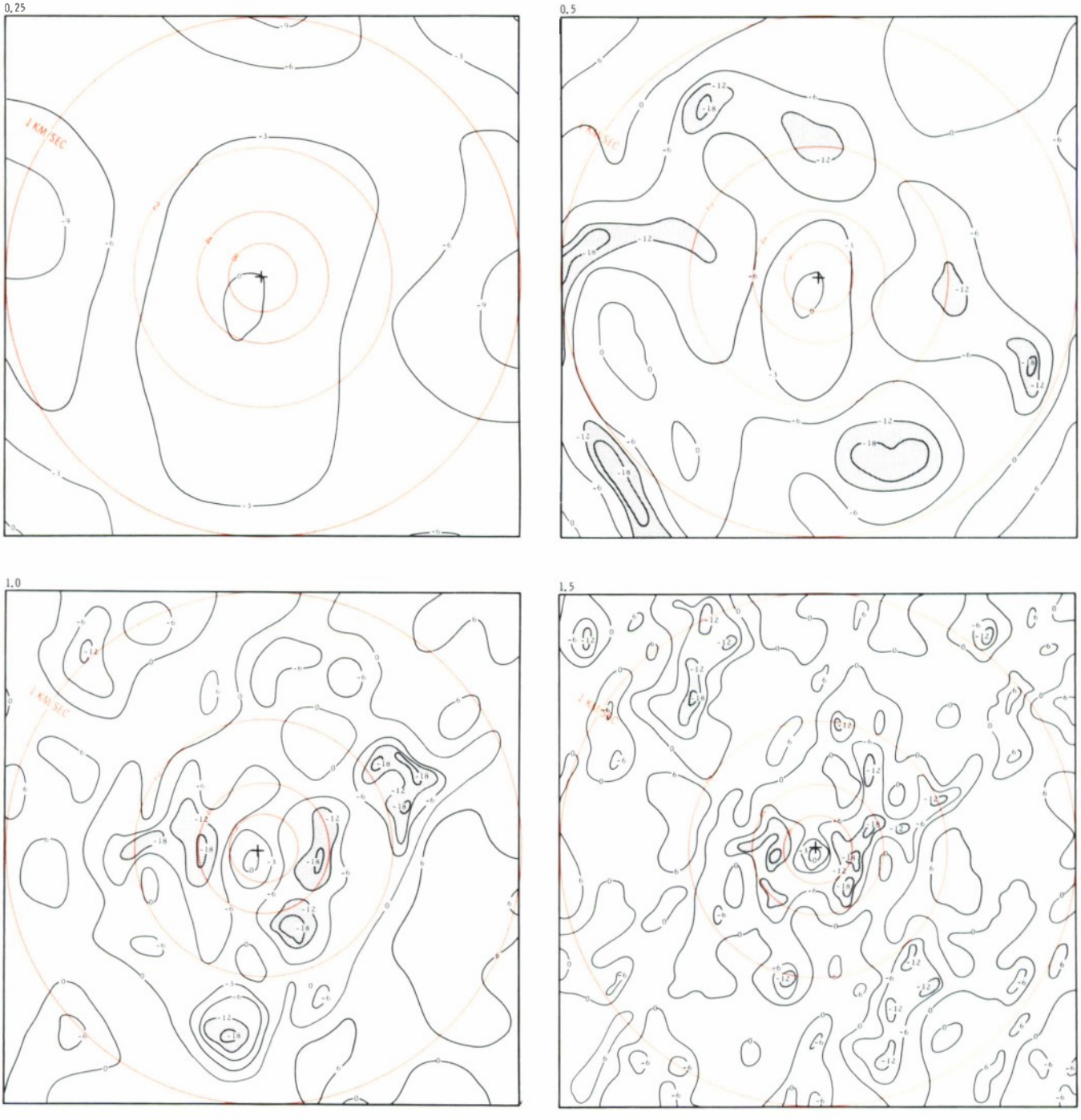

Figure IV-16. The f-$\vec{k}$ Responses of MCF-3

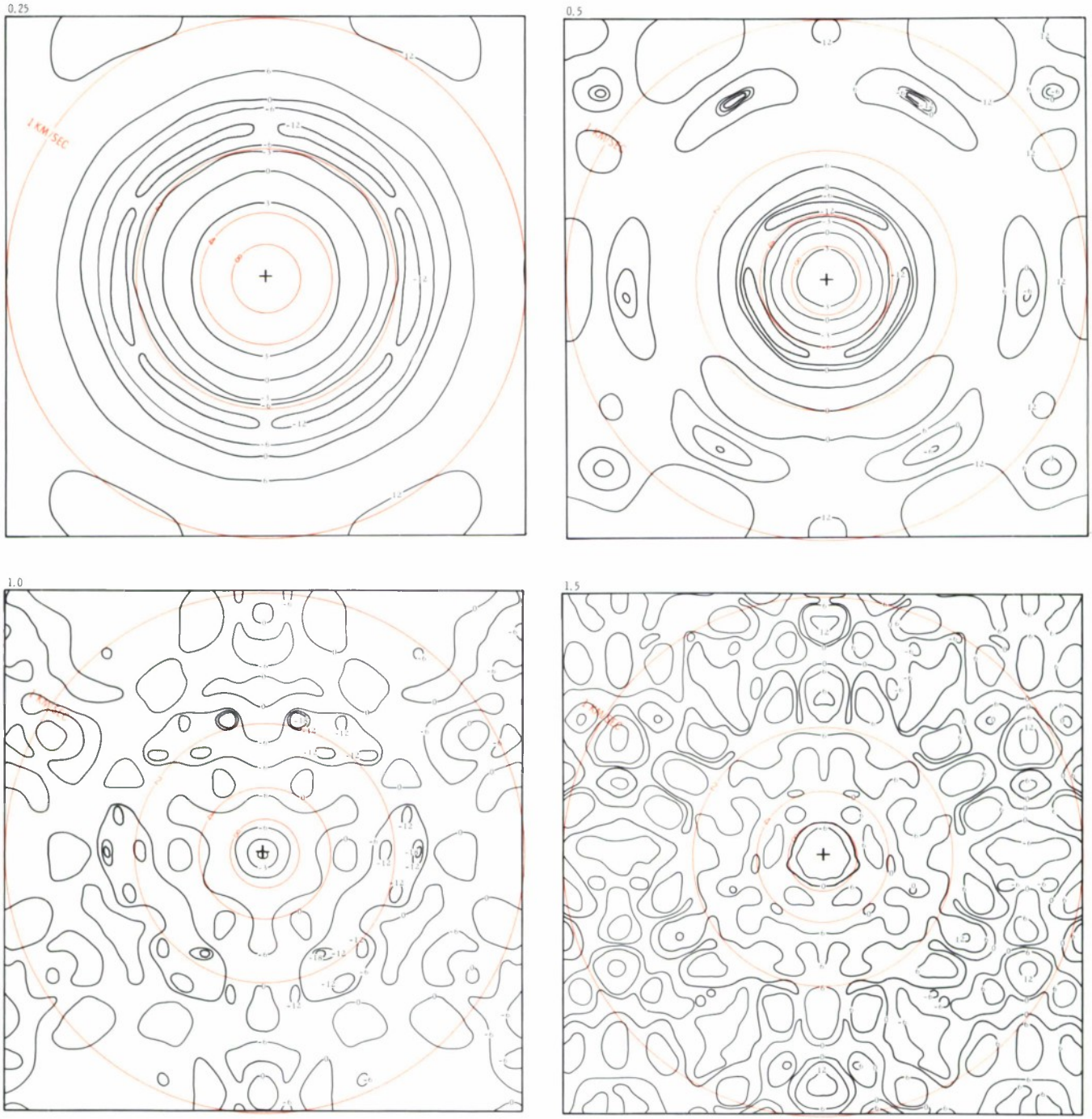

Figure IV-17. The f-$\vec{k}$ Responses of MCF-4

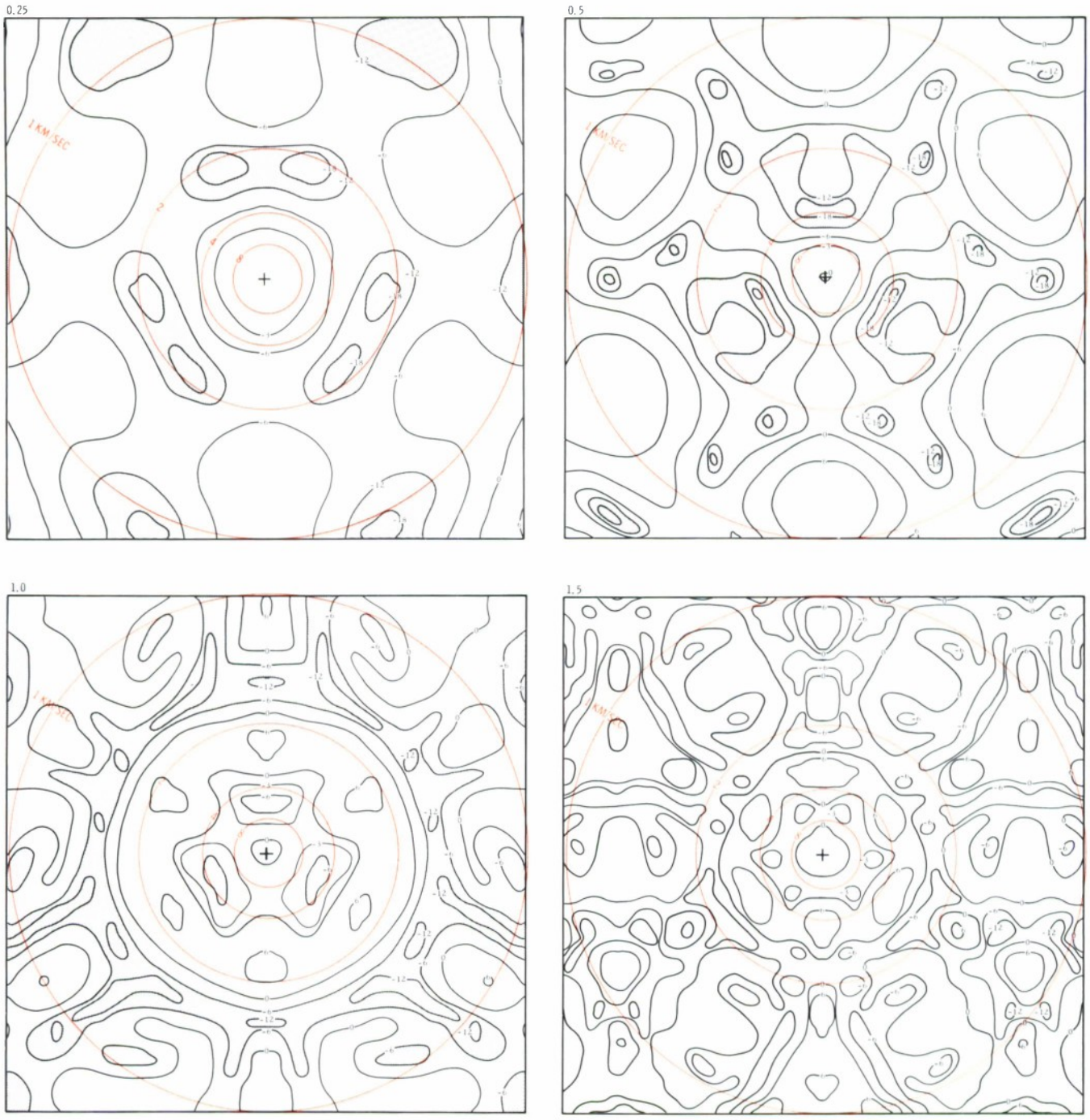

Figure IV-18. The f-$\vec{k}$ Responses of MCF-5

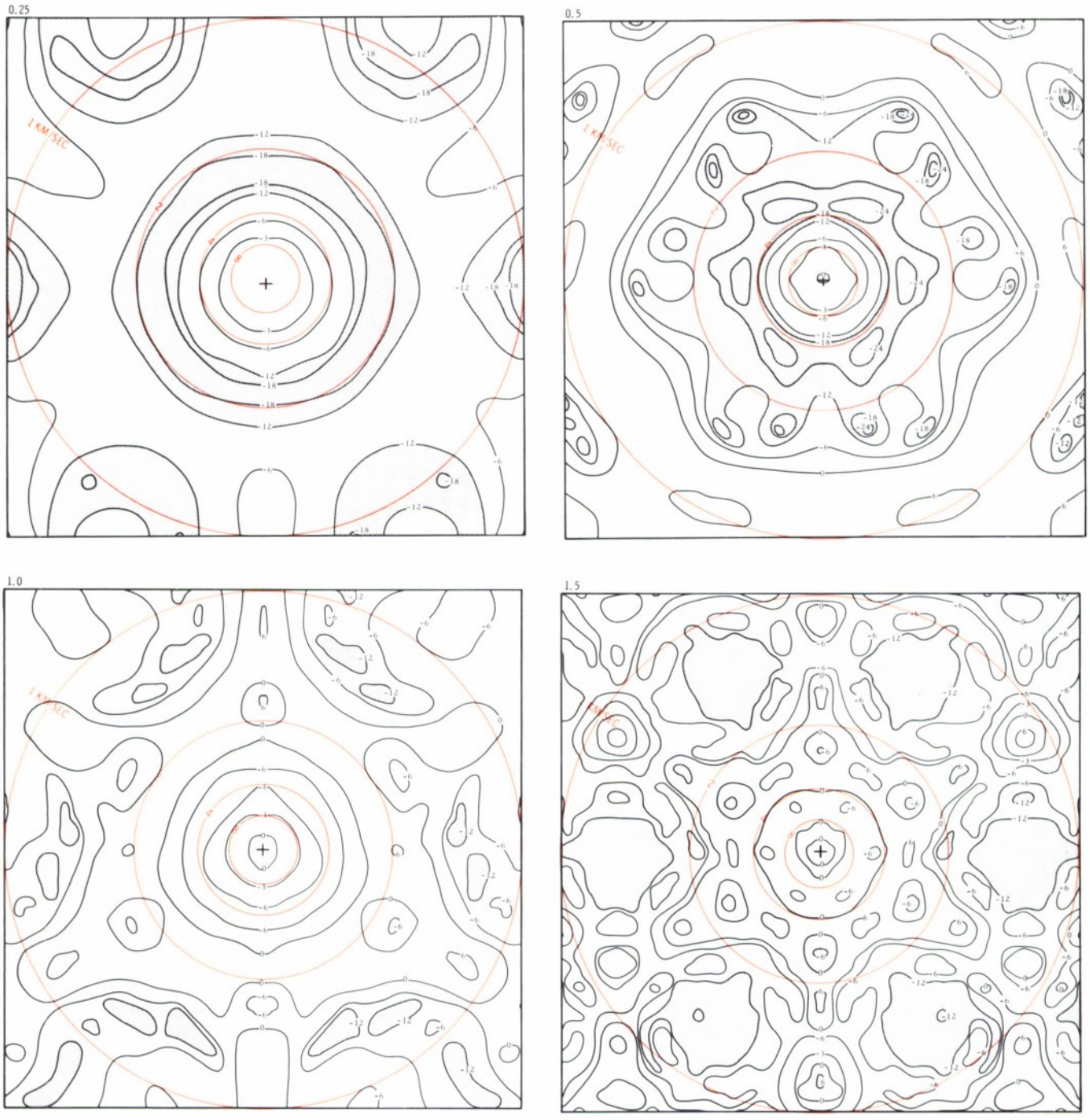

Figure IV-19. The f-$\vec{k}$ Responses of MCF-6

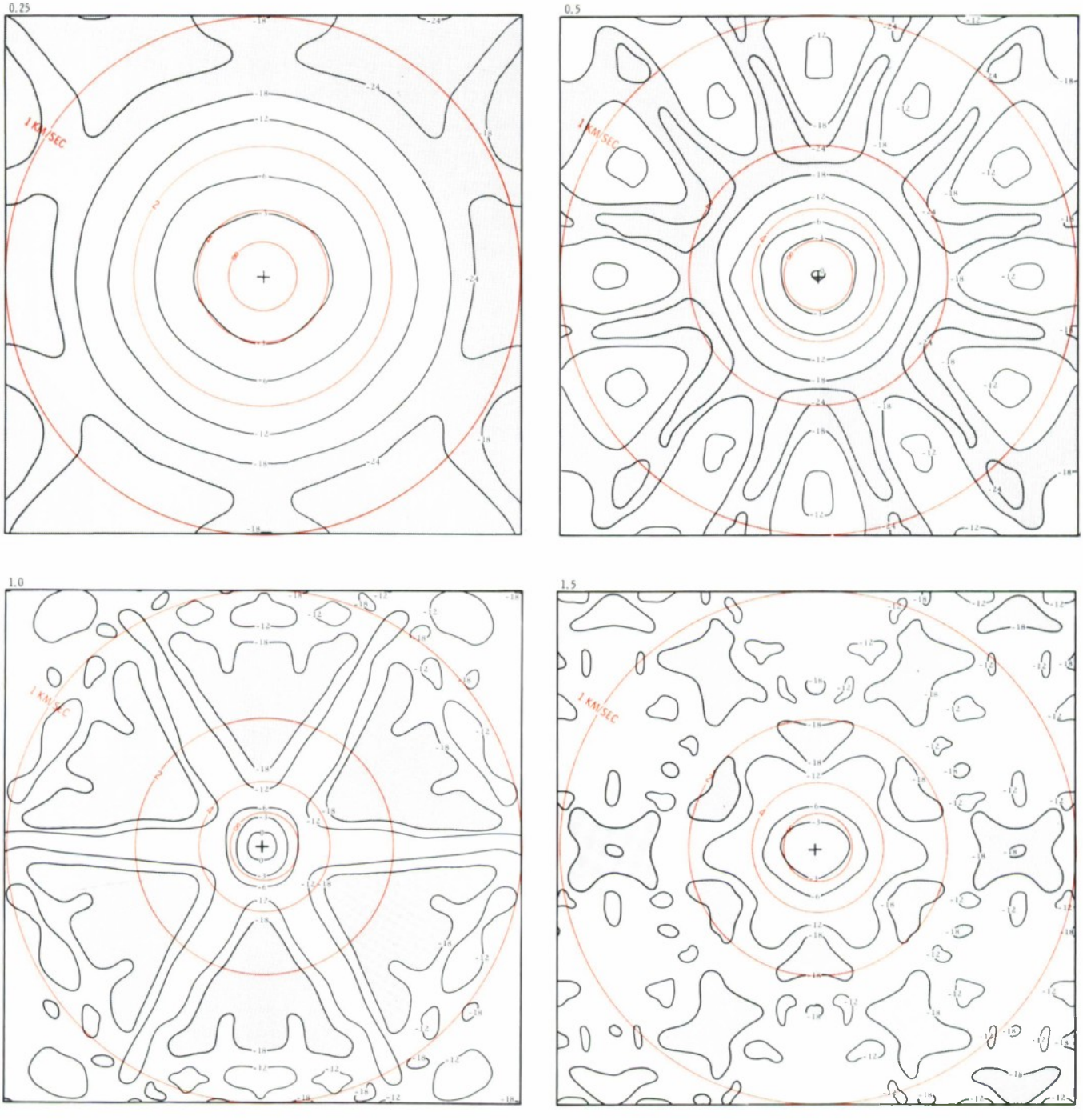

Figure IV-20. The f-$\vec{k}$ Responses of MCF-7

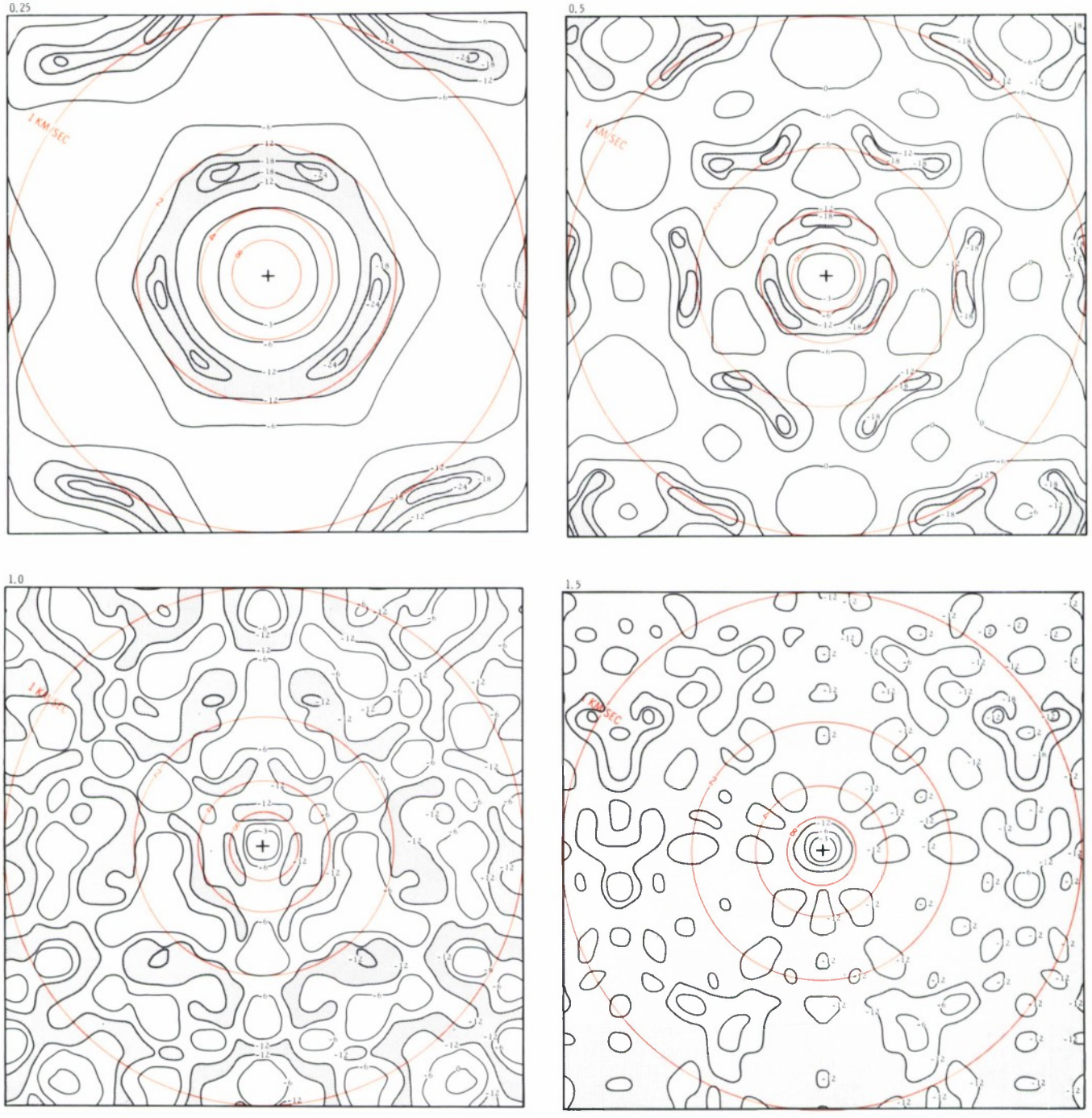

Figure IV-21. The f-$\vec{k}$ Responses of MCF-8

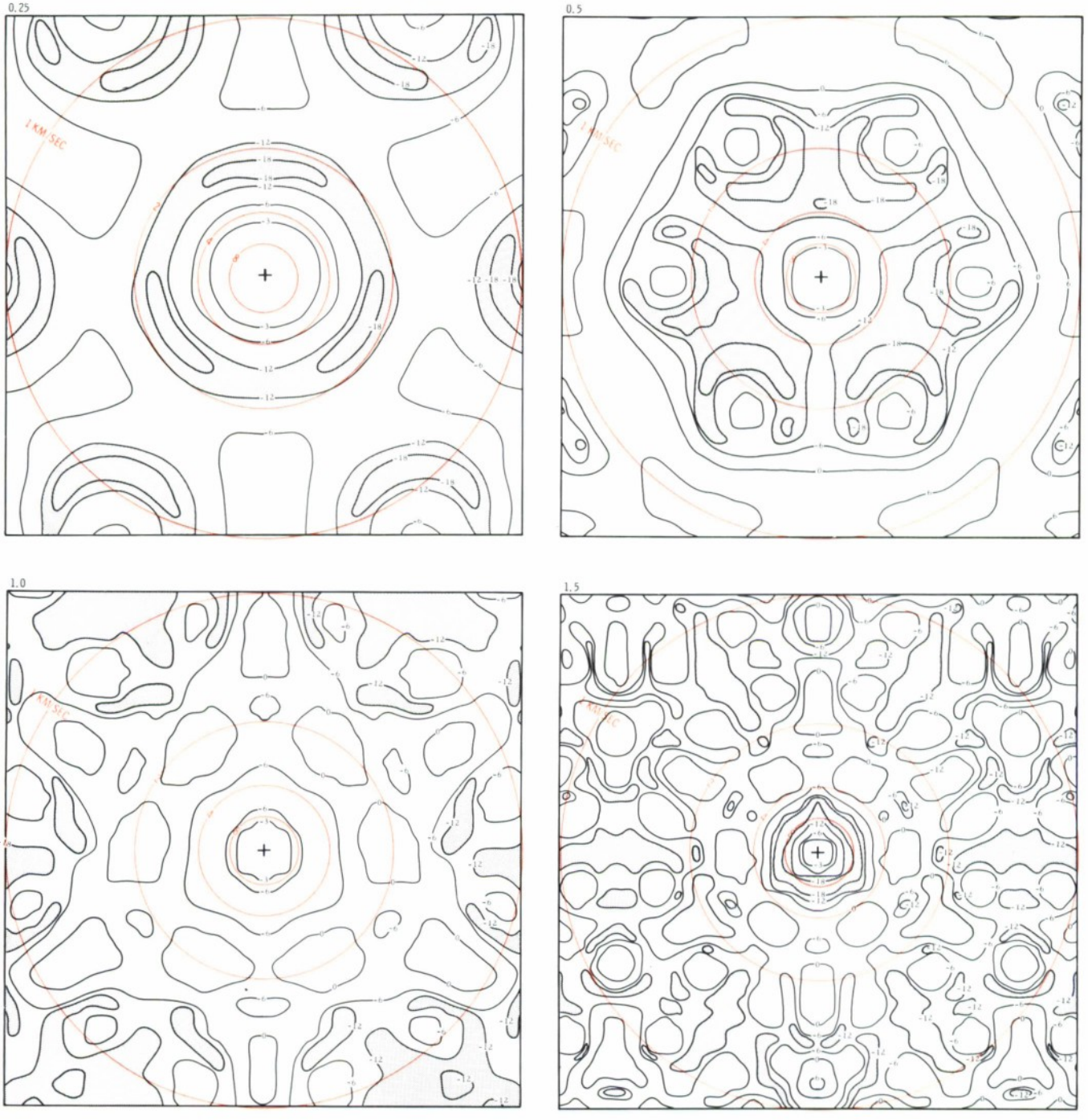

Figure IV-22. The f-$\vec{k}$ Responses of MCF-9

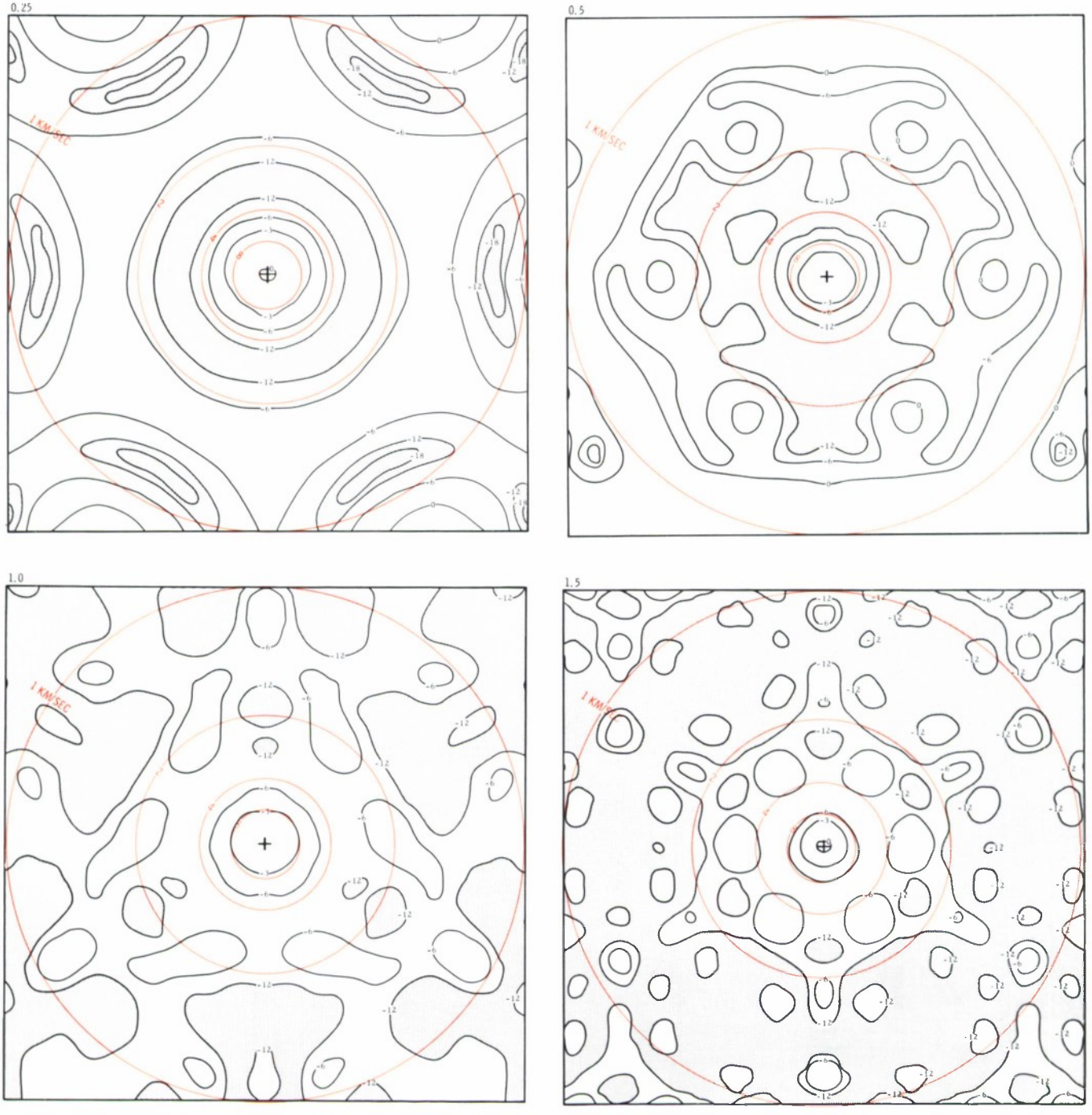

Figure IV-23. The f-$\vec{k}$ Responses of MCF-10

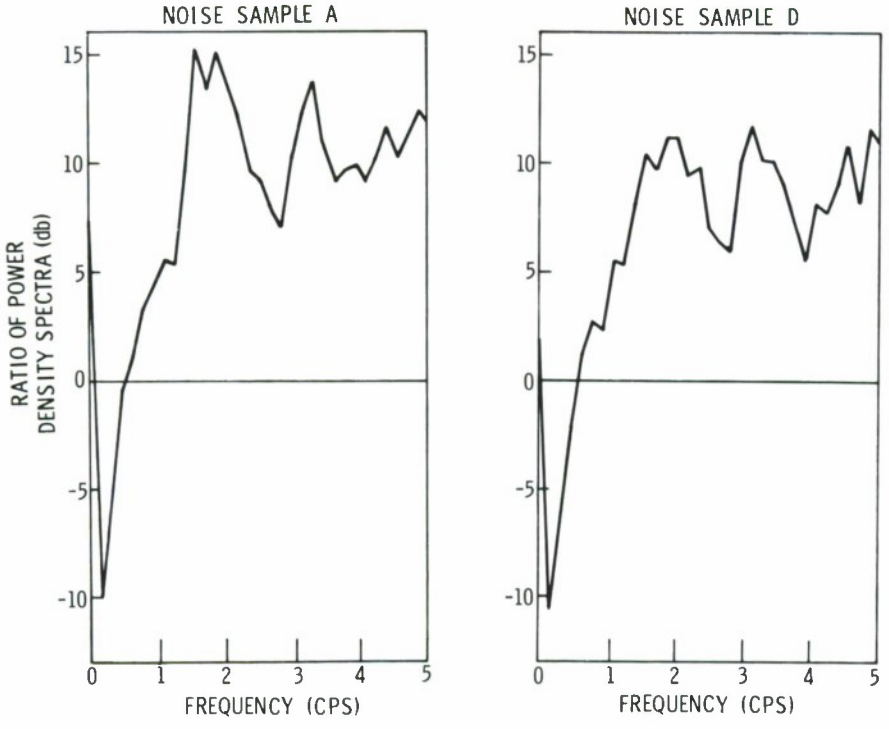

Figure IV-24. MCF-3 Output/Straight Sum

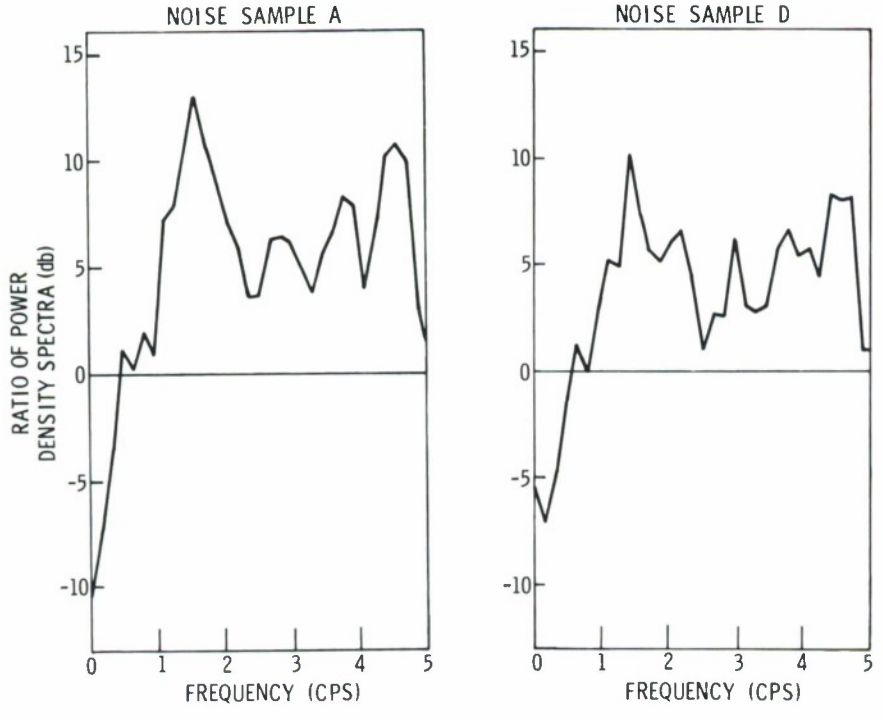

Figure IV-25. MCF-4 Output/Straight Sum

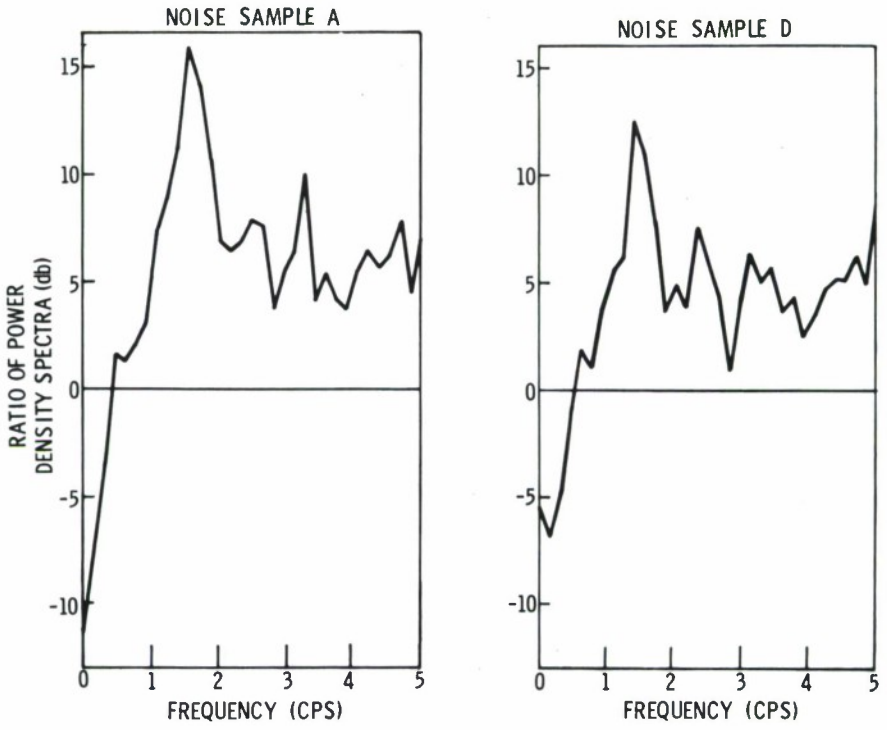

Figure IV-26. MCF-5 Output/Straight Sum

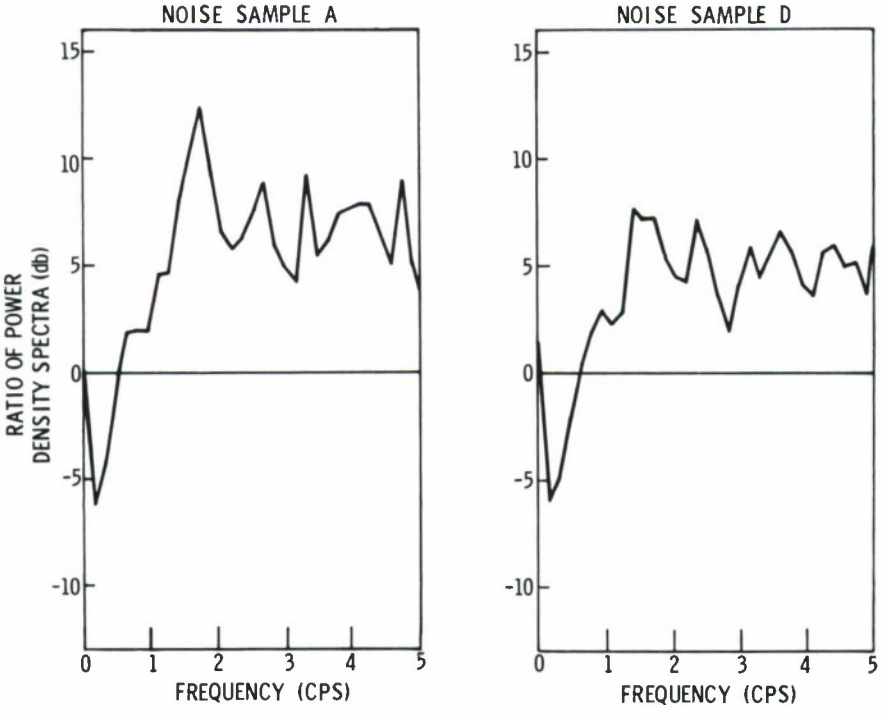

Figure IV-27. MCF-6 Output/Straight Sum

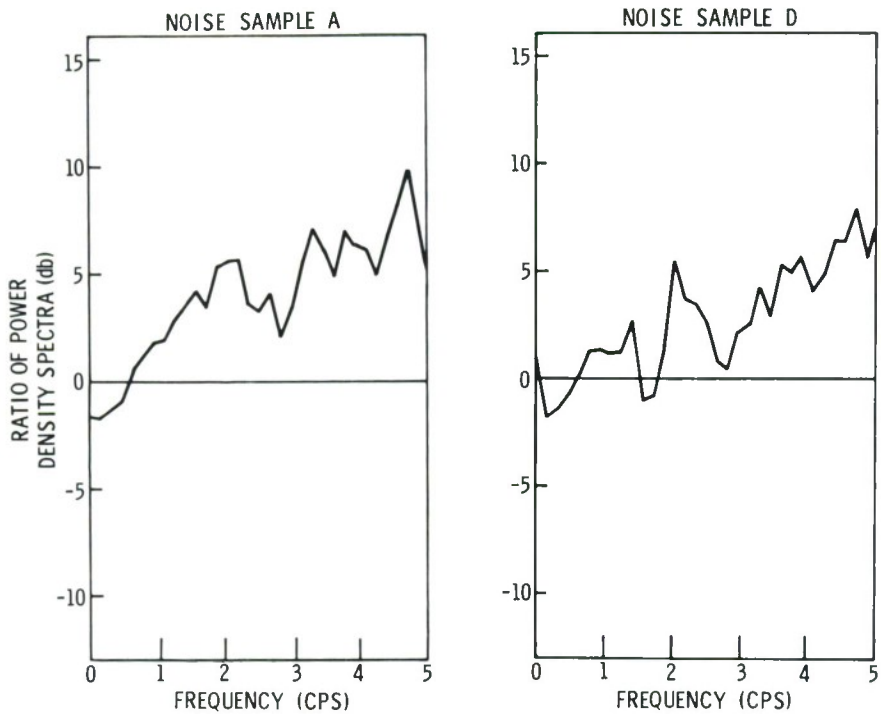

Figure IV-28. MCF-7 Output/Straight Sum

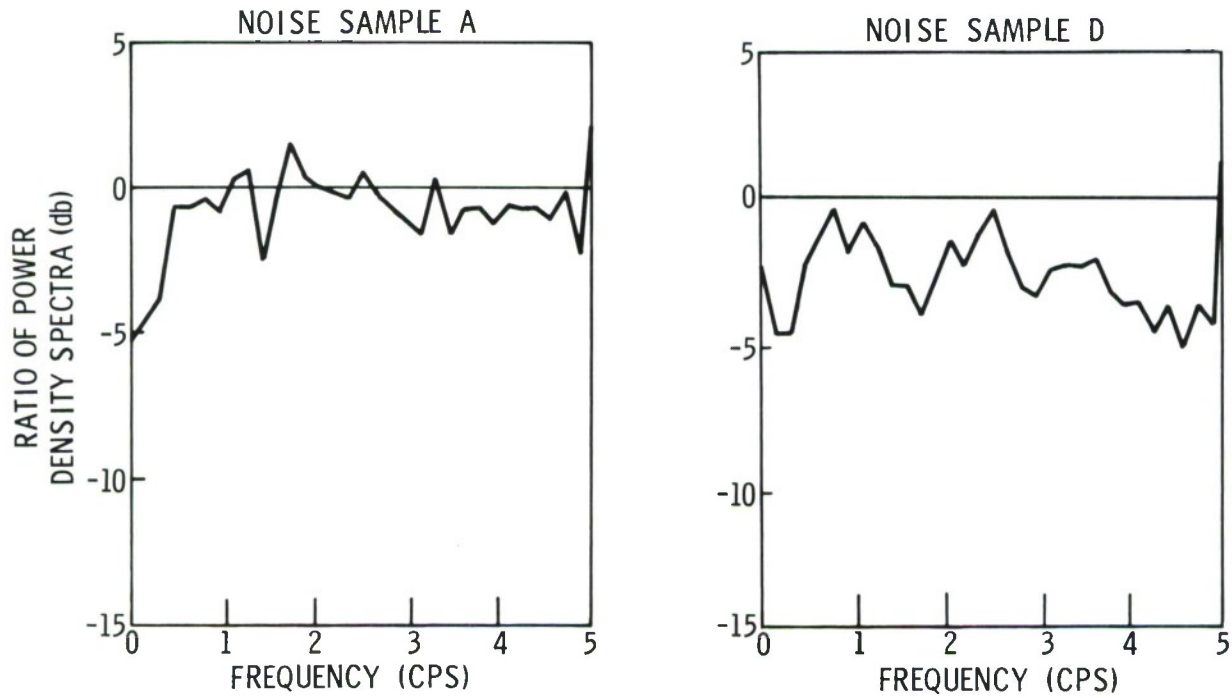

Figure IV-29. MCF-8 Output/Straight Sum

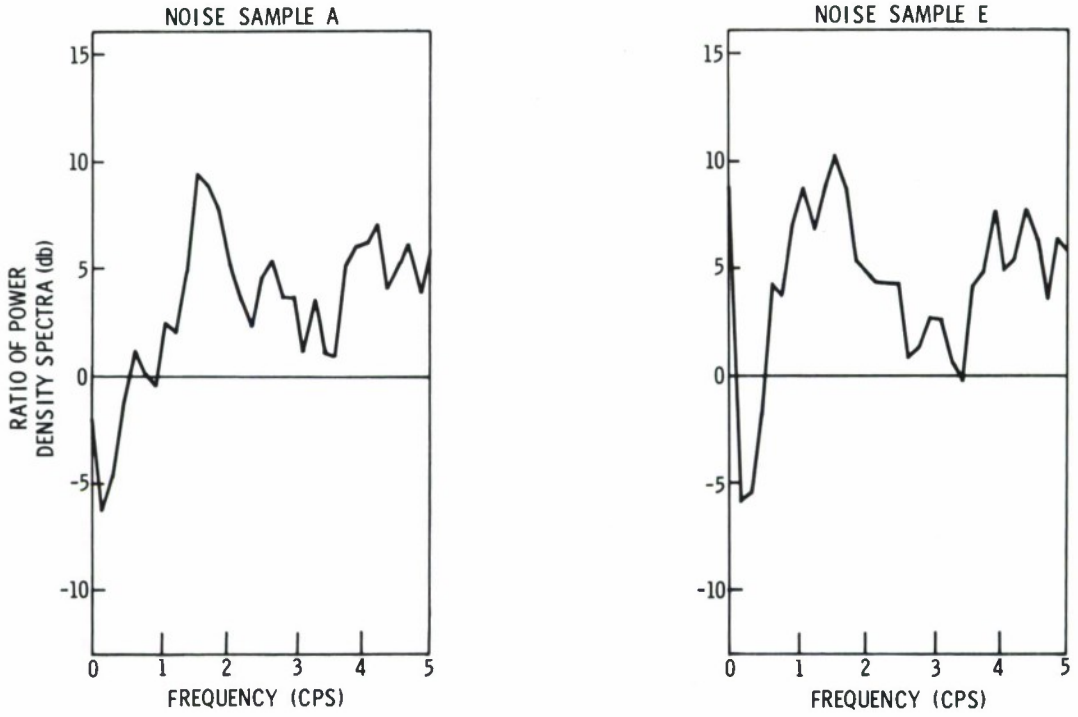

Figure IV-30. MCF-9 Output/Straight Sum

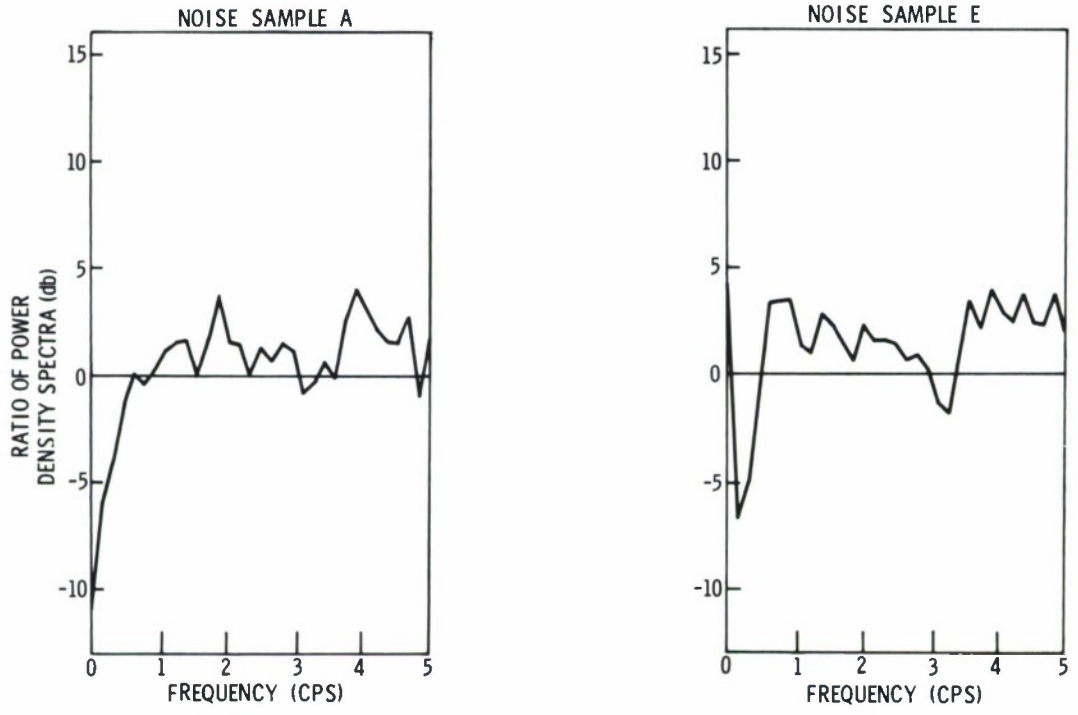

Figure IV-31. MCF-10 Output/Straight Sum

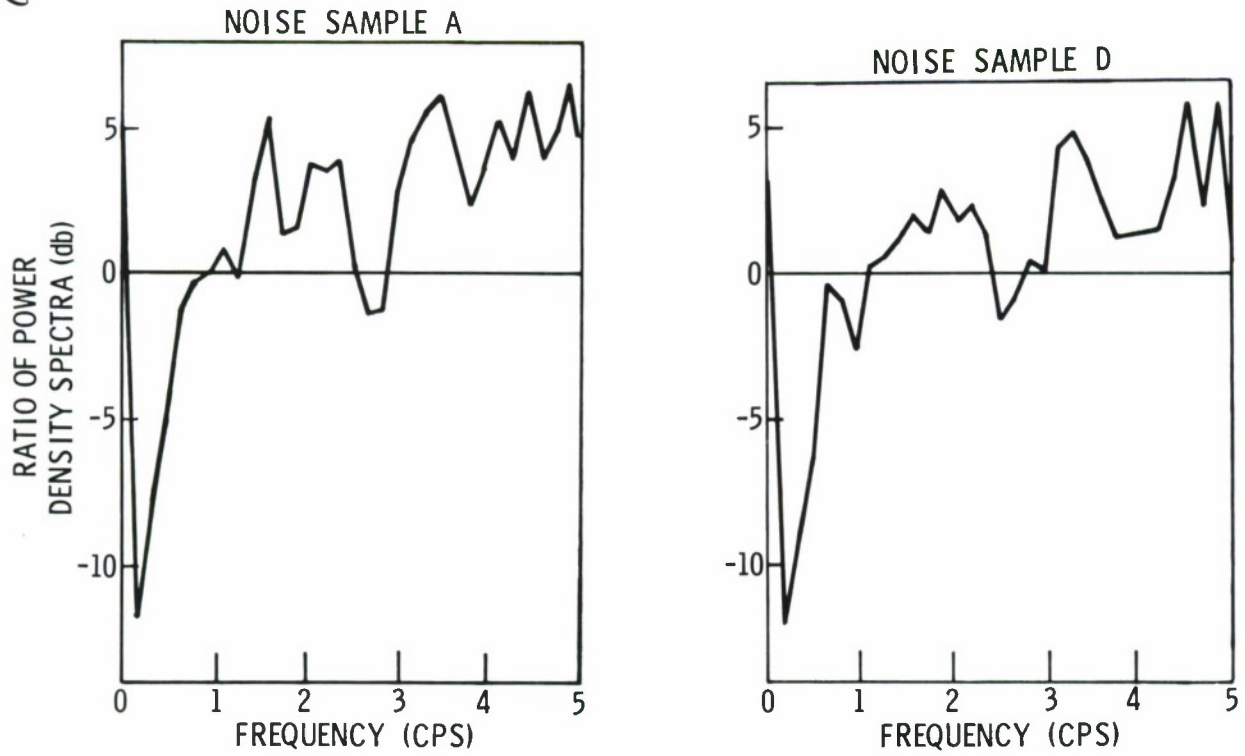

Figure IV-32. MCF-3 Output/CC

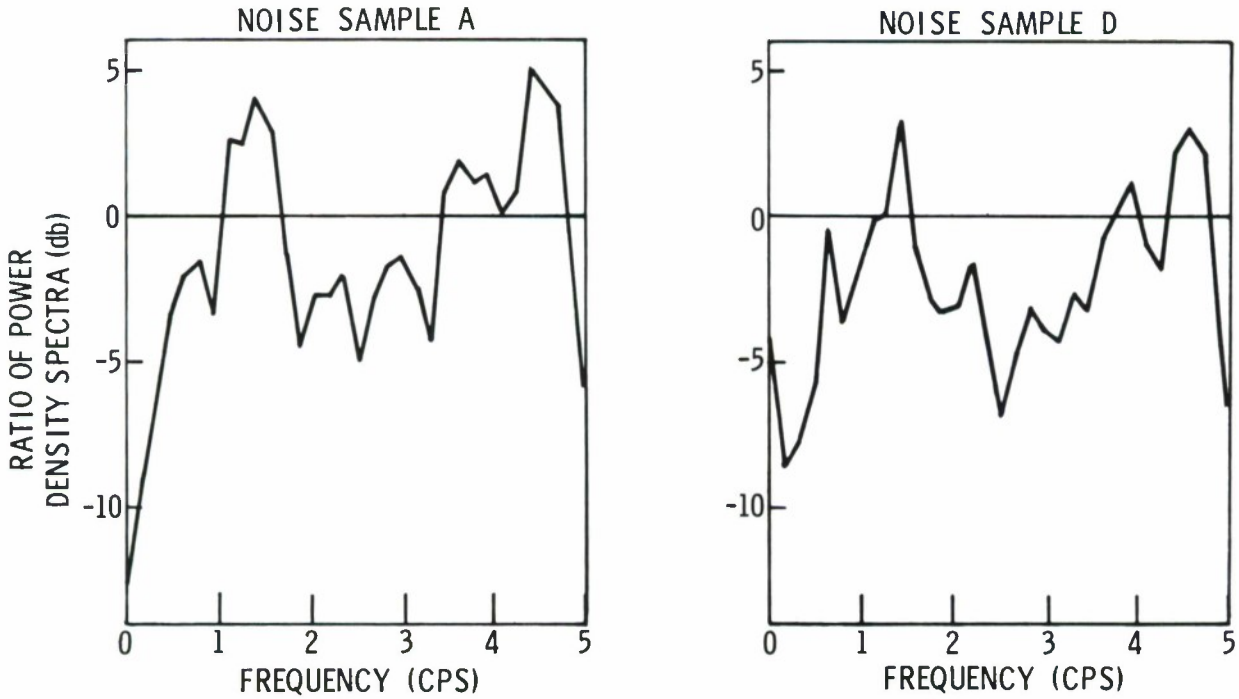

Figure IV-33. MCF-4 Output/CC

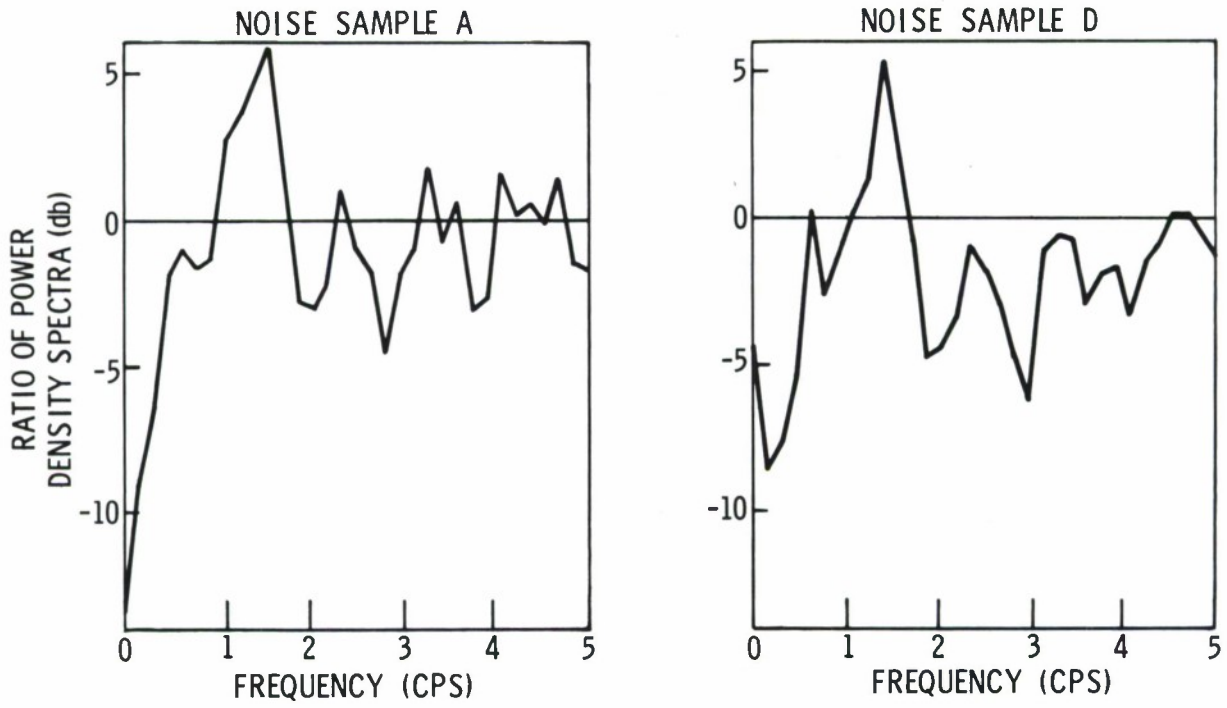

Figure IV-34. MCF-5 Output/CC

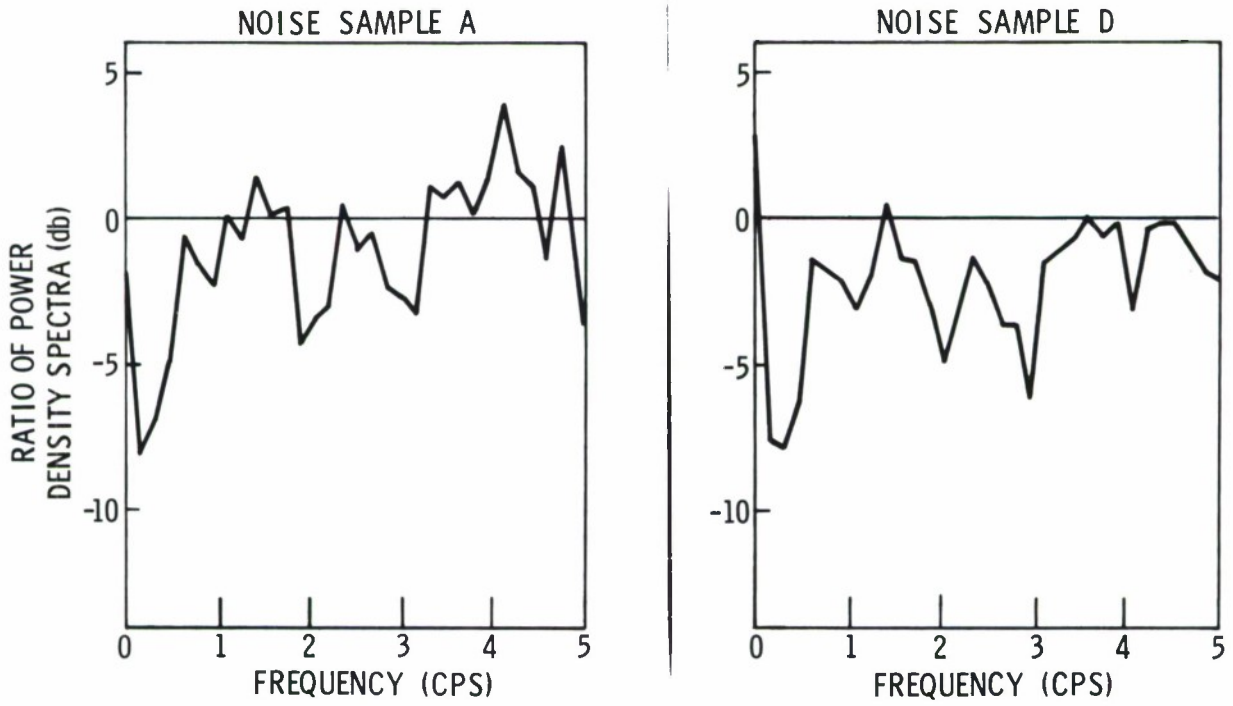

Figure IV-35. MCF-6 Output/CC

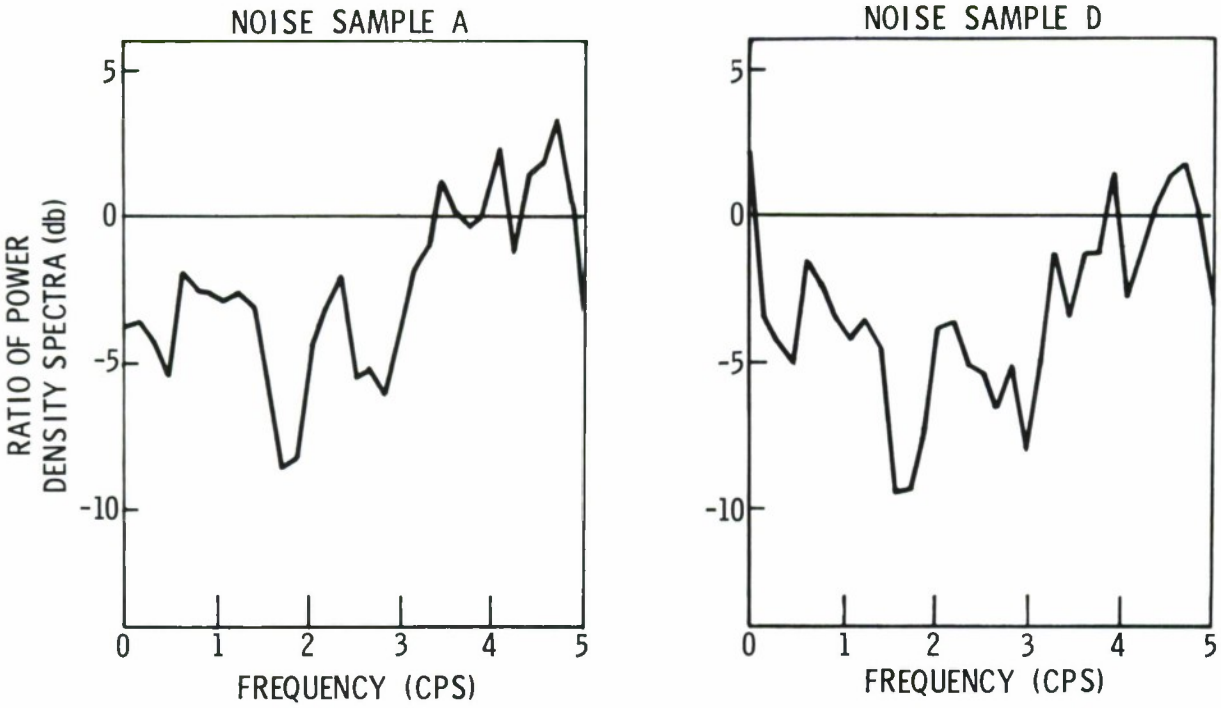

Figure IV-36. MCF-7 Output/CC

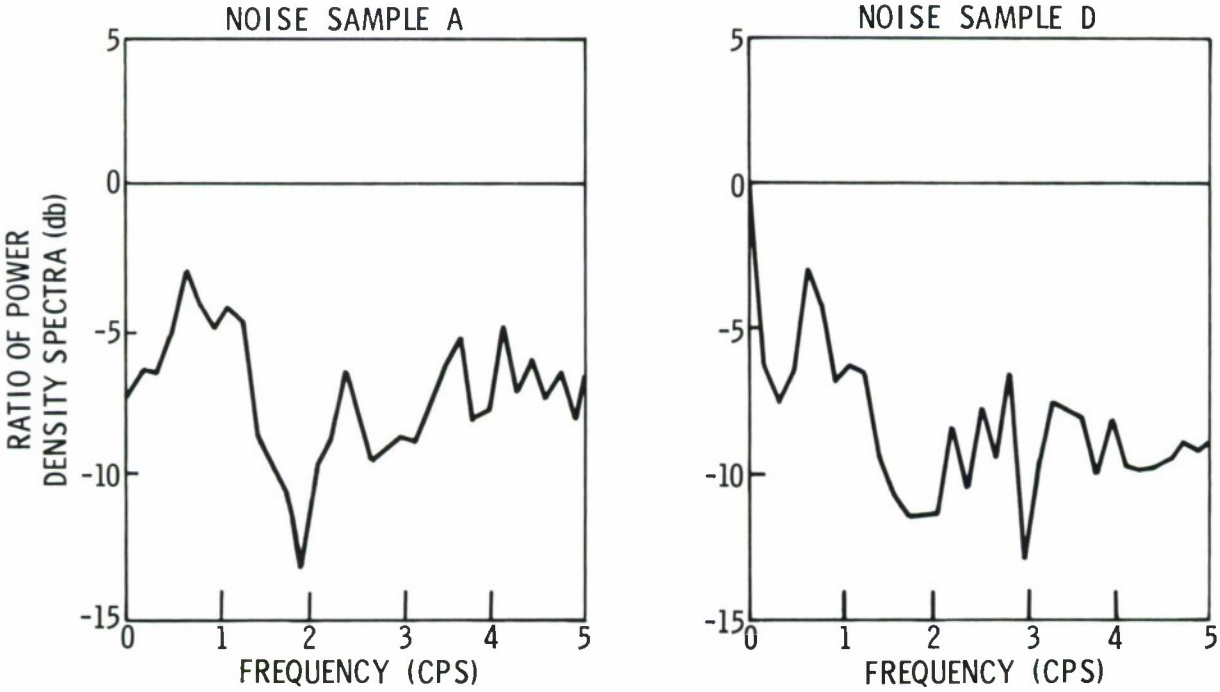

Figure IV-37. MCF-8 Output/CC

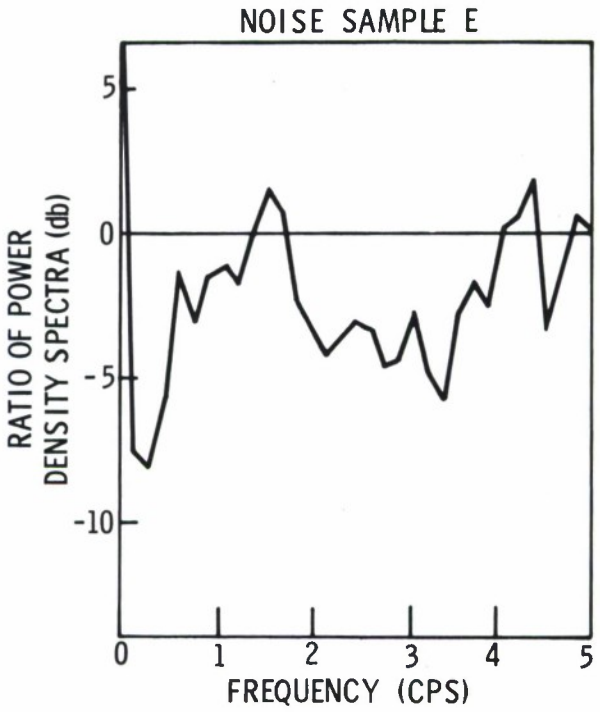

Figure IV-38. MCF-9 Output/CC

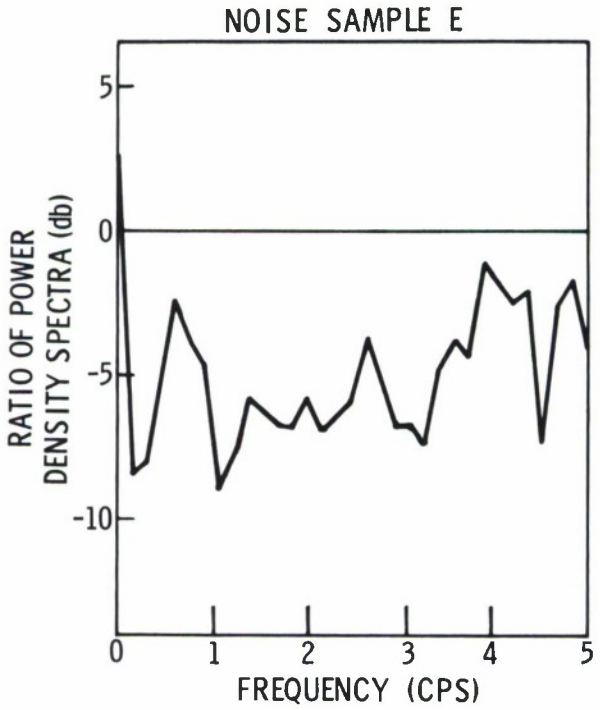

Figure IV-39. MCF-10 Output/CC

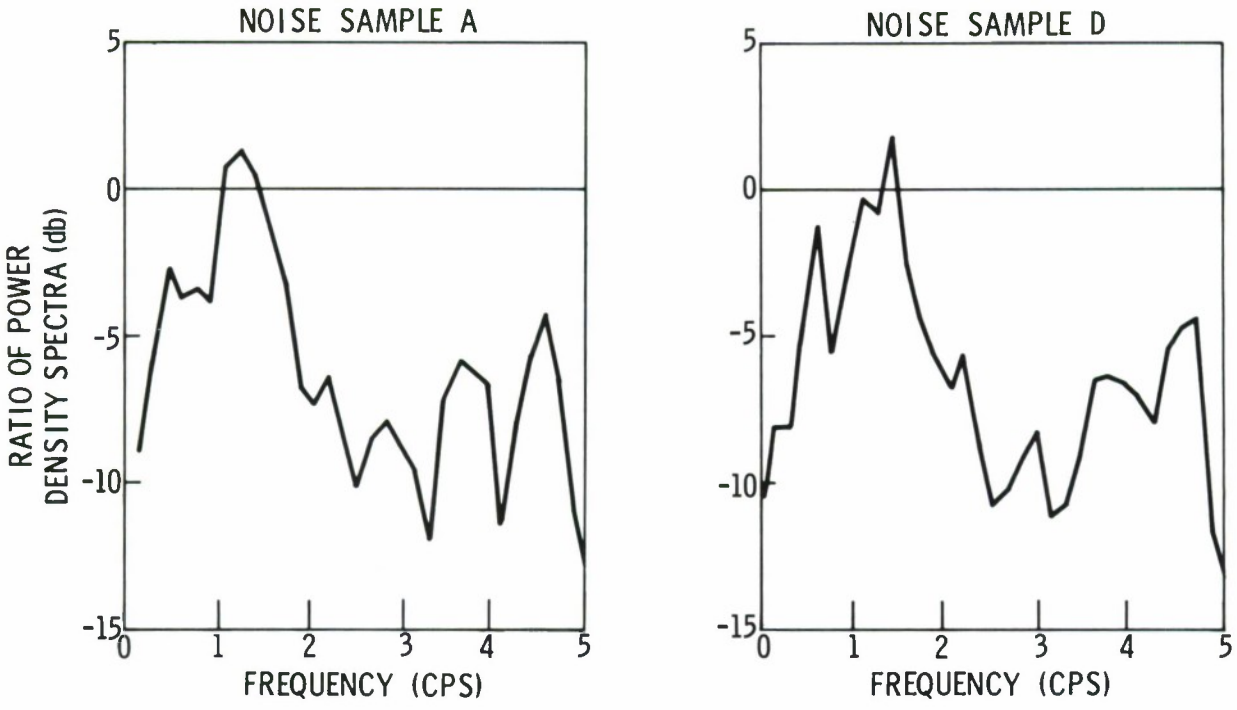

Figure IV-40. MCF-4 Output/Avg

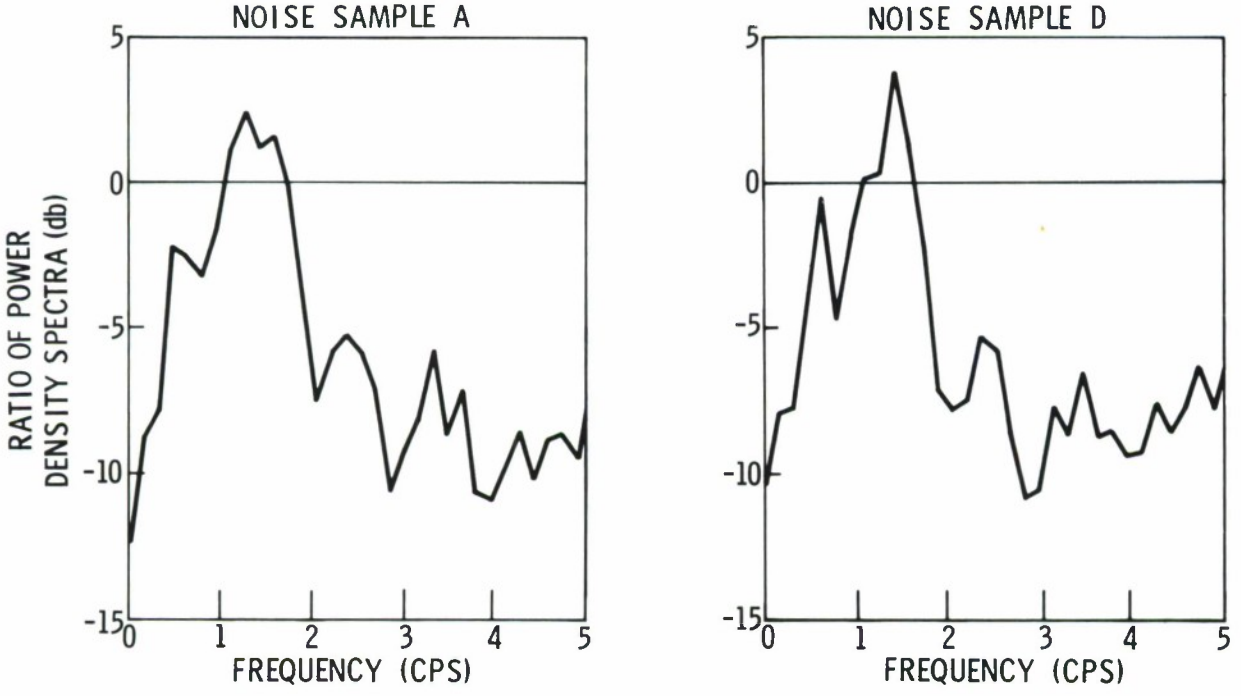

Figure IV-41. MCF-5 Output/Avg

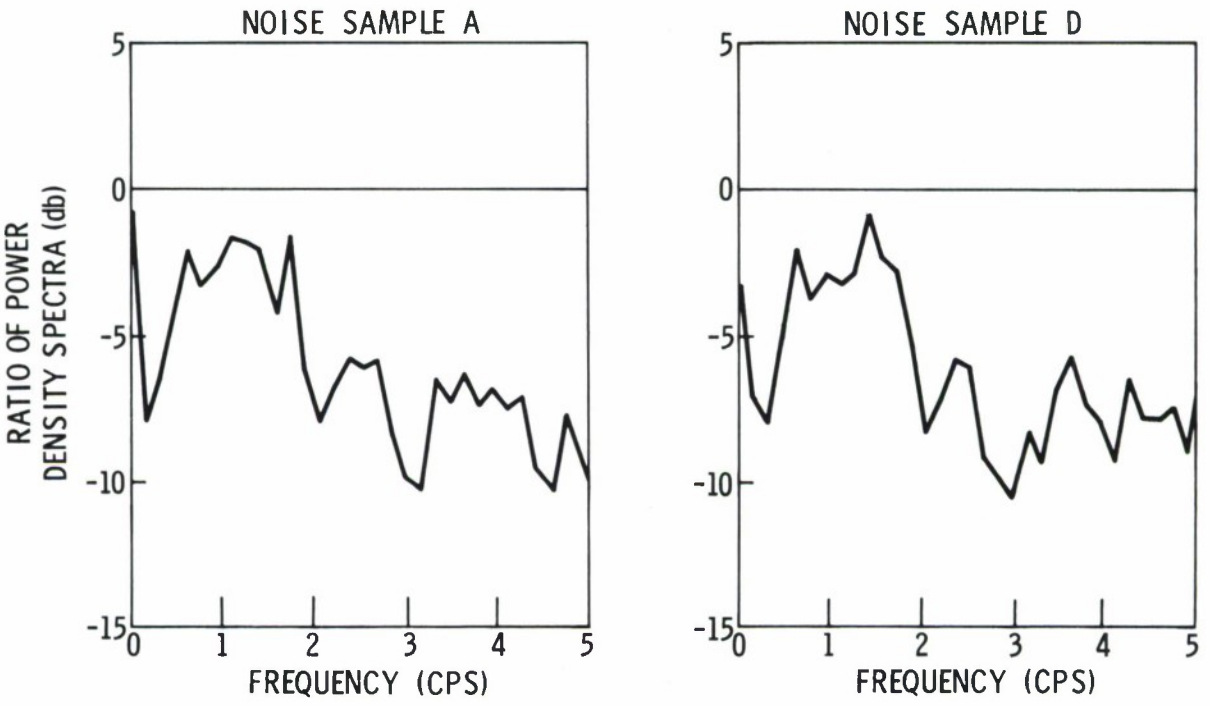

Figure IV-42. MCF-6 Output/Avg

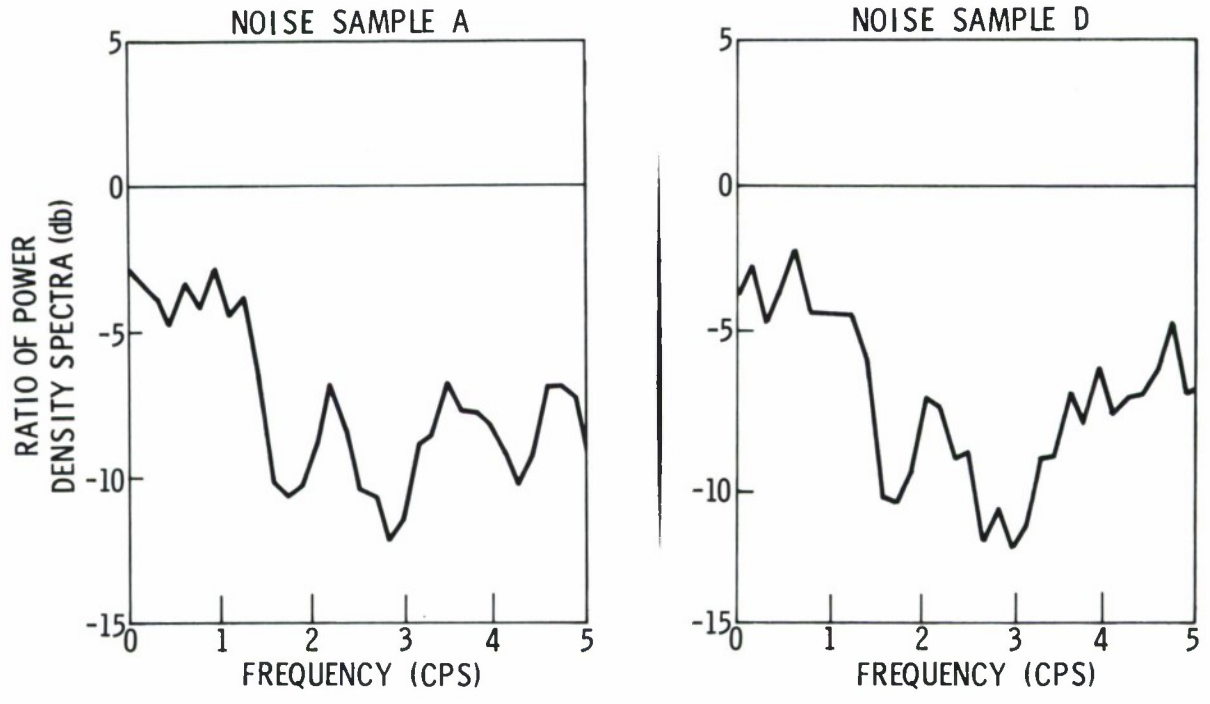

Figure IV-43. MCF-7 Output/Avg

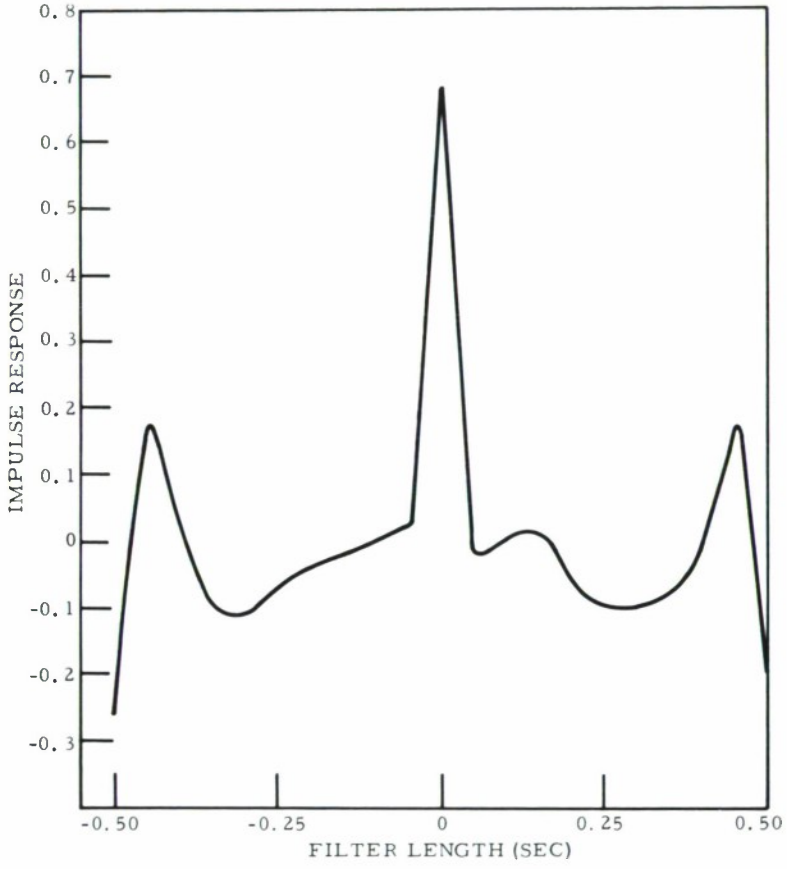

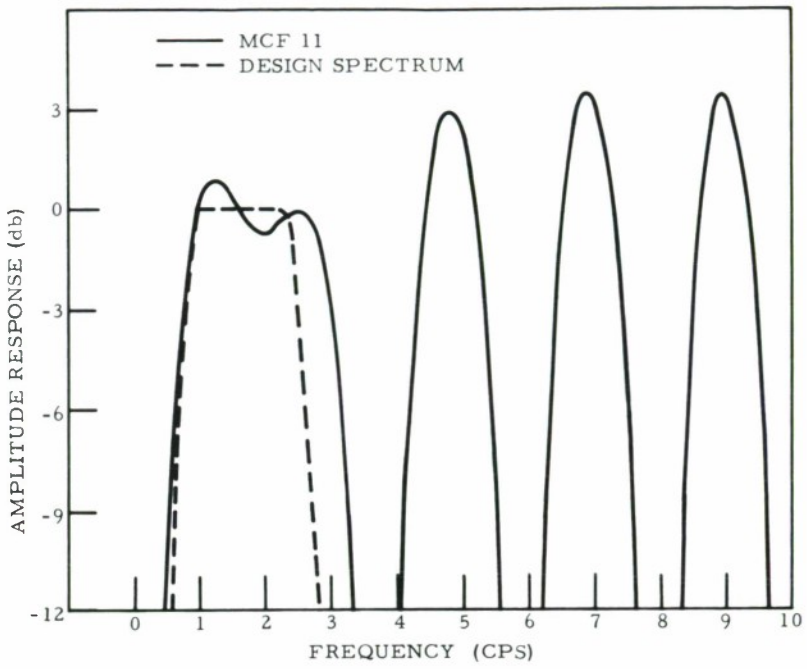

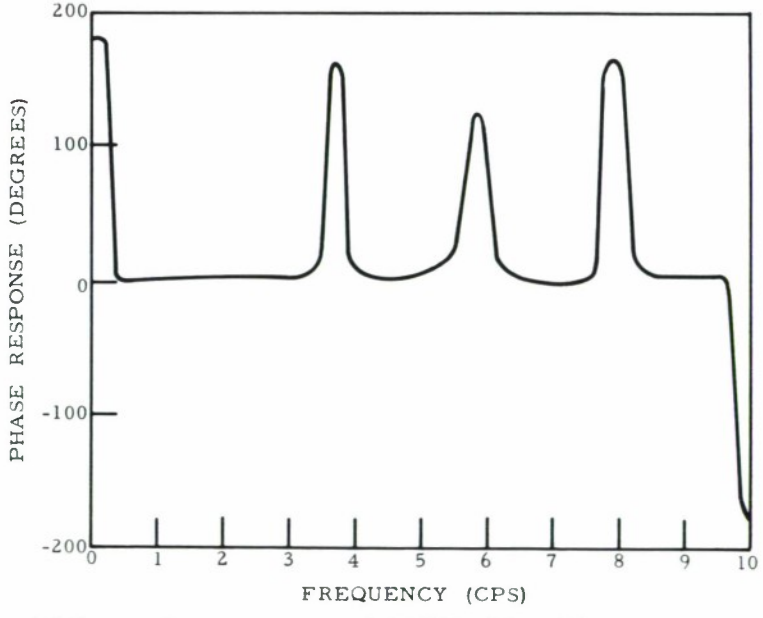

Figure IV-44. Impulse, Amplitude and Phase Responses of MCF-11 with Theoretical Frequency-Domain Shaping Function

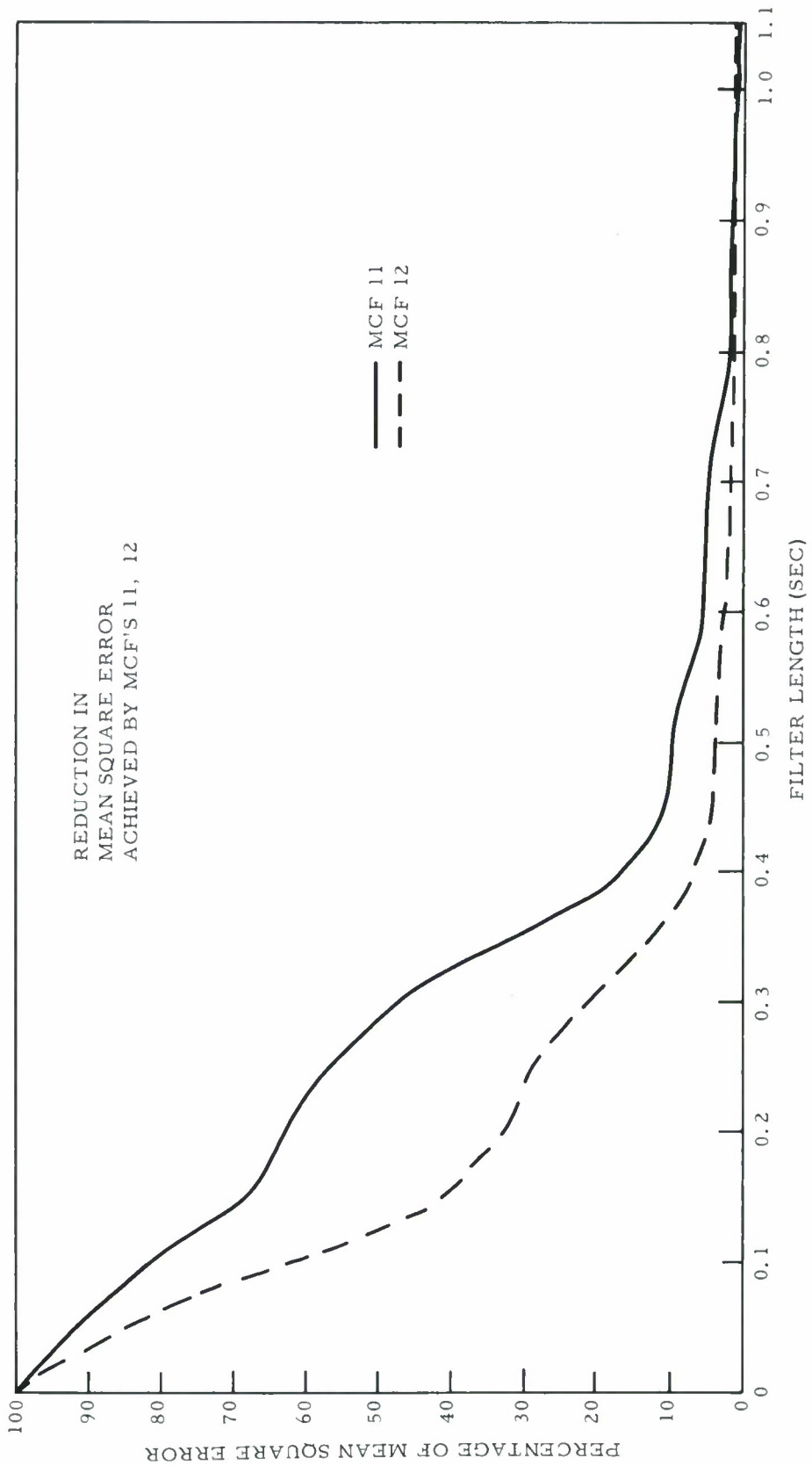

Figure IV-45. Percentage Mean-Square-Error As A Function of Filter Length for the Design of MCF-11,-12

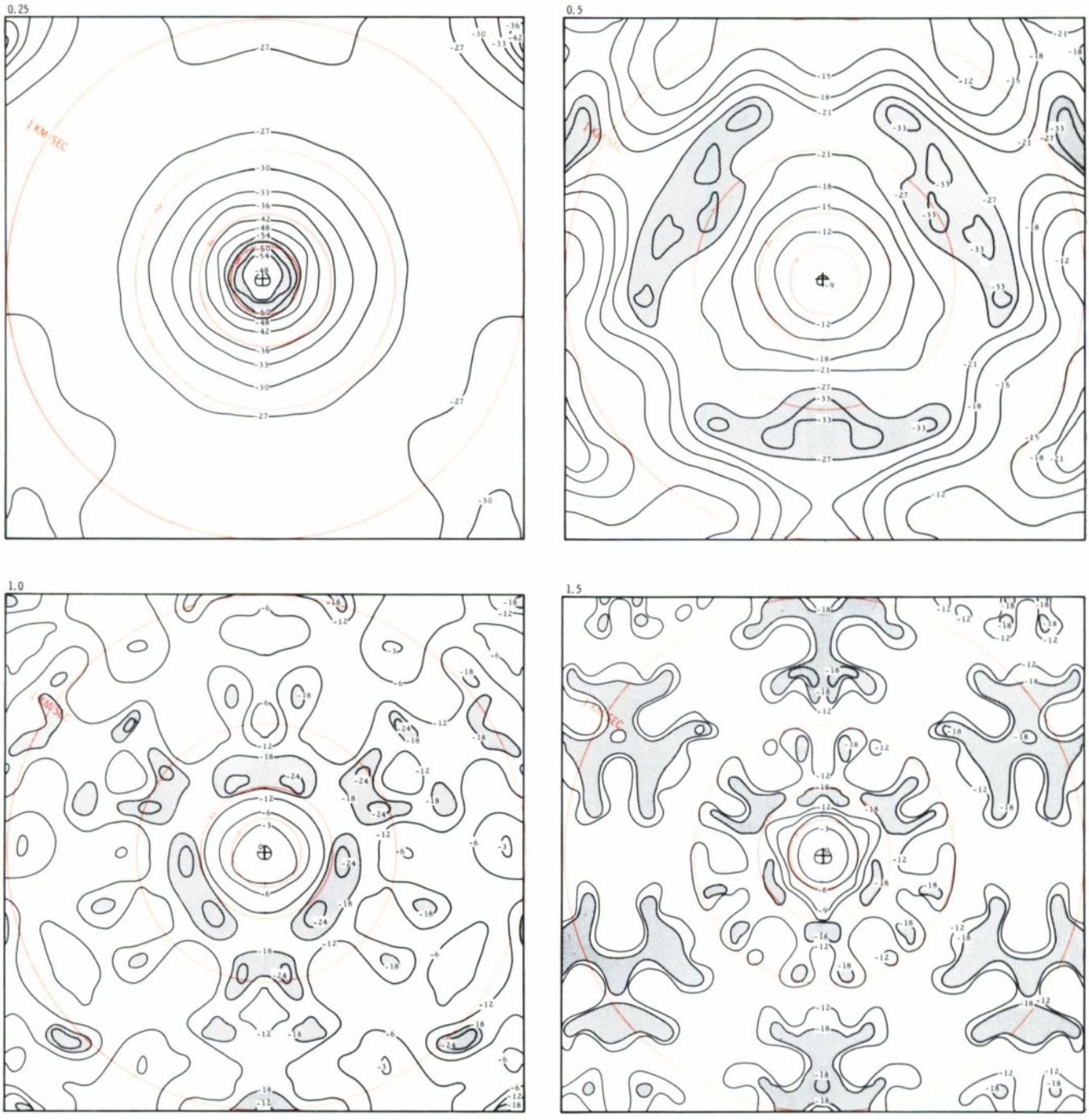

Figure IV-46. Frequency-Wavenumber Responses of MCF-11; f= 0.25, 0.50, 1.00, and 1,50 cps

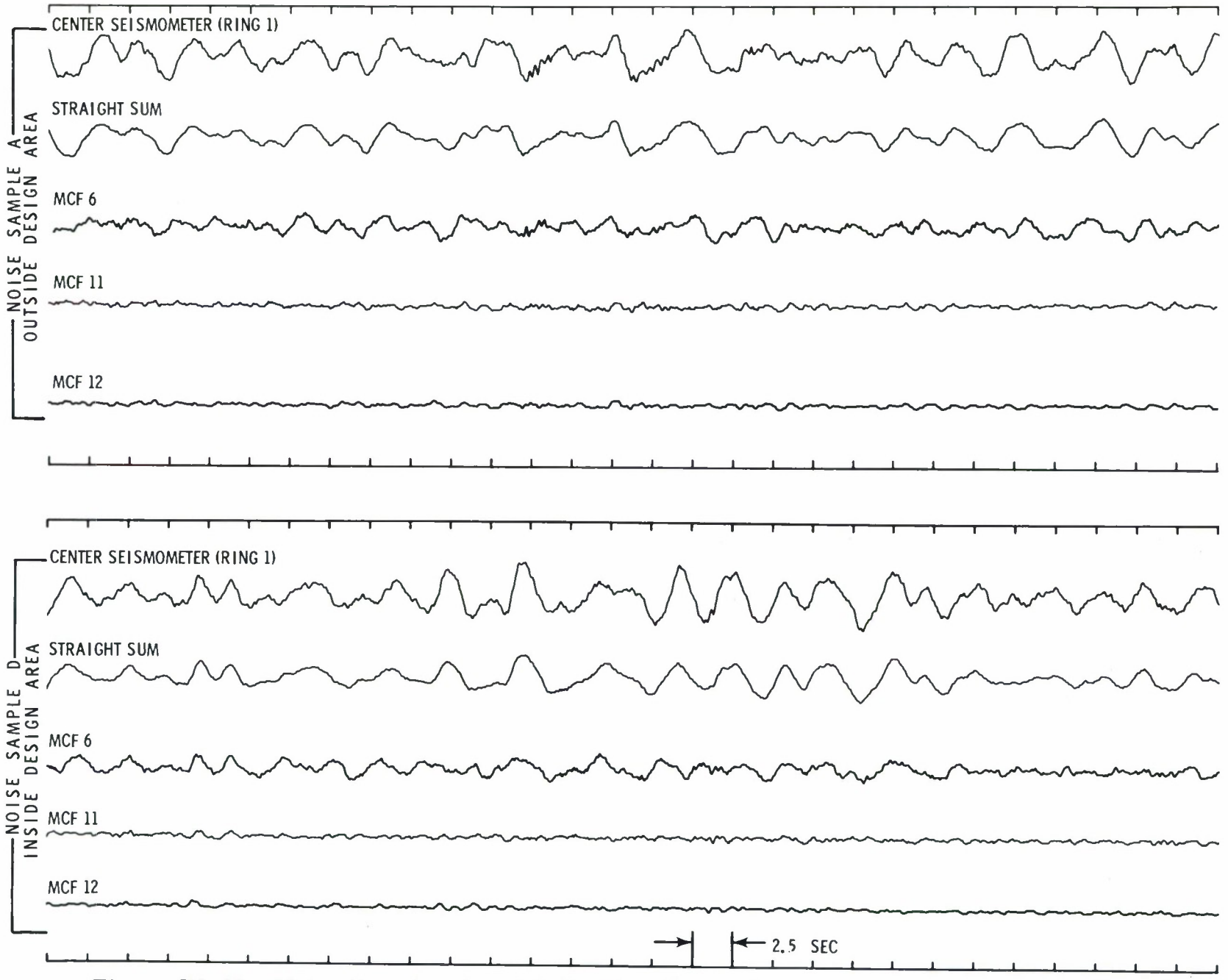

Figure IV-47. Noise Samples A and D Showing Center Seismometer, Straight Sum Output and MCF-6, -11 and -12 Outputs

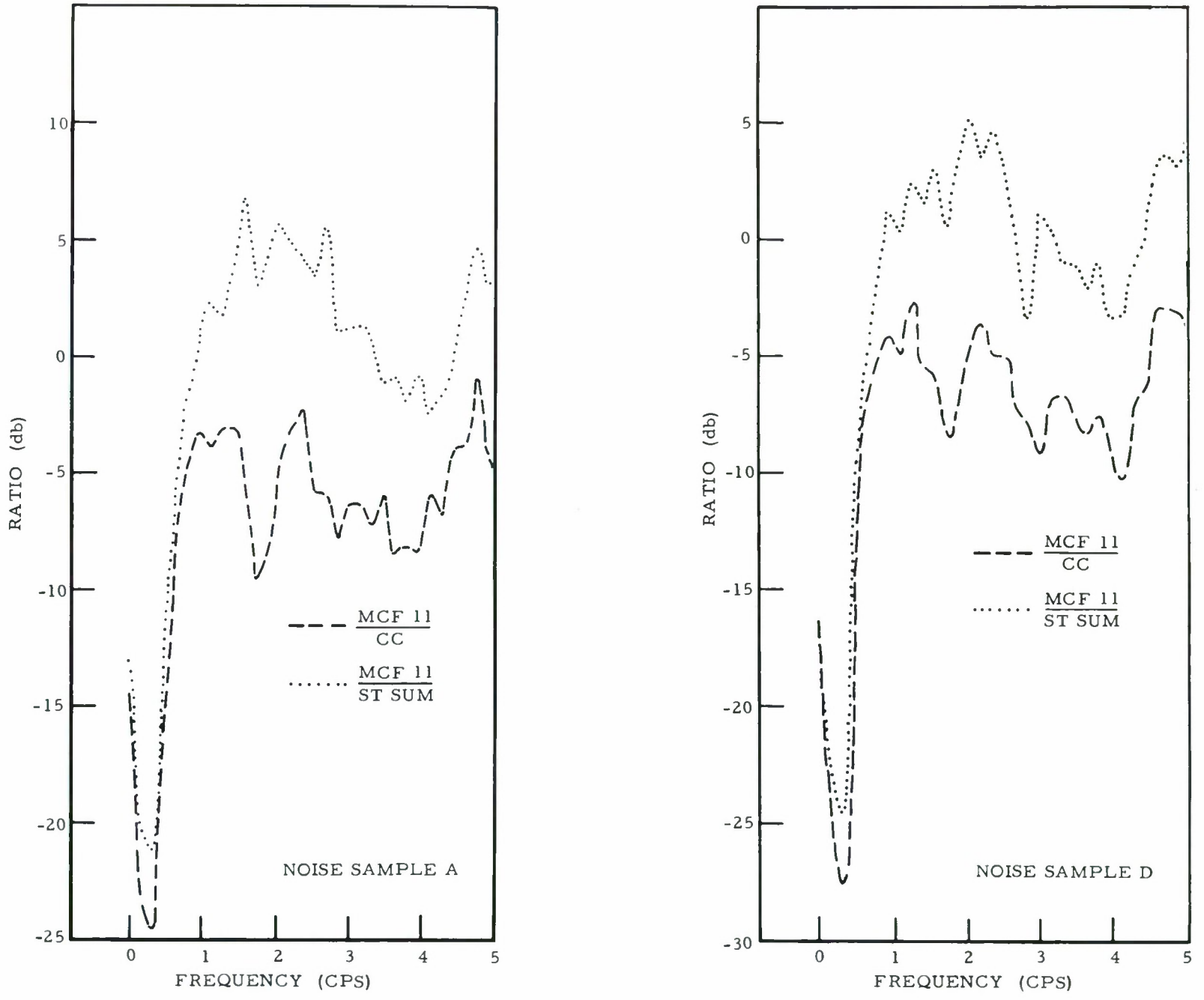

Figure IV-48. Noise Attenuation as a Ratio of Power Density Spectra; MCF-11 Output to Center Seismometer and to Straight Sum Output (Noise Samples A and D)

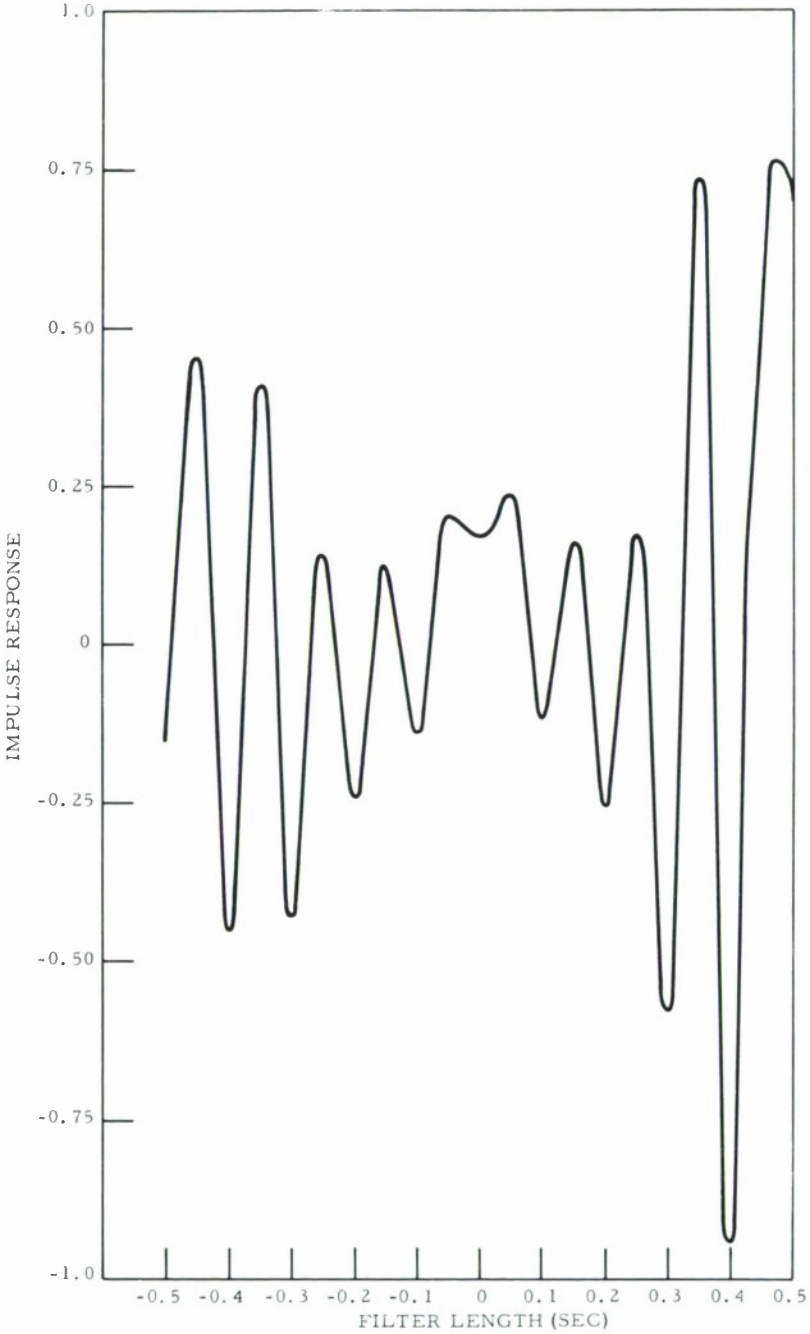

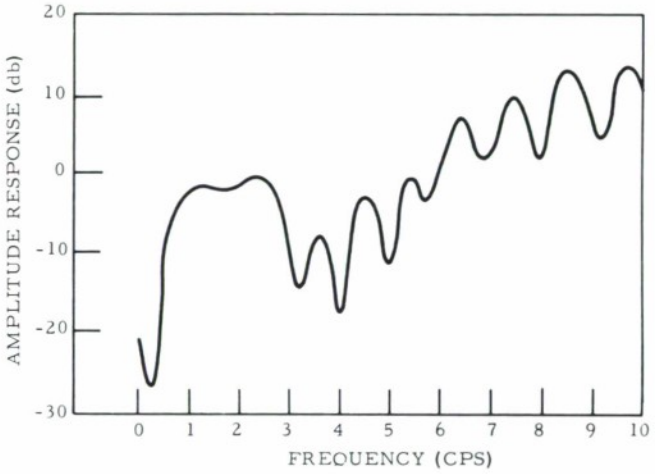

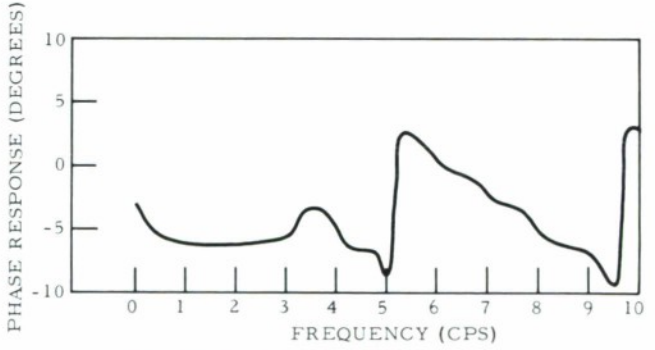

Figure IV-49. Impulse, Amplitude and Phase Response of MCF-12

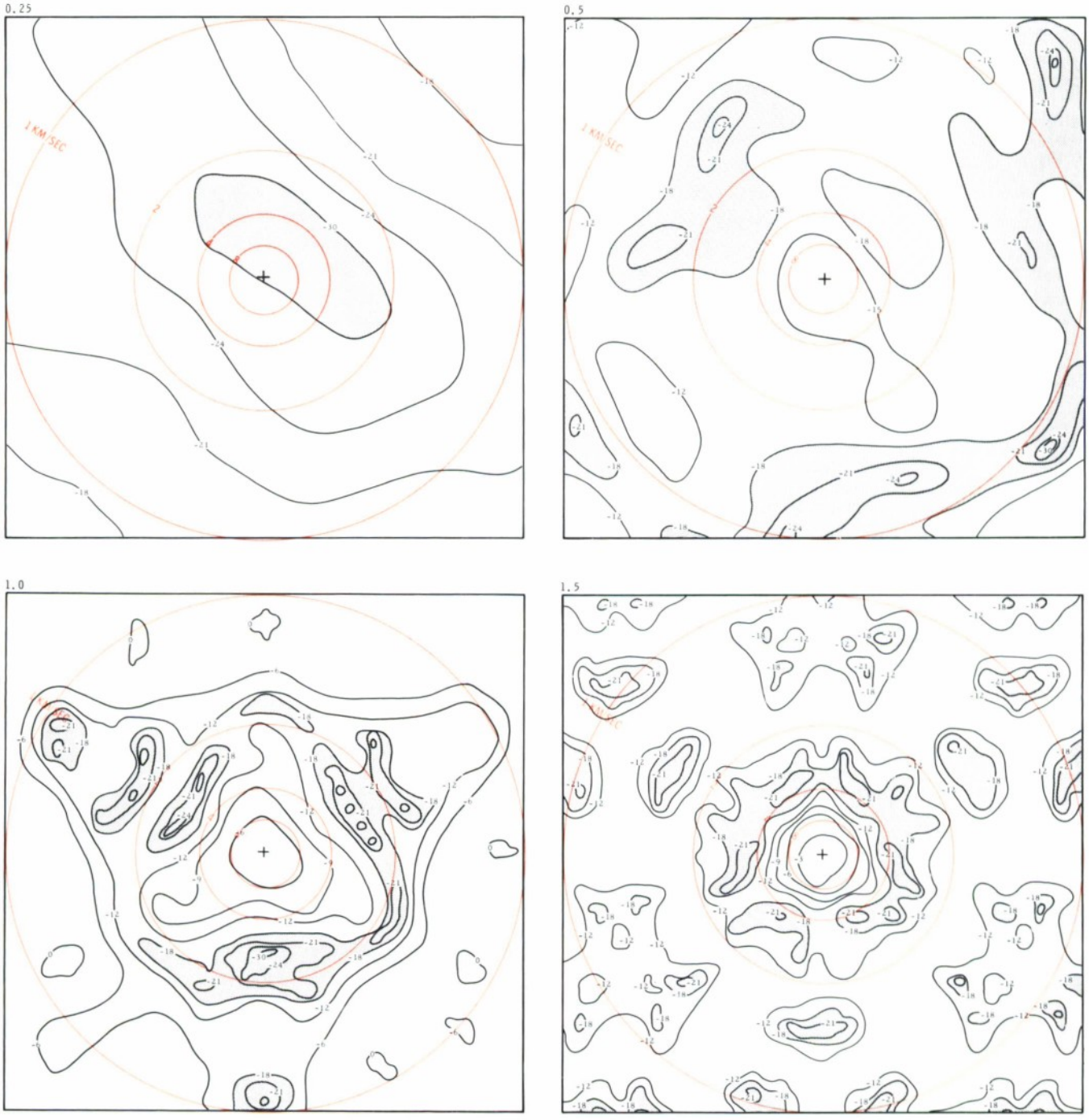

Figure IV-50. Frequency-Wavenumber Responses for MCF-12; f= 0.25, 0.50, 1.0, and 1.50

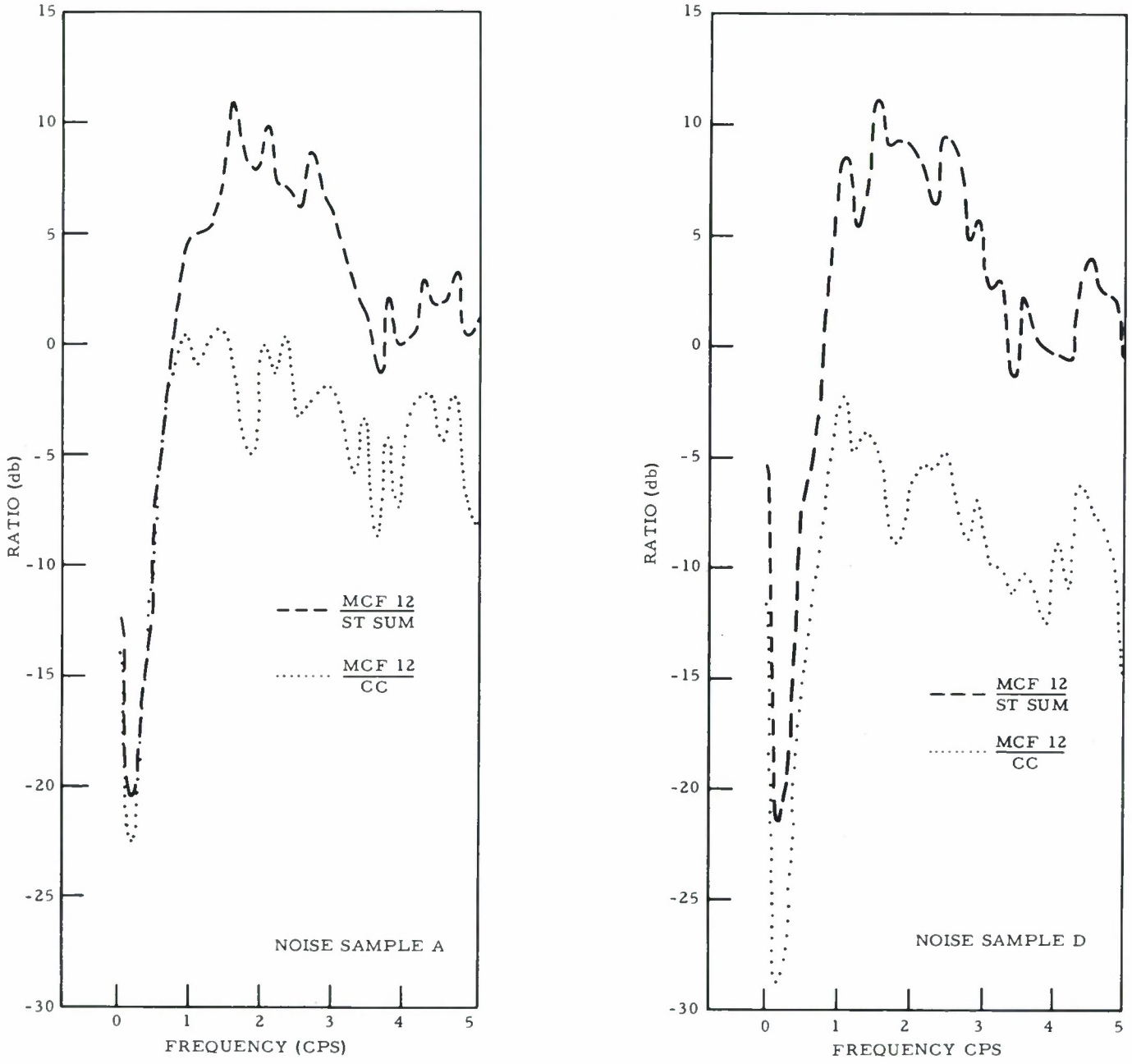

Figure IV-51. Noise Attenuation as a Ratio of Noise Power Density Spectrum of MCF Output to Noise Power Density Spectrum of Center Channel Input (MCF/CC Ratio) for MCF-12

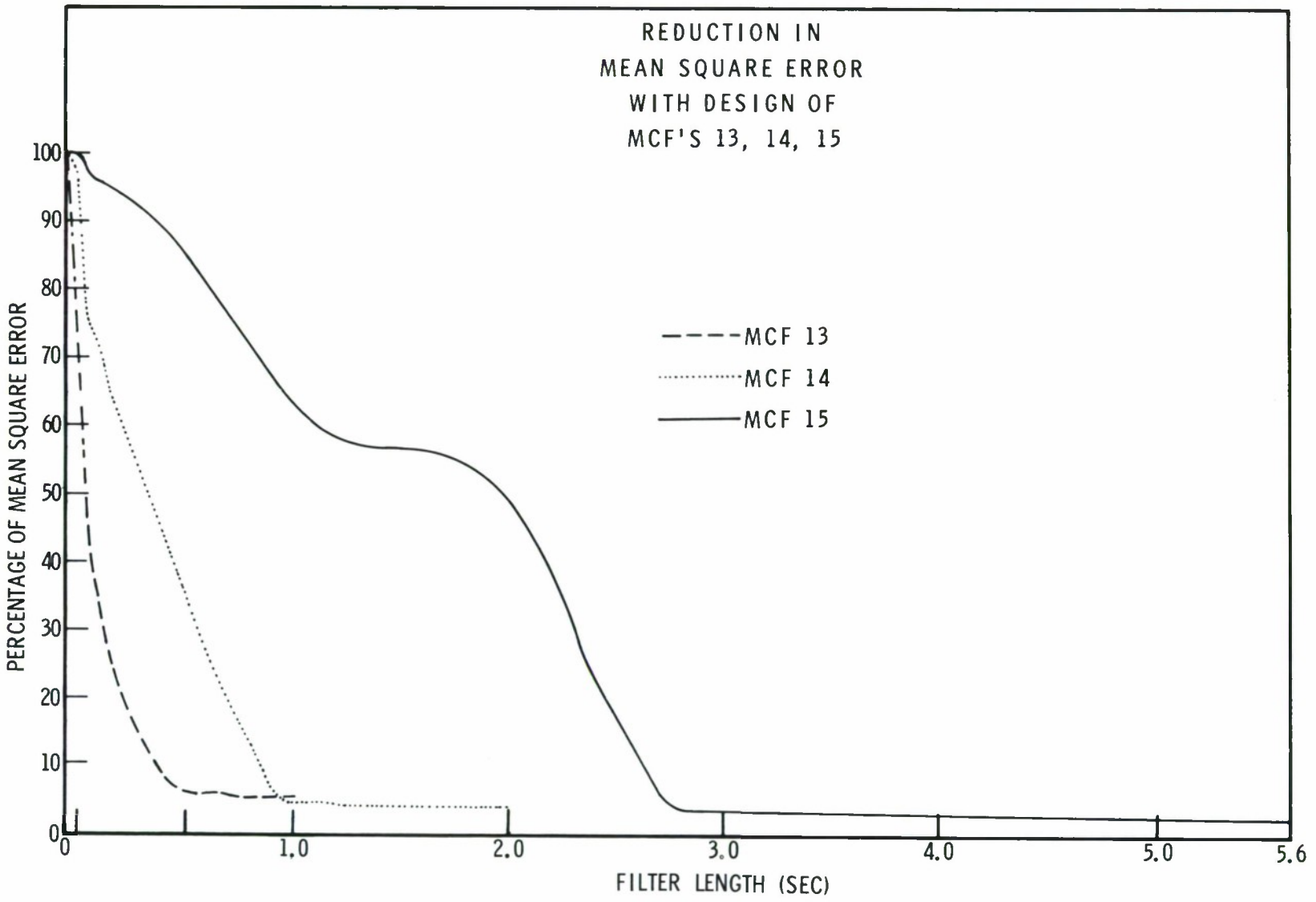

Figure IV-52. Percentage Mean-Square-Error as a Function of Filter Length for the Design of MCF-13, -14 and -15

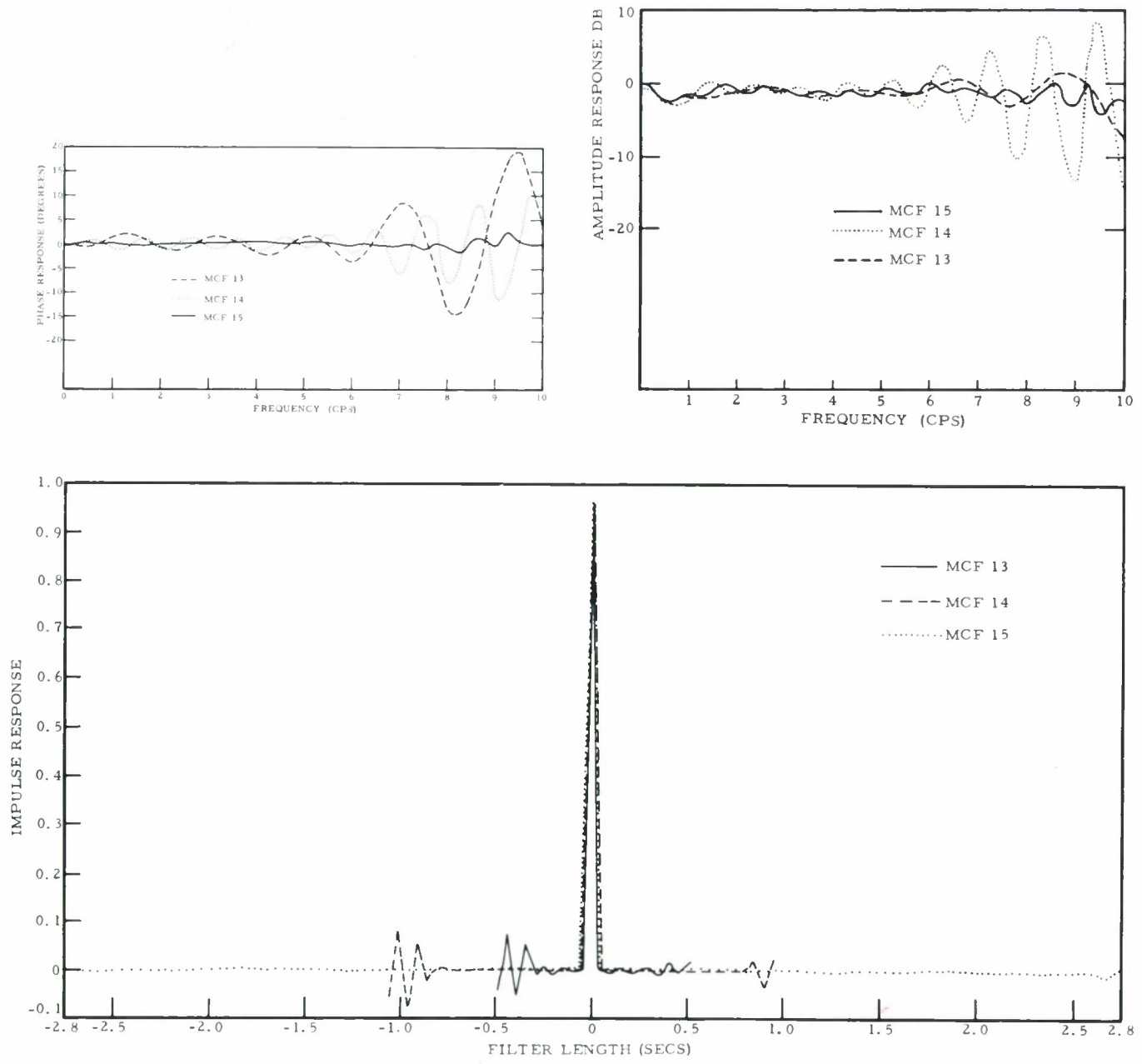

Figure IV-53. Impulse Amplitude and Phase Responses of MCF-13, -14 and -15

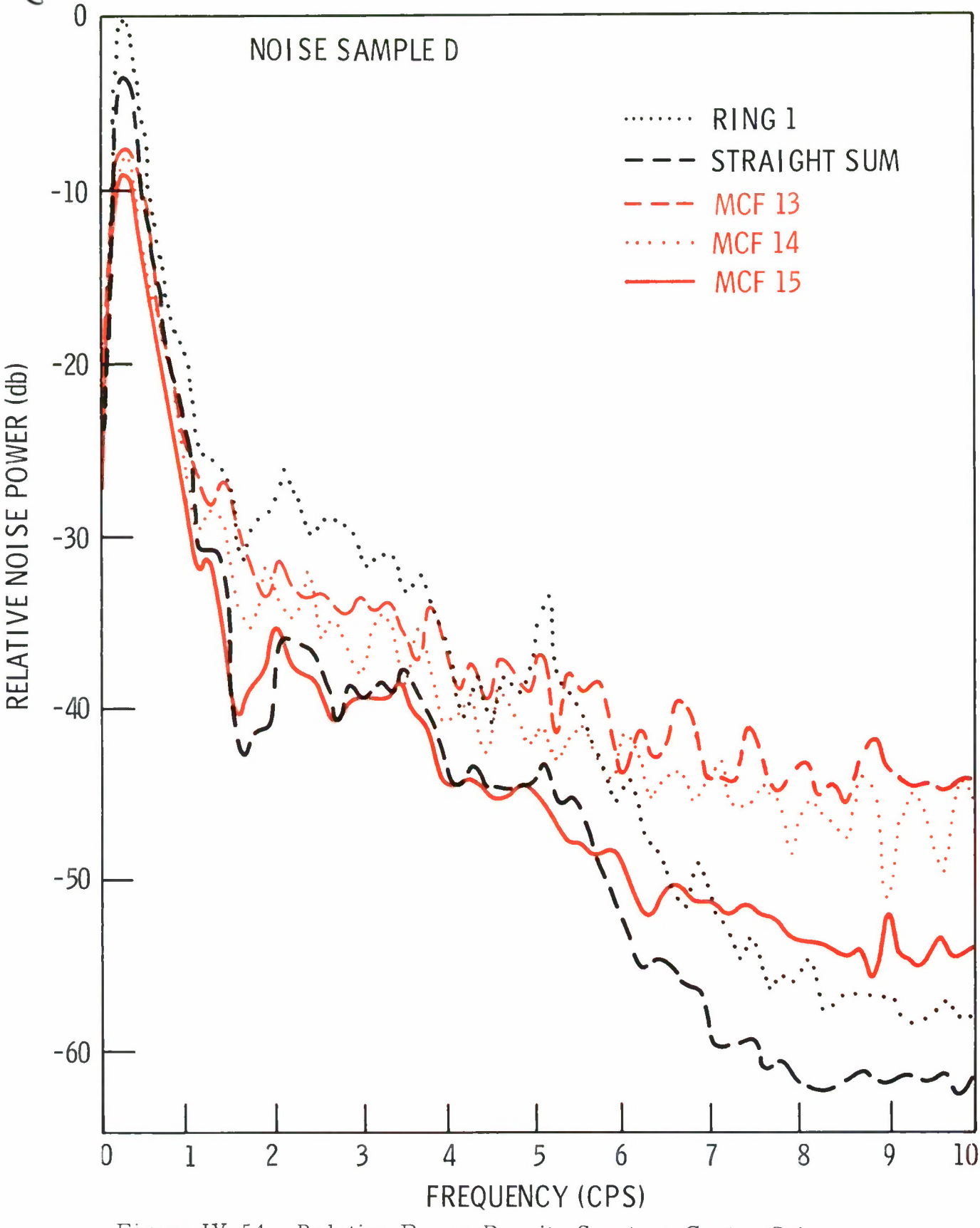

Figure IV-54. Relative Power Density Spectra: Center Seismometer Straight Sum Output, Overlaid with MCF-13, -14 and -15 Outputs

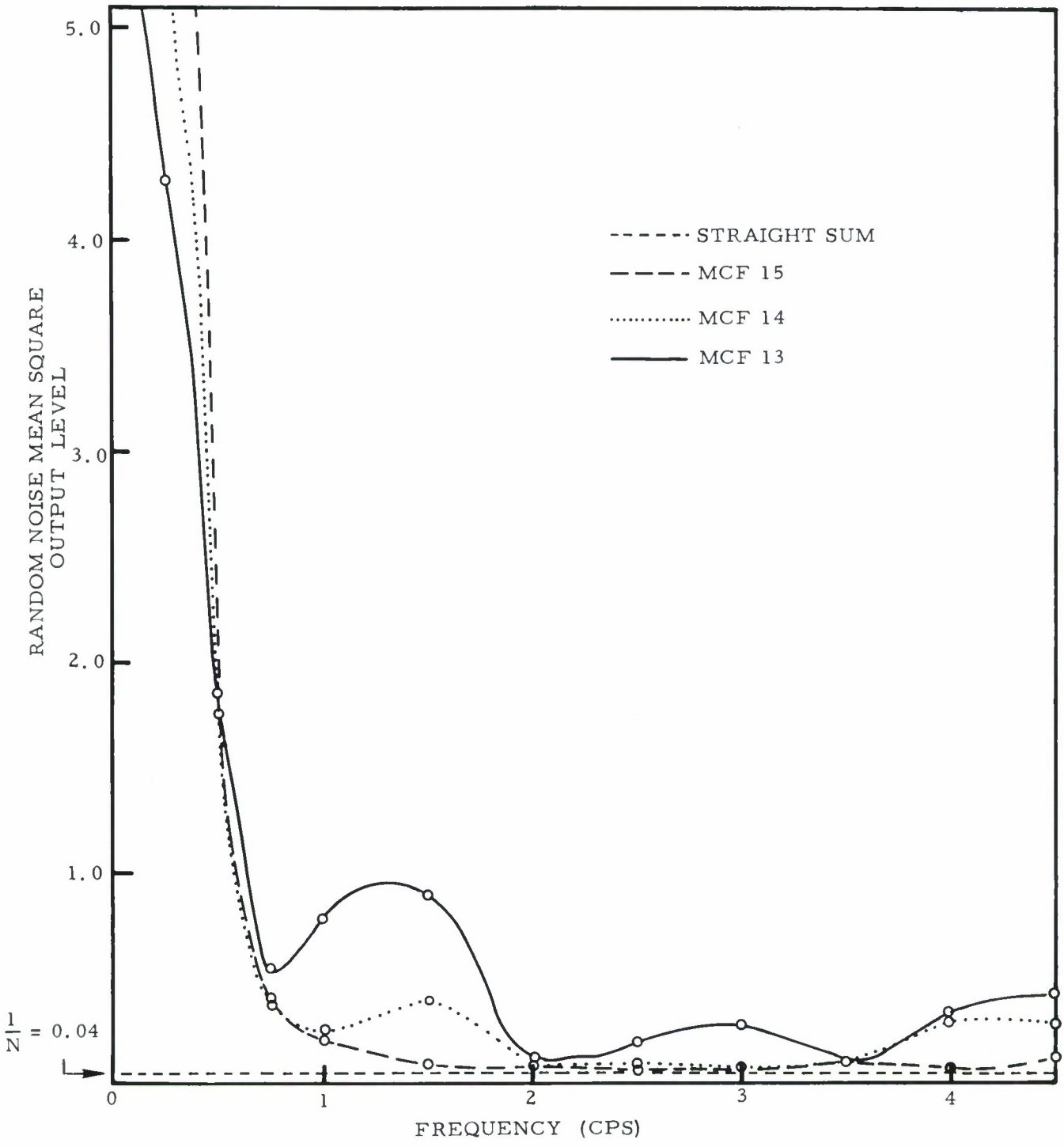

Figure IV-55. Random Noise Response of MCF-13, -14 and -15 as a Frequency Function

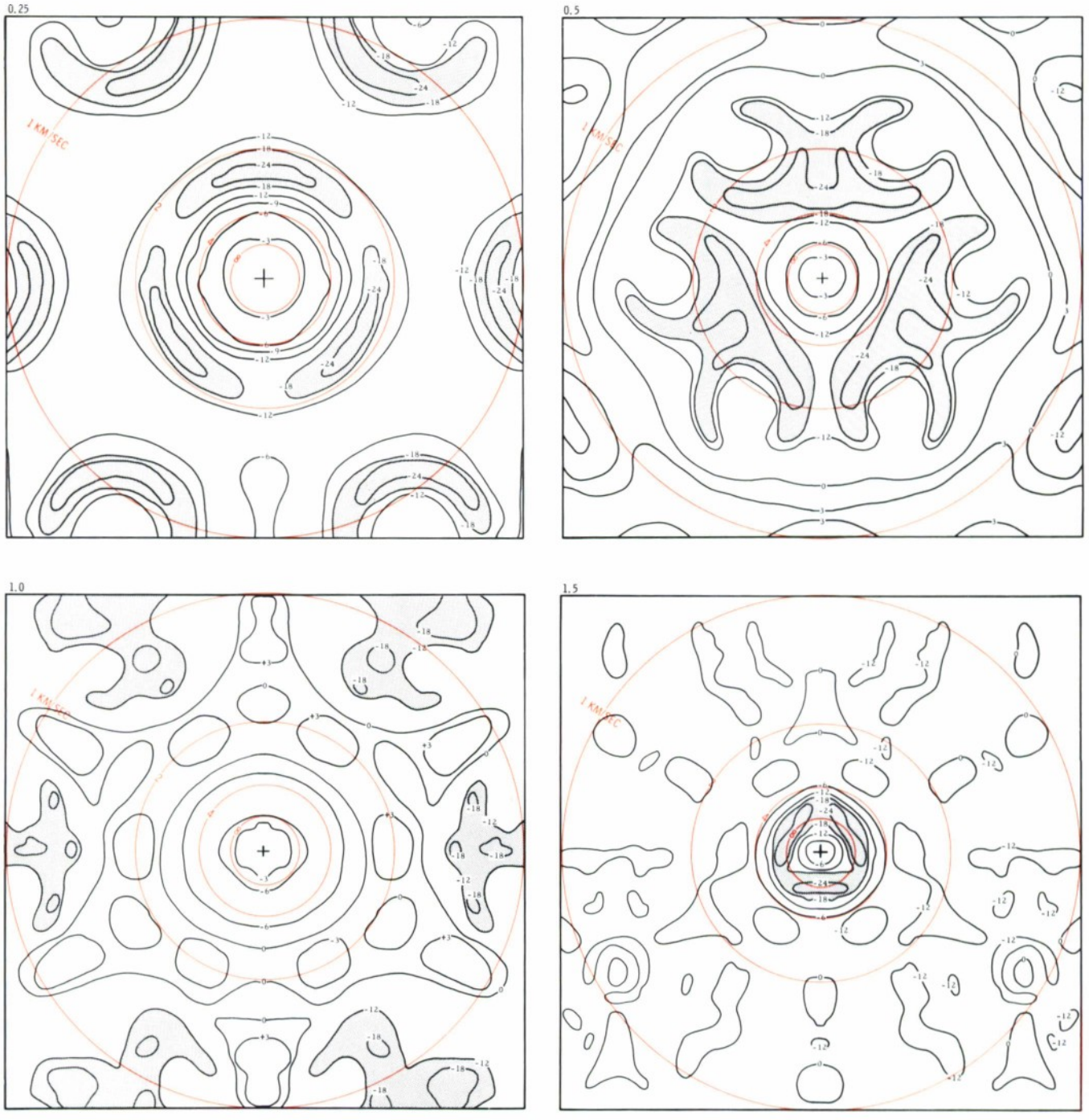

Figure IV-56. Frequency-Wavenumber Responses for MCF-13; f= 0.25, 0.50, 1.0, and 1.50

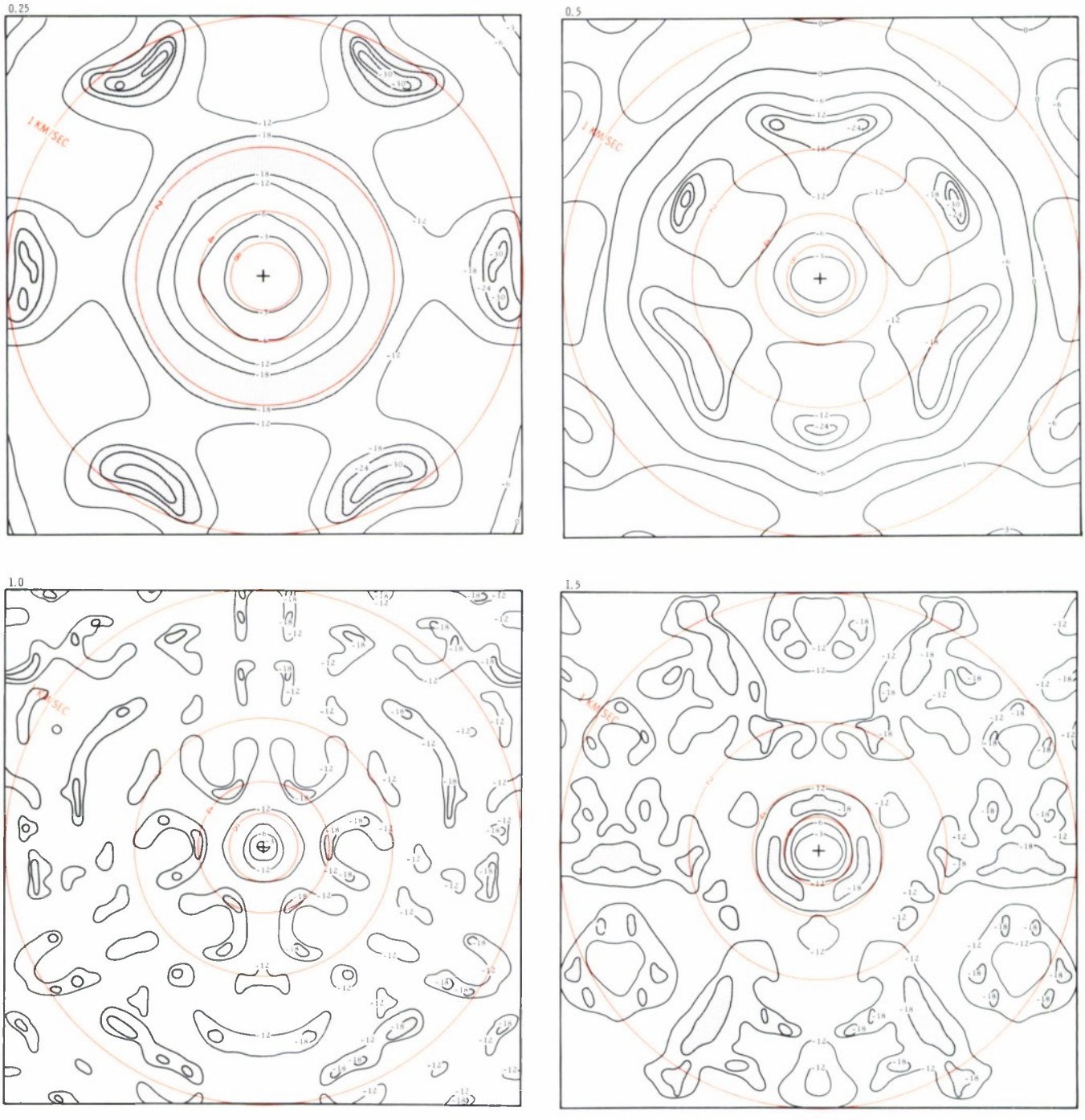

Figure IV-57. Frequency-Wavenumber Responses for MCF-14; f = 0.25, 0.50, 1.0, and 1.50

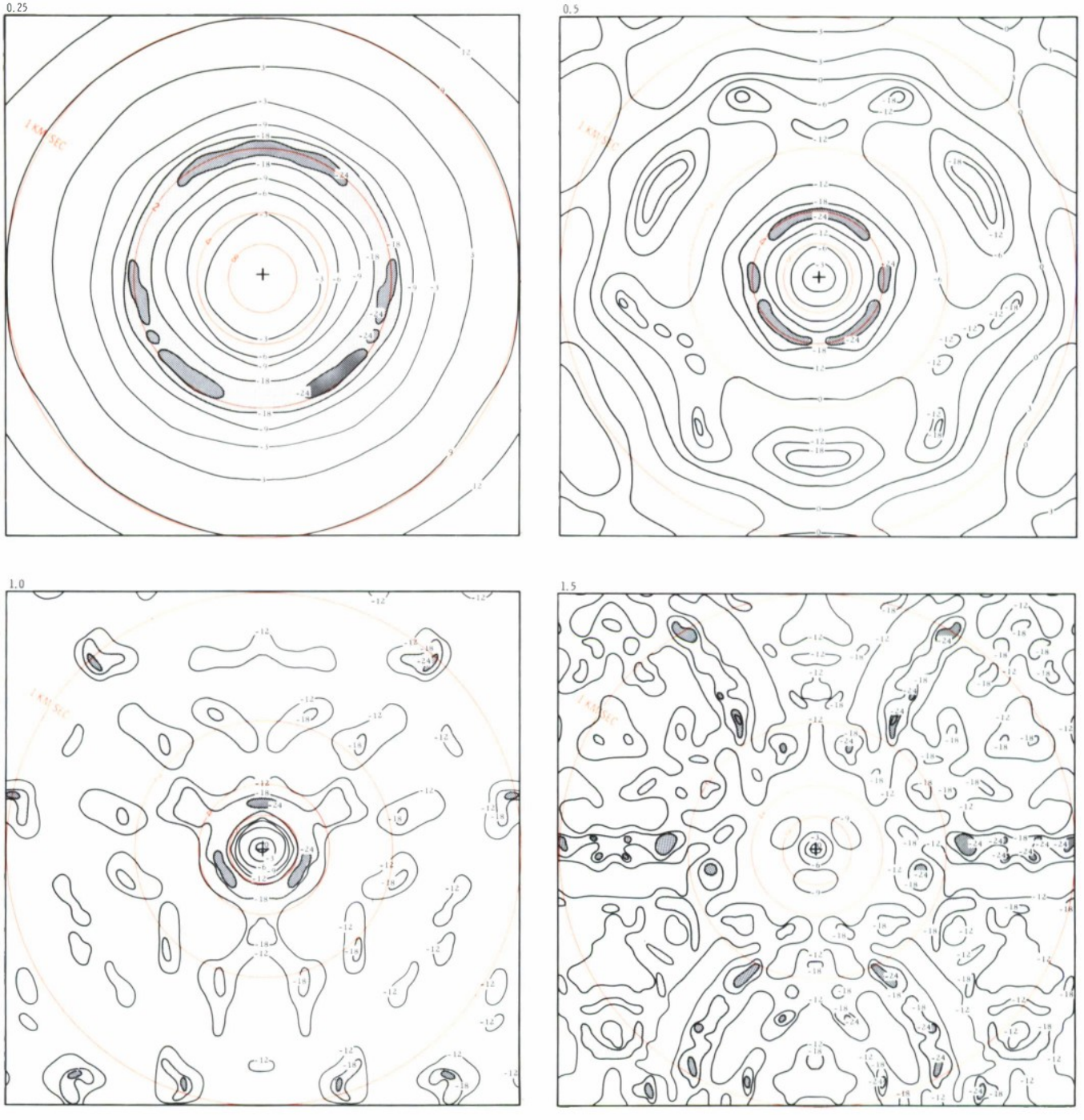

Figure IV-58. Frequency-Wavenumber Responses for MCF-15; f = 0.25, 0.50, 1.0, and 1.50

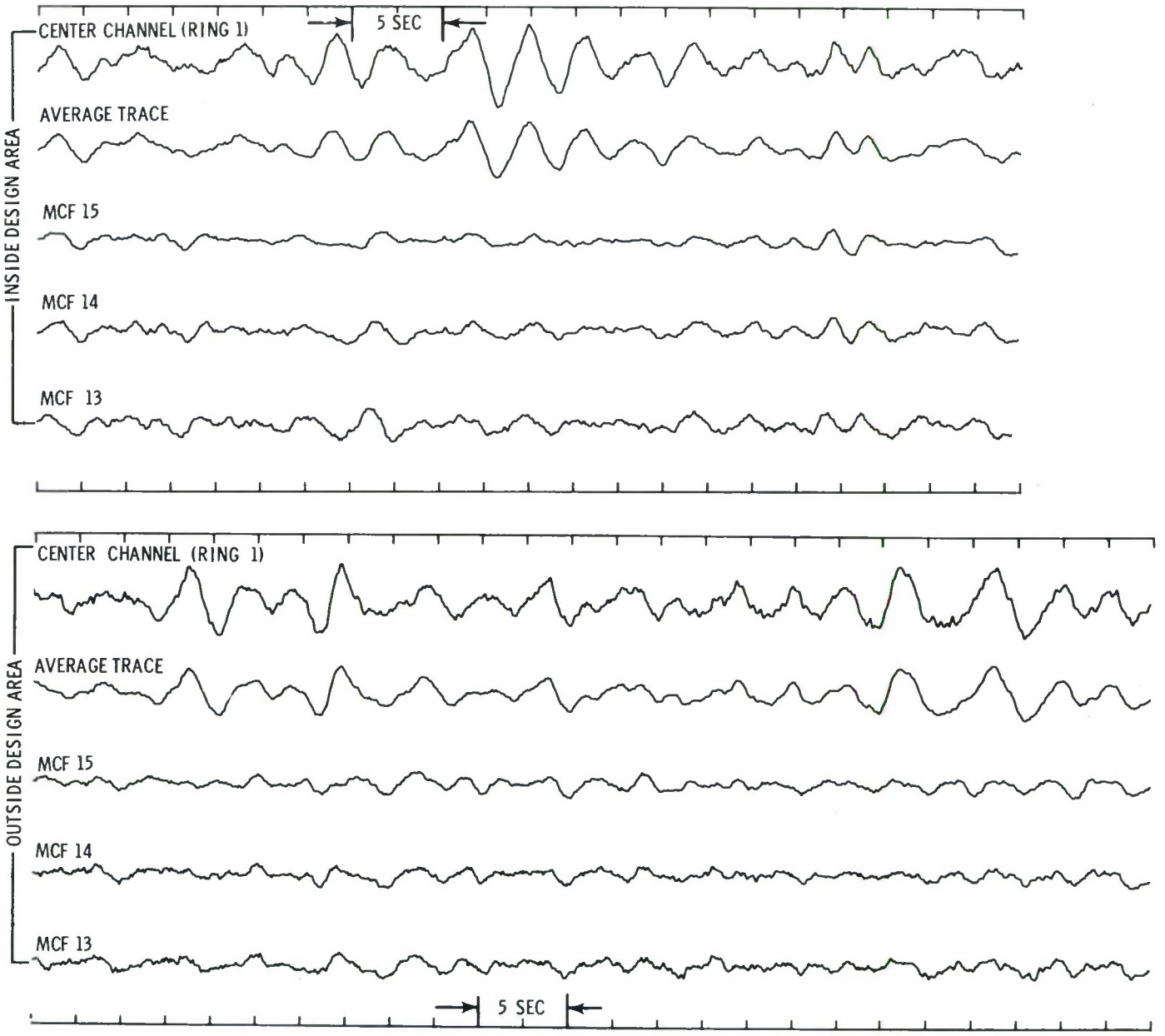

Figure IV-59. Noise Samples B and C Showing Center Seismometer, Straight Sum Output, MCF-13, -14 and -15 Output

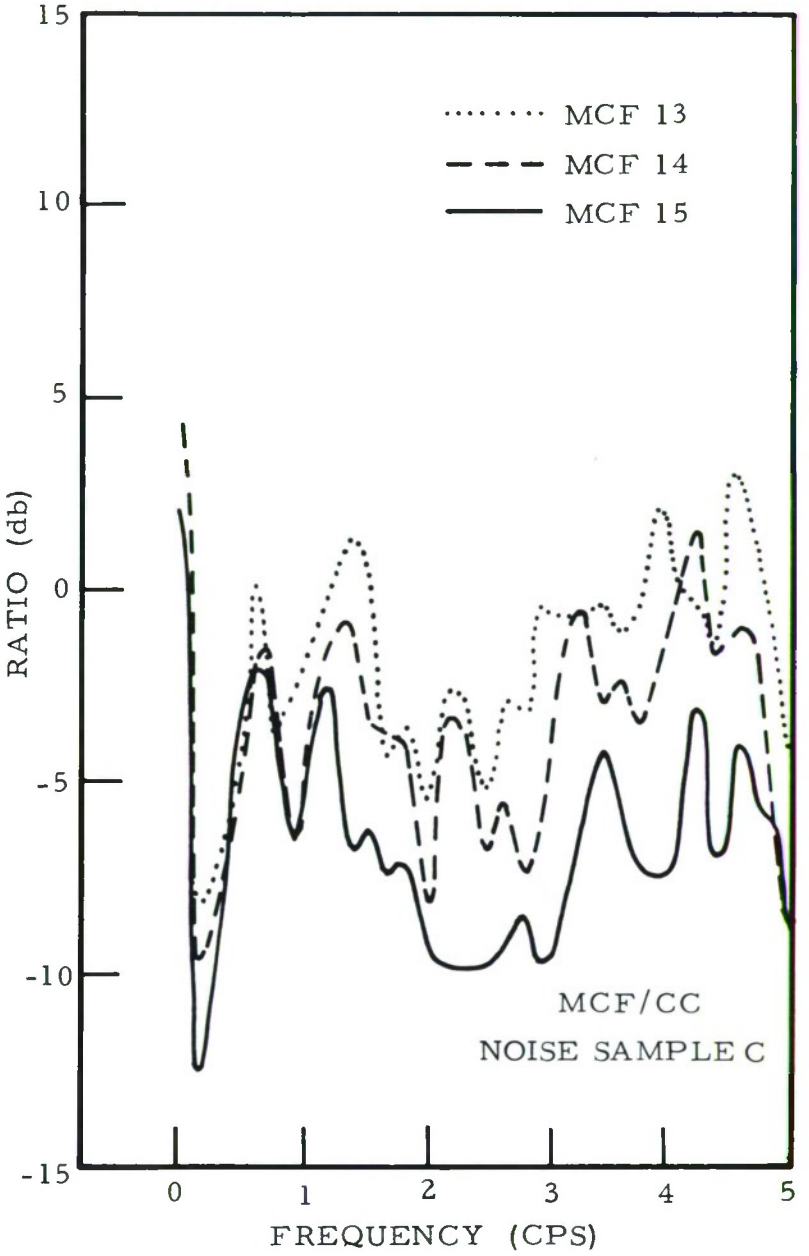

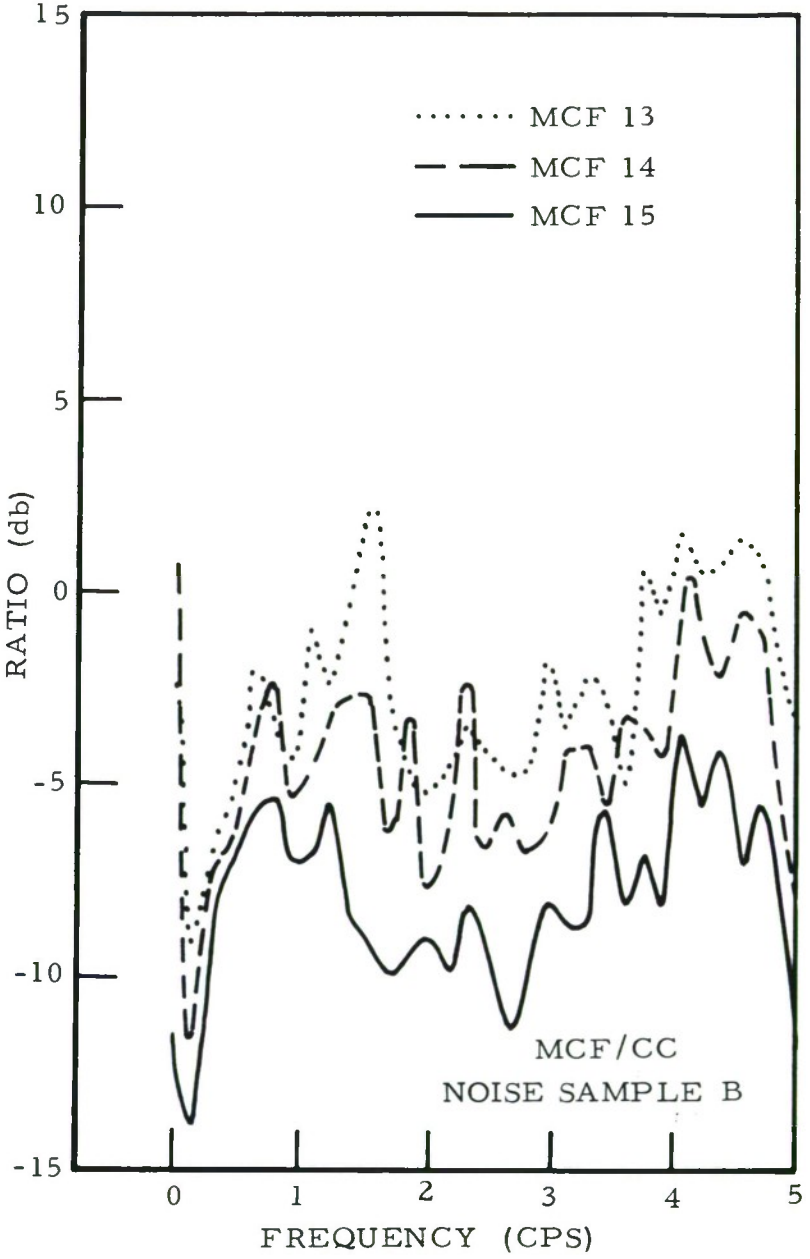

Figure IV-60. Noise Attenuation as a Ratio of Power Density Spectra, MCF-13, -14 and -15 Outputs to Center Seismometer, Noise Sample B and C

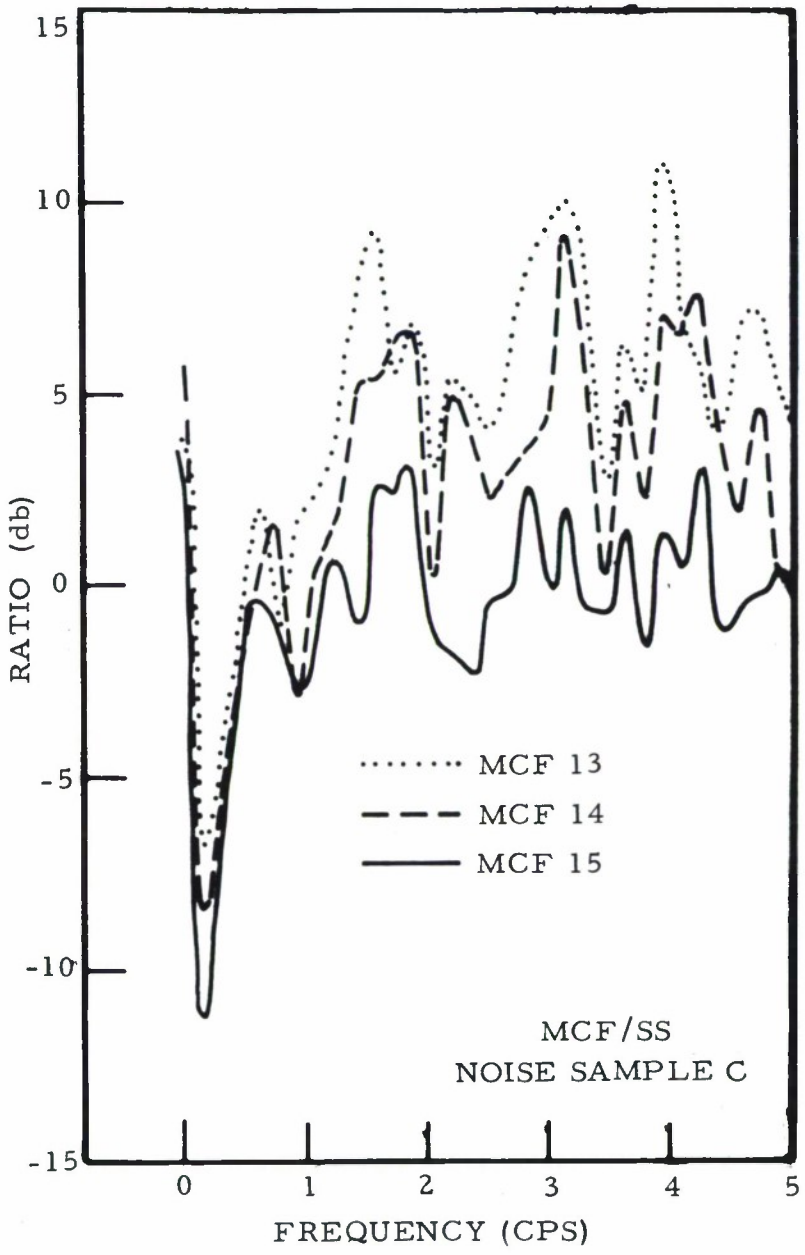

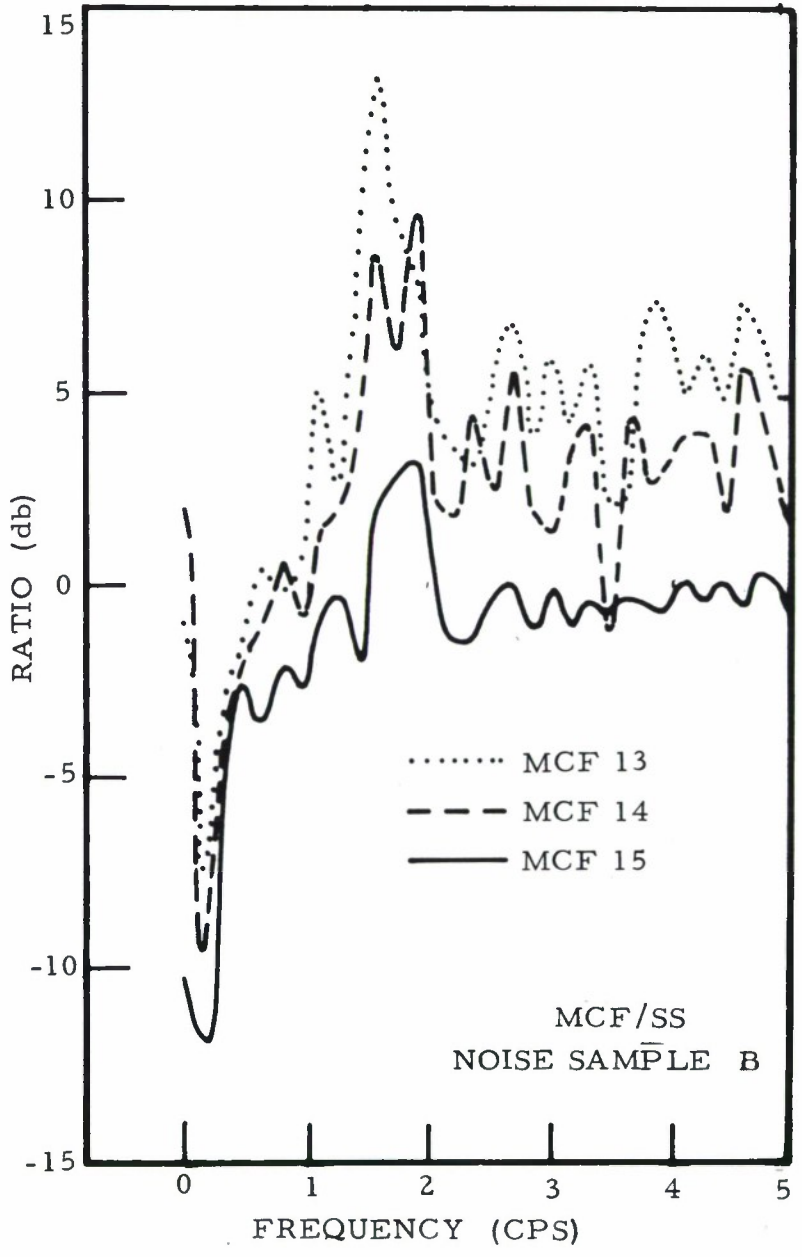

Figure IV-61. Noise Attenuation as a Ratio of Power Density Spectra, MCF-13, -14 and -15 Outputs to Straight Sum Output, Noise Samples B and C

SECTION V

DESIGN AND EVALUATION OF MULTICHANNEL FILTERS AND THE DETECTION PROCESSING PROCEDURE

On the basis of the optimum design techniques determined by the study described in the previous section, one MCF was developed for each of five LASA subarrays. This section presents the design and evaluation of these five filters (MCF-16 through MCF-20) and a brief discussion of their capabilities as detection processors. Another set of filters (MCF-21 through MCF-25) designed with a different signal model are also briefly described in this section. The subarrays for which the filters were designed are C-3, E-2, F-2, F-3, and F-4 (Figure V-1).

A. DESIGN OF THE MULTICHANNEL FILTERS

The type of filter chosen was the 5-ring filter designed from a disk signal model and from measured-noise statistics. As was shown in Section IV, the 5-ring filter performed as well as or better than the 8-ring or the 25-channel maximum-likelihood filter. The disk signal model was shown to offer some improvement over the infinite velocity signal model in maintaining a high, almost flat response to signal over the velocity range from 12 km/sec to infinity. The superiority of the use of measured-noise statistics as opposed to a theoretical noise model was shown in its sharp response to signal in frequency-wavenumber space and in suppressing the noise at low frequencies. As was mentioned before, the averaging of the correlation sets from several noise samples recorded on different days eliminates many of the eccentricities of a single noise sample and produces a filter which operates consistently over a long period of time.

In order to improve the low-frequency noise attenuation, frequency-filtering was used to cut off all information below a certain frequency. The high-frequency attenuation was improved by whitening the noise correlations to reduce the effect of the large low-frequency noise peak in the design of the filters.

The study of the effect of filter length indicated that the gain of a 5.85-sec length over a 2-sec length was insufficient to justify its use. The length of 1.8 sec resulted from the shortening produced in whitening the correlations calculated for a 2-sec filter and seemed to be a good compromise between the 1-sec and 2-sec filters which did not differ greatly in quality.

The large variations in seismometer response within only a few months led to the decision to not include instrument response variations in the signal model.

The filters were designed from an average of several noise correlations sets which were obtained from noise recorded simultaneously at each subarray; however, in some cases the record of a particular sample at a particular subarray was considered to be a poor speciman and was discarded. Table V-1 gives the noise samples that were used in the design of the filters. A 150-sec gate was used in each case, the data being selected generally at the beginning of each 330-sec record.

The signal model corresponds to constant power density over a disk in wavenumber space ($\vec{k}$-space) with a radius corresponding to a horizontal velocity component of 12 km/sec. The power density spectrum was shaped by the autopower density spectrum of the average of the noise autocorrelations of a single subarray to provide a separate signal model for each subarray.

Each signal model was then reshaped to provide the specified frequency filtering. This frequency shaping function, used for all five subarrays, was flat from 1.0 to 3.0 cps, down 10 db at 0.75 and 3.25 cps, down 30 at 0.50 and 3.50 cps, down 50 db at 3.75 cps and equal to 0.0 at all other frequencies from 0.00 to 10.00 cps. The combination of the two shapings produced a signal and noise pair with constant signal-to-noise ratio between 1.00 and 3.00 cps and a signal-to-noise ratio which decreased rapidly to zero outside this band. The ratio of total signal power to total noise power was then set equal to 2.

The second set of filters (MCF-21 through MCF-25) was designed identically as the first set except that the signal model was an infinite velocity model rather than a disk model.

B. MULTICHANNEL FILTER RESPONSES

The responses presented for each filter include the percent mean-square error as a function of filter length for design of the MCF, the impulse response and the frequency response and the frequency-wavenumber response. The frequency response is presented in two parts: the amplitude response and the phase response.

The percent mean-square-error as a function of filter length (Figures V-2 through V-6) shows a total noise power reduction of 96 percent to 98 percent for each filter. The impulse responses of all six filters (Figures V-2 through V-6) are almost identical. The amplitude responses

Table V-1

NOISE SAMPLES USED IN DESIGN OF MCF-16 THROUGH MCF-20

Subarray		C3	E2	F2	F3	F4
MCF No.		16	17	18	19	20
Date	Time (MST)					
11-05-65	03:19-03:25				X	
11-09-65	02:39-02:45					
11-16-65	06:29-06:35				X	
11-20-65	03:40-03:46					
11-23-65	02:19-02:24		X			
11-23-65	05:49-05:55					
11-24-65	03:18-03:24					
12-01-65	10:10-10:15					
03-24-66	12:47-12:55					
03-29-66	11:08-11:16					
03-31-66	13:58-14:06					
04-05-66	16:10-16:18					

X - Indicates that a sample from a particular subarray was not used.

of all the filters are similar: showing a good passband; almost flat from 1.0 to 3.0 cps, as desired; and a drop to about -20 to -30 db above 4.0 cps. The phase responses are flat from 0.5 to 3.5 cps and, in general, oscillate between $0^\circ \pm 5^\circ$ and $180^\circ \pm 5^\circ$ outside this frequency band.

The second set of filters (MCF-21 through MCF-25) was designed to attempt a slight increase in noise rejection at the expense of low velocity signal response. As in the case of the disk signal model filters, the infinite velocity filters have nearly identical responses, so the responses are presented for only one filter, MCF-21, designed for the F-3 subarray. The mean-square-error (Figure V-7) has been reduced to 1.1 percent compared with 2.8 percent for MCF-16 (the disk signal model filter designed for the F-3 subarray). The impulse responses of these two filters are similar as are the frequency responses. One difference in the amplitude responses is that at high frequencies (above 4.0 cps) the response of MCF-21 is down about 30 db compared to approximately 22 db for the MCF-16 response.

The frequency-wavenumber responses of the five filters are shown in Figures V-8 through V-12. As expected from examination of the other responses, there is little difference among the $f\text{-}\vec{k}$ responses. The amplitude responses dropped very low below 1.0 cps, but the lowest point in that band occurred at 0.30 cps. This is why the amplitude responses indicate a greater rejection than the $f\text{-}\vec{k}$ responses show at infinite velocity at 0.25 cps. The difference of 5 to 10 db is easily accounted for by the extreme slope of the amplitude responses at these frequencies. At 1.00 cps, the $f\text{-}\vec{k}$ responses are up to 0 db at infinite velocity and are down less than 1.0 to 1.5 db at 12 km/sec at this frequency and at 1.50 cps. At velocities less than 12 km/sec the responses fall sharply to levels below -12 db. The exact level and velocity at which greatest rejection occurs varies from filter to filter since each filter was designed for a different subarray. At 0.25 cps a rejection ring occurs between 2 and 3 km/sec with about 12 to 15 db more rejection than at infinite velocity. At 0.50 cps the response has risen several decibels while maintaining the same general shape. At 1.00 cps most of the filters are rejecting noise most strongly around 2.5 km/sec and 1.5 km/sec, with typical rejections of 18 db or more. At 1.50 cps these rejection rings are still present but are not as deep as at 1.00 cps.

The $f\text{-}\vec{k}$ response of MCF-21 is shown in Figure V-13. This response is basically the same as that of MCF-16 except for two differences. MCF-21 tends to have 3 to 6 db greater rejection at low velocities than

MCF-16. At high velocities MCF-21 does not have the flat signal response which MCF-16 has at velocities above 12 km/sec. At 1.00 cps the response of MCF-21 is down about 4 db at 12 km/sec. Thus for detection of signals at high velocities above 20 km/sec, the infinite velocity filter would be as good as or better than the disk signal model filter.

The general characteristics which were enhanced by proper selection of design parameters are noticed in the f-$\vec{k}$ responses:

- High rejection over all f-$\vec{k}$ space at low frequencies
- A nearly flat pass region in $\vec{k}$-space corresponding to high velocity signals at frequencies from 1.00 to 3.00 cps
- Sharp falloff of the response at velocities below 12 km/sec
- Good rejection in all directions at low velocities
- A generally isotropic response

C. NOISE ATTENUATION AND SIGNAL DISTORTION

The plots of noise attenuation are shown in Figures V-14 through V-16. These plots show the ratio of the MCF output power density spectrum to the straight summation power density spectrum for the noise immediately preceding one of the signals used in the evaluation of the application of the filters to signals. The three signals are designated by the location of their source as Algeria, Kuriles and Marianas.

The noise used in the plots of noise attenuation was recorded at the subarray for which the MCF applied to that noise was designed. The subarray is identified in parentheses on the figure.

The ratios show that the filters have greater attenuation of noise than the straight sum process at all frequencies below 0.9 or 1.0 cps. The maximum improvement of the filters, compared to the straight sum, occurs between 0.25 and 0.30 cps and is about 25 db in most cases; going as high as 30 db in the case of MCF-20 applied to noise recorded at F-2 preceding the signal from Algeria. The improvement goes as low as 21db in the case of MCF-20 applied to noise recorded at F-2 preceding the signal from the Marianas. From 1.0 to about 4.0 cps, the MCFs have about 3 to 10db less noise rejection than the straight sum process. This difference is probably due to the high proportion of random noise in this band, little of which the MCF can reject when the signal model is a disk in $\vec{k}$-space. At higher

frequencies the filters noise rejection approaches that of the straight sum. At these frequencies the MCF has allowed the signal response to drop to a low value because of the signal response shaping function used in the original design of the MCFs. It should be remembered that for the 25-seismometer LASA subarrays, the straight sum process has a theoretical maximum noise rejection of 14 db.

The MCF outputs for samples containing signals are shown in Figures V-17, V-18 and V-19. The signals are from Algeria, the Kurile Islands and the Mariana Islands, respectively. The figures show no significant signal distortion. A slight precursor can be seen on some of the figures, but it is very small and doesn't present any problem in signal detection.

D. DETECTION PROCESSING

The detection processing procedure consisted of a running autocovariance estimate over the MCF output. For a trace G with elements g_i, A_i was computed for every value of i according to the equation

$$A_i = \frac{1}{N} \sum_{k=0}^{k=N-1} g_{i-k}^2$$

The gate used in these cases was N=50 or a time of 2.5 sec. The outputs are shown in Figures V-20, V-21 and V-22. The first signal arrival is clearly shown as are some of the later phase arrivals. The peak occuring 11 sec after the P-wave peak for the Kurile Islands event corresponds to a pP arrival for the reported 33 km depth. The peak occuring 40 sec after the P-wave peak for the Mariana Islands is unidentified. The reported depth for this event was also 33 km. Strong evidence of teleseismic energy was obtained in each case. The indication at subarray F3 of the Mariana Islands event is especially impressive considering the poor signal-to-noise ratio of this event at F3.

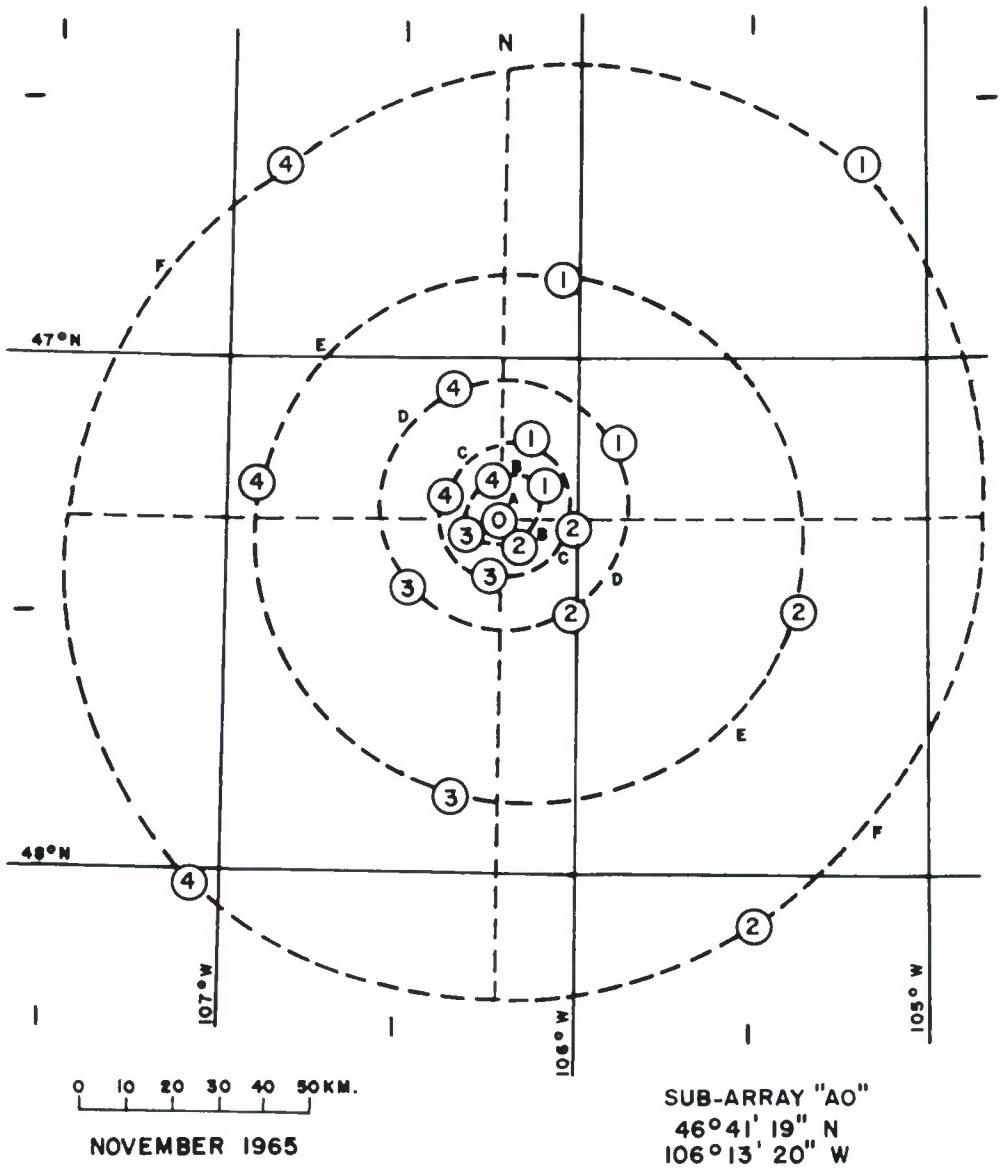

Figure V-1. LASA Subarrays

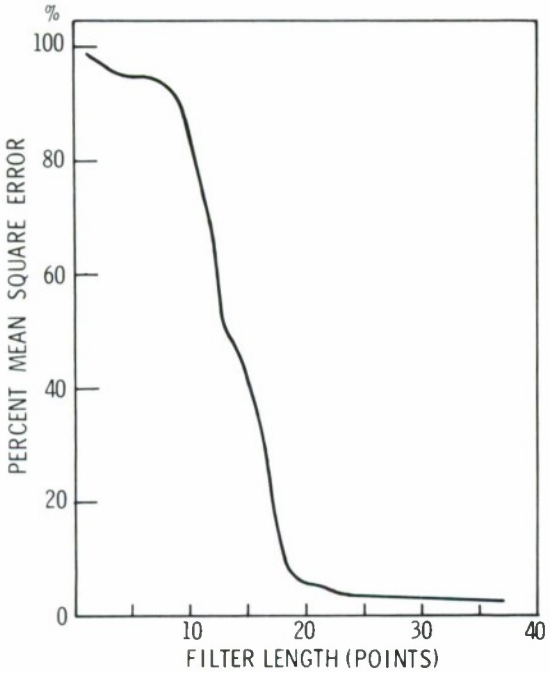

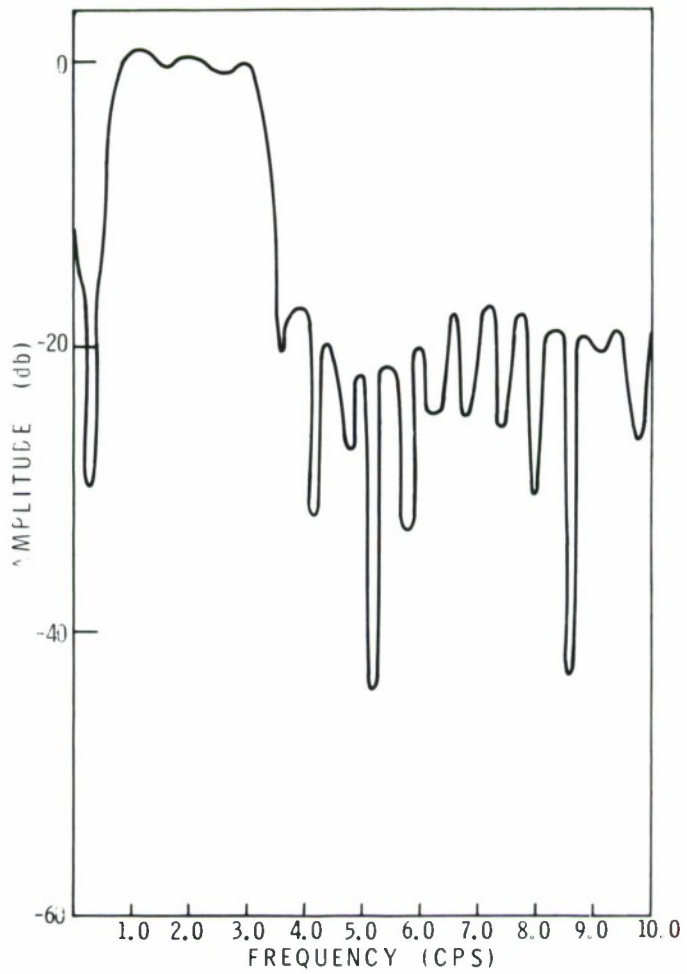

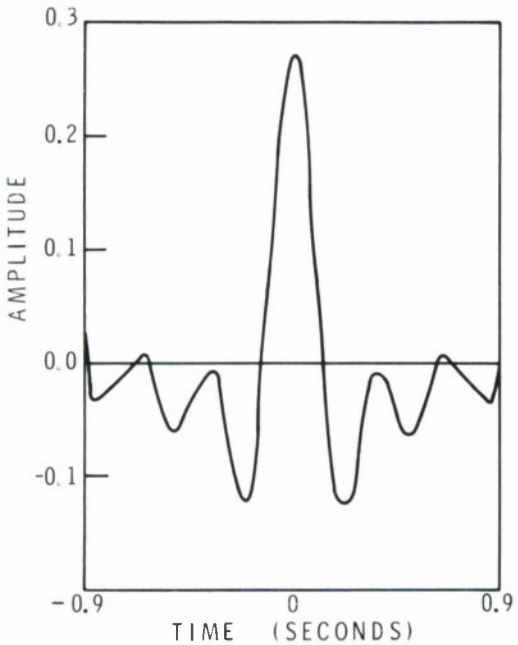

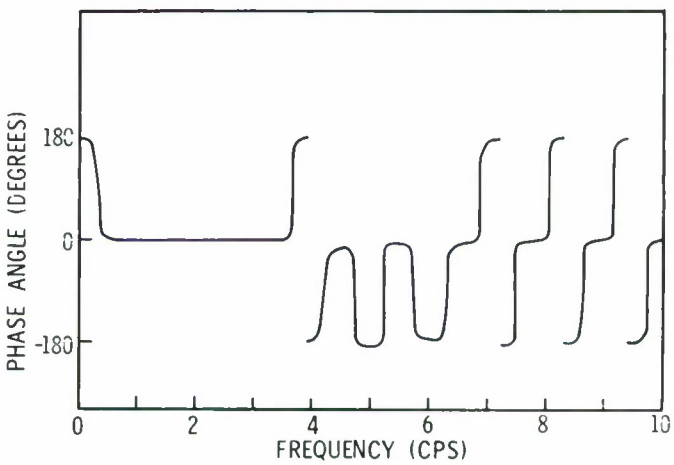

Figure V-2. Mean-Square-Error Vs Filter Length, Impulse Response and Frequency Response of MCF-16

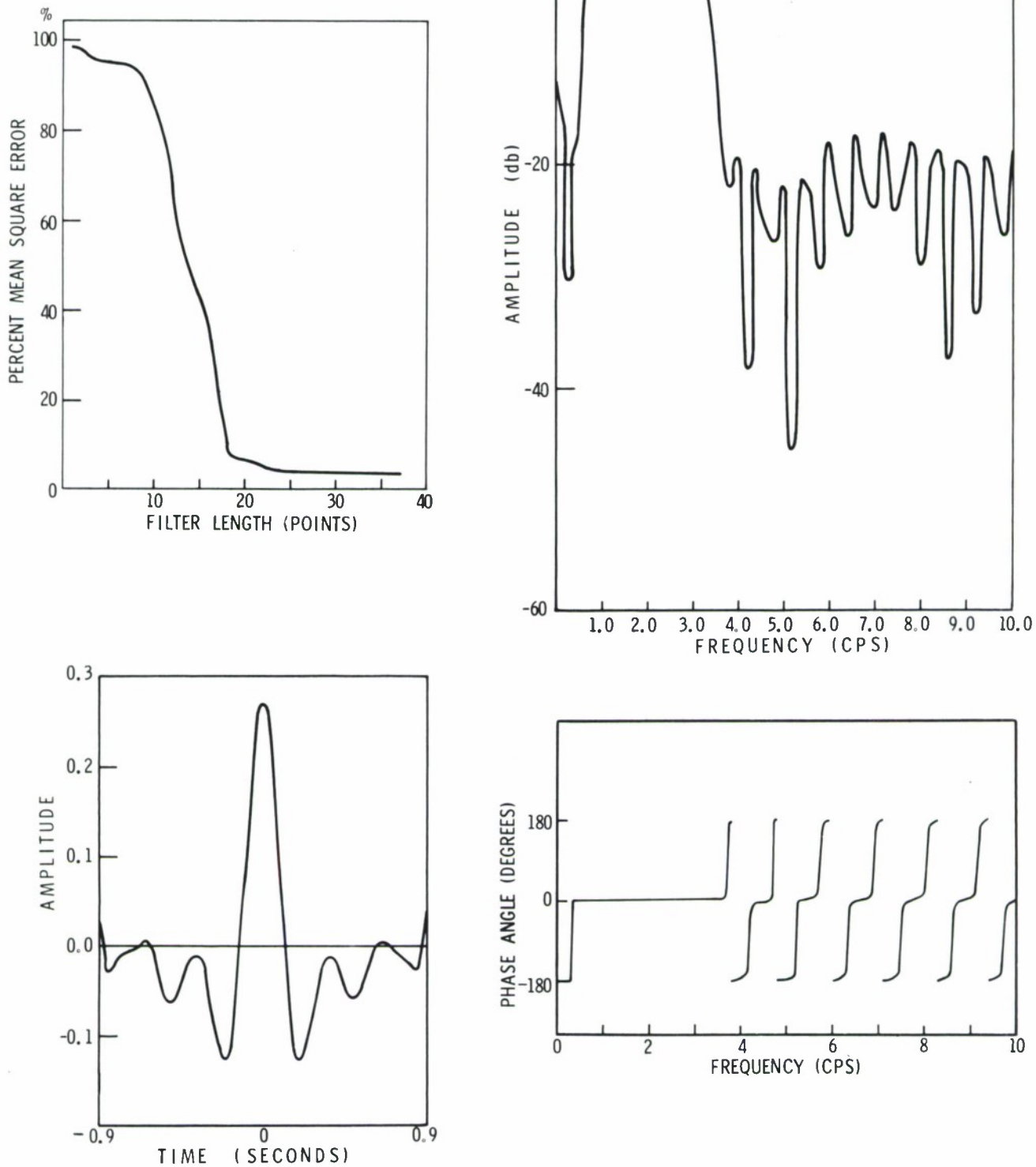

Figure V-3. Mean-Square-Error Vs Filter Length, Impulse Response and Frequency Response of MCF-17

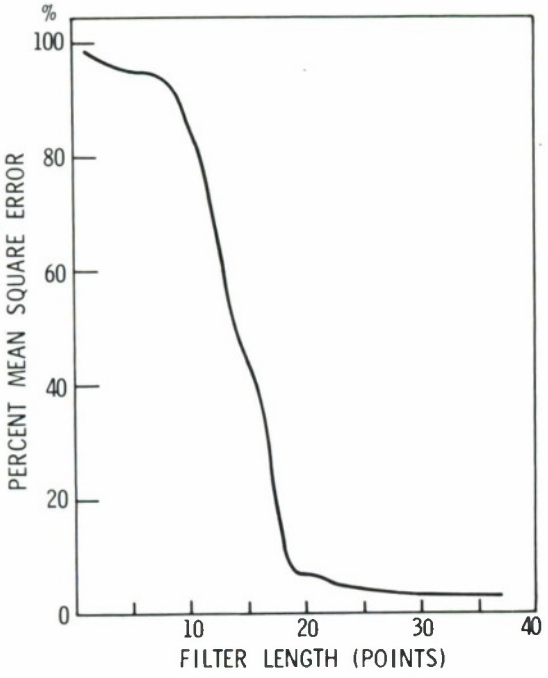

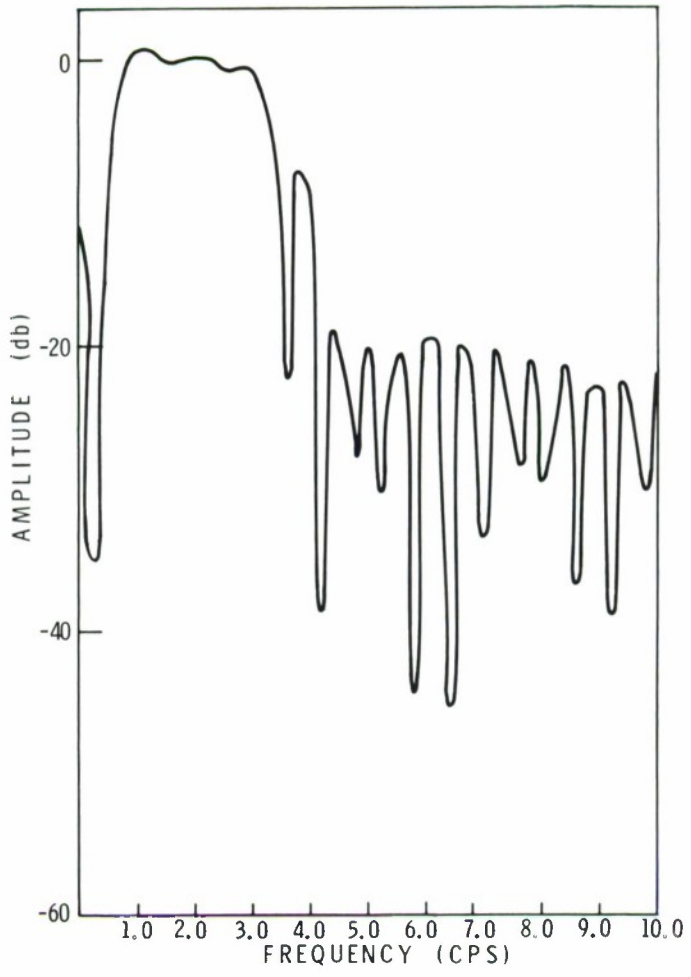

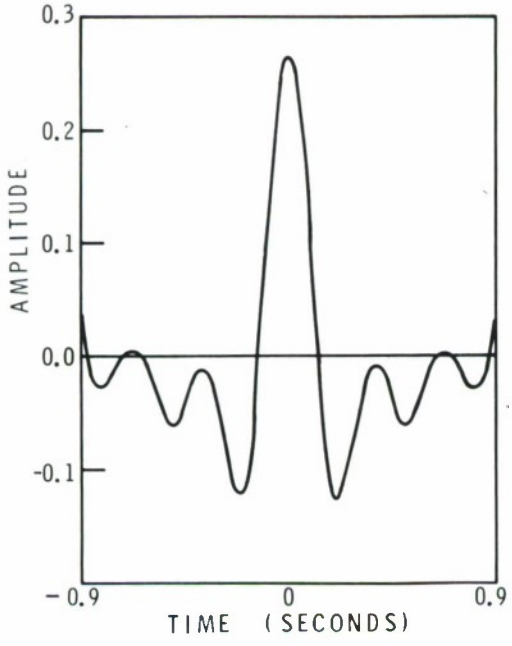

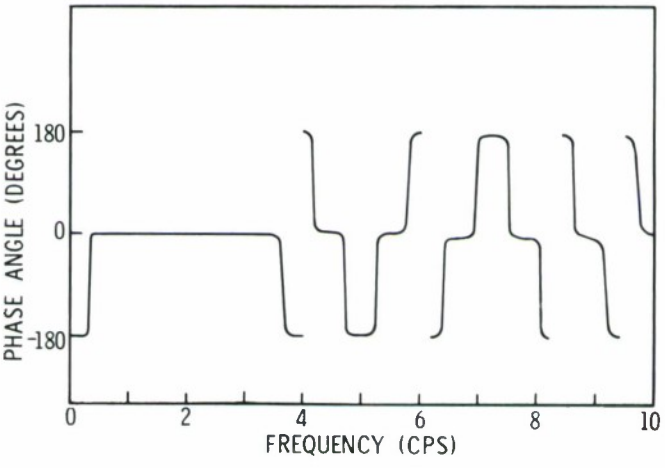

Figure V-4. Mean-Square-Error Vs Filter Length, Impulse Response and Frequency Response of MCF-18

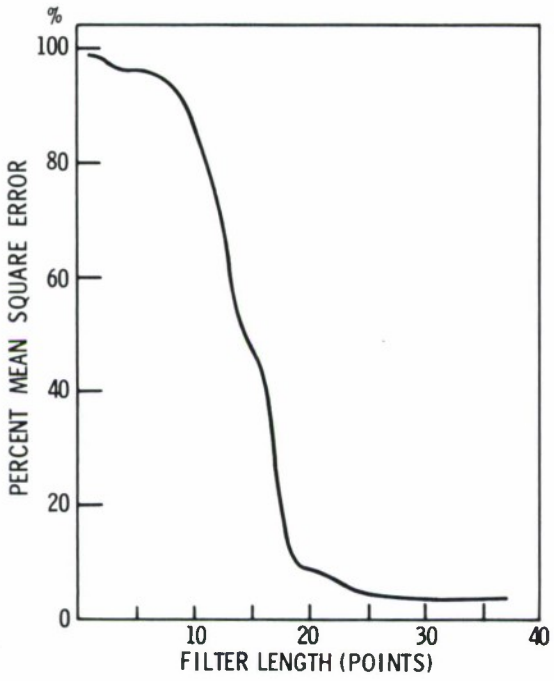

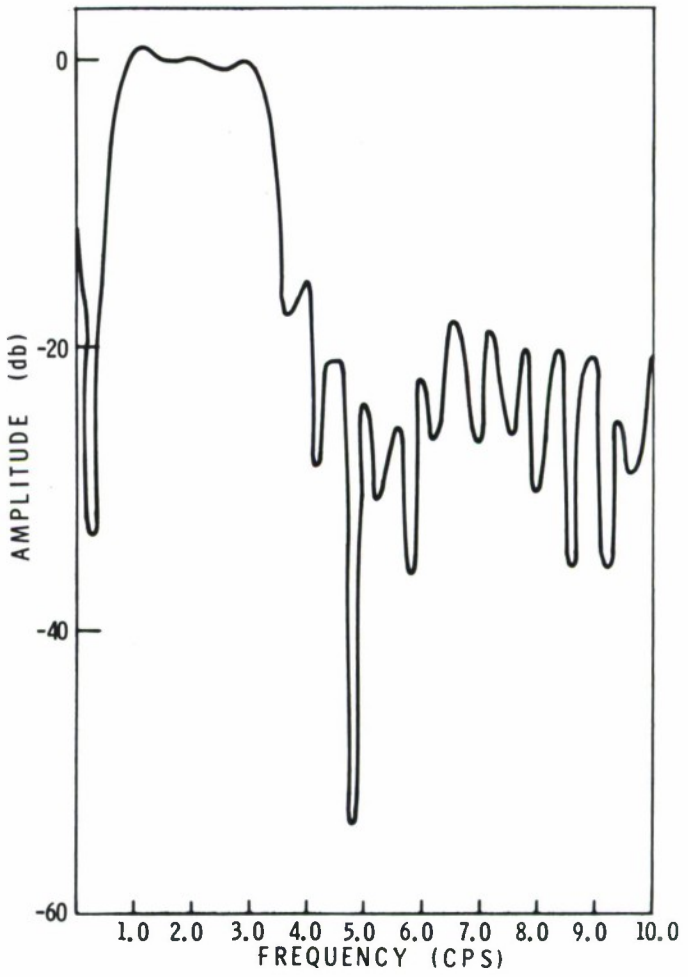

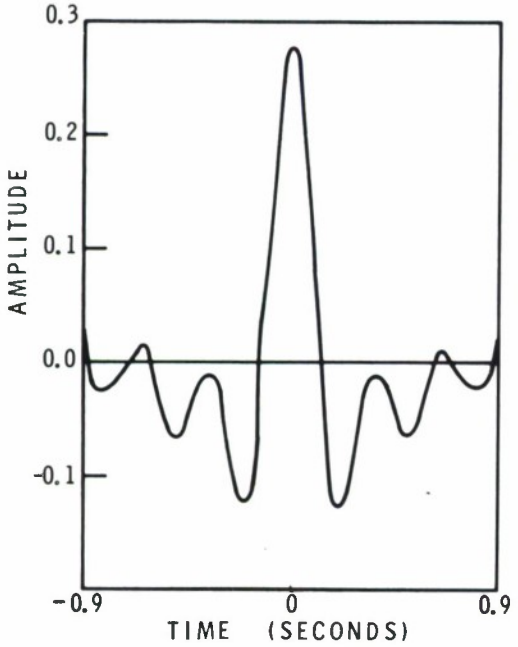

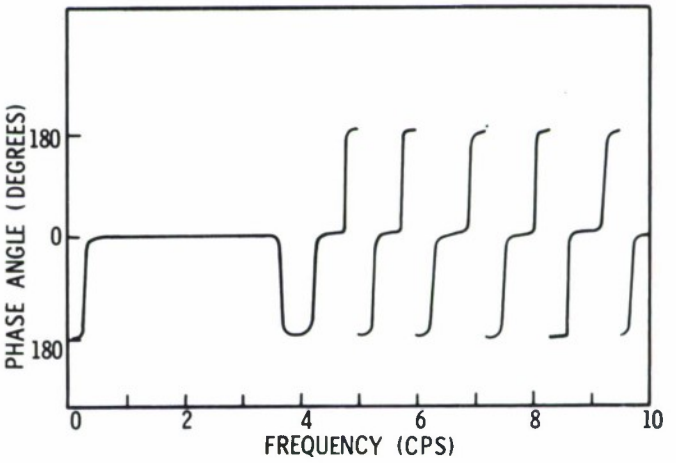

Figure V-5. Mean-Square-Error Vs Filter Length, Impulse Response and Frequency Response of MCF-19

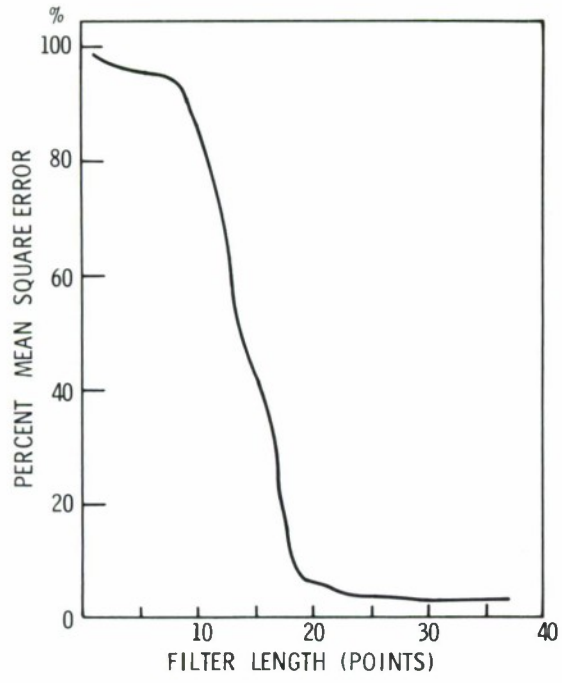

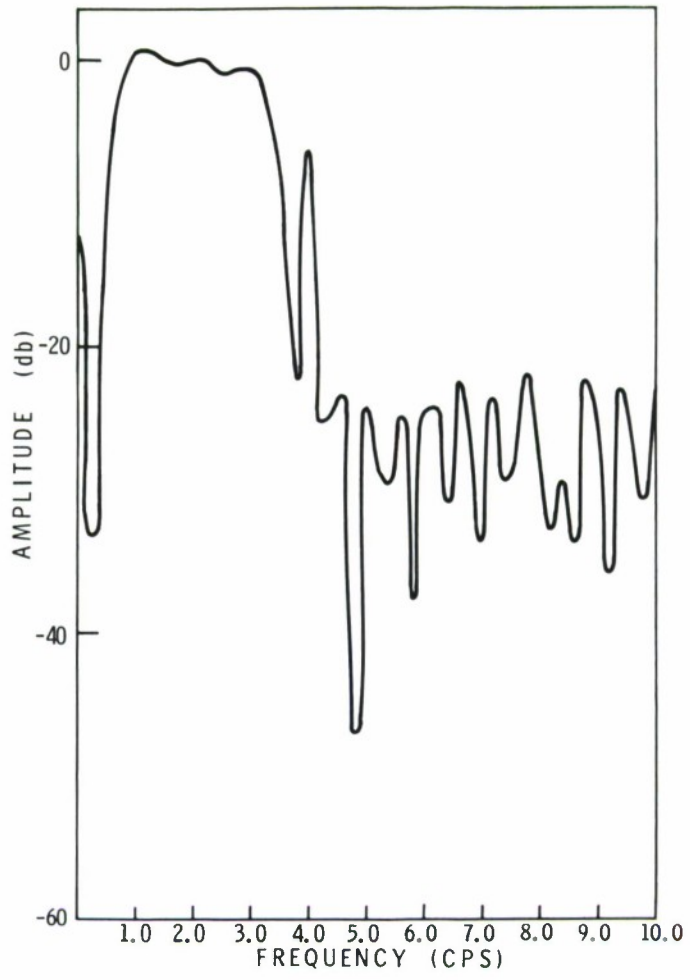

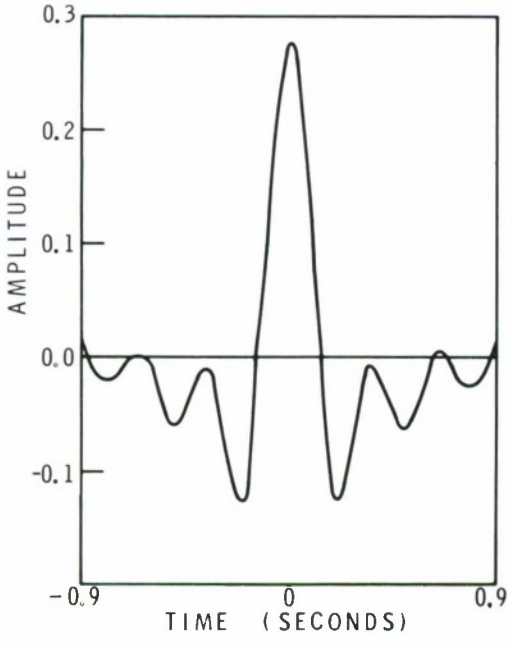

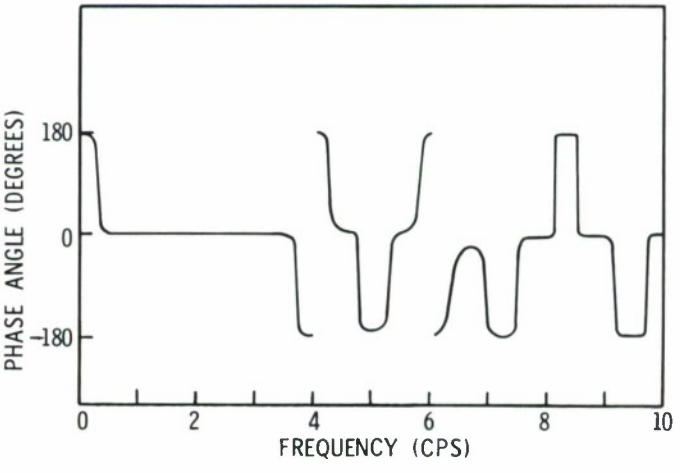

Figure V-6. Mean-Square-Error Vs Filter Length, Impulse Response and Frequency Response of MCF-20

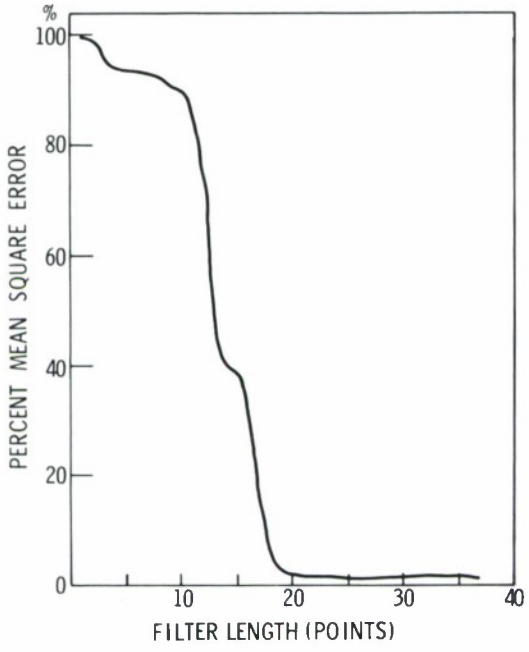

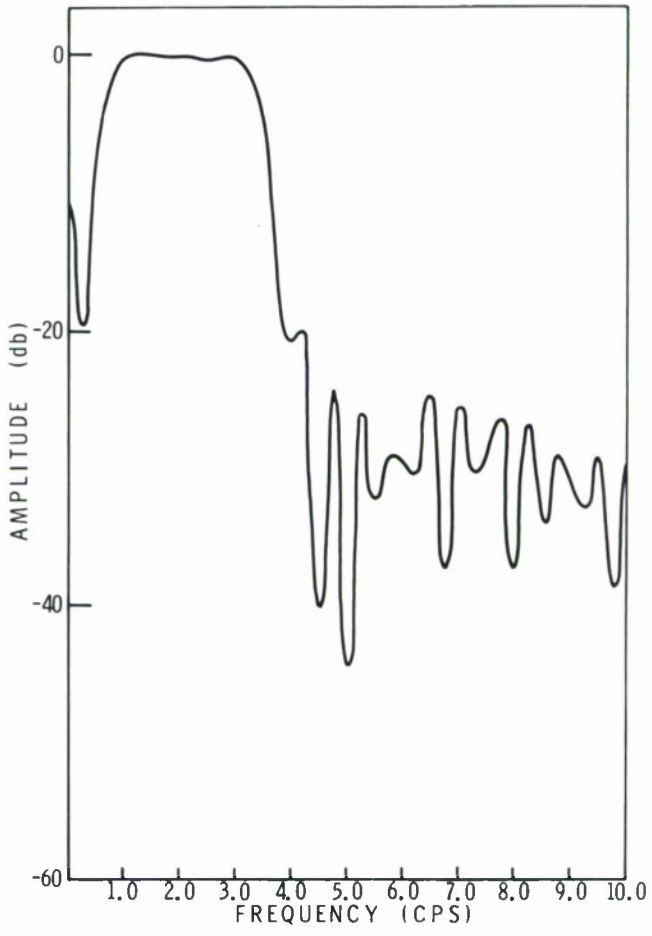

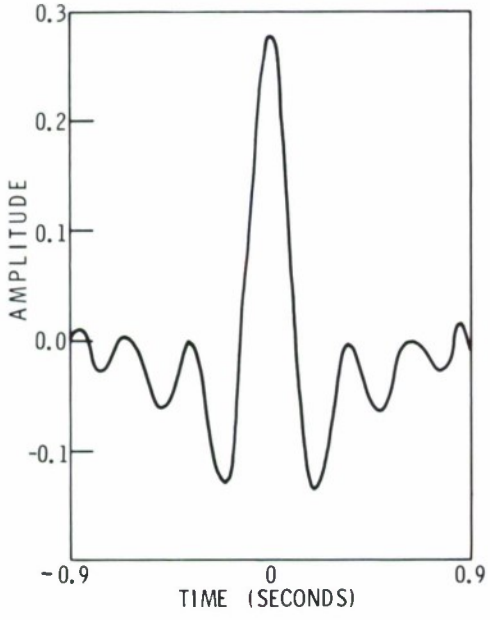

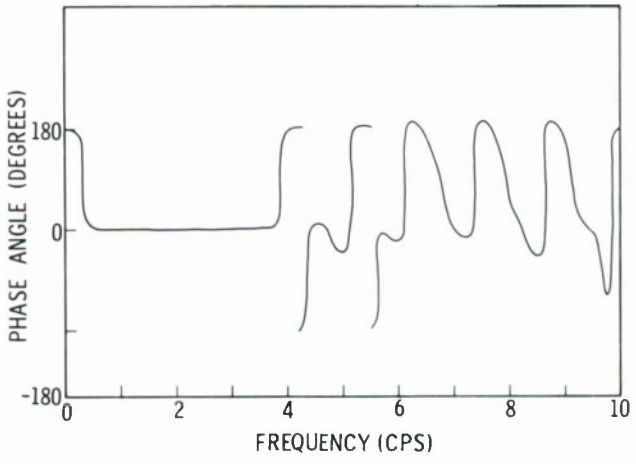

Figure V-7. Mean-Square-Error Vs Filter Length, Impulse Response and Frequency Response of MCF-21

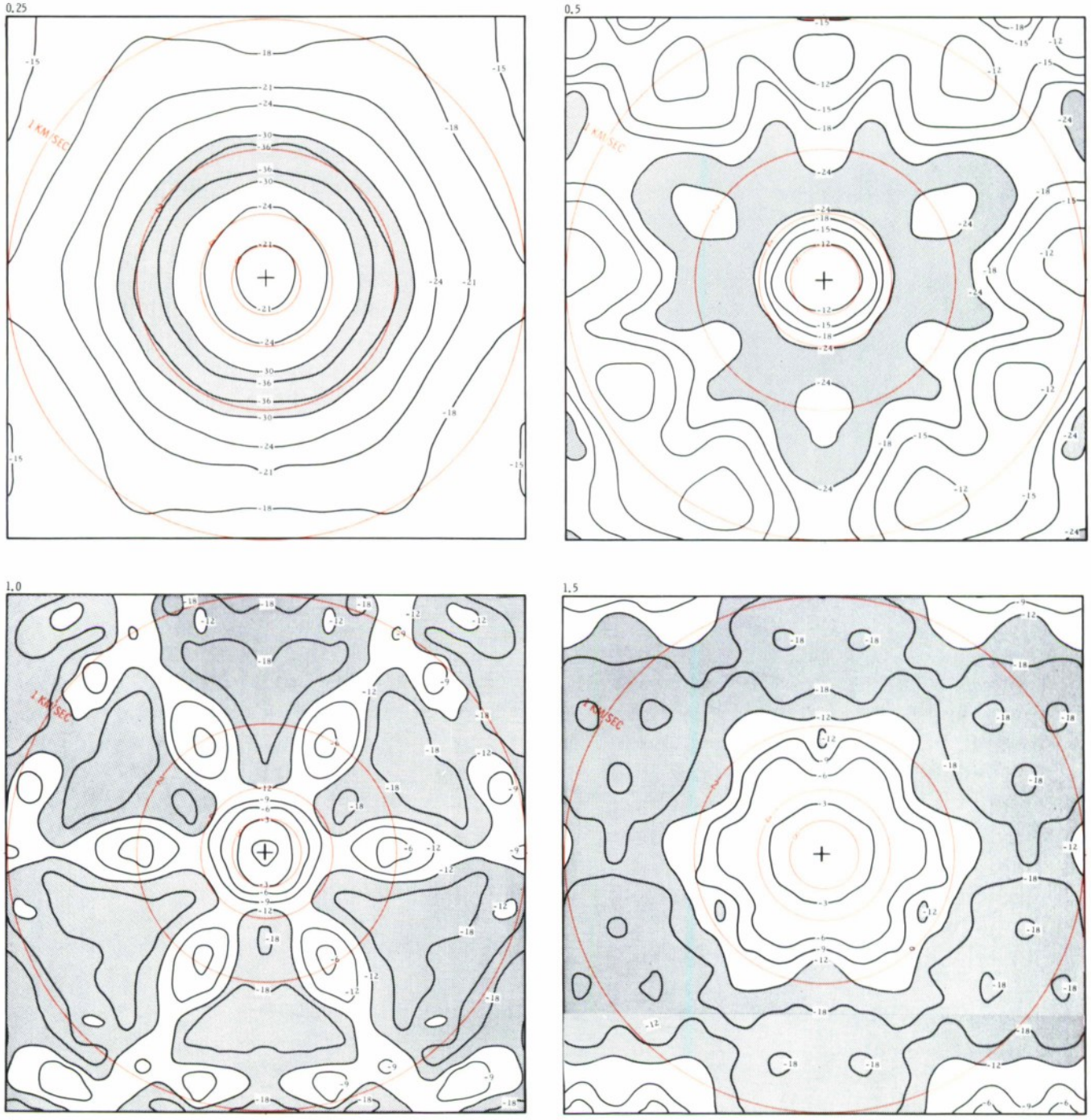

Figure V-8. Frequency-Wavenumber Response of MCF-16; f = 0.25, 0.50, 1.00 and 1.50 cps

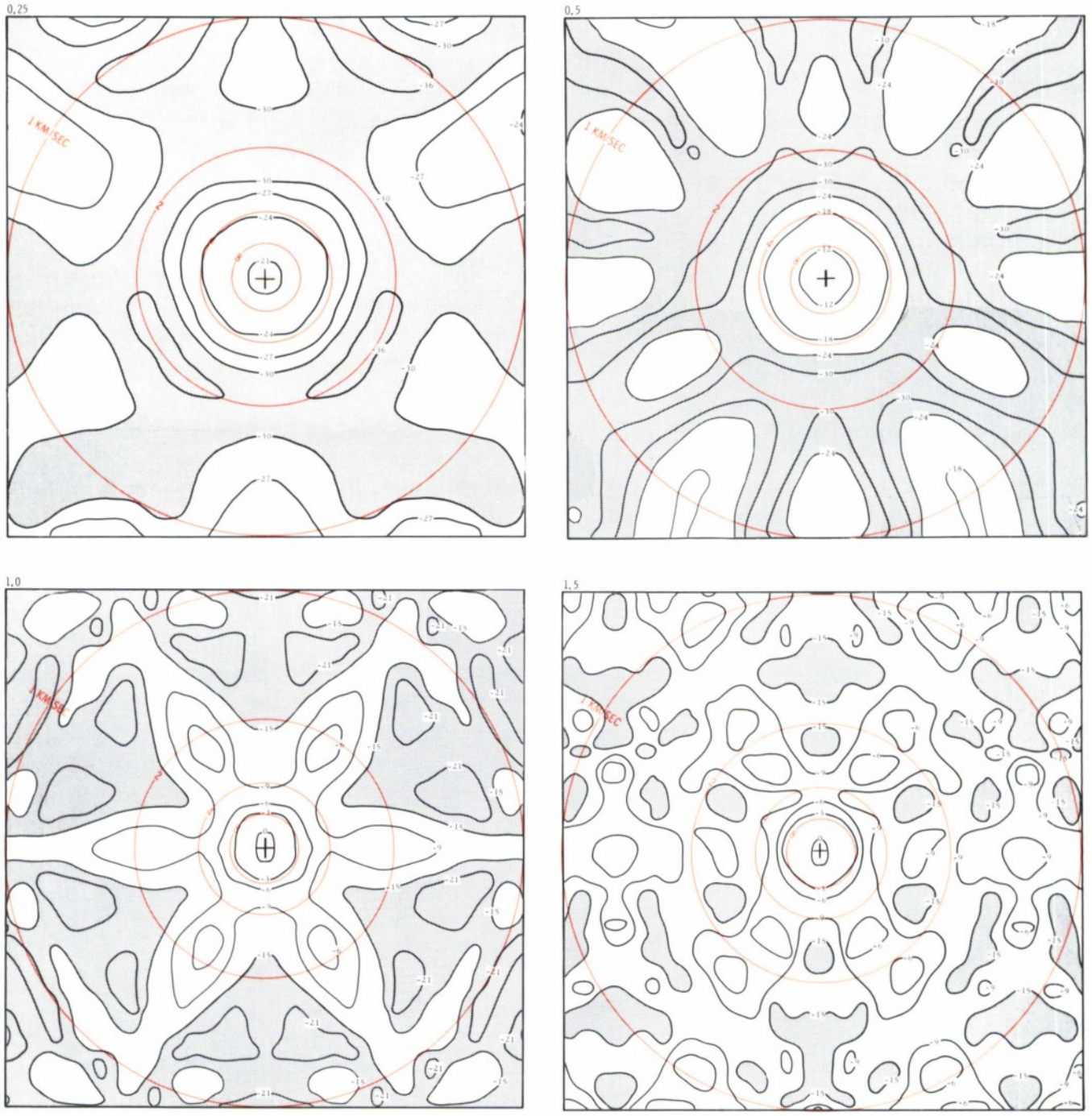

Figure V-9. Frequency-Wavenumber Response of MCF-17; f = 0.25, 0.50, 1.00 and 1.50 cps

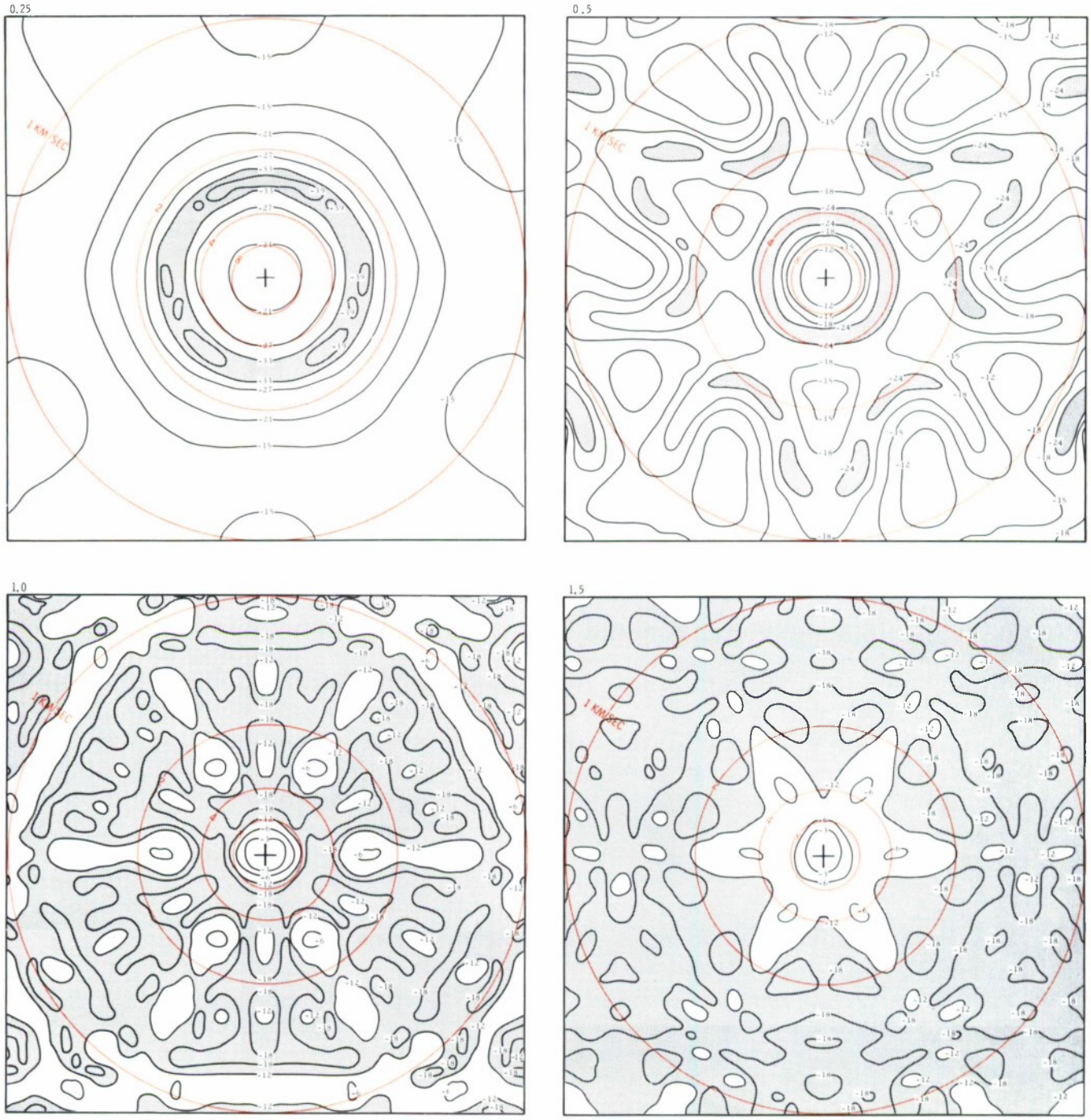

Figure V-10. Frequency-Wavenumber Response of MCF-18; f = 0.25, 0.50, 1.00 and 1.50 cps

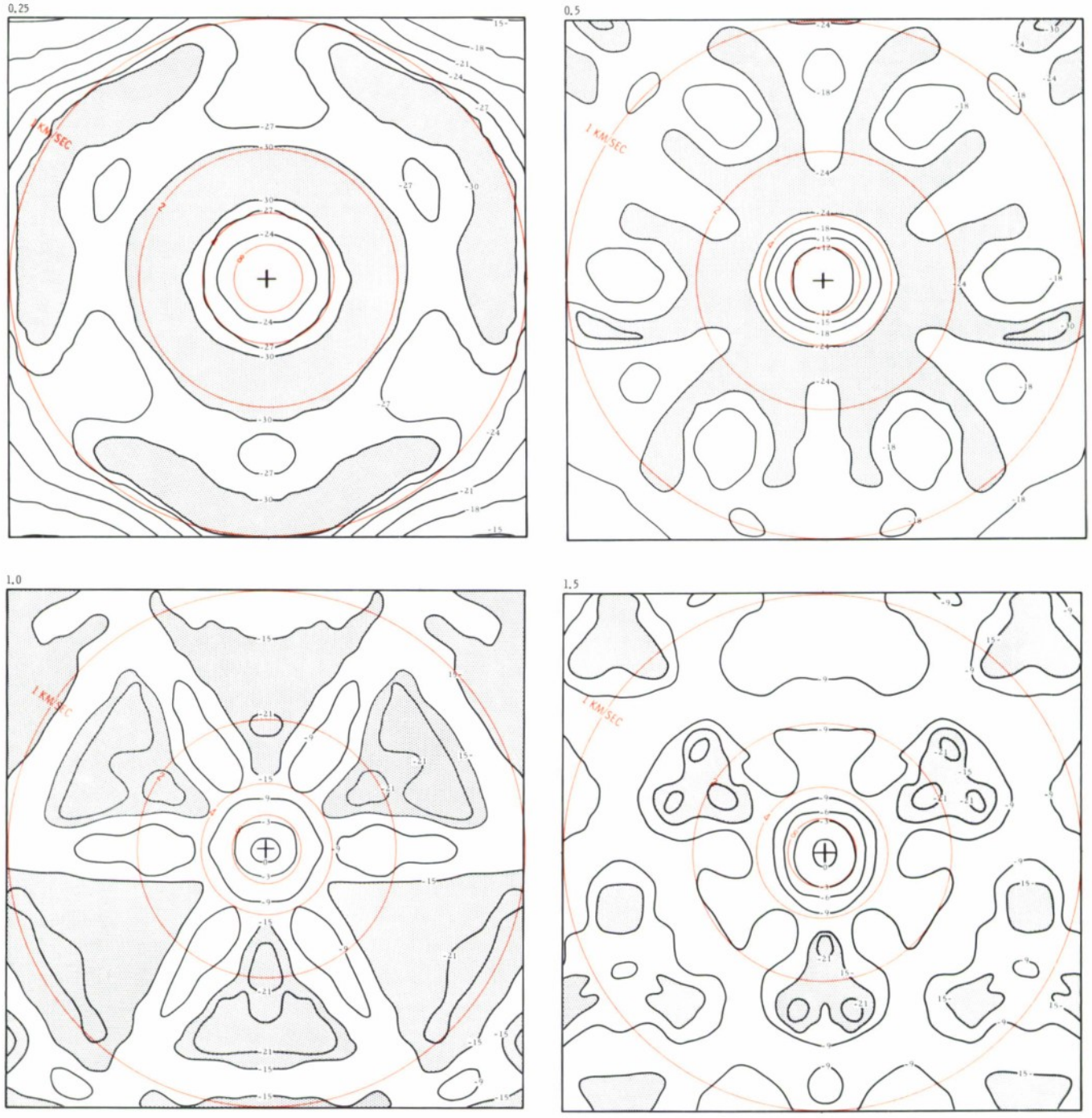

Figure V-11. Frequency-Wavenumber Response of MCF-19; f = 0.25, 0.50, 1.00 and 1.50 cps

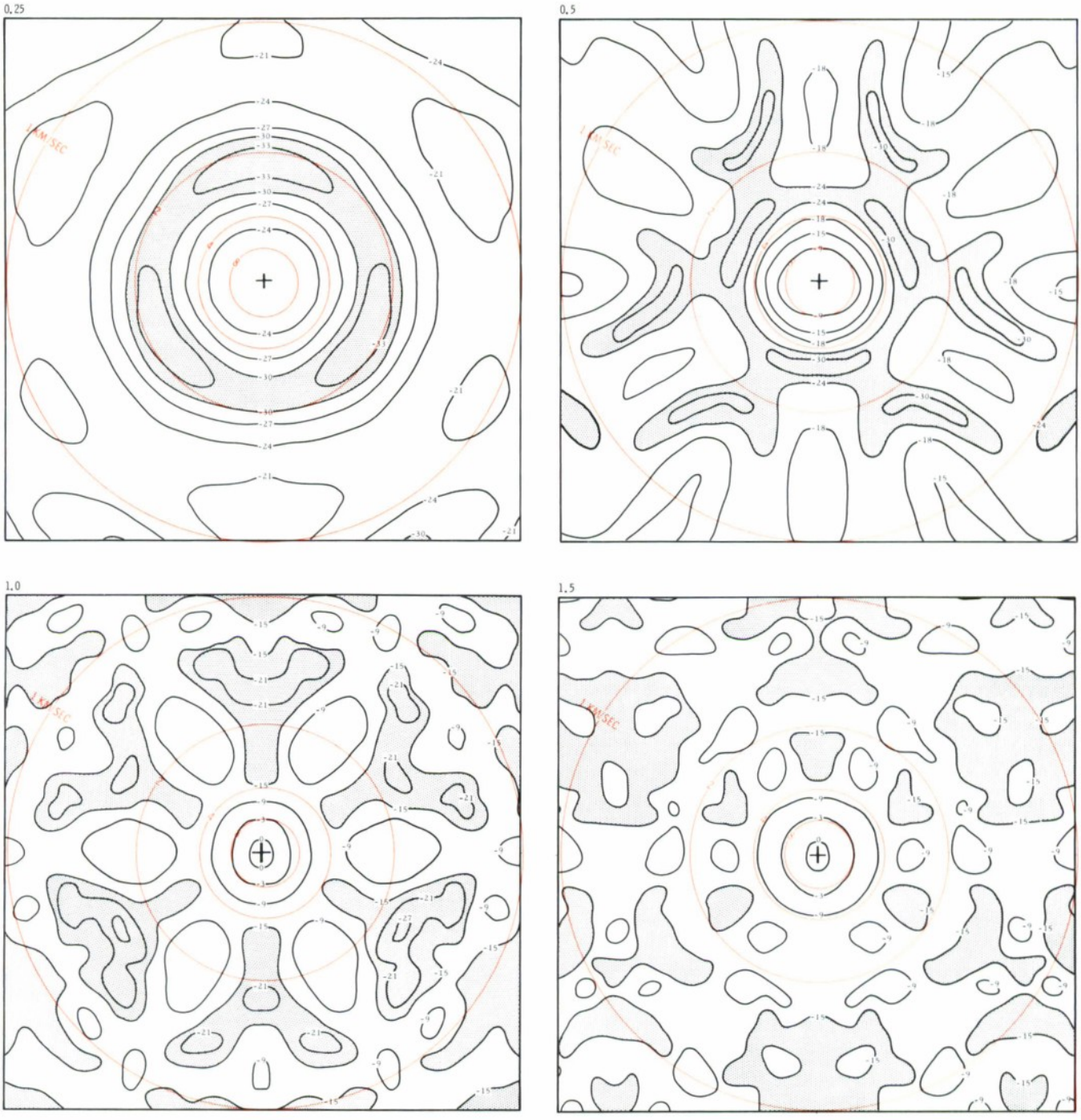

Figure V-12. Frequency-Wavenumber Response of MCF-20; f = 0.25, 0.50, 1.00 and 1.50 cps

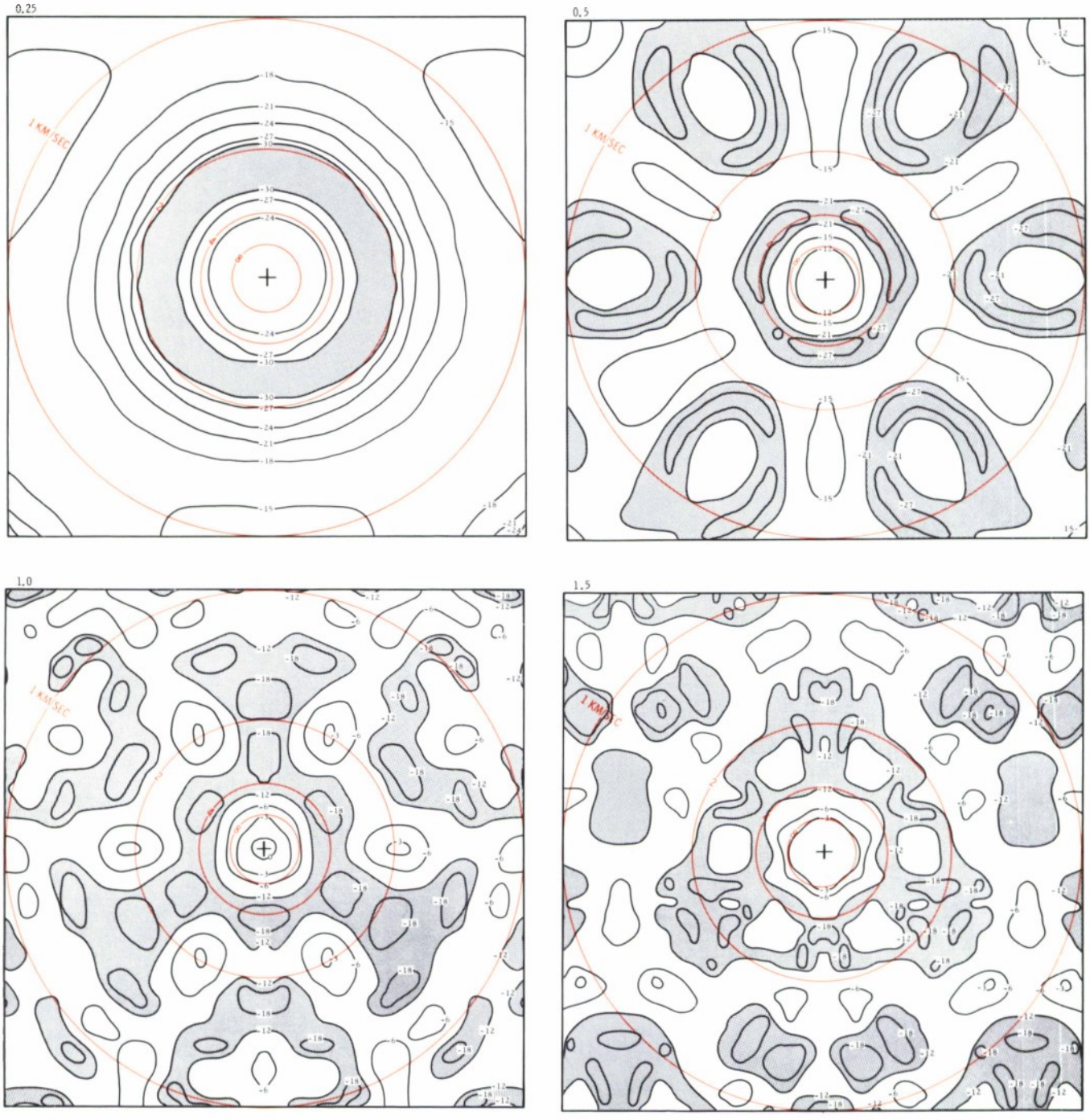

Figure V-13. Frequency-Wavenumber Response of MCF-21; f = 0.25, 0.50, 1.00 and 1.50 cps

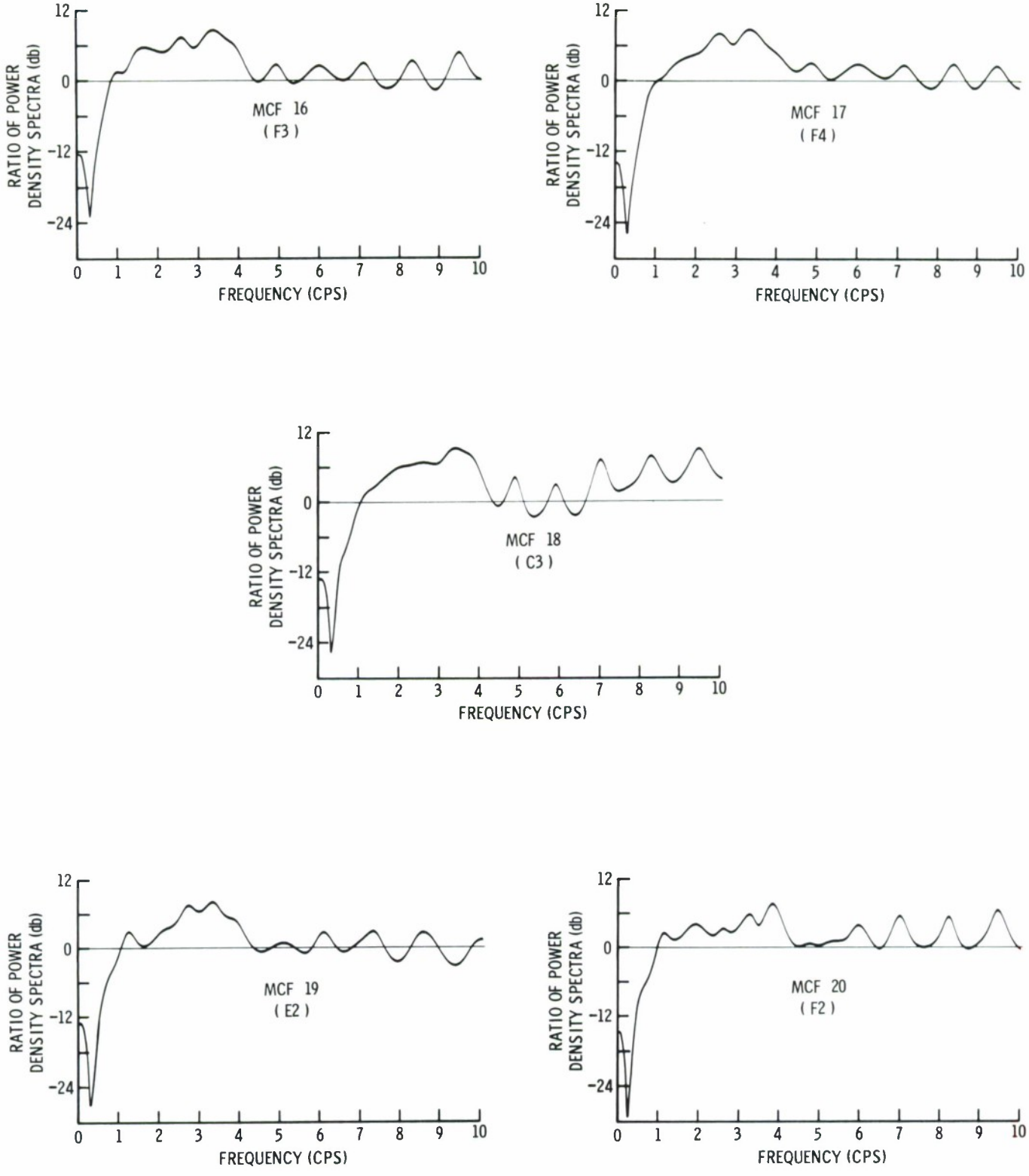

Figure V-14. Ratio of MCF Output Power Density Spectrum to Straight Sum Power Density Spectrum for Noise Immediately Preceding the Algerian Signal. Subarray at Which Noise Was Recorded is Indicated in Parentheses

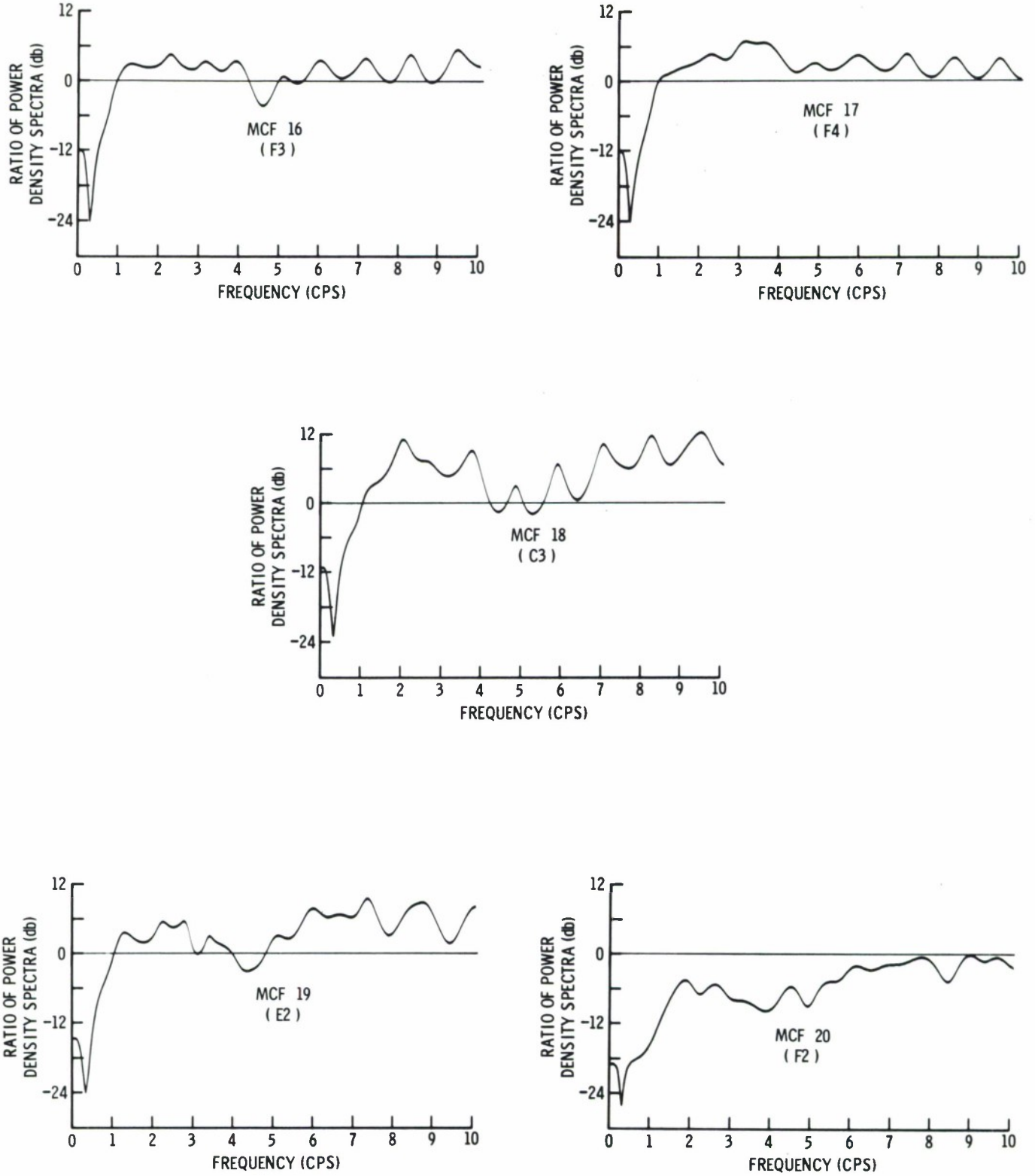

Figure V-15. Ratio of MCF Output Power Density Spectrum to Straight Sum Power Density Spectrum for Noise Immediately Preceding the Kuriles Signal. Subarray at Which Noise Was Recorded is Indicated in Parentheses

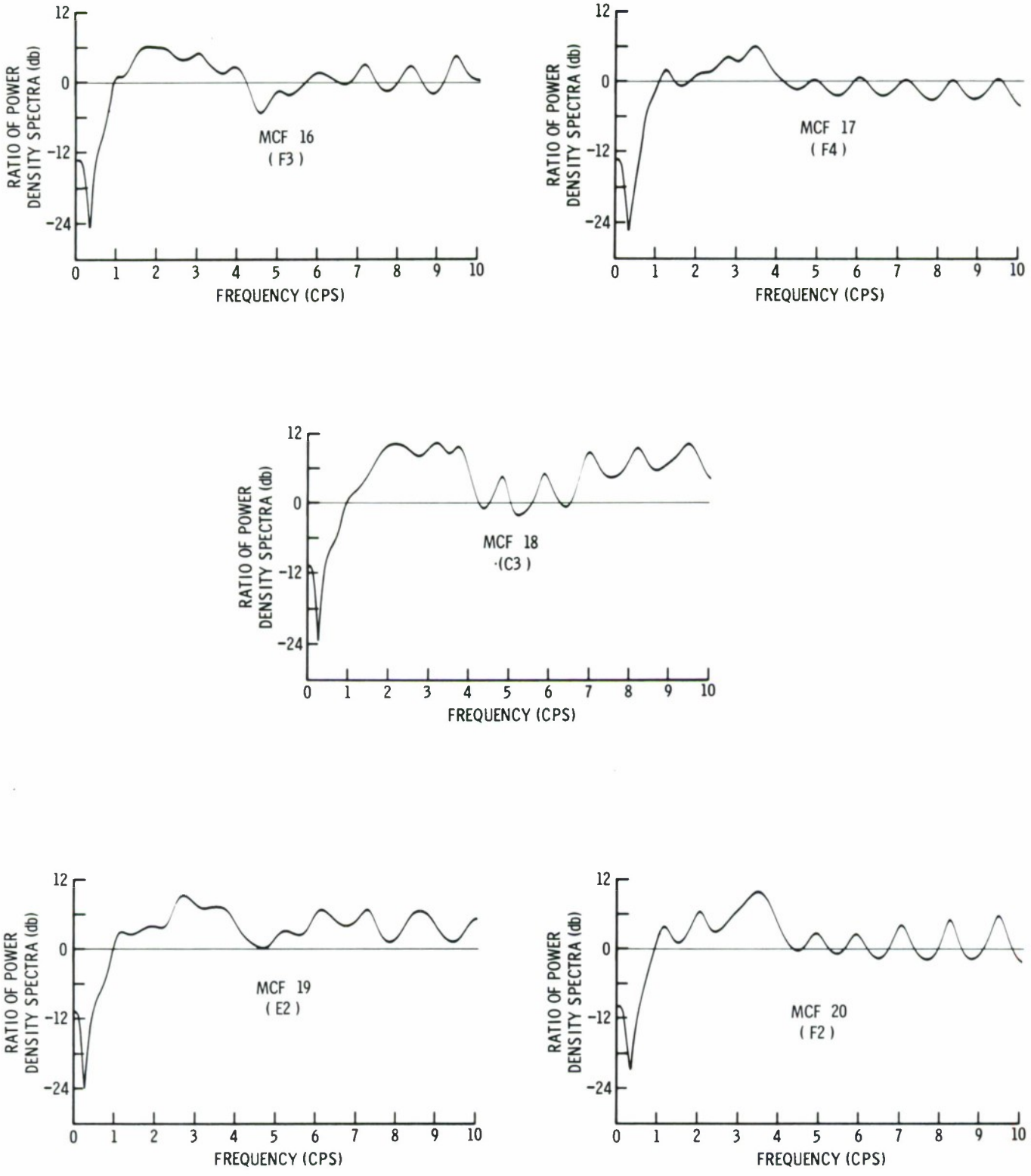

Figure V-16. Ratio of MCF Output Power Density Spectrum to Straight Sum Power Density Spectrum for Noise Immediately Preceding the Marianas Signal. Subarray at Which Noise Was Recorded is Indicated in Parentheses

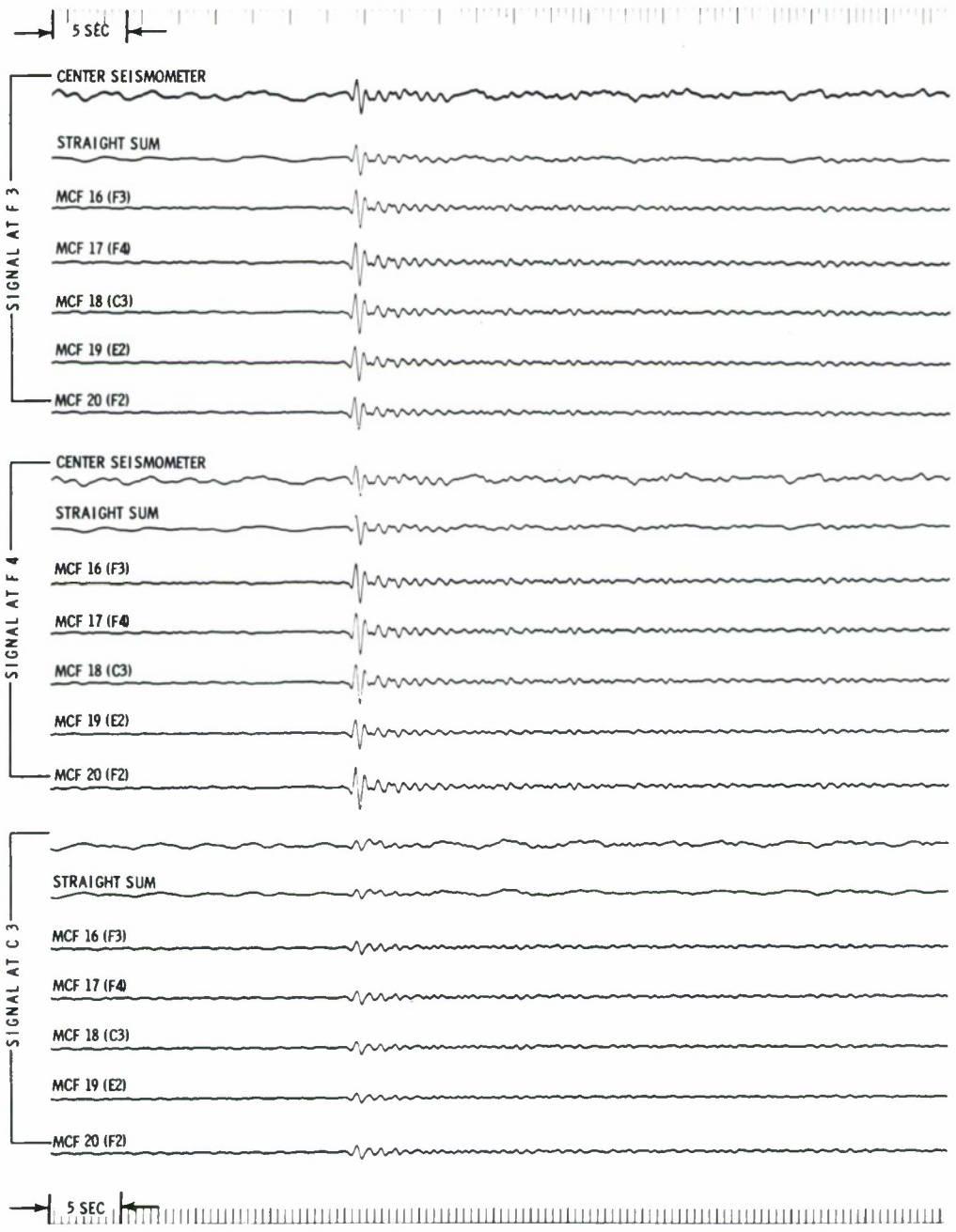

Figure V-17a. MCF Outputs and Reference Traces for Signal from Algeria. The outputs are Shown for Each Filter Applied to the Signal From Each Subarray. The Numbers in Parentheses Indicate the Subarray for Which the Filter was Designed

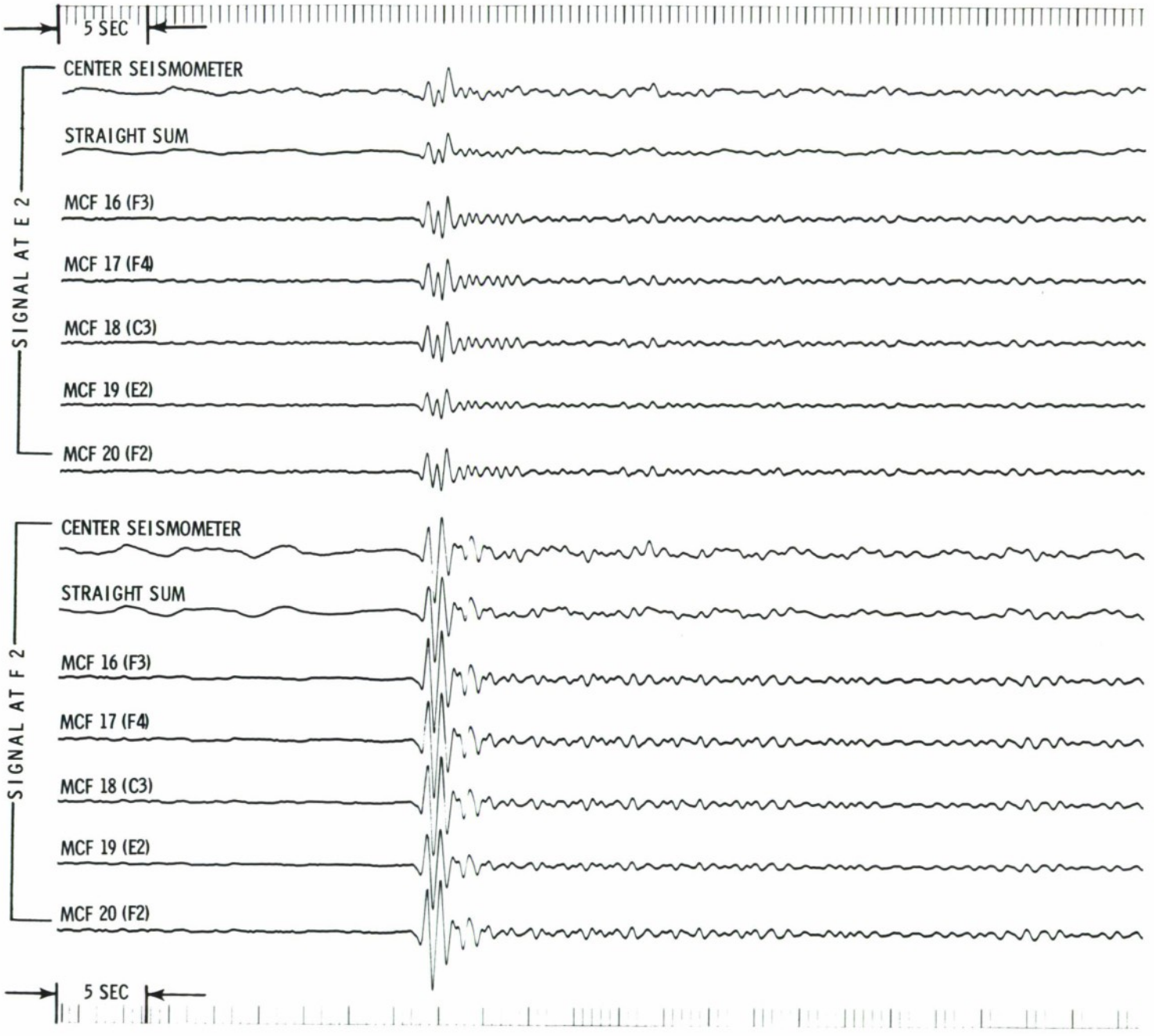

Figure V-17b. MCF Outputs and Reference Traces for Signal from Algeria. The Outputs are Shown for Each Filter Applied to the Signal from Each Subarray. The Numbers in Parentheses Indicate the Subarray for Which the Filter was Designed

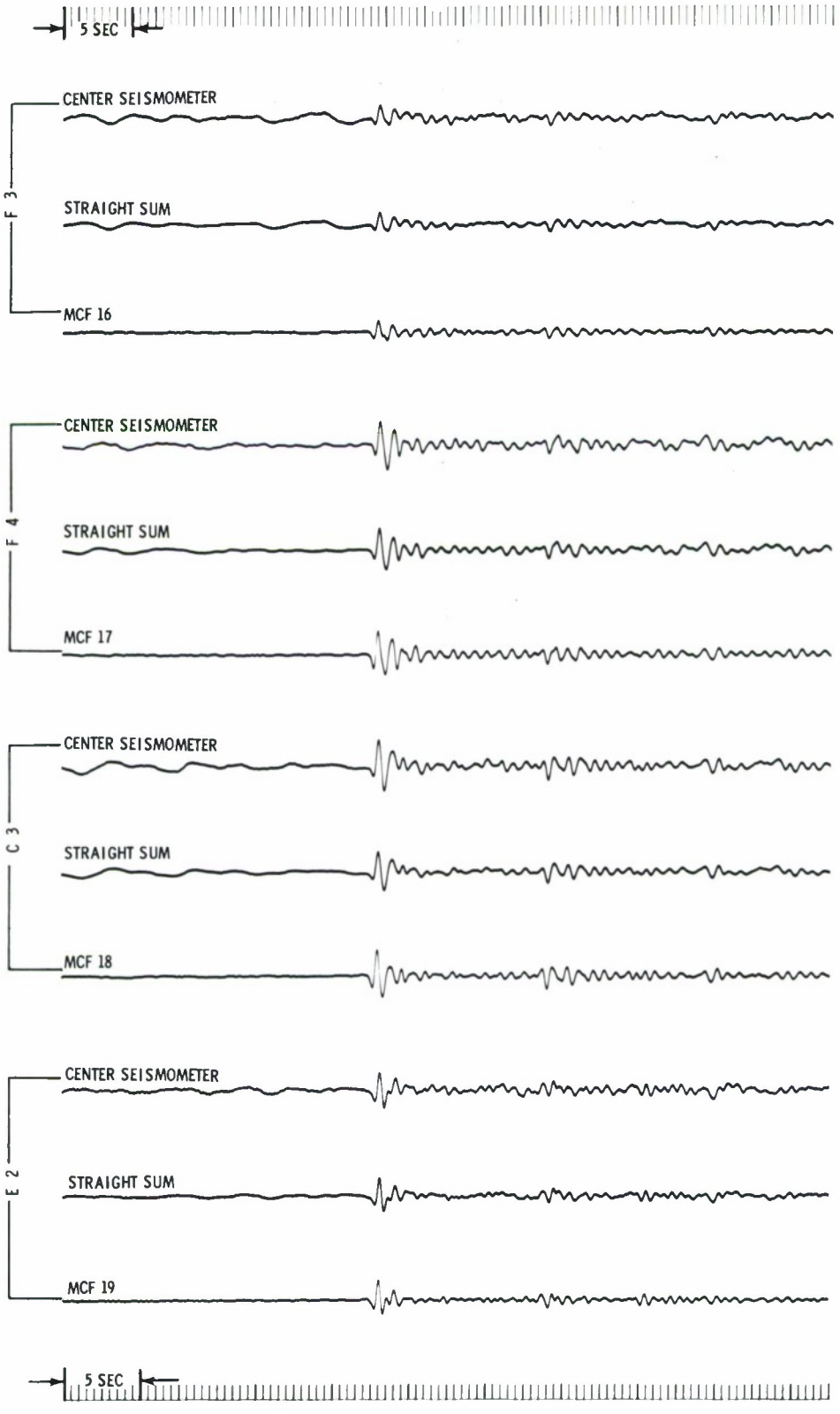

Figure V-18. MCF Outputs and Reference Traces for Signal from the Kurile Islands. The Results are Shown Only for the MCF Applied to Data for the Subarray for Which it was Designed

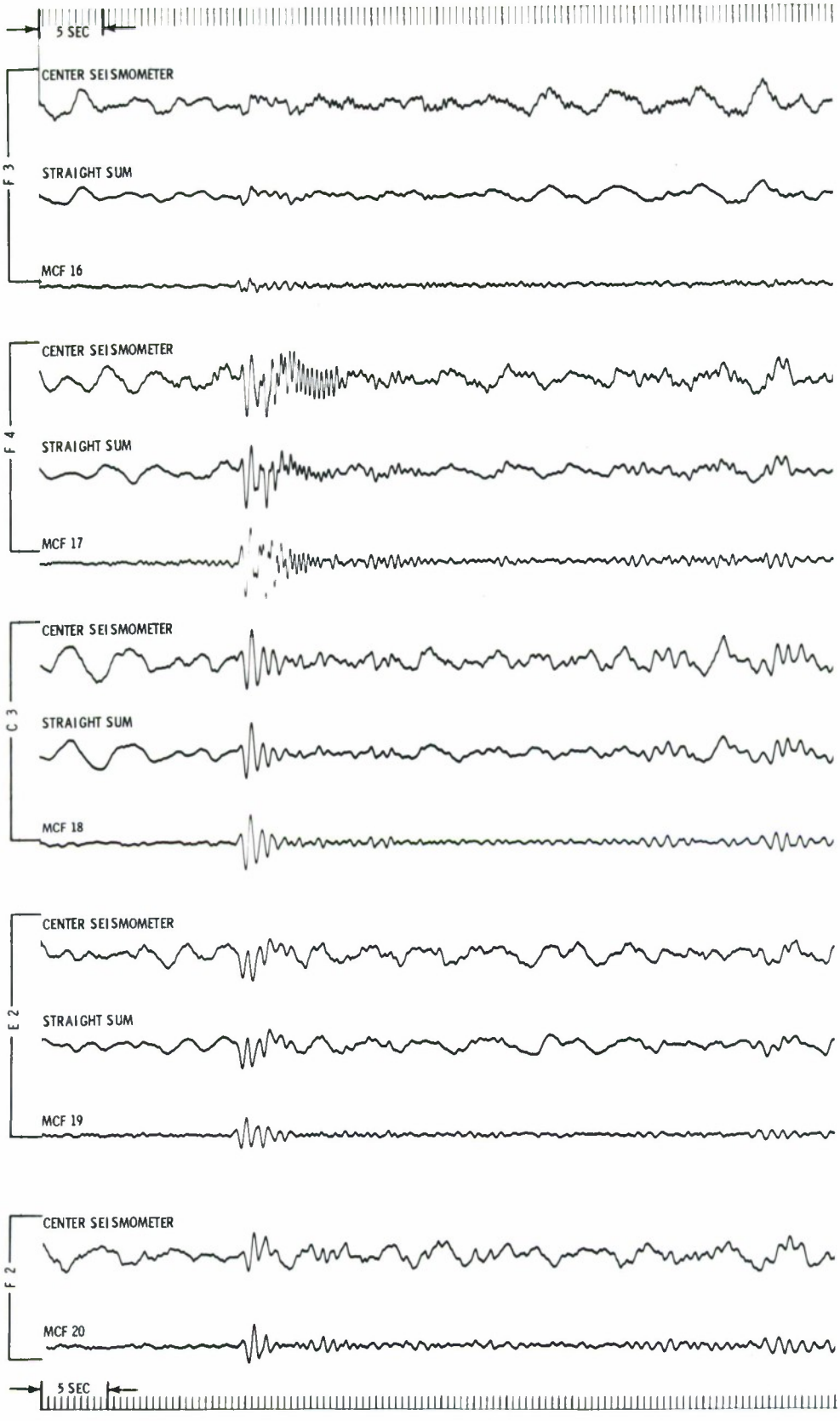

Figure V-19. MCF Outputs and Reference Traces for Signal from the Mariana Islands. The Results are Shown Only for the MCF Applied to Data for the Subarray for Which it was Designed

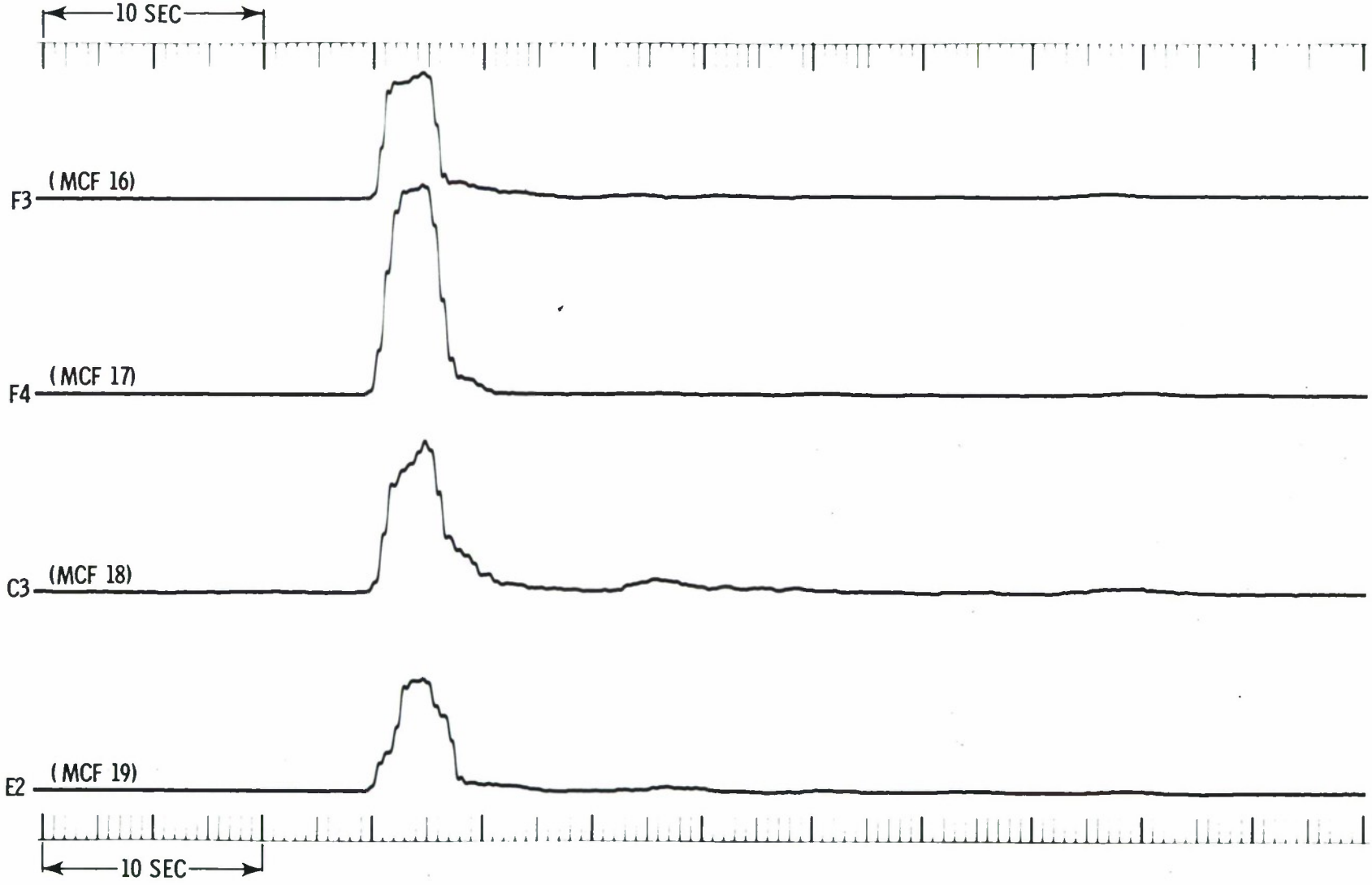

Figure V-20. Outputs of Detection Processor for Each Subarray for Signal from Algeria

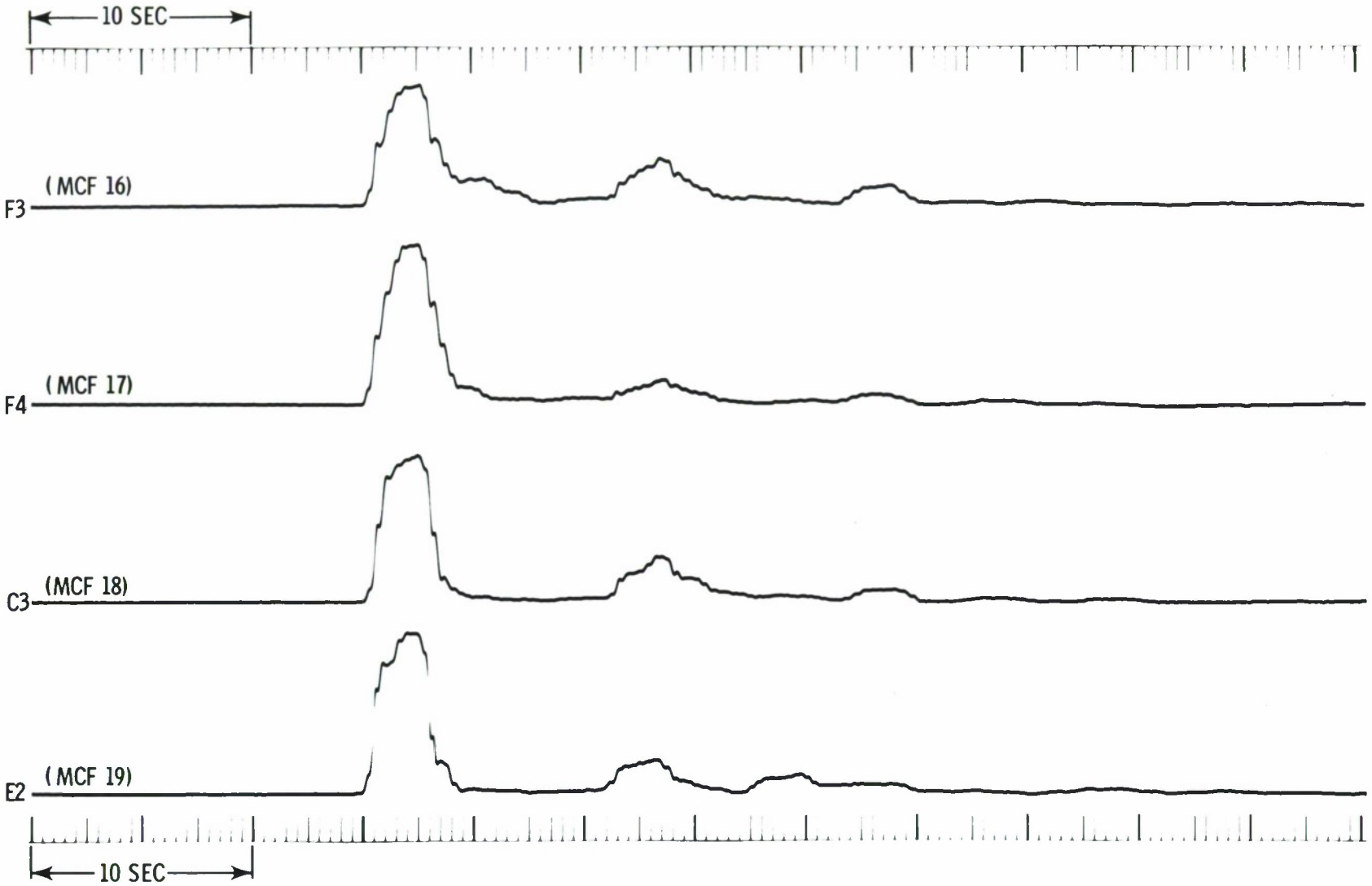

Figure V-21. Outputs of Detection Processor for Each Subarray for Signal from the Kurile Islands

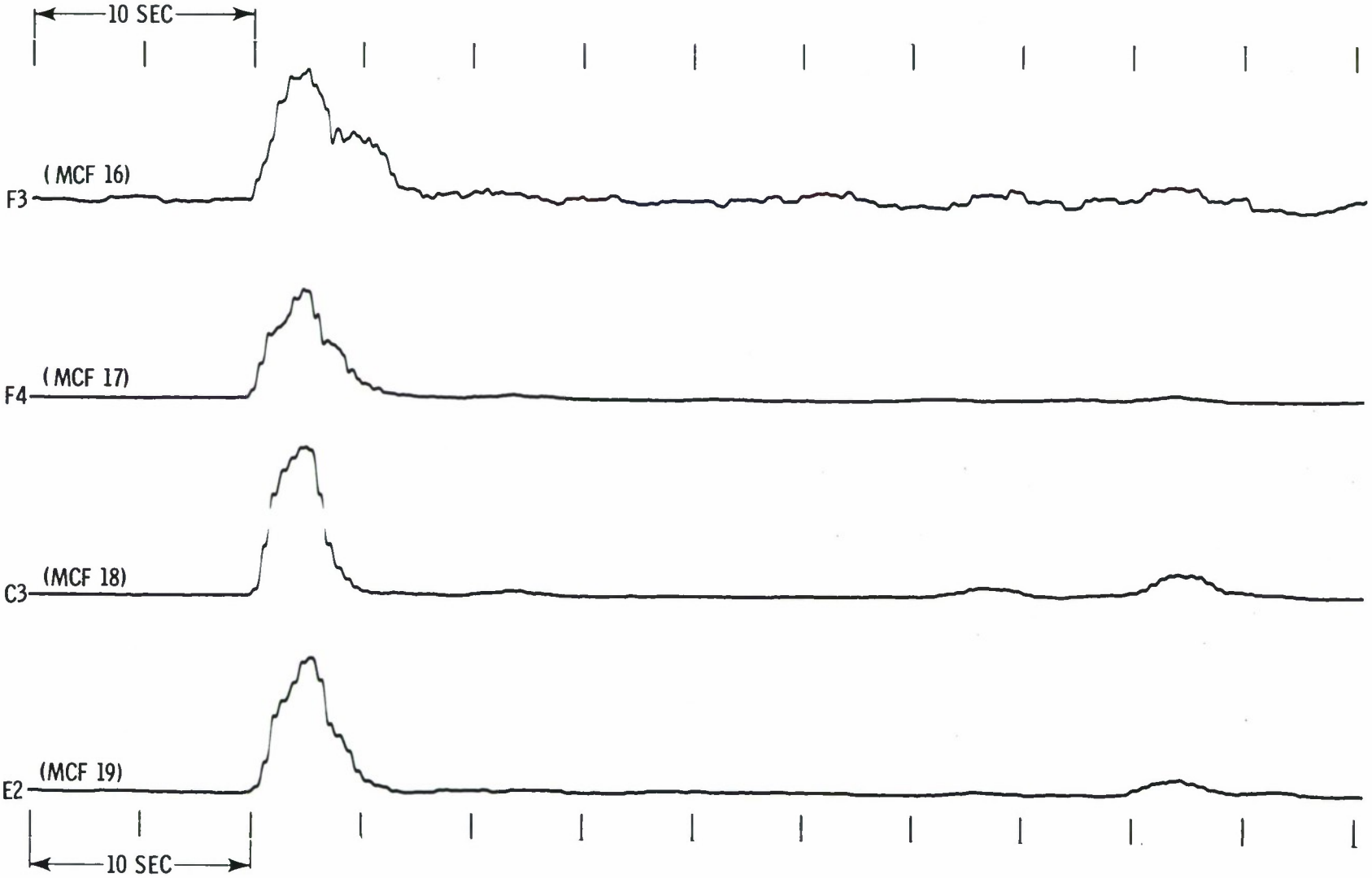

Figure V-22. Outputs of Detection Processor for Each Subarray for Signal from the Mariana Islands

APPENDIX A

AVERAGED NOISE CORRELATION SETS FOR THE FIVE SUBARRAYS

APPENDIX A

AVERAGED NOISE CORRELATION SETS FOR THE FIVE SUBARRAYS

The noise models used in the design of the filters presented in Section V were formed by averaging several ring model correlation sets. The recording date and time of the noise sample for each correlation set is listed in Table V-1. The list consists of seven night noise and five day noise samples. Therefore, to equally represent day and night noise, the day noise samples are multiplied by a factor of 7/5.

Two night noise samples (5 Nov 1965 and 16 Nov 1965) at subarray F-3 and one night noise sample (23 Nov 1965) at subarray E-2 were found to be unusable due to severe non-seismic noise bursts. These samples are excluded from the average.

Figures A-1a through A-5b present the averaged-noise correlation sets for the five subarrays. The correlations are in the order (ring)1*(ring)1, 1*2, ... 1*5, 2*2, ... 2*5, 3*3, ... 3*5, 4*4, 4*5, 5*5, for each subarray. The crosscorrelations are shown from -2.0 sec to +2.0 sec, and the autocorrelations between 0.0 sec and 2.0 sec. Each lag value represents 0.05 sec in time.

Whitening filters were developed for each subarray using the averaged autocorrelation of the center seismometer (ring1). These filters are presented in Table A-1. Each filter was autocorrelated and subsequently convolved with the averaged correlations of that set. The resulting sets of whitened correlations were truncated by the convolution process to between -1.85 sec and +1.85 sec in length, and were used in the MCF design.

The inclusion in this report of the listings of the unwhitened correlation sets is based on the belief that they would be of considerable use to those interested in further study along these lines. Much expensive and relatively non-technical effort was required to assemble, demultiplex, ring-sum, compute and average correlations with such a considerable quantity of data. The availability of this data may expedite further signal detection studies.

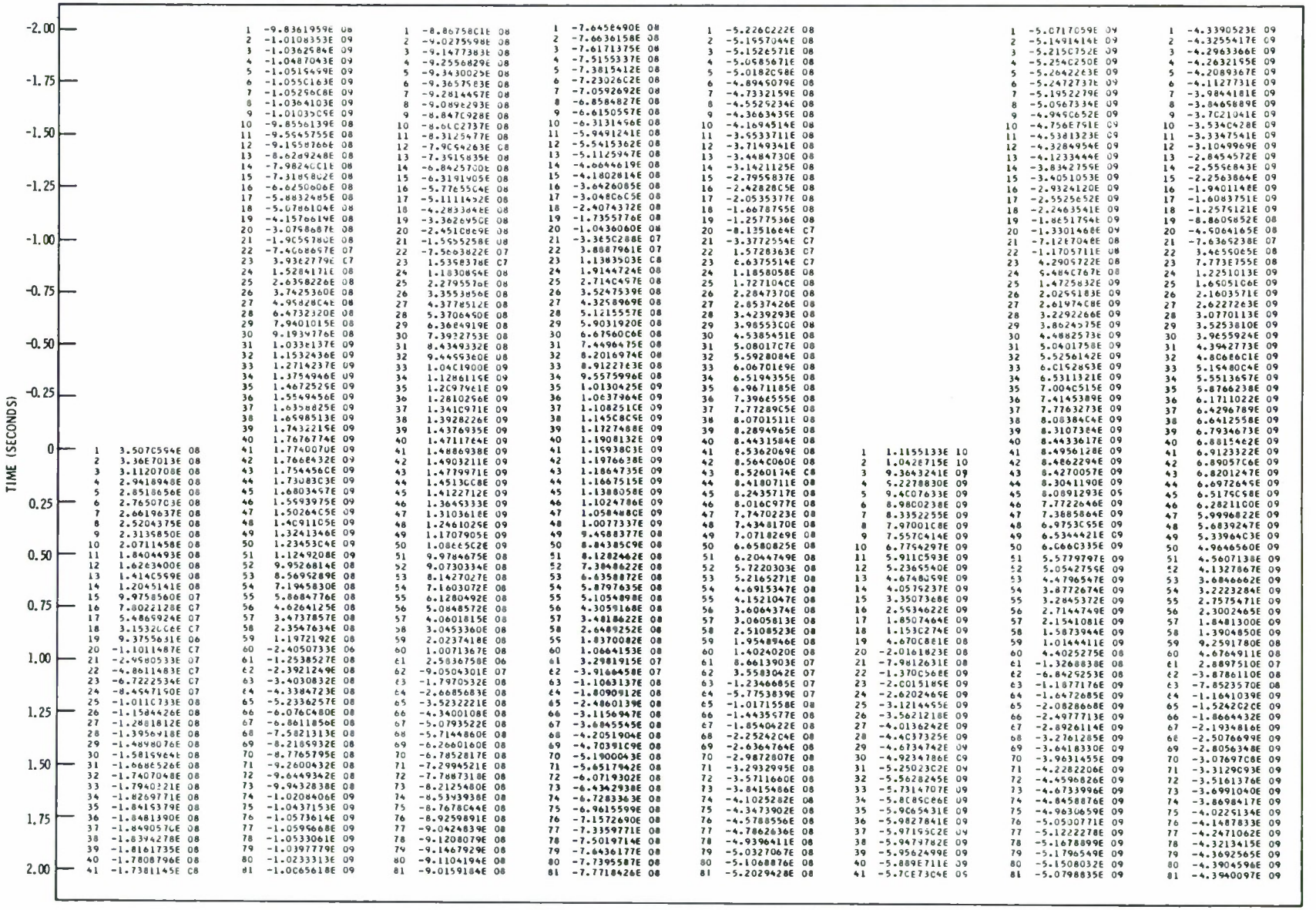

Figure A-1a. Averaged (Day plus Night) Noise Correlation Set for 5-Channel Ring Model of Subarray F-3

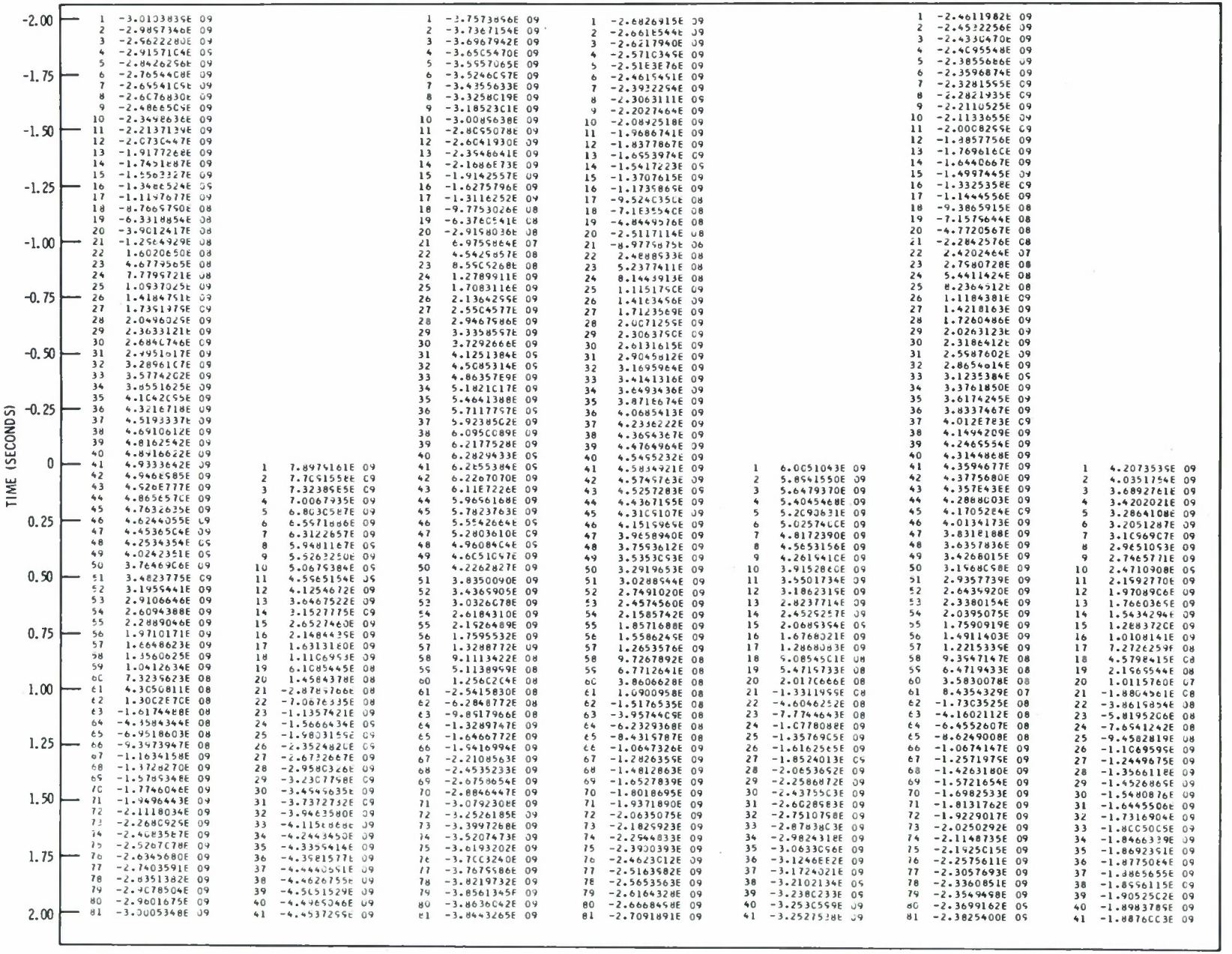

Figure A-1b. Averaged (Day plus Night) Noise Correlation Set for 5-Channel Ring Model of Subarray F-3

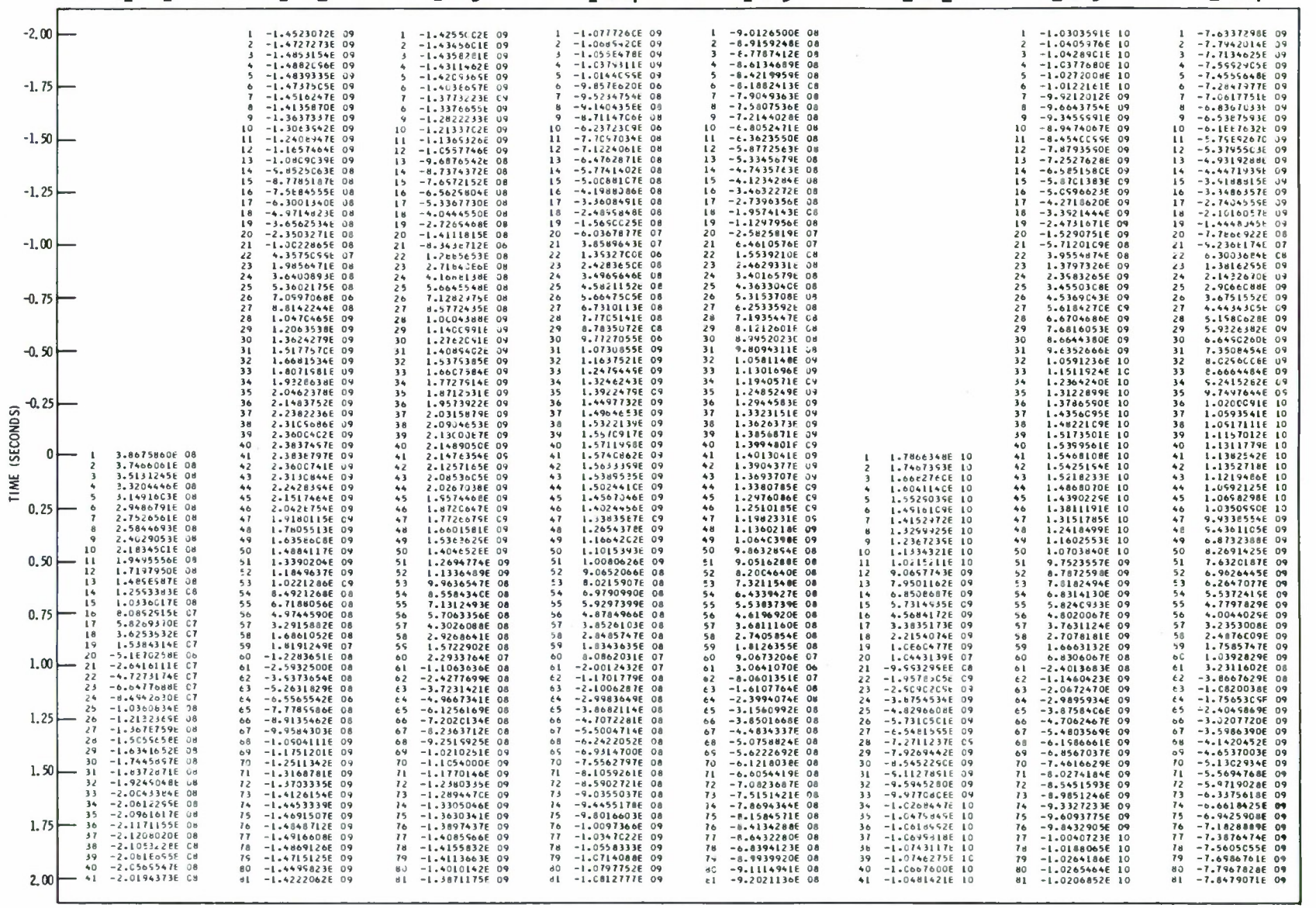

Figure A-2a. Averaged (Day plus Night) Noise Correlation Set for 5-Channel Ring Model of Subarray F-2

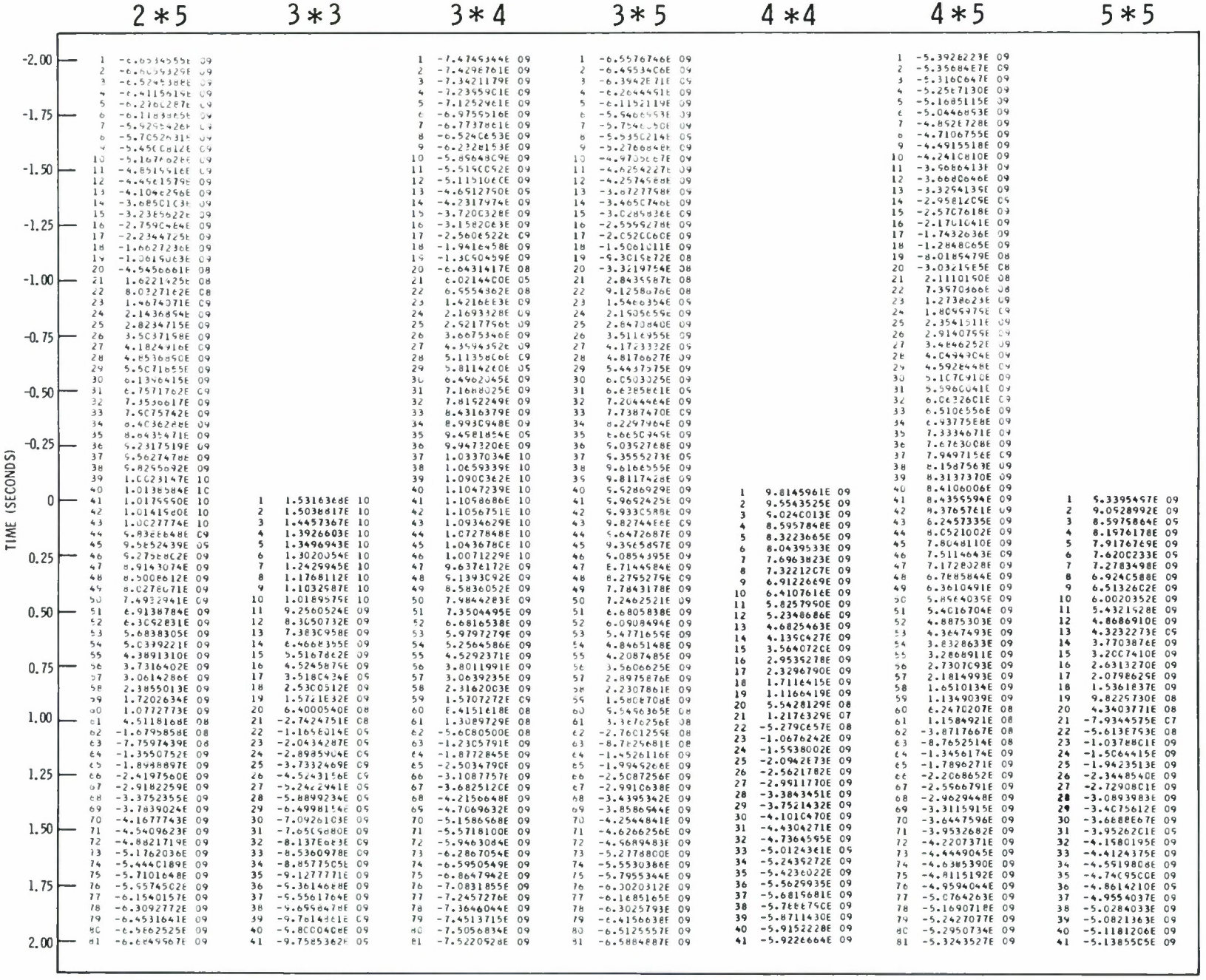

Figure A-2b. Averaged (Day plus Night) Noise Correlation Set for 5-Channel Ring Model of Subarray F-2

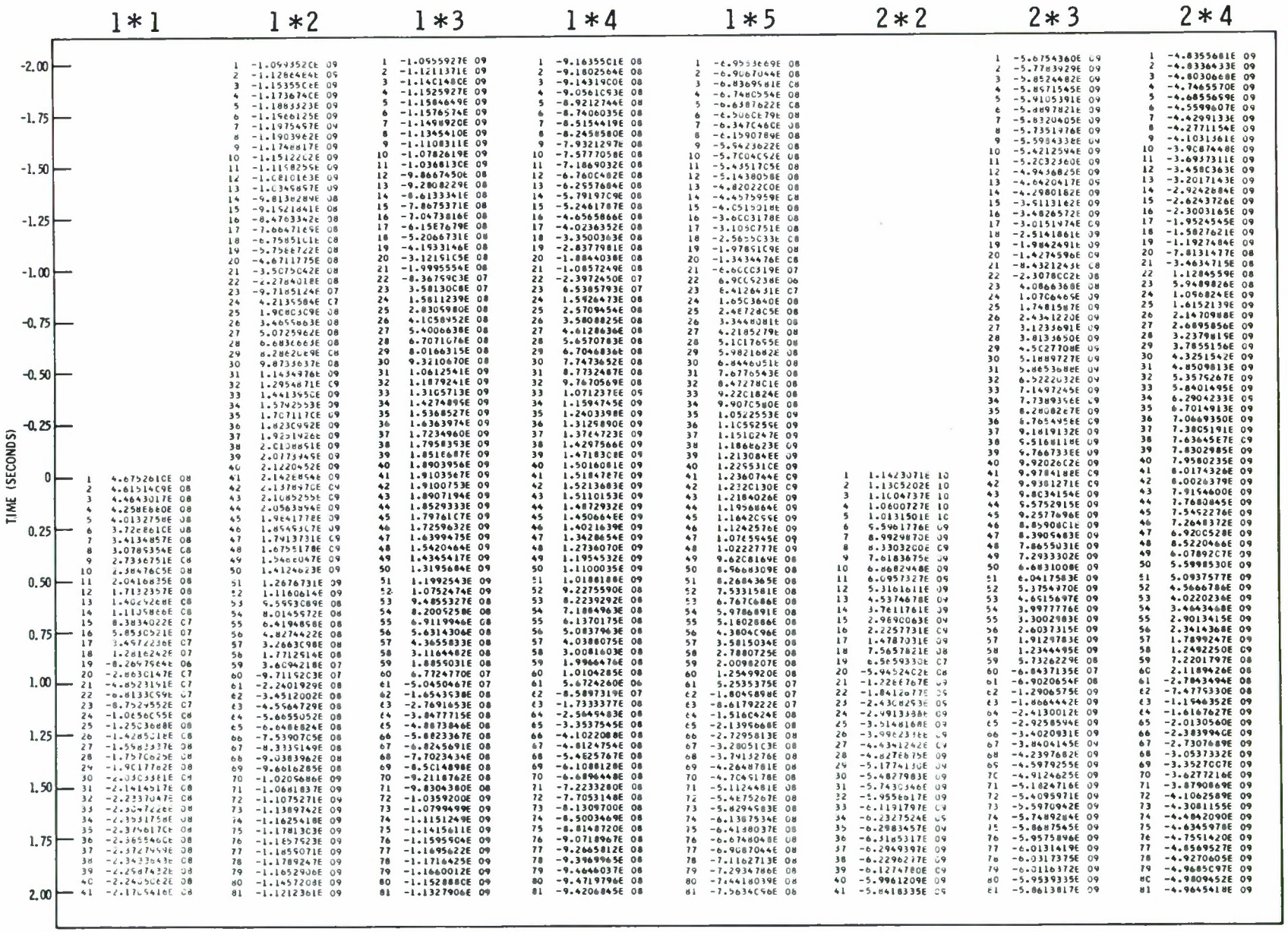

Figure A-3a. Averaged (Day plus Night) Noise Correlation Set for 5-Channel Ring Model of Subarray F-4

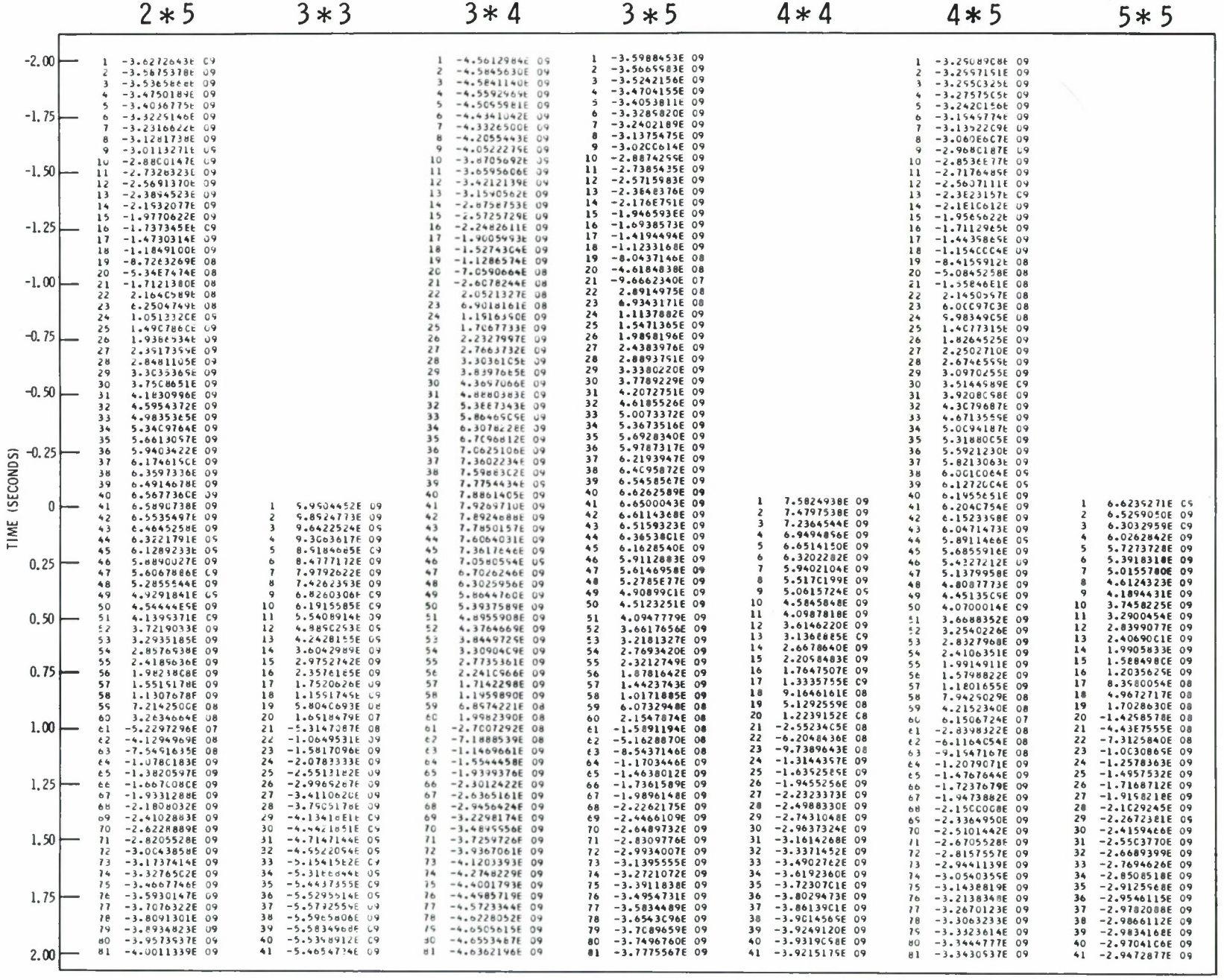

Figure A-3b. Averaged (Day plus Night) Noise Correlation Set for 5-Channel Ring Model of Subarray F-4

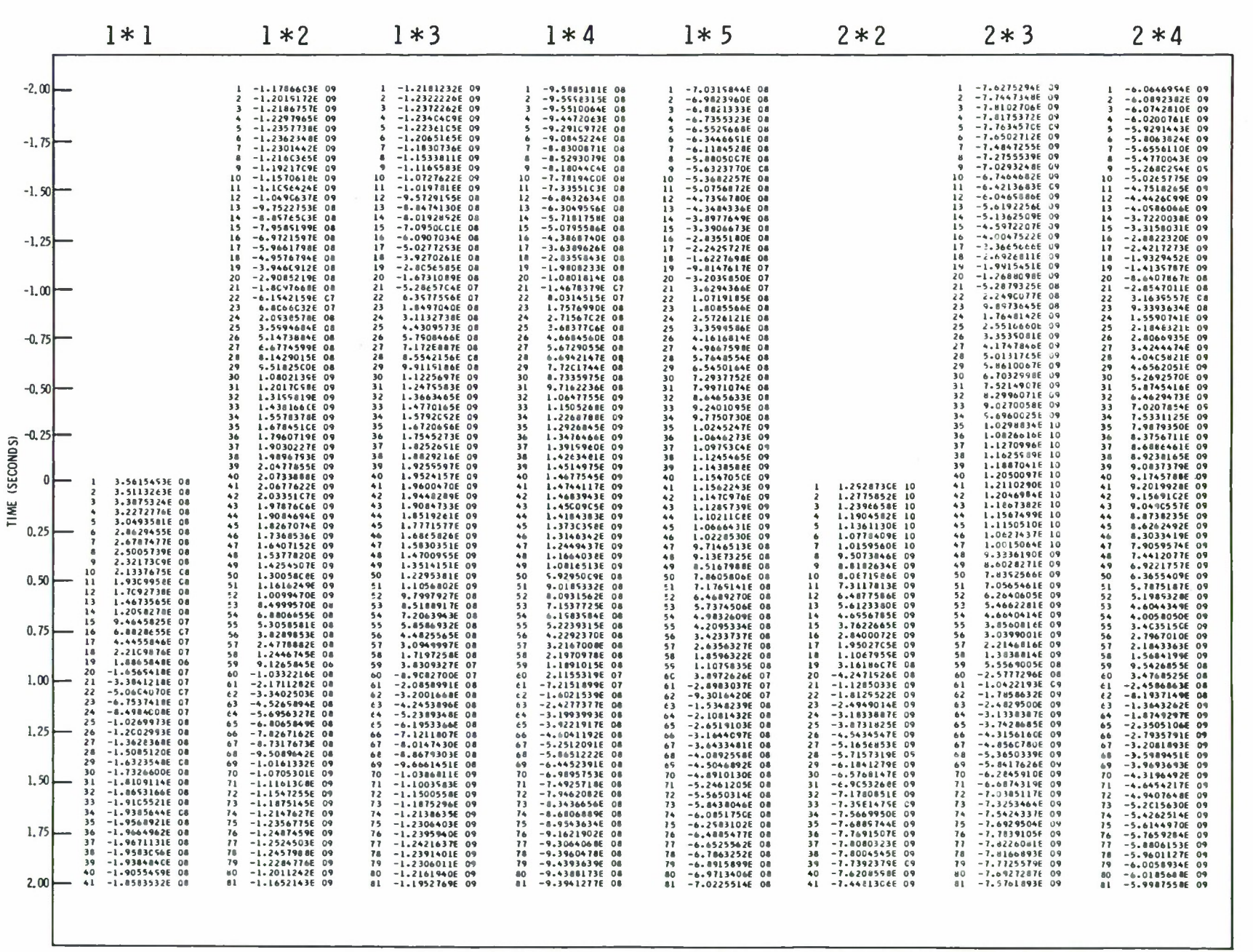

Figure A-4a. Averaged (Day plus Night) Noise Correlation Set for 5-Channel Ring Model for Subarray C-3

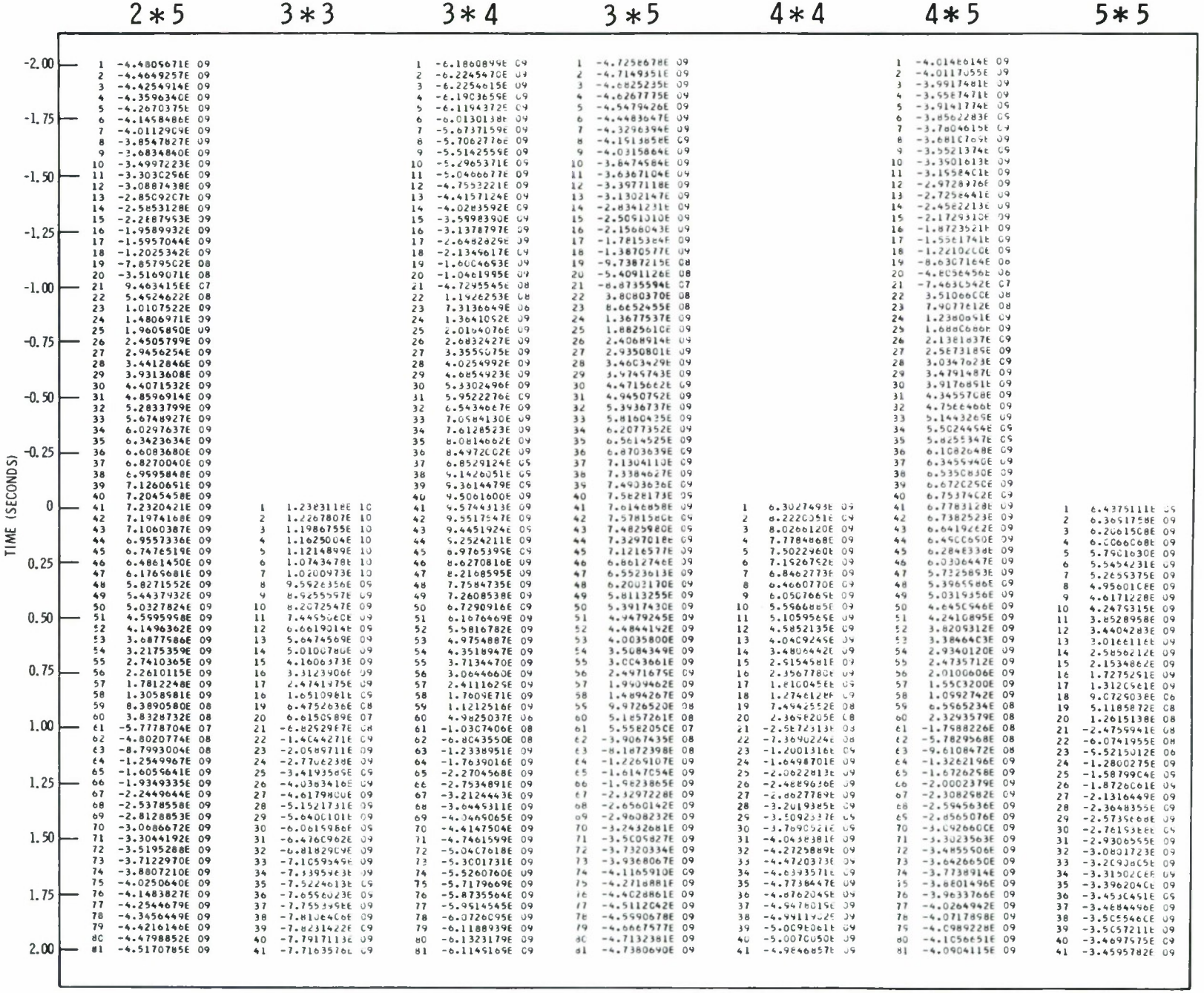

Figure A-4b. Averaged (Day plus Night) Noise Correlation Set for 5-Channel Ring Model of Subarray C-3

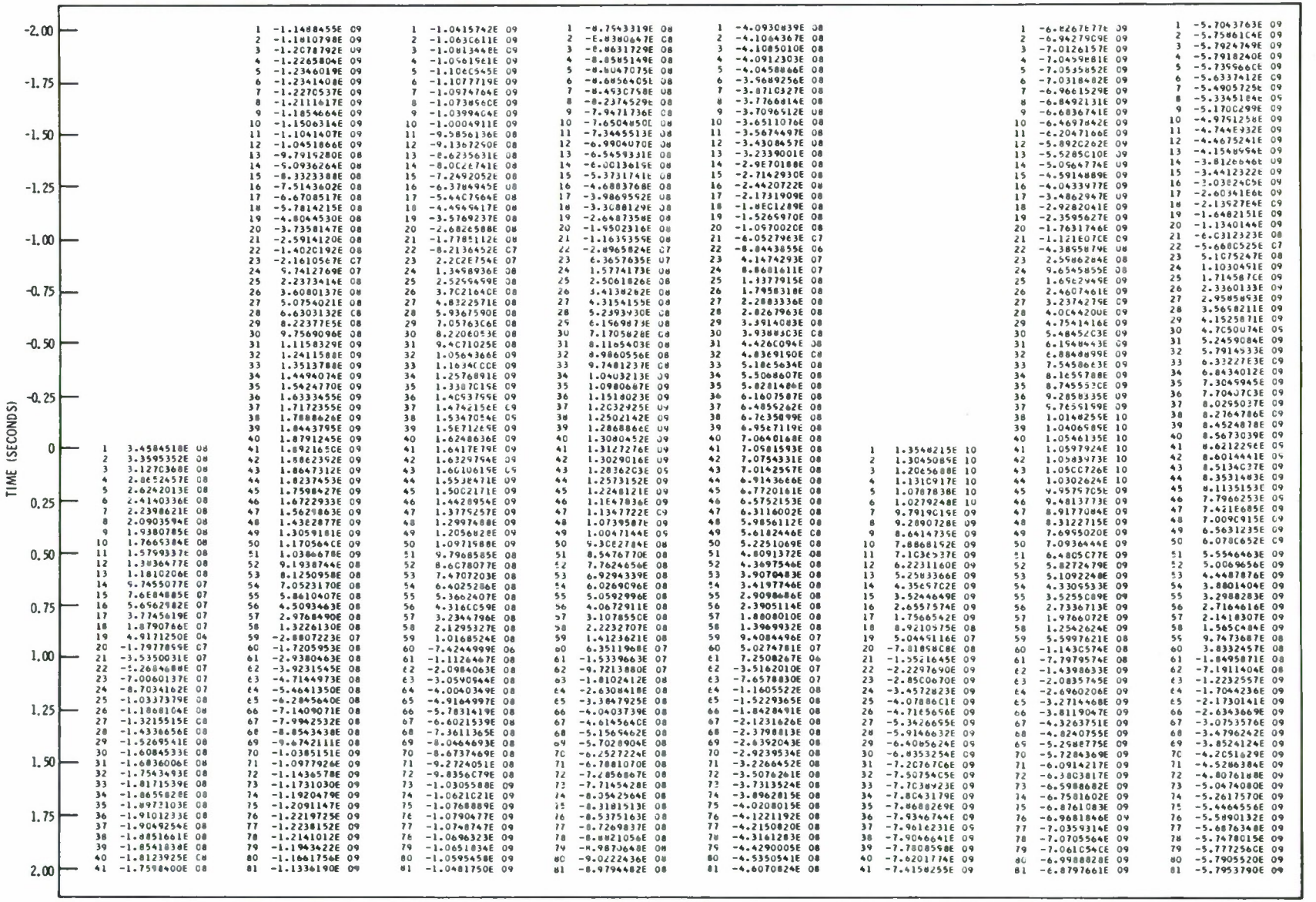

Figure A-5a. Averaged (Day plus Night) Noise Correlation Set for 5-Channel Ring Model for Subarray E-2

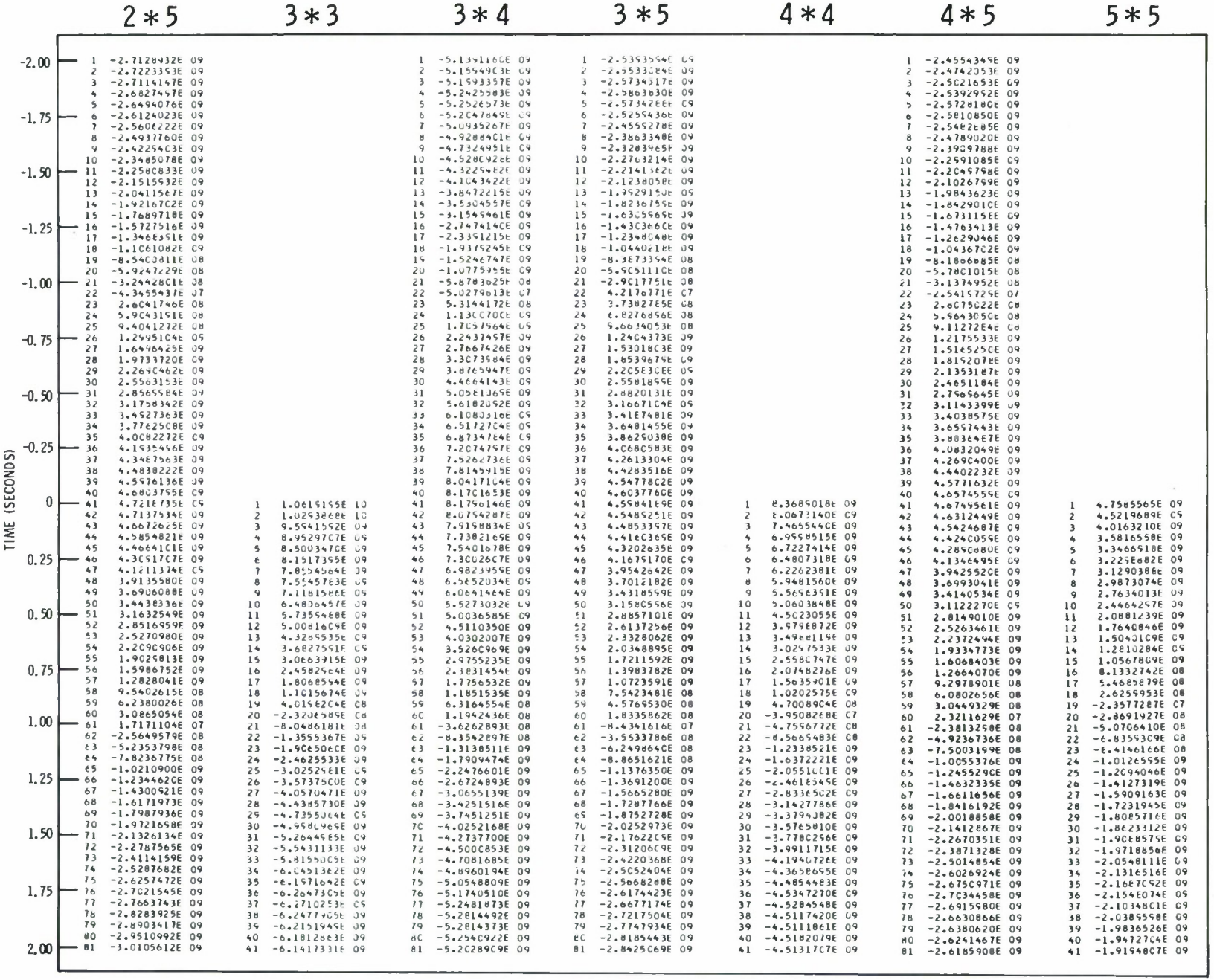

Figure A-5b. Averaged (Day plus Night) Noise Correlation Set for 5-Channel Ring Model of Subarray E-2

Table A-1

WHITENING FILTERS FOR THE FIVE SUBARRAYS

	Subarray C-3		Subarray F-2
1	1.0000000E 00	1	1.0000000E 00
2	-1.0757737E 00	2	-1.2011120E 00
3	-6.4689597E-02	3	3.5605594E-01
4	9.6869609E-02	4	-4.5989817E-02
5	7.2587480E-02	5	-7.7634451E-02

	Subarray F-4		Subarray E-2
1	1.0000000E 00	1	1.0000000E 00
2	-1.1068382E 00	2	-1.3222608E 00
3	-3.3041908E-02	3	5.5108198E-01
4	9.9640668E-02	4	-8.9560338E-02
5	7.2090762E-02	5	-9.5849597E-02

	Subarray F-3
1	1.0000000E 00
2	-1.2276418E 00
3	6.4279133E-01
4	-3.52050C6E-01
5	-2.6365489E-02

APPENDIX B
MULTICHANNEL FILTER WEIGHTS

APPENDIX B
MULTICHANNEL FILTER WEIGHTS

This report has dealt with the design and evaluation of 23 multichannel filters of various types and descriptions. Of these, 13 were described and compared in various ways in Section IV. They are briefly outlined in Table IV-1, presented earlier. The remaining 10 filters were presented in Section V as "final" filters since they incorporated the more desirable features revealed by the Section IV comparisons. This group consists of five disk model filters and five infinite-velocity filters, one for each of the five subarrays.

In anticipation of further study and to complete the MCF presentation, Appendix B presents a complete listing of all MCF filter weights. These are contained in Figures B-1 through B-23.

MCF-3 is a 25-channel filter, MCF-4, -5 and -8 are 8-channel ring models, with all remaining filters corresponding to a 5-channel ring model configuration. In each instance, the channel 1 designation refers to the center seismometer. For MCF-3, the filters are presented in the order corresponding to seismometers 10, 21, 31, 51, 71, 22, 42, 62, 82, 23, 33, 53, 73, 24, 44, 64, 84, 25, 35, 55, 75, 26, 46, 66, and 86.

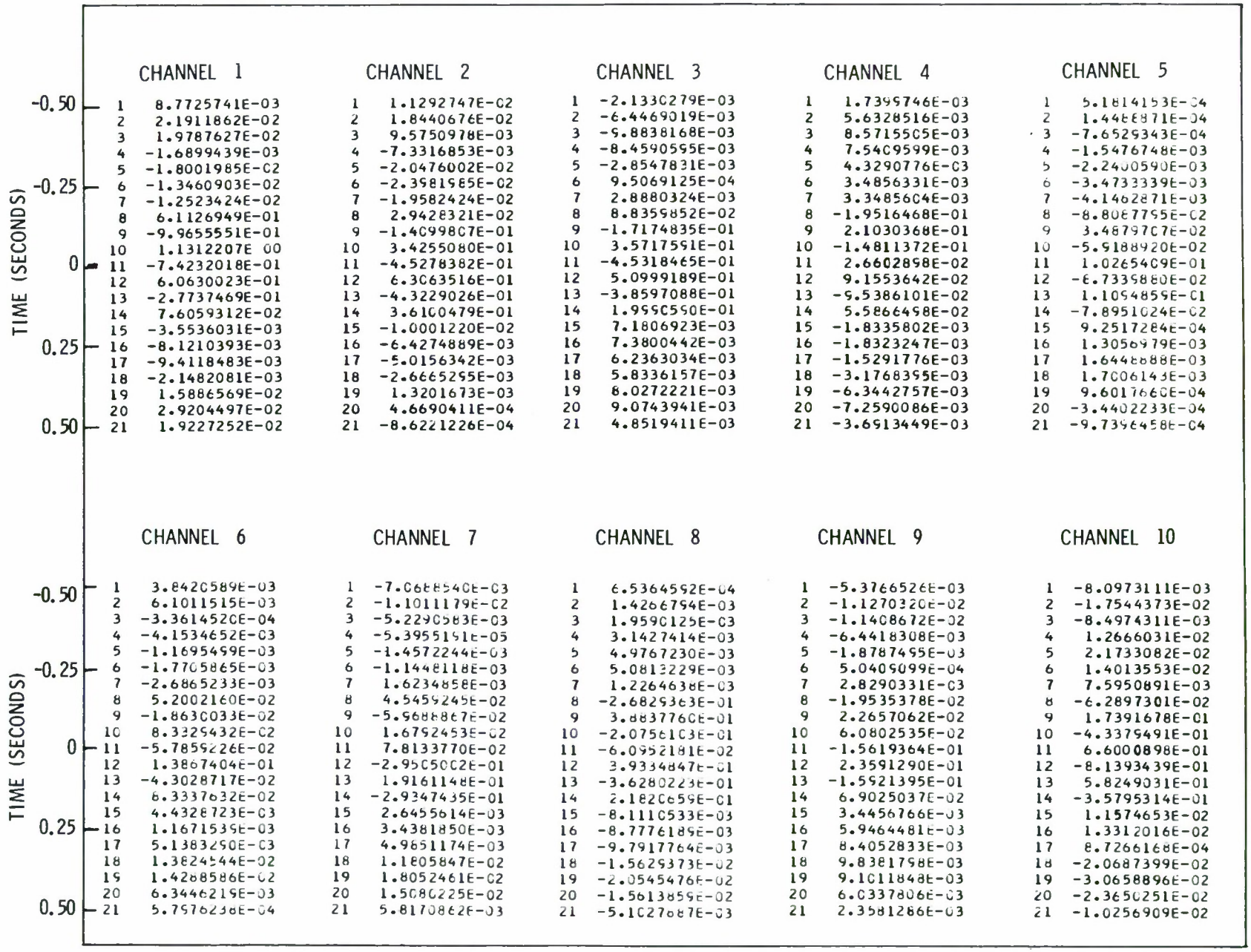

TIME (SECONDS)		CHANNEL 1	CHANNEL 2	CHANNEL 3	CHANNEL 4	CHANNEL 5
-0.50	1	8.7725741E-03	1.1292747E-02	-2.1330279E-03	1.7399746E-03	5.1814153E-04
	2	2.1911862E-02	1.8440676E-02	-6.4469019E-03	5.6328516E-03	1.4468871E-04
	3	1.9787627E-02	9.5750978E-03	-9.8838168E-03	8.5715505E-03	-7.6529343E-04
	4	-1.6899439E-03	-7.3316853E-03	-8.4590595E-03	7.5409599E-03	-1.5476748E-03
	5	-1.8001985E-02	-2.0476002E-02	-2.8547831E-03	4.3290776E-03	-2.2400590E-03
-0.25	6	-1.3460903E-02	-2.3981985E-02	9.5069125E-04	3.4856331E-03	-3.4733339E-03
	7	-1.2523424E-02	-1.9582424E-02	2.8880324E-03	3.3485604E-03	-4.1462871E-03
	8	6.1126949E-01	2.9428321E-02	8.8359852E-02	-1.9516468E-01	-8.8087795E-02
	9	-9.9655551E-01	-1.4099807E-01	-1.7174835E-01	2.1030368E-01	3.4879707E-02
	10	1.1312207E 00	3.4255080E-01	3.5717591E-01	-1.4811372E-01	-5.9188920E-02
0	11	-7.4232018E-01	-4.5278382E-01	-4.5318465E-01	2.6602898E-02	1.0265409E-01
	12	6.0630023E-01	6.3063516E-01	5.0999189E-01	9.1553642E-02	-6.7339880E-02
	13	-2.7737469E-01	-4.3229026E-01	-3.8597088E-01	-9.5386101E-02	1.1094859E-01
	14	7.6059312E-02	3.6100479E-01	1.9995590E-01	5.5866498E-02	-7.8951024E-02
	15	-3.5536031E-03	-1.0001220E-02	7.1806923E-03	-1.8335802E-03	9.2517284E-04
0.25	16	-8.1210393E-03	-6.4274889E-03	7.3800442E-03	-1.8323247E-03	1.3056979E-03
	17	-9.4118483E-03	-5.0156342E-03	6.2363034E-03	-1.5291776E-03	1.6446888E-03
	18	-2.1482081E-03	-2.6665255E-03	5.8336157E-03	-3.1768395E-03	1.7006143E-03
	19	1.5886569E-02	1.3201673E-03	8.0272221E-03	-6.3442757E-03	9.6017660E-04
	20	2.9204497E-02	4.6690411E-04	9.0743941E-03	-7.2590086E-03	-3.4402233E-04
0.50	21	1.9227252E-02	-8.6221226E-04	4.8519411E-03	-3.6913449E-03	-9.7396458E-04

TIME (SECONDS)		CHANNEL 6	CHANNEL 7	CHANNEL 8	CHANNEL 9	CHANNEL 10
-0.50	1	3.8420589E-03	-7.0688540E-03	6.5364592E-04	-5.3766526E-03	-8.0973111E-03
	2	6.1011515E-03	-1.1011179E-02	1.4266794E-03	-1.1270320E-02	-1.7544373E-02
	3	-3.3614520E-04	-5.2290583E-03	1.9590125E-03	-1.1408672E-02	-8.4974311E-03
	4	-4.1534652E-03	-5.3955151E-05	3.1427414E-03	-6.4418308E-03	1.2666031E-02
	5	-1.1695499E-03	-1.4572244E-03	4.9767230E-03	-1.8787495E-03	2.1733082E-02
-0.25	6	-1.7705865E-03	-1.1448118E-03	5.0813229E-03	5.0409099E-04	1.4013553E-02
	7	-2.6865233E-03	1.6234858E-03	1.2264638E-03	2.8290331E-03	7.5950891E-03
	8	5.2002160E-02	4.5459245E-02	-2.6829363E-01	-1.9535378E-02	-6.2897301E-02
	9	-1.8630033E-02	-5.9688867E-02	3.8837760E-01	2.2657062E-02	1.7391678E-01
	10	8.3329432E-02	1.6792453E-02	-2.0756103E-01	6.0802535E-02	-4.3379491E-01
0	11	-5.7859226E-02	7.8133770E-02	-6.0952181E-02	-1.5619364E-01	6.6000898E-01
	12	1.3867404E-01	-2.9550502E-01	3.9334847E-01	2.3591290E-01	-8.1393439E-01
	13	-4.3028717E-02	1.9161148E-01	-3.6280223E-01	-1.5921395E-01	5.8249031E-01
	14	6.3337632E-02	-2.9347435E-01	2.1820659E-01	6.9025037E-02	-3.5795314E-01
	15	4.4328723E-03	2.6455614E-03	-8.1110533E-03	3.4456766E-03	1.1574653E-02
0.25	16	1.1671539E-03	3.4381850E-03	-8.7776189E-03	5.9464481E-03	1.3312016E-02
	17	5.1383290E-03	4.9651174E-03	-9.7917764E-03	8.4052833E-03	8.7266168E-04
	18	1.3824544E-02	1.1805847E-02	-1.5629373E-02	9.8381798E-03	-2.0687399E-02
	19	1.4288586E-02	1.8052461E-02	-2.0545476E-02	9.1011848E-03	-3.0658896E-02
	20	6.3446219E-03	1.5080225E-02	-1.5613859E-02	6.0337806E-03	-2.3650251E-02
0.50	21	5.7976238E-04	5.8170862E-03	-5.1027687E-03	2.3581286E-03	-1.0256909E-02

Figure B-1a. Filter Weight Listings for MCF-3; 25-Channel Maximum-Likelihood MCF

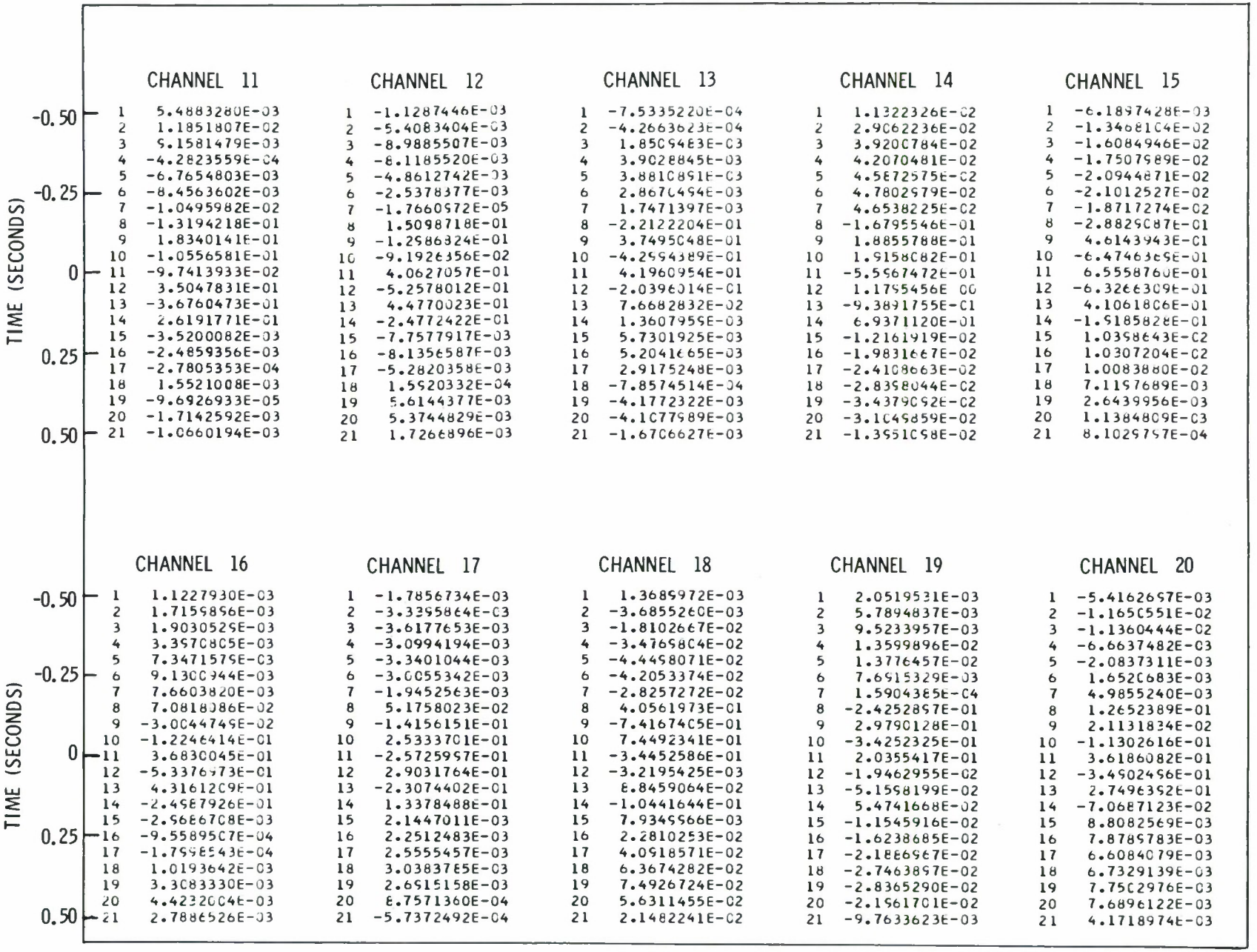

Figure B-1b. Filter Weight Listings for MCF-3; 25-Channel Maximum-Likelihood MCF

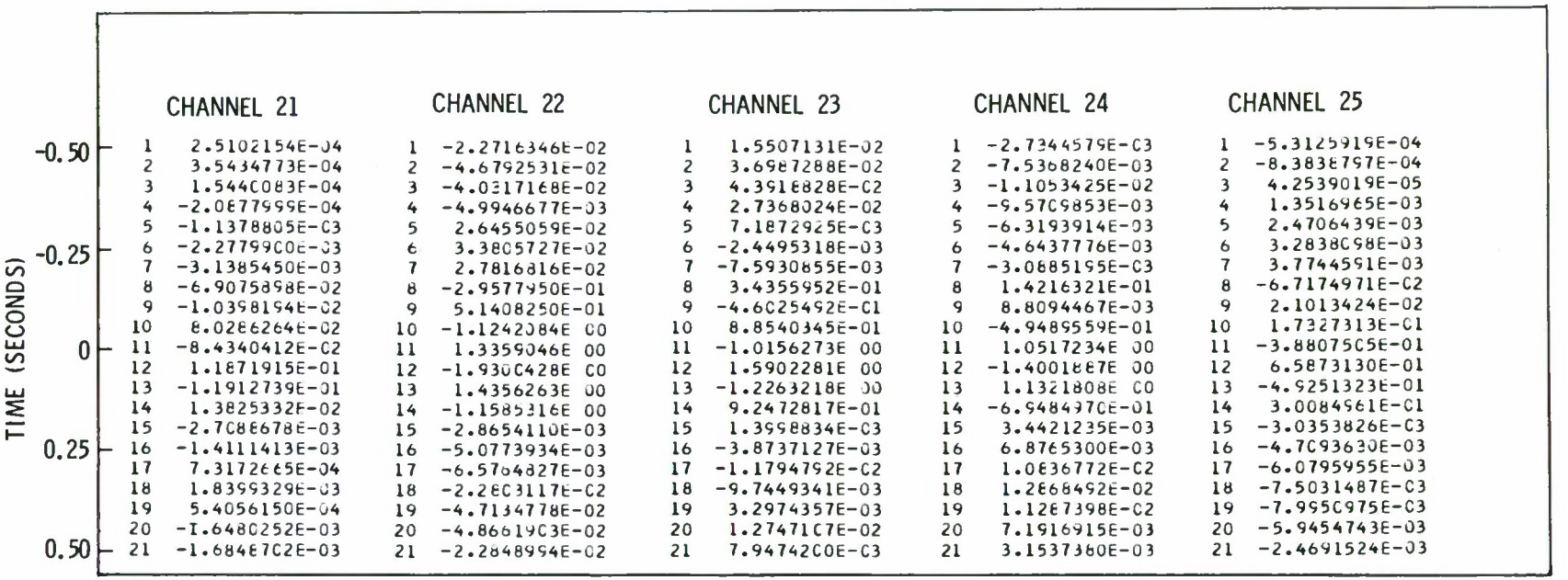

TIME (SECONDS)	CHANNEL 21	CHANNEL 22	CHANNEL 23	CHANNEL 24	CHANNEL 25
	1 2.5102154E-04	1 -2.2716346E-02	1 1.5507131E-02	1 -2.7344579E-03	1 -5.3125919E-04
	2 3.5434773E-04	2 -4.6792531E-02	2 3.6987288E-02	2 -7.5368240E-03	2 -8.3838797E-04
	3 1.5440083E-04	3 -4.0317168E-02	3 4.3918828E-02	3 -1.1053425E-02	3 4.2539019E-05
	4 -2.0877999E-04	4 -4.9946677E-03	4 2.7368024E-02	4 -9.5709853E-03	4 1.3516965E-03
-0.50	5 -1.1378805E-03	5 2.6455059E-02	5 7.1872925E-03	5 -6.3193914E-03	5 2.4706439E-03
	6 -2.2779900E-03	6 3.3805727E-02	6 -2.4495318E-03	6 -4.6437776E-03	6 3.2838098E-03
	7 -3.1385450E-03	7 2.7816816E-02	7 -7.5930855E-03	7 -3.0885195E-03	7 3.7744591E-03
	8 -6.9075898E-02	8 -2.9577950E-01	8 3.4355952E-01	8 1.4216321E-01	8 -6.7174971E-02
	9 -1.0398194E-02	9 5.1408250E-01	9 -4.6025492E-01	9 8.8094467E-03	9 2.1013424E-02
-0.25	10 8.0286264E-02	10 -1.1242084E 00	10 8.8540345E-01	10 -4.9489559E-01	10 1.7327313E-01
	11 -8.4340412E-02	11 1.3359046E 00	11 -1.0156273E 00	11 1.0517234E 00	11 -3.8807505E-01
	12 1.1871915E-01	12 -1.9306428E 00	12 1.5902281E 00	12 -1.4001887E 00	12 6.5873130E-01
	13 -1.1912739E-01	13 1.4356263E 00	13 -1.2263218E 00	13 1.1321808E 00	13 -4.9251323E-01
	14 1.3825332E-02	14 -1.1585316E 00	14 9.2472817E-01	14 -6.9484970E-01	14 3.0084961E-01
0	15 -2.7086678E-03	15 -2.8654110E-03	15 1.3998834E-03	15 3.4421235E-03	15 -3.0353826E-03
	16 -1.4111413E-03	16 -5.0773934E-03	16 -3.8737127E-03	16 6.8765300E-03	16 -4.7093630E-03
	17 7.3172665E-04	17 -6.5764827E-03	17 -1.1794792E-02	17 1.0836772E-02	17 -6.0795955E-03
	18 1.8399329E-03	18 -2.2803117E-02	18 -9.7449341E-03	18 1.2668492E-02	18 -7.5031487E-03
	19 5.4056150E-04	19 -4.7134778E-02	19 3.2974357E-03	19 1.1287398E-02	19 -7.9950975E-03
0.25	20 -1.6480252E-03	20 -4.8661903E-02	20 1.2747107E-02	20 7.1916915E-03	20 -5.9454743E-03
	21 -1.6846702E-03	21 -2.2848994E-02	21 7.9474200E-03	21 3.1537360E-03	21 -2.4691524E-03
0.50					

Figure B-1c. Filter Weights for MCF-3; 25-Channel Maximum-Likelihood MCF

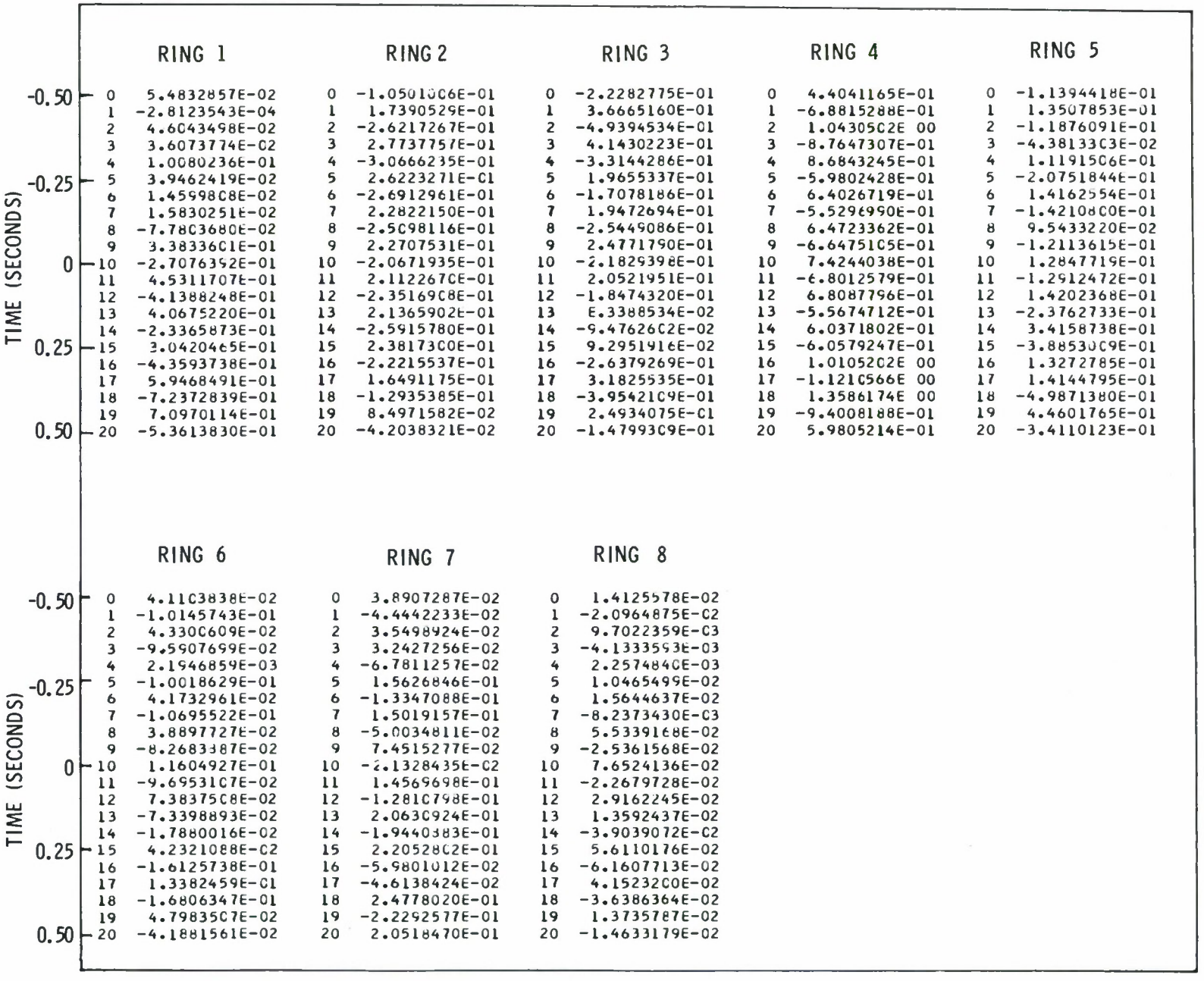

TIME (SECONDS)	RING 1	RING 2	RING 3	RING 4	RING 5
	0 5.4832857E-02	0 -1.0501006E-01	0 -2.2282775E-01	0 4.4041165E-01	0 -1.1394418E-01
	1 -2.8123543E-04	1 1.7390529E-01	1 3.6665160E-01	1 -6.8815288E-01	1 1.3507853E-01
-0.50	2 4.6043498E-02	2 -2.6217267E-01	2 -4.9394534E-01	2 1.0430502E 00	2 -1.1876091E-01
	3 3.6073774E-02	3 2.7737757E-01	3 4.1430223E-01	3 -8.7647307E-01	3 -4.3813303E-02
	4 1.0080236E-01	4 -3.0666235E-01	4 -3.3144286E-01	4 8.6843245E-01	4 1.1191506E-01
	5 3.9462419E-02	5 2.6223271E-01	5 1.9655337E-01	5 -5.9802428E-01	5 -2.0751844E-01
-0.25	6 1.4599808E-02	6 -2.6912961E-01	6 -1.7078186E-01	6 6.4026719E-01	6 1.4162554E-01
	7 1.5830251E-02	7 2.2822150E-01	7 1.9472694E-01	7 -5.5296990E-01	7 -1.4210800E-01
	8 -7.7803680E-02	8 -2.5098116E-01	8 -2.5449086E-01	8 6.4723362E-01	8 9.5433220E-02
	9 3.3833601E-01	9 2.2707531E-01	9 2.4771790E-01	9 -6.6475105E-01	9 -1.2113615E-01
0	10 -2.7076392E-01	10 -2.0671935E-01	10 -2.1829398E-01	10 7.4244038E-01	10 1.2847719E-01
	11 4.5311707E-01	11 2.1122670E-01	11 2.0521951E-01	11 -6.8012579E-01	11 -1.2912472E-01
	12 -4.1388248E-01	12 -2.3516908E-01	12 -1.8474320E-01	12 6.8087796E-01	12 1.4202368E-01
	13 4.0675220E-01	13 2.1365902E-01	13 1.3388534E-02	13 -5.5674712E-01	13 -2.3762733E-01
	14 -2.3365873E-01	14 -2.5915780E-01	14 -9.4762602E-02	14 6.0371802E-01	14 3.4158738E-01
0.25	15 3.0420465E-01	15 2.3817300E-01	15 9.2951916E-02	15 -6.0579247E-01	15 -3.8853009E-01
	16 -4.3593738E-01	16 -2.2215537E-01	16 -2.6379269E-01	16 1.0105202E 00	16 1.3272785E-01
	17 5.9468491E-01	17 1.6491175E-01	17 3.1825535E-01	17 -1.1215566E 00	17 1.4144795E-01
	18 -7.2372839E-01	18 -1.2935385E-01	18 -3.9542109E-01	18 1.3586174E 00	18 -4.9871380E-01
	19 7.0970114E-01	19 8.4971582E-02	19 2.4934075E-01	19 -9.4008188E-01	19 4.4601765E-01
0.50	20 -5.3613830E-01	20 -4.2038321E-02	20 -1.4799309E-01	20 5.9805214E-01	20 -3.4110123E-01

TIME (SECONDS)	RING 6	RING 7	RING 8
	0 4.1103838E-02	0 3.8907287E-02	0 1.4125578E-02
	1 -1.0145743E-01	1 -4.4442233E-02	1 -2.0964875E-02
-0.50	2 4.3306609E-02	2 3.5498924E-02	2 9.7022359E-03
	3 -9.5907699E-02	3 3.2427256E-02	3 -4.1333593E-03
	4 2.1946859E-03	4 -6.7811257E-02	4 2.2574840E-03
	5 -1.0018629E-01	5 1.5626846E-01	5 1.0465499E-02
-0.25	6 4.1732961E-02	6 -1.3347088E-01	6 1.5644637E-02
	7 -1.0695522E-01	7 1.5019157E-01	7 -8.2373430E-03
	8 3.8897727E-02	8 -5.0034811E-02	8 5.5339168E-02
	9 -8.2683387E-02	9 7.4515277E-02	9 -2.5361568E-02
0	10 1.1604927E-01	10 -2.1328435E-02	10 7.6524136E-02
	11 -9.6953107E-02	11 1.4569698E-01	11 -2.2679728E-02
	12 7.3837508E-02	12 -1.2810798E-01	12 2.9162245E-02
	13 -7.3398893E-02	13 2.0630924E-01	13 1.3592437E-02
	14 -1.7880016E-02	14 -1.9440383E-01	14 -3.9039072E-02
0.25	15 4.2321088E-02	15 2.2052802E-01	15 5.6110176E-02
	16 -1.6125738E-01	16 -5.9801012E-02	16 -6.1607713E-02
	17 1.3382459E-01	17 -4.6138424E-02	17 4.1523200E-02
	18 -1.6806347E-01	18 2.4778020E-01	18 -3.6386364E-02
	19 4.7983507E-02	19 -2.2292577E-01	19 1.3735787E-02
0.50	20 -4.1881561E-02	20 2.0518470E-01	20 -1.4633179E-02

Figure B-2. Filter Weight Listings for MCF-4; 8-Ring IV Model MCF

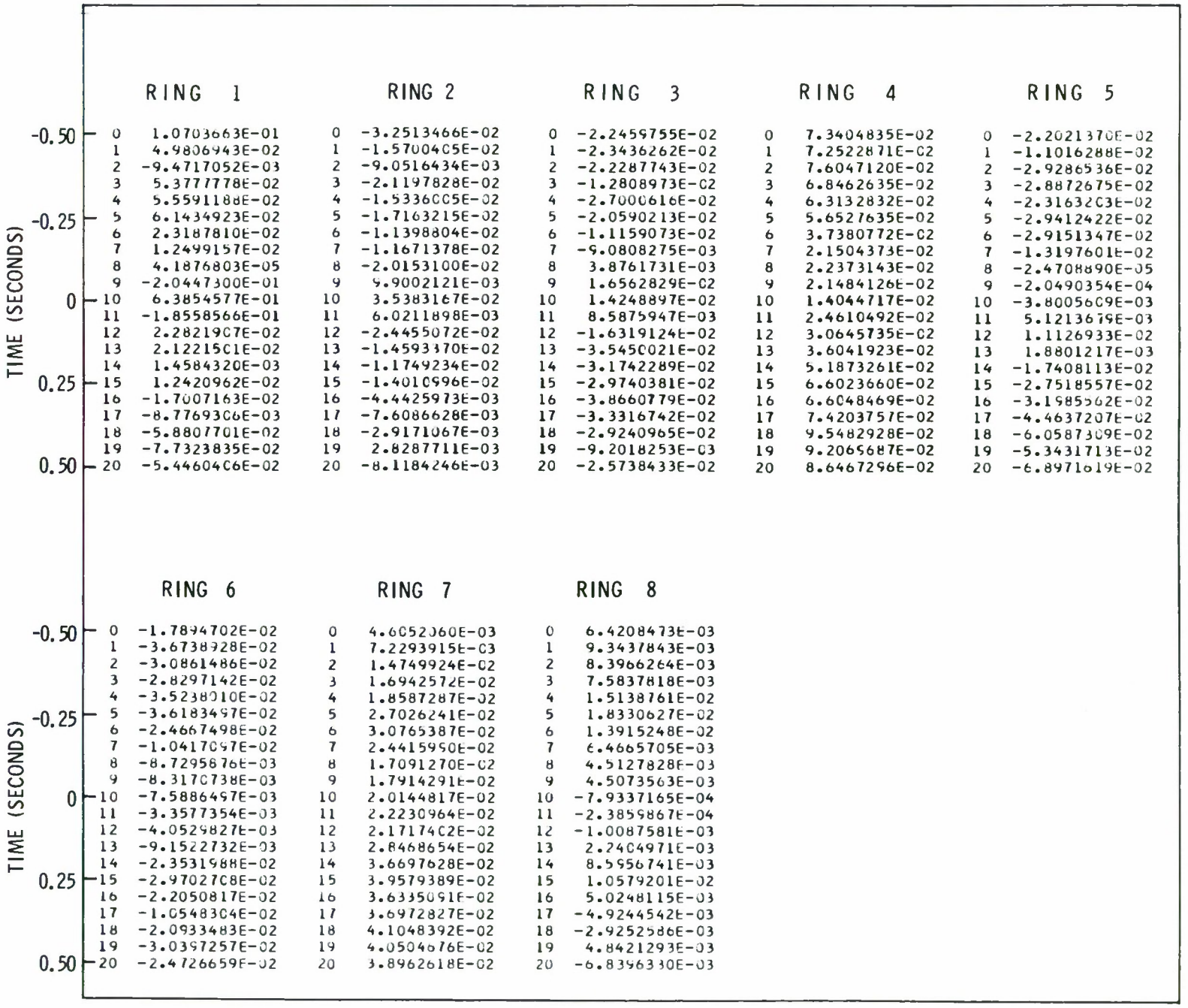

TIME (SECONDS)	RING 1	RING 2	RING 3	RING 4	RING 5
-0.50	0 1.0703663E-01	0 -3.2513466E-02	0 -2.2459755E-02	0 7.3404835E-02	0 -2.2021370E-02
	1 4.9806943E-02	1 -1.5700405E-02	1 -2.3436262E-02	1 7.2522871E-02	1 -1.1016288E-02
	2 -9.4717052E-03	2 -9.0516434E-03	2 -2.2287743E-02	2 7.6047120E-02	2 -2.9286536E-02
	3 5.3777778E-02	3 -2.1197828E-02	3 -1.2808973E-02	3 6.8462635E-02	3 -2.8872675E-02
	4 5.5591188E-02	4 -1.5336005E-02	4 -2.7000616E-02	4 6.3132832E-02	4 -2.3163203E-02
-0.25	5 6.1434923E-02	5 -1.7163215E-02	5 -2.0590213E-02	5 5.6527635E-02	5 -2.9412422E-02
	6 2.3187810E-02	6 -1.1398804E-02	6 -1.1159073E-02	6 3.7380772E-02	6 -2.9151347E-02
	7 1.2499157E-02	7 -1.1671378E-02	7 -9.0808275E-03	7 2.1504373E-02	7 -1.3197601E-02
	8 4.1876803E-05	8 -2.0153100E-02	8 3.8761731E-03	8 2.2373143E-02	8 -2.4708890E-05
	9 -2.0447300E-01	9 9.9002121E-03	9 1.6562829E-02	9 2.1484126E-02	9 -2.0490354E-04
0	10 6.3854577E-01	10 3.5383167E-02	10 1.4248897E-02	10 1.4044717E-02	10 -3.8005609E-03
	11 -1.8558566E-01	11 6.0211898E-03	11 8.5875947E-03	11 2.4610492E-02	11 5.1213679E-03
	12 2.2821907E-02	12 -2.4455072E-02	12 -1.6319124E-02	12 3.0645735E-02	12 1.1126933E-02
	13 2.1221501E-02	13 -1.4593370E-02	13 -3.5450021E-02	13 3.6041923E-02	13 1.8801217E-03
	14 1.4584320E-03	14 -1.1749234E-02	14 -3.1742289E-02	14 5.1873261E-02	14 -1.7408113E-02
0.25	15 1.2420962E-02	15 -1.4010996E-02	15 -2.9740381E-02	15 6.6023660E-02	15 -2.7518557E-02
	16 -1.7007163E-02	16 -4.4425973E-03	16 -3.8660779E-02	16 6.6048469E-02	16 -3.1985562E-02
	17 -8.7769306E-03	17 -7.6086628E-03	17 -3.3316742E-02	17 7.4203757E-02	17 -4.4637207E-02
	18 -5.8807701E-02	18 -2.9171067E-03	18 -2.9240965E-02	18 9.5482928E-02	18 -6.0587309E-02
	19 -7.7323835E-02	19 2.8287711E-03	19 -9.2018253E-03	19 9.2065687E-02	19 -5.3431713E-02
0.50	20 -5.4460406E-02	20 -8.1184246E-03	20 -2.5738433E-02	20 8.6467296E-02	20 -6.8971619E-02

TIME (SECONDS)	RING 6	RING 7	RING 8
-0.50	0 -1.7894702E-02	0 4.6052060E-03	0 6.4208473E-03
	1 -3.6738928E-02	1 7.2293915E-03	1 9.3437843E-03
	2 -3.0861486E-02	2 1.4749924E-02	2 8.3966264E-03
	3 -2.8297142E-02	3 1.6942572E-02	3 7.5837818E-03
	4 -3.5238010E-02	4 1.8587287E-02	4 1.5138761E-02
-0.25	5 -3.6183497E-02	5 2.7026241E-02	5 1.8330627E-02
	6 -2.4667498E-02	6 3.0765387E-02	6 1.3915248E-02
	7 -1.0417097E-02	7 2.4415950E-02	7 6.4665705E-03
	8 -8.7295876E-03	8 1.7091270E-02	8 4.5127828E-03
	9 -8.3170738E-03	9 1.7914291E-02	9 4.5073563E-03
0	10 -7.5886497E-03	10 2.0144817E-02	10 -7.9337165E-04
	11 -3.3577354E-03	11 2.2230964E-02	11 -2.3859867E-04
	12 -4.0529827E-03	12 2.1717402E-02	12 -1.0087581E-03
	13 -9.1522732E-03	13 2.8468654E-02	13 2.2404971E-03
	14 -2.3531988E-02	14 3.6697628E-02	14 8.5956741E-03
0.25	15 -2.9702708E-02	15 3.9579389E-02	15 1.0579201E-02
	16 -2.2050817E-02	16 3.6335091E-02	16 5.0248115E-03
	17 -1.0548304E-02	17 3.6972827E-02	17 -4.9244542E-03
	18 -2.0933483E-02	18 4.1048392E-02	18 -2.9252586E-03
	19 -3.0397257E-02	19 4.0504676E-02	19 4.8421293E-03
0.50	20 -2.4726659E-02	20 3.8962618E-02	20 -6.8396330E-03

Figure B-3. Filter Weight Listings for MCF-5; 8-Ring Disk Model MCF

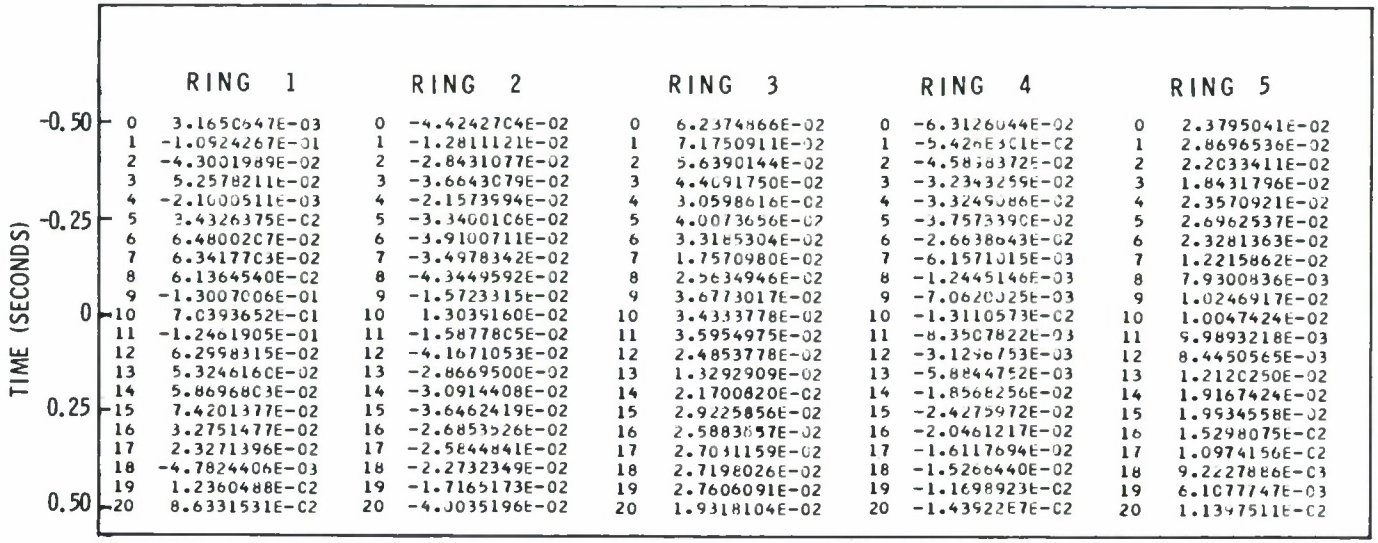

TIME (SECONDS)	RING 1	RING 2	RING 3	RING 4	RING 5
-0.50	0 3.1650647E-03	0 -4.4242704E-02	0 6.2374866E-02	0 -6.3126044E-02	0 2.3795041E-02
	1 -1.0924267E-01	1 -1.2811121E-02	1 7.1750911E-02	1 -5.4206301E-02	1 2.8696536E-02
	2 -4.3001989E-02	2 -2.8431077E-02	2 5.6390144E-02	2 -4.5838372E-02	2 2.2033411E-02
	3 5.2578211E-02	3 -3.6643079E-02	3 4.4091750E-02	3 -3.2343259E-02	3 1.8431796E-02
	4 -2.1000511E-03	4 -2.1573994E-02	4 3.0598616E-02	4 -3.3249086E-02	4 2.3570921E-02
-0.25	5 3.4326375E-02	5 -3.3400106E-02	5 4.0073656E-02	5 -3.7573390E-02	5 2.6962537E-02
	6 6.4800207E-02	6 -3.9100711E-02	6 3.3185304E-02	6 -2.6638643E-02	6 2.3281363E-02
	7 6.3417703E-02	7 -3.4978342E-02	7 1.7570980E-02	7 -6.1571015E-03	7 1.2215862E-02
	8 6.1364540E-02	8 -4.3449592E-02	8 2.5634946E-02	8 -1.2445146E-03	8 7.9300836E-03
	9 -1.3007006E-01	9 -1.5723315E-02	9 3.6773017E-02	9 -7.0620325E-03	9 1.0246917E-02
0	10 7.0393652E-01	10 1.3039160E-02	10 3.4333778E-02	10 -1.3110573E-02	10 1.0047424E-02
	11 -1.2461905E-01	11 -1.5877805E-02	11 3.5954975E-02	11 -8.3507822E-03	11 9.9893218E-03
	12 6.2998315E-02	12 -4.1671053E-02	12 2.4853778E-02	12 -3.1296753E-03	12 8.4450565E-03
	13 5.3246166E-02	13 -2.8669500E-02	13 1.3292909E-02	13 -5.8844752E-03	13 1.2120250E-02
	14 5.8696803E-02	14 -3.0914408E-02	14 2.1700820E-02	14 -1.8568256E-02	14 1.9167424E-02
0.25	15 7.4201377E-02	15 -3.6462419E-02	15 2.9225856E-02	15 -2.4275972E-02	15 1.9934558E-02
	16 3.2751477E-02	16 -2.6853526E-02	16 2.5883857E-02	16 -2.0461217E-02	16 1.5298075E-02
	17 2.3271396E-02	17 -2.5844841E-02	17 2.7031159E-02	17 -1.6117694E-02	17 1.0974156E-02
	18 -4.7824406E-03	18 -2.2732349E-02	18 2.7198026E-02	18 -1.5266440E-02	18 9.2227886E-03
	19 1.2360488E-02	19 -1.7165173E-02	19 2.7606091E-02	19 -1.1698923E-02	19 6.1077747E-03
0.50	20 8.6331531E-02	20 -4.0035196E-02	20 1.9318104E-02	20 -1.4392287E-02	20 1.1397511E-02

Figure B-4. Filter Weight Listings for MCF-6; 5-Ring Disk Model MCF

TIME (SECONDS)	RING 1	RING 2	RING 3	RING 4	RING 5
-0.50	0 2.7097276E-02	0 -6.7727584E-03	0 -8.0922569E-04	0 -6.7077612E-03	0 -1.3602696E-02
	1 6.9140919E-03	1 -2.2843005E-03	1 4.5655914E-03	1 3.6115065E-03	1 3.3383974E-03
	2 7.1182270E-03	2 -4.1522364E-03	2 1.7659764E-03	2 -7.6600302E-05	2 2.6272475E-04
	3 8.5386673E-03	3 -4.8384732E-03	3 1.9358669E-03	3 -2.9765545E-04	3 1.8147254E-03
	4 7.8778715E-03	4 -6.4566199E-03	4 2.4276560E-03	4 -1.2492298E-03	4 2.0464119E-03
-0.25	5 3.8285059E-03	5 -6.2385881E-03	5 8.7595786E-04	5 -2.2768215E-03	5 6.6419994E-03
	6 1.6904287E-02	6 -1.0660456E-02	6 1.5610634E-03	6 -1.1474625E-04	6 7.0530794E-03
	7 -1.4041173E-02	7 -5.0022431E-03	7 -7.9275391E-03	7 1.2577773E-02	7 2.7779501E-03
	8 4.3042625E-02	8 -2.8028636E-02	8 1.0224511E-02	8 9.6948752E-03	8 1.7767662E-03
	9 -1.1186282E-01	9 -1.6581362E-02	9 3.0638842E-02	9 3.0140687E-03	9 1.6104188E-03
0	10 2.7802637E-01	10 1.0949861E-01	10 4.2912409E-03	10 1.8156250E-03	10 2.6889351E-03
	11 -1.1184939E-01	11 -1.6585915E-02	11 3.0642077E-02	11 3.0129135E-03	11 1.6086600E-03
	12 4.3032617E-02	12 -2.8026910E-02	12 1.0222053E-02	12 9.6962407E-03	12 1.7774787E-03
	13 -1.4040482E-02	13 -5.0031222E-03	13 -7.9259416E-03	13 1.2578598E-02	13 2.7783541E-03
	14 1.6899466E-02	14 -1.0659540E-02	14 1.5599394E-03	14 -1.1334879E-04	14 7.0534183E-03
0.25	15 3.8285436E-03	15 -6.2391361E-03	15 8.7454326E-04	15 -2.2772484E-03	15 6.6431729E-03
	16 7.8767414E-03	16 -6.4554075E-03	16 2.4274099E-03	16 -1.2493238E-03	16 2.0473611E-03
	17 8.5374920E-03	17 -4.8386773E-03	17 1.9357928E-03	17 -2.9821710E-04	17 1.8140900E-03
	18 7.1187137E-03	18 -4.1506784E-03	18 1.7674288E-03	18 -7.5746036E-05	18 2.6468411E-04
	19 6.9188973E-03	19 -2.2869540E-03	19 4.5616893E-03	19 3.6070186E-03	19 3.3333578E-03
0.50	20 2.7083959E-02	20 -6.7681000E-03	20 -8.0785155E-04	20 -6.7047030E-03	20 -1.3600707E-02

Figure B-5. Filter Weight Listings for MCF-7; 5-Ring Disk Model MCF

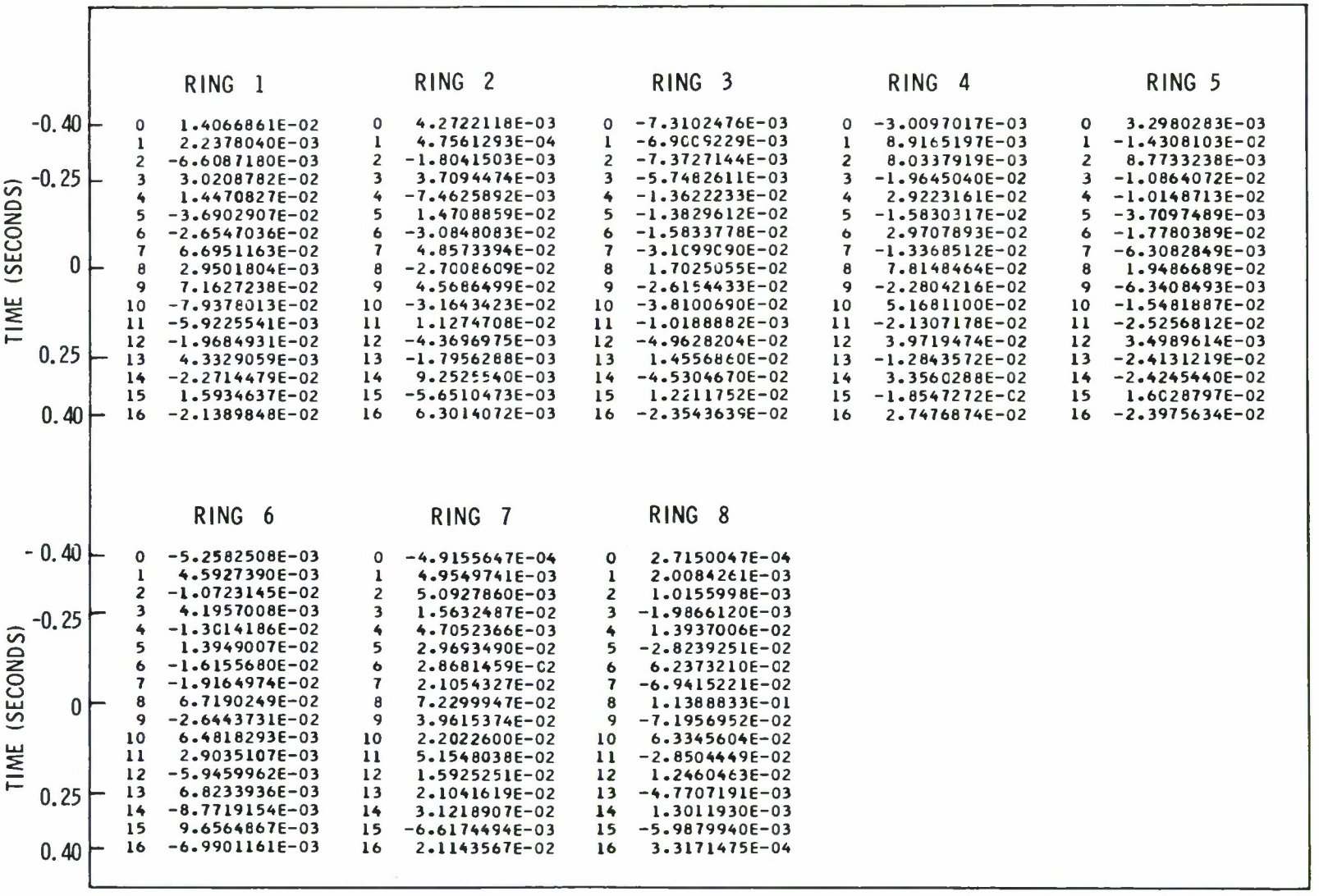

Figure B-6. Filter Weight Listings for MCF-8; 8-Ring IV Model MCF

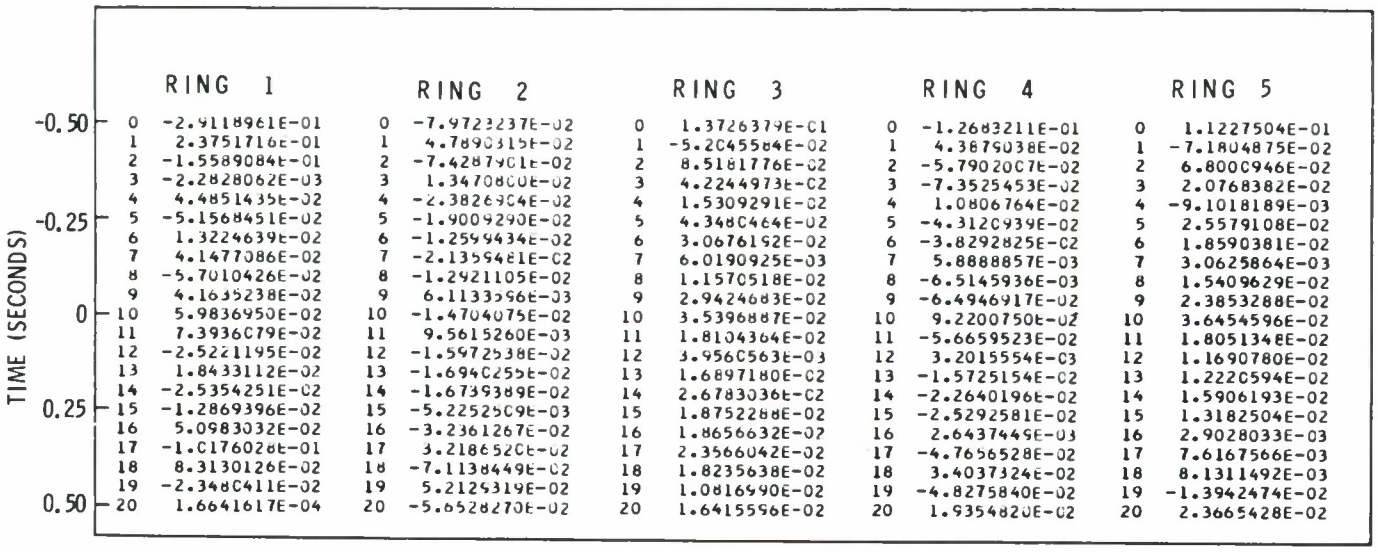

TIME (SECONDS)	RING 1	RING 2	RING 3	RING 4	RING 5
-0.50	0 -2.9118961E-01	0 -7.9723237E-02	0 1.3726379E-01	0 -1.2683211E-01	0 1.1227504E-01
	1 2.3751716E-01	1 4.7890315E-02	1 -5.2045584E-02	1 4.3879038E-02	1 -7.1804875E-02
	2 -1.5589084E-01	2 -7.4287901E-02	2 8.5181776E-02	2 -5.7902007E-02	2 6.8000946E-02
	3 -2.2828062E-03	3 1.3470800E-02	3 4.2244973E-02	3 -7.3525453E-02	3 2.0768382E-02
	4 4.4851435E-02	4 -2.3826904E-02	4 1.5309291E-02	4 1.0806764E-02	4 -9.1018189E-03
-0.25	5 -5.1568451E-02	5 -1.9009290E-02	5 4.3480464E-02	5 -4.3120939E-02	5 2.5579108E-02
	6 1.3224639E-02	6 -1.2599434E-02	6 3.0676192E-02	6 -3.8292825E-02	6 1.8590381E-02
	7 4.1477086E-02	7 -2.1359481E-02	7 6.0190925E-03	7 5.8888857E-03	7 3.0625864E-03
	8 -5.7010426E-02	8 -1.2921105E-02	8 1.1570518E-02	8 -6.5145936E-03	8 1.5409629E-02
	9 4.1635238E-02	9 6.1133996E-03	9 2.9424683E-02	9 -6.4946917E-02	9 2.3853288E-02
0	10 5.9836950E-02	10 -1.4704075E-02	10 3.5396887E-02	10 9.2200750E-02	10 3.6454596E-02
	11 7.3936079E-02	11 9.5615260E-03	11 1.8104364E-02	11 -5.6659523E-02	11 1.8051348E-02
	12 -2.5221195E-02	12 -1.5972538E-02	12 3.9560563E-03	12 3.2015554E-03	12 1.1690780E-02
	13 1.8433112E-02	13 -1.6940255E-02	13 1.6897180E-02	13 -1.5725154E-02	13 1.2220594E-02
	14 -2.5354251E-02	14 -1.6739389E-02	14 2.6783036E-02	14 -2.2640196E-02	14 1.5906193E-02
0.25	15 -1.2869396E-02	15 -5.2252509E-03	15 1.8752288E-02	15 -2.5292581E-02	15 1.3182504E-02
	16 5.0983032E-02	16 -3.2361267E-02	16 1.8656632E-02	16 2.6437449E-03	16 2.9028033E-03
	17 -1.0176026E-01	17 3.2186520E-02	17 2.3566042E-02	17 -4.7656528E-02	17 7.6167566E-03
	18 8.3130126E-02	18 -7.1138449E-02	18 1.8235638E-02	18 3.4037324E-02	18 8.1311492E-03
	19 -2.3480411E-02	19 5.2129319E-02	19 1.0816990E-02	19 -4.8275840E-02	19 -1.3942474E-02
0.50	20 1.6641617E-04	20 -5.6528270E-02	20 1.6415596E-02	20 1.9354820E-02	20 2.3665428E-02

Figure B-7. Filter Weight Listings for MCF-9; 5-Ring IV Model MCF

TIME (SECONDS)	RING 1	RING 2	RING 3	RING 4	RING 5
-0.50	0 -5.9306224E-02	0 -3.0591689E-02	0 5.3041679E-02	0 -9.4038150E-02	0 8.1448901E-02
	1 3.8287552E-02	1 2.2416055E-02	1 -5.2344728E-02	1 9.9042716E-02	1 -7.5657857E-02
	2 -5.7795396E-02	2 -5.6932724E-02	2 1.0269777E-01	2 -1.4730594E-01	2 1.1108101E-01
	3 2.2592504E-02	3 2.5311102E-02	3 -5.7424393E-02	3 6.9070143E-02	3 -4.0570270E-02
	4 -2.4834722E-02	4 -4.2162528E-02	4 7.8724168E-02	4 -8.0796251E-02	4 4.8111330E-02
-0.25	5 6.9242226E-04	5 2.5801569E-03	5 -2.1259182E-02	5 -4.6767184E-04	5 1.8975239E-02
	6 7.7485485E-04	6 -2.1604727E-02	6 3.8557623E-02	6 -3.4531816E-02	6 1.6551511E-02
	7 -1.0816535E-02	7 -7.0672245E-03	7 1.2514623E-02	7 -2.1867528E-02	7 1.8670562E-02
	8 1.0312992E-02	8 -5.3408377E-03	8 1.9422746E-02	8 -3.8308040E-02	8 2.0861941E-02
	9 1.1960440E-02	9 -2.4075155E-04	9 7.2896264E-03	9 -2.7385125E-02	9 1.8125745E-02
0	10 5.9622992E-02	10 5.8492135E-03	10 5.9308040E-02	10 2.8282740E-02	10 5.9097212E-02
	11 9.3943659E-03	11 -1.0839603E-03	11 -4.0456563E-03	11 -1.3623063E-02	11 1.6894694E-02
	12 8.2144306E-03	12 -1.2710288E-03	12 2.3810789E-02	12 -4.1342605E-02	12 1.5670449E-02
	13 -1.9916455E-02	13 -9.6361100E-03	13 6.2428936E-03	13 -7.2382000E-03	13 1.4267605E-02
	14 -3.6876462E-04	14 -3.5176888E-03	14 1.0330852E-02	14 -2.2366786E-02	14 1.4697264E-02
0.25	15 -7.8242446E-03	15 -7.4807252E-03	15 8.4344114E-03	15 -9.6792732E-03	15 9.7524435E-03
	16 -3.8148090E-02	16 -4.3029508E-03	16 5.6618213E-03	16 -2.9793910E-02	16 3.5547126E-02
	17 1.9545075E-02	17 -1.1176499E-03	17 1.0746541E-02	17 1.4965267E-02	17 -2.8726627E-02
	18 -5.8058140E-02	18 -8.5352799E-03	18 1.3462572E-03	18 -4.9920032E-02	18 6.8553382E-02
	19 2.5661930E-02	19 1.4484034E-03	19 9.8199584E-03	19 3.0095497E-02	19 -4.6945991E-02
0.50	20 -3.0936837E-02	20 -6.8353266E-03	20 -3.7016869E-03	20 -3.2577872E-02	20 4.9626350E-02

Figure B-8. Filter Weight Listings for MCF-10; 5-Ring IV Model MCF

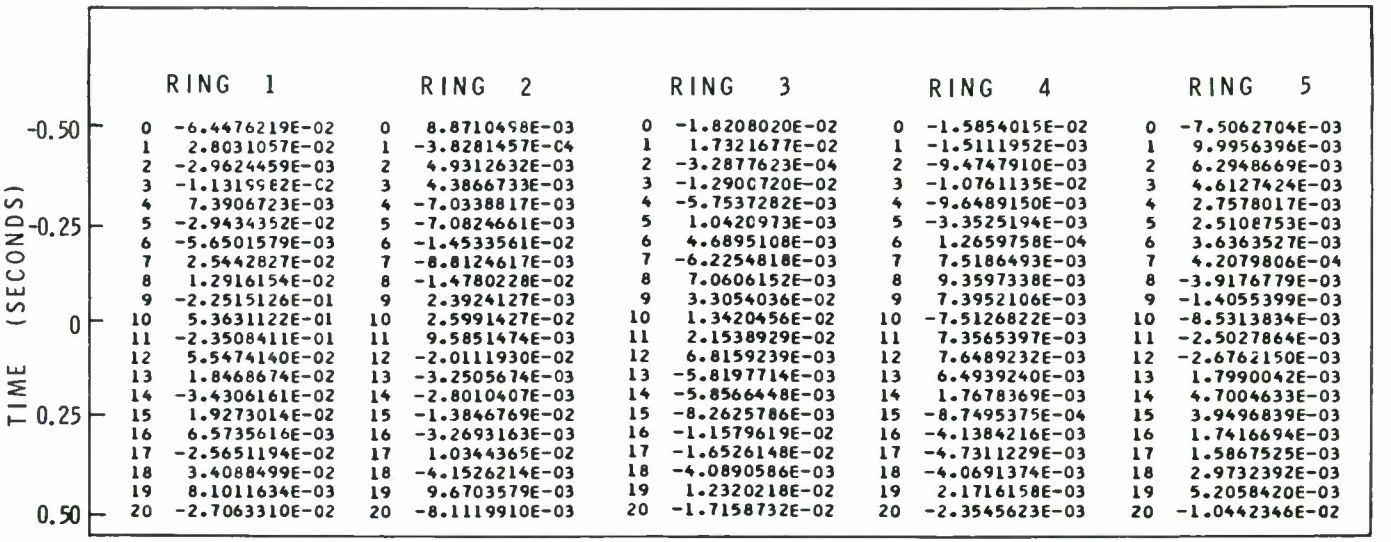

Figure B-9. Filter Weight Listings for MCF-11; 5-Ring Disk Model MCF

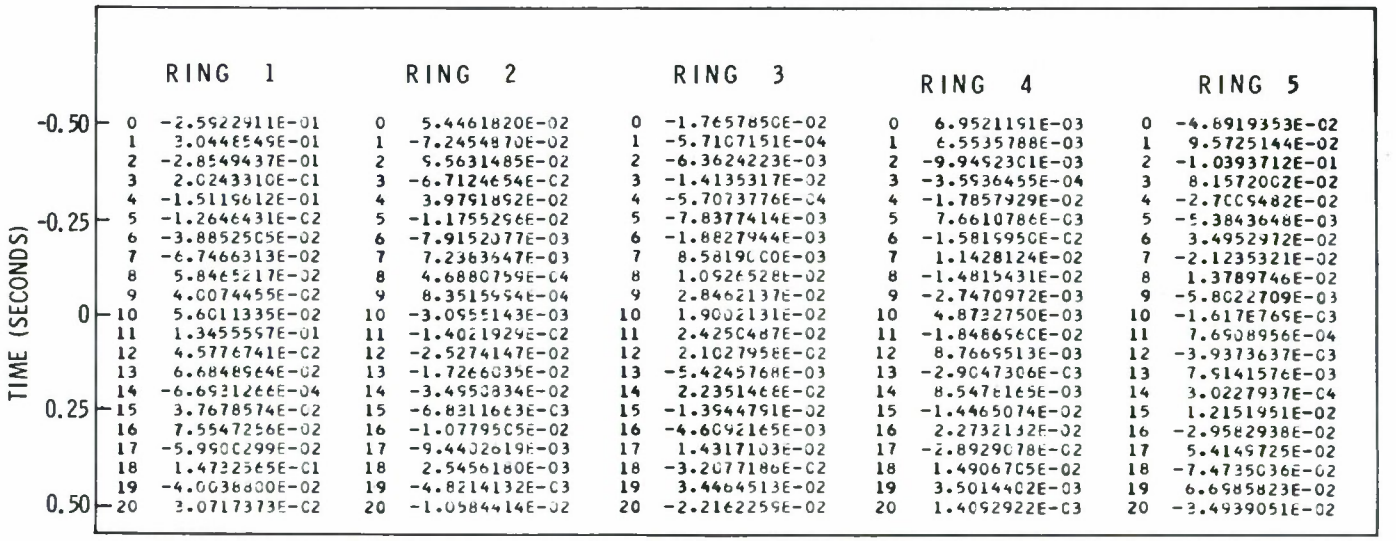

Figure B-10. Filter Weight Listings for MCF-12; 5-Ring Disk Model MCF

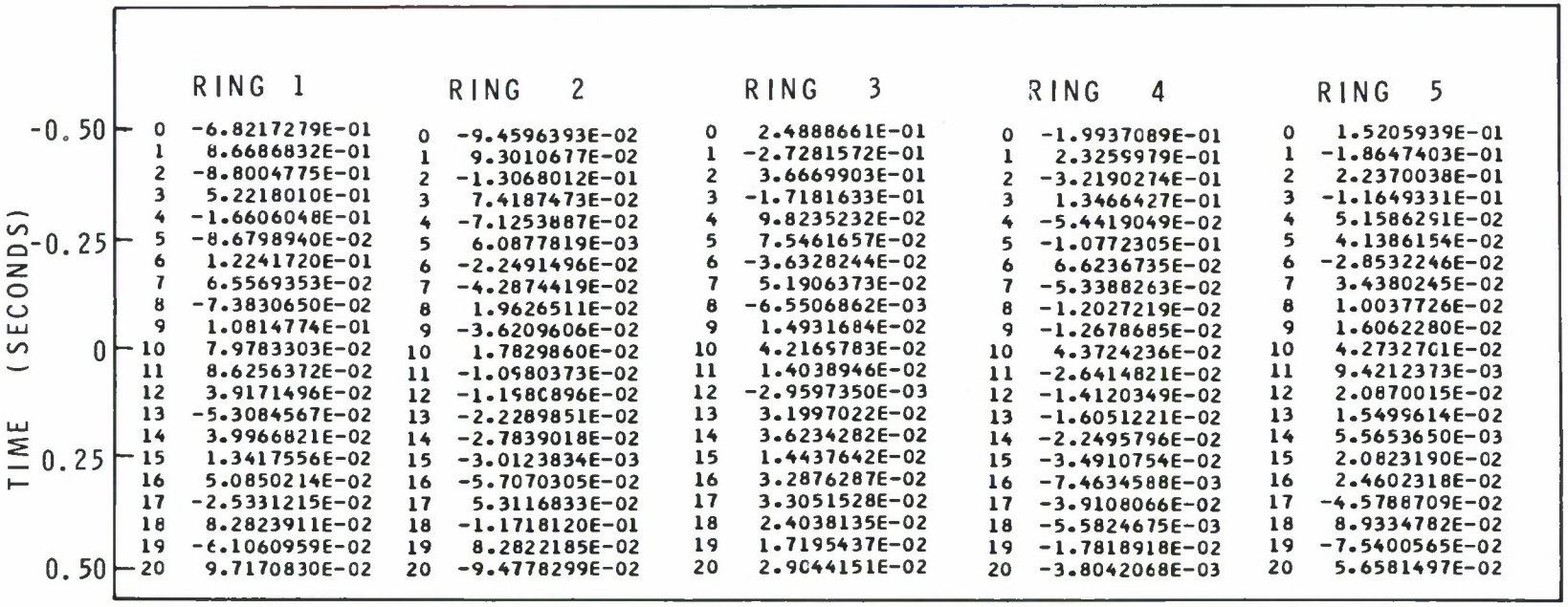

TIME (SECONDS)	RING 1		RING 2		RING 3		RING 4		RING 5	
-0.50	0	-6.8217279E-01	0	-9.4596393E-02	0	2.4888661E-01	0	-1.9937089E-01	0	1.5205939E-01
	1	8.6686832E-01	1	9.3010677E-02	1	-2.7281572E-01	1	2.3259979E-01	1	-1.8647403E-01
	2	-8.8004775E-01	2	-1.3068012E-01	2	3.6669903E-01	2	-3.2190274E-01	2	2.2370038E-01
	3	5.2218010E-01	3	7.4187473E-02	3	-1.7181633E-01	3	1.3466427E-01	3	-1.1649331E-01
	4	-1.6606048E-01	4	-7.1253887E-02	4	9.8235232E-02	4	-5.4419049E-02	4	5.1586291E-02
-0.25	5	-8.6798940E-02	5	6.0877819E-03	5	7.5461657E-02	5	-1.0772305E-01	5	4.1386154E-02
	6	1.2241720E-01	6	-2.2491496E-02	6	-3.6328244E-02	6	6.6236735E-02	6	-2.8532246E-02
	7	6.5569353E-02	7	-4.2874419E-02	7	5.1906373E-02	7	-5.3388263E-02	7	3.4380245E-02
	8	-7.3830650E-02	8	1.9626511E-02	8	-6.5506862E-03	8	-1.2027219E-02	8	1.0037726E-02
	9	1.0814774E-01	9	-3.6209606E-02	9	1.4931684E-02	9	-1.2678685E-02	9	1.6062280E-02
0	10	7.9783303E-02	10	1.7829860E-02	10	4.2165783E-02	10	4.3724236E-02	10	4.2732701E-02
	11	8.6256372E-02	11	-1.0980373E-02	11	1.4038946E-02	11	-2.6414821E-02	11	9.4212373E-03
	12	3.9171496E-02	12	-1.1980896E-02	12	-2.9597350E-03	12	-1.4120349E-02	12	2.0870015E-02
	13	-5.3084567E-02	13	-2.2289851E-02	13	3.1997022E-02	13	-1.6051221E-02	13	1.5499614E-02
	14	3.9966821E-02	14	-2.7839018E-02	14	3.6234282E-02	14	-2.2495796E-02	14	5.5653650E-03
0.25	15	1.3417556E-02	15	-3.0123834E-03	15	1.4437642E-02	15	-3.4910754E-02	15	2.0823190E-02
	16	5.0850214E-02	16	-5.7070305E-02	16	3.2876287E-02	16	-7.4634588E-03	16	2.4602318E-02
	17	-2.5331215E-02	17	5.3116833E-02	17	3.3051528E-02	17	-3.9108066E-02	17	-4.5788709E-02
	18	8.2823911E-02	18	-1.1718120E-01	18	2.4038135E-02	18	-5.5824675E-03	18	8.9334782E-02
	19	-6.1060959E-02	19	8.2822185E-02	19	1.7195437E-02	19	-1.7818918E-02	19	-7.5400565E-02
0.50	20	9.7170830E-02	20	-9.4778299E-02	20	2.9044151E-02	20	-3.8042068E-03	20	5.6581497E-02

Figure B-11. Filter Weight Listings for MCF-13; 5-Ring IV Model MCF

TIME (SECONDS)		RING 1		RING 2		RING 3		RING 4		RING 5
-1.00	0	-4.3715393E-01	0	-8.3014295E-02	0	1.7588862E-01	0	-1.2417196E-01	0	9.5323054E-02
	1	5.2520585E-01	1	8.1938159E-02	1	-1.8701678E-01	1	1.4663661E-01	1	-1.1584876E-01
	2	-5.7545171E-01	2	-1.1787041E-01	2	2.6100725E-01	2	-1.9881174E-01	2	1.3953086E-01
	3	2.6631003E-01	3	6.4348725E-02	3	-1.0838544E-01	3	8.0893438E-02	3	-7.2305797E-02
	4	-1.0437732E-01	4	-5.8615502E-02	4	7.7875611E-02	4	-3.7574593E-02	4	3.2381460E-02
	5	-1.4264196E-01	5	8.9253591E-03	5	6.5177182E-02	5	-6.9149263E-02	5	2.3059231E-02
	6	8.3174811E-02	6	-1.2283350E-02	6	-1.2284197E-02	6	3.0419842E-02	6	-1.8434703E-02
	7	-5.0117075E-02	7	-2.0079255E-02	7	5.8103234E-02	7	-4.0038375E-02	7	1.0797128E-02
	8	-7.7035353E-02	8	1.2990545E-02	8	2.4643196E-02	8	-2.1493528E-02	8	-2.4556076E-03
	9	-1.7081787E-03	9	-2.6693425E-02	9	2.6574712E-02	9	-1.2699408E-02	9	1.3116478E-02
-0.50	10	-6.0648863E-02	10	-6.1104612E-03	10	3.3771829E-02	10	-1.9478739E-02	10	2.2679731E-03
	11	9.5512038E-03	11	-5.8323462E-03	11	3.3616498E-02	11	-3.9084591E-02	11	1.0085595E-02
	12	-4.4188263E-02	12	-1.7644770E-02	12	2.8495086E-02	12	-1.2344482E-02	12	9.6911836E-03
	13	-5.0816417E-02	13	-1.9792631E-03	13	3.8797623E-02	13	-4.2829295E-02	13	1.3373941E-02
	14	-7.0824576E-03	14	-3.0229892E-02	14	4.2526644E-02	14	-3.2793102E-02	14	2.1767855E-02
	15	-2.9243426E-02	15	-1.1418995E-02	15	2.9085170E-02	15	-3.3573625E-02	15	1.9677589E-02
	16	-4.8637786E-02	16	-1.7119986E-02	16	4.5284710E-02	16	-3.7599238E-02	16	1.7535180E-02
	17	3.0072264E-02	17	-3.3565907E-02	17	3.4348335E-02	17	-2.6016336E-02	17	2.0010257E-02
	18	-1.0891191E-01	18	-1.2266103E-02	18	3.5069825E-02	18	-2.6731808E-02	18	2.1271442E-02
	19	6.9998280E-02	19	-2.5283197E-02	19	3.8139881E-02	19	-4.7759147E-02	19	2.3554061E-02
0	20	2.1823620E-02	20	6.0042337E-05	20	6.3874822E-02	20	5.9911164E-02	20	3.2761668E-02
	21	1.0354936E-01	21	-1.5601306E-02	21	3.3007805E-02	21	-6.1469384E-02	21	2.7484509E-02
	22	-5.6808966E-02	22	-2.4757711E-02	22	1.6731644E-02	22	5.2533878E-03	22	1.0815290E-02
	23	3.6336507E-02	23	-2.9729378E-02	23	3.1256461E-02	23	-2.6603977E-02	23	1.9765306E-02
	24	5.4027303E-02	24	-2.4514365E-02	24	1.9357243E-02	24	-1.6603086E-02	24	1.2128675E-02
	25	2.5030774E-02	25	-1.7132680E-02	25	2.2097209E-02	25	-1.6961921E-02	25	6.8754858E-03
	26	5.3167230E-02	26	-2.9900758E-02	26	2.1016704E-02	26	-2.3031731E-02	26	2.3096456E-02
	27	8.1932817E-02	27	-5.8142336E-03	27	1.0780194E-02	27	-1.2340870E-02	27	-6.2768421E-03
	28	1.1478724E-02	28	-2.9487457E-02	28	2.2547661E-02	28	-7.9638862E-03	28	1.2903129E-02
	29	5.9712573E-02	29	-1.5607176E-02	29	1.7486640E-02	29	-1.7363680E-02	29	6.1505818E-03
0.50	30	1.4471437E-02	30	-1.5086464E-02	30	1.6805982E-02	30	-2.2431973E-03	30	-1.6536977E-03
	31	2.3173816E-02	31	-2.6536178E-02	31	2.4741584E-02	31	-8.8444454E-03	31	6.5093779E-03
	32	6.2510710E-02	32	-1.2163661E-02	32	3.2955096E-03	32	3.2636926E-03	32	-3.7375015E-03
	33	2.2644676E-02	33	-1.7408821E-02	33	1.2843357E-02	33	-1.7492826E-03	33	2.7248342E-03
	34	-1.2444735E-02	34	-1.0446789E-02	34	3.6416290E-02	34	-2.0339387E-02	34	-2.9729329E-03
	35	5.7089494E-02	35	-1.4817220E-02	35	-7.9800854E-03	35	2.7656316E-02	35	-1.3627159E-02
	36	1.7521319E-01	36	-4.7225789E-03	36	-5.5363705E-02	36	-1.4581725E-02	36	4.4408046E-02
	37	-2.5446058E-01	37	-2.9535962E-02	37	1.5404932E-01	37	2.1343306E-04	37	-7.9065718E-02
	38	5.4336458E-01	38	8.6948334E-03	38	-2.3369190E-01	38	1.9886304E-02	38	1.0991703E-01
	39	-4.4904586E-01	39	-2.1346473E-02	39	1.9798310E-01	39	-1.3438008E-02	39	-8.3454825E-02
1.00	40	4.2235279E-01	40	3.8489699E-03	40	-1.4153695E-01	40	6.8278313E-03	40	5.8016777E-02

Figure B-12. Filter Weight Listings for MCF-14; 5-Ring IV Model MCF

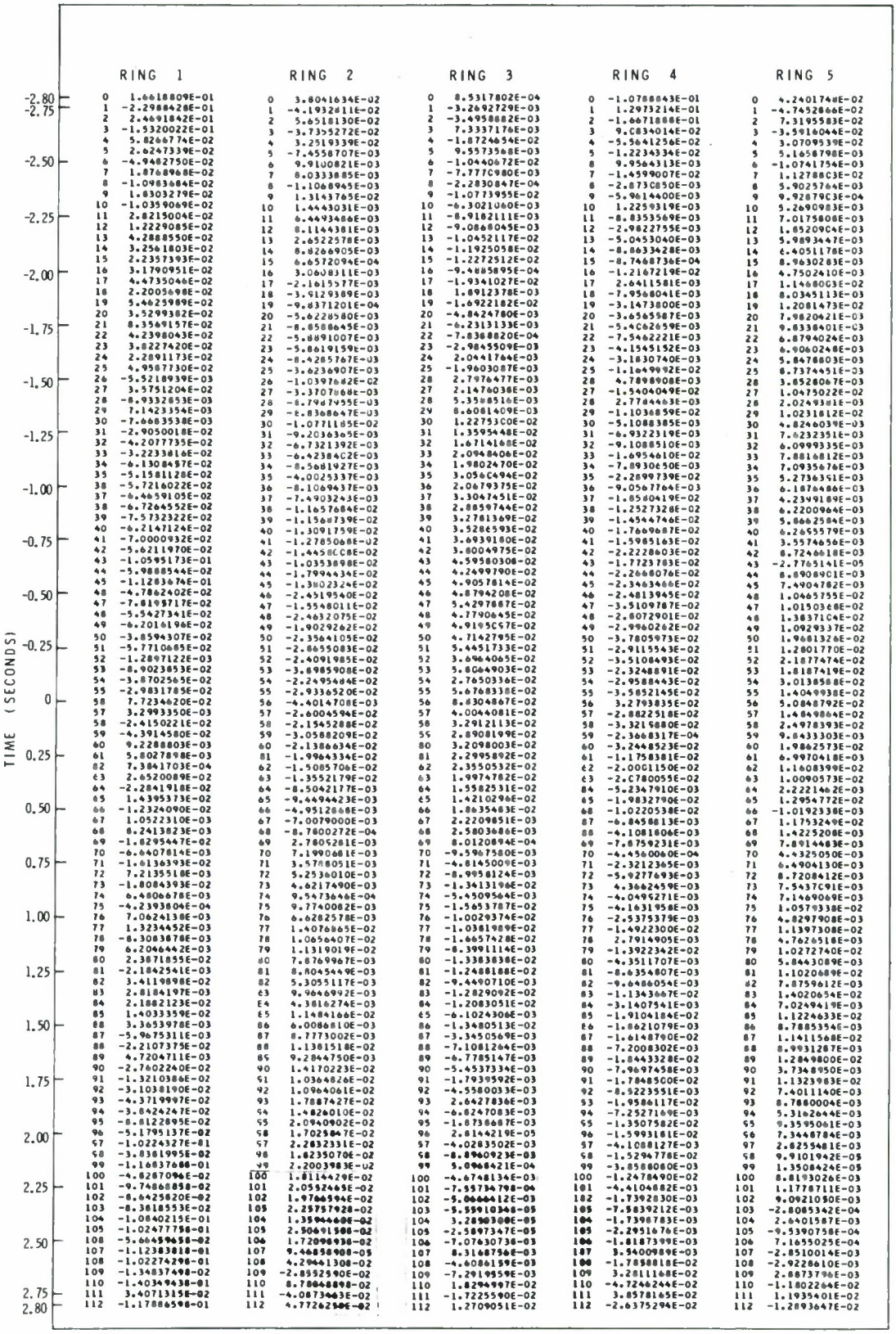

TIME (SECONDS)	RING 1	RING 2	RING 3	RING 4	RING 5
-2.80	0 1.66188809E-01	0 3.80416346E-02	0 8.53178026E-04	0 -1.07888436E-01	0 4.24017446E-02
-2.75	1 -2.29884286E-01	1 -4.19328116E-02	1 -3.26927296E-03	1 1.29732146E-01	1 -4.74528666E-02
	2 2.46918426E-01	2 5.65181306E-02	2 -3.49588826E-03	2 -1.66718886E-01	2 7.31955836E-02
	3 -1.53200226E-01	3 -3.73552726E-02	3 7.33371766E-03	3 9.08340146E-02	3 -3.59160446E-02
	4 5.82667746E-02	4 3.25193396E-02	4 -1.87246546E-02	4 -5.56412566E-02	4 3.07095396E-02
-2.50	5 2.62473396E-02	5 -7.45587076E-03	5 9.55735686E-03	5 -1.22343346E-02	5 5.16587986E-03
	6 -4.94827506E-02	6 9.91008216E-03	6 -1.04406726E-02	6 9.95643136E-03	6 -1.07417546E-03
	7 1.87689686E-02	7 8.03338856E-03	7 -7.77706806E-03	7 -1.45999076E-02	7 1.12788C36E-02
	8 -1.09836846E-02	8 -1.10689456E-03	8 -2.28308476E-04	8 -2.87308506E-03	8 5.90257646E-03
	9 1.83032796E-02	9 1.31437656E-02	9 -1.07739556E-02	9 -5.96144006E-03	9 9.92879C36E-04
-2.25	10 -1.03590696E-02	10 1.44430316E-03	10 -6.30210606E-03	10 1.22593196E-02	10 5.26909836E-03
	11 2.82150046E-02	11 6.44934866E-03	11 -8.91821116E-03	11 -8.83535696E-03	11 7.01758086E-03
	12 1.22290856E-02	12 8.11443816E-03	12 -9.08660456E-03	12 -2.98227556E-03	12 1.85209C46E-03
	13 4.28885506E-02	13 2.65225786E-03	13 -1.04521176E-02	13 -5.04530406E-03	13 5.98934676E-03
	14 3.25618036E-02	14 8.82669056E-03	14 -1.19250586E-02	14 -8.86334286E-03	14 6.40511786E-03
	15 2.23573936E-02	15 6.65720946E-04	15 -1.22725126E-02	15 -8.74687366E-04	15 8.96302836E-03
-2.00	16 3.17909516E-02	16 3.04983116E-03	16 -9.44858956E-04	16 -1.21672196E-02	16 4.75024106E-03
	17 4.47350466E-02	17 -2.16155776E-03	17 -1.93410276E-02	17 2.64115816E-03	17 1.14680C36E-02
	18 2.20056986E-02	18 -3.91293896E-03	18 1.89123786E-03	18 -7.95680416E-03	18 8.03451136E-03
	19 5.46259896E-02	19 -9.83712016E-04	19 -1.69221826E-02	19 -3.14738006E-03	19 1.20814736E-02
	20 3.52993826E-02	20 -5.62285806E-03	20 -4.84247806E-03	20 -3.63655876E-03	20 7.98204216E-03
-1.75	21 8.35691576E-02	21 -8.85886456E-03	21 -6.23131336E-03	21 -5.46262656E-03	21 9.83384016E-03
	22 4.23980436E-02	22 -5.88910076E-03	22 -7.83688206E-04	22 -7.54622216E-03	22 6.87940246E-03
	23 3.82274206E-02	23 -5.86191596E-03	23 -2.98455096E-03	23 -4.15451526E-03	23 6.90602486E-03
	24 2.28911736E-02	24 -8.42857676E-03	24 2.04417646E-03	24 -3.18307406E-03	24 5.84788036E-03
	25 4.95877306E-02	25 -3.62369076E-03	25 -1.96030876E-03	25 -1.16499926E-02	25 8.73744516E-03
-1.50	26 -5.52189396E-03	26 -1.03976426E-02	26 2.79764776E-03	26 4.78988086E-03	26 3.85280676E-03
	27 3.57512046E-02	27 -3.37078686E-03	27 2.14760386E-03	27 -1.54040496E-02	27 1.04750226E-02
	28 -8.93326536E-03	28 -8.79479556E-03	28 5.35588516E-03	28 2.77844636E-03	28 2.02493816E-03
	29 7.14233546E-03	29 -8.83686476E-03	29 8.60814096E-03	29 -1.10368596E-02	29 1.02318126E-02
	30 -7.66883536E-03	30 -1.07711856E-02	30 1.22753C06E-02	30 -5.10883856E-03	30 4.82460396E-03
-1.25	31 -2.90500186E-02	31 -9.20363656E-03	31 1.35959486E-02	31 -6.93223196E-03	31 7.62323516E-03
	32 -4.20777356E-02	32 -6.73213926E-03	32 1.67141686E-02	32 -9.10885106E-03	32 6.09993356E-03
	33 -3.22338166E-02	33 -6.42384626E-03	33 2.09484066E-02	33 -1.69546106E-02	33 7.88186126E-03
	34 -6.13084976E-02	34 -8.56819276E-03	34 1.98024706E-02	34 -7.89306506E-03	34 7.09356766E-03
	35 -5.15811286E-02	35 -4.00253376E-03	35 3.05604946E-02	35 -2.28997396E-02	35 5.27363516E-03
-1.00	36 -5.72160226E-02	36 -8.10694376E-03	36 2.06793756E-02	36 -9.05677646E-03	36 6.18764866E-03
	37 -6.46659106E-02	37 -7.49032436E-03	37 3.30474516E-02	37 -1.05804196E-02	37 4.23491896E-03
	38 -6.72645526E-02	38 -1.16576846E-02	38 2.88597446E-02	38 -1.25273286E-02	38 6.22009646E-03
	39 -7.57323226E-02	39 -1.15687396E-02	39 3.27813696E-02	39 -1.45447466E-02	39 5.86625846E-03
	40 -6.21471246E-02	40 -1.30917596E-02	40 3.52865936E-02	40 -1.76696876E-02	40 6.26555796E-03
-0.75	41 -7.00009326E-02	41 -1.27850686E-02	41 3.69391806E-02	41 -1.59851636E-02	41 3.55746566E-03
	42 -5.62119706E-02	42 -1.44586C86E-02	42 3.80049756E-02	42 -2.22286036E-02	42 8.72466186E-03
	43 -1.05951736E-01	43 -1.03538986E-02	43 4.59580306E-02	43 -1.77237836E-02	43 -2.77651416E-05
	44 -5.98885446E-02	44 -1.79964346E-02	44 4.24997906E-02	44 -2.26680766E-02	44 8.69084016E-03
	45 -1.12833676E-01	45 -1.38023246E-02	45 4.90578146E-02	45 -2.34634666E-02	45 7.49047826E-03
-0.50	46 -4.78624026E-02	46 -2.45195406E-02	46 4.87942086E-02	46 -2.48139456E-02	46 1.04657556E-02
	47 -7.81987176E-02	47 -1.55480116E-02	47 5.42978876E-02	47 -3.51097876E-02	47 1.01503686E-02
	48 -5.54273416E-02	48 -2.46320756E-02	48 4.77906456E-02	48 -2.80729016E-02	48 1.38371C46E-02
	49 -6.20161966E-02	49 -1.90292626E-02	49 4.91956576E-02	49 -2.99602626E-02	49 1.09293376E-02
-0.25	50 -3.85943076E-02	50 -2.35641056E-02	50 4.71427956E-02	50 -3.78059736E-02	50 1.96813266E-02
	51 -5.77106856E-02	51 -2.86550836E-02	51 5.44517336E-02	51 -2.91155436E-02	51 1.28017706E-02
	52 -1.28971226E-03	52 -2.40919856E-02	52 3.69640656E-02	52 -3.51084936E-02	52 1.18774746E-02
	53 -8.90238536E-02	53 -3.89859086E-02	53 5.80649036E-02	53 -2.32488916E-02	53 1.81874196E-02
	54 -3.87025656E-02	54 -2.24954846E-02	54 2.76503366E-02	54 -2.95884436E-02	54 3.01385886E-02
0	55 -2.98317856E-02	55 -2.93365206E-02	55 5.67683386E-02	55 -3.58521456E-02	55 1.40499386E-02
	56 7.72346206E-02	56 -4.40147086E-03	56 8.83048676E-02	56 3.27938356E-02	56 5.08487926E-02
	57 3.29933506E-03	57 -2.60045946E-02	57 4.00440816E-02	57 -2.88225186E-02	57 1.48498646E-02
	58 -2.41502216E-02	58 -2.15452886E-02	58 3.29121136E-02	58 -3.32158806E-02	58 2.49783936E-02
	59 -4.39145806E-02	59 -3.05882096E-02	59 2.89081996E-02	59 -2.36683176E-04	59 9.84333036E-03
0.25	60 9.22888036E-03	60 -2.13866346E-02	60 3.20980036E-02	60 -3.24485236E-02	60 1.98625736E-02
	61 5.80278986E-03	61 -1.99643346E-02	61 2.29958926E-02	61 -1.17583816E-02	61 6.99704186E-03
	62 7.38417036E-04	62 -1.50857066E-02	62 2.35505326E-02	62 -2.00011506E-02	62 1.16083996E-02
	63 2.65200896E-02	63 -1.35521796E-02	63 1.99747826E-02	63 -2.67800556E-02	63 1.00905736E-02
	64 -2.28419186E-02	64 -8.50421776E-03	64 1.55825316E-02	64 -5.23679106E-03	64 2.22214626E-03
0.50	65 1.43953736E-02	65 -9.64944236E-03	65 1.42102966E-02	65 -1.98327906E-02	65 1.29547726E-02
	66 -1.23240906E-02	66 -4.95128686E-03	66 1.86354836E-02	66 -1.02205386E-02	66 -1.01923386E-03
	67 1.05223106E-03	67 -7.00790006E-03	67 2.22098516E-03	67 -8.04588136E-03	67 1.17532496E-02
	68 8.24138236E-03	68 -8.78002726E-04	68 2.58036866E-03	68 -4.10818066E-03	68 1.42252086E-03
	69 -1.82954476E-02	69 2.78052816E-03	69 8.01208946E-04	69 -7.87592316E-03	69 7.89144836E-03
0.75	70 -6.64078146E-03	70 7.19906816E-03	70 -9.59675806E-03	70 -4.45600606E-04	70 4.43250506E-03
	71 -1.61363936E-02	71 3.57880516E-03	71 -4.81450096E-03	71 -2.32123656E-03	71 6.49041306E-03
	72 7.21355186E-03	72 5.25360106E-03	72 -8.99581246E-03	72 -5.92776936E-03	72 8.72084126E-03
	73 -1.80843936E-02	73 4.62174906E-03	73 -1.34131966E-02	73 4.36624596E-03	73 7.54376916E-03
	74 6.48066786E-03	74 9.54736466E-04	74 -5.45095646E-03	74 -4.04952716E-03	74 7.14690696E-03
1.00	75 -4.23936046E-04	75 9.77400826E-03	75 -1.56537876E-02	75 -4.16319586E-03	75 1.05793386E-02
	76 7.06241386E-03	76 6.62825786E-03	76 -1.00293746E-02	76 -2.53753796E-03	76 4.82979086E-03
	77 1.32344526E-03	77 1.40768656E-02	77 -1.03819896E-02	77 -1.49223006E-02	77 1.13973086E-02
	78 -8.30838786E-03	78 1.06564076E-02	78 -1.66574286E-02	78 2.79149056E-03	78 4.76265186E-03
	79 6.20464426E-03	79 1.13190196E-02	79 -8.39911146E-03	79 -1.39223426E-02	79 1.02727406E-02
1.25	80 2.38718556E-02	80 7.87699676E-03	80 -1.33833836E-02	80 -4.35117076E-03	80 5.84430896E-03
	81 -2.18425416E-03	81 8.80454496E-03	81 -1.24881886E-02	81 -8.63548076E-03	81 1.10206896E-02
	82 3.41198986E-02	82 5.30551176E-03	82 -9.44907106E-03	82 -9.64860546E-03	82 7.87596126E-03
	83 2.81841976E-03	83 9.96469926E-03	83 -1.28290926E-02	83 -1.13436676E-02	83 1.40206546E-02
	84 2.18821236E-02	E4 4.38162746E-03	84 -1.20830516E-02	84 -3.14075416E-03	84 7.02494196E-03
1.50	85 1.40333596E-02	E5 1.14841666E-02	85 -6.10243066E-03	85 -1.91041846E-02	85 1.12246336E-02
	86 3.36539786E-03	86 6.00868106E-03	86 -1.34805136E-02	86 -1.86210796E-03	86 8.78853546E-03
	87 -5.96753116E-03	87 8.77730026E-03	87 -3.34505696E-03	87 -1.61487906E-02	87 1.14115686E-02
	88 -2.21073756E-02	88 1.13815186E-02	88 -7.10812646E-03	88 -7.20083026E-03	88 8.99312876E-03
	89 4.72047116E-03	89 9.28447506E-03	89 -6.77851476E-03	89 -1.84433286E-02	89 1.28498006E-02
1.75	90 -2.76022406E-02	90 1.41702236E-02	90 -5.45373346E-03	90 -7.96974586E-03	90 3.73489506E-03
	91 -1.32103866E-02	91 1.03648266E-02	91 -1.79395926E-03	91 -1.78485C06E-02	91 1.13239036E-02
	92 -3.10381906E-02	92 1.09640616E-02	92 -4.55800336E-03	92 -8.92235516E-03	92 7.40111406E-03
	93 -4.37199976E-02	93 1.78874276E-02	93 2.64278366E-03	93 -1.95861176E-02	93 8.78600046E-03
	94 -3.84262476E-02	94 1.48260106E-02	94 -6.82470836E-03	94 -7.25271696E-03	94 5.31626446E-03
2.00	95 -8.81228956E-02	95 2.09409026E-02	95 -1.87386876E-03	95 -1.35075826E-02	95 9.35950616E-03
	96 -5.17951376E-02	96 1.70258476E-02	96 2.81442196E-05	96 -1.59931816E-02	96 7.34487846E-03
	97 -1.02243276E-01	97 2.28323316E-02	97 -4.02835026E-03	97 -4.10881276E-03	97 2.82554816E-03
	98 -3.83619956E-02	98 1.82350706E-02	98 -8.89409236E-03	98 -1.52947786E-02	98 9.91019426E-03
	99 -1.16837686-01	99 2.20039836-02	99 5.09686216-04	99 -3.85880806-03	99 1.35084246-03
2.25	100 -4.82870966-02	100 1.81144296-02	100 -4.67481346-03	100 -1.24784906-02	100 8.81930266-03
	101 -9.74868856-02	101 2.05524696-02	101 -7.55734796-04	101 -4.41048826-03	101 1.17787116-03
	102 -8.64258206-02	102 1.97665946-02	102 -5.06664126-03	102 -1.73928306-03	102 9.09210806-03
	103 -8.38185536-02	103 2.25757926-02	103 -5.55910346-05	103 -7.58392126-03	103 -2.80853426-04
	104 -1.08402156-01	104 1.35944606-02	104 3.28503006-05	104 -1.73987836-03	104 2.64015876-03
2.50	105 -1.02477756-01	105 2.50691506-02	105 -2.58973476-05	105 -2.29516766-03	105 -9.53907586-04
	106 -5.66459656-02	106 1.72096936-02	106 -7.07630736-03	106 -1.81873996-03	106 7.16550256-04
	107 -1.12383816-01	107 9.44858906-05	107 8.31687566-03	107 3.94009896-03	107 -2.85100146-03
	108 -1.02274296-01	108 4.29461306-02	108 -4.60861596-03	108 -1.78588186-02	108 -2.92286106-03
	109 -1.34837496-02	109 -2.85525906-02	109 -7.29195596-03	109 3.28111686-02	109 2.86737966-03
2.75	110 -1.40349636-01	110 8.78648896-02	110 1.82949976-02	110 -4.72462446-02	110 -1.18022646-02
	111 3.40713156-02	111 -4.08734636-02	111 -1.72255906-02	111 3.85781656-02	111 1.19354016-02
2.80	112 -1.17886596-01	112 4.77262506-02	112 1.27090516-02	112 -2.63752946-02	112 -1.28936476-02

Figure B-13. Filter Weight Listings for MCF-15; 5-Ring IV Model MCF

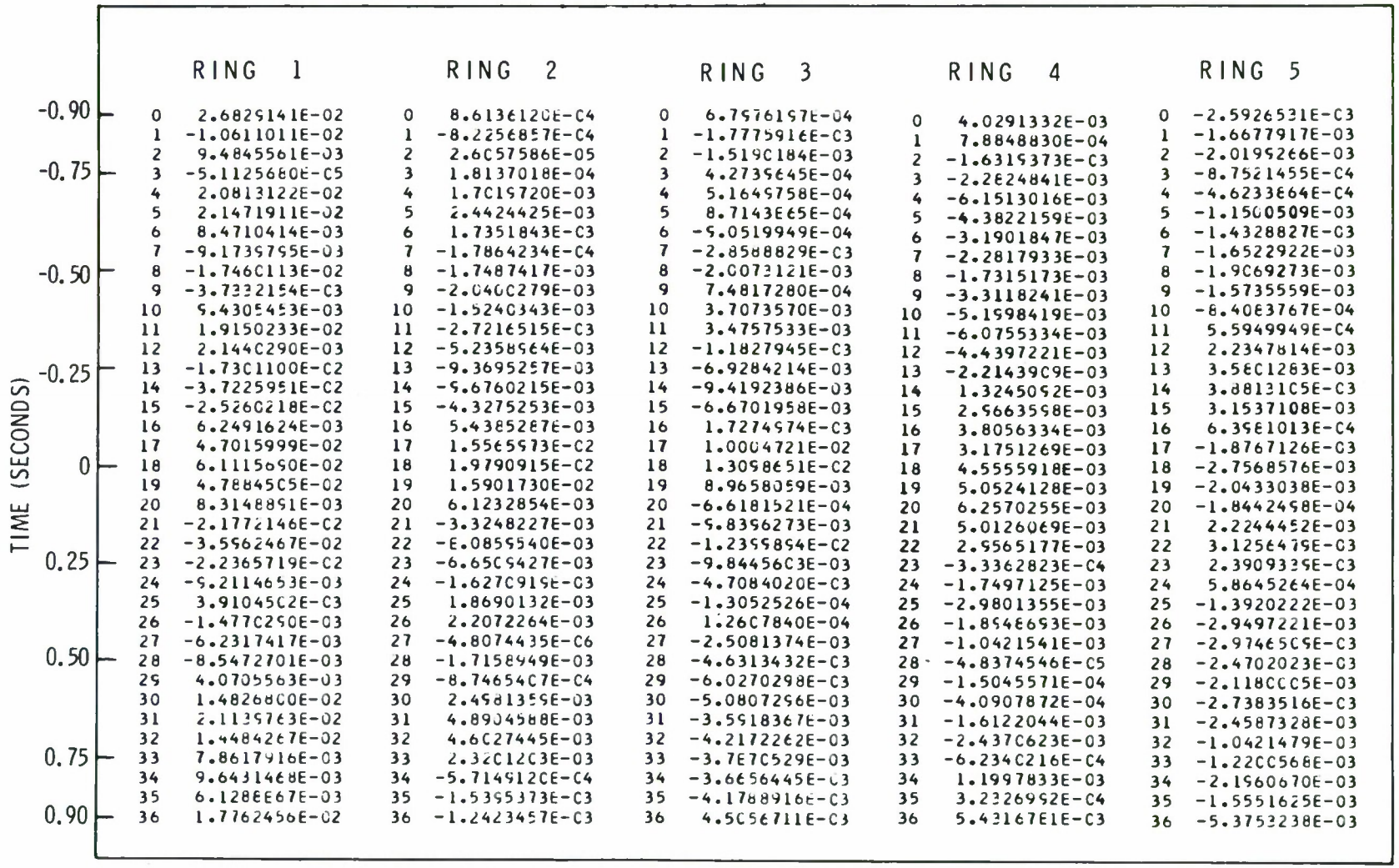

	RING 1	RING 2	RING 3	RING 4	RING 5
0	2.6825141E-02	8.6136120E-04	6.7576197E-04	4.0291332E-03	-2.5926531E-03
1	-1.0611011E-02	-8.2256857E-04	-1.7775916E-03	7.8848830E-04	-1.6677917E-03
2	9.4845561E-03	2.6057586E-05	-1.5190184E-03	-1.6315373E-03	-2.0195266E-03
3	-5.1125680E-05	1.8137018E-04	4.2735645E-04	-2.2824841E-03	-8.7521455E-04
4	2.0813122E-02	1.7019720E-03	5.1649758E-04	-6.1513016E-03	-4.6233664E-04
5	2.1471911E-02	2.4424425E-03	8.7143E65E-04	-4.3822159E-03	-1.1500509E-03
6	8.4710414E-03	1.7351843E-03	-9.0519949E-04	-3.1901847E-03	-1.4328827E-03
7	-9.1739795E-03	-1.7864234E-04	-2.8588829E-03	-2.2817933E-03	-1.6522922E-03
8	-1.7460113E-02	-1.7487417E-03	-2.0073121E-03	-1.7315173E-03	-1.9069273E-03
9	-3.7332154E-03	-2.0400279E-03	7.4817280E-04	-3.3118241E-03	-1.5735559E-03
10	9.4305453E-03	-1.5240343E-03	3.7073570E-03	-5.1998419E-03	-8.4083767E-04
11	1.9150233E-02	-2.7216515E-03	3.4757533E-03	-6.0755334E-03	5.5949949E-04
12	2.1440290E-03	-5.2358564E-03	-1.1827945E-03	-4.4397221E-03	2.2347814E-03
13	-1.7301100E-02	-9.3695257E-03	-6.9284214E-03	-2.2143909E-03	3.5801283E-03
14	-3.7225951E-02	-9.6760215E-03	-9.4192386E-03	1.3245052E-03	3.8813105E-03
15	-2.5260218E-02	-4.3275253E-03	-6.6701958E-03	2.9663598E-03	3.1537108E-03
16	6.2491624E-03	5.4385287E-03	1.7274974E-03	3.8056334E-03	6.3581013E-04
17	4.7015999E-02	1.5565973E-02	1.0004721E-02	3.1751269E-03	-1.8767126E-03
18	6.1115650E-02	1.9790915E-02	1.3098651E-02	4.5555918E-03	-2.7568576E-03
19	4.7884505E-02	1.5901730E-02	8.9658059E-03	5.0524128E-03	-2.0433038E-03
20	8.3148851E-03	6.1232854E-03	-6.6181521E-04	6.2570255E-03	-1.8442458E-04
21	-2.1772146E-02	-3.3248227E-03	-5.8356273E-03	5.0126069E-03	2.2244452E-03
22	-3.5562467E-02	-6.0855540E-03	-1.2355854E-02	2.9565177E-03	3.1256479E-03
23	-2.2365719E-02	-6.6509427E-03	-9.8445603E-03	-3.3362823E-04	2.3909335E-03
24	-9.2114653E-03	-1.6270919E-03	-4.7084020E-03	-1.7497125E-03	5.8645264E-04
25	3.9104502E-03	1.8690132E-03	-1.3052526E-04	-2.9801355E-03	-1.3920222E-03
26	-1.4770250E-03	2.2072264E-03	1.2607840E-04	-1.8546693E-03	-2.9497221E-03
27	-6.2317417E-03	-4.8074435E-06	-2.5081374E-03	-1.0421541E-03	-2.9746509E-03
28	-8.5472701E-03	-1.7158949E-03	-4.6313432E-03	-4.8374546E-05	-2.4702023E-03
29	4.0705563E-03	-8.7465407E-04	-6.0270298E-03	-1.5045571E-04	-2.1180005E-03
30	1.4826800E-02	2.4581359E-03	-5.0807296E-03	-4.0907872E-04	-2.7383516E-03
31	2.1135763E-02	4.8904588E-03	-3.5918367E-03	-1.6122044E-03	-2.4587328E-03
32	1.4484267E-02	4.6027445E-03	-4.2172262E-03	-2.4370623E-03	-1.0421479E-03
33	7.8617916E-03	2.3202123E-03	-3.7E70529E-03	-6.2340216E-04	-1.2200568E-03
34	9.6431468E-03	-5.7149126E-04	-3.6656445E-03	1.1997833E-03	-2.1960670E-03
35	6.1288E67E-03	-1.5395373E-03	-4.1788916E-03	3.2326952E-04	-1.5551625E-03
36	1.7762456E-02	-1.2423457E-03	4.5056711E-03	5.4316761E-03	-5.3753238E-03

Figure B-17. Filter Weight Listings for MCF-16: Final 5-Channel Disk Model; Subarray F-3

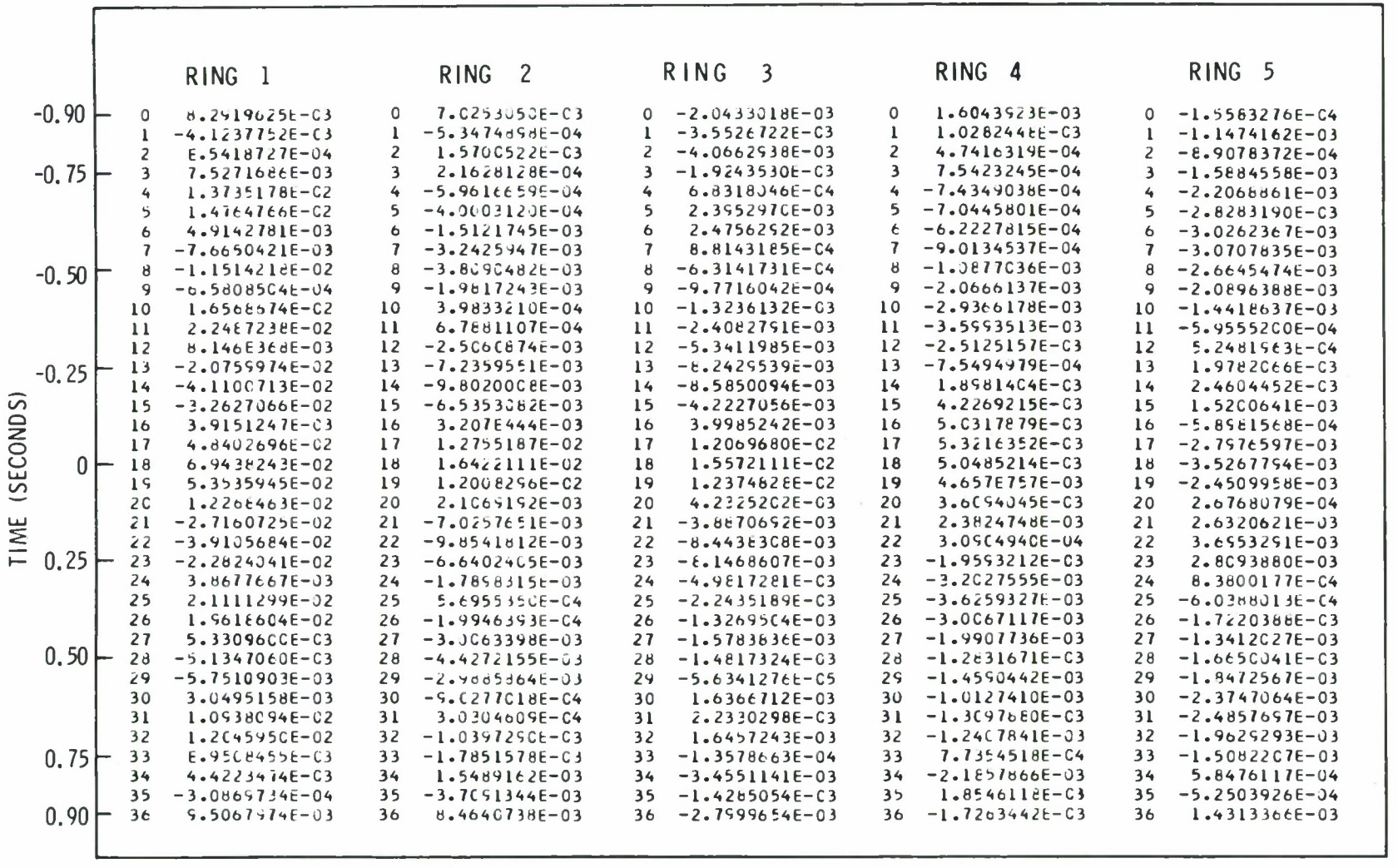

TIME (SECONDS)	RING 1	RING 2	RING 3	RING 4	RING 5
	0 8.2919625E-03	0 7.0253050E-03	0 -2.0433018E-03	0 1.6043923E-03	0 -1.5583276E-04
	1 -4.1237752E-03	1 -5.3474698E-04	1 -3.5526722E-03	1 1.0282446E-03	1 -1.1474162E-03
-0.90	2 8.5418727E-04	2 1.5700522E-03	2 -4.0662938E-03	2 4.7416319E-04	2 -8.9078372E-04
	3 7.5271686E-03	3 2.1628128E-04	3 -1.9243530E-03	3 7.5423245E-04	3 -1.5884558E-03
	4 1.3735178E-02	4 -5.9616659E-04	4 6.8318046E-04	4 -7.4349038E-04	4 -2.2068861E-03
-0.75	5 1.4764766E-02	5 -4.0003120E-04	5 2.3952970E-03	5 -7.0445801E-04	5 -2.8283190E-03
	6 4.9142781E-03	6 -1.5121745E-03	6 2.4756252E-03	6 -6.2227815E-04	6 -3.0262367E-03
	7 -7.6650421E-03	7 -3.2425947E-03	7 8.8143185E-04	7 -9.0134537E-04	7 -3.0707835E-03
	8 -1.1514218E-02	8 -3.8090482E-03	8 -6.3141731E-04	8 -1.0877036E-03	8 -2.6645474E-03
-0.50	9 -6.5808504E-04	9 -1.9817243E-03	9 -9.7716042E-04	9 -2.0666137E-03	9 -2.0896388E-03
	10 1.6568574E-02	10 3.9833210E-04	10 -1.3236132E-03	10 -2.9366178E-03	10 -1.4418637E-03
	11 2.2487238E-02	11 6.7881107E-04	11 -2.4082751E-03	11 -3.5993513E-03	11 -5.9552C0E-04
	12 8.1466368E-03	12 -2.5066874E-03	12 -5.3411985E-03	12 -2.5125157E-03	12 5.2481563E-04
-0.25	13 -2.0759974E-02	13 -7.2359551E-03	13 -8.2429539E-03	13 -7.5494979E-04	13 1.9782066E-03
	14 -4.1100713E-02	14 -9.8020008E-03	14 -8.5850094E-03	14 1.8981404E-03	14 2.4604452E-03
	15 -3.2627066E-02	15 -6.5353082E-03	15 -4.2227056E-03	15 4.2269215E-03	15 1.5220641E-03
	16 3.9151247E-03	16 3.2076444E-03	16 3.9985242E-03	16 5.0317879E-03	16 -5.8581568E-04
	17 4.8402696E-02	17 1.2755187E-02	17 1.2069680E-02	17 5.3216352E-03	17 -2.7976597E-03
0	18 6.9438243E-02	18 1.6422111E-02	18 1.5572111E-02	18 5.0485214E-03	18 -3.5267794E-03
	19 5.3535945E-02	19 1.2008296E-02	19 1.2374628E-02	19 4.6576757E-03	19 -2.4509958E-03
	20 1.2266463E-02	20 2.1069192E-03	20 4.2225202E-03	20 3.6094045E-03	20 2.6768079E-04
	21 -2.7160725E-02	21 -7.0257651E-03	21 -3.8870652E-03	21 2.3824748E-03	21 2.6320621E-03
	22 -3.9105684E-02	22 -9.8541812E-03	22 -8.4436C8E-03	22 3.0904940E-04	22 3.6553291E-03
0.25	23 -2.2824041E-02	23 -6.6402405E-03	23 -6.1468607E-03	23 -1.9593212E-03	23 2.8093880E-03
	24 3.8677667E-03	24 -1.7858315E-03	24 -4.9817281E-03	24 -3.2027555E-03	24 8.3800177E-04
	25 2.1111299E-02	25 5.6955350E-04	25 -2.2435189E-03	25 -3.6259327E-03	25 -6.0388013E-04
	26 1.9616604E-02	26 -1.9946393E-04	26 -1.3269504E-03	26 -3.0067117E-03	26 -1.7220388E-03
	27 5.3309600E-03	27 -3.0063398E-03	27 -1.5783836E-03	27 -1.9907736E-03	27 -1.3412027E-03
0.50	28 -5.1347060E-03	28 -4.4272155E-03	28 -1.4817324E-03	28 -1.2831671E-03	28 -1.6650041E-03
	29 -5.7510903E-03	29 -2.9885364E-03	29 -5.6341276E-05	29 -1.4590442E-03	29 -1.8472567E-03
	30 3.0495158E-03	30 -9.0277018E-04	30 1.6366712E-03	30 -1.0127410E-03	30 -2.3747064E-03
	31 1.0938094E-02	31 3.0304609E-04	31 2.2330298E-03	31 -1.3097680E-03	31 -2.4857697E-03
	32 1.2045950E-02	32 -1.0397250E-03	32 1.6457243E-03	32 -1.2407841E-03	32 -1.9629293E-03
0.75	33 8.9508455E-03	33 -1.7851578E-03	33 -1.3578663E-04	33 7.7354518E-04	33 -1.5082207E-03
	34 4.4223474E-03	34 1.5489162E-03	34 -3.4551141E-03	34 -2.1857866E-03	34 5.8476117E-04
	35 -3.0869734E-04	35 -3.7091344E-03	35 -1.4265054E-03	35 1.8546118E-03	35 -5.2503926E-04
0.90	36 9.5067974E-03	36 8.4640738E-03	36 -2.7999654E-03	36 -1.7263442E-03	36 1.4313366E-03

Figure B-18. Filter Weight Listings for MCF-17: Final 5-Channel Disk Model; Subarray F-4

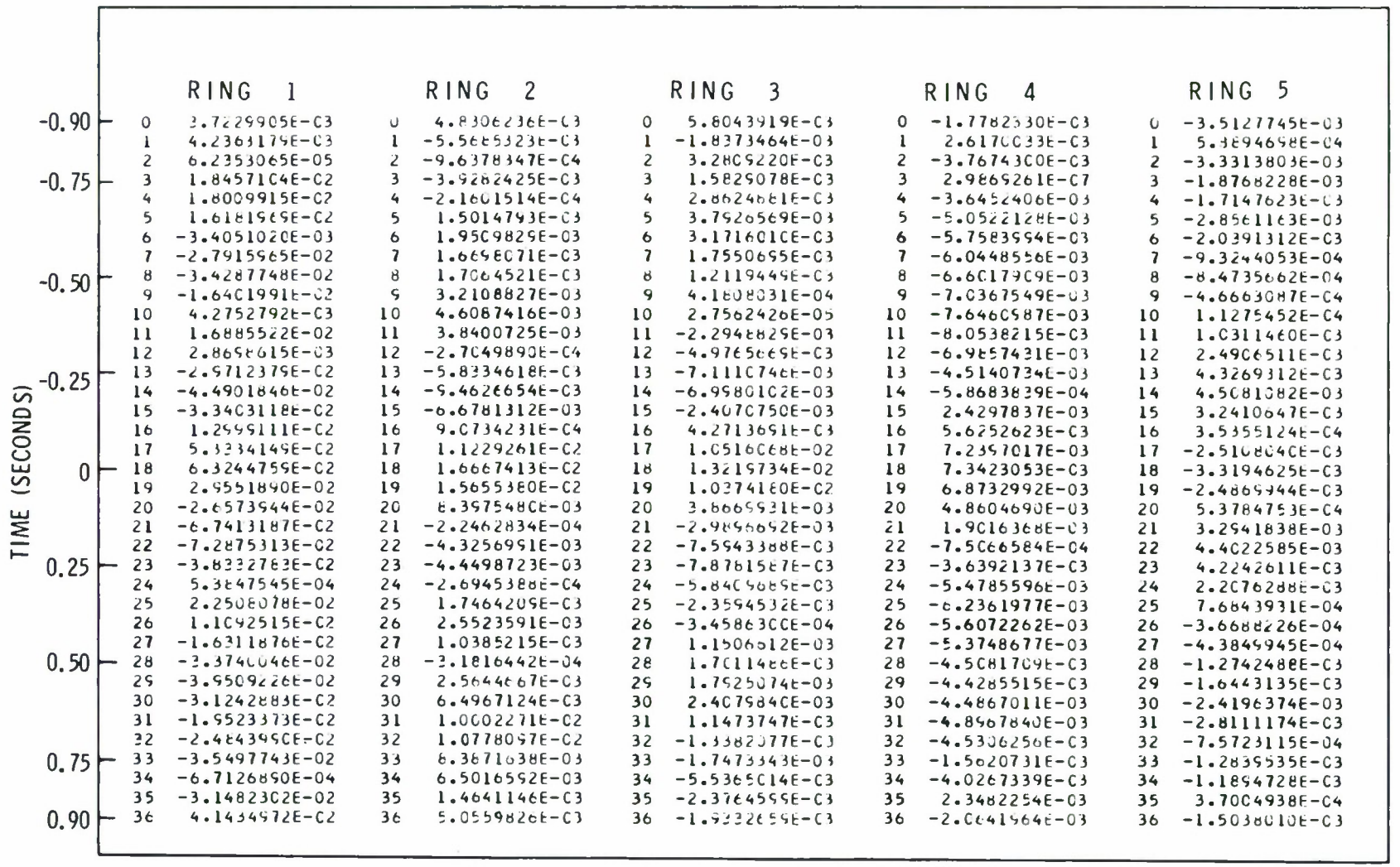

	RING 1	RING 2	RING 3	RING 4	RING 5
0	3.7229905E-03	4.8306236E-03	5.8043919E-03	-1.7782530E-03	-3.5127745E-03
1	4.2363179E-03	-5.5665323E-03	-1.8373464E-03	2.6170033E-03	5.3894698E-04
2	6.2353065E-05	-9.6378347E-04	3.2809220E-03	-3.7674300E-03	-3.3313803E-03
3	1.8457104E-02	-3.9282425E-03	1.5829078E-03	2.9869261E-07	-1.8768228E-03
4	1.8009915E-02	-2.1601514E-04	2.8624661E-03	-3.6452406E-03	-1.7147623E-03
5	1.6181969E-02	1.5014793E-03	3.7926569E-03	-5.0522128E-03	-2.8561163E-03
6	-3.4051020E-03	1.9509829E-03	3.1716015E-03	-5.7583994E-03	-2.0391312E-03
7	-2.7915965E-02	1.6696071E-03	1.7550695E-03	-6.0448556E-03	-9.3244053E-04
8	-3.4287748E-02	1.7064521E-03	1.2119449E-03	-6.6017909E-03	-8.4735662E-04
9	-1.6401991E-02	3.2108827E-03	4.1808031E-04	-7.0367549E-03	-4.6663087E-04
10	4.2752792E-03	4.6087416E-03	2.7562426E-05	-7.6460587E-03	1.1275452E-04
11	1.6885522E-02	3.8400725E-03	-2.2948829E-03	-8.0538215E-03	1.0311460E-03
12	2.8656615E-03	-2.7049890E-04	-4.9765669E-03	-6.9857431E-03	2.4906511E-03
13	-2.9712379E-02	-5.8334618E-03	-7.1110746E-03	-4.5140734E-03	4.3269312E-03
14	-4.4901846E-02	-9.4626654E-03	-6.9580102E-03	-5.8683839E-04	4.5081082E-03
15	-3.3403118E-02	-6.6781312E-03	-2.4070750E-03	2.4297837E-03	3.2410647E-03
16	1.2999111E-02	9.0734231E-04	4.2713691E-03	5.6252623E-03	3.5355124E-04
17	5.3334149E-02	1.1229261E-02	1.0516068E-02	7.2357017E-03	-2.5108804E-03
18	6.3244759E-02	1.6667413E-02	1.3219734E-02	7.3423053E-03	-3.3194625E-03
19	2.9551890E-02	1.5655380E-02	1.0374180E-02	6.8732992E-03	-2.4869944E-03
20	-2.6573944E-02	8.3975480E-03	3.6669531E-03	4.8604690E-03	5.3784753E-04
21	-6.7413187E-02	-2.2462834E-04	-2.9896692E-03	1.9016368E-03	3.2941838E-03
22	-7.2875313E-02	-4.3256991E-03	-7.5943388E-03	-7.5066584E-04	4.4022585E-03
23	-3.8332783E-02	-4.4498723E-03	-7.8761587E-03	-3.6392137E-03	4.2242611E-03
24	5.3647545E-04	-2.6945388E-04	-5.8405685E-03	-5.4785596E-03	2.2076288E-03
25	2.2508078E-02	1.7464209E-03	-2.3594532E-03	-6.2361977E-03	7.6843931E-04
26	1.1092515E-02	2.5523591E-03	-3.4586300E-04	-5.6072262E-03	-3.6688226E-04
27	-1.6311876E-02	1.0385215E-03	1.1506612E-03	-5.3748677E-03	-4.3849945E-04
28	-3.3740046E-02	-3.1816442E-04	1.7011488E-03	-4.5081709E-03	-1.2742488E-03
29	-3.9509226E-02	2.5644867E-03	1.7925074E-03	-4.4285515E-03	-1.6443135E-03
30	-3.1242883E-02	6.4967124E-03	2.4079840E-03	-4.4867011E-03	-2.4196374E-03
31	-1.9523373E-02	1.0002271E-02	1.1473747E-03	-4.8967840E-03	-2.8111174E-03
32	-2.4843950E-02	1.0778097E-02	-1.3382077E-03	-4.5306256E-03	-7.5723115E-04
33	-3.5497743E-02	8.3871638E-03	-1.7473343E-03	-1.5020731E-03	-1.2839535E-03
34	-6.7126890E-04	6.5016592E-03	-5.5365014E-03	-4.0267339E-03	-1.1894728E-03
35	-3.1482302E-02	1.4641146E-03	-2.3764559E-03	2.3482254E-03	3.7004938E-04
36	4.1434972E-02	5.0559826E-03	-1.9232659E-03	-2.0041964E-03	-1.5038010E-03

Figure B-14. Filter Weight Listings for MCF-18: Final 5-Channel Disk Model; Subarray C-3

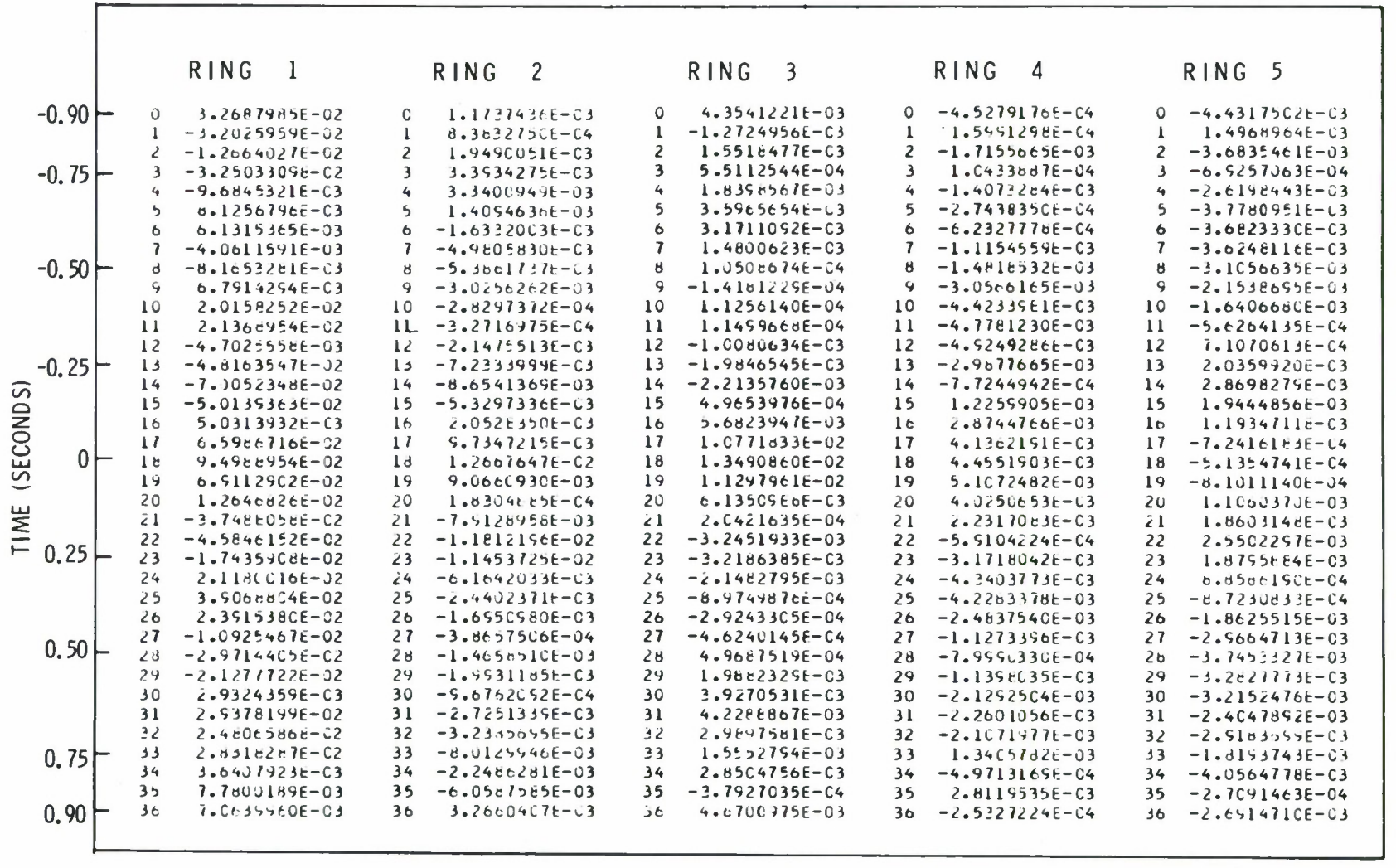

	RING 1	RING 2	RING 3	RING 4	RING 5
0	3.2687985E-02	1.1737436E-03	4.3541221E-03	-4.5279176E-04	-4.4317502E-03
1	-3.2025959E-02	8.3632750E-04	-1.2724956E-03	1.5491298E-04	1.4968964E-03
2	-1.2664027E-02	1.9490051E-03	1.5518477E-03	-1.7155665E-03	-3.6835461E-03
3	-3.2503309E-02	3.3534275E-03	5.5112544E-04	1.0433687E-04	-6.9257063E-04
4	-9.6845321E-03	3.3400949E-03	1.8358567E-03	-1.4073264E-03	-2.6198443E-03
5	8.1256796E-03	1.4094636E-03	3.5965654E-03	-2.7438350E-04	-3.7780951E-03
6	6.1315365E-03	-1.6332003E-03	3.1711052E-03	-6.2327776E-04	-3.6823330E-03
7	-4.0611591E-03	-4.9805830E-03	1.4800623E-03	-1.1154559E-03	-3.6248116E-03
8	-8.1e532e1E-03	-5.3661737E-03	1.0508674E-04	-1.4816532E-03	-3.1056635E-03
9	6.7914254E-03	-3.0256262E-03	-1.4181229E-04	-3.0566165E-03	-2.1538695E-03
10	2.0158252E-02	-2.8297372E-04	1.1256140E-04	-4.4233961E-03	-1.6406680E-03
11	2.136e954E-02	-3.2716975E-04	1.1499668E-04	-4.7781230E-03	-5.6264135E-04
12	-4.7025558E-03	-2.1475513E-03	-1.0080634E-03	-4.5249286E-03	7.1070613E-04
13	-4.8163547E-02	-7.2333994E-03	-1.9846545E-03	-2.9677665E-03	2.0359920E-03
14	-7.0052348E-02	-8.6541369E-03	-2.2135760E-03	-7.7244942E-04	2.8698279E-03
15	-5.0135363E-02	-5.3297336E-03	4.9653976E-04	1.2259905E-03	1.9444856E-03
16	5.0313932E-03	2.0526350E-03	3.6823947E-03	2.8744766E-03	1.1934711E-03
17	6.59e6716E-02	9.7347215E-03	1.0771833E-02	4.1362191E-03	-7.2416183E-04
18	9.49ee954E-02	1.2667647E-02	1.3490860E-02	4.4551903E-03	-5.1354741E-04
19	6.5112902E-02	9.0666930E-03	1.1297961E-02	5.1072482E-03	-8.1011140E-04
20	1.264e826E-02	1.8304e85E-04	6.1350956E-03	4.0250653E-03	1.1066370E-03
21	-3.748E05eE-02	-7.5128958E-03	2.0421635E-04	2.2317063E-03	1.8603148E-03
22	-4.5846152E-02	-1.1812196E-02	-3.2451933E-03	-5.9104224E-04	2.5502297E-03
23	-1.7435906E-02	-1.1453725E-02	-3.2186385E-03	-3.1718042E-03	1.8759e84E-03
24	2.1180016E-02	-6.1642033E-03	-2.1482795E-03	-4.3403773E-03	8.85ee190E-04
25	3.906e8C4E-02	-2.4402371E-03	-8.9749876E-04	-4.2263378E-03	-8.7230833E-04
26	2.3915380E-02	-1.6950980E-03	-2.9243305E-04	-2.4837540E-03	-1.8625515E-03
27	-1.0925467E-02	-3.8657506E-04	-4.6240145E-04	-1.1273396E-03	-2.9664713E-03
28	-2.9714405E-02	-1.4656851E-03	4.9687519E-04	-7.9990330E-04	-3.7453327E-03
29	-2.1277722E-02	-1.9931185E-03	1.9862329E-03	-1.1398035E-03	-3.2827773E-03
30	2.9324359E-03	-9.6762052E-04	3.9270531E-03	-2.1292504E-03	-3.2152476E-03
31	2.9378199E-02	-2.7251339E-03	4.2288867E-03	-2.2601056E-03	-2.4047892E-03
32	2.4e06586E-02	-3.2335655E-03	2.9897581E-03	-2.1071977E-03	-2.9183559E-03
33	2.851e2e7E-02	-8.0129546E-03	1.5527594E-03	1.3405782E-03	-1.8193743E-03
34	3.6407923E-03	-2.2486281E-03	2.8504756E-03	-4.9713169E-04	-4.0564778E-03
35	7.7800189E-03	-6.0587585E-03	-3.7927035E-04	2.8119535E-03	-2.7091463E-04
36	7.0635960E-03	3.2660407E-03	4.0700375E-03	-2.5327224E-04	-2.6514710E-03

Figure B-15. Filter Weight Listings for MCF-19: Final 5-Channel Disk Model; Subarray E-2

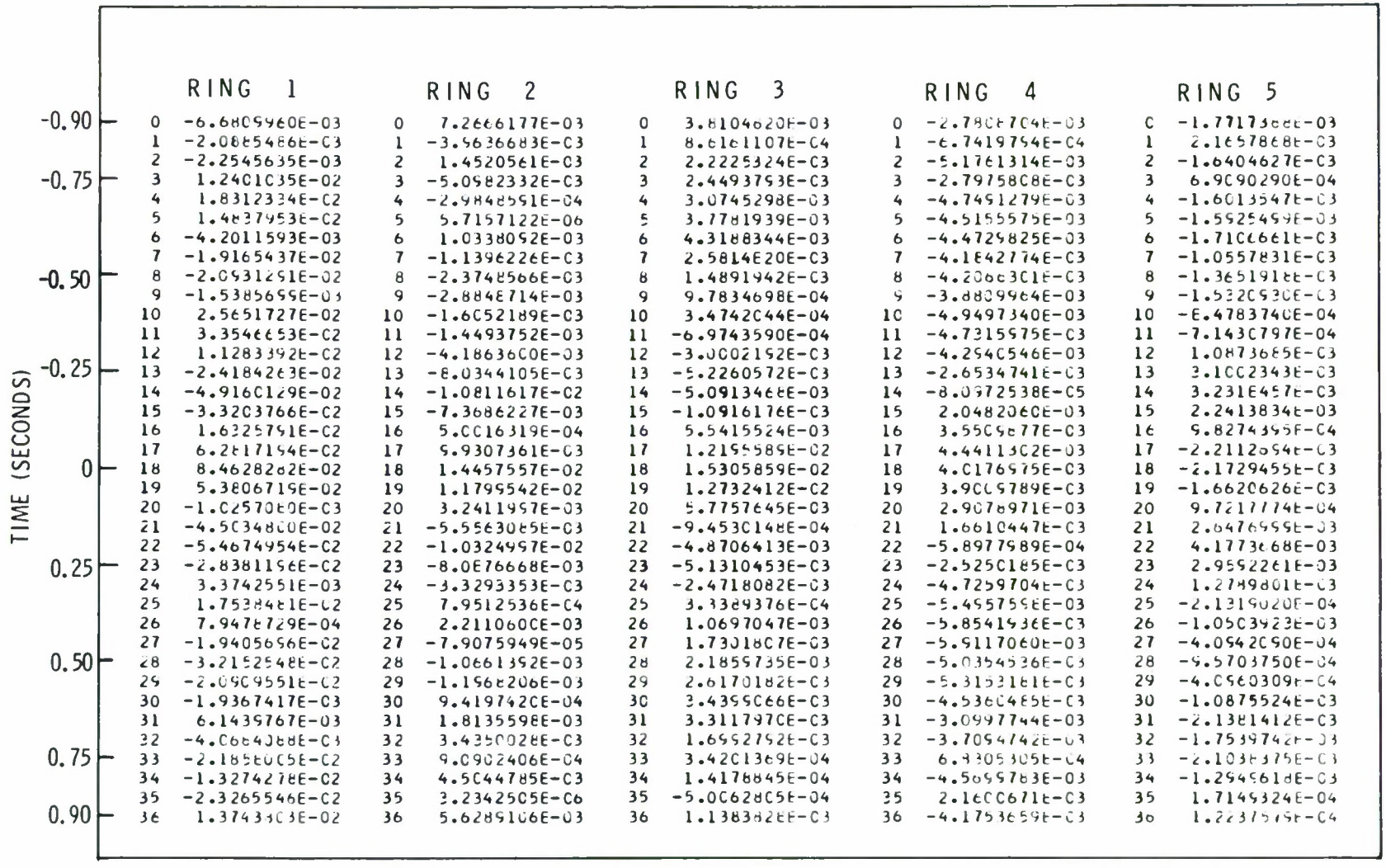

	RING 1		RING 2		RING 3		RING 4		RING 5
0	-6.6809960E-03	0	7.2666177E-03	0	3.8104620E-03	0	-2.7908704E-03	0	-1.7717366E-03
1	-2.0885486E-03	1	-3.9636683E-03	1	8.6161107E-04	1	-6.7419754E-04	1	2.1657868E-03
2	-2.2545635E-03	2	1.4520561E-03	2	2.2225324E-03	2	-5.1761314E-03	2	-1.6404627E-03
3	1.2401C35E-02	3	-5.0582332E-03	3	2.4493793E-03	3	-2.7975808E-03	3	6.9090290E-04
4	1.8312334E-02	4	-2.9848591E-04	4	3.0745298E-03	4	-4.7491279E-03	4	-1.6013547E-03
5	1.4837953E-02	5	5.7157122E-06	5	3.7781939E-03	5	-4.5155575E-03	5	-1.5925459E-03
6	-4.2011593E-03	6	1.0338052E-03	6	4.3188344E-03	6	-4.4729825E-03	6	-1.7100661E-03
7	-1.9165437E-02	7	-1.1396226E-03	7	2.5814E20E-03	7	-4.1E42714E-03	7	-1.0557831E-03
8	-2.0931251E-02	8	-2.3748566E-03	8	1.4891942E-03	8	-4.2066301E-03	8	-1.3651916E-03
9	-1.5385655E-03	9	-2.8848714E-03	9	9.7834698E-04	9	-3.8809964E-03	9	-1.5320530E-03
10	2.5651727E-02	10	-1.6052189E-03	10	3.4742044E-04	10	-4.9497340E-03	10	-E.478374CE-04
11	3.3546653E-02	11	-1.4493752E-03	11	-6.9743590E-04	11	-4.7315575E-03	11	-7.1430797E-04
12	1.1283392E-02	12	-4.1863600E-03	12	-3.0002152E-03	12	-4.2540546E-03	12	1.0873685E-03
13	-2.4184263E-02	13	-8.0344105E-03	13	-5.2260572E-03	13	-2.6534741E-03	13	3.1002343E-03
14	-4.9160129E-02	14	-1.0811617E-02	14	-5.0913466E-03	14	-8.0972538E-05	14	3.2316457E-03
15	-3.3203766E-02	15	-7.3686227E-03	15	-1.0916176E-03	15	2.0482060E-03	15	2.2413834E-03
16	1.6225791E-02	16	5.0016319E-04	16	5.5415524E-03	16	3.5509677E-03	16	9.8274395E-04
17	6.2617154E-02	17	9.9307361E-03	17	1.2195585E-02	17	4.4411302E-03	17	-2.2112054E-03
18	8.4628202E-02	18	1.4457557E-02	18	1.5305859E-02	18	4.0176575E-03	18	-2.1729455E-03
19	5.3806719E-02	19	1.1795542E-02	19	1.2732412E-02	19	3.9005789E-03	19	-1.6620626E-03
20	-1.0257060E-03	20	3.2411957E-03	20	5.7757645E-03	20	2.9078971E-03	20	9.7217774E-04
21	-4.5034800E-02	21	-5.5563065E-03	21	-9.4530148E-04	21	1.6610447E-03	21	2.6476955E-03
22	-5.4674954E-02	22	-1.0324957E-02	22	-4.8706413E-03	22	-5.8977989E-04	22	4.1773668E-03
23	-2.8381156E-02	23	-8.0E76668E-03	23	-5.1310453E-03	23	-2.5250185E-03	23	2.9552261E-03
24	3.3742551E-03	24	-3.3293353E-03	24	-2.4718082E-03	24	-4.7259704E-03	24	1.2749801E-03
25	1.7538481E-02	25	7.9512536E-04	25	3.3369376E-04	25	-5.4957595E-03	25	-2.1319020E-04
26	7.9478729E-04	26	2.2110600E-03	26	1.0697047E-03	26	-5.8541936E-03	26	-1.0503923E-03
27	-1.9405696E-02	27	-7.9075949E-05	27	1.7301807E-03	27	-5.9117060E-03	27	-4.0942090E-04
28	-3.2152548E-02	28	-1.0661352E-03	28	2.1855735E-03	28	-5.0354536E-03	28	-9.5703750E-04
29	-2.0909551E-02	29	-1.1966206E-03	29	2.6170182E-03	29	-5.3153161E-03	29	-4.0960309E-04
30	-1.9367417E-03	30	9.4197420E-04	30	3.4395066E-03	30	-4.5360485E-03	30	-1.0875524E-03
31	6.1439767E-03	31	1.8135598E-03	31	3.3117970E-03	31	-3.0997744E-03	31	-2.1381412E-03
32	-4.0664368E-03	32	3.4350028E-03	32	1.6952752E-03	32	-3.7094742E-03	32	-1.7539742E-03
33	-2.1856005E-02	33	9.0902406E-04	33	3.4201369E-04	33	6.8305305E-04	33	-2.1038375E-03
34	-1.3274278E-02	34	4.5044785E-03	34	1.4178845E-04	34	-4.5699783E-03	34	-1.2949618E-03
35	-2.3265546E-02	35	3.2342505E-06	35	-5.0062805E-04	35	2.1600671E-03	35	1.7149324E-04
36	1.3743303E-02	36	5.6289106E-03	36	1.1383826E-03	36	-4.1753659E-03	36	1.2237545E-04

Figure B-16. Filter Weight Listings for MCF-20: Final 5-Channel Disk Model; Subarray F-2

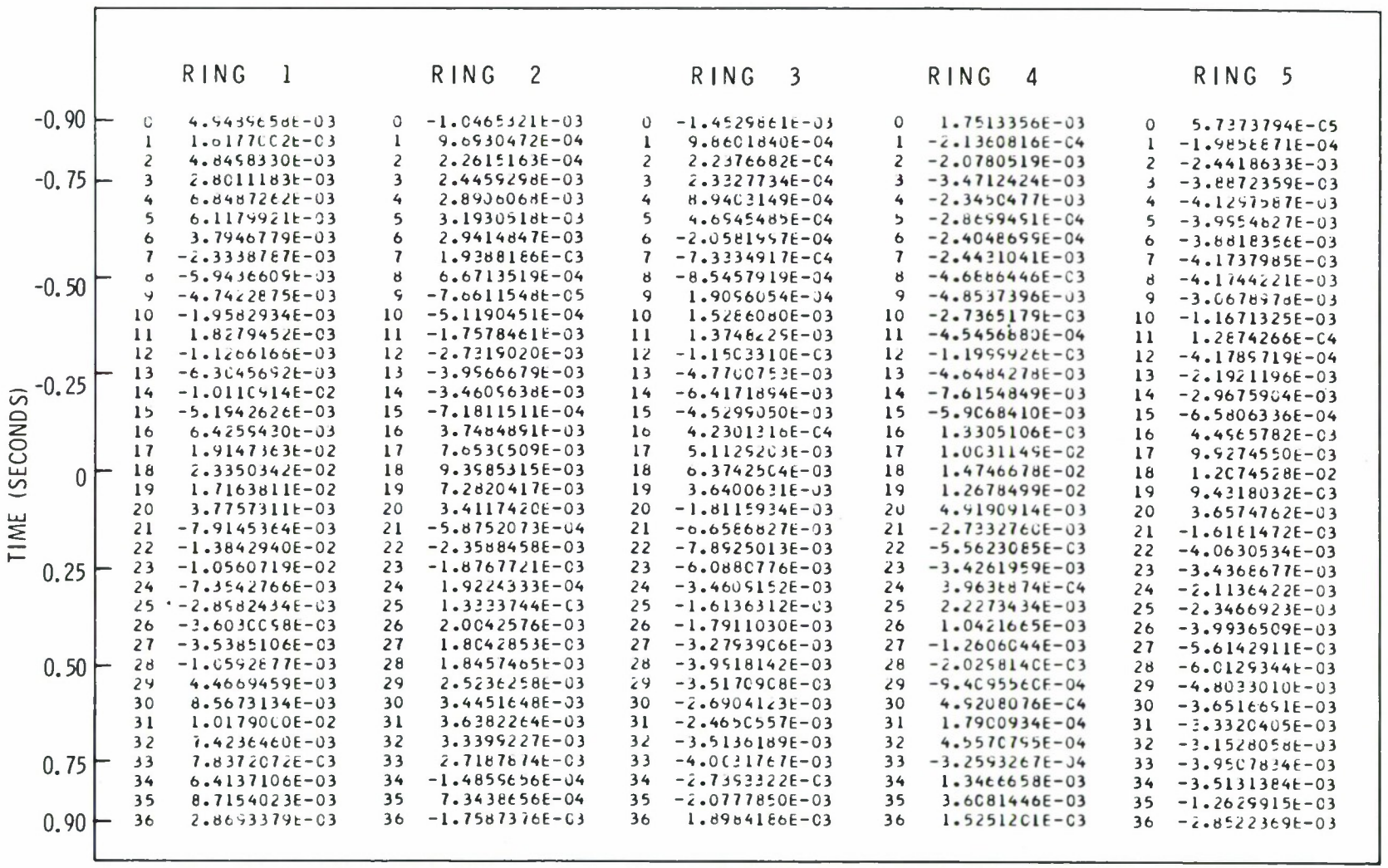

TIME (SECONDS)	RING 1		RING 2		RING 3		RING 4		RING 5	
-0.90	0	4.9439E58E-03	0	-1.0465321E-03	0	-1.4529861E-03	0	1.7513356E-03	0	5.7373794E-05
	1	1.0177CC2E-03	1	9.6930472E-04	1	9.8601840E-04	1	-2.1360816E-04	1	-1.9856871E-04
	2	4.8458330E-03	2	2.2615163E-04	2	2.2376682E-04	2	-2.0780519E-03	2	-2.4418633E-03
-0.75	3	2.8011183E-03	3	2.4459298E-03	3	2.3327734E-04	3	-3.4712424E-03	3	-3.8872359E-03
	4	6.8487262E-03	4	2.890606HE-03	4	8.9403149E-04	4	-2.3450477E-03	4	-4.1297587E-03
	5	6.1179921E-03	5	3.1930518E-03	5	4.6545485E-04	5	-2.8659451E-04	5	-3.9954827E-03
	6	3.7946779E-03	6	2.9414847E-03	6	-2.0581957E-04	6	-2.4048699E-04	6	-3.8818356E-03
	7	-2.3338787E-03	7	1.9388186E-03	7	-7.3334917E-04	7	-2.4431041E-03	7	-4.1737985E-03
-0.50	8	-5.9436609E-03	8	6.6713519E-04	8	-8.5457919E-04	8	-4.6886446E-03	8	-4.1744221E-03
	9	-4.7422875E-03	9	-7.6611548E-05	9	1.9056054E-04	9	-4.8537396E-03	9	-3.0678976E-03
	10	-1.9582934E-03	10	-5.1190451E-04	10	1.5286080E-03	10	-2.7365179E-03	10	-1.1671325E-03
	11	1.8279452E-03	11	-1.7578461E-03	11	1.3748629E-03	11	-4.5456880E-04	11	1.2874266E-04
	12	-1.1266166E-03	12	-2.7319020E-03	12	-1.1503310E-03	12	-1.1999926E-03	12	-4.1785719E-04
-0.25	13	-6.3045692E-03	13	-3.9566679E-03	13	-4.7700753E-03	13	-4.6484278E-03	13	-2.1921196E-03
	14	-1.0110914E-02	14	-3.4605638E-03	14	-6.4171894E-03	14	-7.6154849E-03	14	-2.9675904E-03
	15	-5.1942626E-03	15	-7.1811511E-04	15	-4.5299050E-03	15	-5.9068410E-03	15	-6.5806336E-04
	16	6.4259430E-03	16	3.7484891E-03	16	4.2301316E-04	16	1.3305106E-03	16	4.4965782E-03
	17	1.9147363E-02	17	7.6535509E-03	17	5.1129203E-03	17	1.0031149E-02	17	9.9274550E-03
0	18	2.3350342E-02	18	9.3585315E-03	18	6.3742504E-03	18	1.4746678E-02	18	1.2074528E-02
	19	1.7163811E-02	19	7.2820417E-03	19	3.6400631E-03	19	1.2678499E-02	19	9.4318032E-03
	20	3.7757311E-03	20	3.4117420E-03	20	-1.8115934E-03	20	4.9190914E-03	20	3.6574762E-03
	21	-7.9145364E-03	21	-5.8752073E-04	21	-6.6566827E-03	21	-2.7332760E-03	21	-1.6161472E-03
	22	-1.3842940E-02	22	-2.3588458E-03	22	-7.8925013E-03	22	-5.5623085E-03	22	-4.0630534E-03
0.25	23	-1.0560719E-02	23	-1.8767721E-03	23	-6.0880776E-03	23	-3.4261959E-03	23	-3.4366677E-03
	24	-7.3542766E-03	24	1.9224333E-04	24	-3.4605152E-03	24	3.9638874E-04	24	-2.1136422E-03
	25	-2.8582434E-03	25	1.3333744E-03	25	-1.6136312E-03	25	2.2273434E-03	25	-2.3466923E-03
	26	-3.6030C58E-03	26	2.0042576E-03	26	-1.7911030E-03	26	1.0421665E-03	26	-3.9936509E-03
	27	-3.5385106E-03	27	1.8042853E-03	27	-3.2793906E-03	27	-1.2606044E-03	27	-5.6142911E-03
0.50	28	-1.0592877E-03	28	1.8457465E-03	28	-3.9518142E-03	28	-2.0258140E-03	28	-6.0129344E-03
	29	4.4669459E-03	29	2.5236258E-03	29	-3.5170908E-03	29	-9.4C9556CE-04	29	-4.8033010E-03
	30	8.5673134E-03	30	3.4451648E-03	30	-2.6904123E-03	30	4.9208076E-04	30	-3.6516691E-03
	31	1.0179000E-02	31	3.6382264E-03	31	-2.4650557E-03	31	1.7900934E-04	31	-3.3320405E-03
	32	7.4236460E-03	32	3.3399227E-03	32	-3.5136189E-03	32	4.5570795E-04	32	-3.1528058E-03
0.75	33	7.8372072E-03	33	2.7187874E-03	33	-4.0031767E-03	33	-3.2593267E-04	33	-3.9507834E-03
	34	6.4137106E-03	34	-1.4859656E-04	34	-2.7353322E-03	34	1.3466658E-03	34	-3.5131384E-03
	35	8.7154023E-03	35	7.3438656E-04	35	-2.0777850E-03	35	3.6081446E-03	35	-1.2629915E-03
0.90	36	2.8693379E-03	36	-1.7587376E-03	36	1.8984186E-03	36	1.5251201E-03	36	-2.8522369E-03

Figure B-22. Filter Weight Listings for MCF-21: Final 5-Channel Infinite Velocity Model; Subarray F-3

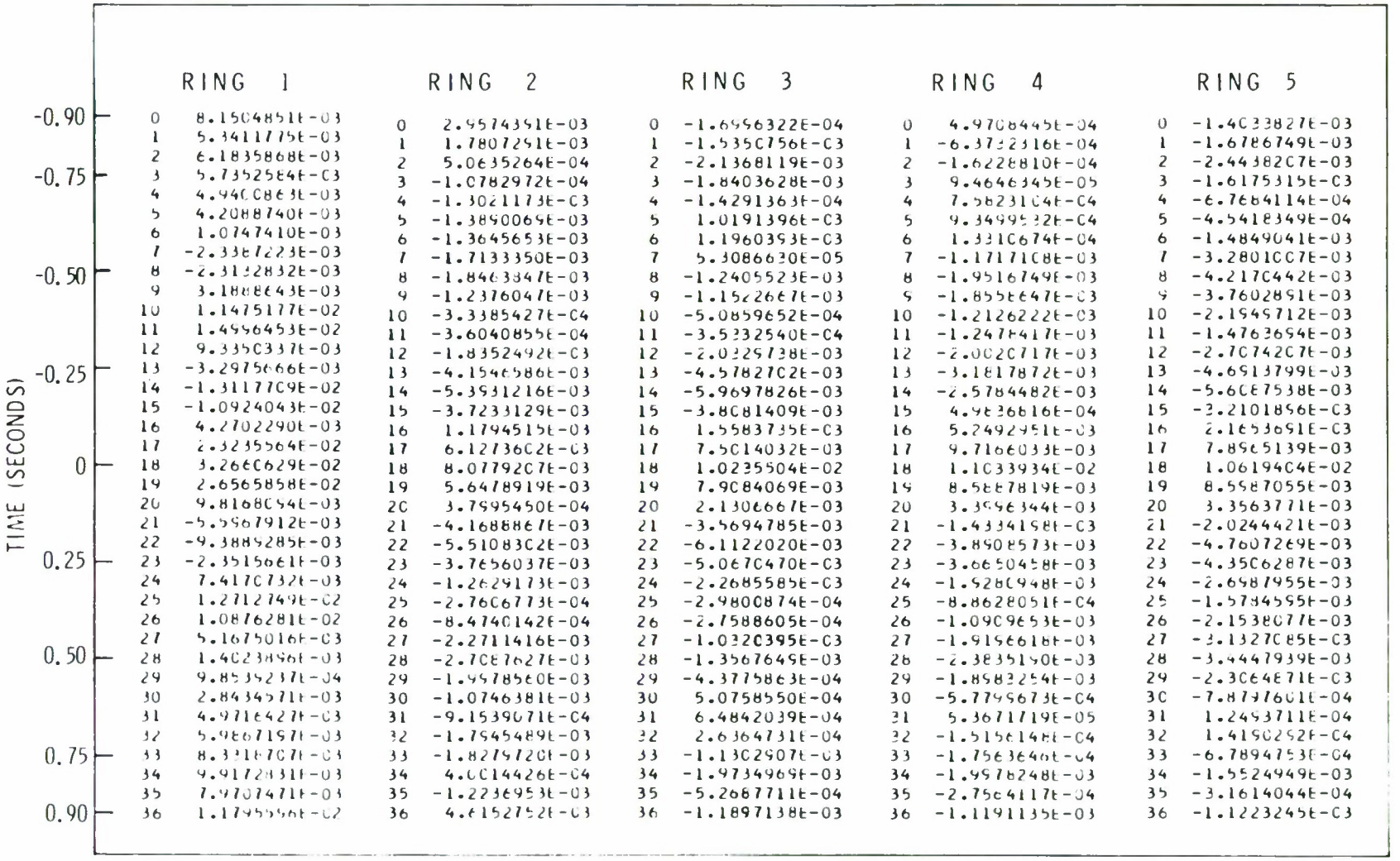

TIME (SECONDS)		RING 1		RING 2		RING 3		RING 4		RING 5
-0.90	0	8.1504851E-03	0	2.9574351E-03	0	-1.6956322E-04	0	4.9706445E-04	0	-1.4033827E-03
	1	5.3411775E-03	1	1.7807251E-03	1	-1.5350756E-03	1	-6.3732316E-04	1	-1.6786749E-03
-0.75	2	6.1835868E-03	2	5.0635264E-04	2	-2.1368119E-03	2	-1.6228810E-04	2	-2.4438207E-03
	3	5.7352564E-03	3	-1.0782972E-04	3	-1.8403628E-03	3	9.4646345E-05	3	-1.6175315E-03
	4	4.9400886E-03	4	-1.3021173E-03	4	-1.4291363E-04	4	7.5823104E-04	4	-6.7684114E-04
	5	4.2088740E-03	5	-1.3890069E-03	5	1.0191396E-03	5	9.3499532E-04	5	-4.5418349E-04
	6	1.0747410E-03	6	-1.3645653E-03	6	1.1960393E-03	6	1.3310674E-04	6	-1.4849041E-03
-0.50	7	-2.3387223E-03	7	-1.7133350E-03	7	5.3086630E-05	7	-1.1717108E-03	7	-3.2801007E-03
	8	-2.3132832E-03	8	-1.8463847E-03	8	-1.2405523E-03	8	-1.9516749E-03	8	-4.2170442E-03
	9	3.1888643E-03	9	-1.2376047E-03	9	-1.1522667E-03	9	-1.8556647E-03	9	-3.7602891E-03
	10	1.1475177E-02	10	-3.3385427E-04	10	-5.0859652E-04	10	-1.2126222E-03	10	-2.1945712E-03
	11	1.4956453E-02	11	-3.6040855E-04	11	-3.5332540E-04	11	-1.2478417E-03	11	-1.4763694E-03
	12	9.3350337E-03	12	-1.8352492E-03	12	-2.0229738E-03	12	-2.0020717E-03	12	-2.7074207E-03
-0.25	13	-3.2975666E-03	13	-4.1546586E-03	13	-4.5782702E-03	13	-3.1817872E-03	13	-4.6913799E-03
	14	-1.3117709E-02	14	-5.3931216E-03	14	-5.9697826E-03	14	-2.5784482E-03	14	-5.6087538E-03
	15	-1.0924043E-02	15	-3.7233129E-03	15	-3.8081409E-03	15	4.9836616E-04	15	-2.2101856E-03
	16	4.2702290E-03	16	1.1794515E-03	16	1.5583735E-03	16	5.2492951E-03	16	2.1653691E-03
	17	2.3235564E-02	17	6.1273602E-03	17	7.5014032E-03	17	9.7166033E-03	17	7.8965139E-03
0	18	3.2660629E-02	18	8.0779207E-03	18	1.0235504E-02	18	1.1033934E-02	18	1.0619404E-02
	19	2.6565858E-02	19	5.6478919E-03	19	7.9084069E-03	19	8.5887819E-03	19	8.5587055E-03
	20	9.8168054E-03	20	3.7995450E-04	20	2.1306667E-03	20	3.3596344E-03	20	3.3563771E-03
	21	-5.5967912E-03	21	-4.1688867E-03	21	-3.5694785E-03	21	-1.4334158E-03	21	-2.0244421E-03
	22	-9.3885285E-03	22	-5.5108302E-03	22	-6.1122020E-03	22	-3.8908573E-03	22	-4.7607269E-03
0.25	23	-2.3515661E-03	23	-3.7656037E-03	23	-5.0670470E-03	23	-3.6650458E-03	23	-4.3506287E-03
	24	7.4177732E-03	24	-1.2629173E-03	24	-2.2685585E-03	24	-1.5280948E-03	24	-2.6987955E-03
	25	1.2712749E-02	25	-2.7606773E-04	25	-2.9800874E-04	25	-8.8628051E-04	25	-1.5784595E-03
	26	1.0876281E-02	26	-8.4740142E-04	26	-2.7588605E-04	26	-1.0909653E-03	26	-2.1538077E-03
	27	5.1675016E-03	27	-2.2711416E-03	27	-1.0320395E-03	27	-1.9156618E-03	27	-3.1327085E-03
0.50	28	1.4023896E-03	28	-2.7087627E-03	28	-1.3567649E-03	28	-2.3835150E-03	28	-3.4447939E-03
	29	9.8535237E-04	29	-1.9978560E-03	29	-4.3775863E-04	29	-1.8583254E-03	29	-2.3064871E-03
	30	2.8434571E-03	30	-1.0746381E-03	30	5.0758550E-04	30	-5.7795673E-04	30	-7.8797601E-04
	31	4.9716427E-03	31	-9.1539071E-04	31	6.4842039E-04	31	5.3671719E-05	31	1.2493711E-04
	32	5.9867197E-03	32	-1.7545489E-03	32	2.6364731E-04	32	-1.5156148E-04	32	1.4150252E-04
0.75	33	8.3318707E-03	33	-1.8279720E-03	33	-1.1302907E-03	33	-1.7563640E-04	33	-6.7894753E-04
	34	9.9172831E-03	34	4.0014426E-04	34	-1.9734969E-03	34	-1.9978248E-03	34	-1.5524949E-03
	35	7.9707471E-03	35	-1.2236953E-03	35	-5.2687711E-04	35	-2.7564117E-04	35	-3.1614044E-04
0.90	36	1.1795596E-02	36	4.6152752E-03	36	-1.1897138E-03	36	-1.1191135E-03	36	-1.1223245E-03

Figure B-23. Filter Weight Listings for MCF-22: Final 5-Channel Infinite Velocity Model; Subarray F-4

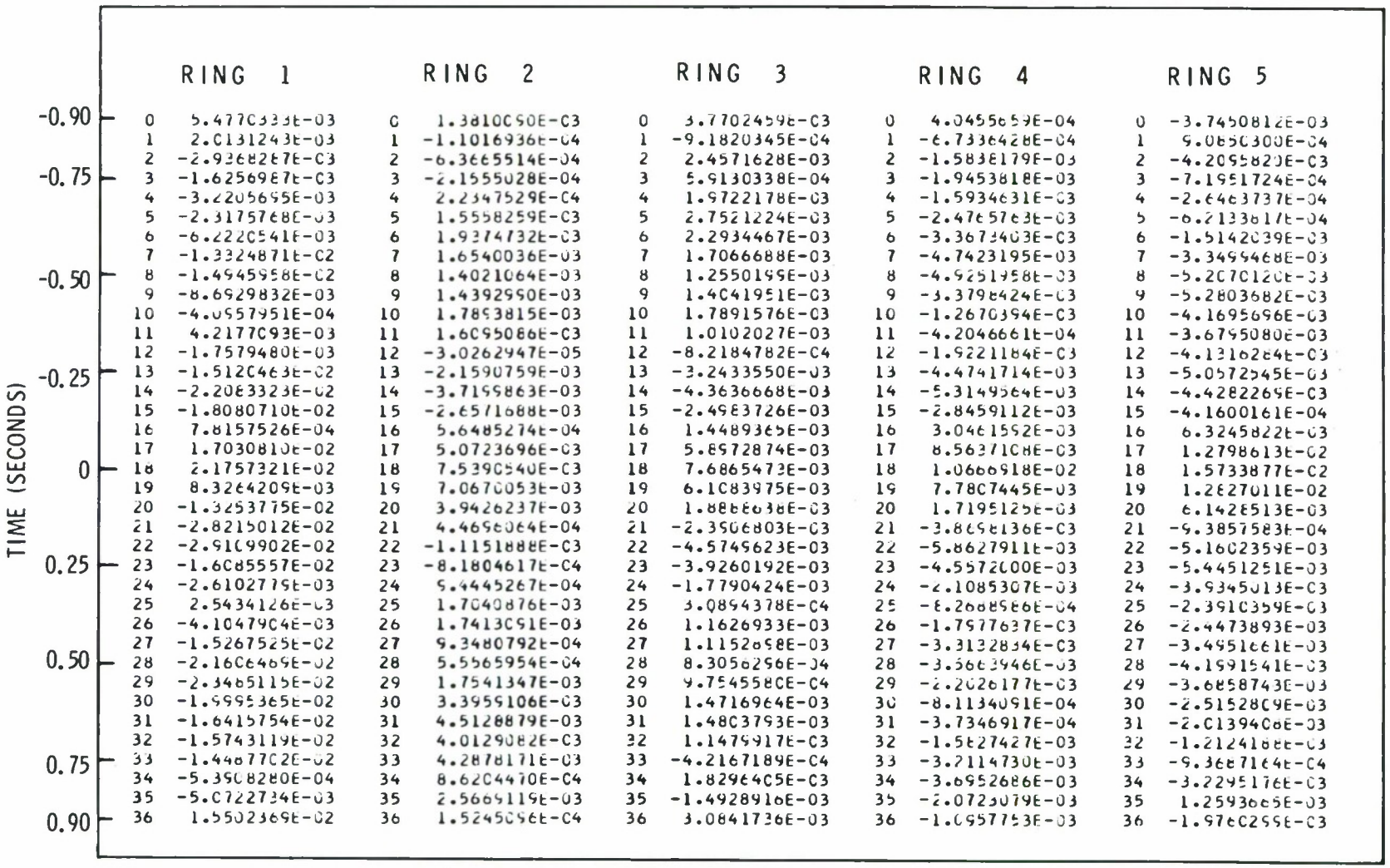

TIME (SECONDS)	RING 1	RING 2	RING 3	RING 4	RING 5
-0.90	0 5.4770333E-03	0 1.3810C50E-03	0 3.7702459E-03	0 4.0455659E-04	0 -3.7450812E-03
	1 2.0131243E-03	1 -1.1016936E-04	1 -9.1820345E-04	1 -6.7336428E-04	1 9.0650300E-04
	2 -2.9268267E-03	2 -6.3665514E-04	2 2.4571628E-03	2 -1.5838179E-03	2 -4.2095820E-03
-0.75	3 -1.6256967E-03	3 -2.1555028E-04	3 5.9130338E-04	3 -1.9453818E-03	3 -7.1951724E-04
	4 -3.2205695E-03	4 2.2347529E-04	4 1.9722178E-03	4 -1.5934631E-03	4 -2.6463737E-04
	5 -2.3175768E-03	5 1.5558259E-03	5 2.7521224E-03	5 -2.4765763E-03	5 -6.2133617E-04
	6 -6.2220541E-03	6 1.9374732E-03	6 2.2934467E-03	6 -3.3673403E-03	6 -1.5142039E-03
	7 -1.3324871E-02	7 1.6540036E-03	7 1.7066688E-03	7 -4.7423195E-03	7 -3.3499468E-03
-0.50	8 -1.4945958E-02	8 1.4021064E-03	8 1.2550199E-03	8 -4.9251958E-03	8 -5.2070120E-03
	9 -8.6929832E-03	9 1.4392990E-03	9 1.4041951E-03	9 -3.3798424E-03	9 -5.2803682E-03
	10 -4.0957951E-04	10 1.7853815E-03	10 1.7891576E-03	10 -1.2670394E-03	10 -4.1695696E-03
	11 4.2177093E-03	11 1.6095086E-03	11 1.0102027E-03	11 -4.2046661E-04	11 -3.6795080E-03
	12 -1.7579480E-03	12 -3.0262947E-05	12 -8.2184782E-04	12 -1.9221184E-03	12 -4.1316284E-03
-0.25	13 -1.5120463E-02	13 -2.1590759E-03	13 -3.2433550E-03	13 -4.4741714E-03	13 -5.0572345E-03
	14 -2.2083323E-02	14 -3.7199863E-03	14 -4.3636668E-03	14 -5.3149564E-03	14 -4.4282269E-03
	15 -1.8080710E-02	15 -2.6571688E-03	15 -2.4983726E-03	15 -2.8459112E-03	15 -4.1600161E-04
	16 7.8157526E-04	16 5.6485274E-04	16 1.4489365E-03	16 3.0461592E-03	16 6.3245822E-03
	17 1.7030810E-02	17 5.0723696E-03	17 5.8972874E-03	17 8.5637108E-03	17 1.2798613E-02
0	18 2.1757321E-02	18 7.5390540E-03	18 7.6865473E-03	18 1.0666918E-02	18 1.5733877E-02
	19 8.3264209E-03	19 7.0670053E-03	19 6.1083795E-03	19 7.7807445E-03	19 1.2627011E-02
	20 -1.3253775E-02	20 3.9426237E-03	20 1.8886038E-03	20 1.7195125E-03	20 6.1426513E-03
	21 -2.8215012E-02	21 4.4696064E-04	21 -2.3506803E-03	21 -3.8698136E-03	21 -9.3857583E-04
	22 -2.9109902E-02	22 -1.1151888E-03	22 -4.5745623E-03	22 -5.8627911E-03	22 -5.1602359E-03
0.25	23 -1.6085557E-02	23 -8.1804617E-04	23 -3.9260192E-03	23 -4.5572000E-03	23 -5.4451251E-03
	24 -2.6102779E-03	24 5.4445267E-04	24 -1.7790424E-03	24 -2.1085307E-03	24 -3.9345013E-03
	25 2.5434126E-03	25 1.7040876E-03	25 3.0894378E-04	25 -8.2688586E-04	25 -2.3910359E-03
	26 -4.1047904E-03	26 1.7413091E-03	26 1.1626933E-03	26 -1.7577637E-03	26 -2.4473893E-03
	27 -1.5267525E-02	27 9.3480792E-04	27 1.1152698E-03	27 -3.3132834E-03	27 -3.4951661E-03
0.50	28 -2.1606469E-02	28 5.5565954E-04	28 8.3056296E-04	28 -3.3663946E-03	28 -4.1991541E-03
	29 -2.3465115E-02	29 1.7541347E-03	29 9.7545580E-04	29 -2.2026177E-03	29 -3.6858743E-03
	30 -1.9995365E-02	30 3.3959106E-03	30 1.4716964E-03	30 -8.1134091E-04	30 -2.5152809E-03
	31 -1.6415754E-02	31 4.5128879E-03	31 1.4803793E-03	31 -3.7346917E-04	31 -2.0139406E-03
	32 -1.5743119E-02	32 4.0129082E-03	32 1.1479917E-03	32 -1.5827427E-03	32 -1.2124188E-03
0.75	33 -1.4467702E-02	33 4.2878171E-03	33 -4.2167189E-04	33 -3.2114730E-03	33 -9.3687164E-04
	34 -5.3908280E-04	34 8.6204470E-04	34 1.8296405E-03	34 -3.6952686E-03	34 -3.2295176E-03
	35 -5.0722734E-03	35 2.5669119E-03	35 -1.4928916E-03	35 -2.0723079E-03	35 1.2593665E-03
0.90	36 1.5502369E-02	36 1.5245056E-04	36 3.0841736E-03	36 -1.0957753E-03	36 -1.9762595E-03

Figure B-19. Filter Weight Listings for MCF-23: Final 5-Channel Infinite Velocity Model; Subarray C-3

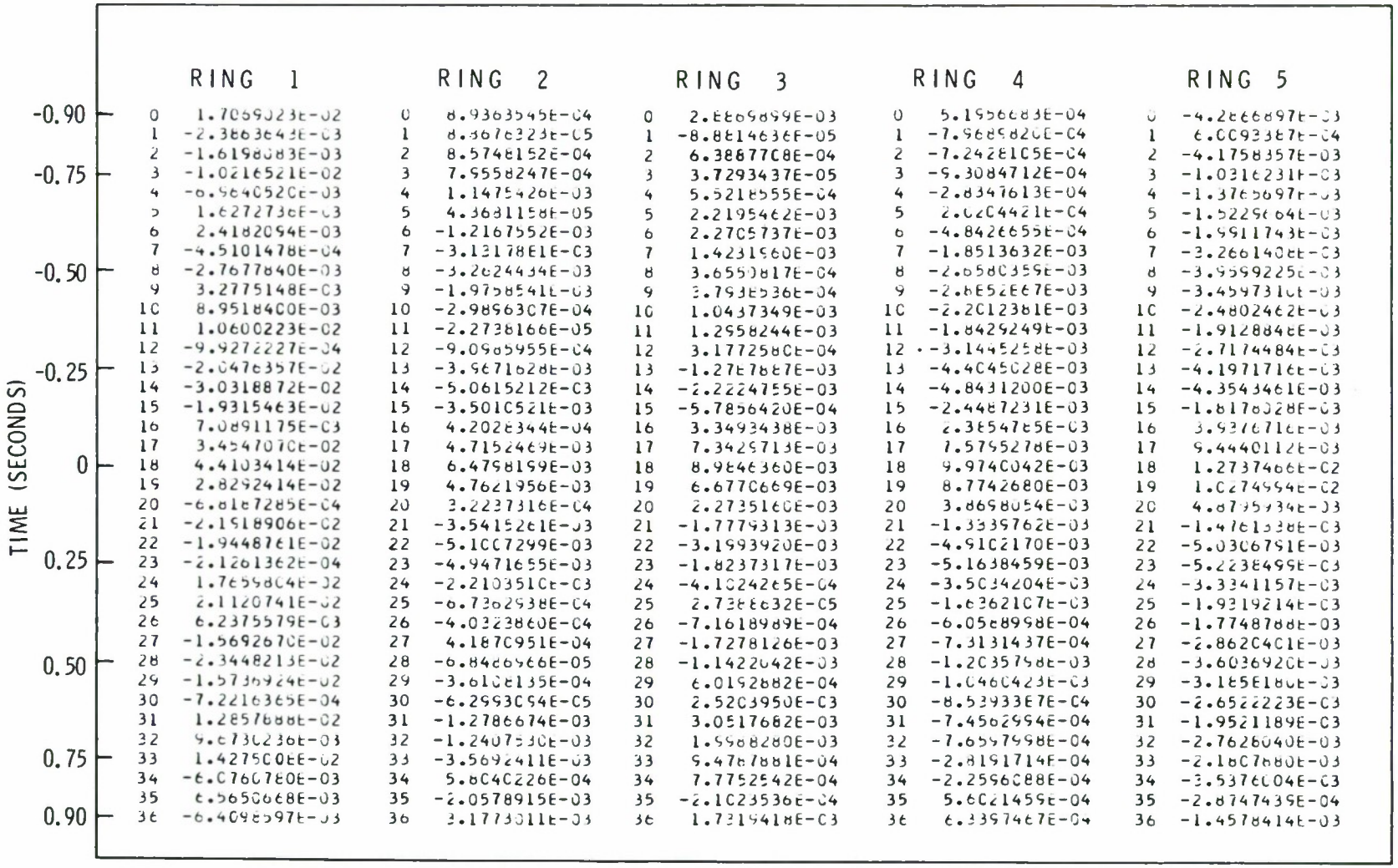

	RING 1		RING 2		RING 3		RING 4		RING 5
0	1.7059023E-02	0	8.9363545E-04	0	2.EE69899E-03	0	5.1956683E-04	0	-4.2666897E-03
1	-2.3663643E-03	1	8.3673223E-05	1	-8.8E14636E-05	1	-7.9685826E-04	1	6.0C933E7E-04
2	-1.6198083E-03	2	8.5748152E-04	2	6.38677C8E-04	2	-7.2428105E-04	2	-4.1758357E-03
3	-1.0216521E-02	3	7.9558247E-04	3	3.7293437E-05	3	-9.3084712E-04	3	-1.0316231E-03
4	-8.9640520E-03	4	1.1475426E-03	4	5.5218555E-04	4	-2.8347613E-04	4	-1.3765697E-03
5	1.6272736E-03	5	4.3681158E-05	5	2.2195462E-03	5	2.02C4421E-04	5	-1.5229E64E-03
6	2.4182094E-03	6	-1.2167552E-03	6	2.27C5737E-03	6	-4.8426655E-04	6	-1.9911743E-03
7	-4.5101478E-04	7	-3.1317861E-03	7	1.4231960E-03	7	-1.8513632E-03	7	-3.2661402E-03
8	-2.7677840E-03	8	-3.2624434E-03	8	3.6550817E-04	8	-2.6580359E-03	8	-3.9599225E-03
9	3.2775148E-03	9	-1.9758541E-03	9	3.793E536E-04	9	-2.8E52E67E-03	9	-3.4597310E-03
10	8.9518400E-03	10	-2.9896307E-04	10	1.0437349E-03	10	-2.2012381E-03	10	-2.4802462E-03
11	1.0600223E-02	11	-2.2738166E-05	11	1.2958244E-03	11	-1.8429249E-03	11	-1.9128846E-03
12	-9.9272227E-04	12	-9.0965955E-04	12	3.177258CE-04	12	-3.1445258E-03	12	-2.7174484E-03
13	-2.0476357E-02	13	-3.9671628E-03	13	-1.27E7867E-03	13	-4.4C45028E-03	13	-4.1971716E-03
14	-3.0318872E-02	14	-5.0615212E-03	14	-2.2224755E-03	14	-4.8431200E-03	14	-4.3543461E-03
15	-1.9315463E-02	15	-3.5010521E-03	15	-5.7856420E-04	15	-2.4487231E-03	15	-1.8176028E-03
16	7.0891175E-03	16	4.2026344E-04	16	3.3493438E-03	16	2.3E547E5E-03	16	3.9376716E-03
17	3.4547070E-02	17	4.7152469E-03	17	7.3429713E-03	17	7.5795278E-03	17	9.4440112E-03
18	4.4103414E-02	18	6.4798159E-03	18	8.9E46360E-03	18	9.9740042E-03	18	1.2737466E-02
19	2.8292414E-02	19	4.7621956E-03	19	6.6770669E-03	19	8.7742680E-03	19	1.0274954E-02
20	-6.8167285E-04	20	3.2237316E-04	20	2.2735160E-03	20	3.8658054E-03	20	4.8795434E-03
21	-2.1518906E-02	21	-3.5415261E-03	21	-1.7779313E-03	21	-1.3339762E-03	21	-1.4761338E-03
22	-1.9448761E-02	22	-5.1007299E-03	22	-3.1993920E-03	22	-4.9102170E-03	22	-5.0306791E-03
23	-2.1261362E-04	23	-4.9471655E-03	23	-1.8237317E-03	23	-5.1638459E-03	23	-5.2238499E-03
24	1.7659804E-02	24	-2.2103510E-03	24	-4.1C242E5E-04	24	-3.5C34204E-03	24	-3.3341157E-03
25	2.1120741E-02	25	-6.7362938E-04	25	2.73EE632E-05	25	-1.6362107E-03	25	-1.9319214E-03
26	6.2375579E-03	26	-4.0323860E-04	26	-7.1618989E-04	26	-6.05E8998E-04	26	-1.7748788E-03
27	-1.5692670E-02	27	4.1870951E-04	27	-1.7278126E-03	27	-7.3131437E-04	27	-2.8620401E-03
28	-2.3448213E-02	28	-6.8466966E-05	28	-1.1422042E-03	28	-1.2C3579BE-03	28	-3.6036920E-03
29	-1.5736924E-02	29	-3.6102135E-04	29	6.0192882E-04	29	-1.0460423E-03	29	-3.1E5E186E-03
30	-7.2216365E-04	30	-6.2993C94E-C5	30	2.52C3950E-C3	30	-8.53933E7E-C4	30	-2.6522223E-03
31	1.2857888E-02	31	-1.2786674E-03	31	3.0517682E-03	31	-7.4562994E-04	31	-1.9521189E-03
32	9.6736236E-03	32	-1.2407530E-03	32	1.9968280E-03	32	-7.6557998E-04	32	-2.7626040E-03
33	1.4275C0EE-02	33	-3.5692411E-03	33	9.4787881E-04	33	-2.8191714E-04	33	-2.1EC7E80E-03
34	-6.C76C7E0E-03	34	5.8C4C226E-04	34	7.7752542E-04	34	-2.2596C88E-04	34	-3.5376C04E-03
35	6.5650668E-03	35	-2.0578915E-03	35	-2.1C23536E-04	35	5.6C21459E-04	35	-2.8747439E-04
36	-6.4098597E-03	36	3.1773011E-03	36	1.7319418E-C3	36	6.3397467E-04	36	-1.4578414E-03

Figure B-20. Filter Weight Listings for MCF-24: Final 5-Channel Infinite Velocity Model; Subarray E-2

TIME (SECONDS)	RING 1		RING 2		RING 3		RING 4		RING 5	
-0.90	0	-8.1164020E-03	0	4.5978525E-03	0	2.2417125E-03	0	-6.7364150E-04	0	-2.7852414E-03
	1	1.6525138E-03	1	-8.3579784E-04	1	4.5286080E-04	1	-6.1287468E-04	1	1.0450354E-03
	2	-4.4682682E-03	2	1.7862653E-03	2	9.2072400E-04	2	-2.9092339E-03	2	-2.7199937E-03
-0.75	3	4.0393833E-03	3	-2.2800925E-03	3	8.3541758E-04	3	-2.4780401E-03	3	3.5633970E-04
	4	4.8671675E-03	4	-4.2726452E-04	4	1.7409457E-03	4	-2.3191639E-03	4	-6.5242808E-04
	5	3.3635525E-03	5	-4.0891677E-04	5	2.6215908E-03	5	-1.8665991E-03	5	-5.5561207E-04
	6	-1.8704612E-03	6	1.9308397E-04	6	3.0405767E-03	6	-1.9134398E-03	6	-2.0687071E-03
	7	-7.2384734E-03	7	-5.7835500E-04	7	1.6908938E-03	7	-2.5961736E-03	7	-3.1290504E-03
-0.50	8	-8.6644630E-03	8	-1.1646645E-03	8	7.7758645E-04	8	-3.5294881E-03	8	-4.3296444E-03
	9	-8.6598569E-04	9	-1.6632192E-03	9	5.3145227E-04	9	-3.0274575E-03	9	-3.5548627E-03
	10	1.0613159E-02	10	-9.7524564E-04	10	7.5750589E-04	10	-2.1650066E-03	10	-1.8653256E-03
	11	1.5861116E-02	11	-8.0890135E-04	11	5.4305533E-04	11	-1.2969576E-03	11	-1.6732305E-03
	12	7.9518365E-03	12	-1.7975687E-03	12	-1.3753555E-03	12	-1.5830356E-03	12	-2.7014033E-03
-0.25	13	-7.0687990E-03	13	-3.4774969E-03	13	-4.0844057E-03	13	-3.2765405E-03	13	-4.4234461E-03
	14	-1.7964363E-02	14	-4.9342045E-03	14	-5.1793573E-03	14	-3.5216633E-03	14	-5.0549339E-03
	15	-1.3181369E-02	15	-3.3285635E-03	15	-2.9041875E-03	15	-1.4886492E-03	15	-2.0866751E-03
	16	8.9786569E-03	16	1.9624234E-04	16	2.3054264E-03	16	3.1395051E-03	16	4.2895850E-03
	17	2.9813704E-02	17	4.5618944E-03	17	7.9523527E-03	17	8.4953554E-03	17	9.5436169E-03
0	18	4.0094078E-02	18	6.4343279E-03	18	1.0455753E-02	18	1.0209251E-02	18	1.2341960E-02
	19	2.7157541E-02	19	5.1215065E-03	19	8.3576402E-03	19	8.2422724E-03	19	9.6840217E-03
	20	2.3629466E-03	20	8.3659954E-04	20	2.8212009E-03	20	2.6717525E-03	20	4.3525391E-03
	21	-1.8049122E-02	21	-3.1025294E-03	21	-1.9822298E-03	21	-2.6731268E-03	21	-1.3923706E-03
	22	-2.2410498E-02	22	-5.2152045E-03	22	-3.8469859E-03	22	-5.2150023E-03	22	-3.5465943E-03
0.25	23	-1.2598726E-02	23	-4.0458141E-03	23	-2.6303222E-03	23	-4.6002642E-03	23	-3.4736405E-03
	24	-3.9432572E-04	24	-1.6350172E-03	24	4.3006012E-05	24	-2.5137572E-03	24	-2.1648966E-03
	25	4.1228918E-03	25	2.3731632E-04	25	1.9540365E-03	25	-1.6706491E-03	25	-1.0878395E-03
	26	-4.0266056E-03	26	1.0640173E-03	26	1.7007177E-03	26	-2.1873175E-03	26	-2.7926451E-03
	27	-1.1520704E-02	27	3.2240998E-04	27	1.2653290E-03	27	-3.9879721E-03	27	-3.7023371E-03
0.50	28	-1.6469179E-02	28	3.0164078E-04	28	1.3814618E-03	28	-4.7352560E-03	28	-4.0592033E-03
	29	-1.1997281E-02	29	2.8624837E-04	29	1.7402318E-03	29	-4.1346057E-03	29	-2.1264746E-03
	30	-5.3831550E-03	30	1.0366214E-03	30	2.4073927E-03	30	-2.9605052E-03	30	-7.6685470E-04
	31	-4.9907321E-03	31	1.0349263E-03	31	1.8106341E-03	31	-1.3155129E-03	31	-1.1254683E-04
	32	-8.1058647E-03	32	1.6336053E-03	32	4.9082953E-04	32	-1.7278044E-03	32	-2.4665717E-04
0.75	33	-1.1100739E-02	33	5.5274588E-04	33	-7.6595183E-04	33	-3.6192153E-04	33	-9.2646444E-04
	34	-6.4972056E-03	34	3.2007274E-03	34	-2.3453794E-04	34	-3.1266097E-03	34	-2.4316243E-03
	35	-4.6232102E-03	35	8.9526580E-04	35	-3.6797699E-04	35	6.5917923E-04	35	2.8695840E-04
0.90	36	3.9897550E-03	36	3.8702573E-03	36	1.1206139E-03	36	-2.5054465E-03	36	-1.6166589E-03

Figure B-21. Filter Weight Listings for MCF-25: Final 5-Channel Infinite Velocity Model; Subarray F-2

APPENDIX C

RELATIVE AMPLITUDE AND PHASE RESPONSES

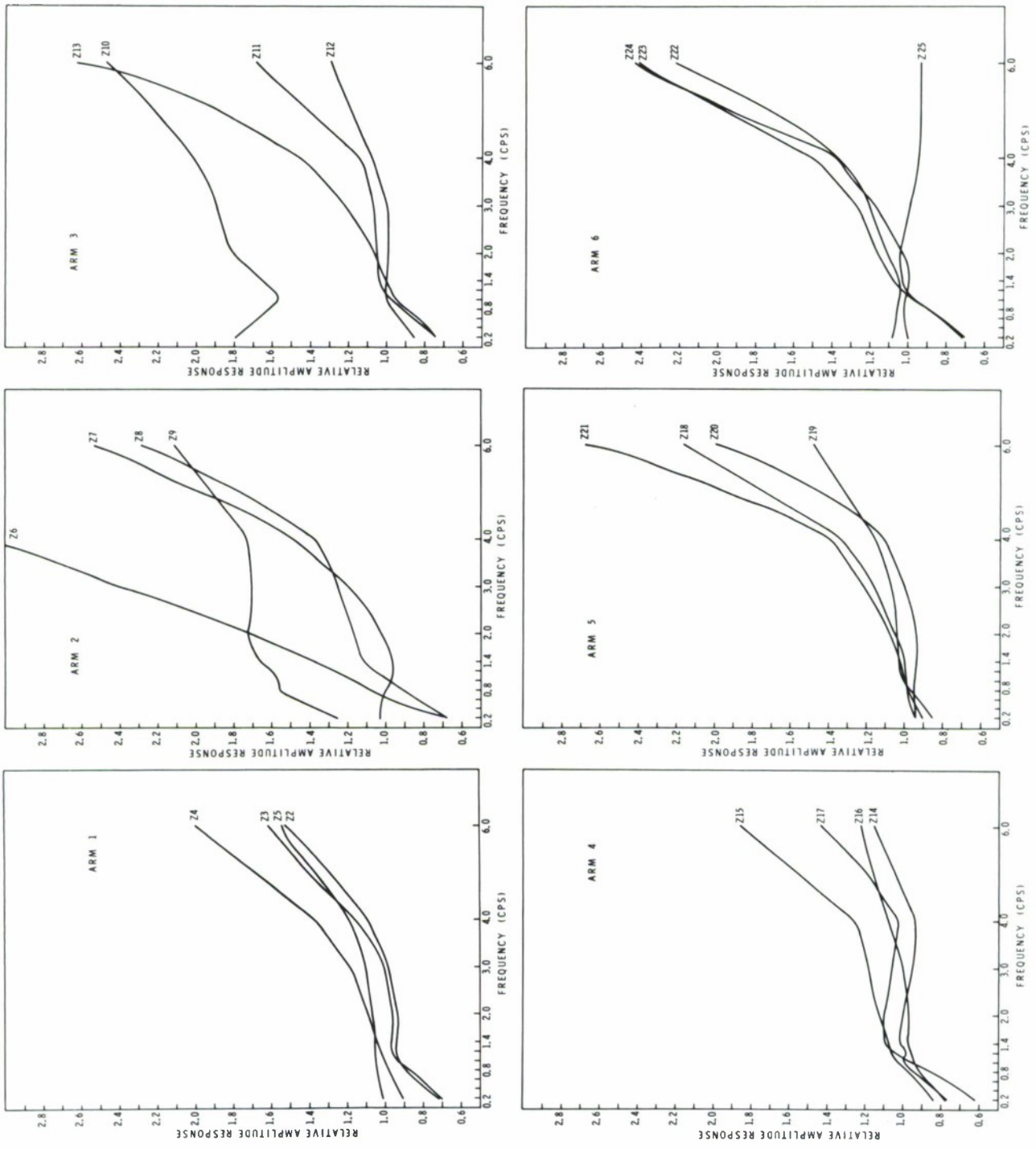

Figure C-1. Relative Amplitude Responses of Subarray F-3

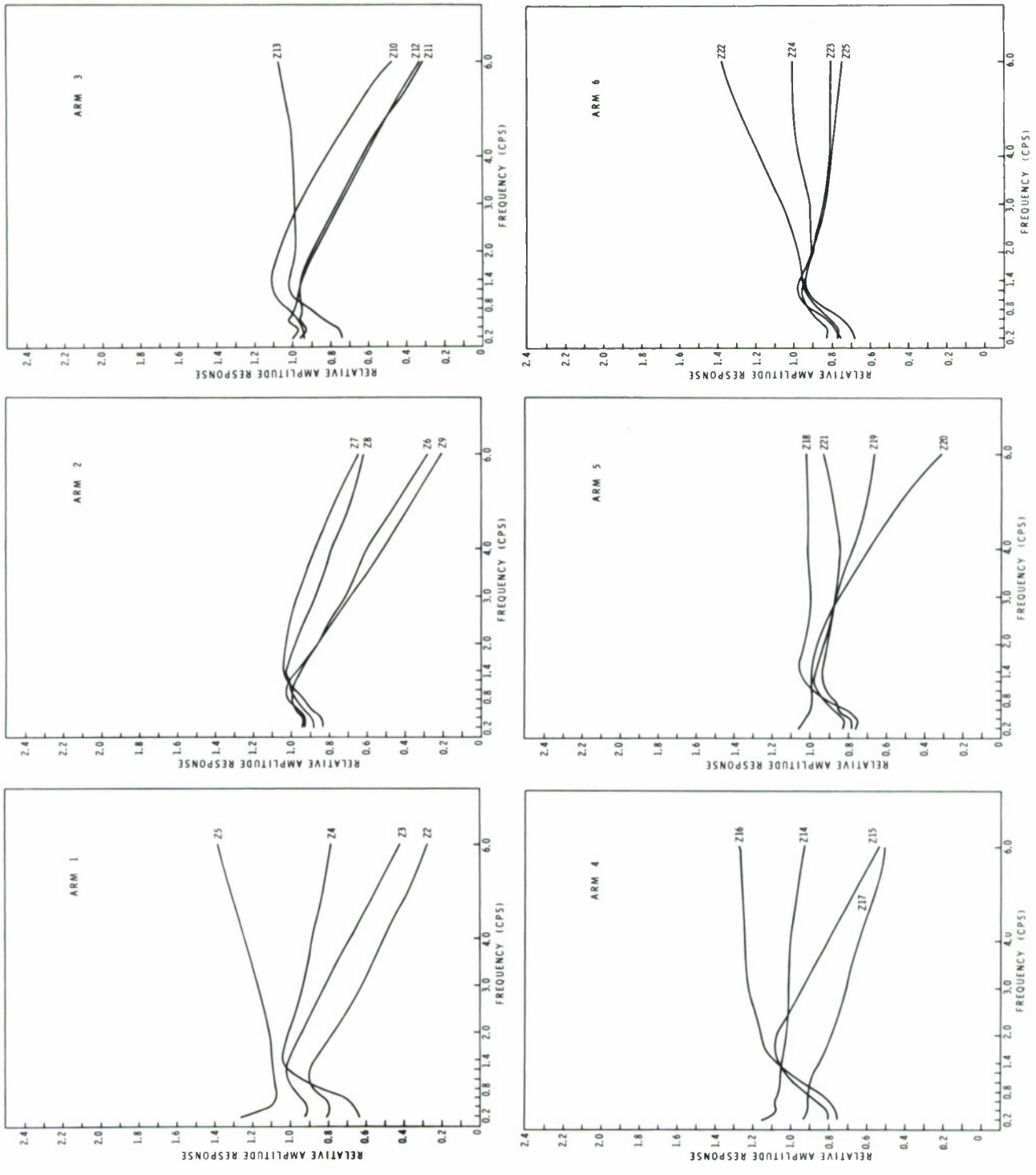

Figure C-2. Relative Amplitude Responses of Subarray F-4

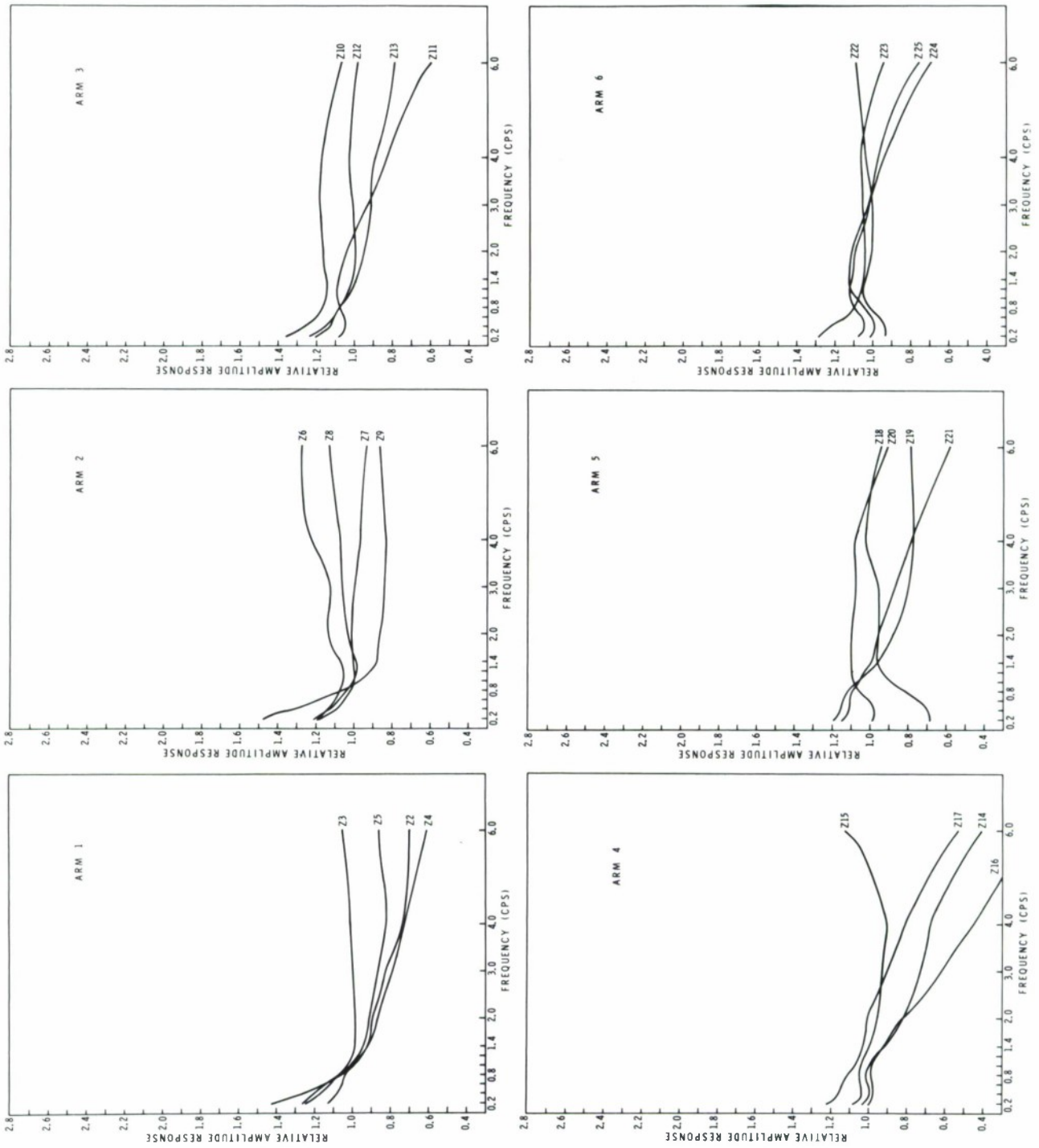

Figure C-3. Relative Amplitude Responses of Subarray C-3

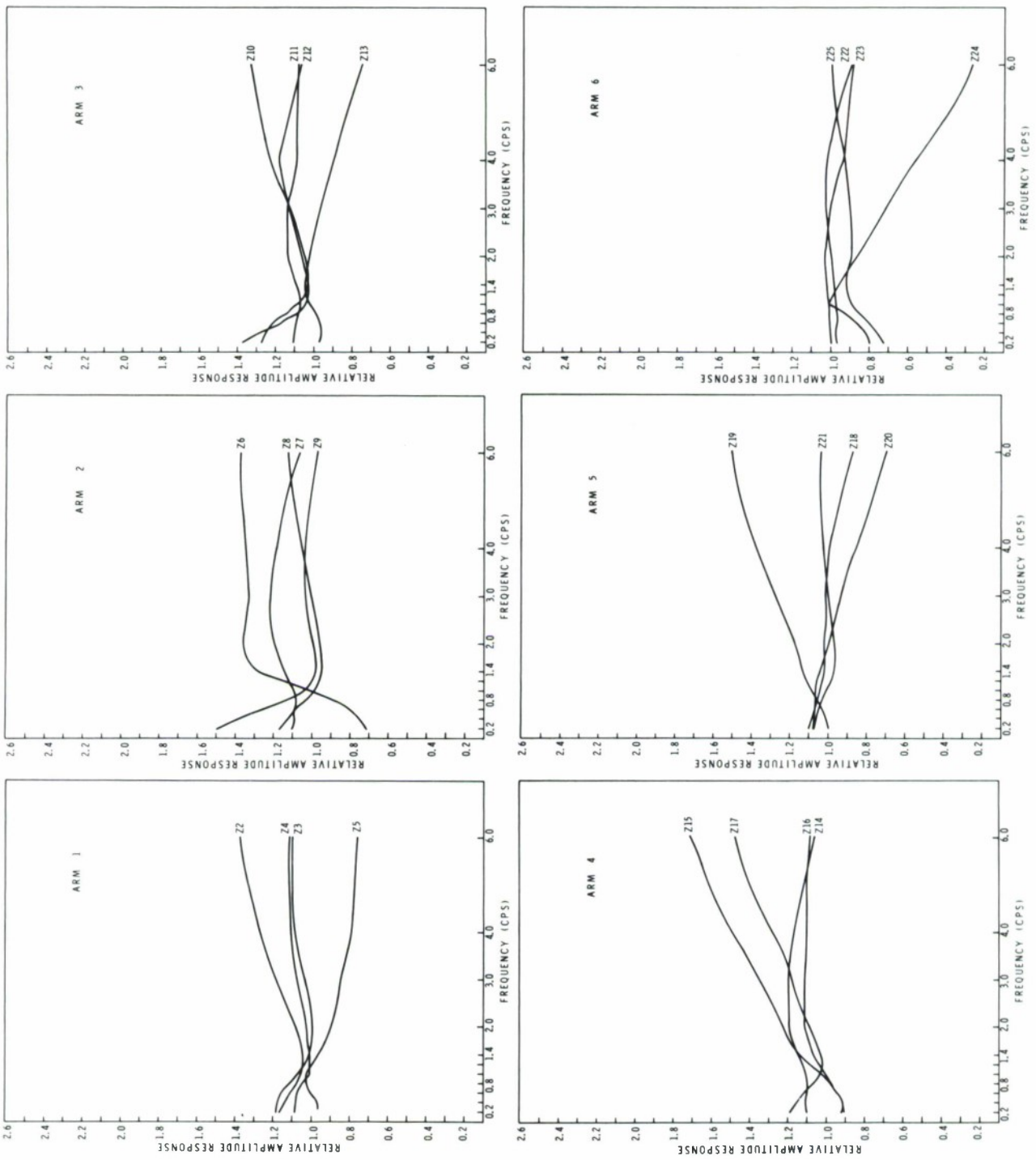

Figure C-4. Relative Amplitude Responses of Subarray E-2

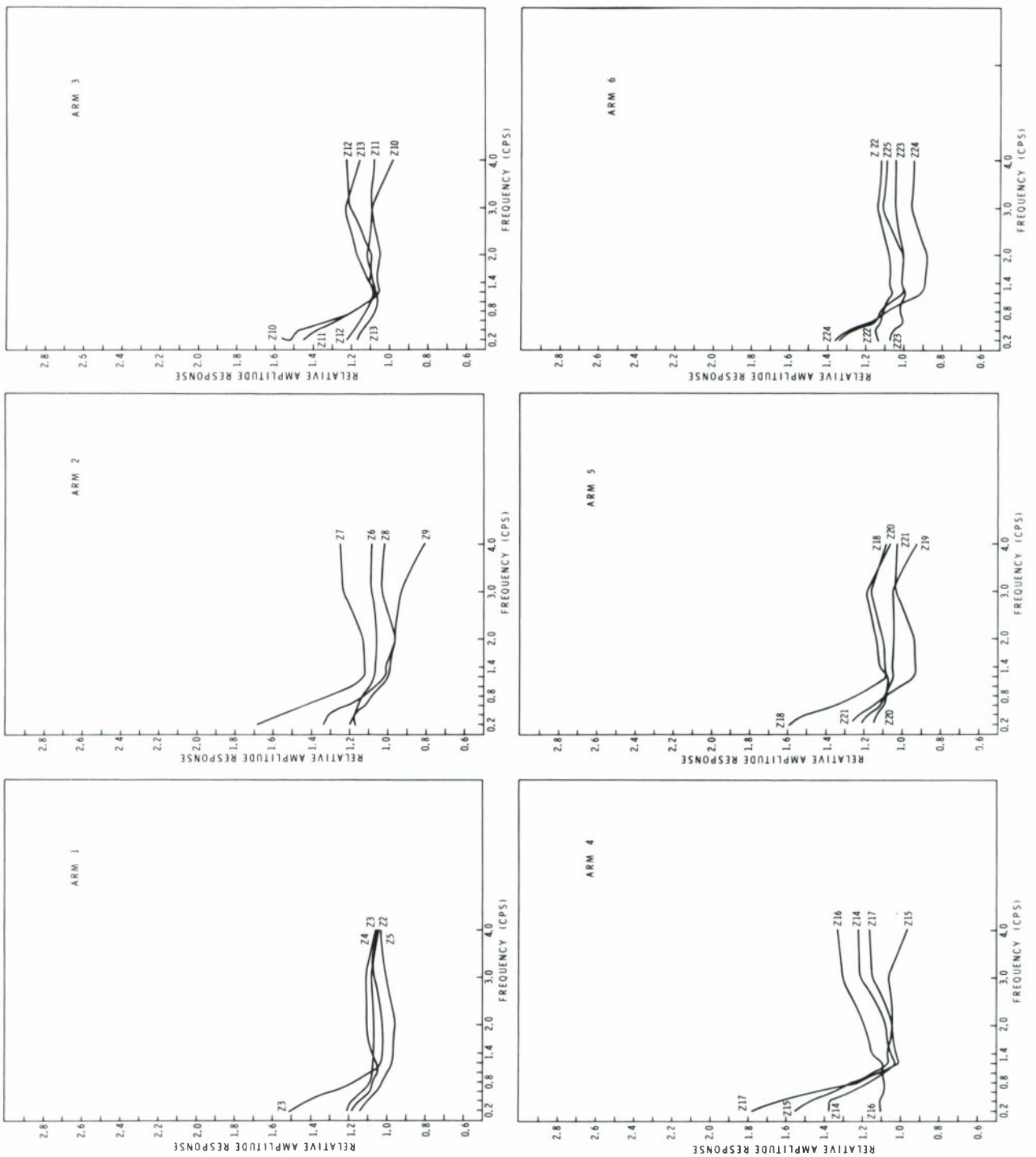

Figure C-5. Relative Amplitude Responses of Subarray F-2

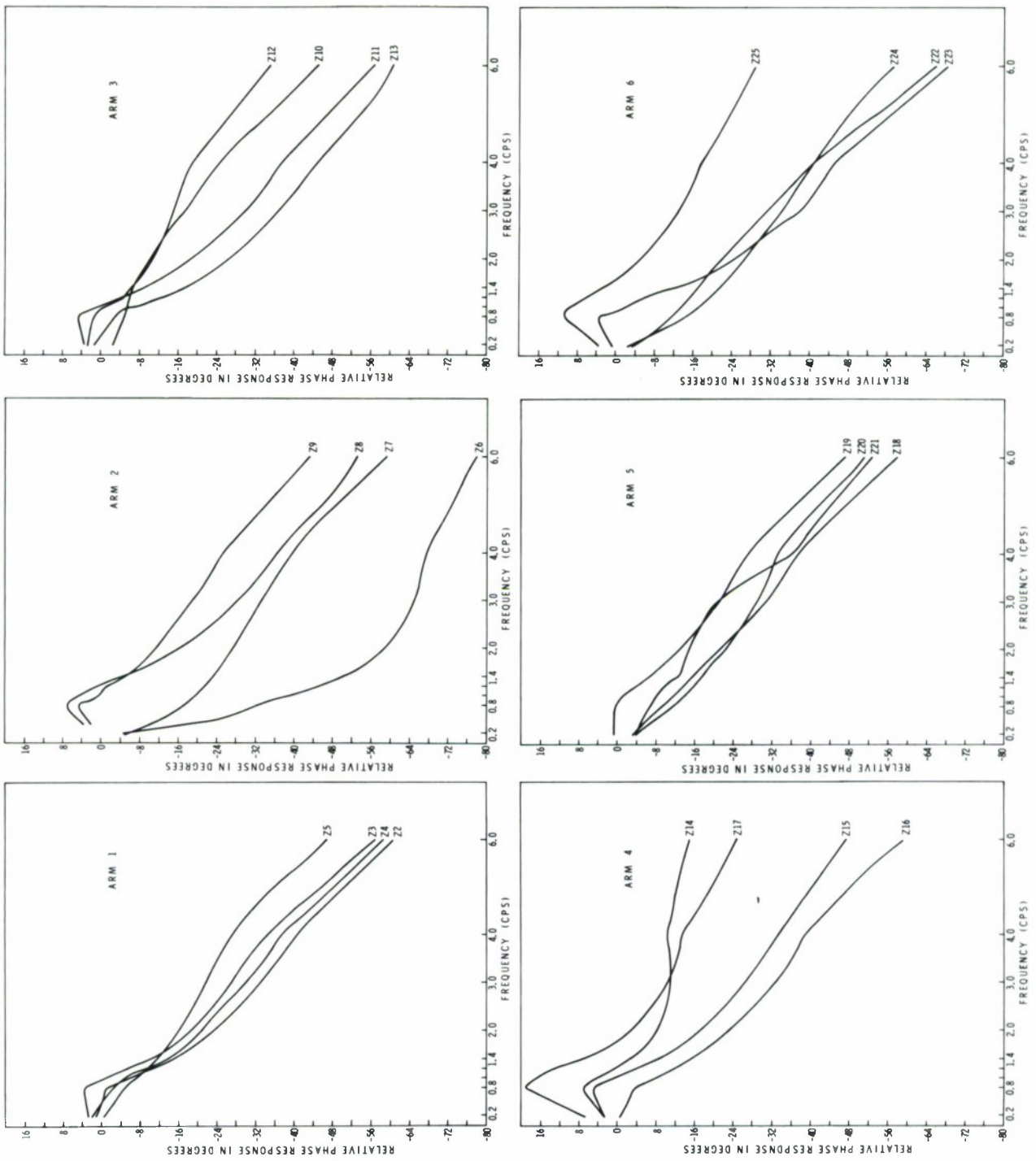

Figure C-6. Relative Phase Responses of Subarray F-3

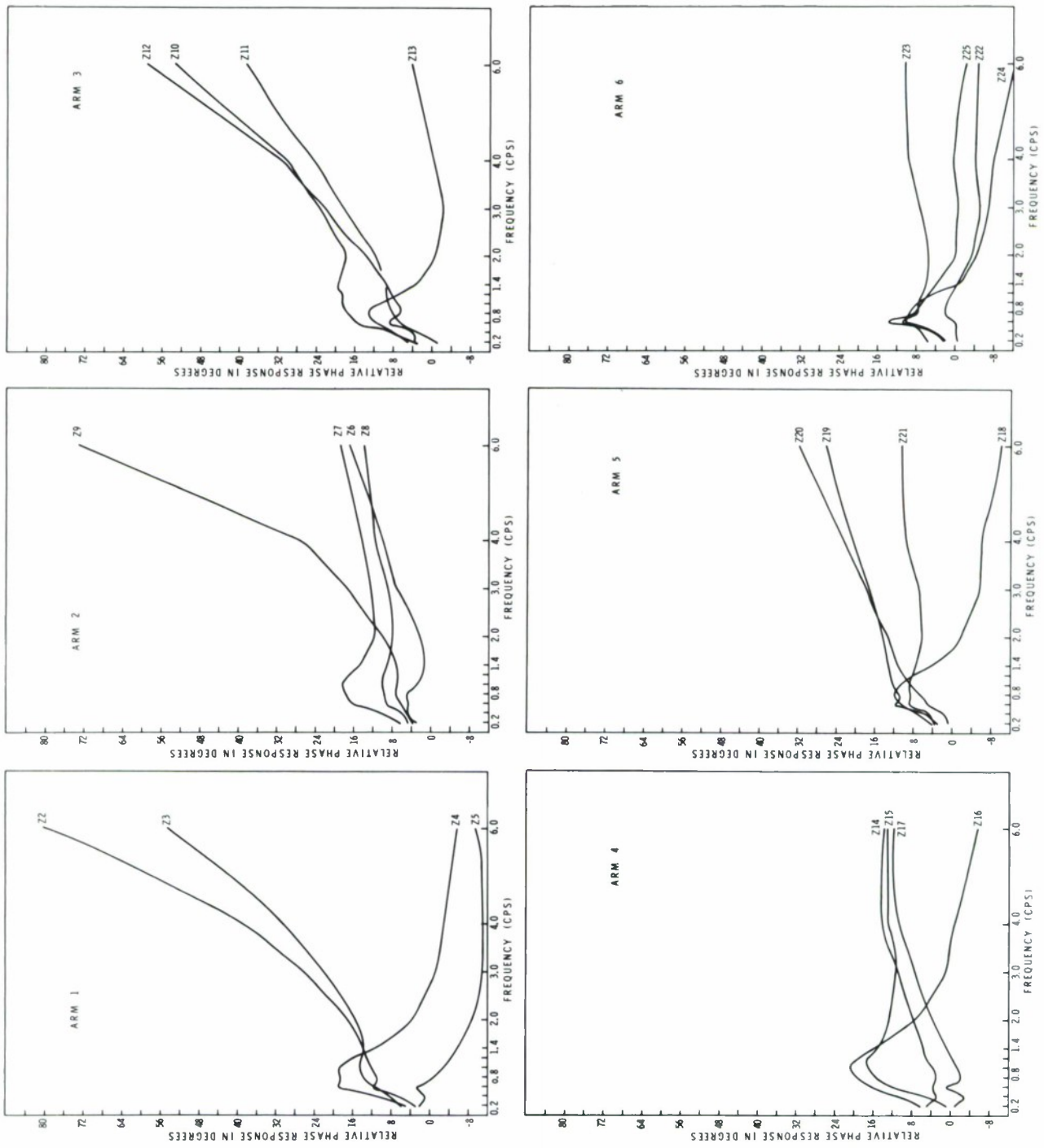

Figure C-7. Relative Phase Responses of Subarray F-4

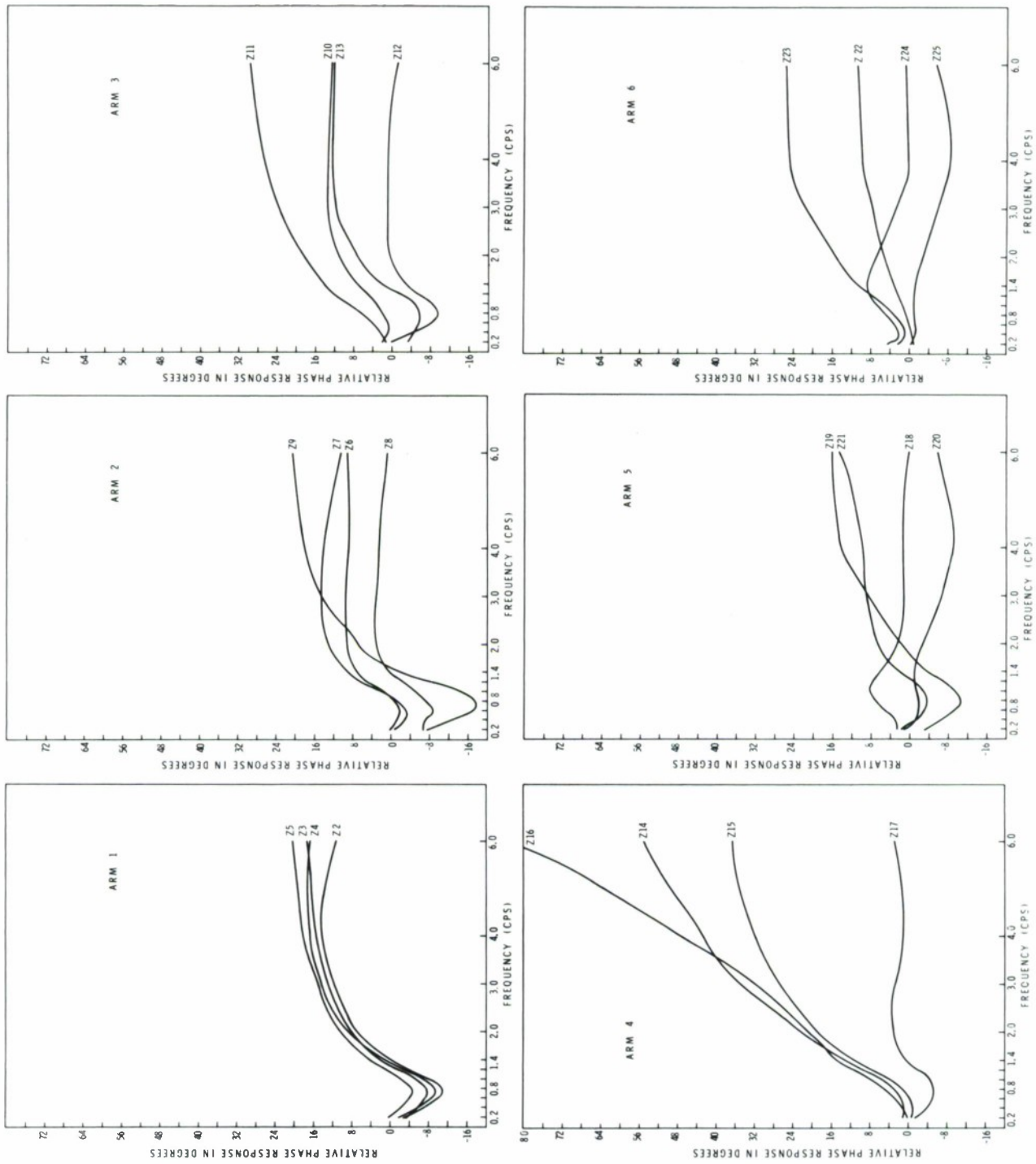

Figure C-8. Relative Phase Responses of Subarray C-3

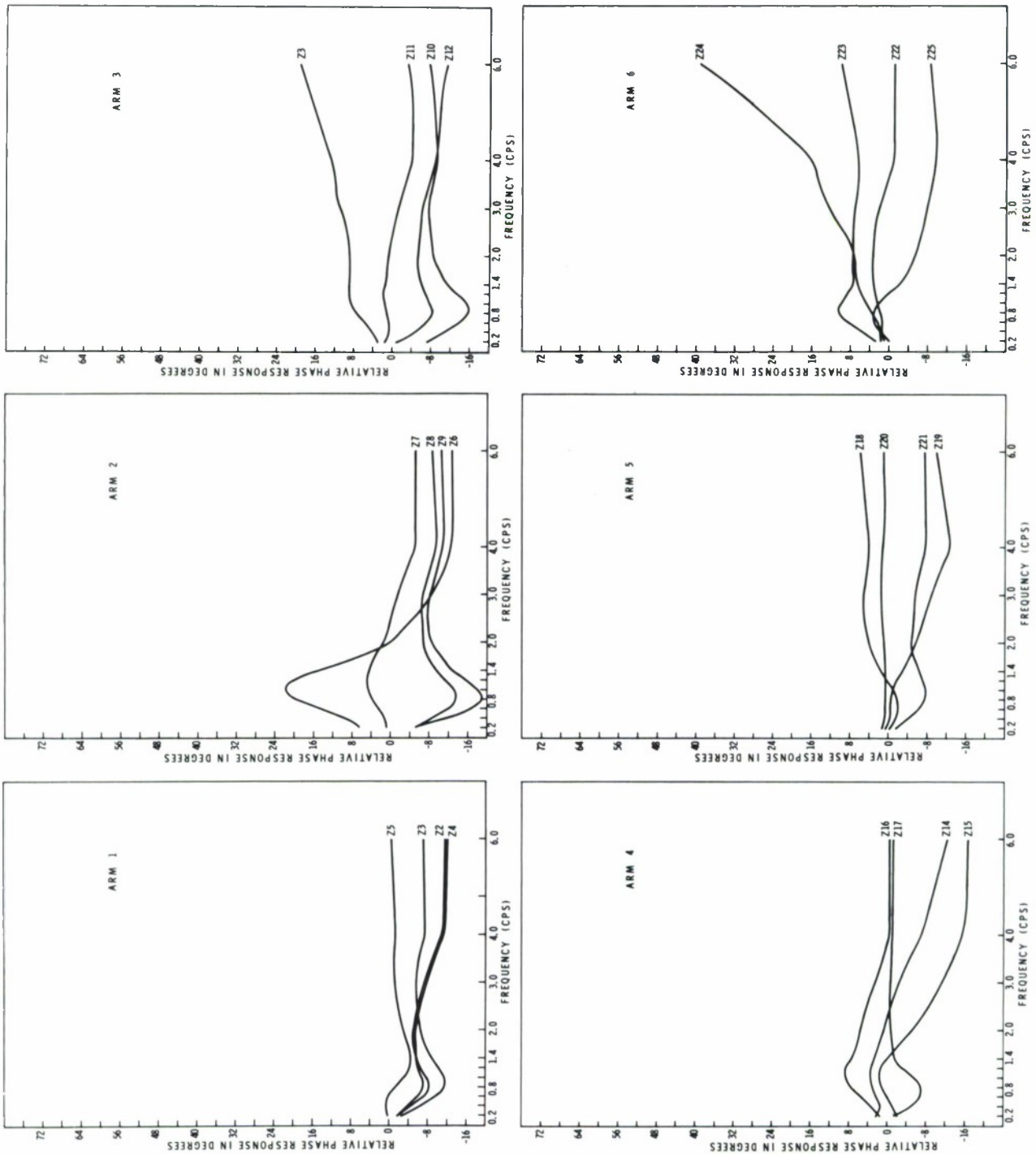

Figure C-9. Relative Phase Responses of Subarray E-2

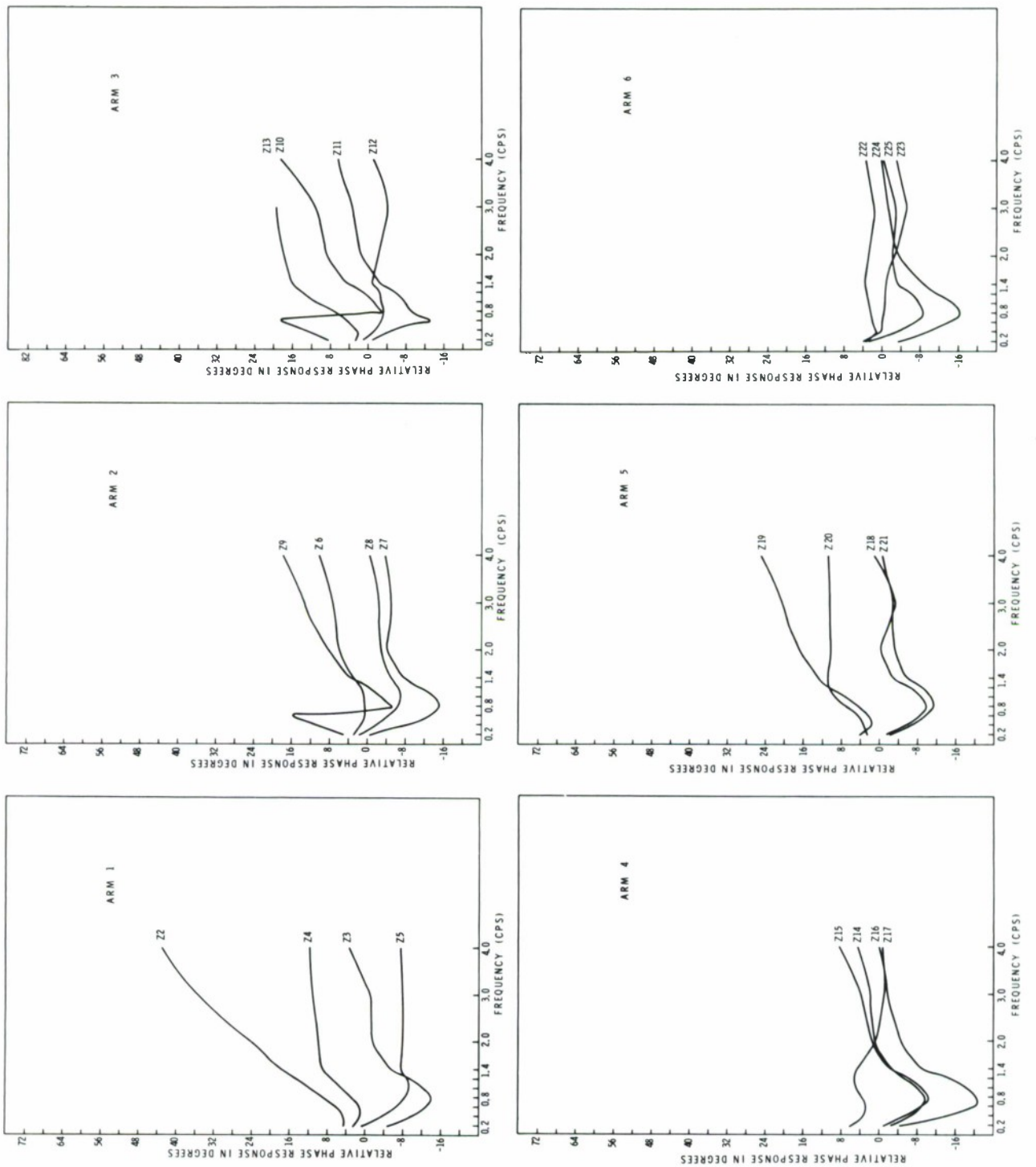

Figure C-10. Relative Phase Responses of Subarray F-2

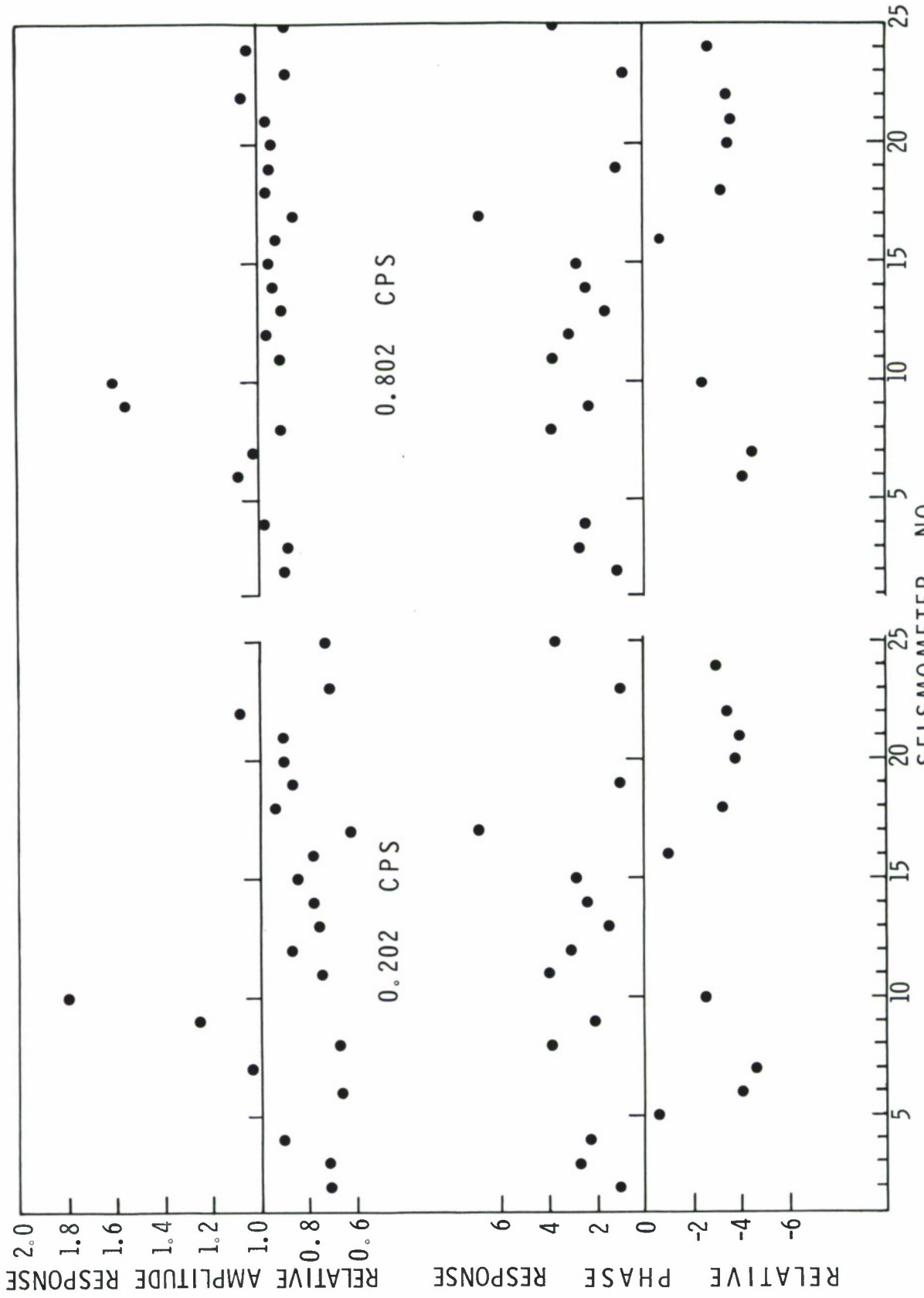

Figure C-11. Relative Phase and Amplitude Responses for Subarray F-3 at Frequencies 0.202 and 0.802 cps

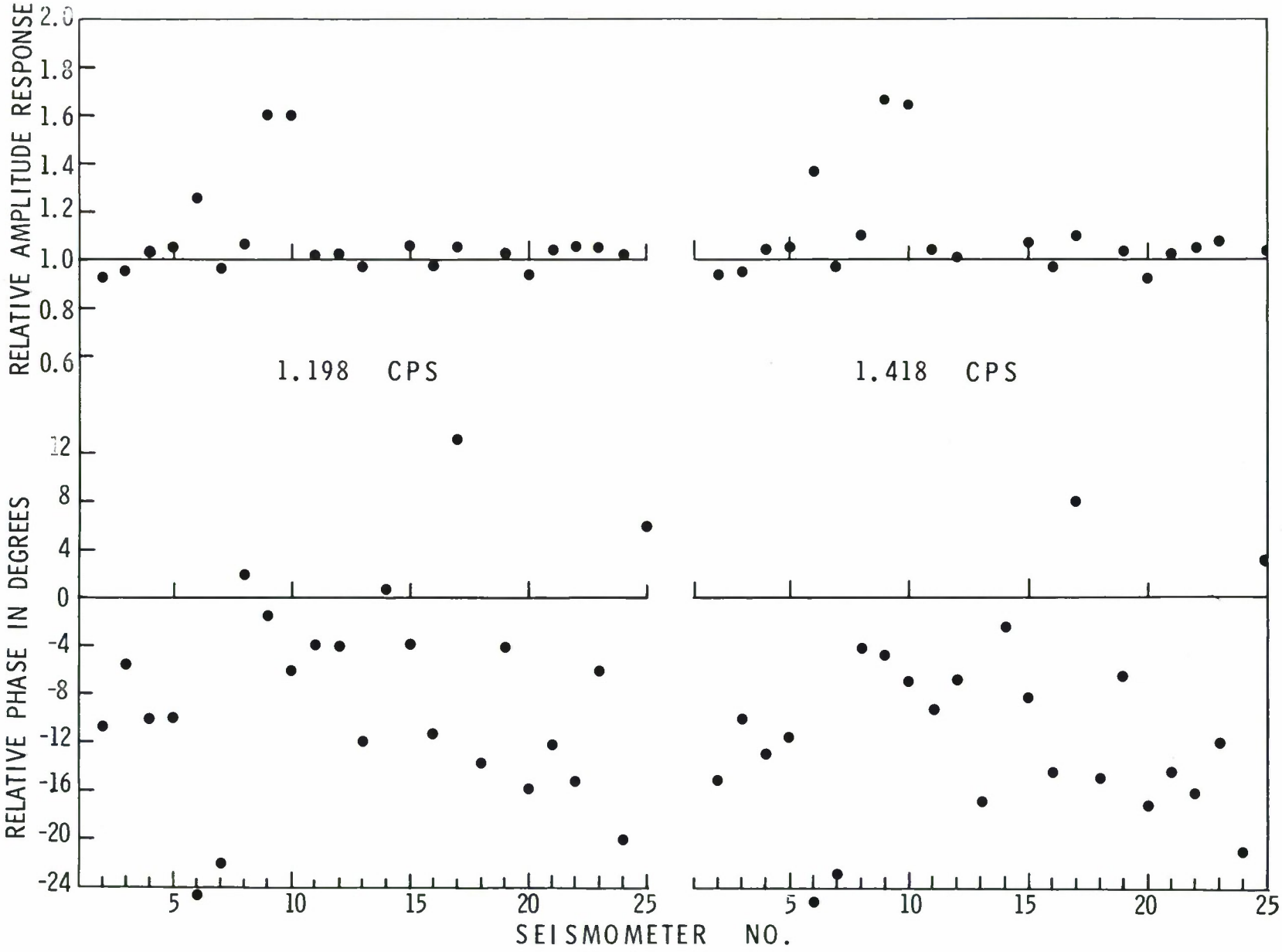

Figure C-12. Relative Phase and Amplitude Responses for Subarray F-3 at Frequencies 1.198 and 1.418 cps

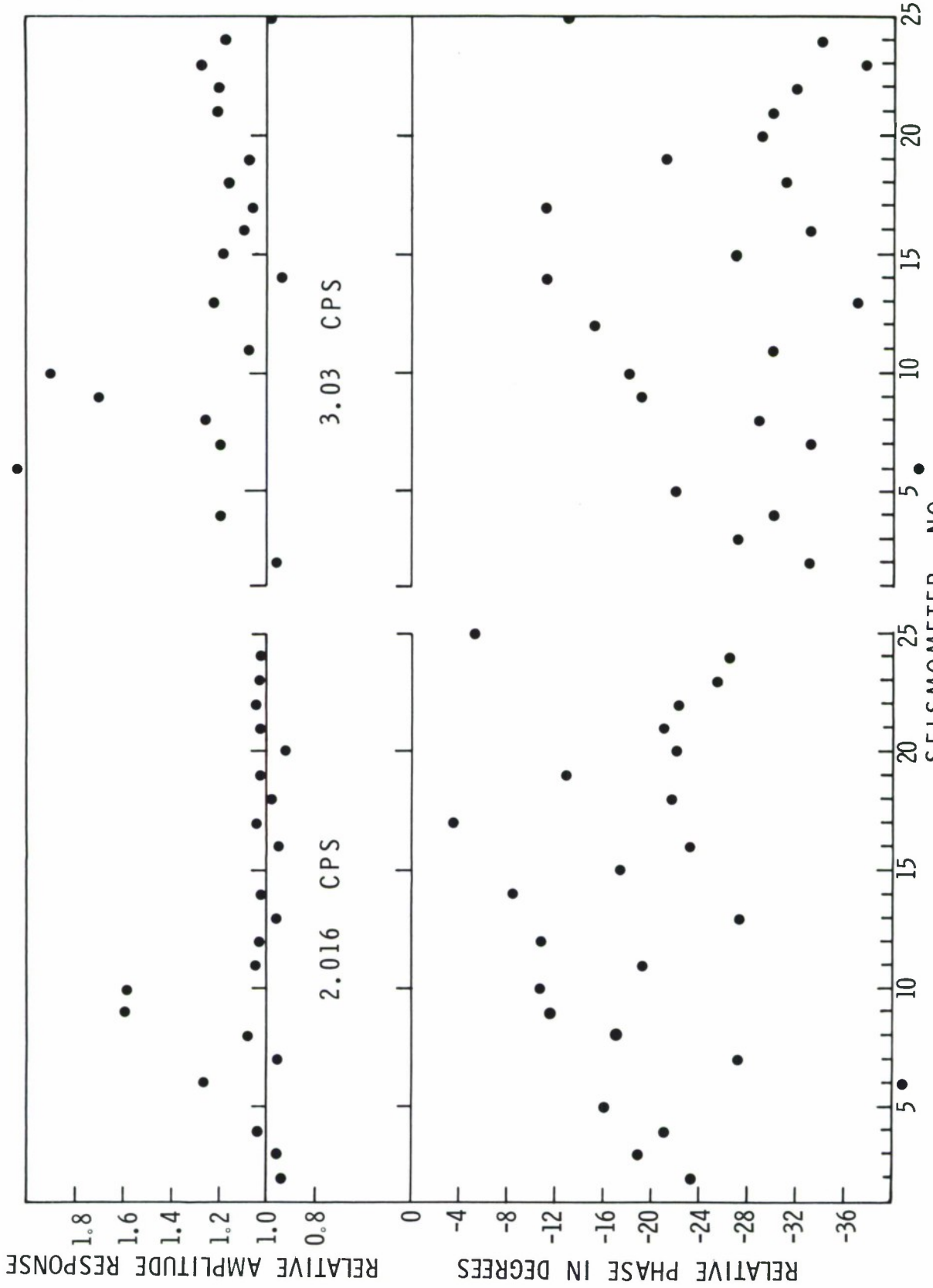

Figure C-13. Relative Phase and Amplitude Responses for Subarray F-3 at Frequencies 2.016 and 3.03 cps

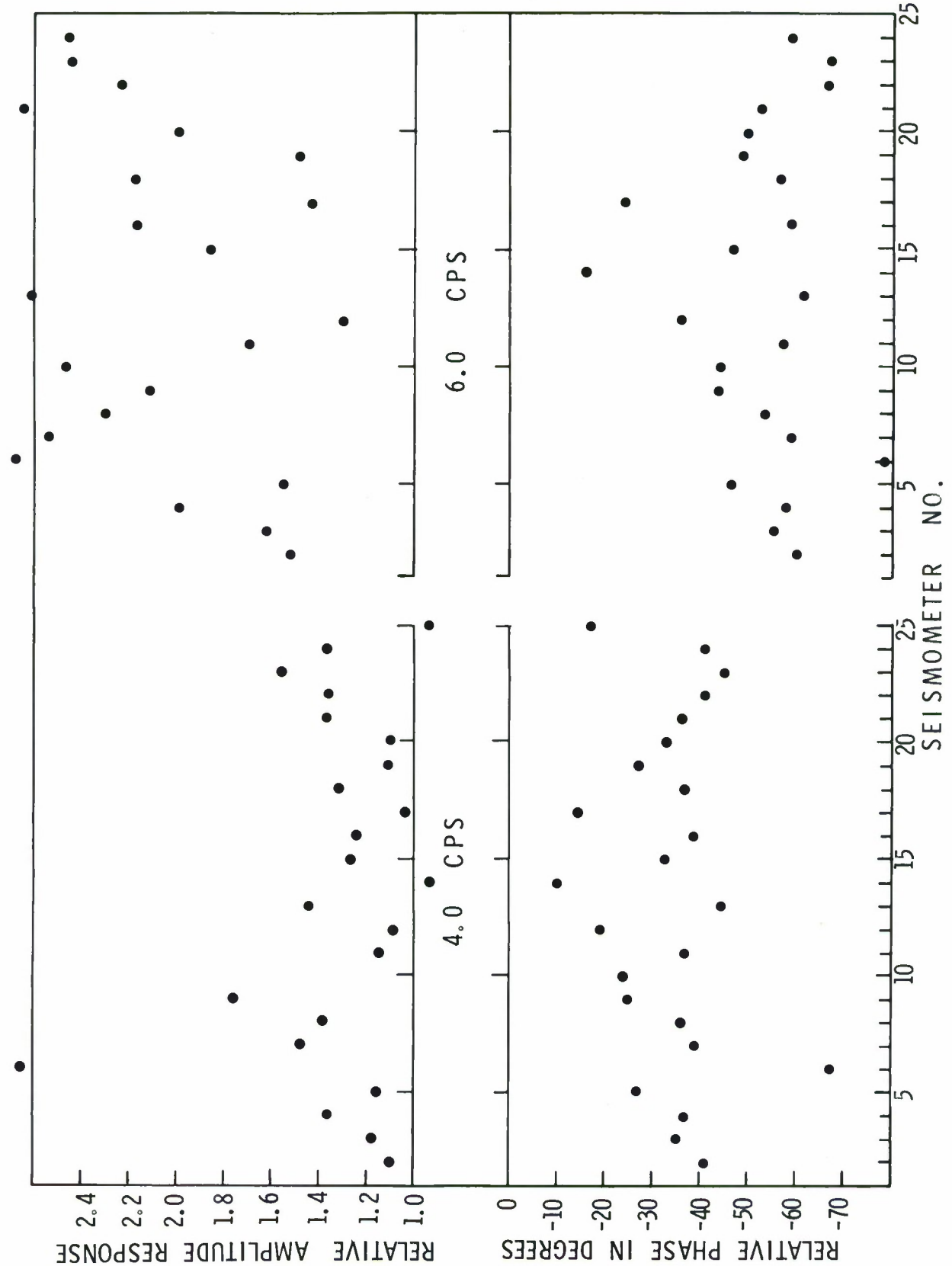

Figure C-14. Relative Phase and Amplitude Responses for Subarray F-3 at Frequencies 4.0 and 6.0 cps

UNCLASSIFIED

Security Classification

DOCUMENT CONTROL DATA – R&D

(Security classification of title, body of abstract and indexing annotation must be entered when the overall report is classified)

1. ORIGINATING ACTIVITY *(Corporate author)*

Texas Instruments Incorporated under Subcontract No. 325 to Lincoln Laboratory, M.I.T.

2a. REPORT SECURITY CLASSIFICATION
Unclassified

2b. GROUP
None

3. REPORT TITLE

LASA Data Analysis and MCF Support Final Report

4. DESCRIPTIVE NOTES *(Type of report and inclusive dates)*

Final Report

5. AUTHOR(S) *(Last name, first name, initial)*

Lake, Harry; Crouch, Don; Harley, Terry
Hair, George; Johnson, Bill; Wrenn, Jim

6. REPORT DATE	7a. TOTAL NO. OF PAGES	7b. NO. OF REFS
31 August 1966	282	5

8a. CONTRACT OR GRANT NO.
AF 19(628)-5167

b. PROJECT NO.
ARPA Order 512

c.

d.

9a. ORIGINATOR'S REPORT NUMBER(S)
Final Report

9b. OTHER REPORT NO(S) *(Any other numbers that may be assigned this report)*
ESD-TR-66-553

10. AVAILABILITY/LIMITATION NOTICES

Distribution of this document is unlimited.

11. SUPPLEMENTARY NOTES

None

12. SPONSORING MILITARY ACTIVITY

Advanced Research Projects Agency, Department of Defense

13. ABSTRACT

With the objective of determining optimum design criteria for predetection multichannel filters for use at the subarray level at the LASA, a study was conducted of the characteristics of the ambient noise fields and instrument responses of five selected subarrays.

Based on the measured characteristics of the noise fields and instrument responses, 14 multichannel filters were developed and compared as to degree of improvement in signal-to-noise ratio. A multichannel filter, of a design determined by the comparison experiments to be optimum for subarray predetection filtering, was developed for each of five subarrays. Five multichannel filters of a slightly different design also were developed. These multichannel filters, and certain others of interest, were punched on paper tape for on-line evaluation with the Digital Multichannel Filter System at LASA.

A processing procedure for detecting signals at either subarray or full-array level is recommended and illustrated by application to selected events at those subarrays under consideration.

14. KEY WORDS

LASA
multichannel filters
noise
signal-to-noise ratio
instrument responses

UNCLASSIFIED

Security Classification